

Monday Morning, October 19, 2015

Atom Probe Tomography Focus Topic

Room: 230A - Session AP+AS+MC+MI+NS-MoM

Atom Probe Tomography of Nanomaterials

Moderator: Daniel Perea, Pacific Northwest National Laboratory

8:20am **AP+AS+MC+MI+NS-MoM1 Correlative Multi-scale Analysis of Nd-Fe-B Permanent Magnet**, *Taisuke Sasaki, T. Ohkubo, K. Hono*, National Institute for Materials Science (NIMS), Japan **INVITED**

(Nd,Dy)-Fe-B based sintered magnets are currently used for traction motors and generators of (hybrid) electric vehicles because of their excellent combination of maximum energy product and coercivity. However, there is a strong demand to achieve high coercivity without using Dy due to its scarce natural resources and high cost. In Nd-Fe-B sintered magnets, thin Nd-rich grain boundary (GB) phase is a key microstructural feature affecting the coercivity. Although Nd-rich phases, e.g. Nd-rich oxides and metallic Nd, located at grain boundary triple junctions affect the formation of the Nd-enriched grain boundary phase during post-sinter annealing, their phase constitution, distribution and orientation relationships are still under debate.

This presentation will introduce examples of advanced characterization works to establish the global microstructural feature that controls the coercivity of Nd-Fe-B sintered magnets, e.g. the clarification of phase constitution and distribution of Nd-rich phases at the grain boundaries by correlative SEM and TEM characterization, and the identification of the structure and chemistry of thin Nd-rich grain boundary phases by high resolution HAADF-STEM and 3D atom probe. We found the coercivity decrease by carbon impurity can be explained by the decrease in the RE (RE: Rare earth) content in the thin Nd-rich grain boundary phase.

9:00am **AP+AS+MC+MI+NS-MoM3 Atom-Probe Tomography of Materials with Dimensions in the Nanometer Range**, *Dieter Isheim*, Northwestern University **INVITED**

Nanometer-sized materials and particles seem to naturally lend themselves for investigation by atom-probe tomography (APT) which provides analytical imaging with subnanometer-scale spatial resolution in three dimensions. The material's characteristic dimensions may already be close to the one required to produce the electric field necessary for analysis by field-evaporation in an atom-probe tomograph and thus analysis seems straight forward. In practice, however, controlled manipulation and positioning of these nanoparticles or nanowires for APT analysis proves challenging since the support structure of an APT tip must be strong enough to resist the mechanical stresses exerted by the high electric fields involved. Additionally, the nanoparticles should ideally not be altered or damaged in the preparation process. These requirements can be met by modern processing techniques that combine suitable deposition methods for packaging nanoparticles in structures that are either ready for analysis, or suitable for subsequent APT tip preparation by a standard technique. Focused-ion-beam (FIB) microscopes equipped with a micro- or nanomanipulator and gas injection systems for electron- or ion-beam induced deposition provide a versatile platform for packaging, cutting, joining, and manipulating nanostructured materials, and thus to capture and target nanoparticles or specific microstructural features for APT analysis. This presentation explores these techniques to characterize a variety of nanometer sized and nanostructured materials, including nanodiamond particles and catalytically grown silicon nanowires.

9:40am **AP+AS+MC+MI+NS-MoM5 Exploring Atom Probe Tomography for Energy Storage and Conversion Materials**, *Pritesh Parikh*, University of California, San Diego, *A. Devaraj*, Pacific Northwest National Laboratory, *S. Meng*, University of California, San Diego

The Sun forms the largest and most abundant source of energy on earth, yet it is not exploited to its full potential. Solar energy is a burgeoning field with a real chance to replace fossil fuels. The intermittent presence of sunlight can be mitigated by combining energy conversion devices such as solar panels with energy storage devices, namely Li ion batteries. A true solution is possible with the integration of both solar panels and batteries. With the general impetus towards adopting renewable sources for large scale energy storage and supply, fundamental studies on solar panels and batteries will provide new clues to design the next generation of energy devices. A Perovskite solar cell is one such technology that has the potential of high efficiency and low processing costs but a clear understanding of the role of different materials and their individual interactions is still lacking. The ability to identify and understand interfaces and multiple layers in a

complex device such as solar cells and batteries is the need of the hour. Here we report on laser assisted atom probe tomography of energy storage and conversion devices to identify the spatial distribution of the elements comprising the various layers and materials. Recent progress and significant challenges for preparation and study of perovskite solar cells and battery materials using laser assisted atom probe tomography will be discussed. This opens up new avenues to understand complex multi-layer systems at the atomic scale and provide a nanoscopic view into the intricate workings of energy materials.

10:00am **AP+AS+MC+MI+NS-MoM6 Atom Probe Tomography of Pt-based Nanoparticles**, *Katja Eder, P.J. Felfler, J.M. Cairney*, The University of Sydney, Australia

Pt nanoparticles are commonly used as catalysts in fuel cells. There are a lot of factors which influence the activity of a catalyst, including the surface structure and geometry [1], d-band vacancy of the metal catalyst [2], the type of metal oxide support [3] and the oxidation state of the surface [4]. It is not yet fully understood in which way these factors influence the activity of the catalyst, since it is experimentally very difficult to get atomic scale information about the distribution of the atoms within such particle with conventional methods like transmission electron microscopy (TEM), scanning electron microscopy (SEM), scanning tunnelling microscopy (STM) and others. Models available which try to explain the structure-activity relationships therefore vary widely and there is much debate in the scientific literature about the underlying mechanisms of catalysis. For this reason it is crucial to conduct more research with methods that are able to obtain chemical information with a resolution on the atomic scale. In the past few years atom probe tomography (APT) has successfully been used in several studies to analyse nanoparticles [4-6]. APT provides a 3D reconstruction of the original specimen, which gives information about the chemical composition and the microstructure at a very high resolution. This method will enable us to have a closer look at the surface and interfaces as well as the composition of individual nanoparticles and solute atoms. In this talk we will present APT results of Pt nanoparticles, describing our efforts to prepare specimens with a reasonable yield and improved throughput compared to earlier studies, as well as some of the approaches used to overcome the difficulties that this challenge presents.

[1] A.R. Tao, S. Habas, P. Yang, Small, 4 (2008) 310-325.

[2] M.-K. Min, J. Cho, K. Cho, H. Kim, Electrochimica Acta, 45 (2000) 4211-4217.

[3] T. Akita, M. Kohyama, M. Haruta, Accounts of chemical research, (2013).

[4] T. Li, E.A. Marquis, P.A.J. Bagot, S.C. Tsang, G.D.W. Smith, Catalysis Today, 175 (2011) 552-557.

[5] Y. Xiang, V. Chitry, P. Liddicoat, P. Felfler, J. Cairney, S. Ringer, N. Kruse, Journal of the American Chemical Society, 135 (2013) 7114-7117.

[6] D.J. Larson, A.D. Giddings, Y. Wu, M.A. Verheijen, T.J. Prosa, F. Roozeboom, K.P. Rice, W.M.M. Kessels, B.P. Geiser, T.F. Kelly, Ultramicroscopy, (2015).

10:40am **AP+AS+MC+MI+NS-MoM8 APT & TEM Observations on Local Crystallization of NbO₂ used in Switching Devices**, *J.-H. Lee*, Pohang University of Science and Technology (POSTECH), Samsung Electronics, Republic of Korea, *J.-B. Seol*, *C.-G. Park*, Pohang University of Science and Technology (POSTECH), National Institute for Nanomaterials Technology (NINT), Republic of Korea **INVITED**

Threshold switching is the basis of electrical or thermal-driven phase change mechanism of oxide layer. That is, some oxide can change their conductivity from the level of insulators to that of metals with above certain current density. Although the mechanism responsible for threshold switching is not fully understood at present, it can be used as a switching device for the solution of sneak leakage problem. In order to apply the bipolar switching materials as the active layer of Resistive-switching Random Access Memory (RRAM), selection device which can minimize the sneak leakage current is needed. Among various candidates, we chose Nb-oxide for the selection device due to its superior compatibility with semiconductor structure. We have elucidated the mechanism of threshold switching of the amorphous NbO₂ layer by using in-situ transmission electron microscopy (TEM) technique combined with atom probe tomography (APT).

In this study, we proved that through an ex-situ experiment using TEM the threshold switching of amorphous NbO₂ accompanies local crystallization. The change in I-V characteristics after electroforming was examined by evaluating the concentration profile. APT combined with in-situ TEM probing technique was performed to understand the threshold switching in

amorphous NbO₂. The local crystallization in amorphous NbO₂ was validated by the observed difference in time-of-flight (ToF) between amorphous and crystalline NbO₂. We concluded that the slower ToF of amorphous NbO₂ (a-NbO₂) compared to that of crystalline NbO₂ (c-NbO₂) is due to the resistivity difference and trap-assisted recombination.

11:20am **AP+AS+MC+MI+NS-MoM10 Correlating Atom Probe Tomography with High-Resolution Scanning Transmission Electron Microscopy and Micro-Photoluminescence Spectroscopy: The Case of III-Nitride Heterostructures**, *Lorenzo Rigutti*, University of Rouen **INVITED**

Correlating two or more microscopy techniques on the same nanoscale object may yield a relevant amount of information, which could not be achieved by other means. In this contribution, we present several results of correlated studies of micro-photoluminescence (μ -PL), high-resolution scanning transmission electron microscopy (HR-STEM) and laser-assisted atom probe tomography (APT) on single nano-objects containing AlGaInN quantum well and quantum dot systems. We will show how this approach can be applied to the study of heterostructure interface definition, presence of defects, carrier localization and optical emission in III-N quantum confined systems [1]. Furthermore, we will show how the use of complementary techniques may be extremely helpful for a correct interpretation of atom probe results [2]. The possible implementation of micro-photoluminescence as an in-situ technique within the atom probe itself will finally be discussed [3].

[1] L. Rigutti et al., *Nano letters* (2014), 14, 107–114.

[2] L. Mancini et al. *J. Phys. Chem. C* (2014) 118, 24136–24151.

[3] L. Rigutti et al., *Ultramicroscopy* (2013), 132, 75–80.

Applied Surface Science

Room: 212D - Session AS-MoM

Quantitative Surface Analysis: Obtaining Quantitative Information in the Face of Material Complexity and Morphology Influences

Moderator: Christopher Szakal, National Institute of Standards and Technology (NIST), Alberto Herrera-Gomez, CINVESTAV-Queretaro, Mexico

8:20am **AS-MoM1 Quantitative XPS of Core-Shell Nanoparticles**, *Cedric Powell*, National Institute of Standards and Technology (NIST), *M. Chudzicki, W.S.M. Werner, W. Smekal*, Technical University of Vienna, Austria

We used the new version of the NIST Database for the Simulation of Electron Spectra for Surface Analysis (SESSA) [1] to simulate XPS spectra of core-shell nanoparticles (NPs). Two series of simulations have been made. First, Cu 2p spectra were simulated using Al K α x-rays for a monolayer of three types of Cu-Au NPs on an Si substrate: (a) an Au shell of variable thickness on a Cu core with diameters of 0.5 nm, 1.0 nm, 2.0 nm, 5.0 nm, and 10.0 nm; (b) a Cu shell of variable thickness on an Au core with diameters of 0.5 nm, 1.0 nm, 2.0 nm, 5.0 nm, and 10.0 nm; and (c) an Au shell of variable thickness on a 1 nm Cu shell on an Au core with diameters of 0.5 nm, 1.0 nm, 2.0 nm, 5.0 nm, and 10.0 nm. For these three morphologies, the outer-shell thickness was varied until the Cu 2p_{3/2} peak intensity was the same (within 2 %) as that found in our previous work with planar Cu/Au morphologies [2]. For each morphology, we performed simulations with elastic scattering switched on and off. We found that elastic-scattering effects were generally strong for the Cu-core/Au-shell and weak for the Au-core/Cu-shell NPs; intermediate elastic-scattering effects were found for the Au-core/Cu-shell/Au-shell NPs. The shell thicknesses required to give the selected Cu 2p_{3/2} peak intensity for the core-shell NPs were less than the corresponding film thicknesses of planar samples since Cu 2p photoelectrons can be detected from the sides and, for the smaller NPs, bottoms of the NPs.

Second, we determined effective attenuation lengths (EALs) for Cu 2p_{3/2} photoelectrons from NPs consisting of a Cu core of diameters 0.5 nm, 1 nm, 2 nm, 5 nm, and 10 nm and a Cu shell with thicknesses between 0.25 nm and 3.75 nm. The EAL was determined from the Cu 2p_{3/2} intensity from the core with no shell and from the Cu 2p_{3/2} intensity from the core that was attenuated by a Cu shell of specified thickness. These EALs varied systematically with both Cu-core diameter and Cu-shell thickness. While the inelastic mean free path of Cu 2p_{3/2} photoelectrons (at 534 eV) in Cu is 1.12 nm, the EALs for a 10 nm Cu core varied from 0.53 nm to 0.65 nm as the Cu-shell thickness increased from 0.25 nm to 3.75 nm. In contrast, the EALs for a 0.5 nm Cu core increased from 0.78 nm at a shell thickness of

0.25 nm to a maximum value of 0.86 nm for a shell thickness of 0.75 nm and then decreased to 0.81 nm for a shell thickness of 3.75 nm. These changes show the important roles of NP morphology, NP dimensions, and elastic scattering in determining shell thicknesses by XPS.

[1] <http://www.nist.gov/srd/nist100.cfm>.

[2] C. J. Powell, S. Tougaard, W. S. M. Werner, and W. Smekal, *J. Vac. Sci. Technol. A* 31, 021402 (2013).

8:40am **AS-MoM2 The Satellites of the 2p Core Level of Transition-Metals**, *Alberto Herrera-Gomez*, CINVESTAV-Queretaro, Mexico

The shake-up satellites in XPS spectra are due to intrinsic energy losses as the photoelectron leaves the hosting atom. The first row transition metals, either in the metallic or in the oxide form (and sometimes in both), display clear shake-up features in the corresponding 2p core level. They are difficult to quantify because the shape of the main 2p peaks of these elements are highly asymmetric and the spectra contains a large background contribution. In fact, there is a frequent correlation between the presence of satellites and a large background intensity and, also, a large peak shape asymmetry. Through newly developed procedures it has been possible to properly fit all these core levels. In addition to those already described in the literature, the procedures allowed for pinpointing previously unreported shake-up satellites. A common feature of the satellites is that their spin-orbit splitting exhibits a remarkable difference with the associated to the main peak, suggesting angular-dependent correlation effects.

9:00am **AS-MoM3 Quantitative Analysis of Advanced Commercial Glasses for Display Technologies**, *Cody Cushman*, Brigham Young University, *N.J. Smith, Corning, T. Grehl, P. Bruener*, ION-TOF GmbH, Germany, *M.R. Linford*, Brigham Young University

A series of complex, multicomponent commercial glasses used in advanced display applications was exhaustively analyzed by X-ray photoelectron spectroscopy (XPS), time-of-flight secondary ion mass spectrometry (ToF-SIMS), low energy ion scattering (LEIS), Rutherford backscattering (RBS), atomic force microscopy (AFM), and spectroscopic ellipsometry, where the purpose of this study was to quantify the compositions and properties of these materials. XPS revealed the compositions of the upper ca. 10 nm of the glasses, which differed substantially from each other. Angle resolved XPS suggested some segregation of some elements to the surfaces. These results were confirmed by LEIS, which conclusively identified the elements at the true surfaces of the materials in a quantitative fashion. Like XPS, ToF-SIMS probed the near surface regions of the materials. However, it also identified elements that were beyond the detection limit of XPS. In addition, ToF-SIMS was used with XPS to quantitatively determine the concentration of –OH groups at the surfaces of the glasses via the SiOH⁺/Si⁺ ratio. Atomic force microscopy (AFM) showed that the materials were all extremely flat, with roughnesses on the order of 1 nm. Spectroscopic ellipsometry from 200 – 1700 nm was used to determine the optical properties (quantitative dispersion relationships) of the glasses. These techniques provided a comprehensive analysis of these glass samples. In addition, the glasses were subjected to various cleaning procedures (plasma, wet chemical cleans, etc.) and other surface treatments. The same suite of analytical techniques was then used to show conditions that led to changes or no changes in the compositions of the glasses, and these changes were quantified.

9:20am **AS-MoM4 New Horizons in Practical Applications of Sputter Depth Profiling**, *W.F. Stickler, C.N. Young, M.D. Johnson*, HP, *A.A. Ellsworth, Amy Walker*, University of Texas at Dallas

In the application of x-ray photoelectron spectroscopy the use of sputter depth profiling is one of the routinely used methods for analysis. Most industrial laboratories study a wide variety of material systems such as polymers or inorganic thin films and many of these material systems require analysis not just of the as received surface, but also of and through the depth of a thin film. Historically, mono atomic argon has been the ion source of choice in XPS, but even at low ion energies mono atomic argon will damage not only polymer systems converting them into amorphous carbon but also damage inorganic materials by creating, for example, intermediate oxides. In recent years other ion sources have become routinely available such as C60⁺ and most recently, gas cluster ion sources. From a practical standpoint, it is important to understand the sputter induced chemistry that may be created by these various sources and the trade-offs for applying these different primary ion sources for routine surface chemical analyses. The effects of preferential sputtering and chemical changes or reactions of metal oxides will be discussed. Several different material systems are examined and discussed by comparing the information obtained using mono atomic argon, an argon gas cluster source and a C60⁺ ion gun for enhancing and clarifying ‘routine’ analyses. The different types of samples to be discussed will include niobium oxides, titanium nitride and multilayer thin films.

9:40am **AS-MoM5 ASSD 30th Anniversary Lecture: Sensitivity Factors in XPS: Where Do They Come From and How Accurate Are They?**, *John Grant*, University of Dayton **INVITED**

The most common method for quantitative analysis in X-ray Photoelectron Spectroscopy (XPS) incorporates relative sensitivity factors. In the 1970s and 1980s, several research groups studied the relative intensities of photoelectron lines and attempted to generate tables of relative sensitivity factors. Calculations were also made of ionization cross-sections using Mg and Al K α x-rays, and experimental measurements were often compared to theory. The seminal measurements were made by Wagner and co-workers, who used two different types of electron energy analyzers from two different manufacturers and compared the results with theory and with other measurements. They found that the agreement in data from the two instruments on the same compounds was good, and they generated a table of empirically derived sensitivity factors. Today, many XPS analysts still use the relative sensitivity factors from Wagner's work, particularly if they use an instrument where the sensitivity factors were not provided. An early ASTM round-robin on XPS measurements on catalysts by 12 laboratories found a large spread in measured peak intensity ratios, even for instruments of the same manufacture, concluding that a calibration procedure for the intensity response of instruments was needed. A later ASTM round-robin on pure Au and Cu concluded that the spread in intensity ratios was typically a factor of ten. Based on these results, Seah spearheaded studies on instrument transmission functions and developed a method so that the relative instrument response function between two different analyzers was better than 5%. In 1990, he published standard reference spectra for XPS and claimed all instruments may be calibrated absolutely to an accuracy of $\pm 2\%$. The National Physical Laboratory (NPL) developed and sold a procedure for generating an instrument transmission function, but it was not widely adopted. At least one manufacturer developed a model for measuring the transmission function in their instruments and measures it on each instrument before shipping it to the purchaser. A digital database of spectra was also developed at NPL, and could have provided a set of relative sensitivity factors for XPS, but it was never sold. It is important to know the origin of the sensitivity factors supplied by manufacturers and any limits placed on their applicability. By measuring spectra from a number of reference compounds one can quickly learn how reliable they are. For the most accurate measurements, one should measure relative sensitivity factors from standard compounds that match as closely as possible the compositions of unknowns.

10:40am **AS-MoM8 Ar⁺ and Cluster Ion Depth Profiling for Quantitative XPS Inorganic Thin Film Analysis**, *Jennifer Mann, J.F. Moulder, S.R. Bryan, J.S. Hammond*, Physical Electronics

A successful XPS sputter depth profile should accurately identify layer thickness and composition of materials as a function of depth within film structures. In the case of inorganic thin films, monoatomic argon ion beam depth profiling continues to be the preferred choice despite issues with preferential sputtering, material migration, and chemical reduction that may occur during the sputter process to alter the apparent profile of the analyzed material [1-3].

The introduction of C₆₀ cluster ion beam and argon gas cluster ion beam (GCIB) sputtering in recent years provided the capability of successful depth profiling of polymer and organic materials as well as thin film structures while preserving the stoichiometry and chemical structures [4,5].

Currently, there is great interest in establishing the viability of these cluster ion sources as an alternative to Ar⁺ ion beam sources for analyzing inorganic semiconductor and glass films, with particular interest in a possible improvement in the quantitative accuracy of the depth profile results compared to Ar⁺ depth profiling [6,7].

The XPS depth profile of a thin film of the semiconductor material Indium Gallium Zinc Oxide (IGZO) was acquired with Ar⁺, C₆₀⁺ and GCIB ion guns. The film thickness and composition was characterized by RBS. Preferential sputtering of the In through the thin film depth profiles was observed with all three ion sources. The highest level of preferential sputtering of In was observed with the Ar⁺ source while the C₆₀⁺ source produced a relatively constant composition through the depth profiles and the most consistent with the expected elemental composition. The sputter volume per incident ion, the resulting interface width and the sputter crater roughness for the three different ion sources was also evaluated.

Similar evaluations for additional thin film oxide samples will also be presented. The results for these comparative studies suggest that depending on the composition of the inorganic oxide thin films, cluster ion sources may provide superior quantitative depth profiling for inorganic oxide thin film samples as well as organic thin film samples.

References

[1] J. B. Malherbe, S. Hofmann and J. M. Sanz, *App. Surf. Sci.*, 1986, 27, 355.

[2] R. K. Brow, *J. of Vac. Sci. Technol. A*, 1989, 7, 1673.

[3] V. Smentkowski, *Prog. in Sur. Sci.*, 2000, 64, 1.

[4] T. Nobuta, T. Ogawa, *J. of Mater. Sci.*, 2009, 44, 1800.

[5] C. M. Mahoney, *Mass Spec. Rev.*, 2010, 29, 247.

[6] Y. Yamamoto, K. Yamamoto, *Mater. Sci. Eng.*, 2011, 18, 022005.

[7] D. Kobayashi, Y. Yamamoto, T. Isemura, *Sur. and Inter. Anal.*, 2013, 45, 113.

11:00am **AS-MoM9 Preservation of Chemical States in Mixed Material Surfaces when Profiling with Noble Gas Clusters**, *Christopher Deeks, J.P.W. Treacy, P. Mack, T.S. Nunney*, Thermo Fisher Scientific, UK

The technique of X-ray Photoelectron Spectroscopy (XPS) is valued within the surface science community because it offers chemical quantification combined with surface specificity. The inherent surface sensitivity is due to the short mean free path of electrons (several nanometres) within solid media. Deducing the chemical composition of layers and interfaces at greater depths is achieved through milling the topmost layers by bombardment with argon ions. It has been well established, however, that milling with monoatomic argon ions can cause sputter-induced damage at the surface, which in turn leads to a loss of chemical state information.

Surface etching with large clusters of argon enables the rapid collection of depth profiles from organic materials and removal of contamination from metal oxides while maintaining the chemical character of a material. Due to the relatively low energy per atom, however, the etch rates of most inorganic materials with these large clusters is not conducive to a high sample throughput. The implementation of smaller gas clusters allows higher energies per atom to be used, leading to increased rates of etching whilst preserving the chemical information that is lost when using monoatomic argon.

Here we shall discuss how using a wider range of *ion energies per atom* enables more effective depth profiling of a wide variety of surface materials. We will present data from mixed inorganic and organic samples to show the benefits of these reduced cluster sizes.

11:20am **AS-MoM10 Photoemission from Complex Material Systems: Obtaining Quantitative Information**, *Robert Opila, J. Church*, University of Delaware **INVITED**

Photoemission is still a rapidly developing technique for surface analysis of complex systems using advancing physical and software technologies. In this talk we will consider two applications of electron spectroscopy taking advantage of hardware and software innovations.

Recently, the adaptation of XPS studies to synchrotron beamlines has produced a new technique – Variable Kinetic Energy XPS (VKE-XPS). VKE-XPS collects XPS data at multiple photon energies, and by doing so, also varies the likelihood of detection of electrons from buried layers. Compositional depth information can be extracted from VKE-XPS data sets by statistically sifting through the data using likelihood calculations assigned to each randomly generated depth profile. We have deployed a new algorithm, Bayes-Sim, which applies a Bayesian statistical approach to establish the framework for a belief system for each compositional simulation. Optimization of the search is carried out using a simulated annealing schedule, which assists in avoiding only locally optimized configurations. The Bayes-Sim algorithm has been encapsulated in a distributable, open-source graphical user interface J-FAB. These improvements were used to study high dielectric materials

Some of the most advanced chemical analytical techniques have been applied to study the degradation of paint pigments from artists in the post-impressionist era (late to early 20th century). The capability to investigate chemical speciation and elemental mapping in micro-samples is enabled only by the spatial resolution and high brilliance of synchrotron techniques like XANES and SR-FTIR. Fairly sophisticated data analyses for synchrotron beam lines have been encapsulated in easy to use software packages thereby complimenting the burgeoning field of art in science with the tools needed to tackle complex problems. In this work degradation of paintings by Munch and Matisse will be discussed.

Characterization of Biological and Biomaterials Surfaces (1)

Moderator: Dan Graham, University of Washington, Joe Baio, Oregon State University

8:20am BI+AS-MoM1 Characterizing the Dissociative Properties of Surface-Bound Biomolecules by *In Vacuo* XPS, Kenan Fears, Naval Research Laboratory

In vacuo X-ray photoelectron spectroscopy (XPS) was used to determine the dissociation constant for pH-tunable, peptide nanostructures on a gold substrate. To validate these protocols, dissociation constants of GG-X-GG and X₅ peptides (X = G, D, H, or K), and bovine albumin (BSA) and fibronectin (FN) were measured for comparison with published values. Drops of biomolecules in 100 mM sodium phosphate buffers (pH 1-12) were deposited on gold substrates and allowed to dry at room temperature. Due to the ca. +1.3 eV shift in binding energy (BE) of protonated amines, pK values of basic amino acids were calculated by plotting the fraction of protonated amines as a function of solution pH. Similarly, the BE of carboxyl groups shifted ca. -1.3 eV upon deprotonation. While C 1s spectra were convoluted by the multiple chemical states of carbon present in the samples, the ratio of the C 1s components centered at BE=289.0 ± 0.4 and BE=287.9 ± 0.3 proved to reliably assess deprotonation of carboxyl groups. The pK values for the Asp (3.1 & 2.4), His (6.7), and Lys (11.3 & 10.6) peptides, and the pI of BSA (4.8) and FN (5.7), were consistent with published values; thus, validating the pK value obtained for our surface-bound nanostructures using these methods.

9:00am BI+AS-MoM3 Quantifying the Surface Chemistry and Overlayer Thickness of Functionalized Nanoparticles, David Castner, University of Washington **INVITED**

Nanoparticles exhibit unique surface properties and require well-controlled surface properties to achieve optimum performance in complex biological or physiological fluids. Despite the widespread appreciation of the unique properties of high surface area nanoparticles there is a surprising lack of detailed surface characterization of these materials, especially for nanoparticles used in biomedical applications. This is in part because nanoparticles present significant challenges for surface characterization. Thus, there is a need to develop rigorous and detailed surface analysis methods for characterizing the surface of nanoparticles. Model systems with well-defined, systematic variations of surface properties are an excellent starting point for developing comprehensive, multi-technique surface characterization methodologies. We have developed methods for quantifying the thickness and structure of carboxylic acid (COOH) SAM functionalized Au nanoparticles (AuNPs) using XPS, SESSA and LEIS. The size, shape, and size distribution of the AuNPs was determined by TEM. Additional surface properties were characterized using ToF-SIMS and FTIR spectroscopy.

These methods were then extended to the covalent attachment of proteins to AuNPs functionalized with OEG SAMs. For the OEG functionalized AuNPs the type of end group (OH vs. OCH₃) doesn't have a significant effect on the SAM thickness and structure, but the size of the AuNP does. The C11 alkyl portion of the thiol molecules was well ordered on all surfaces (flat, 14nm and 40nm). In contrast, the OEG portion of the thiol molecules was better ordered and more densely packed on the 40nm AuNPs compared to the 14nm AuNPs. LEIS measurements showed OEG SAMs had a thickness of 2.0 nm on the 14nm AuNPs compared to 2.6 nm on the 40nm AuNPs. Protein G was immobilized onto the HO-terminated OEG SAMs via carbonyl diimidazole chemistry. On flat Au surfaces XPS showed a monolayer of Protein G was covalently immobilized with little non-specific adsorption. On AuNPs a monolayer of Protein G could also be immobilized, but significant non-specific adsorption was detected.

Recent studies on NPs with Au cores and Ag shells have shown that it is important to account for non-spherical particle shapes of the Ag shell and off-center locations of the Au cores to obtain good agreement between the SESSA and XPS results. Both deviations from ideal core-shell spherical particles result in higher than expected XPS Au concentrations, with the off-center Au cores having the largest contribution to this effect for the particular core-shell NPs examined in this study.

9:40am BI+AS-MoM5 Structure-Function Relation in Gizzard Plates of Cephalaspidean Gastropod, M. Shepelenko, V. Brumfeld, E. Klein, Weizmann Institute of Science, Israel, H. Lubinevsky, Israel Oceanographic & Limnological Research (IOLR) and National Institute of Oceanography, L. Addadi, S. Weiner, Sidney Cohen, Weizmann Institute of Science, Israel

Processing food is an essential function of all organisms. Although grinding of food is typically done by teeth, there are a number of species that perform this action in the muscular stomach or gizzard. This places unique demands on the food processing mechanism, a study of which provides fascinating insights into compositional, structural, and mechanical design of the organism at the nanoscale. The Cephalaspidean gastropods are common marine mollusks with a specialized digestive apparatus containing 3 hardened plates of millimeter size inside the gizzard. The gizzard plates are reported to either grind or crush shelled prey. In this study we apply a variety of techniques including micro-CT, scanning electron microscopy with energy dispersive x-ray spectroscopic analysis, infrared and Raman spectroscopies, powder x-ray diffraction and nanoindentation to understanding the manner in which the gizzard plates of the cephalaspidean *Philine quadripartita* function in the overall digestion process. We determined that the gizzard plates, used to crush the shelled prey, have distinct structure and composition which promote optimal performance of their function. Specifically, the plate composition, a mixture of amorphous calcium carbonate and amorphous calcium phosphate embedded in a chitinous matrix, varies systematically with depth into the plate. The corresponding elastic moduli and hardness of the plates vary accordingly. In contrast to typical teeth, for which the surface comprises the stiffest and hardest material, the hardest and stiffest layer of the gizzard plates is below the working surface. Analysis of the elasticity index (H/E) of the gizzard plates, and comparison with sea urchin teeth, which we have extensively studied in the past, provided interesting insights into the connection between the biological function and mechanical properties of the gizzard plates. Sea urchin teeth, which serve a grinding function, exhibit higher wear resistance and stiffness than gizzard plates which are used for crushing. Nonetheless, the difference in toughness between the two, as determined by comparison of respective in elasticity indices, is relatively small.

10:00am BI+AS-MoM6 Photothermal AFM-IR of Bacteria on Polymer Films: Impact of Cantilever Damping on Quantitative IR Measurements, Daniel Barlow, J.C. Biffinger, Naval Research Laboratory, A.L. Cockrell, Nova Research, M. Lo, K. Kjoller, D. Cook, Anasys Instruments, W. Kyung Lee, P.E. Pehrsson, Naval Research Laboratory, W.J. Goodson, Air Force Research Laboratory, J.N. Russell, Jr., Naval Research Laboratory

Synthetic polymers can be prone to degradation in microbial and other biological environments, often through enzymatic activity. Quantitative assays are important to characterize these degradation mechanisms and accurately correlate relationships with environmentally dependent microbial physiology. For microbial degradation of polyurethane films, conventional FTIR microscopy has been previously applied in quantitative assays with micron - scale spatial resolution. Photothermal AFM-IR offers the potential to extend this analysis to the nanoscale, allowing early degradation processes and mechanisms relative to single microbes to be quantified. As a first step towards this, we have used AFM-IR to characterize a known polyurethane degrading microbe (*Pseudomonas fluorescens*, Pf01) grown on films of a polyether - polyurethane (PU) formulation known to resist enzymatic degradation. This allowed us to conduct preliminary AFM-IR assessments with a relevant microbe and polymer, but without additional complications from biodegradation. Height images of air-dry samples showed the growth procedure in liquid media resulted in monolayer Pf01 biofilm clusters on top of the ~250 nm PU layer, providing a conducive model system for AFM-IR in an ATR configuration. Both bacteria and PU spectral signatures were detectable by AFM-IR spectroscopy and showed generally good agreement with FTIR. However, PU AFM-IR absorption intensities were observed up to 2x higher in regions covered by dried bacteria, versus uncovered regions, even though the PU thickness was uniform over the substratum. This was due to damping variations which were reflected in the cantilever ring-down and attributed to differences in loss modulus and tip - sample adhesion for the two materials. This shows that local cantilever damping can be an important property to assess in AFM-IR analysis of combined biological / polymer samples, a factor that has received little attention thus far. Analysis of the cantilever ring-down will be discussed regarding extraction of damping parameters for normalization of the IR signal.

10:40am **BI+AS-MoM8 Where's Waldo? 3D Localization of Polymer Nanoparticles in Cells using ToF-SIMS**, *Daniel Graham*, University of Washington, *J.T. Wilson*, Vanderbilt University, *J. Lai*, *L.J. Gamble*, *P.S. Stayton*, *D.G. Castner*, University of Washington

Polymeric nanoparticles have shown promise for delivery of therapeutics intracellularly. The diversity of polymer chemical and physical properties enables a wide range of cellular targeting and applications. We have initiated a project investigating the use of 3D ToF-SIMS imaging to localize and characterize polymer nanoparticles within cells. Though other imaging modalities can localize polymer nanoparticles in cells, ToF-SIMS presents the advantage of localization combined with chemical characterization of the particles and the surrounding cell. However, the ability to locate polymer nanoparticles in cells is complicated by the fact that most polymers are made of organic elements such as C, N, and O and produce secondary ion fragments that are the same as those generated from the surrounding cell. Herein we will demonstrate a method we have developed to isolate polymer nanoparticle signal from cell signal and generate 3D images of nanoparticle clusters within cells. Initial results with polymer nanoparticles targeted for endosomal uptake showed punctate localization of nanoparticle clusters within areas consistent with endosomal localization. Areas enriched in nanoparticles could be localized in spite of peak overlap of polymer and cellular signals.

11:00am **BI+AS-MoM9 XPS and ToF-SIMS Analysis of Functionalized Nanoparticles: Effects of Sample Cleaning and Preparations**, *R. La Spina*, *V. Spampinato*, *I. Ojea*, *F.J. Rossi*, *D. Gilliland*, *Giuseppe Ceccone*, European Commission, Joint Research Centre, IHCP, Italy

It is recognized that detailed physico-chemical characterization of nanomaterials is becoming increasingly important both from the technological and from health and safety point of view. Moreover, an incomplete characterisation may inhibit or delay the scientific and technological impact of nanoscience and nanotechnology. However, nanomaterials characterization based on individual instrumental methods is a very challenging issue because their stability, coating and environmental effects may lead to outputs that are not very easy to interpret unequivocally. For this reason multiple analysis methods are needed to understand the nature of nanomaterials, especially if we consider that surface and interfaces are critical to the behaviours of nano-sized materials [1].

Surface chemical analysis methods, such as X-ray Photoelectron Spectroscopy (XPS) and Time of Flight Secondary Ion Mass Spectrometry, can provide an important contribution to more fully characterizing nanomaterials, so these methods should be more generally applied as part of a characterisation set of tools for nanomaterials and nanoparticles synthesized for different applications [2].

In this work, we have investigated the surface chemistry of nanoparticles, gold (AuNPs) and silica (SiO₂NPs), functionalized with different thiols. In particular, the effects of sample cleaning by centrifugation and dialysis have been studied. Moreover, the challenges and problems related to sample preparation for the surface analysis will be also addressed and discussed. The different steps of sample cleaning have been characterised by DLS, CPS and SEM, whilst the surface chemistry has been mainly assessed by XPS. Our results indicate that the cleaning process may influence the functionalization process. For instance, the AuNPs functionalized with CF₃ terminated SAMs shows differences in the efficiency depending upon sample cleaning.

Finally, preliminary results about the behaviour of AuNPs-CF₃ in protein solution (HSA) will be also presented.

[1] Baer D, et al., *Anal. Bioanal. Chem.*, **2010**, 396(3), 983–1002

[2] Grainger D and Castner D, *Adv. Mater.*, **2008**, 20, 867–877

11:20am **BI+AS-MoM10 Engineered Surfaces for Bio-Relevant Applications**, *Marlon Walker*, NIST, *A. Vaish*, University of Delaware, *D. Vanderah*, NIST/Institute for Bioscience and Biotechnology Research

Polydopamine (PDA) is a useful bio-inspired coating for surface modification. Substrates from noble metals such as gold to semiconductors such as silicon can be modified to exhibit useful biomimetic properties that may not be available on the underlying surface. However, conditions of preparation can lead to wide variability in the attributes (such as roughness) of the generated surface, and can affect subsequent functionalization and applicability. Wider adoption of the routine use of PDA is hindered by this uncertainty of the nature of the prepared surface. We present strategies for greater control of the properties of a PDA coating, which could lead to enhanced predictability of surface attributes and greater utility in surface engineering strategies.

11:40am **BI+AS-MoM11 Breast Cancer Tumor Metabolism Investigated with ToF-SIMS**, *Lara Gamble*, *B.M. Bluestein*, *D.J. Graham*, University of Washington

Imaging time-of-flight secondary ion mass spectrometry (ToF-SIMS) was utilized to analyze 21 breast tissue biopsy samples. Eighteen of the biopsy samples were obtained at diagnosis and three after neoadjuvant therapy. Principal component analysis (PCA) was used to reduce the spectral data and determine major variants in the data. PCA analysis of the mass spectral data was used to test for correlation to phenotypes (ER+/PR+, HER2+, and ER-/PR-/HER2-) as well as determine the chemical changes pre and post neoadjuvant therapy.

PCA imaging analysis of the ToF-SIMS tumor tissue images showed that the combination of PCA and ToF-SIMS imaging was able to distinguish different tissue regions that correspond with similar regions in H&E stained serial tissue slices from the same block. Most notably the stromal and cellular regions could be distinguished by imaging PCA. Utilizing regions of interest (ROIs), chemical make-up of stromal regions from different tumor biopsy samples was compared.

While the cellular region showed the clearest separation for pre and post treatment chemistry, spectral PCA analysis of the stromal region shows better separation in scores plots when comparing different tumor types. Chemical analysis of the stromal regions also separated out chemical differences in triple negative tumor samples (with five different triple negative rated tumors investigated to date). In an initial sample set, the pCR (patient complete recovery) and 'near' pCR samples both score negatively in the PC2 scores plot. The key fatty acids associated with pCR samples are myristic acid (14:0), palmitic acid (16:0), stearic acid (18:0) and a 20:3 fatty acid as well as fragments of sphingomyelin and various triglycerides. The main peaks associated with the non-pCR samples were fatty acid 18:1 (consistent with oleic acid) along with cholesterol and vitamin E related peaks. Coincidentally these peaks correlate well with the loadings from the pre neoadjuvant therapy treatment samples, while the highest loadings from the pCR samples correlate with the post treatment tissue loadings.

Electronic Materials and Processing

Room: 211A - Session EM+AS+SS-MoM

Rectenna Solar Cells, MIM Diodes, and Oxide Interfaces

Moderator: John Conley, Oregon State University, Dale Kotter, RedWave Energy, Inc.

8:20am **EM+AS+SS-MoM1 Harvesting Energy with Optical Rectennas: Challenges and Innovations**, *Garret Moddel*, University of Colorado and RedWave Energy, Inc., *S. Joshi*, *B. Pelz*, *A. Belkadi*, *S. Yuan*, University of Colorado at Boulder, *P. Brady*, *D. Kotter*, RedWave Energy, Inc. **INVITED**

Optical rectennas are of interest for radiant heat and light energy harvesting, and ultra-fast detectors that work for terahertz waves up through visible-light wavelengths. The devices work under constraints that are different from those of either microwave rectennas or conventional solar cells. These antenna-coupled diodes incorporate micron-scale antennas and diodes that must operate at frequencies in the tens to hundreds of terahertz, but the antenna size and diode speed are not the most daunting challenges. The current produced by the antenna – particularly for rectennas operating at close to visible-light frequencies – samples the diode at discrete voltages described by a quantum approach instead of at continuously varying voltages described by classical electromagnetic theory – which makes for a fascinating theory of operation. The consequence is a quantum limit to the power conversion efficiency, similar to the Shockley-Queisser limit for conventional solar cells. The optical frequency and intensity determine whether the rectenna operation can be described classically or must involve a quantum analysis. Because rectennas gather current from the entire antenna, if the light is not spatially coherent cancellation occurs, resulting in reduced efficiency. This limits the amount of power received by each diode, which further limits the diode rectification efficiency. Over the last decade the number of groups investigating various parts of rectenna technology has grown from almost none to at least 50. This growing community of researchers, with innovative solutions, is needed to meet optical rectenna challenges and enable a practical technology. Some emerging solutions will be presented.

9:00am **EM+AS+SS-MoM3 Demonstration of Traveling-Wave Metal-Insulator-Metal Diodes for 28 THz (10.6 μ m) Rectennas**, *Bradley Pelz*, University of Colorado at Boulder, *G. Moddel*, University of Colorado at Boulder and Redwave Energy

Lumped element rectennas encounter an efficiency limitation above several terahertz due to the RC time constant of an MIM diode. A traveling-wave diode (TWD) takes advantage of nanoscale geometries to achieve a lower capacitance than that of a lumped element diode. The TWD behaves as a MIM transmission line for surface plasmons in which the rectification occurs as the wave travels down its length. Due to the distributed nature of the rectifier, the impedance seen by the antenna is the characteristic impedance of the transmission line. COMSOL simulations have shown this gives a reactive component of diode impedance that is substantially smaller than either the real component of the characteristic impedance for the TWD or the reactance from the parallel plate capacitance of an equivalently sized lumped element MIM diode. This allows for a much higher coupling efficiency from the antenna than in the case of a lumped element diode, and a substantially reduced RC time constant.

To obtain a resistance that matches that of the antenna simulations show that the TWD requires a width of 100 nm or less, which is too small for conventional lithography techniques. This small critical dimension was achieved using a germanium shadow mask technique. After fabrication, the DC junction characteristics were measured using a four-point technique. The open circuit voltage of these unbiased devices was measured under 28 THz illumination using a CO₂ laser and a lock-in amplifier. The TWD coupled to a bow tie antenna showed both polarization and power dependence. Since these measurements were completed at zero bias, the response could not have been bolometric, and the device must have been operating in energy harvesting mode.

9:20am **EM+AS+SS-MoM4 Basic Efficiency Limits for Rectenna Solar Power Conversion**, *Heylal Mashaal, J.M. Gordon*, Ben-Gurion University of the Negev, Israel

The prospect of employing aperture rectennas for solar power conversion will be explored in this presentation. Sunlight is commonly viewed as incoherent – hence seemingly unsuitable for antenna harvesting – but all electromagnetic radiation exhibits spatial coherence on a sufficiently small scale. The first direct measurement of the spatial coherence of sunlight will be presented, and the ramifications for using optical concentrators that can effectively replace orders of magnitude of antenna and rectifier elements will be discussed.

Rooted in the partial spatial coherence of sunlight, a derivation of the thermodynamic limit for coherence-limited solar power conversion will be presented – an expansion of Landsberg’s elegant basic bound, originally limited to incoherent converters at maximum flux concentration. The results do not depend on a particular conversion strategy. As such, they pertain to systems that span geometric to physical optics.

Last, a basic upper bound will be presented for the ability to rectify the broadband signals using a full wave rectification scheme.

Our findings indicate promising potential for rectenna power conversion.

9:40am **EM+AS+SS-MoM5 Coherence Effects in Periodic Arrays of Nano-Antennas used for Energy Harvesting and Self-Imaging**, *Peter Lerner*, SciTech Associates, LLC, *P.H. Cutler, N.M. Miskovsky*, Penn State University

Coherence effects in periodic arrays of nano-antennas used for energy harvesting and self-imaging

P. B. Lerner [1], N. M. Miskovsky^{1,2}, P. H. Cutler^{1,2}

Modern technology allows the fabrication of antennas with a characteristic size comparable to the electromagnetic wavelength in the optical region. [1] This has led to the development of new technologies using nanoscale rectifying antennas (rectennas) for solar energy conversion and sensing of terahertz, IR and visible radiation. For example, a rectenna array can collect incident radiation from an emitting source and the resulting conversion efficiency and operating characteristics of the device will depend on the spatial and temporal coherence properties of the absorbed radiation. For solar radiation, the intercepted radiation by a micro- or nano-scale array of devices has a relatively narrow spatial and angular distribution. Using the Van Cittert-Zernicke Theorem, we show that the coherence length (or radius) of solar radiation on an antenna array is, or can be, tens of times larger than the characteristic wavelength of the solar spectrum, i.e., the thermal wavelength, $\lambda_T = 2\pi\hbar c / (k_B T)$, which for T=5000K is about 2 microns. Such an effect is advantageous, making possible the rectification of solar radiation with nanoscale rectenna arrays, whose size is commensurate with the coherence length. Furthermore, using the van Cittert-Zernicke Theorem, we also examine the blackbody radiation emitted from an array of antennas at temperature T, which can be quasi-coherent and lead to a modified self-image, analogous to the Talbot-Lau self-imaging

process [2] but with thermal rather than monochromatic radiation. This coherence of the antennas’ blackbody radiation can also introduce an angular spectrum, which may be concentrated (enhanced) along certain spatial directions, giving rise to additional features not present in the original array. The self-emitted thermal radiation may be important as a non-destructive means for quality control of the array.

[1] Miskovsky, N. M., P. H. Cutler, A. Mayer, B. L. Weiss, B. Willis, T. E. Sullivan, and P. B. Lerner (2012) Nanoscale Devices for Rectification of High Frequency Radiation from the Infrared through the Visible: A New Approach, *Journal of Nanotechnology*, Article ID 512379, 19 pages, <http://dx.doi.org/10.1155/2012/512379>.

[2] Gori, F. (1979) Lau Effect and Coherence Theory, *Optics Communications*, 31(1), 4.

1 SciTech Associates, Woodland Drive, State College, 16803.

2 Physics Department (emeritus), Penn State University, University Park, 16802.

10:00am **EM+AS+SS-MoM6 Metamaterial Enhanced Rectenna for Efficient Energy Harvesting**, *D. Lu, Won Park*, University of Colorado Boulder, *P. Brady*, Redwave Energy Inc.

Rectenna solar cell offers an important alternative to the conventional semiconductor solar cell technology. Direct rectification of electromagnetic radiation faces many challenges one of which is the high frequency of operation. Thermal emission from hot bodies peaks at 10 ~ 100 THz while solar radiation has its maximum at around 600 THz. One may circumvent this difficulty if sufficiently strong thermal radiation is available at lower frequencies. In general, thermal emission is described well by the theory of blackbody radiation while the property of the non-black surface is characterized by its emissivity. When the surface supports surface waves, however, the properties of thermal emission can deviate substantially from the blackbody radiation, offering a new avenue for engineering thermal emission. For example, spatially coherent and spectrally selective thermal emission may be achieved. The presence of surface waves also means enhanced local density of states near the surface, which consequently leads to strongly modified thermal emission intensity and spectrum in the near field. In this paper, we report a metamaterial design to achieve enhanced thermal emission at 1 THz.

Two types of metamaterial designs were investigated: a 1D array of parallel trenches and a 2D array of holes etched on copper. The metamaterial surface was designed to support surface waves resembling the surface plasmon on metal surface. Numerical simulations by the finite element method confirmed the presence of surface waves and strong electric field near the surface at 1 THz. The strongly enhanced electric field is the direct consequence of enhanced local density of states. To further confirm the surface modes can be excited by thermal emission, we also conducted finite-difference time-domain simulations in which thermal emission was calculated by using the fluctuation dissipation theorem. Once the enhanced thermal emission is confirmed, a bowtie antenna was placed close to the metamaterial surface to capture the enhanced thermal emission in the near field. The antenna was optimized to maximize the electromagnetic energy delivered to the antenna gap. Since the antenna should couple efficiently with the surface modes, the optimal antenna design became quite different from the free space bowtie antenna operating at the same frequency. The optimized metamaterial and antenna design resulted in an antenna voltage of 10 mV at 1 THz, three orders of magnitude larger than the free space antenna. Such a large enhancement makes the metamaterial approach a highly promising route to efficient energy harvesting with rectenna.

11:00am **EM+AS+SS-MoM9 Modeling of and Power from Nb-NbOx-based Nanorectenna Arrays**, *Richard M. Osgood*, US Army NSRDEC, *J. Xu, G.E. Fernandes*, Brown University, *M. Rothschild, K. Diest*, MIT Lincoln Laboratory, *M. Kang, K.B. Kim*, Seoul National University, Republic of Korea, *L. Parameswaran*, MIT Lincoln Laboratory, *P. Periasamy*, IBM, *M. Chin*, Army Research Laboratory, *S. Kooi*, MIT Institute for Soldier Nanotechnologies, *S. Giardini*, US Army NSRDEC, *R. O’Hayre, P. Joghee*, Colorado School of Mines

We investigate arrays of “microrectennas” (with sub-micron features tuned for the near- and short-wave infrared) consisting of “stripe-teeth” metamaterial antennas conducting vertically through the coupled, underlying metal-insulator-metal (MIM) diode into a metallic substrate. Stripes, with cross-stripe resonances, conduct current out of the array, while antenna-like teeth break left-right symmetry and concentrate a high vertical electric field (E_z) at the end of the teeth at their antenna resonance. If plasmonic field enhancement and concentration reduce the capacitance and/or increase the effective voltage across the MIM diode, new research and development of large-area ultrafast optical rectennas will be enabled, requiring patterning and alignment of only the top metal layer.

Stripe-teeth arrays were designed, fabricated, and analyzed both experimentally and theoretically. Substrates were layers (“ground planes”) of Nb and Al, and a Au nanowire array patterned using novel high-throughput e-beam technology.¹ Substrates were oxidized/anodized, or had oxides deposited, to form microantenna-coupled MIM diodes consisting of Al-Al₂O₃-Al, Au/Ti-NbO_x-Nb, Al-Al₂O₃-Au, Ag/Ti-NbO_x-Nb, Ag/Ti-NiO-Ni, Pt-NbO_x-Nb, after deposition of top metal layers of Ag/Ti, Au/Ti, Pt, and Al (only a few nm of Ti). Conduction through 10-25 nm thick oxide layers in the MIM diodes occurred via quantum mechanical tunneling and thermionic emission, with asymmetric barrier heights all less than 1 V except for the Al-Al₂O₃-Al diodes. The Au-Al₂O₃-Al system required modeling the “hot spot” from top metal protrusions into the Al₂O₃ barrier layers and in close (tunneling) proximity to the ground plane, probably because of the surface roughness and variation in Al₂O₃ thickness; the planar-planar MIM diode model was inapplicable in this case.

The top metal was patterned into the stripe-teeth arrays. Reflective Al substrates provided sharp optical antenna resonances while Nb layers produced broader, weaker antenna resonances due to Nb absorption, similar to stripe-only arrays reported in Ref. 2. We also report the result of visible light (514 nm – 630 nm) laser illumination of Nb/NbO_x/Ag(Ti) stripe-teeth arrays, including the observation of a short-circuit current and open-circuit voltage, in response to power densities in the range 80 W/cm².

1. H. S. Lee, *et. al.*, “Electron beam projection nanopatterning using crystal lattice images obtained from high resolution transmission electron microscopy”, *Adv. Mats.* **19** 4189 (2007).

2. Wu, C., *et.al.* “Large-area wide-angle spectrally selective plasmonic absorber,” *Phys. Rev. B*, Vol. 84, 075102-7, 2011.

11:20am **EM+AS+SS-MoM10 Metal-Insulator-Insulator-Metal Diodes for Rectenna Applications**, *Shijia Lin, N. Murari, J.F. Conley, Jr.*, Oregon State University

A metal-insulator-metal (MIM) tunnel diode has a capacitor-like structure with a thin insulating layer sandwiched by two metals. Because of their potential for femtosecond-fast transport when dominated by tunnel transport, MIMs are of interest for rectenna based solar cells, hot electron transistors, and IR detectors. The common strategy to achieving rectification in MIM devices relies on the use of dissimilar work function metal electrodes to produce an asymmetric electron tunneling barrier with polarity dependent tunneling probability. The performance of single layer MIM devices is limited by the workfunction difference that can be achieved between the electrodes and the metal-insulator band offsets. Small electron affinity oxides are limited by high V_{ON}. Large electron affinity dielectrics have small V_{ON}, but tend to have limited asymmetry due to thermal emission dominated conduction. An alternative approach to controlling asymmetry is to use nanolaminate pairs of insulators with different bandgaps and band offsets to produce asymmetric tunnel barrier metal-insulator-insulator-metal (MIIM) diodes. Asymmetry in MIIM devices may be enhanced by step tunneling¹ or defect enhanced direct tunneling.²

In this work, we investigate asymmetry in HfO₂/Nb₂O₅ bilayer insulator MIIM diodes. HfO₂ and Nb₂O₅ were deposited via atomic layer deposition (ALD) using tetrakis (ethylmethylamino) hafnium (TDMAHf) and niobium ethoxide metal precursors, respectively with H₂O as the oxidant. Nanolaminate films were deposited at a chamber temperature of 250°C in one continuous run without breaking vacuum. Sputtered TaN or amorphous metals were used as the bottom electrode and evaporated Al dots were used as a top electrode. MIIM I-V asymmetry and non-linearity are shown to be a function of stack thickness, relative layer thickness, and insulator layer position with respect to the electrodes. Overall, bilayer insulators are shown to be an effective method of enhancing the performance of MIIM tunnel diodes.

1. N. Alimardani and J.F. Conley Jr, *Appl. Phys. Lett.* **102**, 143501 (2013).

2. N. Alimardani and J.F. Conley, Jr., *Appl. Phys. Lett.* **105**, 082902 (2014).

11:40am **EM+AS+SS-MoM11 Built-in Potential in Fe₂O₃-Cr₂O₃ Superlattices for Improved Photoexcited Carrier Separation**, *Tiffany Kaspar, D.K. Schreiber, S.R. Spurgeon, S.A. Chambers*, Pacific Northwest National Laboratory

Hematite, α-Fe₂O₃, is an ideal photocatalyst to split water as a source of H₂ fuel because it is non-toxic, Earth-abundant, stable in aqueous environments, and possesses a bandgap in the visible wavelength range (~2.1 eV). However, fast photogenerated electron-hole recombination, facilitated in part by slow carrier transport kinetics, has long been identified as a major obstacle in the utilization of hematite photocatalysts. A direct method to reduce photogenerated carrier recombination is to employ heterojunctions to spatially separate excited electrons and holes. Our approach is to engineer built-in electric fields by exploiting the band alignment characteristics of epitaxial Fe₂O₃/Cr₂O₃ heterojunctions. The Fe₂O₃-Cr₂O₃ system exhibits non-commutative band offsets which differ by

approximately 0.4 eV depending on the order of deposition. The non-commutative band offset properties of Fe₂O₃-Cr₂O₃ interfaces can be utilized in a superlattice structure, deposited by oxide molecular beam epitaxy, to build up an intrinsic electric field; this potential may be sufficient to spatially separate photogenerated electrons and holes. We demonstrate precise control over the Fe₂O₃-Cr₂O₃ interface structure with atomic-resolution atom probe tomography and scanning transmission electron microscopy. Direct evidence that Fe₂O₃-Cr₂O₃ superlattice layers generate an intrinsic built-in potential is observed with x-ray photoelectron spectroscopy. The individual interfacial band offset values, and thus the overall potential, can be tailored by altering the cation stoichiometry at the interfaces. Doping the component layers to improve transport characteristics requires a deep understanding of the dopant-induced electronic structure changes. To illustrate how the built-in potential in optimized Fe₂O₃-Cr₂O₃ superlattice structures can be harnessed to drive holes to the surface and electrons into the bulk, photoconductivity and photochemical degradation results will be presented.

Energy Frontiers Focus Topic

Room: 211B - Session EN+AS+EM+NS+SE+SS+TF-MoM

Solar Cells I

Moderator: Jason Baxter, Drexel University, Chintalapalle Ramana, University of Texas at El Paso

8:20am **EN+AS+EM+NS+SE+SS+TF-MoM1 Elevated Temperature Phase Stability of CZTS-Se Thin Films for Solar Cells**, *E. Chagarov, K. Sardashti*, University of California at San Diego, *D.B. Mitzi*, Duke University, *R.A. Haight*, IBM T.J. Watson Research Center, *Andrew C. Kummel*, University of California at San Diego

Density-functional theory simulations of CZTS, CZTSe and CZTS_{0.25}Se_{0.75} photovoltaic compounds have been performed to investigate stability of CZTS_{0.25}Se_{0.75} alloy vs. decomposition to CZTS, CZTSe and other secondary compounds. The Gibbs energy for vibration contribution was estimated by calculating phonon spectra and thermodynamic properties at finite temperatures. It was demonstrated that CZTS_{0.25}Se_{0.75} alloy is stabilized not by enthalpy of formation but by vibration and mixing contributions to the Gibbs energy. A set of phase diagrams was built in multidimensional space of chemical potentials at 300K and 900K temperatures to demonstrate alloy stability and boundary compounds at various chemical conditions. The Gibbs energy gain/loss for several decomposition reactions was calculated as a function of temperature with/without Cu/Zn intermixing and vibration contributions to the Gibbs energy demonstrating CZTS_{0.25}Se_{0.75} that even defect-free (no Cu/Zn intermixing) CZTS_{0.25}Se_{0.75} can be stable at typical processing temperatures.

8:40am **EN+AS+EM+NS+SE+SS+TF-MoM2 Chemical and Electrical Characterization of Polycrystalline CZTS,Se and CIGS,Se Grain Boundaries by NanoAuger and Kelvin Probe Force Microscopy (KPFM)**, *Kasra Sardashti*, UC San Diego, *P.D. Antunez, R.A. Haight*, IBM T.J. Watson Research Center, *A.C. Kummel*, UC San Diego

Polycrystalline Copper-zinc-tin-sulfide/selenide (CZTS,Se) compounds have received wide research interest due to their potential as inexpensive absorber materials composed of earth-abundant elements. Photovoltaic devices fabricated on CZTS,Se have reached conversion efficiencies of 12.6 %. One of the key parameters to further boost the conversion efficiency is to control the concentration of recombination sites at the surface, secondary phase interfaces and in the grain boundaries. To determine the presence of secondary phases on the surface and composition of grain boundaries, this work has employed Auger nanoprobe electron spectroscopy (NanoAuger) with 8nm lateral resolution combined with high resolution ambient Kelvin Probe Force Microscopy (KPFM) with dual-lock-in setup. NanoAuger was performed in planar and cross-sectional modes on CZTS,Se surfaces before and after top surface oxide removal by NH₄OH clean. Elemental maps before and after NH₄OH clean show Sn-/O-rich and Cu-poor grain boundaries suggesting that grain boundaries are terminated by tin-oxide (SnOx). Secondary phases such as SnSe and ZnSe were observed in the cross-sectional maps. Kelvin probe force microscopy (KPFM) on the cleaned surfaces showed that SnOx-terminated grain boundaries have 80-200 mV larger work function than grains, resulting in upward band bending between grains and grain boundaries. The upward band bending accompanied by the large valence band offset between the SnOx and CZTS,Se lead to relatively large energy barriers for both electrons and holes to travel into the grain boundaries and recombine. Comparison with the elemental maps for CIGSe (with device efficiencies as high as 18%) revealed the absence of the grain boundary oxide passivation.

9:40am **EN+AS+EM+NS+SE+SS+TF-MoM5 Spin Coating Thin Film CZTS for Efficient, Low-Cost Solar Cells on Flexible Glass Substrates**, *D. Kava, J. Galindo, C.O. Sana, S. Shahriar, Deidra Hodges*, University of Texas at El Paso

Photovoltaic's contribution to energy production continues to grow as costs continue to decrease. As silicon cells approach their limits, other materials are emerging. The development of $\text{Cu}_2\text{ZnSnS}_4$ (CZTS) thin film solar cells using non-vacuum liquid-based spin coating techniques have been previously investigated. The focus of this paper is the optimization of p-type CZTS thin film solar cells onto flexible substrates. Flexible solar panel costs are higher than their traditional counterparts. CZTS currently reports only a 3.2% efficiency on flexible glass, while the record for CZTS on non-flexible substrates is 12.6%. The cells are created using a single solution ink sol-gel method. All metals are dissolved in a single step prior to deposition onto substrates (nickel foil and coming willow glass) as a thin film. Coming Willow glass is a new material introduced recently to the market, while nickel is an inexpensive flexible reflective foil. The Coming Willow glass is coated with a molybdenum layer as a reflective back contact layer. By using a single step and a solution deposition method, lower production cost are achievable. For thin film deposition, we used a non-vacuum spin coater (WS650 spin processor, Laurell Technologies) with an optimized spin coat programming. Annealing took place under vacuum in a RTP furnace while time, temperature and ramp functions were varied. The other layers of the device consists of cadmium sulfide n-type window layer and a zinc oxide doped with aluminum transparent top contact layer. Characterization and analysis of the thin films were performed using Raman spectroscopy, scanning electron microscope (Zeiss NEON 40), X-ray diffraction (Phillipps X'Pert), profilometer (Veeco Dektak 150), UV-Vis-NIR Spectrophotometer (Cary 5000), Hall Effect measurement system (HMS3000) and 4 point probe (Lucas Labs) measurements. Results show CZTS thin film solar cells on flexible glass is obtainable.

10:00am **EN+AS+EM+NS+SE+SS+TF-MoM6 Band Gap Profile of Cu(In,Ga)(Se,S) 2 Thin Films via High-Resolution Reflection Electron Energy Loss Spectroscopy**, *Sung Heo, H.I. Lee, J.B. Park, G.S. Park*, Samsung Advanced Institute of Technology, Republic of Korea, *D.H. Lee, J.G. Nam*, Samsung, Republic of Korea, *H.J. Kang*, Chungbuk National University, Republic of Korea, *B.D. Choi*, Sungkyunkwan University, Republic of Korea

$\text{Cu}(\text{In,Ga})\text{Se}_2$ (CIGS)-based solar cells was investigated with an aim of enhancing cell performance because these cells provided high conversion efficiency at relatively low cost. The efficiency of CIGS cells has recently approached 19.7% at small sizes. In general, $\text{Cu}(\text{In}_{1-x}\text{Ga}_x)(\text{Se}_{1-y}\text{S}_y)_2$ (CIGSS) composition profiles are double-graded, and they can improve the open-circuit voltage (V_{OC}) and the efficiency of solar cells because band gaps increase toward both the surface (i.e., with the increase of sulfur) and the bottom (i.e., with the increase of gallium). It is important to accurately measure the band gap at the top and the bottom of the CIGSS cell. Nevertheless, the band gap profile measurement of the CIGSS as a function of depth is challenging.

In this study, we obtained the depth profile of the CIGSS cell using the quantitative Auger Electron Spectroscopy method, for which the relative sensitivity factor was corrected using the inductively coupled plasma-atomic emission spectrometry (ICP-AES) method. We also measured the band gap directly using high-resolution reflection electron energy loss spectroscopy (HR-REELS) with a monochromatic electron gun, which has low electron energy at 300 eV.

For the direct measurement of a band gap profile, HR-REELS spectra were obtained as a function of depth during Ar ion sputtering at 3.0 kV. The band gap profile shows a double-graded band gap as a function of depth. The band gap values are 1.32 eV at the surface (E_{g1}), 1.08 eV at the depth between 0.3 and 0.7 μm ($E_{\text{g min.position}}$), and 1.50 eV at the depth of about 2.2 μm (E_{g2}), respectively. Our findings suggest a new analytical method which directly determines the band gap profile as function of depth.

10:40am **EN+AS+EM+NS+SE+SS+TF-MoM8 Spatial Atmospheric ALD of Zinc Oxysulfide Buffer Layers for CIGS Solar Cells**, *C. Frijters, P.J. Bolt, P. Pooldt, Andrea Illiberi*, Solliance/TNO, Netherlands

Copper Indium Gallium di-Selenide (CIGS) solar cells are a promising approach in photovoltaic technology, having low production costs, high conversion efficiencies (> 20 %), as well as the possibility to manufacture them on flexible substrates. State-of-the-art in CIGS solar cells manufacturing is to use a stack of CdS, intrinsic ZnO (*i*-ZnO) and an Al-doped ZnO TCO on top of the CIGS film. Replacement of CdS by a non-toxic Cd-free layer with wider band gap (> 2.4 eV) would a) decrease the production cost by avoiding the expensive treatment of toxic wastes and b) increase the overall cell efficiency by enhancing the quantum efficiency in the blue range. Moreover, the use of a "soft" and highly conformal

deposition technique is preferred to improve the electrical properties of the buffer layer/CIGS interface.

In this paper we present spatial atmospheric atomic layer deposition of a Zn(O,S) buffer layer as CdS replacement for CIGS solar cells. Spatial ALD is emerging as an industrially scalable deposition technique at atmospheric pressure which combines the advantages of temporal ALD, i.e. excellent control of film composition and uniformity on large area substrates, with high growth rates (up to nm/s). Films are grown by sequentially exposing the substrate to oxygen and sulfur precursors (H_2O , H_2S) and the zinc metal precursor (i.e., DEZn). By controlling the kinetics of surface reactions between evaporated precursors and reactive sites at the film surface, the composition of Zn(O,S) can be precisely tuned. The incorporation of S into ZnO results in a bowing of the band gap in the range from 3.3 eV (ZnO) to 2.7 (S/O+S ~ 0.5) and 3.4 eV (ZnS), as measured by spectrophotoemetry. The morphology of the $\text{Zn}(\text{O}_{x-1}\text{S}_x)$ films varies from polycrystalline (for $0 < x < 30$ and $70 < x < 100$) to amorphous ($30 < x < 70$), as measured by X-ray diffraction. CIGS solar cells with a Spatial ALD Zn(O,S) buffer layer show an increased spectral response around 400 nm compared to solar cells with a CdS buffer layer. The solar cells with the Zn(O,S) buffer layer had an efficiency of 15.9 %, compared to 15.5 % for the reference solar cells with a CdS buffer layer.

11:00am **EN+AS+EM+NS+SE+SS+TF-MoM9 Deep Level Electron Traps in Epitaxial CuInSe_2 Probed using Photo-Modulated X-ray Photoelectron Spectroscopy**, *Nicole Johnson*, University of Illinois at Urbana-Champaign, *P. Aydogan*, Bilkent University, Turkey, *A. Rockett*, University of Illinois at Urbana-Champaign, *S. Suzer*, Bilkent University, Turkey

Performance in a variety of electronic devices is largely controlled by minority carrier charge capture on point defects. To date there is no experimental method to directly identify these point defects in a chemically specific fashion. Photo-modulated X-ray Photoelectron Spectroscopy (XPS) utilizes the chemical and charge sensitivity of XPS to identify changes in peak shape due to changing atomic charge state from capture of light-generated minority carriers. Epitaxial thin films of CuInSe_2 (CIS) were chosen as a case study for this technique because their defect chemistry is still relatively unknown as compared to traditional solar cell materials. The 500-1000nm thick films were grown by a hybrid sputtering and evaporation technique on GaAs(001) substrates at 600-700°C. Aligned surface morphology features matching the substrate geometry in scanning electron microscopy (SEM) images indicate epitaxial growth, which was confirmed by x-ray diffraction (XRD). A layer of CdS was deposited on the CIS via chemical bath deposition to protect the CIS surface from oxidation in storage and to duplicate the heterojunction used in solar cells. Prior to loading in the XPS, the CdS was etched off to expose a Cd doped CIS surface for analysis. The photo-modulated XPS used monochromatic AlK α x-rays with a 532 nm laser as the illumination source. Under illumination, each film constituent was observed to exhibit unique binding energy shifts. Based on their peak shifts relative to the surface photovoltage profile, Cd and In were found to be right at the surface while Cu and Se were deeper into the film, consistent with a Cd-doped, In-rich surface. The technique is therefore shown to provide a chemically-sensitive depth profile non-destructively that can be obtained even on a relatively rough sample. Additionally, shape changes in the Se 3d doublet spectra indicate electron capture in a deep trap state that is likely due to cation vacancies. Measurements at varying temperatures indicate air-induced surface recombination states are passivated by annealing at 80C, allowing the surface photovoltage to persist. At 230C, an irreversible change happens in the surface properties such that the surface photovoltage gets much smaller and reverses sign. This work was supported by a joint NSF-TUBITAK collaborative research project (NSF Grant No: 1312539 TUBITAK Grant No: 212M051).

11:20am **EN+AS+EM+NS+SE+SS+TF-MoM10 The Role of ZnTe Buffer Layers on the Performance and Stability of CdTe Solar Cells**, *Jiaojiao Li*, Colorado School of Mines, *A. Abbas*, Loughborough University, UK, *D.M. Meysing, J.D. Beach, D.R. Diercks*, Colorado School of Mines, *M.O. Reese, T.M. Barnes*, National Renewable Energy Laboratory, *C.A. Wolden*, Colorado School of Mines, *J.M. Walls*, Loughborough University, UK

The use of ZnTe buffer layers at the back contact of CdTe solar cells has been credited with contributing to recent improvements in both record cell efficiency and module stability. To better understand the underlying reasons high resolution transmission microscopy (HR-TEM) and atom probe tomography (APT) were used to study the evolution of the back contact region before and after rapid thermal activation of this layer. During activation the 150 nm ZnTe layer, initially nanocrystalline and homogenous, transforms into a bilayer structure consisting of an amorphous region in contact with CdTe characterized by significant Cd-Zn interdiffusion, and a crystalline layer that shows evidence of grain growth

and twin formation. This graded layer may passivate interface defects and account for the improved open circuit voltage and fill factor that accompanies the RTP activation step. Copper, co-evaporated uniformly within ZnTe, is found to segregate dramatically after rapid thermal activation, either collecting near the ZnTe/Au interface or forming Cu_xTe clusters in CdTe at defects or grain boundaries near the interface. Further examination of the Cu_xTe clusters revealed that they are encased in a thin layer of Zn, and it is postulated that this structure may limit the extent of diffusion into CdTe and play an important role in device stability.

11:40am EN+AS+EM+NS+SE+SS+TF-MoM11 **The Performance and Durability of Broadband Anti-Reflection Coatings for Thin Film CdTe Solar Cells**, *G. Womack, P.M. Kaminski, John Walls*, Loughborough University, UK

Light reflection from the glass surface of a photovoltaic (PV) module is a significant source of energy loss for crystalline silicon and all types of thin film PV devices. The reflection at the glass and air interface accounts for ~4% of the total energy. Single layer anti-reflection coatings using magnesium fluoride or porous silica with sufficiently low refractive index have been reported but these are only effective over a narrow range of wavelengths. In this paper we report on the design, deposition and testing of multilayer broadband anti-reflection coatings that reduce the weighted average reflection over the wavelength range used by thin film CdTe devices to ~1.22% resulting in a useful 3.6% increase in photocurrent. In this study we have used multilayer stacks consisting of silica and zirconia layers deposited using a reactive magnetron sputtering process. Details of the stack design, sputtering process parameters and the optical and micro-structural properties of the layers are provided.

Thin film CdTe devices pose a special problem because the anti-reflection coating is applied to one side of the glass while device layers are deposited directly on to the opposite glass surface in the superstrate configuration. In thin film CdTe production, the glass is exposed to high temperature processes during the absorber deposition and during the cadmium chloride activation treatment. If glass pre-coated with a broadband anti-reflection coating is to be used then the coating must withstand temperatures of up to ~550°C. Surprisingly, our studies have shown that multilayer silica/zirconia anti-reflection coatings on soda lime glass remain unaffected by temperatures up to 600 °C at which point mild crazing is observed. This is an important observation since it means that low cost glass which is pre-processed with a broadband anti-reflection coating by glass manufacturers is potentially useable in thin film CdTe module production

In-Situ Spectroscopy and Microscopy Focus Topic
Room: 211C - Session IS+AS+SS-MoM

Fundamental Studies of Surface Chemistry of Single Crystal and Nanomaterials under Reaction Conditions

Moderator: Franklin (Feng) Tao, University of Kansas, Zili Wu, Oak Ridge National Laboratory

8:20am IS+AS+SS-MoM1 **Hot Electron In-Situ Surface Chemistry at Oxide-Metal Interfaces. Foundations of Acid-Base Catalysis**, *Gabor Somorjai*, University of California, Berkeley **INVITED**

The development of Catalytic Metal-Semiconductor Nanodiodes (CMSN) to measure the flow of electrons excited during exothermic catalytic reactions at the metal interface proved that oxidation on platinum generates a steady flux of hot electrons [1]. Evidence is presented that the steady state of chemi-current is correlated to the turnover frequency and that the exothermic hot electron production during reactions on transition metal particles may be widespread. The CO/O₂ and H₂/O₂ reactions were studied most frequently by this method and semiconductors included TiO₂, GaN, CoO_x, NbO_x and TaO_x. Charge transport between the metal and oxide interfaces also influences the product distribution of multipath reactions. These were shown in the hydrogenation of furfural and croton aldehyde at platinum/TiO₂ interfaces as compared to the platinum/silica interfaces [2]. The oxide-metal interfaces appear to produce ions, which carry out reactions that have long been called by the organic chemistry community as acid base catalysis. The typical catalytic structure is mesoporous oxide that is produced to hold the metal nanoparticles. The structures produce high surface area oxide metal interfaces and this is a catalytic architecture for acid base catalysis. Studies in changing the transition metal oxide using a single metal of platinum as nanoparticles, shows the tremendous amplification effect of the oxide metal interfaces in the reactions such as the carbon monoxide oxidation. Platinum alone produces on silica three orders

of magnitude less CO₂ by the CO oxidation process than on cobalt oxide, that is the most active of these acid base oxide metal interface catalytic systems [3]. Nevertheless, not just cobalt oxide, but nickel oxide, manganese oxide, and iron oxide, produces much higher activity for this reaction than platinum alone. In other reactions, when n-hexane isomerization or cyclisation reactions studied, the pure oxides niobium or tantalum do not produce any reaction other than cracking two smaller molecular fragments. However, at the platinum-oxide interfaces with niobium oxide or tantalum oxide, almost 100% selectivity for isomerization could be achieved [4]. Thus it appears that charge catalysis plays a very important role, which is equal in importance to the role of pure metal covalent catalysis that produces molecules without any apparent charge flow. Generation of hot electron flows and the catalytic activity of two-dimensional arrays of colloidal Pt nanoparticles with different sizes are investigated using catalytic nanodiodes. Pt nanoparticles of smaller size lead to higher chemi-current yield, which is associated with the shorter travel length for the hot electrons, compared with their inelastic mean free path [5]. In many oxide supports microporous sites are used, which are less than 1 nm in size and do not allow the larger platinum nanoparticles inside these pores. In that case, the metal that is used to create the catalysts are deposited on the outside surface of the microporous support. This sort of system, where the metal is outside, but the acidic microporous oxides are inside, can be active only by a spill over of the reaction intermediates from the metal to the oxide - and this is quite well known. However if the micropores are substituted by mesopores in the oxide phase the metal nanoparticles can go inside and then single site oxide-metal interface catalysis commences. These two different catalytic processes, where both the oxide and the metal are catalytically active, deserve attention and distinction.

9:00am IS+AS+SS-MoM3 **In-situ GISAXS/GIXAS Characterization of Co_{1-x}Pt_x Bimetallic Clusters under H₂ and CO + H₂ Mixture**, *Bing Yang*, Material Science Division, Argonne National Laboratory, *G. Khadra, J. Tuailon-Combes*, Institut Lumière Matière, University Lyon & CNRS, France, *E. Tyo*, Material Science Division, Argonne National Laboratory, *S. Seifert*, X-ray Science Division, Argonne National Laboratory, *X. Chen*, Department of Mechanical Engineering, Northwestern University, *V. Dupuis*, Institut Lumière Matière, University Lyon & CNRS, France, *S. Vajda*, Material Science Division, Argonne National Laboratory

CoPt alloy particles have recently attracted great interests for their excellent catalytic and magnetic properties. The alloy phase of cobalt and platinum may create dual-functional sites at the mixed interface which enables novel catalytic properties and synergic effect at nanometer scale. In-situ characterization is thus essential to probe the structure and composition of bimetallic clusters under reaction conditions in a catalytic process of interest.

Co_{1-x}Pt_x bimetallic clusters with atomic-precise Pt/Co atomic ratio (x=0, 0.25, 0.5, 0.75, 1) were synthesized using mass-selected low energy clusters beam deposition (LECBD) technique and soft-landed onto the amorphous alumina thin film prepared by atomic layer deposition (ALD). The median diameter of size-selected Co_{1-x}Pt_x alloy clusters is 3nm with size dispersion lower than 10 % according to transmission electron microscopy (TEM). Utilizing X-ray photoemission spectroscopy (XPS), the oxidation state of as-made clusters as well as the aged particles after extended exposure to air was characterized. After exposure to air, both cobalt and platinum species in the bimetallic clusters are found to be oxidized, while the shift of their covalent state exhibits a non-linear correlation with their atomic composition (Pt/Co).

Utilizing *in-situ* grazing incidence small-angle X-ray scattering and X-ray absorption spectroscopy (GISAXS/GIXAS), the evolution of particle size/shape and the oxidation state of the individual metals are monitored under atmosphere reaction conditions. The as-made Co_{1-x}Pt_x clusters were first pretreated with hydrogen and further exposed to CO and H₂ mixture up to 225°C. The change in the oxidation state of Co and Pt of the supported bimetallic clusters exhibited a non-linear dependency on the Pt/Co atomic ratio. For example, low Pt/Co ratio (x≤0.5) facilitates the formation of Co(OH)₂, whereas, high Pt/Co ratio (x=0.75) stabilizes Co₃O₄ composition instead, due to the formation of Co@Pt core-shell structure where the platinum shell inhibits the reduction of cobalt in the core of the Co_{1-x}Pt_x alloy clusters.

In this work, we have demonstrated *in-situ* measurement of particle size/shape and the oxidation state of supported Co_{1-x}Pt_x bimetallic clusters under operating conditions, and elucidated the different surface structure and chemical state with respect to their atomic ratio. The obtained results indicate ways for optimizing the composition of binary alloy clusters for catalysis.

9:20am **IS+AS+SS-MoM4 Novel Surface Oxide on Pt(111) as the Active Phase for NO and CO Oxidation Studied with the ReactorSTM, Matthijs van Spronsen*, J.W.M. Frenken, I.M.N. Groot, Leiden University, Netherlands**

Platinum finds its main application as a car catalyst to control the emission of exhaust gases. Although automotive catalysis has been extensively investigated, challenges still exist. One of the challenges arises when increasing the oxygen/fuel ratio. Under oxygen-rich reaction conditions, much uncertainty exist about the structure of the active surface phase. This is even true for the Pt(111) surface, which is the facet lowest in energy and the simplest model catalysts available.

An early *operando* Scanning Tunneling Microscopy (STM) study [1] showed a stepwise increase in CO oxidation activity at oxygen-rich conditions. This increase concurred with a dramatic and instantaneous morphology change. From the STM images, the atomic structure could not be resolved, but roughening on a long length scale was observed. Under similar conditions, Surface X-ray Diffraction found the formation of thin, bulk-like α -PtO₂ [2]. Surprisingly, a theoretical study concluded that this oxide is inert to CO oxidation [3].

With the high-pressure, high-temperature ReactorSTM [4], we studied the oxidation of Pt(111) both by exposing to O₂ and to NO oxidation conditions.

Upon oxidation with O₂ (1.0 bar, 423-523 K), we found a stable surface oxide consisting of triangles assembled in a 'spoked-wheel' superstructure. In addition, we found a second structure consisting of a lifted-row pattern. The two structures were coexisting on different regions on the surface. The lifted-row structure was becoming more predominant at higher O₂ pressure. We propose that both oxides share the same building block, which are expanded Pt oxide rows.

After evacuation of the reactor, the ordered structures disappeared, although some remnants remained. The surface oxidation is a clear example of the pressure-gap effect. Furthermore, lower-temperature (291-323 K) experiments did not yield any ordered structure showing the dependence on atomic mobility.

Exposure of Pt(111) to NO and O₂ or exposure to NO₂ resulted in the formation of a mixture of small domains of both the spoked-wheel and the lifted-row structures.

The surface oxidation was accompanied with roughening of terraces. This is attributed to relaxation of adsorbate-induced stress on the surface. Identical roughness development was previously found under CO oxidation conditions [1]. Therefore, we argue that a surface oxide was also the relevant structure under CO oxidation conditions.

[1] Bobaru, PhD thesis, Leiden University, 2006

[2] Ackermann, PhD thesis, Leiden University, 2007

[3] Li & Hammer, Chem. Phys. Lett., 409, 1, 2005

[4] Herbschleb, *et al.*, Rev. Sci. Instrum., 85, 083703, 2014

9:40am **IS+AS+SS-MoM5 In Operando Study of Dimethyl Methylphosphonate Degradation Over Metallic and Oxidized Cu(111) Surfaces via Ambient-Pressure X-ray Photoelectron Spectroscopy, Lena Trotochaud, A.R. Head, Lawrence Berkeley National Laboratory (LBNL), Y. Yu, University of Maryland, O. Karlioglu, M. Hartl, LBNL, B. Eichhorn, University of Maryland, H. Bluhm, LBNL**

Filtration systems for absorption and decomposition of chemical warfare agents (CWAs) are the first line of defense against exposure to these toxic compounds. Composite materials (such as ASZM-TEDA) commonly used in filtration systems consist of high-surface-area carbon supports impregnated with various metals and metal oxides. Despite decades of work to develop highly effective and versatile filtration materials with long-term usability, little is known about the mechanisms of CWA degradation by material surfaces and catalyst deactivation and poisoning, in part due to the challenges involved with spectroscopic characterization of catalyst surfaces under operating conditions. Enabling the rational design of more advanced filtration and decomposition materials for broad-spectrum protection against CWAs and other toxic industrial compounds requires a sophisticated understanding of the chemical mechanisms behind CWA sorption and degradation on the molecular scale.

We will present the surface spectroscopic study of metallic and oxidized Cu(111) single crystal surfaces for catalytic decomposition of dimethyl methylphosphonate (DMMP), a CWA simulant. Ambient-pressure X-ray photoelectron spectroscopy (APXPS) enables examination of these surfaces during DMMP adsorption and decomposition. Initial experiments indicate that adsorption of DMMP on Cu(111) is observed at pressures as low as 1×10^{-7} Torr, and degradation of DMMP is observed at this pressure and higher

(60 mTorr) at room temperature. Possible mechanisms of DMMP degradation and deactivation of the surface will also be discussed.

10:00am **IS+AS+SS-MoM6 Bridging the Pressure and Materials Gap between Surface Science and Catalysis: Probing the Surface of Metal Oxide Nanoparticles under Reaction Conditions, Maria Kipreos, M. Foster, University of Massachusetts, Boston**

Traditionally, surface science employs ultra-high vacuum, cryogenic conditions and well defined crystal planes; however, heterogeneous catalysis and photocatalysis occur in ambient conditions with complex substrates composed of several crystal planes. Consequently, materials and pressure gaps exist that need to be bridged in order to better understand the surface chemistry of catalysts under reaction conditions. Metal oxide particles employed in catalysis contain a complex matrix of crystal planes, metal/oxygen bonds, metal/hydroxyl bonds, and oxide/water interactions. We utilize *in situ* Diffuse Reflectance Infrared Fourier Transform Spectroscopy (DRIFTS) to monitor reactions from ambient to high pressures between gaseous adsorbates (water, formic acid, and methanol) and metal oxide particles (TiO₂ and ZnO, semiconductors and ZrO₂, an insulator) commonly used as components of catalysts. The internal and external scattering of light that occurs in DRIFTS is well suited for analysis of reactions on the surface of metal oxide nanoparticles. Spectral shifts in frequency, peak area and width values, and absorbance values are used to interpret the structure and reactivity of the surface. Additionally, the use of Confocal Raman Spectroscopy aids in determining the structural variability in these substrates. The use of gaseous probes and these instrumental techniques provides a better understanding of the structure and reactivity of solid nanoparticles surfaces.

10:40am **IS+AS+SS-MoM8 The Use of Integrated Operando, In Situ and DFT Techniques to Unravel the Steps of Heterogeneous Catalytic Reactions, Fabio Ribeiro, W.N. Delgass, J. Greeley, R. Gouder, J. Miller, Purdue University, W.F. Schneider, University of Notre Dame**
INVITED

Our quest to understand catalysis is limited by our ability to observe the active site while it is turning over. To facilitate this task we developed model catalysts where the active sites are deposited on the external surface area of an appropriate support. Effective characterization, however, happens only with the simultaneous measurement of the rate of reaction while the catalyst is in operation, called *operando* measurements. The application of *operando* techniques is becoming a more common tool to help unravel catalytic functions. Our group has custom-built an *operando* reactor for the measurement of X-ray absorption spectroscopy. While *operando* measurements are a major improvement, they provide a static picture of a system that is actually dynamic. Dynamic techniques where the catalyst kinetic and structural properties can be followed simultaneously with a time resolution of a fraction of a turnover are the techniques of choice. We will show examples using a transmission FTIR cell we developed. The great advantage and sometimes necessity of performing experiments in the dynamic and *operando* modes will be discussed. The help from theory will also be illustrated.

11:20am **IS+AS+SS-MoM10 In Situ XPS Of Graphene-Catalyst Interactions During Chemical Vapor Deposition, Robert Weatherup, Lawrence Berkeley National Laboratory**

Critical to controlling the growth of graphene and carbon nanotubes during chemical vapor deposition (CVD) is a detailed understanding of the role of the catalyst, however this remains incomplete due the wide parameter space. Here we investigate the dynamics of graphene-catalyst interactions during CVD using time- and depth-resolved X-ray photoelectron spectroscopy [1-2], *in situ* scanning tunneling microscopy [3] and grand canonical Monte Carlo simulations coupled to a tight-binding model [1]. We focus on Ni(111) as a model catalyst surface and probe *in-operando* a wide range of hydrocarbon exposure pressures (10^{-6} - 10^{-1} mbar). The key atomistic mechanisms of graphene formation on Ni are thereby revealed and our data highlights an interdependency between the distribution of carbon close to the catalyst surface and the strength of the graphene-catalyst interaction.

The strong interaction of epitaxial graphene with Ni(111) causes a depletion of dissolved carbon close to the catalyst surface, which prevents additional layer formation leading to a self-limiting graphene growth behavior for low exposure pressures (10^{-6} - 10^{-3} mbar). Increasing the hydrocarbon pressure further (to $\sim 10^{-1}$ mbar) leads to weakening of the graphene-Ni(111) interaction accompanied by additional graphene layer formation, mediated by an increased concentration of near-surface dissolved carbon. We also reveal that the growth of more weakly adhered, rotated graphene on Ni(111) is linked to an initially higher level of near-surface carbon compared to the case of epitaxial graphene growth. We relate these results to the simple kinetic growth model that we have previously established [6] and use them to consistently explain previous graphene CVD results in the literature. The

* Morton S. Traum Award Finalist

key implications for graphene growth control and their relevance to carbon nanotube growth are thereby highlighted.

References

- (1) Weatherup et al. *J. Am. Chem. Soc.* 2014, 136, 13698-13708
- (2) Weatherup et al. *Nano Lett.* 2011, 11, 4154-4160
- (3) Patera et al. *ACS Nano* 2013, 7, 7901-7912
- (4) Weatherup et al. *ACS Nano* 2012, 6, 9996-10003

11:40am **IS+AS+SS-MoM11 Mechanism Study for Salen Ligand Homogeneous Catalyst in a Heterogeneous Catalysis System**, *Niclas Johansson, S. Chaudhary, A.R. Head, O. Snezhkova, J.N. Andersen, J. Knudsen, J. Schnadt*, Lund University, Sweden

Surface-immobilization of transition metal complexes otherwise used as homogeneous catalysts, i.e. in the same (solution) phase as the reactants and products, and their use as heterogeneous catalysts has been an active field of research for many years. The attractiveness of the idea of surface-immobilization lies in the potential to significantly increase the efficiency and selectivity of heterogeneous catalysts [1], the ease of catalyst and product separation [1], and the fact that the need for solvents and highly oxidizing agents might be eliminated in the heterogeneous system.

Here we direct our attention towards the transition metal Mn(III)-salen complex [R,R(-)-N,N'-Bis(3,5-di-*t*-butylsalicylidene), 1,2-cyclohexane diaminomanganese(III)chloride] which have been shown to be very effective homogeneous catalysts for enantioselective epoxidation of unfunctionalised olefins. Yet, while much research has been done to investigate the salen complexes' catalytic properties in the homogeneous phase, very few surface science studies have been performed [2,3].

Here we report a study starting from standard UHV conditions and bridging the pressure gap into more realistic conditions. Here, we will show UHV spectra coupled to Torr-range Ambient Pressure X-ray Photoelectron Spectroscopy (APXPS).

We investigated propylene (C₂H₆) epoxidation reaction using surface-deposited Mn(III)-Salen on Au(111) as catalyst. With APXPS we were able to follow the electronic structure changes during reaction conditions in a gas mixture of propylene and oxygen. The spectra acquired show gas phase interactions and changes was found that were specific to the gas mixture. Surprisingly, O 1s spectra acquired at room temperature shows CO₂ which indicates complete oxidation of propylene. This result was further confirmed with a mass spectrometer in direct connection with the reaction chamber. Indeed, the complexes are active even in a heterogeneous system supporting the possibility of transferring homogeneous catalysts into heterogeneous catalytical systems.

References

- [1] C. Copéret and J.-M. Basset, *Adv. Synth. Catal.* 349, 78 (2007)
- [2] K. Lâmel et al, *Nano Lett.* 10, 2965 (2010)
- [3] A. Schwartz et al., *J. Phys. Chem. C* 117, 1105 (2013)

Advanced Surface Engineering

Room: 212A - Session SE+AS+NS+TR-MoM

Nanostructured Thin Films and Coatings

Moderator: Robert Franz, Montanuniversität Leoben, Austria, Andrey Voevodin, Air Force Research Laboratory

8:20am **SE+AS+NS+TR-MoM1 Reactively Sputter Deposited Ternary AlN-based Coatings**, *Joerg Patscheider*, Empa, Switzerland, *E. Lewin*, Uppsala University, Sweden

The protection of surfaces against preventing premature failure by abrasion-resistant nitride coatings has been investigated and put into daily operation ever since. Despite these efforts, the wide range of available protective coatings cannot be used, when glass and other optically transparent materials have to be protected due to the opacity of transition metal nitrides for visible light. For such applications thin films based on Al-A-N with additions of elements from group 14 with A = Si, Ge or Sn are attractive candidate materials, as their transparency in the visible range opens new opportunities of applications. Furthermore, the addition of these elements causes the formation of solid solutions and of nanocomposites, leading to enhanced hardness in the case of A = Si and Ge. Once nanocomposites are formed, enhanced hardness of more than 30 GPa is observed in the case of Al-Si-N and more than 20 GPa for Al-Ge-N and Al-Sn-N. The choice of the additional A element allows for the preparation of highly transparent coatings for the case of Si and the control of color in the range from yellow to red by tuning of the UV absorption edge in the case of Ge and Sn. The

role of deposition conditions and their implications on the structure these ternary nitride coatings will be discussed.

8:40am **SE+AS+NS+TR-MoM2 Mo₂BC Coatings for Metal Forming: Interactions Between Tool Surface and Aluminium by Theory and Experiment**, *Jochen Schneider*, RWTH Aachen University, Germany, *H. Bolvardi*, Oerlikon Balzers, Liechtenstein, *D. Music*, RWTH Aachen University, Germany

Low temperature growth strategies for Mo₂BC coatings are reviewed and initial theoretical and experimental data pertaining to the applicability of these coatings during forming of Al based alloys are discussed. A Mo₂BC(040) surface was exposed to O₂. The gas interaction was investigated using *ab initio* molecular dynamics and x-ray photoelectron spectroscopy (XPS) of air exposed surfaces. The calculations suggest that the most dominating physical mechanism is dissociative O₂ adsorption whereby Mo - O, O - Mo - O and Mo₂ - C - O bond formation is observed. To validate these results, Mo₂BC thin films were synthesised utilizing high power pulsed magnetron sputtering and air exposed surfaces were probed by XPS. MoO₂ and MoO₃ bond formation is observed and is consistent with here obtained *ab initio* data. Additionally, the interfacial interactions of O₂ exposed Mo₂BC(040) surface with an Al nonamer is studied with *ab initio* molecular dynamics to describe on the atomic scale the interaction between this surface and Al to mimic the interface present during cold forming processes of Al based alloys. The Al nonamer was disrupted and Al forms chemical bonds with oxygen contained in the O₂ exposed Mo₂BC(040) surface. Based on the comparison of here calculated adsorption energy with literature data, Al - Al bonds are shown to be significantly weaker than the Al - O bonds formed across the interface. Hence, Al-Al bond rupture is expected for a mechanically loaded interface. Therefore the adhesion of a residual Al on the native oxide layer is predicted. This is consistent with experimental observations. The data presented here may also be relevant for other oxygen containing surfaces in a contact with Al or Al based alloys for example during forming operations.

9:00am **SE+AS+NS+TR-MoM3 Molecular Dynamics Simulations of TiN/TiN(001) Growth**, *Daniel Edström, D.G. Sangiovanni, V. Chirita, L. Hultman*, Linköping University, Sweden, *J.E. Greene, I. Petrov*, University of Illinois at Urbana Champaign

The Modified Embedded Atom Method (MEAM) interatomic potential within the classical Molecular Dynamics (MD) framework enables realistic, large-scale simulations of important model materials such as TiN. As a step toward understanding atomistic processes controlling the growth of TiN on a fundamental level, we perform large-scale simulations of TiN/TiN(001) deposition using a TiN MEAM parameterization which reproduces experimentally-observed surface diffusion trends, correctly accounts for Ehrlich barriers at island step edges [1], [2], and has been shown to give results in excellent qualitative and good quantitative agreement with *Ab Initio* MD based on Density Functional Theory (DFT) [3], [4]. 85% of a monolayer of TiN is deposited on 100x100 atom TiN(001) substrates at a rate of 1 Ti atom per 50 ps, resulting in simulation times of 212.5 ns. The TiN substrate is maintained at a typical epitaxial growth temperature, 1200 K during deposition using N:Ti flux ratios of 1:1, 2:1, and 4:1 and incident energies of 2 and 10 eV to probe the effects of N₂ partial pressure and substrate bias on TiN(001) growth modes. We observe nucleation of Ti_xN_y molecules; N₂ desorption; the formation, growth and coalescence of mixed <100>, <110>, and <111> faceted islands; as well as intra- and interlayer mass transport mechanisms. For equal flux ratios at 2 eV incidence energy, islands begin to form atop existing islands at coverages ≥ 0.25 ML, leading to 3D multilayer growth. Increasing the N:Ti flux ratio shifts the growth mode to layer-by-layer growth and changes the stoichiometry from under- to over-stoichiometric. We discuss the implications of these results on thin film growth and process tailoring. Our classical MD predictions are supported and complemented by DFT-MD simulations.

[1] D. G. Sangiovanni, D. Edström, L. Hultman, V. Chirita, I. Petrov, and J. E. Greene, "Dynamics of Ti, N, and TiN_x (x=1-3) ad molecule transport on TiN(001) surfaces," *Phys. Rev. B*, vol. 86, no. 15, p. 155443, 2012.

[2] D. Edström, D. G. Sangiovanni, L. Hultman, V. Chirita, I. Petrov, and J. E. Greene, "Ti and N adatom descent pathways to the terrace from atop two-dimensional TiN/TiN(001) islands," *Thin Solid Films*, vol. 558, pp. 37-46, 2014.

[3] D. G. Sangiovanni, D. Edström, L. Hultman, I. Petrov, J. E. Greene, and V. Chirita, "Ab initio and classical molecular dynamics simulations of N₂ desorption from TiN(001) surfaces," *Surf. Sci.*, vol. 624, pp. 25-31, 2014.

[4] D. G. Sangiovanni, D. Edström, L. Hultman, I. Petrov, J. E. Greene, and V. Chirita, "Ti adatom diffusion on TiN(001): Ab initio and classical molecular dynamics simulations," *Surf. Sci.*, vol. 627, pp. 34-41, 2014.

9:20am **SE+AS+NS+TR-MoM4 Stress Design of Multi-layered Coatings, Wolfgang Seidl**, Christian Doppler Laboratory for Application Oriented Coating Development at the Institute of Materials Science and Technology, Vienna University of Technology, 1040 Vienna, Austria, *M. Arndt*, Oerliko Balzers, Oerlikon Surface Solutions AG, 9496 Balzers, Liechtenstein, *P. Polcik*, Plansee Composite Materials GmbH, 86983 Lechbruck am See, Germany, *P.H. Mayrhofer*, Vienna University of Technology, Austria

Residual stresses within physical vapour deposited coatings are a major concern, as they are often the origin of failure and delamination. Furthermore, stresses, which typically scale with the thickness, limit the thickness of the coating. With increasing stresses, the interface region is increasingly stressed and weakened, promoting delamination and buckling effects. CrN coatings are known to allow for moderate compressive or even tensile stresses, enabling the preparation of coating thicknesses above 20 μm . Although CrN coatings exhibit excellent tribological and wear resistance properties, their thermal stability with respect to Cr-N dissociation is limited to 900 $^{\circ}\text{C}$, which limits their application field. However, several applications require higher thermal stability in combination with relatively thick ceramic coatings. Therefore, we study in detail the requirements to develop nitride-based coatings with thicknesses exceeding 20 μm .

The residual stresses of arc evaporated TiN, CrN, TiAlN, CrAlN, and TiAlTaN coatings, prepared with an industrial sized coating plant (Balzers Oerlikon INNOVA), are investigated as a function of their thicknesses by measuring the curvature of one-side coated Si(100) cantilevers. Based on these studies we developed multilayer arrangements of TiN/CrN, TiAlN/CrN, TiAlN/CrAlN, and TiAlTaN/CrAlN thick coatings. Their stresses are designed through variations in bilayer period and arrangements of the cathodes at the sidewalls of the industrial chamber.

The individual coatings and multilayers are additionally investigated with respect to growth morphology (by cross sectional scanning electron microscopy), hardness and indentation moduli (by nanoindentation), structure and crystallographic phases (by X-ray diffraction).

9:40am **SE+AS+NS+TR-MoM5 Atomistic Guided Development of Hard Coatings and Thin Films for Severe Applications, Paul Mayrhofer**, Vienna University of Technology, Austria **INVITED**

This work summarizes recent developments on applying thin film structure and architecture concepts to hard coatings for optimized performance in various application fields.

The hardness of materials rapidly decreases at elevated temperatures as generally the density of structural defects, such as point defects, dislocations, and grain boundaries, decreases. Additional strengthening can be provided by age-hardening mechanisms, which originate from decomposition-processes of supersaturated phases to form new obstacles retarding plastic deformation. Furthermore important is the resistance against oxidation and corrosive attack.

By using ab initio calculations and sophisticated experimental methods we will have a detailed insight into various mechanisms responsible for excellent mechanical strength, thermal stability and oxidation resistance properties of Ti-Al-N based hard coatings. For these materials we will also compare the effect of various architecture and alloying concepts with e.g., Y, Zr, Hf, Nb, and Ta.

Another important class of hard coatings is based on the material systems CrN and Cr-Al-N. After a short overview on ab initio and experimental studies in comparison to their sister system Ti-Al-N, we will have a small excursion on the influence of architecture – using the model system CrN/AlN multilayers or their superlattices – on the mechanical properties and especially fracture toughness. Furthermore, based on recent ab initio investigations suggesting that the inherent fracture toughness of CrN can be increased by alloying with Mo or W, we will explore in detail the challenges in studying Cr-Mo-N or Cr-W-N materials by ab initio and experiments.

The various thin film structure and architecture concepts allow the utilization of multifunctional properties facilitating the development of next generation's hard coatings.

10:40am **SE+AS+NS+TR-MoM8 Crystallographic Stabilization of δ -WC Thin Films by Alloying with B, using Reactive Magnetron Sputtering of W in Trimethylboron (CH_3)₃B, Hans Högberg, L. Tengdelius, M. Samuelsson, G. Greczynski, F. Eriksson, L. Hultman**, Linköping University, Sweden

The hardness, oxidation resistance, and high temperature stability of hexagonal δ -WC (B_h) in cemented carbide is a key component in metal cutting. Such a property envelop suggest many potential thin film applications. However, the literature shows that thin film growth of δ -WC by for instance magnetron sputtering is complicated typically resulting in

the deposition of films containing the phase γ -WC (B_l) with a carbon content lower than nominal, i.e. WC_{1-x} . As the properties of this phase is less favorable compare to those of δ -WC, growth of WC_{1-x} must be avoided in an optimized thin film material. In this study, we attempt to promote the formation of δ -WC films by alloying with B. Our hypothesis is that the preferred growth of WC_{1-x} films depends on the preference of C to occupy octahedral sites found in the B_l structure and where the larger B atom may act to stabilize the B_h structure by better filling out the larger trigonal prism interstitials in this structure. We use reactive magnetron sputtering of W, using trimethylboron (CH_3)₃B (TMB) as C and B precursor. The 5 min depositions were carried on Si(100) substrates in a Kr plasma held at a constant pressure of 0.53 Pa. The gaseous TMB was introduced close to the substrates. The influence of TMB flow, ranging from 1-10 mln, was studied for a growth temperature of 500 $^{\circ}\text{C}$. Also, the influence of growth temperature, from room temperature to 900 $^{\circ}\text{C}$, was investigated for a constant TMB flow of 10 mln. X-ray photoelectron spectroscopy shows that the content of B and C scales with the flow into the plasma with no B and ~ 3 at.% C at 1 mln and 6.5 at.% B and 17.8 at.% C at 10mln. In contrast, temperatures up to 600 $^{\circ}\text{C}$ show no impact on the B and C content in the films, while higher temperatures give a solid state reaction with the substrate. X-ray diffraction shows broad peaks indicative of small grain sizes and with peaks at 2θ angles matching those of the phases WC_{1-x} or W. In the in the temperature range 300 to 600 $^{\circ}\text{C}$, 100-textured WC_{1-x} films are deposited and with a shift to a weak 111 orientation at lower temperatures. At 500 $^{\circ}\text{C}$, TMB flows of 5 to 10 mln results in the growth of 100-textured WC_{1-x} films, while lower flows yield W films. Films are deposited with thicknesses up to ~ 1000 nm, corresponding to a deposition rate of 3.3 nm/s. The microstructure is generally fine-grained, but with broken columns at 500 and 600 $^{\circ}\text{C}$ and a TMB flow of 1 mln. The mechanical properties of the films will be reported.

11:00am **SE+AS+NS+TR-MoM9 Epitaxial and Polycrystalline WN_x and MoN_x Films Deposited by Reactive DC Magnetron Sputtering, Brian Oszdolay, K. Balasubramanian**, Rensselaer Polytechnic Institute, *C.P. Mulligan*, U.S. Army Armament Research Development & Engineering Center, Benét Laboratories, *M.J. Guerette, L. Huang, D. Gall*, Rensselaer Polytechnic Institute

WN_x layers, 1.45- μm -thick, were deposited by reactive magnetron sputtering on MgO(001), MgO(111), and Al₂O₃(0001) in 20 mTorr N₂ at $T_s = 500$ -800 $^{\circ}\text{C}$. X-ray diffraction ω - 2θ scans, ω -rocking curves, ϕ scans, and reciprocal space maps show that all layers deposited from 500-700 $^{\circ}\text{C}$ exhibit the cubic rock-salt structure, with a relaxed lattice constant that decreases from 4.299 to 4.171 \AA as the N-to-W ratio decreases from $x = 1.20$ for $T_s = 500$ $^{\circ}\text{C}$ to $x = 0.83$ for $T_s = 700$ $^{\circ}\text{C}$, as measured by energy dispersive and photoelectron spectroscopies. $T_s = 500$ -600 $^{\circ}\text{C}$ yields a polycrystalline 111-textured microstructure on all substrates. In contrast, deposition at 700 $^{\circ}\text{C}$ results in epitaxial growth of WN(111) and WN(001) on MgO(111) and MgO(001), respectively, while deposition on Al₂O₃(0001) yields a 111-preferred orientation, misoriented cubic WN grains as well as N-deficient BCC W. $T_s = 800$ $^{\circ}\text{C}$ causes nitrogen loss and WN_x layers with primarily BCC W grains and $x = 0.04$ -0.06. The measured elastic modulus ranges from 110-260 GPa for $T_s = 500$ -700 $^{\circ}\text{C}$ and decreases with increasing N-content, and increases to 350 GPa for $T_s = 800$ $^{\circ}\text{C}$. For samples deposited at $T_s = 700$ $^{\circ}\text{C}$, nanoindentation on WN on MgO(001), MgO(111), and Al₂O₃(0001) provides hardness values of 9.8 ± 2.0 , 12.5 ± 1.0 , and 10.3 ± 0.4 GPa, and elastic moduli of 240 ± 40 , 257 ± 13 , and 242 ± 10 GPa, respectively. The corresponding shear moduli measured by Brillouin light scattering are 127 ± 2 GPa, 121 ± 2 GPa and 115 ± 2 GPa. MoN_x layers, 1- μm -thick, deposited on MgO(001) also exhibit a cubic rock salt structure with x decreasing from 1.18 for $T_s = 500$ and 600 $^{\circ}\text{C}$ to $x = 0.76$ for $T_s = 800$ $^{\circ}\text{C}$ but remaining approximately constant for $T_s = 800$ -1000 $^{\circ}\text{C}$. Layers with $T_s > 700$ $^{\circ}\text{C}$ contain both epitaxial MoN_x(001) and 111-oriented grains. The out-of-plane lattice constant decreases from 4.22 to 4.18 \AA for 111 oriented grains and from 4.17 to 4.06 \AA for epitaxial 001-oriented grains, as T_s is increased from 700 $^{\circ}\text{C}$ to 1000 $^{\circ}\text{C}$.

11:20am **SE+AS+NS+TR-MoM10 Phase Stability and In Situ Growth Stresses in Thin Cu/Nb Multilayered Films, Qianying Guo, L. Wan, R.L. Martens, G.B. Thompson**, University of Alabama

As the length scale of individual layers are reduced in a Cu/Nb multilayer, fcc to bcc and bcc to fcc transformations were noted for Cu and Nb respectively. These transitions have been modeled using a thermodynamic phase diagram where interfacial and volumetric energy considerations determine stability and the bilayer thickness of the multilayer is a state variable for predicting those transformations. Using HRTEM, the evolution of the interface from incoherent-to-semicoherent-to-coherent is determined and related to the structural component of the interfacial energy reduction that drives the crystalline transformations. When equal thicknesses of each layer were < 1 nm, the layers underwent an additional transformation from a crystalline to amorphous structure. This has been rationalized by the

positive enthalpy of mixing between these two species as they intermixed during the sputter deposition process. The chemical intermixing and local clustering at and near the interface has been quantified by atom probe tomography. These phase transformations have been related to real-time, intrinsic growth stress measurements. All of the multilayers were in a compressive stress state, but a notable reduction in the compressive stress value occurred with each transformation. The collective characterization of the film, via TEM, atom probe, and stress evolution, have provided insights into the structural stability of crystalline phases at the nanoscale.

11:40am **SE+AS+NS+TR-MoM11 Droplets in Cathodic Arc Evaporated (Al,Cr)₂O₃-based Coatings and the Nucleation of Dedicated Crystalline Structures**, *Christian M. Koller*, CDL AOS, TU Wien, Austria, *R. Hahn*, TU Wien, Austria, *J. Ramm*, Oerlikon Balzers, Oerlikon Surface Solutions AG, Liechtenstein, *S. Kolozsvári*, Plansee Composite Materials GmbH, Germany, *P.H. Mayrhofer*, CDL AOS, TU Wien, Austria
Corundum-type Al₂O₃ coatings demonstrate excellent thermo-mechanical properties, giving rise to widespread applications as protective films on, e.g., cutting inserts or components. These coatings are typically synthesised by chemical vapour deposition (CVD) at temperatures of 900 °C or higher, which excludes temperature sensitive substrates. Physical vapour deposition (PVD) proved to be a suitable method for low temperature synthesis of nitrides with excellent properties. However, the growth of single-phased corundum-type α -Al₂O₃ by PVD is still a difficult task under standard production conditions. In general, a mixed phase composition of metastable cubic phases is observed, which influence the thermo-mechanical performance of the coating. The utilisation of targets produced by powder metallurgical methods allows for the combination of aluminium with other elements, suitable to promote dedicated crystal structures as demonstrated by AlCr and more recently AlCrFe, where dense crystalline coatings with an increased amount of hexagonal phase fractions were realised. Although the alloying with Cr and Fe is a promising concept with good prospects, the mechanism to form the hexagonal structure in these materials is yet not understood. Therefore, the aspect of layer-nucleation is investigated in more detail. A significant part of hexagonal crystallites in (Al,Cr,Fe)₂O₃ coatings is triggered by nucleation onto small particles incorporated in the coating. They originate from the cathode surface and are generated during the cathodic arc process. Cathode surface modifications, macroparticle incorporation and the associated coating microstructures are elucidated by detailed X-ray diffraction and electron microscopy studies. Implications on the coatings' properties and possible technological concepts are discussed.

Surface Science

Room: 113 - Session SS+AS+EN-MoM

Synthesis, Structure and Characterization of Oxides

Moderator: Sylvie Rangan, Rutgers, the State University of New Jersey

8:20am **SS+AS+EN-MoM1 Oxygen Uptake on Rh(111)**, *Daniel Killelea*, *J. Derouin*, *R.G. Farber*, Loyola University Chicago

Rhodium surfaces are of high utility for the partial oxidation of small molecules. We present results from a study of the uptake of gas-phase oxygen atoms on the Rh(111) surface. A combination of temperature programmed desorption (TPD), Auger electron spectroscopy (AES), and scanning tunneling microscopy (STM) were used to determine the total amount of oxygen, the oxygen surface coverages, and the surface structures, respectively. Our findings suggest that oxygen atoms are readily incorporated in to the near-surface region on Rh(111) while retaining low oxygen surface coverages and structures. We further studied how the surface changes when the subsurface oxygen atoms emerge to the surface. These findings provide insight to the formation of bulk oxides, and show that high-coverages of oxygen are not necessary for absorption of oxygen into the selfedge.

8:40am **SS+AS+EN-MoM2 Formation of Subsurface Oxygen and Surface Oxides on Ag(111) by Atomic Oxygen**, *Jonathan Derouin**, *R.G. Farber*, *D.R. Killelea*, Loyola University Chicago

Understanding the interaction of oxygen with transition metal surfaces is important in many areas including corrosion and catalysis. The oxygen/silver system in particular has been studied extensively both experimentally and theoretically. Interest is driven largely by the role of silver in two widely used industrial reactions: the epoxidation of ethylene to produce ethylene oxide and the partial oxidation of methanol to produce

formaldehyde. In addition, the oxygen/silver system can serve as a model for the dissociative chemisorption of diatomic molecules on close packed metal surfaces. Despite extensive research, the oxygen/silver system is still not well understood. To better understand this system, we use UHV-STM, AES and TPD to study the adsorption of atomic O on an Ag(111) crystal. Atomic O is generated by thermally cracking molecular O. By varying the power of the thermal cracker we are able to change the flux of atomic O reaching the Ag surface. Higher atomic O fluxes produce O structures which desorb at significantly higher temperatures than structures produced with lower O fluxes. We then use UHV-STM to further characterize the various oxide structures produced.

9:00am **SS+AS+EN-MoM3 Surface and Bulk Properties of Pure and Mixed Titania**, *Matthias Batzill*, University of South Florida **INVITED**
Titanium oxide in its different polymorphs remains a model system for structure property relationships in simple oxides. In this talk we address issues related to both the bulk and the surface properties of TiO₂. Measuring the photocatalytic activity of anatase- and rutile- epitaxial films we conclude that charge carriers excited deeper in the bulk contribute to the surface photocatalytic activity for anatase compared to rutile [1]. This difference may be an important factor for explaining the generally higher photocatalytic activity of anatase-TiO₂. In the second part of the talk, surface properties are presented on the example of rutile TiO₂(011). The (011) surface orientation is less frequently studied compared to the (110) surface. Under UHV-conditions the (011) surface reconstructs into a complex 2x1 structure. We investigate the stability of this reconstruction under chemical adsorption. We find that for strongly adsorbing molecules the surface restructures to enable stronger adsorption. We show that this restructuring is strongly anisotropic resulting in quasi-1D adsorbate structures [2]. The instability of the rutile TiO₂(011)-2x1 surface may also be exploited for the formation of unique mixed oxide surfaces. This we demonstrate with iron oxide, which forms an ordered mixed TiFeOx surface oxide layer. Such mixed oxide surface may also form by impurity segregation from the bulk and thus may be a common surface structure in Fe-doped TiO₂.

[1] "Why is anatase a better photocatalyst than rutile? - Model studies on epitaxial TiO₂ films" T. Luttrell, S. Halpegamage, J.G. Tao, A. Kramer, E. Sutter, M. Batzill *Sci. Rep.* 4, 4043 (2014).

[2] "Adsorbate Induced Restructuring of TiO₂(011)-(2x1) Leads to One-Dimensional Nanocluster Formation" Q. Cuan, J. Tao, X.Q. Gong, M. Batzill *Phys. Rev. Lett.* 108, 106105 (2012).

9:40am **SS+AS+EN-MoM5 Characterizations of Non-polar Polar Interfaces: Cr₂O₃ on ZnO (0001) and (000-1)**, *Xiaodong Zhu*, *M.D. Morales-Acosta*, *J. Shen*, *F.J. Walker*, *J. Cha*, *E.I. Altman*, Yale University
The growth of non-polar Cr₂O₃ on oppositely poled ZnO surfaces was characterized to determine how the polar substrate influences the properties of the non-polar film. Photoelectron spectroscopy (XPS and UPS), electron diffraction (RHEED and LEED), High-resolution transmission electron microscopy (HRTEM), X-ray diffraction (XRD) and X-ray reflectivity (XRR) have been performed to determine the growth mode, film quality and interfacial electronic properties are influenced by the substrate polarization. The growth is 2D; however, the films appear initially disordered on both substrates. With increasing film thickness, the films ordered with a well-defined epitaxial relationship. The HRTEM and XRD/XRR results for thicker films confirm a clear interface and well-defined lattice structure near the interface and throughout the film, indicating that above a critical thickness the entire film reorganizes into an ordered structure. The polar interfaces show a small but noticeable band offset that decayed with increasing film thickness. Statistical analysis of UPS valence band spectra revealed an enhanced density of states near the Fermi level for Cr₂O₃ on the positive surface consistent with stabilization of the positive interface by charge transfer; in contrast, no significant valence band differences were observed between bulk Cr₂O₃ and thin Cr₂O₃ thin layers on the negative surface. The results will be compared with those obtained for ZnO/Cr₂O₃/ ZnO (0001) and (000-1) to determine if the interfacial properties are sensitive to how the interface is formed.

10:40am **SS+AS+EN-MoM8 Exploring Iron Oxide Clusters and Films Supported on HOPG with HREELS and AES**, *Joel Langford*, University of California, Irvine, *F. Rosner*, Technical University of Munich, Germany, *J. Kwon*, *J.C. Hemminger*, University of California, Irvine

We are using High Resolution Electron Energy Loss Spectroscopy (HREELS) and Auger Electron Spectroscopy (AES) to investigate nanoclusters and films of iron oxide supported on highly oriented pyrolytic graphite (HOPG). For the films, two AES oxidation profiles were generated by annealing in oxygen. One profile was at a constant sample temperature of 500 K with varying exposure, the other by varying sample temperature while keeping exposure at a constant 1000 L. Both oxidation profiles

* Morton S. Traum Award Finalist

saturate at an AES O/Fe ratio of 1.2. This ratio is below the O/Fe ratio of magnetite (Fe₃O₄), and hematite (Fe₂O₃) indicating incomplete oxidation of the film. Additional evidence for incomplete film oxidation comes from the absence of Fuchs-Kliwer phonons in the HREEL spectra. For the nanoclusters we are investigating two systems; polydispersed iron oxide nanoclusters on HOPG, and platinum nanoclusters supported on iron oxide nanoclusters. The polydispersed nanoclusters are more susceptible to oxidation than the film as evident by the higher AES O/Fe ratio and the presence of Fuchs-Kliwer phonons in the HREEL spectra. The platinum nanoclusters are synthesized on the iron oxide nanoparticles by an ex-situ photodeposition technique and therefore adventitious carbon is adsorbed prior to transfer into the UHV chamber. To remove the adventitious carbon we annealed in oxygen at a sample temperature of 1000 K. HREEL spectra show that the annealing procedure removes adventitious carbon because of the absence and appearance of a CO resonance before and after cleaning, respectively. HREEL spectra after low temperature CO adsorption and as a function of subsequent anneal temperature will be presented.

11:00am **SS+AS+EN-MoM9 Computational Materials Design[®]: Ionic Conduction in Rare-Earth-Metal Oxides from the First Principles-based Studies**, *Susan Aspera, M. Sakae, M. Alaydrus, T.P.T. Linh, N.H. Linh, H. Nakanishi*, Osaka University, Japan, *H. Kasai*, Akashi College, Japan

Solid oxide fuel cells (SOFC) have been one of the most promising technologies to tap alternative sources of energy. This technology utilizes abundant fuel materials such as H₂, CH₄ and other hydrocarbon materials to lessen our dependence on non-renewable fossil fuels that are nearly depleting. It takes into advantage the efficiency brought about by high kinetics of reaction at the electrolyte sides occurring at high working temperature. With this, ceramic based materials are often used as electrolyte and electrode materials. However, the working temperature of SOFCs is often too high (700°C to 1000°C). This limits the application of SOFCs and consequently high cost of producing durable materials for high working temperature. Recently, research related to this technology focuses on materials that work at intermediate temperature (IT-SOFC). This entails finding/designing materials that have high ionic conductivity at IT-SOFC working temperature.

Recent developments in computational simulation techniques, coupled with the rapid progress in computer efficiency, make first principles-based COMPUTATIONAL MATERIALS DESIGN (CMD[®]) a relevant field in the world of surface science and condensed matter physics. In this scheme, quantum mechanical calculations are performed to design promising materials and, understand the necessary mechanisms for the realization of an efficient technological device. Here, we employed the CMD[®] process and density functional theory-based analysis to study the atomic and electronic properties of several rare-earth-metal oxides (Pr₂NiO₂, La₂GeO₅, LaGaO₃ and CeO₂) which has potential application in IT-SOFC. These materials are known to have different structures according to symmetry, and the mechanism by which O ion conducts, i.e. via oxygen vacancies (O_{vac}) migration or O interstitial migration. The O ion migration path is dependent on the structure of the material, and the corresponding activation energy barrier for oxygen ion migration (E_{ac}) is affected by the concentration of O_{vac} and the presence of dopants, for O ion conduction via vacancies. In most of these systems, dopants with the same ionic radius as the host materials create high probability for O_{vac}, which then affects ionic conductivity, and the E_{ac} is found to be least for dopants with ionic radius near to that of the host material. Furthermore, as ionic migration is sensitive to the atomic structure, E_{ac} is partly due to the structural alteration brought about by the presence of impurities such as dopants and creation of heterostructure interfaces. With these understanding, we can comment on the methods by which ionic conductivity can be enhanced in these materials.

11:20am **SS+AS+EN-MoM10 Modeling and Characterization of Exemplar Sealing Glasses to Develop Chemistry-Structure-Property Relationships**, *Michael Brumbach, T. Zeidler, T. Alam, M. Rodriguez, L. Criscenti, M. Kalan, A. Mirabal, D. Bencoe, K. Ewsuk*, Sandia National Laboratories

The performance of joining materials in many applications, such as glass-to-metal seals in solid oxide fuel cells and medical devices, require improvements in glass properties for greater reliability. In this work, simple sealing glass compositions have been used to develop experimentally-validated molecular models. The goal is to understand glass chemistry and structure such that modeling can be used to guide glass design, for manufacturability, and optimized performance. The coupled modeling and experimental work will be discussed.

Technological glasses are used in many applications where inorganic joining is required. Applications of joining glasses include glass in glass-to-metal seals (in solid oxide fuel cells or medical components), glass-bonded ceramics (such as debase aluminas), and low temperature co-fired ceramic

(LTCC) packaging for microelectronics. For these applications, well-controlled processing conditions and high reliability in the end-product are of paramount importance. To better understand materials performance and reliability our objective is to develop experimentally-validated simulation tools to predict and control glass chemistry-structure property relationships. These tools will be used to predict structure-function relationships in bulk glasses and at joining interfaces.

Results from experimental characterization of several barium aluminosilicate glasses will be discussed. Solid-state NMR, lab-based and synchrotron X-ray scattering, and EXAFS have been used to determine structural characteristics of the exemplar glasses. Comparison of experimental results to molecular dynamics modeling of the three-component glass will be presented. Additional simulations of glass properties and comparisons to measurements will also be discussed.

Sandia National Laboratories is a multi-program laboratory managed and operated by Sandia Corporation, a wholly owned subsidiary of Lockheed Martin Corporation, for the U.S. Department of Energy's National Nuclear Security Administration under contract DE-AC04-94AL85000.

Thin Film

Room: 111 - Session TF+AS+SS-MoM

Self-Assembled Monolayers, Layer-by-Layer, etc.

Moderator: Han Zuilhof, Wageningen University, Netherlands

8:20am **TF+AS+SS-MoM1 The Effects of Embedded Dipoles in Aromatic Self-Assembled Monolayers**, *Sven Schuster*, Universität Heidelberg, Germany, *T. Abu-Husein*, Universität Frankfurt, Germany, *D.A. Egger, I. Hehn*, Graz University of Technology, Austria, *M. Kind*, Universität Frankfurt, Germany, *E. Zojer*, Graz University of Technology, Austria, *A. Terfort*, Universität Frankfurt, Germany, *M. Zharnikov*, Universität Heidelberg, Germany

Self-assembled monolayers (SAMs) are frequently used as intermediate films to modify charge-carrier injection from metal-electrodes into an organic semiconductor. This is usually achieved by use of the terminal dipolar groups comprising the SAM-ambient interface and affecting, at the same time, the growth chemistry of the semiconductor. Here we suggest an alternative approach, viz. embedding dipolar element into the molecular backbone, which allows decoupling the dipole control and the interfacial chemistry. As molecular backbone we use oligophenyl moiety which provides a suitable structural match to most organic semiconductors. As polar unit we use pyrimidine, varying its orientation in the molecular backbone and, consequently, the direction of the embedded dipole moment. The electronic and structural properties of these embedded-dipole SAMs are thoroughly analyzed using a number of complementary characterization techniques combined with quantum-mechanical modeling. We show that such mid-chain substituted monolayers are highly interesting from both fundamental and application viewpoints, as the dipolar groups are found to induce a potential discontinuity inside the monolayer, electrostatically shifting the energy levels in the regions above and below the dipoles relative to one another. These SAMs also allow for tuning the substrate work function in a controlled manner independent of the docking and interfacial chemistry. In addition, a mixture of the embedded-dipole molecules with opposite orientations of dipoles makes possible a fine tuning of the work function between the ultimate values, associated with a particular dipole orientation. Quantum-mechanical modeling in conjunction with x-ray photoelectron spectroscopy experiments provides insight into the molecular organization of such mixed monolayers.

8:40am **TF+AS+SS-MoM2 IR Spectroscopic studies of Molecular Thin Films exhibiting Spontaneous Dipole Alignment**, *Alexander Rosu-Finsen*, Heriot-Watt University, UK, *J. Lasne*, Heriot-Watt University, France, *A. Cassidy, D. Field*, Aarhus University, Denmark, *M.R.S. McCoustra*, Heriot-Watt University, UK

In recent years, observations of the presence of a spontaneous and powerful static electric field within thin films of molecular solids have been reported by Field and co-workers [1]. These electric fields, which can approach 10⁸ V m⁻¹ or more, are believed to arise from alignment of the molecular dipoles in the thin films. Seeking to provide an independent means of observing this phenomenon of the "spontelectric phase", the first new electrically-unique, structural phase to have emerged in decades, we have used reflection-absorption infrared spectroscopy (RAIRS) to investigate thin films of nitrous oxide (N₂O). The presence of a static electric field within the thin film, the defining characteristic of spontelectrics, is demonstrated through the observed temperature dependence of longitudinal-transverse optical

(LO-TO) splitting in RAIR spectra, using an analysis based on the vibrational Stark effect [2]. Tentative evidence for the surface-templating of the growth of the spontelectric phase will be presented from RAIRS studies of solid carbon monoxide (CO) on a range of water substrates (porous amorphous solid water, compact amorphous solid water and crystalline water) [3].

[1] Spontaneous electric fields in solid films: spontelectrics. D. Field, O. Plekan, A. Cassidy, R. Balog, N.C. Jones and J. Dunger, *Int. Rev. Phys. Chem.*, 2013, **32**, 345-392.

[2] Spontaneously electrical solids in a new light. J. Lasne, A. Rosu-Finsen, A. Cassidy, M. R. S. McCoustra and D. Field, *Phys. Rev. Lett.*, submitted.

[3] Templating dipole alignment in solid carbon monoxide on water ice surfaces. A. Rosu-Finsen, J. Lasne, A. Cassidy, D. Field and M. R. S. McCoustra, *Phys. Rev. Lett.*, in preparation.

9:00am **TF+AS+SS-MoM3 Coordination-Based Molecular Assemblies as Electrochromic Materials: Ultra-High Switching Stability and Coloration Efficiencies^[1]**, *Michal Lahav*, Weizmann Institute of Science, Israel

Layer-by-Layer (LbL) deposition, combined with metal-ligand coordination, has served as a powerful tool for generating functional architectures.^[2] Such systems might find interesting applications in molecular electronics, sensor, solar cells and data storage. More significantly, owing to their interesting electrochromic (EC) behavior, they are promising candidates for use in smart windows and display devices. In this study we used a dip-coating process to generate molecular assemblies (MA) from metal polypyridyl complexes cross-linked with PdCl₂. These polypyridyl complexes are considered ideal chromophores for fabricating electrochromic materials, due to their excellent stability and light absorption that greatly depends on their oxidation state.^{[3],[4]} The number of pyridine moieties of the chromophores is varied to control (i) the materials' stability, (ii) color, (iii) redox-chemistry, and (iv) the film growth (i.e., linear vs. exponential). We also observed that minor structural differences (i.e., the pyridine-bipyridine bond order) at the molecular level become apparent when the stability and electrochromic properties are examined (Figure 1). The MAs exhibit high coloration efficiencies and are extremely stable: they are thermally robust and have exceptionally high (spectro)electrochemical activity. Furthermore, we demonstrated the formation of a first-generation solid-state set-up.^{[1],[5]}

1) S. Shankar, M. Lahav, M. E. van der Boom, *J. Am. Chem. Soc.* **2015**, *137*, Just Accepted Manuscript.

2) R. J. Mortimer, *Annu. Rev. Mater. Res.*, **2011**, *41*, 241.

3) G. de Ruiter, M. Lahav, M. E. van der Boom, *Acc. Chem. Res.*, **2014**, *47*, 3407-3416.

4) G. de Ruiter, M. Lahav, H. Keisar, M. E. van der Boom, *Angew. Chem., Int. Ed.* **2013**, *52*, 704-709.

5) M. E. van der Boom, M. Lahav, S. Shankar, US Patent 61/906,565, **2013**.

9:20am **TF+AS+SS-MoM4 New Approaches to the Preparation of Well-defined Metal Films on Top of Self-assembled Monolayers**, *Michael Zharnikov*, Universität Heidelberg, Germany

Self-assembled monolayers (SAMs) can be potentially used as ultrathin insulating dielectric layers or intermediate films in different electronic and spintronic devices. Whereas the bottom electrode in such assemblies is represented by the metal substrate, the top electrode should be prepared at the SAM-ambience interface. Regretfully, the formation of a well-defined metal film on top of the SAMs is a non-trivial task, since the metal atoms deposited onto the SAM-ambient interface do not stay there, but penetrate into the monolayer and diffuse to the metal substrate following a strong thermodynamical drive. Here I discuss three new approaches to suppress the above penetration and diffusion, taken a representative ferromagnetic metal, nickel, as a test adsorbate. The first approach relies on irradiation-induced cross-linking of a thiol-substituted aromatic SAM. Whereas 2D-polymerization of such a SAM prevents penetration of the metal atoms into the monolayer, the thiol groups at the SAM-ambient interface serve as nucleation centers for the growing "top" film. The second approach, relying on SAMs of perfluoroterphenyl-substituted alkanethiols, utilizes a chemical reaction between the SAM constituents and adsorbate atoms. The primary process is the Ni mediated loss of fluorine atoms followed by extensive cross-linking between the partly defluorinated molecular backbones. The stability of these backbones and the rapid development of the cross-linking are the key components to hinder the metal penetration. Finally, the penetration of deposited metal atoms into a SAM can be nearly completely inhibited by the preliminary formation of palladium-chloride seeding layer at the SAM-ambience interface. The palladium atoms in the seeding layer serve as nucleation centers for the growing metal film, staying at its bottom during the growth. In contrast, the chlorine atoms are transferred from

palladium to the deposited metal, staying on the top of the growing metal film and serving as surfactants.

9:40am **TF+AS+SS-MoM5 N-Heterocyclic Carbenes as Novel Ligands for Self Assembled Monolayers on Gold**, *Cathleen Crudden*, Queen's University, Canada **INVITED**

The use of N-heterocyclic carbenes (NHCs) to modify homogeneous metal catalysts is widespread, however despite the versatility of these complexes, the high metal-NHC bond strength and oxidative stability of NHC-ligated metals, and the ease of synthesis of NHCs, there have been only a handful of reports of mostly ill-defined surfaces functionalized by NHCs.

We will describe the use of NHCs to form self-assembled monolayers on gold surfaces. In particular, films prepared by the deposition of 1,3-dihydro-1,3-bis(isopropyl)benzimidazol-2-ylidene, show molecular ordering on the surface and remarkable stability. They show no decomposition upon heating for 24 hrs in THF, in boiling in water for 24hrs or upon treatment with acid (pH 2) or base (pH 12). Incredibly, they even survive largely after 24 hr exposure to hydrogen peroxide. This remarkable increase in stability relative to thiol-based SAMs will greatly increase the number of reagents and conditions to which the SAMs can be exposed.

The use of these films in SPR-based biosensing will be described, as will novel methods for the preparation of such films that can be carried out in air on the bench top.

10:40am **TF+AS+SS-MoM8 Improved Stability of Ag Thin Films due to Several Organic Surface Monolayers**, *Midori Kawamura*, Kitami Institute of Technology, Japan, *C. Kudo, T. Sasaki, Y. Abe, K.H. Kim, T. Kiba*, Kitami Institute of Technology

Due to excellent physical properties, Ag thin films have been used as low-e coating, optical mirror, and so on. It is necessary to prevent degradation of the Ag films in air or humid atmosphere. For the purposes, it has been reported that several metal oxide nanolayers and organic monolayers are effective to make Ag thin films stable. Previously, we reported that modification of Ag films with 3-mercaptopropyltrimethoxysilane (MPTMS) monolayer can improve durability of the Ag films after environmental tests because strong bonds were formed between thiol moiety and Ag films, and also between silanol moiety and glass substrate. In the present study, we attempted to use other type of organic molecules, namely straight chain alkylthiols, such as 1-octadecanethiol (1-ODT), 1-dodecanthiol (1-DT) for protection of Ag film surface and compared with MPTMS.

Ag thin films (10nm) were deposited on clean glass substrates by vacuum evaporation. Then monolayer of 1-ODT and 1-DT were formed over the Ag thin films by solution method. The samples were kept in a constant temperature and humidity chamber (40 degree Celsius and 90 RH%) for a week. The electrical resistance, surface morphology, optical transmittance were measured before and after the test. Ag film without the monolayer, and that with MPTMS were also examined for comparison.

The surface roughness of the Ag film without the monolayer drastically increased from 2.7 nm to 27 nm after the test. However, the increase was within 1nm on Ag films with 1-DT and 1-ODT surface layers. These changes were smaller than that on Ag film with MPTMS surface layer. By the measurement of electrical resistivity, it was found that increase in the resistivity after the test was very much suppressed in the Ag film with these monolayers. In addition, optical transmittance measurement showed that transmittance spectrum of Ag films with these monolayers did not change after the test. These results accord with the Ag film morphology change. Consequently, excellent passivation effect of 1-DT and 1-ODT surface monolayers on Ag films was confirmed.

11:00am **TF+AS+SS-MoM9 Electronic Structures of the Biaxially-strained GaSb(111) Films**, *Takuya Hatayama*, The University of Electro-Communications (UEC-Tokyo), Japan, *A. Akaishi*, The University of Electro-Communications (UEC-Tokyo), *J. Nakamura*, The University of Electro-Communications (UEC-Tokyo), Japan

III-V compound semiconductors have been extensively researched as alternative channel materials of complementary metal-oxide-semiconductor devices because of their superior carrier mobility[1]. In particular, GaSb is one of the promising p-channel materials, because its hole transport properties are significantly improved compared to Si. Recently, Ohtake *et al.* Have reported that high-quality GaSb films can be epitaxially grown on the Si(111) substrate using the InAs buffer layer[2]. The lattice constant in the plane of growth for the thin GaSb epilayer inherits the lattice constant of InAs, causing an inherent strain in the GaSb film. As a result, the electronic structure of the GaSb film can be modified. In this study, we evaluate the electronic properties of the strained GaSb bulk and the (111) films, especially the band gap formation, the effective mass, and the electronic conductivity, using first-principles calculations within the density functional theory. In general, the local density approximation (LDA) is commonly

applied to the exchange correlation term. However, it has been well-known that the band gap of semiconductors is significantly underestimated with LDA. In order to rectify the underestimation of the band gap and to correctly evaluate electronic dispersions at band edges, we use the hybrid functional proposed by Heyd-Scuseria-Ernzerhof (HSE06) for the exchange-correlation term[3]. The spin-orbit interaction is also included.

We assume the biaxial strain parallel to the GaSb (111) plane. For the bulk with a direct band gap at ambient pressure, GaSb becomes an indirect band gap material under the compressive biaxial strain. The biaxial strain makes the twofold-degenerate heavy-hole and light-hole bands split into two bands at the Gamma point of the valence band. Interestingly, under the biaxial tensile strain, the effective mass of holes becomes anisotropic. We will also report on changes in electronic properties of the GaSb (111) ultrathin films under the biaxial strain.

[1] J. A. del Alamo, *Nature* **479**, 317 (2011)

[2] A. Ohtake, T. Mano, N. Miyata, T. Mori, and T. Yasuda, *Appl. Phys. Lett.* **104**, 032101 (2014)

[3] J. Heyd, G. E. Scuseria, and M. Ernzerhof, *J. Chem. Phys.* **118**, 8207 (2003); *ibid* **124**, 219906E (2006)

11:20am **TF+AS+SS-MoM10 How to Repel Polymer Adsorption on Flat Surfaces?**, *Zhanhua Wang, S.P. Pujari, M.M.J. Smulders, H. Zuilhof*, Wageningen University, Netherlands

Organic monolayers or polymer brushes, often in combination with surface structuring, are widely used to prevent nonspecific adsorption of polymeric or biological material on sensor and microfluidic surfaces. Here we show for the first time how robust, covalently attached alkyne- derived monolayers or ATRP-produced polymer brushes, with a varying numbers of fluorine atoms, on atomically flat Si(111), effectively repel a wide range of apolar polymers without the need for micro- or nanostructuring of the surface. We have studied the antifouling property of fluoro-hydro monolayers and of fluorine-containing polymer brushes towards a range of commonly used polymers/plastics with comparable molecular weight in non- aqueous solvent, and have investigated the effect of polymer molecular weight on the fouling behavior. These studies relied on a range of characterization methods: wettability studies, ellipsometry, X- ray photoelectron spectroscopy (XPS) and atomic force microscopy (AFM). We developed a novel surface morphology survey by AFM characterization that can accurately quantify the degree of fouling.

These studies consistently displayed that especially the mono-fluorinated (F1) monolayer shows excellent anti- fouling behavior, even more so than e.g. corresponding monolayers with perfluorinated alkyl tails. In this presentation the causes of this unprecedented and surprising finding are discussed. Second, we will focus on polymer brush properties that further reduce the adsorption of polymers. These findings and analysis offer significant potential for antifouling applications of ultrathin and covalently bound fluorine- containing coatings for a range of micro- and nanotechnological applications.

11:40am **TF+AS+SS-MoM11 Symmetric Attachment of Annulated Aromatic Hydrocarbons in Self-assembled Monolayers by Use of Oxazoles**, *C. Partes*, University of Frankfurt, Germany, *S. Schuster, T. Wächter*, University of Heidelberg, Germany, *Martin Kind*, University of Frankfurt, Germany, *M. Zharnikov*, University of Heidelberg, Germany, *A. Terfort*, University of Frankfurt, Germany

Self-assembled monolayers (SAMs) have proven to be powerful tools for tuning surface properties because of the uncomplicated method of their preparation and the high variability of their organic moieties. The suitability of SAMs in applications like, e.g., organic electronics is frequently investigated. An aim for the use of SAMs is the reduction of injection barriers that occur at the interfaces between organic semiconductors and technologically relevant substrates like gold or silicon.

A SAM ideal for this purpose should exhibit a high vertical conductivity. In view of this, we investigated several aromatic and araliphatic SAMs, e.g. terphenyl-terminated monolayers on gold [1]. In a more recent ansatz, we have examined SAMs bearing annulated moieties such as anthracene, which in contrast to oligophenyls are entirely planar [2]. However, as a consequence of the asymmetric substitution of anthracene to the thiol anchor group it is hardly possible to alter the tilt angle of these thiolate molecules within the SAMs [2].

To overcome this drawback, we extended the annulated system of the SAM-forming thiols with an oxazole unit, which allows for a quasi-symmetric attachment to the anchor group. This restores the possibility to influence the tilt angle of the aromatic units using the so-called odd-even effect in SAMs.

Here, we like to present preliminary results on preparation and structural properties of SAMs made from aromatic oxazole thiols on gold surfaces.

REFERENCES

[1] Shaporenko, A.; Brunnbauer, M.; Terfort, A.; Grunze, M.; Zharnikov, M./J. Phys. Chem. B/108, 14462-14469 (2004).

[2] Dauselt, J.; Zhao, J.; Kind, M.; Binder, R.; Bashir, A.; Terfort, A.; Zharnikov, M./J. Phys. Chem. C/115, 2841-2854 (2011).

Monday Afternoon, October 19, 2015

Atom Probe Tomography Focus Topic

Room: 230A - Session AP+AS-MoA

Current and New Research Fields for Applications of Atom Probe Tomography

Moderator: Baishakhi Mazumder, Center for Nanophase and Materials Sciences Oak Ridge National Laboratory, Oak Ridge, TN 37831, USA

2:20pm **AP+AS-MoA1 APT Studies of the Embrittlement of Fe-Cr Ferrite**, *Mattias Thuvander*, Chalmers University of Technology, Sweden, *J. Odqvist*, *P. Hedström*, KTH Royal Institute of Technology, Sweden
INVITED

Ferrite containing more than a few percent chromium is susceptible to embrittlement when subjected to elevated temperatures for sufficiently long periods of time. The phenomenon is often called '475°C embrittlement', indicating the temperature at which the effect is most rapid. The embrittlement is an issue for several important types of steel, including corrosion resistant ferritic steel, duplex stainless steel, cast austenitic steel and austenitic weldments, and limits their maximum service temperature (to about 300°C). The volume fraction of ferrite ranges from 100% in ferritic steel, to about 50% in duplex steel, down to 5-25% in austenitic castings and weldments (for which the presence of some ferrite is needed to avoid solidification cracking). The reason behind the embrittlement is the phase separation into two bcc-phases, Cr-rich α' and Fe-rich α , as can be seen in the binary Fe-Cr phase diagram. The phase separation results in an increase in strength and hardness but a decrease in ductility. Depending on Cr-content and temperature, the phase separation occurs by nucleation and growth (typically for low Cr contents) or by spinodal decomposition (typically for high Cr contents). Spinodal decomposition is an interesting phenomenon in physical metallurgy and it has been extensively studied for a long time. The phase separation occurs on the nanometer scale and during the early stages the concentration variations are subtle. Therefore, it is a challenging mechanism to study experimentally. Atom probe tomography (APT) is a well-suited technique, as small concentration variations on a small scale can be measured, also in the case when the phase separation has a complex 3D-structure, which is the case for spinodal decomposition. In this presentation, APT methodology for studying spinodal decomposition will be discussed. Also, results from several investigations concerning phase separation kinetics will be presented. For example, the influence of stress on spinodal decomposition in duplex steels, the influence of homogenization temperature on spinodal decomposition in binary Fe-Cr and the behavior of different ternary Fe-Cr-X systems will be addressed.

3:00pm **AP+AS-MoA3 Comparing APT Mass Spectral Ranging for Compositional Accuracy: A Case Study with Cast Duplex Stainless Steels**, *Daniel Perea*, *A. Eaton*, *J. Liu*, Pacific Northwest National Laboratory, *S. Mburu*, *S. Schwarm*, *R. Kollis*, *S. Ankem*, University of Maryland

The mass spectrum of an atom probe tomographic analysis is a superposition of correlated mass-to-charge-state peaks and uncorrelated background counts. The compositional accuracy of a volume of material measured via atom probe tomographic analysis is dependent upon the manner in which the individual mass spectral peaks are ranged for integration. However, an accurate calculation of composition can be challenging due to a combination of complicated peak shapes, peak overlap, and background counts. Using data from both the α -ferrite and γ -austenite phases of a cast duplex stainless steel, we illustrate a methodology to account for the background counts, as well as to deconvolute overlapping peaks, in order to calculate composition that we compare to energy dispersive x-ray spectroscopy measurements.

3:20pm **AP+AS-MoA4 Chemical Imaging of Atmospheric Aerosols using Atom Probe Tomography and Multi-Modal Characterization**, *Jia Liu*, *M.I. Nandasiri*, *L. Gordon*, *G. Kulkarni*, *V. Shuthanandan*, Pacific Northwest National Laboratory, *S.A. Thevuthasan*, Qatar Environment and Energy Research Institute, Qatar, *A. Devaraj*, Pacific Northwest National Laboratory

Global climate is significantly dictated by small particulates in the atmosphere known as aerosols. These atmospheric aerosol particles when subjected to certain humidity and temperature conditions can induce heterogeneous ice nucleation, which is directly sensitive to aerosol surface structure and chemistry. These ice nuclei are the precursors to snow fall and precipitation. Often natural atmospheric aerosols are found to be coated

with sulfates and organic molecules. Elucidating the mechanism responsible for ice nucleation on coated or bare atmospheric aerosols requires understanding the structure, composition and chemical state of coated and bare aerosols. At EMSL we are developing a multimodal approach for imaging bare and coated aerosols utilizing a combination of atom probe tomography (APT), imaging X-ray photoelectron spectroscopy (XPS), focused ion beam scanning electron microscopy (FIB-SEM) and transmission electron microscopy (TEM). Imaging XPS provides the composition and chemical state of organic or inorganic elements within the top 5nm of the surface of aerosol particles with a spatial resolution of ~ 3 μm . FIB-SEM aids in understanding the morphology and porosity of particles both on the surface and sub-surface. TEM provides the atomic scale structural information and laser assisted APT provides sub-nanoscale compositional mapping of aerosols. TEM and APT are sub-single particle analysis techniques and can complement the individual aerosol particle measurements provided by the single particle laser ablation time of flight mass spectrometry (SPLAT). All these techniques provide specific multiscale chemical and structural information about the aerosol particles from the macro- to the atomic-scale. Specific examples from multimodal chemical imaging of mineral dust aerosols coated with varying concentration of sulfuric acid or organics will be presented along with the direct insights gained through this approach for improving ice nucleation parameterizations.

3:40pm **AP+AS-MoA5 Combining Atom Probe Tomography with TKD and FIB for Comprehensive Characterization of High Performance Materials**, *Sophie Primig*, University of New South Wales, Australia, *K. Babinsky*, *P. Haslberger*, *C. Hofer*, *D. Lang*, *C. Turk*, Montanuniversität Leoben, Austria
INVITED

Despite the increasing interest in atom probe tomography, this technique has so far almost exclusively been applied for chemical analyses of materials at the atomic scale. As nowadays the frontiers of material science are more and more being pushed towards the nanostructure, advanced comprehensive characterization techniques which provide both chemical and crystallographic information are required. For the crystallographic analysis of atom probe specimens several complementary techniques such as transmission electron microscopy have been applied that all have their advantages and drawbacks. Different approaches try to establish crystallographic information directly from the atom probe data itself which is still computationally challenging and not always possible. Another recently proposed straightforward way of quickly obtaining crystallographic information is the application of transmission Kikuchi diffraction on atom probe tips prior to the atom probe experiment. This procedure has so far only been successfully applied for positioning of grain boundaries close to the apex of the tips via focused ion beam milling.

The aim of the current study is to show applications of transmission Kikuchi diffraction on atom probe specimens of high performance materials and to demonstrate the strengths as well as the limits of these two complementary techniques. Four examples are shown which include boron segregation at prior austenite grain boundaries in a heat treatable steel, interlath retained austenite films with cementite in a bainitic steel, molybdenum carbides in a molybdenum alloy, and the preparation of grains with well-defined crystal directions in the tip axis of an iron-cobalt-molybdenum alloy.

4:20pm **AP+AS-MoA7 Atom Probe Tomography Studies of FeCo Nanocomposite Soft Magnetic Materials**, *A. Leary*, *V. Degeorge*, *V. Keylin*, Carnegie Mellon University, *Arun Devaraj*, *J. Cui*, Pacific Northwest National Laboratory, *M. Mchenry*, Carnegie Mellon University

Nanocomposite soft magnetic materials exhibit high magnetization and low coercivity for application in power electronics, motors, and sensors. The composite nature of these materials, created by thermal annealing of rapidly solidified metallic glasses, offers many options to tune desired material properties. Grain sizes below ~ 30 nm are relevant to average the magnetocrystalline anisotropy between neighboring grains within an exchange volume. Chemical partitioning during devitrification creates variations in local composition compared to the nominal alloy composition. These variations impact material properties such as magnetostriction, Curie temperature, and grain size. Local composition measurements of annealed nanocomposites by Atom Probe Tomography link observed magnetic properties to the material structure. The impacts of chemical partitioning on diffusion limited grain growth, intergranular coupling at high temperature, and induced anisotropy are discussed.

Applied Surface Science

Room: 212D - Session AS-MoA

Practical Surface Analysis I: Interpretation Challenges

Moderator: Karen Gaskell, University of Maryland, College Park, Alan Spool, HGST, a Western Digital Company

2:20pm **AS-MoA1 ASSD 30th Anniversary Lecture: XPS: Three Challenges and an Opportunity**, *James Castle*, University of Surrey, UK **INVITED**

The 3 challenges refer to ambitions that have been on the books for many years:

1, to obtain XPS data from individual sub-micro particles using a laboratory instrument. Cazaux (1975) scanned an electron beam across the reverse of an Al foil holding the particles. A similar arrangement was adopted by Jenkins and Castle (1994). Their object was to examine the interface region of microtomed thin sections of adhesive joints. Useful parameters were determined but this, reverse-side excitation of x-rays is not easily adapted for use in a laboratory instrument. Recently Castle et al (2013) have returned to the subject using an Auger spectrometer. The particles are scattered on Al or Mg foil from which X-rays are produced by the impact of an electron beam close to the particle. Examples will be given

2, the need to make the Auger Parameter (AP) more intuitive. The AP, Wagner (1974), depends on the relaxation energy of the chemical structure. It is so easily determined but yields a number that is so readily forgettable! Mg has a value of 2488eV whilst Ca is 644eV. West and Castle (1982) showed how a universal scale for the AP might be produced. The zero point is that for a non-polarisable lattice. Since the refractive index (RI) also depends on lattice polarizability the zero-point can be found using the value of $RI = 1$ on a suitable plot and thus elements placed on a common scale. More recently (2002), Castle et al used the method to compare AP'S for V and O for a series of compounds. It is concluded that a universal scale would greatly benefit those in applied surface chemical analysis.

3, is codifying the procedures that would enable manufacturers to give a first estimate of near-surface structure from the survey scan: helping to plan the detail scans which follow the survey. Castle and Baker (1999) gave an indication of how this might be approached and a very detailed set of rules was published by Castle (2007) An ISO standard for recognition of a C1s peak as contamination is being developed by ISO TC201. With this, manufacturers should have the confidence that any automated data processing will have the backing of users.

The **opportunity** would bring to fruition the vision of those members of ASSD when they launched Surface Science Spectra as a Journal and a database in 1993. As a Journal it is still unique in our field and is much valued for its provision of reference spectra for materials of current interest. The opportunity is to provide a searchable data base of peak energies for all elements in the diverse set of 1000 materials included in the 22 volumes now available.

3:00pm **AS-MoA3 Results from a VAMAS Inter-Laboratory Comparison on the Measurement of Composition of Organic Mixtures in Depth Profiling**, *Alexander Shard*, National Physical Laboratory, UK

Argon cluster sources for 3D analysis of organic materials are starting to become routinely used in material analysis. Most new XPS and SIMS instruments are now equipped with such sources and are finding widespread use in both academia and industry. The purpose of a depth profile is to measure the distribution of chemical species and therefore it is important to assess the ability of various techniques and approaches to provide this information. One of the most popular analytical methods to combine with cluster beam sputtering is SIMS. This method provides excellent specificity, high sensitivity in most cases and enables discrimination of compounds that cannot be matched by other methods such as XPS. However, there are a number of factors that prevent organic SIMS from being quantitative. For XPS there is a well-established route to obtain chemical compositions, which is its primary advantage in organic depth profiling.

Until recently, organic SIMS data could be used to identify compounds, and could only measure concentrations in special cases. The major limiting factor in SIMS is the 'matrix effect' which has not been the subject of any substantive or coordinated investigation since the genesis of organic SIMS analysis in the 1980s. Fortunately, the ability provided by argon cluster sources to perform nearly damage-free profiles of organic materials allows us to begin to address this effect.

Mixed molecular materials of known composition have been made with sufficient precision and stability for a reliable analysis to be performed. The materials demonstrate, unambiguously, that matrix effects are significant in

molecular SIMS experiments, but also that these effects can be measured and described. It is found that the matrix effects are remarkably consistent between laboratories and appear to depend upon two main factors: the identity of the secondary ion and; the analytical source used. Furthermore, it is possible to establish normalization schemes that compensate for the matrix effect whilst also eliminating the other major source of error in quantitative SIMS: instability and drift in the primary beam current.

This talk will describe VAMAS project A3(g), the SIMS matrix effect and implications in the quantitative analysis of SIMS depth profiles. These effects are not restricted to compositional analysis but also have a profound influence on the apparent position of interfaces, often contributing the major source of uncertainty to the measurement of the thickness of an organic layer.

3:20pm **AS-MoA4 In Operando Studies of High Temperature, Heterogeneous Electrocatalysis on a Lanthanum Strontium Manganite-based Solid Oxide Electrochemical Cell**, *Aaron Geller, B. Eichhorn*, University of Maryland, College Park

Near ambient X-ray photoelectron spectroscopy (APXPS) was used for *In Operando* studies on lanthanum strontium manganite (LSM, $La_{0.8}Sr_{0.2}MnO_{3-z}$) electrodes, one of the most popular materials currently in use on solid oxide electrochemical cells (SOCs). SOCs consisting of two LSM electrodes on a yttria-stabilized zirconia (YSZ) electrolyte were probed in an oxygen atmosphere (0.5 Torr) at ~ 600 °C under open circuit voltage (OCV) and polarized conditions. Polarization promotes the oxygen reduction reaction (ORR, cathodic reaction) on one LSM electrode and oxygen evolution reaction (OER, anodic reaction) on the other. Through use of an area detector, electrochemically-induced phenomena on the surface of the cell such as surface potential mapping, Sr segregation, and changes in the Mn oxidation state were observed and spatially resolved to within 20 microns.

By tracking shifts in the La 4d and Sr 3d peaks under polarization relative to OCV, local surface potentials of each LSM electrode were determined and it was observed that the majority of electrochemical activity, signified by a sharp potential drop, was located at the LSM/YSZ interface (shifts in the Zr 3d peaks were used to determine the local potential of YSZ). Several challenges in interpretation were found, the most surprising of which was a potential separation between the lanthanum and strontium components of the LSM lattice which were expected to exhibit the same potential under bias. Instead, the lattice La was driven to a higher potential than the lattice Sr on both electrodes. Furthermore, it was found that lattice Sr was relatively depleted under bias on each electrode, though the effect was more pronounced on the OER side. Sr 3d spectra also showed two different species under bias, lattice Sr and surface-segregated SrO, with the surface species shifted to a higher potential than the lattice Sr species. The data analysis process of these complex systems presented several challenges as well, which will be discussed.

3:40pm **AS-MoA5 Building the Link Between XPS Data and Functional Properties of Materials**, *Kateryna Artyushkova, I. Matanovic, S. Kabir*, University of New Mexico, *B. Kieffer*, New Mexico State University, *A. Serov, P. Atanassov*, University of New Mexico **INVITED**

Building structure-to-property relationships is one of the most often attempted research tasks in today's chemistry of materials. Often relationships are directly dependent and easy to identify. In complex, nano-structured functional materials, those correlations are intertwined and multi-directional. Predicting macroscopic property of interest, such as activity, wettability, stability, etc., based on correlation with materials surface chemistry is challenging but yet accomplishable.

The relationship between functional property and the chemical structure of materials is typically established through correlations between performance metrics parameters and various spectroscopic techniques, including XPS, XANES, XPES, TOF-SIMS, and Mössbauer spectroscopy. The primary advantage of XPS in the characterization of heterogeneous multicomponent nanostructures is the ability to discriminate between different surface oxidation states and chemical environments. However, the assignment of XPS peaks in highly heterogeneous materials is not straightforward. A significant improvement in the assignment of peaks at various binding energies could be achieved using reference materials, yet, many relevant reference materials do not exist. State-of-the-art computations allow the determination of BE shifts for specific defect chemistries and geometries, providing valuable information for processing and interpretation of spectra data.

In this talk, I will discuss approaches towards structure-to-property relationships derived for energy-related materials, such as electrocatalysts for fuel cell and biocatalysts for microbial fuel cells. I will discuss multivariate approaches towards correlating XPS data with performance characteristics and binding energy shift calculations using DFT for interpreting XPS spectra. Application of XPS instrumentation with in-situ

capabilities to study materials under conditions relevant to their application will be also discussed.

4:20pm AS-MoA7 Multitechnique Characterization of Protein G B1 Orientation on Surfaces, Elisa Harrison, G. Interlandi, D.G. Castner, University of Washington

The orientation of adsorbed proteins on surfaces has been shown to influence biological responses, so research and development of biotechnological applications (e.g., sandwich ELISAs) have focused on controlling the orientation of each protein layer. However, characterizing protein orientation has been a challenge. The goal of this research is to address these challenges by developing methodology to study multilayer protein systems. Specifically, we aim to determine the orientation of protein G B1, an IgG antibody-binding domain of protein G, on various surfaces and the effect of its orientation on antibody binding using a variety of surface-sensitive tools and simulations. We propose that binding selectivity will increase for well-ordered protein films due to high availability of binding domains. To achieve control over surface properties, we have utilized four types of self-assembled monolayers (SAMs) to control protein orientation: N-Hydroxysuccinimide-terminated SAMs and dodecanethiol SAMs to immobilize protein G B1 in a random orientation and maleimide-terminated SAMs and bare gold to immobilize cysteine mutants of protein G B1 in a well-ordered orientation. Developing methods using surface-sensitive, label-free tools, such as XPS, ToF-SIMS, and quartz crystal microbalance with dissipation monitoring, provide detailed information of the adsorbed proteins, such as composition, coverage, and orientation. Additionally, computational methods to predict the orientation of proteins on surfaces can help to interpret and complement experimental techniques. In this work, we describe the development of a simulator to determine protein orientation on a surface using Monte Carlo (MC) simulations. We chose two proteins to test the MC simulator: LK α 14 peptide and protein G B1. We chose LK α 14, a 14-mer consisting of only leucine and lysine amino acid residues, as a benchmark because of its predictable structure and orientation on hydrophobic surfaces. To test the MC simulator on a more complex system, we used protein G B1. Preliminary MC simulations show that protein G B1 is likely to interact with a graphene surface through residues Met1, Val21, Ala48, and the hydrophobic part of Lys10 on terminal ends of the protein. We will extend the MC algorithm to predict the orientation of additional protein/surface combinations and validate using experimental results. While the systems explored thus far are model systems that are far less complex compared to biological systems of the real world, we aim to develop methodology using state-of-the-art tools that can be continuously improved to help expand our knowledge of, and possibly control, biomolecules on surfaces.

4:40pm AS-MoA8 Investigation of Composition and Structure of Functionalized Carbon Materials, Svitlana Pylypenko, K.N. Wood, Colorado School of Mines, A.A. Dameron, National Renewable Energy Laboratory, R. O'Hayre, Colorado School of Mines

While significant efforts has been placed on understanding the role of nitrogen in real, application based environments utilizing high surface area carbon supports, a lack of knowledge exists in understanding the specific functionalities and their role in improving performance. In this work we expand the understanding of nitrogen functionalized high surface area carbon supports by focusing on the careful analysis of the distribution of nitrogen functionalities through XPS and other complementary techniques, such as Raman and NEXAF spectroscopies. Functionalization of several high-surface carbons was performed using nitrogen ion implantation using a variety of ion implantation parameters. The results contained herein show that increasing implantation time only marginally elevates nitrogen concentration, forming mostly single defect structures. Increasing the beam current results in formation of more complex defect structures containing clustered multi-nitrogen defects, similar to those observed in carbon nitride materials. We also show that higher nitrogen dosage levels create a more homogeneous distribution of nitrogen functionalities, regardless of initial carbon material or the resulting nitrogen concentration.

5:00pm AS-MoA9 How to Make Amorphous Carbon Stable: An *In Situ* XPS and NEXAFS Investigation of Thermally-Induced Structural Evolution of Amorphous Carbon Surfaces, Filippo Mangolini, Ecole Centrale de Lyon - LTDS, France, J. Hilbert, J.B. McClimon, J.R. Lukes, R.W. Carpick, University of Pennsylvania

Silicon oxide-doped hydrogenated amorphous carbon (a-C:H:Si:O) coatings are fully amorphous thin-film materials consisting of two interpenetrating networks, one being a hydrogenated amorphous carbon (a-C:H) network and the other a silica glass network. At temperatures above 150°C, pure a-C:H films undergo a rapid degradation that starts with the evolution of hydrogen and is followed by the conversion of sp³ bonds to sp² [1]. However, a-C:H:Si:O exhibits much lower susceptibility to oxidative degradation, and higher thermal stability compared to a-C:H. This makes a-

C:H:Si:O attractive for many applications, including next generation hard disk drives, which require overcoat materials that are thermally stable up to temperatures above 500°C. Although it is well-established that a-C:H:Si:O possesses superior thermal stability and oxidation resistance relative to a-C:H, the scientific basis for this behavior is not understood. To investigate this, a combined *in situ* X-ray photoelectron spectroscopy (XPS) and near-edge X-ray absorption fine structure (NEXAFS) spectroscopy study was performed. Changes in the surface chemistry and bonding configuration of a-C:H:Si:O (e.g., silicon oxidation state, carbon hybridization state) were accessed *in situ* at temperatures up to 450°C. A novel methodology for processing NEXAFS spectra, which makes it possible to account for the presence of a carbonaceous contamination layer on an air-exposed material, was developed [2]. This allowed quantitative evaluation of the carbon hybridization state in the film as a function of the annealing temperature. Upon high vacuum annealing, two thermally-activated processes could be determined to take place in a-C:H:Si:O by assuming a Gaussian distribution of activation energies with mean value E and standard deviation σ : a) ordering and clustering of sp² carbon ($E \pm \sigma = 0.22 \pm 0.08$ eV); and b) conversion of sp³- to sp²-bonded carbon ($E \pm \sigma = 2.7 \pm 1.0$ eV). The experimental results are in qualitative agreement with the outcomes of molecular dynamics simulations performed using the ReaxFF potential. To determine the environmental dependence of the surface structural evolution of a-C:H:Si:O, the results of the *in situ* XPS/NEXAFS investigation were compared to those for a-C:H:Si:O samples heated in air, showing a strong effect of atmospheric oxygen. These results provide guidance for designing modified materials able to meet ever-increasing performance requirements of coatings for demanding applications.

1. F. Mangolini, F. Rose, J. Hilbert, R.W. Carpick, Applied Physics Letters, 103, 161605, 2013

2. F. Mangolini, J.B. McClimon, F. Rose, R.W. Carpick, Analytical Chemistry, 86, 12258, 2014

5:20pm AS-MoA10 A Comparative Study of the Native Oxide on 316L Stainless Steel by XPS and ToF-SIMS, Sabrina Tardio, M.-L. Abel, University of Surrey, UK, R.H. Carr, Huntsman PU, J.E. Castle, J.F. Watts, University of Surrey, UK

AISI 316L is an austenitic stainless steel which is widely used in applications that require a degree of resistance to crevice and/or pitting corrosion. The L identifier of 316L indicates lower carbon content than the standard 316 grade, a characteristic which reduces the susceptibility to sensitization (grain boundary carbide precipitation) and for this reason it is widely used in heavy gauge welded components. The corrosion resistance of stainless steel is a result of the presence of a thin oxide layer on its surface. The passivation of stainless steel takes place in atmospheric conditions which yields a film that is self-healing on localised damage. The oxide, naturally formed in the atmosphere, is generally referred to as the native oxide and it is affected by environmental factors and, for that reason, different methods are often employed to modify the oxide layer to make it suitable for particular applications. This steel is also widely used as a substrate for adhesion; it is one of the "technological surfaces" on which organic coatings are applied. In this context, differences in the chemistry of the surface, as a consequence of different treatments, will influence the degree and modality of interaction of the adhesives with this metal. Many works have studied stainless steel with the aim of understanding more about the modification of this oxide layer, but few have addressed the composition of the passive film in its air-formed or water exposed state. In this work, attention is focused on the composition of the native oxide and changes in its chemistry brought about by water exposure. The native oxide film on stainless steel is very thin, of the order of 2 nm, and known to be readily modified by immersion in aqueous media. In this paper, XPS and ToF-SIMS are employed to investigate the nature of the film in the air-formed and water emmersed states. The film is described in terms of oxide, hydroxide and water content. The preferential dissolution of iron is shown to occur on immersion. It is shown that a water absorbed layer and a hydroxide layer are present above the oxide-like passive film. The concentrations of water and hydroxide appear to be higher in the case of exposure to water. A secure method for the peak fitting of Fe2p and Cr2p XPS spectra of such films on their metallic substrates is described. The importance of XPS survey spectra is underlined and the feasibility of C₆₀⁺ SIMS depth profiling of a thin oxide layer is shown.

Biomaterial Interfaces

Room: 211D - Session BI+AS-MoA

Characterization of Biological and Biomaterials Surfaces (2)

Moderator: Joe Baio, Oregon State University, Dan Graham, University of Washington

2:20pm BI+AS-MoA1 Characterization of Protein G B1 Immobilized Gold Nanoparticles using Time of Flight Secondary Ion Mass Spectrometry and X-ray Photoelectron Spectroscopy, *Yung-Chen Wang**, D.G. Castner, University of Washington

Nanoparticles (NPs) have been widely used in many fields of science due to their unique physical properties. While many applications of NPs such as imaging probes or drug carriers often require the conjugation of proteins or biomolecules, the surface interactions between NPs and biomolecules remains underexplored. For example, the immobilization of immunoglobulin G (IgG) onto NP surfaces is critical for the development of many immunosensors and drug delivery nanocarriers. Notably, the orientation of the immobilized IgG can have a significant impact on clinical outcomes of nanocarriers by impacting its biostability and efficacy. One approach to control the proper orientation of IgG is by utilizing the IgG Fc tail binding proteins.

In this work, Protein G B1, a protein that will selectively bind to the Fc tail of IgG, was immobilized onto gold NPs (AuNPs) functionalized with maleimide and oligo-(ethylene glycol)(OEG) self-assembled monolayers (SAMs). Protein G B1 was immobilized on AuNPs using either carbonyldiimidazole (CDI) chemistry or maleimide-cysteine interaction. We use the surface sensitive analysis techniques of x-ray photoelectron spectroscopy (XPS) and time of flight-secondary ion mass spectrometry (ToF-SIMS) to characterize the immobilization of protein G B1. Unlike conventional NP characterization techniques such as dynamic light scattering (DLS) and UV/Vis, XPS and ToF-SIMS can provide additional information on the surface elemental composition, protein coverage and orientation.

XPS analysis confirmed the CDI activation of the OEG-SAMs AuNPs by detecting the nitrogen containing active intermediate and the attenuation of gold signal. After incubation with protein, the immobilization of the protein was demonstrated by the increased nitrogen signal on the surface. ToF-SIMS analysis also confirmed the successful functionalization, CDI activation, and protein immobilization by identifying signature secondary ions from each step of the protein immobilization process.

By comparing the ratio of secondary ion intensity originating from opposite ends of the protein, it was possible to determine the orientation of immobilized protein G B1. As expected, the non-site specific CDI chemistry did not lead to a specific protein orientation on the AuNPs. In contrast to CDI chemistry, we expect to control the orientation of the immobilized protein using maleimide functionalized AuNPs and cysteine mutants of Protein G B1 through site-specific carbon-sulfur interaction.

Overall, the systematic characterizations in this study will provide detail information of protein-NP interactions and serve as a platform for controlling the orientation of IgG on AuNPs.

2:40pm BI+AS-MoA2 Controlled Molecular Mechanisms of Engineered Solid Binding Proteins on Surfaces, *Christopher So*, National Research Council postdoc cited at Naval Research Laboratory, *S. Walper*, US Naval Research Laboratory, *R. Stine*, Nova Research, *D.E. Barlow*, *K. Wahl*, US Naval Research Laboratory

Persistent and uncontrolled aggregation of proteins at surfaces remains a major challenge for biocompatibility, fouling, and biosensing. To fully realize the rich properties of proteins at interfaces, a critical link between displayed protein sequence and surface assembly mechanisms is required. Here we use rational protein mutations combined with *in situ* microscopy and spectroscopy methods to demonstrate that manipulation of solid binding and intermolecular interactions by proteins can dictate their surface behavior and induce nanostructure formation. We use streptavidin (SA) as a robust scaffold to control the density and localization of aromatic residues, expected to interact with surfaces such as graphite and graphene through π -bonding. The surface adapted SAs are generated by placing aromatic side chains of varying polarity (Phenylalanine, Tyrosine, Tryptophan) along three putative permissive sites in a coplanar arrangement. The effects of these mutations on bulk solution structure, surface-associated structure, as well as surface affinity, orientation and spatial organization are studied *in situ* using attenuated total reflectance (ATR) infrared spectroscopy (IR)

* ASSD Student Award Finalist

with linear polarization (LP), fluid-mode atomic force microscopy (AFM), and circular dichroism (CD). We have found that our simple modifications to mSA have little effect on the solution state of the protein, while having a pronounced effect on affinity and secondary structure in the adsorbed state. Through fabricating graphene-coated ATR-IR prisms, we find that unmodified mSA exhibits an ordered beta sheet structure at surfaces, while tryptophan modifications to mSA (Trp-mSA) induces a more disordered structure. We quantify by temporal ATR-IR spectra a *ca.* 4.5x enhancement in sticking probability for Trp-mSA over mSA to graphene. Fluid-mode AFM studies on graphite support a surface-mediated coarsening mechanism: while mSA forms no obvious surface structures, Trp-mSA aggregates and forms islands 10-50 nm in size over the course of an hour. Such disordered SA aggregates provide high affinity sites for slow lateral island growth processes, giving rise to a bi-modal exponential adsorption curve for Trp-mSA but absent in mSA. Ultimately, defining the molecular basis of protein self-assembly and the impact of displayed chemistries at liquid-solid interfaces will enable rationally designed biological surface coatings and engineered biointerfaces with tailorable functionalities.

3:00pm BI+AS-MoA3 Molecular-Level Surface Analysis Demonstrates the Impact of Detergent Selection on Decellularized Tissues, *Adam Taylor*, University of Washington, *L.J. White*, University of Nottingham, UK, *D.M. Faulk*, *L.T. Saldin*, University of Pittsburgh, *D.G. Castner*, University of Washington, *S.F. Badylak*, University of Pittsburgh, *B.D. Ratner*, University of Washington

Decellularized matrix scaffolds may be prepared through a range of techniques. Detergents are frequently used in decellularization protocols due to their ability to solubilize cell membranes and dissociate DNA from proteins. Whilst removal of cellular material is regularly assessed, the impact of detergent selection on extracellular matrix (ECM) structure and composition is less commonly investigated. Time-of-flight secondary ion mass spectrometry (ToF-SIMS) is a powerful surface analysis technique to probe biological structures with high mass resolution and surface specificity, and has previously been used to distinguish decellularized ECM by anatomical location or culture conditions. The objective of this study was to utilize ToF-SIMS to investigate the influence of detergent selection upon a representative decellularized tissue, specifically the basement membrane complex (BMC) of porcine urinary bladder matrix (UBM) prepared by treatment with 1% SDS, 4% deoxycholate, 8 mM CHAPS or 3% Triton X-100 for 24 hours.

Principal components analysis (PCA) revealed spectral differences between treatment groups. High mass peaks associated with specific detergent fragments were observed on the scaffolds exposed to SDS and deoxycholate. Peaks indicative of phospholipid membranes were observed in all samples, but to a greater extent with scaffolds not exposed to detergent. We further probed these data sets to investigate how detergent selection impacts proteinaceous ECM components. Using a reduced peak list of known characteristic amino acid fragments, PCA distinguished native bladder tissue from decellularized UBM and highlighted spectral differences between UBM treated with ionic vs. charge-neutral detergents. Notably, the basement membrane surface of UBM prepared with ionic detergents SDS and deoxycholate yielded less intense characteristic peaks from hydrophobic amino acids than UBM treated with charge neutral detergents CHAPS and Triton X-100. Harsher detergents may denature protein structure and break protein-protein interactions through binding of their hydrophobic tail to hydrophobic amino acid residues. Such damage is hypothesized to cause sub-optimal *in vitro* and *in vivo* responses. We further examined cell-matrix interactions of human urothelial cells seeded on the BMC of UBM, investigating how detergent exposure affected cell proliferation and permeability of the cell monolayer. An understanding of the effects of detergent exposure on the structure, composition and surface molecular functionality of decellularized scaffolds will facilitate a rational strategy for successful recellularization and subsequent positive clinical outcomes.

3:20pm BI+AS-MoA4 Liquid Repelling Surfaces Based on Candle Soot are Non-Fouling, *Lars Schmu*ser, *M. Paven*, *N. Encinas*, Max Planck Institute for Polymer Research, Mainz, Germany, *D.J. Graham*, *D.G. Castner*, University of Washington, *D. Vollmer*, *H.J. Butt*, *T. Weidner*, Max Planck Institute for Polymer Research, Mainz, Germany

Super non-fouling surfaces resist protein adhesion and have a broad field of possible application like implant technology, drug delivery, bio-compatible materials, biosensors and marine coatings. Non fouling properties can be fabricated by using liquid repelling surfaces, which minimize the contact area of water soluble particles with the non fouling surface. For a surface to be "amphiphobic" – to repel a range of liquids including oil and water – requires a micro to nanometer scale surface roughness in combination with a hydrophobic coating. Paven et al. (1) described the production of an amphiphobic surface with remarkably low production requirements. This surface is made of a glass slide, candle soot

and 2 commercially available chemicals which are deposited via chemical vapor deposition. Soot deposition and chemical vapor deposition can be applied to a broad variety of substrate shapes, such as the inner wall of tubes. This makes the soot coating a promising tool for blood compatible material design for stents and tubing including applications such as dialysis. Here we present a protein adsorption study onto these amphiphobic surfaces made of candle soot. Since even nanograms per cm² levels of protein on biomaterial surfaces can cause detrimental effects for patients, we employed surface sensitive spectroscopic methods, X-ray photoelectron spectroscopy (XPS) and time of flight secondary ion mass spectrometry (ToF-SIMS) to quantify protein adsorption. We did not detect any adsorbed proteins within a detection limit of better than 1 ng/cm² of adsorbed proteins, which demonstrates the super non-fouling property of soot-coated surfaces. Interestingly, the naturally amphiphobic cuticle ("skin") of springtails – small ancient arthropods who live in soil – use an approach very similar to the artificial soot surfaces to achieve protein repellency: Nanometer roughness with hydrophobic coatings. We will discuss XPS, ToF-SIMS and fluorescence microscopy studies quantifying the amount of protein adsorbed onto these surfaces.

1. M. Paven *et al.*, Super liquid-repellent gas membranes for carbon dioxide capture and heart–lung machines. *Nat Commun*4, (2013).

3:40pm **BI+AS-MoA5 Time-of-Flight Secondary Ion Mass Spectrometry Investigations of the Pancreatic Islet Tumor Microenvironment**, *Blake Bluestein*, Department of Bioengineering, University of Washington, *F.M. Morrish, D. Hockenbery*, Fred Hutchinson Cancer Research Center, *L.J. Gamble*, Department of Bioengineering, University of Washington

Imaging time-of-flight secondary ion mass spectrometry (ToF-SIMS) provides chemical information with subcellular spatial resolution. In this work, imaging ToF-SIMS is used to analyze tumor microenvironments from mouse model (*Myc/p53*^{-/-}) biopsies with *Myc*-dependent inducible and regressible pancreatic β -cell neoplasia. The *Myc* oncogene is overexpressed in many human cancers and has major effects on cellular metabolism, including lipid metabolism. While imaging ToF-SIMS analysis of tumor tissue will provide a new perspective by visualizing tumor progression/regression, the system itself can also act as a model system for investigating stroma-tumor interactions in cancerous tissues.

Pancreatic tissues were harvested and frozen in optimal cutting temperature (OCT) at 6 days post *Myc* induction. 4 μ m cryosections were serially cut, with one used for H&E staining, one for ToF-SIMS analysis, and another for immunohistochemistry. High mass and high spatial resolution data was acquired with the pulsed 25 keV Bi₃⁺ ion beam rastered over a 1 mm x 1 mm area (1280 x 1280 pixels). ROIs of the tumor and stromal tissue were then investigated further with imaging principal components analysis (PCA) to identify peaks that correspond to species of interest. Regions identified by analysis and PCA were cross-referenced against immunohistochemical and H&E images to differentiate tumor areas from the surrounding tissue.

ToF-SIMS data suggests a preferential uptake of fatty acids 18:3 and 18:2 within the tumor. The 6 day *Myc*-induced islet tumor exhibits a signal of 14:0, possibly a product of de novo fatty acid synthesis within the tumor. The tumor also exhibits an increased localization of sphingomyelin fragments and vitamin E compared to the surrounding tissue. Interestingly, the data shows an absence of Mg⁺ within the islet tumor and small, higher signal regions on the periphery of the tumor. These peripheral tumor regions also show an increased, localized signal of CN⁻, CNO⁻, C₇H₁₀O⁺, and Fe⁺, but further histologic correlations are needed to discern if these structures are inflammatory zones, mitochondrial dense regions, or related to vasculature. Once these localized areas have been defined, a comparison to the chemistry identified by ToF-SIMS may aid in interpreting the *Myc* oncogene and its effect on pancreatic β -cell neoplasia. PCA was applied to image data and revealed different chemistries within the tumor and surrounding tissue. PCA was also applied to selected tumor region images to spatially and chemically analyze within the tumor to compare chemistries between different tumor sizes, where tumor size is potentially indicative of different tumor stage development.

4:00pm **BI+AS-MoA6 Paper-based Device for Home Phenylalanine Monitoring from a Sample of Whole Blood**, *R. Robinson, Elaine Fu*, Oregon State University

Paper microfluidics is a rapidly growing subfield of microfluidics that makes use of paper-like porous materials to create devices for use in low-resource settings. Advantages of the use of porous materials include capillary flow, removing the need for equipment for pumping fluids, and lower material costs compared to traditional microfluidics-based devices composed of silicon or glass. In the current presentation, we describe the development of a paper-based device for home therapy monitoring. For persons with phenylketonuria (PKU), maintaining a restricted level of phenylalanine (Phe) in the body is a continuing challenge. Given the large

inter-person variation in Phe metabolism, maintaining nutritional therapy can be a lengthy and difficult process that would be aided by the ability to perform real-time monitoring of Phe levels. Adherence to diet therapy is an even greater challenge for young children, adolescents, and women during pregnancy, and for these groups in particular, rapid feedback could be critical in tailoring a diet to be optimal for each individual. Current tests for Phe require a high-resource laboratory environment and are not suitable for the rapid detection of Phe levels and feedback to the patient that is needed for effective monitoring of PKU therapy. Our solution is a semi-quantitative, paper-based device that is rapid, easy to use, and low cost for patient home use. Device operation is based on simple user steps. The user applies whole blood (40 mL) to a plasma separation membrane, which filters out the cellular components of the blood and releases plasma to two downstream glass fiber pads. There, Phe in the sample and NAD⁺, catalyzed by the enzyme phenylalanine dehydrogenase, react to form Phe-pyruvate, NADH, and NH₃. At 6 min, the user folds the card closed and fluid is transferred to a final glass fiber detection pad, in which NADH, nitroblue tetrazolium, and methoxy phenazine methosulfate react to form NAD⁺ and a purple-colored product. The device is read at ~7.5 min. Visibly distinct signal intensities are generated from whole blood samples containing 0 (normal), 3.75 (slightly elevated), and >7.5 mg/dL (substantially elevated) spiked-in Phe. Thus, this test may allow users to distinguish between normal versus elevated levels of blood Phe on a rapid timescale that could inform their diet therapy. The assay exhibited reasonable reproducibility with coefficients of variation between 11 and 24%. A focus of the presentation will be on the controlled patterning and drying of biochemical reagents in porous materials for later rehydration on the device, which is key to the robust operation of the device.

4:20pm **BI+AS-MoA7 Multivalent Probes for Tuneable 'Superselective' Targeting**, *G.V. Dubacheva*, CIC biomaGUNE, Spain, *T. Curk*, University of Cambridge, UK, *R. Auzély-Velty*, Cermav, Cnrs, France, *D. Frenkel*, University of Cambridge, UK, **Ralf Richter**, CIC biomaGUNE & University Grenoble Alpes, Spain **INVITED**

A basic requirement in biomedical research is the ability to specifically target cells and tissues. Targeting typically relies on the specific binding of a 'ligand' on a tailor-made probe to a 'receptor' on the desired cell or tissue. Conventional probes efficiently distinguish a cell surface displaying the receptor from others that do not. They exhibit limited selectivity, however, when the surfaces to be distinguished display a given receptor at different densities.

Based on theoretical arguments, it has been proposed that multivalent probes that bind several receptors simultaneously can sharply discriminate between different receptor densities. Here, we present an experimental model system that demonstrates such 'superselective' targeting. To this end, recent achievements of synthetic chemistry and surface characterization were combined to create well-defined multivalent polymers and surfaces that interact with each other through highly specific host/guest interactions. With this model system, we show that superselective binding can be tuned through the design of the multivalent probe to target a desired density of binding sites. We develop an analytical model that provides simple yet quantitative predictions to tune the polymer's superselective binding properties by its molecular characteristics such as size, valency, and affinity.

This work opens up a route toward the rational design of multivalent probes with defined superselective targeting properties for practical applications in life sciences (analytics, diagnostics and therapy). It also provides mechanistic insight into the regulation of multivalent interactions in biology, notably the superselective targeting of the extracellular matrix polysaccharide hyaluronan to its main cell surface receptor CD44.

5:00pm **BI+AS-MoA9 Targeted Ultrathin Silica Nanoshells as HIFU Sensitizing Agents for In Vivo LnCAP Prostate Tumor Removal**, *James Wang, A. Liberman, C. Barback, S. Blair, R. Mattrey, W. Trogler, A.C. Kummel*, UC San Diego

Diagnostic ultrasound (US) is a prevalent medical imaging modality due to its low-cost, high resolution, and therapeutic capability when coupled with high intensity focused ultrasound (HIFU) systems. 500 nm rigid silica ultrathin nanoshells were synthesized as a chemically stable US tumor marking contrast agent with continuous *in vivo* US imaging lifetime. Iron (III) was included into the silica shell network to promote biodegradability from serum transferrin proteins. It was shown previously that the removal of iron from the silica shell network via transferrin fragments the nanoshells for effective biodegradation. Folate was conjugated to the surface of the silica nanoshells via the 3-aminopropyltriethoxysilane (APTES) linker. Folate has been shown in the literature to bind to prostate specific membrane antigen (PSMA) with a high binding affinity due to folate hydrolase activity. Conjugating the silica nanoshell surface with folate targets the ultrathin silica nanoshells towards the LnCAP tumor where PSMA is significantly up-regulated. The surface modified ultrathin silica

nanoshells were filled with liquid perfluorocarbon (PFC) which underwent acoustic droplet vaporization (ADV) during US insonation. The phase transition of PFC from liquid to vapor generated a large amount of PFC microbubbles that created contrast during US imaging. *In vitro* experiments with US have demonstrated that the ultrathin silica nanoshells can be imaged for at least 3 hours under color Doppler imaging, exhibiting a continuous US imaging lifetime. *In vivo* experiments have shown that folate conjugated silica nanoshells were able to accumulate and persist within the tumor region for up to 12 days post-injection, observable with US imaging. Surface conjugation with polyethylene glycol (PEG) increased the ultrasound signal at the tumor by increasing the particles accumulating at the tumor site. When exposed to high intensity focused ultrasound (HIFU), the particles were able to enhance the HIFU power and liquefy tumor tissue. With particles present, the HIFU duty cycle can be lowered to 2 %, minimizing tissue thermal deposition. By synthesizing ultrathin silica nanoshells with a folate-conjugated surface, it has been demonstrated that folate-conjugated ultrathin rigid silica nanoshells can accumulate in the LnCAP tumor persistently for 12 days. PEGylation of the particles further increase the particle accumulation concentration in the tumor, acting as a HIFU sensitizing agent for ultrasound histotripsy. Through intelligent surface modification, liquid PFC filled silica particles can act as a multi-functional theranostic agent for ultrasound diagnosis.

5:20pm **BI+AS-MoA10 Transparent Field Effect Sensor with Nanostructured Amorphous In-Ga-Zn-O Wires**, Xiaosong Du, Y. Li, J. Motley, G. Herman, Oregon State University

Amorphous In-Ga-Zn-O (a-IGZO) materials have a wide range of applications in high performance electronic devices, from the active material in thin film transistors for flat-panel displays and as the transducer for field effect sensors. A key benefit of a-IGZO over amorphous silicon is that it enables low processing temperatures, while retaining relatively large electron mobilities, low operating voltages, and very low off currents. In this study, we have fabricated a-IGZO films with well-defined nanostructures using colloidal lithography. These nanostructured a-IGZO films were then patterned into wires using electrohydrodynamic printing of an etch resist followed by wet chemical etching. We have characterized these nanostructured a-IGZO wires using field effect test structures to evaluate their electronic properties. To improve selectivity and stability of the nanostructured a-IGZO wires for sensing applications we have functionalized the back-channel surface with molecular receptors, where glucose oxidase was successfully attached as a sensing enzyme. Depletion/accumulation of carriers in the a-IGZO back-channel was observed upon reaction of the glucose oxidase with the analyte, which leads to significant changes in the sensors electronic signals. Continuous monitoring of glucose concentration can be achieved by measuring a direct change in channel conductance, turn on voltage shift, and/or electrical hysteresis. The results obtained for nanostructured a-IGZO wires will be compared to blanket a-IGZO films, where we have found that the nanostructured a-IGZO wires provide a significant enhancement in sensitivity to subtle changes in glucose concentrations in physiological buffers. These results provide insight into a route to develop low-cost transparent biochemical sensors based on the emerging a-IGZO technology.

Electronic Materials and Processing

Room: 211A - Session EM+AS+SS-MoA

MIM Diodes, Functional Oxides, and TFTs

Moderator: Pat Brady, RedWave Energy, Inc., John Conley, Oregon State University

2:20pm **EM+AS+SS-MoA1 Engineered Tunnel-Barrier Terahertz Rectifiers for Optical Nantennas**, Ivona Mitrovic, N. Sedghi, A.D. Weerakkody, J.F. Ralph, S. Hall, J.S. Wrench, P.R. Chalker, University of Liverpool, UK, Z. Luo, S. Beeby, University of Southampton, UK

Thin film metal-insulator-metal rectifying devices using double, triple or quadruple insulator layers are currently the focus of attention for the development of next-generation optical nantennas for infrared energy harvesting. The interest is driven by their distinctive attributes, such as nanoscale footprint, room temperature operation, zero bias voltage requirement, and ease of integration with Complementary Metal Oxide Semiconductor technology. Highly asymmetric and nonlinear current-voltage (IV) behaviour at low applied voltages is critical for this application. In this paper, we present comprehensive experimental and theoretical work on tunnel-barrier rectifiers comprising double ($\text{Ta}_2\text{O}_5/\text{Al}_2\text{O}_3$ and $\text{Nb}_2\text{O}_5/\text{Al}_2\text{O}_3$) and triple ($\text{Ta}_2\text{O}_5/\text{Nb}_2\text{O}_5/\text{Al}_2\text{O}_3$) insulator configurations engineered to enhance low voltage nonlinearity. There are two mechanisms that allow metal-insulator-insulator-metal (MIIM)

rectifiers to have a high nonlinearity while keeping the resistance low: (i) resonant tunnelling, and (ii) step tunnelling. This paper focuses on the former approach. A modified multi-layer Tsu-Esaki method has been used for IV calculations on the transmission coefficient by the transmission matrix method. The theoretical work indicates that the onset of resonant tunneling in MIIM and MIIM rectifiers can be adjusted to be close to zero volts by appropriate choice of work function difference of the metal contacts, the thickness of insulator layers, and the depth of the quantum well. The double and triple insulator rectifiers were fabricated using atomic layer deposition (ALD) and rf magnetron sputtering, while different metal contacts including Al, Ta, W, Nb, Cr and Ag were defined by photolithography or shadow mask and deposited by e-beam and thermal evaporation. The thickness, band gap, surface roughness, band offsets and work functions have been extracted from variable angle spectroscopic ellipsometry, atomic force microscopy, x-ray and inverse photoelectron spectroscopy on fabricated devices to ascertain the quality of the interfaces and to measure barriers. The key rectifier properties, asymmetry, nonlinearity and responsivity have been assessed from current voltage measurements performed in the range 293-370 K. A superior low voltage asymmetry (18 at 0.35 V) and responsivity (9 A/W at 0.2 V) has been observed for fabricated bilayer $\text{Ta}_2\text{O}_5/\text{Al}_2\text{O}_3$ and $\text{Nb}_2\text{O}_5/\text{Al}_2\text{O}_3$ MIIM devices respectively, in advance of state-of-the-art experimental values. The results demonstrate ALD and rf sputtered tunnel-barrier rectifiers which enhance low voltage nonlinearity and have the potential to be employed in optical nantennas for infrared energy harvesting.

2:40pm **EM+AS+SS-MoA2 MIM Diodes for RF Energy Harvesting**, A.A. Khan, A. Syed, F. Ghaffar, Atif Shamim, King Abdullah University of Science and Technology

Metal Insulator Metal (MIM) diodes that work on fast mechanism of tunneling have been used in a number of very high frequency applications such as (Infra Red) IR detectors and optical Rectennas for energy harvesting. Their ability to operate under zero bias condition as well as the possibility of realizing them through additive techniques makes them attractive for (Radio Frequency) RF applications. However, two major issues namely, high surface roughness at the metal-insulator junction which effects the reliability of the diode, and very high resistance (typically in Mega Ohms) which complicates its matching with RF antenna have prevented its wide spread use in RF rectennas.

In this work, various metal deposition methods such as sputtering and electron beam evaporation are compared in pursuit of achieving low surface roughness. Amorphous metal alloy has also been investigated in terms of its low surface roughness. Zinc oxide has been studied for its suitability as a thin dielectric layer for MIM diodes. Finally, comprehensive RF characterization of MIM diodes has been performed in two ways: 1) by standard S-parameter methods, and 2) by investigating their rectification ability under zero bias operation.

It is concluded from the Atomic Force Microscopy (AFM) imaging that surface roughness as low as sub 1 nm can be achieved reliably from crystalline metals such as copper and platinum. This value is comparable to surface roughness achieved from amorphous alloys, which are non-crystalline structures and have orders of magnitude lower conductivities. Relatively lower resistances of the order of 1 Kilo Ohm with a sensitivity of 1.5 V^{-1} have been obtained through DC testing of devices with MIM diode structure of platinum/zinc oxide/titanium. Finally, RF characterization reveals that input impedances in the range of 300 Ω to 25 Ω can be achieved in the low GHz frequencies (from 0.5-10 GHz). From the rectification measurements at zero bias, a DC voltage of 4.7 mV has been obtained from an incoming RF signal of 0.4 W at 2.45 GHz, which indicates the suitability of these diodes for RF rectenna devices without providing any bias. These preliminary results indicate that with further optimization, MIM diodes are attractive candidates for RF energy harvesting applications.

3:00pm **EM+AS+SS-MoA3 Diode Structure Based on Carbon Materials for Ultra high Frequency Driving**, JaeEun Jang, Daegu Gyeongbuk Institute of Science and Technology (DGIST), Republic of Korea

If the antenna can be designed to absorb wavelengths in the range of a few hundred THz with multi-antenna array design, it results in high conversion efficiency due to power production from various light sources between ultraviolet (UV) and infrared (IR) radiation that is often thought of as heat and exists beyond the visible range for humans. One of the problems in this idea, however, is the nature of visible or IR light to oscillate at ultra-high frequencies. Therefore, a rectifier working at such an ultra-high frequency should be developed with a highly efficient coupling between antenna and light. Because Schottky diode is limited to frequencies less than \sim THz level, nanometer size MIM diode structure has been suggested as alternative design. Two different metals have used normally to make an asymmetric

characteristic of current-voltage. However the work function difference between the metals cannot produce a high asymmetry, which causes a poor rectifier performance, even though the structure can be driven in THz range. To solve this issue, we used a structural asymmetric MIM design. The planar asymmetric design using various metals or graphene showed better asymmetric I-V characteristics than that of simple MIM structure. In addition, for the vertical aligned design, single multi-wall carbon nanotube was formed as one electrode to get high tunneling current caused by the structural effect of sharp tip. The structural asymmetry can make a different field density states to the metals, which induces a high rectify characteristics. The contrast ratio between the forward and the reverse bias is $\sim 10^4$ level. The estimated cut-off frequency is about 4.74THz. The electrical characteristics are stable up to 423K.

3:20pm **EM+AS+SS-MoA4 Optical Rectenna Arrays using Vertically Aligned Carbon Nanotubes**, *Baratunde Cola*, Georgia Institute of Technology

The response of a multiwall carbon nanotube to visible light has been reported to be consistent with conventional radio antenna theory. Researchers have proposed that this result might be exploited to realize an optical rectification device – that is, a device that converts free-propagating electromagnetic waves at optical frequencies to localized d.c. electricity. However, an experimental demonstration of this concept requires that the multiwall carbon nanotube antenna be coupled to a diode that operates on the order of 1 petahertz (switching speed on the order of a femtosecond). Ultralow capacitance, on the order of a few attofarads, could allow a diode to operate at these frequencies; and the development of metal-insulator-metal tunnel junctions with nanoscale dimensions has emerged as a potential path to diodes with ultralow capacitance, but these structures remain extremely difficult to fabricate and couple to a nanoscale antenna reliably. Here we demonstrate optical rectification by engineering metal-insulator-metal tunnel diodes at the tips of multiwall carbon nanotubes, which act as the antenna and metallic electron emitter in the diode. This performance is achieved using diode areas based on the diameter of a single carbon nanotube (about 10 nanometers), geometric field enhancement at the carbon nanotube tips, and a low work function semi-transparent top metal contact. Using vertically-aligned arrays of the diodes, we measure d.c. open-circuit voltage and short-circuit current at visible and infrared electromagnetic frequencies that is due to a rectification process, and quantify minor contributions from thermal effects. Our devices show evidence of photon-assisted tunneling, and exhibit zero-bias diode responsivity on the order of 0.1 amps per Watt and zero-bias differential resistance as low as 100 ohm-centimeter squared under illumination. Additionally, power rectification is observed under simulated solar illumination. Numerous current-voltage scans on different devices, and between 5-77 degrees Celsius, show no detectable change in diode performance, indicating a potential for robust operation.

3:40pm **EM+AS+SS-MoA5 World Record Tunable Microwave Dielectrics**, *C.H. Lee*, Cornell University, *N.D. Orloff*, National Institute of Standards and Technology (NIST), *T. Birol*, *Y. Zhu*, *Y. Nie*, Cornell University, *V. Goian*, Institute of Physics ASCR, *R. Haislmaier*, Pennsylvania State University, *J.A. Mundy*, Cornell University, *J. Junquera*, Universidad de Cantabria, *P. Ghosez*, Université de Liège, *R. Uecker*, Leibniz Institute for Crystal Growth, *V. Gopalan*, Pennsylvania State University, *S. Kamba*, Institute of Physics ASCR, *L.F. Kourkoutis*, *K.M. Shen*, *D.A. Muller*, Cornell University, *I. Takeuchi*, University of Maryland, College Park, *J.C. Booth*, National Institute of Standards and Technology (NIST), *C.J. Fennie*, **Darrell Schlom**, Cornell University **INVITED**

The miniaturization and integration of frequency-agile microwave circuits—relevant to electronically tunable filters, antennas, resonators, phase shifters and more—with microelectronics offers tantalizing device possibilities, yet requires thin films whose dielectric constant at GHz frequencies can be tuned by applying a quasi-static electric field. Appropriate systems, e.g., $\text{Ba}_x\text{Sr}_{1-x}\text{TiO}_3$, have a paraelectric-to-ferroelectric transition just below ambient temperature, providing high tunability. Unfortunately such films suffer significant losses arising from defects. Recognizing that progress is stymied by dielectric loss, we start with a system with exceptionally low loss— $\text{Sr}_{n+1}\text{Ti}_n\text{O}_{3n+1}$ phases—where $(\text{SrO})_2$ crystallographic shear planes provide an alternative to point defect formation for accommodating non-stoichiometry. Guided by theoretical predictions, we biaxially strain a $\text{Sr}_{n+1}\text{Ti}_n\text{O}_{3n+1}$ phase with $n = 6$ to introduce a ferroelectric instability and create a new type of tunable microwave dielectric. This tunable dielectric exhibits a world record figure of merit at room temperature and frequencies up to 125 GHz. Our studies also reveal details about the microscopic growth mechanism of these phases, which are relevant to preparing atomically precise oxide interfaces to these and other Ruddlesden-Popper phases.

4:20pm **EM+AS+SS-MoA7 Bandgap Engineering and Application of SiZnSnO Amorphous Oxide Semiconductor**, *Sang-Yeol Lee*, Cheongju University, Republic of Korea **INVITED**

The band gap of the amorphous SiZnSnO (SZTO) semiconductor has been controlled by bandgap engineering using Si ratio. The addition of small amount of Si in SZTO channel layer can change the position of Fermi level in band gap. By investigating the ultraviolet photoelectron spectroscopy (UPS) characteristics, it is verified that Si atoms can modify the Fermi energy level of SZTO thin films. Carrier generation originated from the oxygen vacancy could modify the Fermi level in the band gap of oxide thin films since Si could be an oxygen vacancy suppressor. This is also related with the origin of defect state which was observed to be involved with the creation of oxygen vacancies. Since it is not so easy to derive directly the change of the Fermi energy level in the energy band gap of amorphous oxide semiconductor, no report of the relation between the Fermi energy level in the energy band gap of oxide semiconductor and the device stability of oxide thin film transistors has been reported. We derive directly band gap and Fermi energy level by using the ultraviolet photoelectron spectroscopy (UPS) characteristics, Kelvin probe (KP) and electron energy loss spectroscopy (EELS). The instability mechanism of amorphous oxide thin film transistors based on the band parameter of oxide semiconductor will be discussed and applied to display applications.

5:00pm **EM+AS+SS-MoA9 Self-aligned Vertical ZnO-based Circuits by Spatial ALD**, *Shelby Nelson*, *C.R. Ellinger*, *L.W. Tutt*, Eastman Kodak Company

Metal oxide thin-film transistors (TFTs) are becoming the mainstream for display backplanes. These TFTs are fabricated with traditional photolithographic techniques, typically on rigid substrates. In our lab, we explore approaches that are more “print-compatible”, with broad alignment tolerance and no small-gap mask features. We deposit zinc oxide (ZnO) semiconductors, aluminum oxide (Al_2O_3) dielectrics, and aluminum-doped zinc oxide conductors by the fast, atmospheric pressure, large-area-compatible, spatial atomic layer deposition (SALD) process. In addition to depositing good-quality thin-film transistor layers at temperatures at and below 200 °C, this process can work with a wide variety of rough and deformable substrates.

Here we describe vertical TFT and circuit architectures that unite process simplicity with high performance. The liberal design rules result from vertical transistors with self-aligned source and drain contacts that define the sub-micron channel length. Using 10-micron design rules for both the minimum line/space dimensions and for alignment tolerances, we have fabricated 9-stage ring oscillators with greater than 1 MHz oscillation frequency, at supply voltage below 6 V. Starting with a gate layer with a re-entrant profile on the edge, these devices use spatial ALD to conformally coat the Al_2O_3 gate dielectric and ZnO semiconductor, and a line-of-sight deposition process such as evaporation for the aluminum electrodes. Individual device characteristics as well as circuit performance will be discussed.

5:20pm **EM+AS+SS-MoA10 Geometrically Asymmetric Tunneling Nanostructures by Atomic Layer Deposition**, *Jie Qi*, *X. Jiang*, *B.G. Willis*, University of Connecticut

Geometrically asymmetric tunneling nanostructures are of interest to make ultra-high frequency diodes for applications in detection and solar energy harvesting. Atomic layer deposition (ALD) is one of the most promising techniques for fabrication of tunneling nanostructures. In previous work, it has been demonstrated that individual metal-vacuum-metal (MVM) tunnel junctions with a gap distance of 1-2 nm can be fabricated by selective-area ALD of Cu onto Pd templates. However, optimizing nonlinearity and scaling up to large arrays of tunneling devices both introduce new challenges that include achieving precise control of nucleation and good quality conformal growth on sharply defined asymmetric nanostructures.

In this study, the fabrication of large arrays of MVM tunnel junctions is investigated using selective-area ALD. Nano-patterned Pd nanostructures with sharp asymmetric features are prepared as seed layers for planar, geometrically-asymmetric junctions on SiO_2 / silicon substrates by high-resolution electron beam lithography. Selective-area ALD applied to patterned Pd nanostructures allows tuning the size of junctions to nanometer dimensions. Microscopy and chemical analysis are used to evaluate nanostructure morphology, tunnel junction uniformity, and selective area growth characteristics. In-situ electrical measurements are used to measure DC current-voltage curves and nonlinearity. It was found that film nucleation and growth selectivity can be greatly affected by different pre-deposition sample treatments. UV/Ozone (UVO) cleaning and hydrogen annealing before ALD both enhance the nucleation of Cu thin films on Pd seed layers. In addition, UVO treatment promotes selective growth on Pd vs. SiO_2 areas while boiling samples in water to hydroxylate SiO_2 surface area contributes to a loss of selectivity. In-situ measured electrical data

during ALD growth demonstrate a gradual convergence to tunneling with sub-nm control provided by the ALD method. However, control of tunneling non-linearity and geometric asymmetry is complicated by an incomplete understanding of the growth mechanism and the morphology evolution of nanostructures. There is a compromise between conditions that promote good ALD growth and those that maintain geometric asymmetry. We conclude with suggestions to promote growth, maintain sharp asymmetric features, and achieve non-linear tunneling characteristics.

Energy Frontiers Focus Topic

Room: 211B - Session EN+AS+EM+NS+SE+SS+TF-

MoA

Solar Cells II

Moderator: Adrie Mackus, Stanford University

2:20pm EN+AS+EM+NS+SE+SS+TF-MoA1 **Influence of Annealing Temperature in the Bulk Defect Formation in Perovskite Thin Films.** *Weina Peng, B.X. Anand, L.-H. Liu, S.C. Sampat, B.E. Bearden, A.V. Malko, Y.J. Chabal*, University of Texas at Dallas

Perovskites are emerging as front-runners for solar cell applications because of their superior optoelectronic properties. Over the past few years the grain size of perovskites has been continuously improved from several hundred of nanometers to a few millimeters which resulted in better solar conversion efficiencies. In addition to surface and grain boundary related defects, perovskites are prone to the formation of bulk defects as well. However the role of bulk defects in the determination of photovoltaic performance of perovskites is rarely explored. To this end we investigate the impact of annealing temperature on the defect density in polycrystalline $\text{CH}_3\text{NH}_3\text{PbI}_3$ thin films of ~ 1 micron average grain size prepared using vapor assisted solution process (VASP). The photoluminescence (PL) intensity and lifetime show systematic reduction when the annealing temperature is increased from 150°C to 200°C. A rough estimate of the defect state density obtained using fluence dependent PL measurements reveal a 5 fold increase in defect density for a 25°C increase in annealing temperature although the average grains size stays unchanged. Furthermore, surface passivation of perovskite films using Al_2O_3 via atomic layer deposition leads to an improvement in PL intensity and lifetime. But the PL quantum efficiency, as well as the lifetime, of the surface passivated 200°C annealed sample remains significantly lower than that of the un-passivated 150°C annealed sample indicating that the majority of the defects states we observe in the high temperature annealed samples originate from bulk defects. Thus the present study shows that minimizing the number of bulk defects, in addition to surface defects, is very important in the realization of highly efficient perovskite solar cells.

3:00pm EN+AS+EM+NS+SE+SS+TF-MoA3 **Tandem Solar Cells Using Perovskites, Silicon and CIGS.** *M.D. McGehee, Tomas Leijtens*, Stanford University **INVITED**

The efficiency of perovskite solar cells has soared from a few percent to over 20% in the last 3 years. They are very attractive for multijunction solar cell applications because the bandgap of perovskite semiconductors can be easily tuned in the range of 1.55 to 2.2 eV and the open circuit voltage of the cells is large. We have made highly efficient semitransparent perovskite solar cells using silver nanowire meshes as the top electrode. These cells can be used in combination with either silicon or copper indium gallium diselenide solar cells to make four-terminal and two-terminal tandems. We will also present detailed characterization of perovskite semiconductors made with different processing conditions to show what needs to be done to minimize recombination and make the solar cells stable.

3:40pm EN+AS+EM+NS+SE+SS+TF-MoA5 **Lifetime, Mobility, and Diffusion of Photoexcited Carriers in Ligand-Exchanged Lead Selenide Nanocrystal Films Measured by Time-Resolved Terahertz Spectroscopy.** *G.W. Guglietta*, Drexel University, *B.T. Diroll, E.A. Gaulding, J.L. Fordham*, University of Pennsylvania, *S. Li*, Drexel University, *C.B. Murray*, University of Pennsylvania, *Jason Baxter*, Drexel University

Colloidal semiconductor nanocrystals have been used as building blocks for electronic and optoelectronic devices ranging from field effect transistors to solar cells. Properties of the nanocrystal films depend sensitively on the choice of capping ligand to replace the insulating synthesis ligands. Thus far, ligands leading to the best performance in transistors result in poor solar cell performance, and vice versa. To gain insight into the nature of this dichotomy, we used time-resolved terahertz spectroscopy measurements to study the mobility and lifetime of PbSe nanocrystal films prepared with five common ligand-exchange reagents. Non-contact terahertz spectroscopy

measurements of conductivity were corroborated by contacted van der Pauw measurements of the same samples. The films treated with different displacing ligands show more than an order of magnitude difference in the peak conductivities and a bifurcation of time-dynamics. Inorganic chalcogenide ligand-exchanges with sodium sulfide (Na_2S) or ammonium thiocyanate (NH_4SCN) show high THz mobilities above $25 \text{ cm}^2\text{V}^{-1}\text{s}^{-1}$, which is desirable for transistors, but nearly complete decay of transient photocurrent within 1.4 ns. The high mobility with NH_4SCN and Na_2S exchanges is more than offset by their short lifetimes and results in diffusion lengths of only ~ 200 nm. In contrast, ligand exchanges with 1,2-ethylenediamine (EDA), 1,2-ethanedithiol (EDT), and tetrabutylammonium iodide (TBAI) show $\sim 5\times$ lower mobilities but much longer carrier lifetimes, with $\sim 30\%$ of photoexcited carriers remaining for >10 ns. The long lifetimes with EDA, EDT, and TBAI yield diffusion lengths of at least 500 nm, which is approaching the film thickness desired for strong light absorption in solar cells. This bifurcated behavior may explain the divergent performance of field-effect transistors and photovoltaics constructed from nanocrystal building blocks with different ligand exchanges.

4:00pm EN+AS+EM+NS+SE+SS+TF-MoA6 **iCVD Synthesis and Integration of Poly(vinylpyrrolidone) and Poly(4-vinylpyridine) as Polymer Electrolytes in Dye Sensitized Solar Cells.** *Yuriy Y. Smolin, S. Janakiraman, A.J. Sauter, M. Soroush, K.K.S. Lau*, Drexel University

Initiated chemical vapor deposition (iCVD) is used to synthesize and integrate poly(4-vinylpyridine) (P4VP) and polyvinylpyrrolidone (PVP) as polymer electrolytes within the mesoporous TiO_2 photoanode of dye sensitized solar cells (DSSCs). DSSCs with conventional liquid electrolytes are prone to leakage and evaporation, which hinders DSSC durability and field implementation. In addition, liquid electrolytes lead to significant electron recombination within the cells that limit DSSC performance. In contrast, polymer electrolytes do not suffer from the practical disadvantages and could potentially enhance the cell's I-V behavior.

However, in order to enable good contact between the TiO_2 electrode and the polymer electrolyte, a major obstacle is the difficulty in achieving good pore filling of the polymer into the mesoporous TiO_2 layer. Mesoscale pore diameter, high aspect ratio, and tortuous pore structure of the photoanode along with liquid surface tension, poor wettability, and solute steric hindrance make pore filling extremely limited when using liquid techniques. This leads to poor electrical contact and lower efficiency. To overcome the challenges of pore filling, we directly synthesized polymer electrolytes inside the pore volume of the photoanode using the solvent-free technique of iCVD. iCVD relies on the vapor delivery of monomer and initiator, which facilitates infiltration into the porous TiO_2 substrate, and by controlling the relative rates of diffusion and surface polymerization through iCVD process parameters, uniform and conformal growth of polymer is achieved. The pore filling of the polymer electrolyte into 5–10 μm photoanodes using iCVD is typically 90–100% which is significantly better than that achievable with liquid techniques like spin coating.¹

In this work, we will show that iCVD P4VP and PVP polymer electrolytes can be effectively integrated within TiO_2 mesoporous photoanodes to produce enhanced DSSCs. By varying the polymer electrolyte chemistry including the use of a crosslinking agent during iCVD to stabilize the resulting polymer structure, DSSC I-V characteristics, such as open-circuit voltage, short-circuit current density and fill factor, are tuned.² To gain a better understanding on the effect of the polymer electrolyte, experimental techniques such as linear sweep voltammetry, intensity modulated spectroscopy, and impedance spectroscopy are used. Mathematical modeling of DSSC behavior is also performed to relate these experimental observations with the dynamics of the operation of the cell.

1. S. Nejadi and K. K. S. Lau, *Nano Lett.*, 2010, 11, 419-423.

2. Y. Y. Smolin et al., *J. Power Sources*, 2015, 274, 156-164.

4:20pm EN+AS+EM+NS+SE+SS+TF-MoA7 **Interfacial Effects on Device Performance in Organic Solar Cells.** *Huanxin Ju, J.F. Zhu*, University of Science and Technology of China, *D.S. Ginger*, University of Washington

The better understanding of the underlying mechanisms is essential for the further development of highly efficient organic photovoltaics (OPVs) devices. In this paper, the transient photovoltage (TPV) and charge extraction (CE) measurements in combination with the synchrotron radiation photoemission spectroscopy (SRPES) were used to gain insights into the correlation between the microscopic interfacial properties and macroscopic device performance. The OPV devices based on PCDTBT: PC_{70}BM with Ca interlayer were studied as a reference system to investigate the interfacial effects on device performance. The charge carrier decay dynamics demonstrated that the device with the Ca interlayer exhibited a lower recombination constant (k_{rec}) than that only with the Al cathode at a given charge carrier density (n). In addition, the interfacial energy band structures indicated that the strong dipole moment produced by the Ca

interlayer can facilitate electron extraction as well as drive hole away at the cathode/polymer interface, resulting in retarding interfacial recombination losses. Finally, we examined the device performance with the Ca interlayer to find that the efficiency is improved by 28% as compared to that without the Ca interlayer, which shows good correlation with the observed interfacial properties.

4:40pm **EN+AS+EM+NS+SE+SS+TF-MoA8 Tungsten-Titanium Mixed Oxide Thin Films for Improved Structural and Optical Properties for Solar Driven Applications**, *Mirella Vargas*, The University of Texas at El Paso, *N.R. Murphy*, Air Force Research Laboratory, *R.V. Chintalapalle*, The University of Texas at El Paso

Tungsten oxide (WO_3) is a well-established *n*-type semiconductor possessing unique optical and electronic properties. WO_3 has become the most interesting inorganic material for electrochromic applications due to the reversible spectral absorption properties associated with WO_3 . WO_3 thin films and nanostructures exhibit an optical band gap that permits efficient use of the solar spectrum including absorption in the blue part of the visible region and the ultraviolet region, as well as a high transmission region that extends from the near-infrared (IR) to the visible spectrum. Coupled with good electronic transport properties, photosensitivity, and chemical integrity, WO_3 -based materials are attractive for applications related to sustainable energy production including energy efficient windows and architecture, photoelectrochemical (PEC) water-splitting, photocatalysis and solar cells. Anion or cation doping into WO_3 has been extensively studied as this offers the opportunity to tailor the transport properties that may influence the efficiency of solar driven devices. Titanium doping into WO_3 has proven to enhance the electrochromic response and the cyclic lifetime by a factor of five in PEC devices. In the present case a systematic investigation of progressively increasing the Ti content in the W-Ti target for reactive sputtering has been employed to tune the structure, chemistry, and properties of the films. Tungsten-titanium (W-Ti) mixed oxide thin films were fabricated using reactive sputtering of W-Ti alloy targets with Ti content ranging from 0 to 30 wt.%. X-ray photoelectron spectroscopy confirms the existence of W and Ti in their highest oxidation states of +6 and +4, respectively. Quantification of binding energy shifts for W and Ti core-level transitions confirms the formation of WO_3 - TiO_2 composite oxide films. Optical analyses made from spectrophotometry measurements indicate a decrease in band gap with a discrete amount of Ti incorporation. The band gap decreases with increasing Ti from 3.0 eV to 2.5 eV. Such films are expected to have the possibility for tuning the electrical conductivity while retaining the optical transparency to make them efficient for photoelectrochemical cells and photovoltaics.

5:00pm **EN+AS+EM+NS+SE+SS+TF-MoA9 Potential Resolution to the "Doping Puzzle" in Pyrite FeS_2** , *X. Zhang, M. Li, L. O'Brien, J. Walter, M. Manno, F. Mork, J. Kakalios, Eray Aydil, C. Leighton*, University of Minnesota

In principle, pyrite FeS_2 is one of the most suitable photovoltaic materials for sustainable low-cost, large-scale solar cell manufacturing because it has high absorbance in the visible and comprises earth-abundant inexpensive elements. However, current efficiencies of solar cells based on pyrite FeS_2 have not exceeded 2.8%. Early research on this material concluded that unintentionally doped FeS_2 thin films are *p*-type and subsequent solar cell work evolved based on this presumption. In fact, it is now widely accepted that FeS_2 thin films almost always exhibit *p*-type conduction even though single crystals are typically found to be *n*-type. This discrepancy between single crystals and thin films is perplexing and to date this puzzle remains unexplained. In this talk we reexamine the conclusion that undoped FeS_2 films are predominantly *p*-type and provide an explanation for this "doping puzzle" in pyrite. Using a combination of Hall effect, thermopower, and temperature-dependent resistivity measurements on a large set of well characterized single crystals and thin films, we show that the widely accepted predominant *p*-type behavior in pyrite films may, in fact, be an artifact of hopping conduction and should be revisited. Specifically, both Hall effect and thermopower measurements establish that all of our high-mobility ($>1 \text{ cm}^2\text{V}^{-1}\text{s}^{-1}$) films and single crystals are *n*-type. Temperature-dependent resistivity measurements on these high mobility films and crystals establish diffusive electronic transport. We find that films with lower mobility ($4 \times 10^{-2} - 1 \text{ cm}^2\text{V}^{-1}\text{s}^{-1}$) also show *n*-type Hall effect but exhibit a *p*-type Seebeck coefficient, leading to a discrepancy in the measured carrier type. Temperature-dependent resistivity measurements on these intermediate mobility films show a transition from diffusive to hopping transport. Finally, both Hall and Seebeck coefficients are strongly suppressed and invert in the lowest mobility thin films ($<4 \times 10^{-3} \text{ cm}^2\text{V}^{-1}\text{s}^{-1}$) indicating apparent *p*-type conduction. Temperature-dependent resistivity measurements establish unambiguous hopping behavior in these lowest mobility films. Based on this evolution of Hall and Seebeck coefficients with carrier mobility, and the well-known suppression of the Hall and Seebeck effects in conductors with hopping electronic transport, we

conclude that the apparent crossover from *n*-type to *p*-type with decreasing mobility is, in fact, an artifact of hopping conduction.

Work supported by the NSF under DMR-1309642, in addition to the University of Minnesota NSF MRSEC under DMR-1420013.

5:20pm **EN+AS+EM+NS+SE+SS+TF-MoA10 Interparticle Contact Radius and Electron Transport in Thin Films Comprised of Nanocrystals**, *Elijah Thimsen, D. Lanigan*, Washington University, St. Louis

Thin films comprised of nanocrystals are being explored for a variety of applications that involve electron transport. For traditional applications such as photovoltaic solar cells, the goal is often to utilize solution processing to make an inexpensive thin film that essentially behaves as a bulk material with diffusive transport. For other applications, such as neuromorphic computing, variable range hopping (VRH) transport is more desirable because it enables a given nanocrystal to have orders of magnitude more nearest neighbors than it physically touches. It is of paramount importance that the structure-property relationships that control electron transport mechanism be elucidated. Previous work has demonstrated that interparticle separation distance affects charge carrier mobility. However, for films comprised of nanocrystals that are physically touching, what is the effect of contact radius? In this work, we present a systematic experimental study of the effect of interparticle contact radius on the electron transport mechanism in thin films comprised of heavily-doped ZnO nanocrystals embedded in Al_2O_3 . As the contact radius increased, the electron transport mechanism crossed over from VRH to diffusive conduction. For large contact radius between nanocrystals, the room-temperature electron mobility in the film approached the local mobility within a nanocrystal, approximately $10 \text{ cm}^2 \text{V}^{-1} \text{s}^{-1}$. The conclusion is that for nanocrystals that are physically touching, the interparticle contact radius determines the transport mechanism. With the ability to control the electron transport mechanism in films comprised of ZnO nanocrystals, we performed an exploratory study of the Hall effect in these materials. Hall effect measurements are of great utility and are routine for determining charge carrier mobility and type, but the interpretation of data for materials that exhibit VRH has been difficult in the past. For well-connected ZnO nanocrystals that exhibit diffusive conduction, the Hall coefficient was independent of temperature, as expected for the high doping level. Alternatively, for films with small contact radius between nanocrystals, which exhibited a VRH transport mechanism, we observed an anomalous behavior of the Hall coefficient at low temperature (100 to 200 K). Surprisingly, for films that exhibited VRH, the magnitude of the Hall coefficient increased exponentially with decreasing temperature, in stark contrast to the conventional wisdom that the Hall effect is suppressed for VRH.

In-Situ Spectroscopy and Microscopy Focus Topic Room: 211C - Session IS+AS+SA+SS-MoA

Ambient Pressure X-ray Photoelectron Spectroscopy Studies for Catalytic and Energy Materials in Gas Phase

Moderator: Peter Crozier, Arizona State University, Franklin (Feng) Tao, University of Kansas

2:20pm **IS+AS+SA+SS-MoA1 In situ Electron Spectroscopy for Energy Science**, *Robert Schlögl*, Fritz-Haber-Institut der Max-Planck-Gesellschaft, Germany **INVITED**

The use of volatile renewable electricity in larger amounts in our energy systems requires grid-scale technologies for integration electricity in material energy carrier streams. Several systemic options always suffer from our conceptual weakness to convert free electrons in chemical bonds. This can be achieved with accumulators for limited applications and should be done through water splitting and synthesis of solar fuels in almost unlimited applications. Complex interfacial chemistry is the underlying scientific challenge. To tackle this old challenge with new concepts it is essential to improve our ability to study chemical, electronic and geometric structures of nanoscopic objects in-situ meaning under operation conditions. A whole train of dedicated instrumentation from specimen formation, data acquisition and auxiliary analyses plus sample manipulation is necessary for this task. The presentation gives some aspects of priority challenges and uses examples of operation studies of water splitting catalysts and of CO₂ reduction systems to illustrate the present status of insight. In the outlook the possibilities of the novel experiment EMIL at BESSY will be discussed.

3:00pm **IS+AS+SA+SS-MoA3 Catalysis on Singly Dispersed Bimetallic Sites on Oxide Support**, *Luan Nguyen*, University of Kansas, *A. Frenkel*, Yeshiva University, *J. Li*, Tsinghua University, China, *F. Tao*, University of Kansas

Reaction events of heterogeneous catalysis occur on specific catalytic sites. Atoms of a catalytic site arrange in a specific geometric/electronic configuration for adsorbing/dissociating reactant molecules and subsequent coupling to form product molecules. Bimetallic catalysts play significant roles in chemical and energy transformations due to their tunable catalytic properties through ligand, geometric, bi-functional, or lattice strain effect.

When a bimetallic site (M_1A_n , M and A: metal elements, $n \geq 1$) is one of the continuous sites on the surface of a bimetallic NP, this site is in a metallic state. However, when M_1A_n sites are *separately* anchored on a surface of a transition metal oxide support, these isolated bimetallic sites are in cationic state. Such change in electronic structure could cause these bimetallic sites to have stronger chemisorption to reactant or/and intermediate molecules, thus facilitating its dissociation and subsequent coupling. In addition, singly dispersed of metal M in M_1A_n minimizes the potential binding configurations of reactant molecules hence may enhance catalytic selectivity toward a specific reaction pathway. Here we present singly dispersed bimetallic catalyst Rh_1Co_3 prepared on Co oxide support, which exhibits 100% selectivity for the production of N_2 in NO reduction with CO.

Preparation of isolated bimetallic sites Rh_1Co_3 on Co_3O_4 nanorods begins with the formation of hydroxide species $Rh(OH)_n$ on the surface of Co_3O_4 , followed by calcination at 150°C in O_2 to form Rh-O-Co bonds between singly dispersed $Rh(OH)_n$ species and the surface of Co_3O_4 , and concluded with a carefully controlled reduction to remove oxygen atoms between Rh and Co and thus a simultaneous formation of Rh-Co bonds. In-situ ambient pressure X-ray photoelectron spectroscopy (AP-XPS) was used to monitor the oxidation and reduction steps and to avoid over or under-reduction.

Formation of singly dispersed Rh atoms was visualized using HAADF-STEM. The bonding environment of Rh to three Co atoms was confirmed using in-situ EXAFS. For reduction of NO with CO, Rh_1Co_3/CoO exhibits high activity at 110 °C with 100% selectivity toward N_2 production. In contrast, Rh-Co alloy NP/CoO has much lower activity and selectivity (10%) under the same condition. In-situ AP-XPS investigation shows that Rh atoms are at cationic state instead of metallic state. Along with this, DFT calculations suggest that a strong adsorption of intermediate N_2O molecules on Rh_1Co_3 site prevents its desorption as a byproduct and provides a dissociation pathway of N_2O to N_2 with a low activation barrier (~0.21 eV), thus leading to a 100% selectivity to N_2 production.

3:20pm **IS+AS+SA+SS-MoA4 Oxidation and Recovery of WC Thin Film Surfaces**, *E. Monazami*, University of Virginia, *J.B. McClimon*, University of Pennsylvania, *N. Johansson*, *P. Shayesteh*, *S. Urpelainen*, *J. Schnadt*, Lund University, Sweden, *Petra Reinke*, University of Virginia

Transition metal carbide (TMC) surfaces are coveted as catalytic materials, electrodes and hard protective coatings. A bottleneck in their use is surface oxidation, which leads to a decay in performance. Our work establishes the feasibility of surface recovery by using a carbon-rich WC layer where recarburization of the surface is initiated by an annealing step. Thin carbon-rich tungsten carbide layers are grown by co-deposition of W and C_{60} on a $MgO(001)$ surface at 1100 K. The MgO substrate serves as a diffusion barrier for carbon, and the films have a well-defined carbon inventory controlled by the deposition rates of the reactants. The film surfaces were studied by in-situ Scanning Tunneling Microscopy and Spectroscopy. Raman spectroscopy confirmed the presence of highly defective graphitic carbon. The oxidation-recarburization (O-R) cycles were studied in the ambient pressure endstation SPECIES at MAX-Lab (J. Synchr. Rad. 701, 19 (2012)) in a pressure of 0.3 mbar of O_2 . Oxidation with $p(O_2)$ of 10^{-5} mbar were performed at SPECIES for direct comparison to low $p(O_2)$ STM experiments.

The carbon-rich WC films exhibit a relatively rough surface, which allows only in a few instances true atomic resolution, but graphite as well as graphene layers can be identified. Oxidation at $T > 550$ K leads to etching of surface carbon and the growth of a W-oxide layer and STS maps show the oxide evolution. The oxidation in the low $p(O_2)$ pressure regime progresses slowly and the surface carbide is recovered by annealing.

The use of the SPECIES endstation enabled a quantitative study of the O-R cycles including a detailed analysis of the respective bonding environments which are modified at different times in the O-R cycle. The oxidation in the ambient pressure environment was monitored using the ratio of W-carbide to W-oxide in the W4f core level during the reaction. The steady state thickness of oxide is a function of sample temperature and order of annealing cycles. The surface carbide concentration can be fully recovered in a subsequent annealing step, and repeated O-R cycles were performed. The O-R process is controlled by the interplay between surface oxidation, oxygen and carbon diffusion and our results will be modeled with a simple

set of transport equations. We will discuss the role of different bonding environments as we move through the O-R cycle and compare UHV and ambient pressure results up to 800 K. These results clearly illustrate that carbon-rich tungsten carbide materials can be used to achieve a long term use of carbide surfaces in catalysis and fuel cell applications.

supported by NSF-Division of Materials Research (Ceramics) DMR-100580, STINT award.

3:40pm **IS+AS+SA+SS-MoA5 Microscopy, Spectroscopy, and Reactivity of Surfaces in Vacuum and under Ambient Reaction Pressures**, *Miquel Salmeron*, *B. Eren*, Lawrence Berkeley National Laboratory **INVITED**

The goal of surface science research is to provide atomic level understanding of the structural and dynamic properties of surfaces, a goal particularly relevant for chemical applications, including catalysis, photochemistry, batteries and fuel cells. With X-ray Photoemission Spectroscopy (XPS) and X-ray absorption Spectroscopy (XAS) we determine composition and electronic structure. With Scanning Tunneling Microscopy (STM) we image atoms and molecules as they adsorb, diffuse and react on single crystal surfaces. To study surfaces in the presence of gases, in the Torr to Atmospheres range, which is relevant to practical catalysis, new instrumentation is needed. Over the last years we developed high pressure STM, XPS and XAS, to study surfaces under high coverage of adsorbates in equilibrium with gases near ambient pressures and temperature. Using a combination of these techniques I will show how under these conditions the structure of surfaces and the adsorbed layers can be very different from that at low coverage, or even at high coverage but at low temperature. Adsorbates can induce dramatic restructuring of the surface, as I will show in the case of CO induced restructuring of Cu surfaces and the reactions with Oxygen.

4:20pm **IS+AS+SA+SS-MoA7 Novel Solutions for Ambient Pressure and In Situ Photoelectron Spectro-Microscopy**, *Hikmet Sezen*, *M. Amati*, *L. Gregoratti*, Elettra-Sincrotrone Trieste, Italy

A technique based on photoelectron spectroscopy (PES) providing simultaneously spectroscopy and microscopy capabilities and being compatible with ambient pressure conditions is still missing. Ambient pressure PES (APPES), based on differential pumping of the electron energy analyzer, offers an optimal spectroscopic solution to overcome pressure barrier for surface related studies[1]. Unfortunately, APPES has very limited spatial resolution. On the other hand, a better than 100 nm spatial resolution scanning photoelectron microscope (SPEM), where the X-ray beam is demagnified down to a 130 nm spot by Zone Plate Fresnel optics and the sample scanned under the focused beam, is accessible from a few synchrotrons. A direct adaptation of the APPES approach to SPEM technique is not possible because of geometric constraints, stabilities and sustainability of the x-ray optics under near ambient pressures, and mechanical stability of the photoelectron detection system under such severe pumping conditions. In this presentation we will introduce two novel solutions for near-ambient pressure SPEM with ~100 nm spatial resolution and compatible with in-situ/operando conditions operated at ESCAmicroscopy beamline at Elettra synchrotron facility.

Dynamic high pressure (DHP) is the one of our near-ambient pressure SPEM solution. The technique is based on generating high pressure pulsed gas packets directed to the sample. Under influence of gas pulses the sample falls a few mbar pressure in a burst instant, then gas packets dilute into the SPEM chamber to yield a 1×10^{-5} mbar background pressure. From the test results a 10^{-3} - 10^{-2} mbar equivalent static pressure was felt by Si and Rh samples during in-situ oxidation reaction.[2] It is available for users.

Effusive cell is another solution for near-ambient pressure SPEM. The sample is encapsulated with a vacuum sealed cell and located just 30-50 μm behind of a 200 μm diameter size pinhole. The focused x-ray beam are scanning the sample through the pinhole. The generated photoelectrons come out from the same pinhole and are able to reach the electron energy analyzer. Due to the geometric orientation of energy analyzer and the pinhole we can achieve ca. a $200 \times 100 \mu m^2$ aerial point of view on the sample. The pressure inside the cell can be raised up to mbar range while the pressure in the main chamber kept around 1×10^{-5} mbar which is the safety limit for SPEM system. An encapsulated filament is behind the sample for heating, and other electrical connections are ready for biasing of sample, and thermocouple connections.

[1] D. F. Ogletree, et al. Rev. Sci. Instrum. 73, 3872 (2002)

[2] M. Amati, et al. J. Instrum. 8, 05001 (2013)

4:40pm **IS+AS+SA+SS-MoA8 In Situ Studies of Partial Oxidation of Methanol to Hydrogen on Isolated Bimetallic Site Pt₁Zn_n**, *Shiran Zhang, L. Nguyen*, University of Kansas, *A. Frenkel*, Yeshiva University, *J. Liu*, Arizona State University, *F. Tao*, University of Kansas

Partial oxidation of methanol to hydrogen and carbon dioxide offers a novel route in converting liquid fuel to hydrogen for fuel-cell systems and thus has been widely investigated in the past decade. One important category of heterogeneous catalysts for catalyzing this reaction is bimetallic nanoparticles which consist of continuous bimetallic sites in a metallic state. Isolation of such bimetallic sites through anchoring them on oxide could offer distinctly different catalytic performance in contrast to continuous sites on bimetallic nanoparticles.

Here we reported an isolated bimetallic site Pt₁Zn_n supported on ZnO which offers an extremely high catalytic activity with high selectivity for transformation of methanol to hydrogen with oxygen. It was prepared through a restructuring of singly dispersed Pt atoms on ZnO with reducing treatment. The formed isolated Pt atoms on ZnO was characterized with high-angle annular dark-field scanning transmission electron microscopy (HAADF-STEM) along the projected [10-10] of ZnO as well as the corresponding structural model (Figure 1). The bright spots show single dispersion of Pt atoms. The offset of Pt atoms to the Zn atom row suggests Pt atoms are on the column of oxygen atoms, which indicates the bonding of Pt atom to Zn atoms. Photoemission features of Pt4f of the catalyst during catalysis were tracked with ambient pressure X-ray photoelectron spectroscopy (AP-XPS) using monochromated Al K α (Figures 2). The resultant partial reduced state of Pt atoms under reaction condition is consistent with the electronic state of Pt in Pt₁Zn_n bimetallic site.

Catalytic performance of the formed isolated Pt₁Zn_n bimetallic site in partial oxidation of methanol was evaluated and compared with Pt-Zn bimetallic nanoparticle catalyst (Figure 3). Isolated Pt₁Zn_n bimetallic site catalyst exhibits much higher activity per active site and selectivity to H₂ than Pt-Zn nanoparticle catalyst in transformation of methanol to hydrogen through partial oxidation. The cationic nature of these isolated bimetallic site in contrast to the metallic nature of active sites on a nanoparticle could be responsible for the differences in catalytic performance. This study illustrates that isolation of continuous bimetallic sites on a nonmetallic support is a new opportunity to tune catalytic performance of bimetallic catalysts.

5:00pm **IS+AS+SA+SS-MoA9 New Developments in Small Spot and Imaging Near Ambient Pressure XPS**, *Andreas Thissen*, SPECS Surface Nano Analysis GmbH

Over the last 15 years, Near Ambient Pressure (NAP-) XPS has demonstrated its promising potential in a wide variety of applications. Starting from the Catalysis and Ice paradigm, the focus has shifted towards solid-liquid interfaces, liquid jets and in-situ electrochemistry. Initially, the experiments had to be carried out using advanced synchrotron sources to reach reasonable count rates. But now, the SPECS PHOIBOS 150 NAP offers optimized transmission for electrons, even at pressures up to and above 100mbar, so researchers can now use it with conventional X-ray and UV sources in their own laboratories. Because of the widened application fields, standard XPS is now also attainable when combined with easily adjustable monochromated X-ray sources that offer stable operation, small excitation spots, and high photon flux densities, even in Near Ambient Pressure conditions. The latest designs and results are presented showing small spot performance for spot sizes < 30 μ m, while also showcasing the latest implementations of imaging NAP-XPS that uses a new concept allowing for lateral resolved measurements without a compromise in count rate and usability. Highlighting on how sample environments (in situ cells for gases and liquids, electrochemical cells, gas inlets) and integration are both absolutely essential to obtain relevant results from well-defined samples, the presentation will demonstrate the use of NAP-XPS systems for high throughput-XPS measurements, as well as a variety of applications.

5:20pm **IS+AS+SA+SS-MoA10 In Situ Measurement of the Abundances and Temperatures of the Constituents of Semiconductor Manufacturing Plasmas via Terahertz Absorption Spectroscopy: Comparison with Theoretical Models**, *Yaser Helal, C.F. Neese, F.C. De Lucia*, The Ohio State University, *A. Agarwal, B. Craver, P.R. Ewing, P.J. Stout, M.D. Armacost*, Applied Materials, Inc.

Plasmas used by the semiconductor manufacturing industry are similar in pressure, temperature, and electron density to those used for the laboratory study of astrophysical neutrals, ions, and radicals. Thus, methods developed over several decades in the submillimeter/terahertz spectral region are directly applicable. Important attributes of terahertz absorption spectroscopy are that it can provide from first principles, without need for calibration, absolute concentrations and temperatures. Furthermore, since there are no intrusive probes, terahertz observations do not impact or change the plasma under study. Such measurements provide details and

insight into the interactions and reactions occurring within the plasma and their implications for semiconductor manufacturing processes. In this work, a continuous wave, 0.5 – 0.75 THz absorption spectrometer was developed and used to study the processes in a commercial inductively coupled plasma (ICP) etch chamber. Because of the relatively long wavelength of the terahertz radiation, diffraction is more serious than in the optical regime. As a result, an important part of this work was the development of optical strategies to couple this spectrometer to the plasma reactor using its existing viewports. Comparisons of the experimental results with predictions from equipment models for ICPs will also be presented for Ar/CF₄/CHF₃ with varying pressures, powers, and gas mixture ratios. Comparisons such as this provide a basis for validating and improving models, whose development is a complex and difficult science in itself. The results presented in this talk show that terahertz rotational spectroscopy can provide unique and easy to interpret information about manufacturing plasmas and is a useful development tool for process, theoretical and physical models, and the improvement of etch methods.

Nanometer-scale Science and Technology Room: 212B - Session NS+AS+SP-MoA

Optical Spectroscopy at the Nanoscale Moderator: Craig Prater, Anasys Instruments

2:20pm **NS+AS+SP-MoA1 Nanoscale Infrared Spectroscopy Characterization of Amyloid Aggregate Structure**, *Francesco Simone Ruggeri*, Ecole Polytechnique Fédérale de Lausanne (EPFL), Switzerland, *T. Muller*, University of Cambridge, UK, *D. Galante*, CNR, Italy, *T.P.J. Knowles*, University of Cambridge, UK, *H. Lashuel*, Ecole Polytechnique Fédérale de Lausanne (EPFL), Switzerland, *C. D'Arrigo*, CNR, Italy, *G. Dieter*, Ecole Polytechnique Fédérale de Lausanne (EPFL), Switzerland

INVITED

Aging of world population has increased the onset of several neurodegenerative disorders (ND). These diseases are connected with insoluble fibrillar proteins aggregates, termed Amyloid. During their aggregation, starting monomeric proteins undergo internal structural rearrangement bringing to fibrils with a final universal cross β -sheet quaternary structure. This structure is independent by the monomeric initial one and it is the fingerprint of amyloid and related diseases. Previously, the final fibrillar cross- β sheet structures were considered the cause of the illnesses. Nowadays, there is strong evidence that the intermediate oligomeric stages of fibrillation could be the cytotoxic one and most of the research groups are investigating the early stages of fibrillation and the inter-conversion of monomers into fibrils. Infrared spectroscopy is a key method for studying conformational properties of proteins and their structural conversion during amyloid fibrillation. Unfortunately, this and others bulk techniques are just able to give average information of the heterogeneous aggregating amyloid solution. To study the chemical structure of amyloid species at the nanoscale, we utilized a thermomechanical detection technique based on atomic force microscopy (nanoIR). If an IR pulse is absorbed by a sample, the local temperature rises and leads to a local thermal expansion. This deformation excites mechanical resonances of the AFM cantilever, in contact with the sample, allowing simultaneously acquiring topography, nanoscale chemical IR maps and/or spectra. We focused on the study of different amyloidogenic proteins, as α -synuclein, lysozyme and $\alpha\beta$ 42. We measured chemical spectra and IR maps of monomeric and fibrillar aggregates. For the first time, we distinguished chemically different amyloid structures at the single aggregate nanometer scale. Nanoscale chemical characterization of amyloidogenic structures as oligomers, protofibrils and fibrils is central to understand how proteins misfold and aggregate, to unravel the structural rearrangement of monomers inside amyloid fibrils and to target pharmacological approach to ND.

3:00pm **NS+AS+SP-MoA3 Recent Progress in Tip-Enhanced Mid-Infrared Photoexpansion Nanospectroscopy**, *M. Jin, F. Lu, Mikhail Belkin*, The University of Texas at Austin

INVITED

Mid-infrared absorption spectroscopy in the molecular fingerprint region (1/ λ ~600-4000 cm⁻¹) is widely used for chemical identification and quantitative analysis. The ability to perform mid-infrared spectroscopy with nanometer spatial resolution is highly desired for applications in chemical, materials, and life sciences. Nanoscale mid-infrared spectra can be obtained by detecting mechanical forces exerted by sample on an atomic force microscope (AFM) tip upon sample light absorption and photoexpansion. The first demonstration that photoexpansion of bulk polymers can be detected by AFM and used for mid-infrared nanospectroscopy was by Alexander Dazzi and co-workers [1]. However, only relatively thick polymer samples (approximately 50-nm-thick or thicker) produced

detectable cantilever deflections in these experiments, even when mid-infrared optical intensity was close to sample damage. We demonstrated that the sensitivity of mid-infrared photoexpansion nanospectroscopy, also known as AFM-IR, may be improved by several orders of magnitude if we send low-power laser pulses at a repetition frequency that is tuned in resonance with the mechanical vibrational frequency of an AFM cantilever and if we further employ tip-enhancement of the optical field below a sharp gold-coated AFM tip. As a result, monolayer sensitivity and 25 nanometer spatial resolution was achieved for molecular imaging in air [2]. We will discuss details of these experiments and recent progress of this technique, including development of background suppression methods that may lead to further enhancement in sensitivity and progress towards achieving photoexpansion nanospectroscopy of samples in aqueous environment that requires mitigation of liquid damping of cantilever vibration and strong infrared absorption.

[1] A. Dazzi, R. Prazeres, F. Glotin and J.M. Ortega, *Opt. Lett.* 30, 2388 (2005).

[2] F. Lu, M. Jin and M.A. Belkin, *Nature Photonics* 8, 307 (2014).

3:40pm **NS+AS+SP-MoA5 Nano-photonic Phenomena in van der Waals Heterostructures, Dmitri Basov**, University of California San Diego **INVITED**

Layered van der Waals (vdW) crystals consist of individual atomic planes weakly coupled by vdW interaction, similar to graphene monolayers in bulk graphite. These materials can harbor superconductivity and ferromagnetism with high transition temperatures, emit light and exhibit topologically protected surface states. An ambitious practical goal is to exploit atomic planes of vdW crystals as building blocks of more complex artificially stacked heterostructures where each such block will deliver layer-specific attributes for the purpose of their combined functionality. We investigated van der Waals heterostructures assembled from atomically thin layers of graphene and hexagonal boron nitride (Hbn). We observed a rich variety of optical effects due to surface plasmons in graphene and hyperbolic phonon polaritons in Hbn. We launched, detected and imaged plasmonic, phonon polaritonic and hybrid plasmon-phonon polariton waves in a setting of an antenna based nano-infrared apparatus. Peculiar properties of hyperbolic phonon polaritons in Hbn enabled sub-diffractive focusing in infrared frequencies. Because electronic, plasmonic and phonon polaritonic properties in van der Waals heterostructures are intertwined, gate voltage and/or details of layer assembly enable efficient control of nano-photonic effects. I will also discuss an ability to manipulate plasmonic response of in these structures at femto second time scales that we have demonstrated using a novel technique of pump-probe nano-infrared spectroscopy.

4:20pm **NS+AS+SP-MoA7 Ultrahigh Vacuum Tip-Enhanced Raman Spectroscopy and Fluorescence of a Self-Assembled Porphyrin Monolayer, Naihao Chiang***, N. Jiang, Northwestern University, D. Chulhai, Pennsylvania State University, E. Pozzi, M.C. Hersam, Northwestern University, L. Jensen, Pennsylvania State University, T. Seideman, R.P. Van Duyne, Northwestern University

The study of ultrahigh vacuum tip-enhanced Raman and fluorescence spectroscopy (UHV-TERS/TEF) has been raised to an unprecedented level. UHV-TER and TEF spectra for a self-assembled meso-tetrakis-(3,5-di-tert-butylphenyl)-porphyrin (H_2TBPP) on Ag(111) have been observed with five different laser excitations in the Q-band region. The observed TERS spectra are complemented by the time-dependent density functional theory (TDDFT) simulations. Chemical information of different vibronic excited states is revealed. The observed TEF spectra suggest a weak coupling of H_2TBPP to the surface due to the t-butyl groups. Therefore, the strong tip-enhancement is sufficient to overcome the quenching effect of the metal substrate. This study demonstrates the potential of combining TERS and TEF for studying surface-mounted porphyrins, thus setting the stage for future investigation into porphyrin-based photovoltaics and photocatalysis.

4:40pm **NS+AS+SP-MoA8 Nano-Optical Spectroscopic Imaging of Monolayer MoS_2 , Wei Bao§**, UC Berkeley, N. Borys, Lawrence Berkeley National Lab, C. Ko, J. Suh, W. Fan, UC Berkeley, A. Thron, Lawrence Berkeley National Lab, Y. Zhang, A. Buyanin, UC Berkeley, J. Zhang, S. Cabrini, P. Ashby, A. Weber-Bargioni, Lawrence Berkeley National Lab, S. Tongay, Arizona State University, S. Aloni, D. Ogletree, Lawrence Berkeley National Lab, J. Wu, UC Berkeley, M.B. Salmeron, Lawrence Berkeley Lab, UC Berkeley, P. Schuck, Lawrence Berkeley National Lab

With their remarkable electrical and optical properties, two dimensional (2D) monolayer transition metal dichalcogenide (ML-TMDC) semiconductors are ideal building blocks for atomically thin, flexible optoelectronic devices. Yet their performance falls far below theoretical

expectations, particularly for critical factors such as carrier mobility and quantum yield. Overcoming these problems requires a fundamental understanding of the optoelectronic properties of these materials at the nanoscale, which is best obtained with optical microscopy and spectroscopy tools with spatial resolution below the diffraction limit. Here, we use the recently-developed “Campanile” nano-optical probe¹ to spectroscopically image for the first time key optoelectronic properties in ML- MoS_2 with deeply sub-wavelength resolution – i.e., at a resolution commensurate with characteristic distances such as the exciton diffusion length. We find that synthetic ML- MoS_2 is composed of two distinct optoelectronic regions: a locally-ordered but mesoscopically heterogeneous interior, where photoluminescence (PL) intensity correlates with the local ratio of the exciton and trion populations, and an unexpected edge region ~300 nm wide of energetically disordered states. In addition, we directly visualize the spatially-varying optical properties of inter- and intra- flake grain boundaries and quantify the characteristic length over which they quench excitons. Complimentary Nano-Auger elemental analysis reveals that the optically “defective” grain boundary and edge regions are sulfur-deficient. The nanoscale structure-property relationships established here have broad implications for the development of atomically thin transistors, quantum optical components, photodetectors and light-emitting devices based on high-quality ML-TMDCs.

1 Bao, W. Mapping local charge recombination heterogeneity by multidimensional nanospectroscopic imaging, 1317-1321 (2012).

5:00pm **NS+AS+SP-MoA9 Hybrid Peak-force Tapping/near-field s-SNOM Microscope for Nano-chemical and Nano-mechanical Imaging of Proteins and Other Nanoscale Systems, Martin Wagner**, Bruker Nano Surfaces, K. Carneiro, S. Habelitz, University of California, T. Mueller, Bruker Nano Surfaces

Infrared spectroscopy can give valuable information on chemical composition, but far-field techniques such as FTIR spectroscopy are limited in spatial resolution. s-SNOM is a well-established near-field technique [1] that can overcome this diffraction limit, allowing an improvement in spatial resolution down to 10 nm.

Our s-SNOM instrument is based on an atomic force microscope whose tip is illuminated with a quantum cascade laser. Field-resolved detection of the scattered light measures absorption [2]. We have combined the instrument with peak-force tapping, a technique that allows Pn-level force control between tip and sample. Besides being able to image fragile material systems, one can extract valuable nano-mechanical information such as adhesion or modulus with molecular resolution [3].

Here, amongst other brief examples, we study an amelogenin sample. Amelogenin is a protein that is critical to dental enamel formation [4,5]. In the presence of calcium and phosphate ions it self-assembles into ordered, self-aligned nanoribbon bundles. Since the ordering is similar to the one observed in phosphate-based apatite crystals that comprise dental enamel, it is likely that the bundles form a template for these crystals. To help clarify that open question, we map the distributions of phosphate and hydroxyapatite nanocrystals within the bundles consisting of <30 nm narrow nanoribbons that have only a height of a few nm down to 1nm.

We present correlated topography, near-field and nano-mechanical data. While the presence of phosphate could be identified using s-SNOM absorption maps, no apatite nanocrystals with higher modulus than the ribbons were observed in peak-force tapping. This indicates that for these in vitro preparation conditions apatite crystals have not formed yet, but also highlights the high chemical sensitivity of the instrument.

In summary, using a novel combination of near-field imaging and peak-force tapping we study the phosphate distribution and crystallization in protein samples. Our findings help to understand the formation processes of dental enamel and the role of amelogenin protein.

[1] F. Keilmann, Hillenbrand R., *Phil. Trans. R. Soc. Lond. A* 362, 787 (2004)

[2] X. Xu, A. Tanur, G. Walker, *J. Phys. Chem. A* 117, 3348 (2013)

[3] F. Rico, C. Su, S. Scheuring, *Nano Lett.* 11, 3983 (2011)

[4] O. Martinez-Avila et al., *Biomacromolecules* 13, 3494 (2012)

[5] B. Sanii et al., *J Dent Res* 93 (9), 918 (2014)

* NSTD Student Award Finalist

Atom Probe Tomography Focus Topic

Room: 211D - Session AP+AS-TuM

New Applications of Atom Probe Tomography

Moderator: Arun Devaraj, Pacific Northwest National Laboratory

8:00am AP+AS-TuM1 **Development of Atom Probe Tomography for Studying Nuclear Corrosion Issues**, *Daniel Schreiber*, Pacific Northwest National Laboratory **INVITED**

Material degradation and corrosion create significant challenges to nuclear energy production, both in terms of the structural integrity of plant components and also in the long-term disposal of high-level radioactive waste. For structural materials, stress corrosion cracking (SCC) continues to be a prominent issue for Ni-base alloys in the high temperature (~320 °C in pressurized water reactors) corrosive reactor environment. Despite decades of research, there has yet to be a consensus on the fundamental mechanisms that control SCC response. On the other hand, the long-term disposition of high-level nuclear waste generated by nuclear energy production continues to be an open question. Vitrification of high-level waste into a relatively stable form (e.g. borosilicate glass) is being actively pursued. However, disagreement exists about the long-term stability of the glass if/when exposed to ground water in a geologic repository due to an ill-defined rate-limiting process controlling glass dissolution. In both cases, high-resolution microscopy techniques including atom probe tomography (APT) provide unique opportunities to test various mechanistic theories with unprecedented spatial resolution and chemical sensitivity. Such studies have only recently been made possible through the advancement of site-specific focused ion beam (FIB) sample preparation methods and pulsed-laser APT systems, creating a unique environment for revolutionary discoveries.

In this talk, I will discuss the development of APT methods for characterizing SCC microstructures in select model and commercial alloys and also for characterizing the dissolution of model vitrified nuclear waste glasses. The corrosion of metals and the dissolution of glass present unique but overlapping challenges in sample preparation, data acquisition and data interpretation that will be discussed in detail. Highlights will be presented in both cases on how APT is changing the way we view the fundamental mechanisms dictating SCC of metals and glass alteration.

8:40am AP+AS-TuM3 **Using Aqueous Solutions by Cryo-Fixation As a Matrix for Analyzing Materials in APT**, *Stephan Gerstl, B. Scherrer*, ETH Zürich, Switzerland, *J.M. Cairney*, University of Sydney, Australia, *R. Spolenak, R. Wepf*, ETH Zürich, Switzerland **INVITED**

Atom probe tomography has progressively engaged the world of materials characterization with 3-dimensional nanometer-level maps of various dense materials. These atom maps have been the attraction of the technique because they enable new perspectives and analysis of solid materials literally atom by atom. The analysis of soft organic materials, even aqueous solutions, has however been a long-standing issue as it is impaired by contamination, uncertain phase formation, and questionable observed states. These outcomes have been interrogated, retested, and re-analyzed to better understand the artifacts involved. Here we present the development steps achieved together with the APT results obtained of three aqueous based solutions: a water-based citrate solution, a 1:1 water-ethanol mixture, and a commercially available marginally alcoholic beverage. These aqueous solutions were chosen so as to exhibit differences in their mass-spectrum response due to their dissimilarities. The methodologies enabling these analyses require arresting the liquids so they are stable in vacuum environments, sharpening them to a needle geometry, and transporting them between chambers whilst not altering their structural integrity; all steps being done close to LN₂ temperatures. The main challenge was with contamination, which needs to be minimized and separated from the material of interest in the analysis. The cryo-fixation method involves plunge freezing the region of interest (ROI) in cryogenic liquids, sharpening the ROI in a FIB fitted with a cryogenically cooled stage, and field evaporating it in a retrofitted cryo-transfer enabled LEAP 4000X-HR.

All aqueous specimens could be analyzed successfully; with the resulting amounts of ROI analyzed being small (only a thin film is probed due to sample geometry), trends and fluctuations in ion concentrations have been interrogated and will be presented.

The application space of this technique will be considered in terms of using fluids as matrices and designing the experiments to increase the volume of soft materials analyzed.

11:00am AP+AS-TuM10 **Atom Probe Tomography Investigation of TiSiN Thin Films Made Possible by ¹⁵N Isotopic Substitution**, *David Engberg*, Linköping University, Sweden, *L.J.S. Johnson*, Sandvik Coromant, Sweden, *M.P. Johansson-Jöesaar*, SECO Tools AB, Sweden, *M. Odén*, Linköping University, Sweden, *M. Thuvander*, Chalmers University of Technology, Sweden, *L. Hultman*, Linköping University, Sweden

TiSiN is one of the most important materials for commercial wear resistant coatings on cutting tools. Understanding of the growth and structure of these coatings has become increasingly important for optimizing their performance. Yet knowledge regarding the solid solubility, distribution, and stoichiometry of SiN_y has been lacking in the complex metastable TiN-SiN structure. Atom probe tomography (APT) in combination with analytical electron microscopy provides a way to attain compositional information in 3D on the nanometer scale. However, mass spectrum overlaps of N and Si ions have so far prevented such APT analyses. By growing TiSiN coatings with ¹⁵N using cathodic arc deposition, we show that the mass spectrum overlaps of Si and N can be largely avoided. TiSi¹⁵N films of two compositions, Ti_{0.81}Si_{0.19}¹⁵N and Ti_{0.92}Si_{0.08}¹⁵N in a predominantly cubic structure, have been studied using APT. We find evidence of Si-Si clustering on the nanometer scale, while there are no indications of overstoichiometric SiN_y (y ≈ 1).

11:20am AP+AS-TuM11 **Investigating the Alternating Cation/Anion Compositions in a High-Voltage Li-Mn-Rich Oxide Electrode during First Charge-Discharge Cycle using Atom Probe Tomography**, *Baishakhi Mazumder, D. Mohanty, C. Daniel, D. Wood III*, Oak Ridge National Laboratory

High-voltage layered lithium and manganese-rich (LMR) oxides are potential cathodes for high-energy-density lithium-ion batteries for electric vehicles. Unfortunately, structural transformation during charging and discharging in these oxides leads to undesired phenomena, such as voltage fade during subsequent cycles and lower columbic efficiency in the first cycle, that remain stumbling blocks for practical usage. Understanding the micro-structural changes during the first cycle is critical to obtaining fundamental insight regarding the activation mechanism(s) related to the first cycle capacity loss. In this work, Atom Probe Tomography (APT) has been employed to obtain the 3D microstructural and sub-nm-level compositional information of LMR oxides during the first cycle to resolve the activation mechanism(s) that lead to structural transformation.

The greatest challenge for APT analysis from the actual electrode materials is the complexity in creating needle-shaped specimens. Owing to the discontinuous geometry of the electrode, which is characterized by non-uniform interconnected channels, it is extremely difficult to make a structurally stable needle for controlled field evaporation. Micro-fractures and irregular evaporation due to differences in evaporation fields between the composite elements during APT analysis is also challenging. Additionally, experimental parameters, including tip temperature, laser energy, and detection rate, all strongly impact the field-evaporation and subsequent data analysis. By overcoming these challenges, reliable and reproducible data has been obtained after optimizing the experimental parameters and developing a reliable procedure to prepare stable samples. Mass spectra reveal molecular complexes M_xO_y for M=Ni,Mn,Co, while the Li appears predominantly as elemental ions. The 3D distributions as well as the compositions of each element were obtained for each sample at different states of charge during the first cycle. These data provides insight towards understanding the structural rearrangements during the first charge-discharge cycle that correlates with the first cycle irreversible capacity loss.

1) M.M. Thackeray, et al., J. Mat. Chem. 17 3112 (2007)

2) D. Mohanty, et al., Chem. Mat. 26 6272 (2014)

Research supported by CNMS, which is a DOE Office of Science User Facility. LMR material was obtained from Argonne National Laboratory. The electrodes/cell fabrication, and cell testing were carried out at the DOE's Battery Manufacturing R&D Facility at Oak Ridge National Laboratory, which is supported by VTO within the core funding of the ABR subprogram. Authors thank Dr. Jianlin Li at ORNL for fabricating electrodes.

Applied Surface Science

Room: 212D - Session AS+NS-TuM

Chemical/Molecular Information from Sub-micron Features and Materials

Moderator: Carl Ventrice, Jr., SUNY Polytechnic Institute, David Carr, Physical Electronics USA

8:40am AS+NS-TuM3 **ASSD 30th Anniversary Speaker: Defect Detection and Characterization in Wafer Processing and Magnetic Storage Technologies – Then, Now and (maybe) the Future.** *Christopher Brundle*, C R Brundle and Associates **INVITED**

Some 30 years ago defects (“particles”) in wafer processing were unacceptable for sizes in the um range. Today the specification is 23nm and will soon be 19nm. These numbers are, of course, directly related to the ever decreasing dimensions of semiconductor devices. This paper gives a historical overview of the evolution of the techniques used in defect detection and characterization for both Development and Manufacturing over this period, and what might be needed in the future.

In Magnetic Storage key dimensions have decreased at a similar pace and similar defect and quality control issues obtain. Some of these will also be discussed, if there is time.

Examples are presented where possible, but there is an understandable difficulty in obtaining release for real examples of defects concerning current forefront technology!

9:20am AS+NS-TuM5 **Characterisation of Glass-To-Metal Interfaces using FIB and STEM.** *Paul Yates*, University of Surrey, UK

Components needing electrical feed through seals are frequently made with glass-to-metal seals and have been for many years. They are often made with stainless steel and silicate glasses but, in order to save weight or for biomedical uses, titanium components are sometimes required. Silicate free glasses are required due to the deleterious reaction that occur between titanium and silicate glasses. The reactions in these systems are not fully understood. When characterising the interfaces and assessing interface quality the standard approach is to use cross sections and characterise with scanning electron microscopy and energy-dispersive x-ray spectroscopy. Although this can reveal micrometer scale processes it can not reveal the nano scale reactions that determine the bonding across the interface in many cases. In this work focussed ion beam milling and scanning transmission electron microscopy are used to attain nano scale information about selected areas of the interface between titanium and a strontium boroaluminate glass-ceramic. Additionally, reactions between the glass-ceramic and Kovar (Fe-29Ni-17Co), a common glass sealing alloy, are characterised. Oxidation of the Kovar surface creates an oxide, characterised with x-ray photoelectron spectroscopy and x-ray diffraction, that improves bonding across the interface compared to the native oxide.

9:40am AS+NS-TuM6 **X-ray Structural Analysis of Self-assembled Nano-Dielectrics.** *Li Zeng, A. Walker*, Northwestern University, *R. Turrisi*, University of Milano-Bicocca, Italy, *M.C. Hersam, T.J. Marks, M.J. Bedzyk*, Northwestern University

Organic thin-film transistors (OTFTs) are viewed as the new generation thin-film transistors (TFT) for future low-cost, printable, structural flexible electronics, and related processable solution-based organic and inorganic semiconductors. However, one major limitation of OTFTs is that the organics semiconductors exhibit relatively low carrier mobility, which requires high operating voltage in order to achieve an operational drain current. One route to reduce the operation voltage is to increase the capacitance of the dielectric layer as the drain current increases linearly with respect to the dielectric capacitance for constant operating voltages and channel dimensions. A class of materials called self-assembled nano-dielectrics (SAND) with phosphoric acid-functionalized organic precursors sandwiched between ultrathin layers of high-*k* inorganic oxide materials has been synthesized and applied in the TFT field. These materials show exceptionally large capacitance, excellent insulating properties, and are also suitable for ambient atmosphere fabrication. The hybrid nature of these materials utilizing the distinct properties of both the organic and inorganic components can be incorporated into the low-operating voltage semiconductor-based OTFTs to enhance the performance.

Despite the impressive performance and flexibility of SANDs, some fundamental aspects of dielectric behavior remain unexplored. Particularly, the behavior of the Br⁻ counteranions that are paired with the phosphonic acid-based -electron (PAE) cationic building blocks are poorly understood. It is believed that the location, distribution of the Br⁻ counteranions, as well as their response to applied AC and DC electric fields, are critical to the

behavior of the dielectric in device-like environments. Therefore, long-period X-ray Standing Wave (LP-XSW), which is a powerful technique sensitive to heavy atom distributions, was used to characterize a three-layer SAND structure deposited on synthetic Si/Mo multilayer substrates. The elemental distributions of Br and reference elements were extracted from the analysis of XSW data. These accurate measurements are important for better understanding counteranion distributions, charge transport, dipole-semiconductor interactions, and future device modeling and engineering.

11:00am AS+NS-TuM10 **Multimodal Imaging for Physical and Chemical Surface Characterization using a Combined Atomic Force Microscopy-Mass Spectrometry Platform.** *Olga Ovchinnikova*, Oak Ridge National Laboratory **INVITED**

The functionality of materials is largely determined by the mechanisms that take place at sub-micron length scales and at interfaces. In order to understand these complex material systems and further improve them, it is necessary to measure and map variations in properties and functionality at the relevant physical, chemical, and temporal length scales. The goal of multimodal imaging is to transcend the existing analytical capabilities for nanometer scale spatially resolved material characterization at interfaces through a unique merger of advanced scanning probe microscopy, mass spectrometry and optical spectroscopy. Combining atomic force microscopy (AFM) and mass spectrometry (MS) onto one platform has been demonstrated by our group as a method for high resolution spot sampling and imaging of substrates. To advance this basic approach and to expand its capabilities we now have incorporated Band-Excitation (BE) to allow us to measure nanomechanical properties of a sample by measuring the contact resonance frequency shift. In this presentation, I will discuss the benefits of a multimodal imaging system and demonstrate our results for polymeric systems, biological plant and animal tissue, and bacterial colonies. I will also talk about future developments to incorporate spectroscopic measurements into the platform.

This work was supported by the Division of Chemical Sciences, Geosciences, and Biosciences, Office of Basic Energy Sciences, United States Department of Energy. ORNL is managed by UT-Battelle, LLC for the U.S. Department of Energy under contract DE-AC05-00OR22725.

11:40am AS+NS-TuM12 **Understanding the TERS Effect with On-line Tunneling and Force Feedback Using Multiprobe AFM/NSOM with Raman Integration.** *A. Lewis*, The Hebrew University of Jerusalem and Nanonics Imaging Ltd, Israel, *Rimma Dekhter, P. Hamra, Y. Bar-David, H. Taha*, Nanonics Imaging Ltd, Jerusalem, Israel

Tip enhanced Raman scattering (TERS) has evolved in several directions over the past years. The data from this variety of methodologies has now accumulated to the point that there is a reasonable possibility of evolving an understanding of the underlying cause of the resulting effects that could be the origin of the various TERS enhancement processes.

The objective of this presentation is to use the results thus far with atomic force microscopy (AFM) probes with noble metal coating, etching, transparent gold nanoparticles with and without a second nanoparticle [Wang and Schultz, ANALYST 138, 3150 (2013)] and tunneling feedback probes [R. Zhang et. al., NATURE 498, 82 (2013)]. We attempt at understanding this complex of results with AFM/NSOM multiprobe techniques. Results indicate that TERS is dominated by complex quantum interactions. This produces a highly confined and broadband plasmon field with all *k* vectors for effective excitation. Normal force tuning fork feedback with exposed tip probes provides an excellent means to investigate these effects with TERS probes that we have shown can circumvent the vexing problem of jump to contact prevalent in conventional AFM methodology and permit on-line switching between tunneling and AFM feedback modes of operation.

12:00pm AS+NS-TuM13 **High Resolution CREM for Electrical Characterization of Thin Oxide Layers.** *Hagai Cohen, A. Givon*, Weizmann Institute of Science, Israel

The chemically resolved electrical measurements technique (CREM) has already been proven very useful in studies of nanometric layered structures. CREM exploits the chemical contrast across a studied system to probe the local, domain specific, electrostatic potential in a non-contact manner. As such, its spatial resolution is usually determined by the studied structure itself, other than the probe size; a fact imposing severe limitations when nm, or even sub-nm, resolution is requested. In the present work we show that this inherent limitation can be overcome. Improved CREM resolution is established, with which a principal progress is demonstrated in the access to fine details of the electrical properties of nanometric SiO₂ layers grown on SiC substrates.

Photocatalysis

Moderator: Jason Baxter, Drexel University, Manjula Nandasiri, Pacific Northwest National Laboratory

8:00am EN+AS+EM+SE+SS-TuM1 **Ultra-dense Hydrogen and Low Energy Nuclear Reactions**, Sveinn Ólafsson, Science Institute, Physics Department University of Iceland, L. Holmlid, University of Gothenburg, Sweden

For over the last 25 years the science of cold fusion/LENR has been researched around the world with slow pace of progress. Modest quantity of excess heat and signatures of nuclear transmutation and helium production have been confirmed in experiments and theoretical work has resulted in a flora of possible theoretical scenarios. [1-2]

Here we present energy production in several stages of surface processes that result first in the formation of Rydberg matter of Hydrogen [3] that can later condense in a new ultra-dense Hydrogen phase with 2.3 pm short bond distances. This phase is nuclear active showing break-even fusion reaction [7] under 100mW laser pulsing and slow spontaneous fusion occurring without laser pulsing[4,5,6]. The experimental work in around 30 publications is briefly reviewed and latest experimental results presented and discussed.

In that work high-energy particles are detected from the spontaneous processes using scintillation and other similar detectors. Both spontaneous line-spectra and a spontaneous broad energy distribution similar to a beta-decay distribution are observed indicating detection of particles such as muons. The broad distribution is concluded to be due to nuclear particles, giving straight-line Kurie-like plots. They are observed even at a distance of 3 m in air and have a total rate of 10^7 - 10^{10} s⁻¹. In the talk the link of these observation to Low energy nuclear reactions (LENR) or so called cold fusion will be discussed experimentally and theoretically.

1. The science of low energy nuclear reaction.

Storms E. World Scientific Publishing Company; 2007.

2. The explanation of low energy nuclear reaction.

Storms E. Ienergy Press; 2014.

3. Review paper: Experimental Studies and Observations of Clusters of Rydberg Matter and Its Extreme Forms Leif Holmlid. *J Clust Sci* (2012) 23:5–34

4. Spontaneous ejection of high-energy particles from ultra-dense deuterium D(0)

Leif Holmlid and Sveinn Ólafsson

Volume 40, Issue 33, 7 September 2015, Pages 10559–10567)

5. Charged particle energy spectra from laser-induced processes: nuclear fusion in ultra-dense deuterium D(0) Leif Holmlid and Sveinn Ólafsson submitted 2015.

6. Muon detection studied by pulse-height energy analysis: Novel converter arrangements

Leif Holmlid and Sveinn Ólafsson. *Rev. Sci. Instrum.* 86, 083306 (2015);

7. Heat generation above break-even from laser-induced fusion in ultra-dense deuterium

Leif Holmlid. *AIP Advances* 5, 087129 (2015);

8:20am EN+AS+EM+SE+SS-TuM2 **Optical and Surface Properties of Semiconductor Nanowires for Solar Fuels**, Eleonora Frau, J. Vukajlovic, A. Dalmau-Mallorqui, A. Fonctuberta i Morral, E. Alarcon Llado, Ecole Polytechnique Fédérale de Lausanne (EPFL), Switzerland

Semiconductor nanowires (NWs) are filamentary crystals with new properties from their bulk counterparts. Their large versatility makes them excellent candidates as building blocks for contributing to solving the energy problem in the near future. In this work, we will assess two main properties of semiconductor NWs that have an impact to solar energy conversion.

First, it is known that light is strongly absorbed by NW arrays since light resonances give rise to effective absorption cross-sections that are much larger than the geometrical ones. Optical resonances depend on NW geometry and dielectric environment, and can result into absorption effective diameters up to 25 times larger than the geometrical for certain wavelengths. We have used finite-difference time-domain (FDTD) electromagnetic simulations to understand and design NW-based sunlight scavengers. For instance, a GaAs NW array that is only covering 3% of the surface can generate more photocurrent than a planar film, considering a

30% reflectivity (see figure1). Also that thanks to optical resonances, an indirect-bandgap material such as Si is capable of absorbing most of the light within a 2um long NW array that only covers 7% of the device surface.

On the other hand, it is also known that surface states and traps detriment device performances. However, in case where solar energy is directly converted into fuel (such as hydrogen) in a photoelectrochemical (PEC) cell, the large surface-to-volume ratio of NW forests is an important asset. Since the electrochemical reactions happen at the semiconductor surface, NWs enable the use of low-cost catalysts (e.g. MoSx) even though they exhibit lower performances than noble metals (e.g. Pt). In order to assess the effects of nanostructuring photo-electrodes for solar fuel generation, we have studied photo-cathodes based on Silicon nanopillar structures. The photo-cathodes were fabricated by using a top-down approach and their diameters range from ~200 to 900nm and lengths ~2um. We observe that reducing the size of the nanostructure, increases the overpotential, and thus the overall efficiency (see figure 2). By coating the surface with thin TiO₂ layers, the performance is improved in terms of overpotential and fill factor. We explain these findings by using an electrico-kinetic model of the semiconductor-water junction. We find that the TiO₂ layers actually act as a hole blocking layer, preventing recombination.

8:40am EN+AS+EM+SE+SS-TuM3 **Engineering Surfaces and Interfaces for Photoelectrochemical (PEC) Water-Splitting**, Thomas Jaramillo, J.D. Benck, Stanford University, J. Kibsgaard, SLAC National Accelerator Laboratory, T.R. Hellstern, C.J. Hahn, P. Chakthranont, R. Britto, K.D. Fong, Stanford University **INVITED**

The talk will focus on engineering surfaces and interfaces for solar photoelectrochemical (PEC) water-splitting for the direct, renewable production of H₂. In particular, this talk begin by describing research efforts to develop H₂ evolution catalysts that are active, stable, and comprised of only earth-abundant elements, including transition metal sulphides, phosphides, and phosphosulfides.¹⁻³ Next, we will describe recent efforts to integrate these catalysts onto semiconductor surfaces to provide corrosion protection as well as enhanced interfacial catalysis for PEC water-splitting.⁴ This talk will focus on the need for high turnover frequency (TOF) catalysts, which ultimately enable the greatest flexibility in designing optimum interfaces for high performance devices.

[1] J. Kibsgaard, T.F. Jaramillo, F. Besenbacher, "Building an appropriate active site motif into a hydrogen evolution catalyst with thiomolybdate [Mo₃S₁₃]²⁻ clusters," *Nature Chemistry*, 6 (2014) 248.

[2] J.D. Benck, T.R. Hellstern, J. Kibsgaard, P. Chakthranont, T.F. Jaramillo, "Catalyzing the Hydrogen Evolution Reaction (HER) with Molybdenum Sulfide Nanomaterials," *ACS Catalysis*, 4 (2014) 3957.

[3] J. Kibsgaard and T.F. Jaramillo, "Molybdenum Phosphosulfide: An Active, Acid-Stable Earth-Abundant Catalyst for the Hydrogen Evolution Reaction," *Angewandte Chemie*, 53 (2014) 14433.

[4] J.D. Benck, S.C. Lee, K.D. Fong, J. Kibsgaard, R. Sinclair, T.F. Jaramillo, "Designing active and stable silicon photocathodes for solar hydrogen production using molybdenum sulfide nanomaterials," *Advanced Energy Materials*, 4 (2014) 1400739.

9:20am EN+AS+EM+SE+SS-TuM5 **Bulk and Surface Effects of Incorporating Titanium Into Hematite Thin Films to Improve Photoelectrochemical Water Splitting**, Anthony Abel, A.M. Patel, Drexel University, I.G. Torregrosa, Utrecht University, Netherlands, B. Opananont, J.B. Baxter, Drexel University

Hematite (α -Fe₂O₃) has emerged as a promising photoanode material for photoelectrochemical (PEC) water splitting due to its chemical stability, earth-abundance, low cost, and suitable band gap for both water splitting and visible light absorption. However, poor charge separation due to low hole mobility and high recombination rate, and sluggish oxygen evolution reaction kinetics have limited its potential as an economical water-splitting catalyst. Here, we investigate titanium incorporation into hematite photoanodes and provide insight into the role of Ti⁴⁺ in improving PEC performance. Planar hematite thin films (~45 nm thick) were deposited by successive ionic layer adsorption and reaction (SILAR) of FeOOH on an FTO/glass substrate and subsequent annealing to induce phase transition to α -Fe₂O₃, and titanium was incorporated up to 10% Ti/(Ti+Fe) by either modification of the SILAR solution (SM: α -Fe₂O₃) or solid-state diffusion (SSD: α -Fe₂O₃) during the annealing process. PEC measurements revealed substantial improvements in both charge separation efficiency and hole injection into the electrolyte, increasing photocurrent from nearly zero to ~0.6 mAcm⁻² under 1-sun irradiation at 1.23 V_{RHE}. Mott-Schottky analysis indicated a 100 mV cathodic shift in the flat band potential upon doping with Ti⁴⁺ regardless of fabrication method, but a 100-fold increase in carrier density only in SM: α -Fe₂O₃ films, resulting in a high 20 % separation efficiency at 1.23 V_{RHE} with optimized 5 % Ti/(Ti+Fe) in the modified SILAR solution. Electrochemical impedance spectroscopy showed a 4x

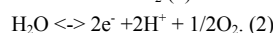
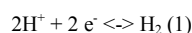
increase in the surface state capacitance peak near the water oxidation onset potential, possibly due to reduced Fermi level pinning as a result of more efficient hole injection into the electrolyte. More importantly, doping with titanium resulted in a 100-fold decrease in the charge transfer resistance from surface states to the electrolyte, revealing the strong influence of Ti^{4+} on interfacial kinetics. Further surface modification with an ultrathin FeOOH surface passivation layer raised the plateau photocurrent to ~ 0.8 mA/cm² at 1.23 V_{RHE}, representing a 3x improvement over previous reports of SILAR-deposited hematite films and comparable with record performance for planar hematite deposited using high vacuum synthesis techniques.

9:40am **EN+AS+EM+SE+SS-TuM6 Iron Oxide Nanoparticle Growth on Highly Oriented Pyrolytic Graphite (HOPG) and Photocatalytic Properties of Pt on Iron Oxide**, Jayde Kwon, J.C. Hemminger, University of California, Irvine

Highly oriented pyrolytic graphite (HOPG) is an ideal substrate to study the fundamental growth mechanism of iron oxide independent from substrate effects. Platinum on iron oxide is a model heterogeneous catalyst with importance to biotechnology and solar cell applications. Selective growth of iron oxide nanoparticle (NP) either on step edges of HOPG or oxygen plasma treated HOPG by physical vapor deposition (PVD) will be presented. The successful selective iron oxide NP growth was validated by scanning electron microscopy (SEM), transmission electron microscopy (TEM), and X-ray photoelectron spectroscopy (XPS). The development of the NP array system is highly significant in that it can provide an ideal template for theoretical calculations for fundamental metal growth studies. Pt nanoparticles were subsequently deposited on the iron oxide nanoparticles using a selective photodeposition technique. The application of these nano-systems (Pt nanoparticles on iron oxide nanoparticles) towards photocatalysis of methylene blue will be presented. Although iron oxide is a promising semiconductor photocatalyst, it suffers from a short hole diffusion length, low electrical conductivity and a high rate of electron hole recombination. However, this bimetallic system using platinum deposited on iron oxide overcomes these barriers. A novel method was developed using small quantities of Pt on iron oxide to significantly enhance methylene blue decomposition. This system is also being explored as a catalytic model for water-gas shift reactions.

11:00am **EN+AS+EM+SE+SS-TuM10 Interface Design for Efficient and Stable Photoelectrochemical Water Splitting**, Joel Ager, Lawrence Berkeley National Laboratory **INVITED**

Solar photoelectrochemical (PEC) water splitting is potential future carbon-neutral energy source which could dramatically change the landscape of global energy generation and storage. The half reactions for water splitting are as follows:



The free energy change for the overall reaction, $H_2O \leftrightarrow H_2 + 1/2O_2$ corresponds to 1.23 eV per electron transferred; however, typically >1.5 V is required to overcome kinetic limitations, particularly for the O_2 evolution reaction. The most commonly used approach for integrated solar water splitting employs photocathodes (H_2 or hydrocarbon producing) and photoanodes (O_2 producing) linked in a tandem geometry [1].

The interface challenges required to demonstrate a practical system which is both efficient and stable under operation are substantial and severe. In addition to constructing interfaces, either solid-solid or solid liquid, which achieve the desired photovoltaic charge separation, the surfaces of these photoelectrodes can be a failure point under sustained operation due to corrosion. We have found that the use of nanoscale conformal oxide layers can greatly reduce corrosion rates. Moreover, it is possible to achieve both high performance and lifetime by the use of protection layers which are also tuned for selective carrier contact.

Examples of such a strategy will be shown for photocathodes [2-5] and for photoanodes [5]. Recent work on p-type transparent oxides (p-TCOs) used as selective hole contacts for photoanodes will be emphasized. For example, it will be shown that using $NiCo_2O_4$ as the p-TCO and n-type Si as a prototypical light absorber, a rectifying heterojunction capable of light driven water oxidation can be created. By placing the charge separating junction in the Si using a np^+ structure and by incorporating a highly active Ni-Fe oxygen evolution catalyst, efficient light-driven water oxidation can be achieved. The generality of the p-TCO protection approach is demonstrated by multi-hour, stable, water oxidation with n-InP/p- $NiCo_2O_4$ heterojunction photoanodes.

Acknowledgements. This material is based upon work performed by the Joint Center for Artificial Photosynthesis, a DOE Energy Innovation Hub, supported through the Office of Science of the U.S. Department of Energy under Award Number DE-SC0004993.

References.

1. J. W. Ager *et al.*, *Energy Environ. Sci.* (2015). DOI:10.1039/C5EE00457H
2. M. H. Lee *et al.*, *Ang. Chemie Int. Edition* **51** 10760 (2012).
2. Y. Lin *et al.*, *Nano Letters* **13** 5615 11 (2013)
3. Y. Lin *et al.*, *J. Phys. Chem. C* **119**, 2308 (2015).
4. J. Yang *et al.*, *J. Amer. Chem. Soc.* **136** 6191 (2014).

11:40am **EN+AS+EM+SE+SS-TuM12 Buried, Hetero, and p-i-electrolyte III-V Photoelectrochemical Junctions with Significantly Enhanced Photocurrent Onset Potentials**, James Young, H. Doscher, J. Turner, T. Deutsch, National Renewable Energy Laboratory

To approach the maximum achievable solar-to-hydrogen (STH) conversion efficiencies with photoelectrochemical (PEC) devices, it is necessary to employ the lowest possible band gap (E_g) absorbers that can still provide sufficient voltage to drive water splitting at high rates (1.7-1.8 V for 25% STH). The record 12.4% STH was achieved by a GaInP₂/GaAs PEC/photovoltaic (PV) tandem device while an all solid state GaInP₂/GaAs PV/PV tandem produces an open-circuit voltage that approaches 2.4 V. Since GaAs ($E_g = 1.4$ eV) is the current-limiting junction in these devices, it can be substituted by InGaAs with $E_g = 1.0$ eV to reach 25% STH. The current-for-voltage tradeoff of using lower- E_g absorbers moves toward the constraint of insufficient voltage for spontaneous water splitting. To address this approaching constraint, we investigate several alternative device structures at the III-V/electrolyte interface that show photocurrent onset potential enhancements of a few hundred mV. We will present band diagram calculations and electrochemical measurements to discuss the voltage performance of these structures.

12:00pm **EN+AS+EM+SE+SS-TuM13 X-ray Absorption Studies on the Li-S Battery Cathode Side**, Yifan Ye, University of Science and Technology of China, A. Kawase, Lawrence Berkeley National Laboratory, H.X. Ju, University of Science and Technology of China, E. Cairns, Lawrence Berkeley National Laboratory, J.-H. Guo, Lawrence Berkeley Lab, University of California, Berkeley, J.F. Zhu, University of Science and Technology of China

As increasing global energy consumption in the coming days, sustainable, clean energy technologies are highly desirable. The high theoretical specific capacity of 1675 mA·h/g for elemental S has prompted intense effort to study the Lithium-Sulfur batteries. With the application of cetyltrimethyl ammonium bromide (CTAB), modified sulfur-graphene oxide (S-GO) nano-composite based Li/S batteries exhibited a very high initial discharge capacity of 1440 mA·h/g of sulfur at 0.2C with excellent rate capability of up to 6C for discharge and 3C for charge while still maintaining high specific capacity. And the batteries demonstrated cycling performance up to 1500 cycles with extremely low decay rate of 0.039% per cycle. With the introduction of CTAB, the performance of the GO-S based Li-S battery has been improved significantly, thus it is important to figure out the role of CTAB played in the system. During the synthesis process of the cathode materials, S and Na₂S were used as the precursors, the ratio of S/Na₂S is crucial to the components of the precursors. Moreover, the sequence of mixing GO/CTAB solution with precursor solution is a key point to effective cathode synthesis procedure. Understanding these information helps to optimize the methodology for the controllable synthesis of desired cathode material that can be used to fabricate an efficiency and well-performed Li/S battery. S K-edge X-ray absorption spectroscopy (XAS) is applied to study the chemical species evolution during the GO-S-CTAB cathode material synthesis. The influences on the cathode materials related to the battery performance are monitored by S K-edge XAS. The research revealed the interaction between CTAB and GO, S, Na₂S and Na₂S_x. It indicated that CTAB can physical adsorbed on Na₂S_x molecules by bonding with the terminal S atoms of Na₂S_x chains, and this kind of bonding can convert to chemical C-S bonding with heating treatment. Thus the interaction of CTAB with GO, formed C-S between CTAB and S and interaction of GO and S provided a tight tri-layer structure which can immobilize the S particles on GO sheet and finally enhanced the battery performance. The information from this work proved the importance of Na₂S:S ratio, CTAB/GO adding procedure in the fabrication process, and we can easily apply XAS to optimize these recipe. And moreover, this work proved strong evidence that XAS tools can be used to do the initial characterization on the battery performance before real cycling procedure.

In-Situ Spectroscopy and Microscopy Focus Topic
Room: 211C - Session IS+AS+SA+SS-TuM

In-situ Studies of Solid-liquid Interfaces

Moderator: Anatoly Frenkel, Yeshiva University, Franklin (Feng) Tao, University of Kansas

8:20am **IS+AS+SA+SS-TuM2 Water at Ionic Liquid Interfaces Probed by APXPS, John Newberg, Y. Khalifa, A. Broderick, University of Delaware**

Ionic liquids (ILs) have a wide array of applications in biotechnology, coatings, synthesis, separations, and energy sciences. Many of these processes involve either IL-solid or IL-vapor interactions. It is therefore critical we understand the fundamental interfacial properties of ILs on a molecular level. Due to the ubiquity of water, its influence on the properties of ILs has been the focus of many bulk studies and, more recently, surface science studies. Here we will highlight the use of a recently commissioned ambient pressure X-ray photoelectron spectroscopy setup in our laboratory and its application in characterizing the interfacial region of hydrophilic and hydrophobic ILs upon interaction with water vapor as a function of increasing pressure.

8:40am **IS+AS+SA+SS-TuM3 Probing the Liquid-Solid Interface of polycrystalline Pt in 1.0 M KOH using Ambient Pressure Photoemission Spectroscopy and "Tender" X-rays, Marco Favaro, B. Jeon, P.N. Ross, Z. Hussain, J. Yano, Z. Liu, E.J. Crumlin, Lawrence Berkeley National Laboratory (LBNL)**

With the previous success in soft X-ray AP-XPS gas-solid interface^{1a-c} probing, researchers have started to gain insights into the liquid-solid boundaries^{1d}. Taking the cue from these new research frontiers, we have developed on BL 9.3.1 at the Advanced Light Source (LBNL) a new liquid phase AP-XPS system (based on a Scienta R4000 HiPP-2 analyzer) that will shed new light on the understanding of the chemical changes at the electrode surfaces during normal working conditions, leading to a great enhancement of our knowledge on the most important processes in energy conversion and storage^{2a,b}. The combination of this new system with synchrotron radiation in the "tender" X-ray region (between 2 and 7 keV), allows us to probe the interface between thin liquid and solid phases using high kinetic energy photons and then, thanks to the *in operando* approach, directly track the phenomena occurring at the electrode liquid-solid interface during the electrochemical reactions of interest. The technique developed at BL 9.3.1 allows the study of both gas-liquid and liquid-solid interfaces, for pressures up to a hundred of Torr^{2a}.

In order to deeply investigate the possibilities offered by this new technique and, at the same time, to establish a benchmark, a reference material such as polycrystalline Pt has been studied in 1.0 M KOH electrolyte. In this talk we will demonstrate that it is possible to have fine control of the applied potential^{2a,b}, measuring the core level binding energy shift of the oxygen *1s* and potassium *2p* photoemission lines, according to the applied external potential. Moreover we will discuss the observation, under *in operando* conditions, of the changes of the surface oxidation state^{2b} of Pt triggered by the applied potential. Thanks to the innovative experimental approach, we have observed the *in situ* formation of Pt(II) and Pt(IV) species during the oxygen evolution reaction (OER), as well as the reversibility of the surface chemistry passing from anodic to cathodic potentials (up to the hydrogen evolution reaction, HER).

[1] a. Lu et al., *Sci. Rep.* **2**, 715 (2012); b. Zhang et al., *Nat. Mat.* **9**, 444 (2010); c. Axnanda et al., *Nano Lett.* **13**, 6176 (2013); d. Starr et al., *Chem. Soc. Rev.* **42**, 5833 (2013); e. Mudiyansele et al., *Angew. Chem. Int. Ed.* **52**, 5101 (2013).

[2] a. S. Axnanda, E. Crumlin et al., *Sci. Rep.*, accepted; b. E. Crumlin et al., *in preparation*.

9:00am **IS+AS+SA+SS-TuM4 Toward Ambient Pressure Electron Spectroscopy with Conventional XPS Instrumentation, Andrei Kolmakov, National Institute of Standards and Technology (NIST)**

The current state of the art instrumentation for ambient pressure electron spectroscopy requires highly specialized sophisticated laboratory equipment or dedicated synchrotron radiation facilities. The limited access to these equipment impedes *in situ* (*in vivo*) studies under realistic conditions in catalysis, energy, environmental and bio-(medical) fields. We propose a new sample platform which enables ambient pressure XPS to be conducted using conventional XPS instrumentation. The core of the sample platform is microchannel environmental cells sealed with electron transparent, molecularly impermeable, mechanically and chemically stable graphene

layer. The channels can be impregnated with liquids or gases and yet be vacuum compatible. Two major wafer scale fabrication strategies: (i) transferred graphene and (ii) as grown graphene layer were described. The coverage yield, membrane cleanness and leaking rates were comparatively studied. The feasibility tests of the platform included *in situ* XPS and electron microscopy studies of the water radiolysis and electrochemical processes taking place at liquid electrolyte-solid interface.

9:20am **IS+AS+SA+SS-TuM5 Solvation and Chemistry at the Interface: Near Ambient Pressure Electron Spectroscopy Studies of Aqueous Solution Interfaces, John Hemminger, University of California, Irvine**
INVITED

We have combined liquid-jet photoelectron spectroscopy coupled with classical molecular dynamics simulations to study the composition and chemistry of the liquid/vapor interface of aqueous solutions. Our experiments take advantage of the variable x-ray energy capability of synchrotron radiation and the kinetic energy dependence of the electron inelastic mean free path to carry out experiments with different probe depths. At low x-ray energy the low energy photoelectrons are detected primarily from the surface region of the solution. At higher x-ray energy our experiments probe more deeply into the solution. This allows us to directly compare the liquid/vapor interface with the bulk of the aqueous solution. We will present recent results on aqueous solutions of organonitrile compounds (acetonitrile and propionitrile). Our experiments and MD simulations show that both acetonitrile and propionitrile accumulate at the liquid/vapor interface—even though both nitriles are fully miscible with water. We have also studied the salting in and salting out effects for nitriles in water. We also have studied the effect of ion size on the surface propensity of cations in alkali halide aqueous solutions.

11:00am **IS+AS+SA+SS-TuM10 In situ Single-molecule Microscopy of Photoelectrocatalysis for Solar Water Oxidation, Peng Chen, Cornell University**
INVITED

This talk will present our recent results in using single-molecule super-resolution fluorescence microscopy to image photoelectrochemical reactions on single semiconductor nanostructures *in situ* under photoelectrochemical water oxidation conditions. We separately image hole and electron induced reactions, driven by light and electrochemical potential, and map the reactions at single reaction temporal resolution and nanometer spatial resolution. We also correlate the surface hole and electron reactivity with the local water oxidation efficiency using sub-particle level photocurrent measurements. By depositing oxygen evolution catalysts in a spatially controlled manner, we further identify the optimal sites for catalyst deposition for photocurrent enhancement and onset potential reduction.

11:40am **IS+AS+SA+SS-TuM12 In Situ and Operando AP-XPS for the Oxidation State of Pd at Solid/Liquid Interface, Beomgyun Jeong, M. Favaro, P.N. Ross, Z. Hussain, Lawrence Berkeley National Laboratory (LBNL), Z. Liu, Shanghai Institute of Microsystem and Information Technology, China, B.S. Mun, J. Lee, Gwangju Institute of Science and Technology, Republic of Korea, E.J. Crumlin, Lawrence Berkeley National Laboratory (LBNL)**

A catalyst is defined as a substance that enhances a reaction rate without changing its chemical state. However, often the chemical state of a catalyst surface undergoes changes during the reaction, leading to the degradation of catalyst performance. These phenomena are particularly significant in electrocatalysis in which reaction occurs at solid/liquid interface with electrical potential as an activation energy to drive the reaction. In order to understand the mechanism of catalyst degradation, it is important to have a capability to observe the chemical states of electrode and various chemical species in electrolyte during the reaction taking place at the solid/liquid interface. In order to explore this region, we have developed a new experimental approach [1], using ambient pressure XPS (AP-XPS) coupled with "tender" X-rays (in the range between 2.5 and 7.0 keV) at the Advanced Light Source BL 9.3.1, Lawrence Berkeley National Laboratory. Because of the relatively high kinetic energy of the incoming photons, "tender" X-rays allow probing solid/liquid interfaces through thin electrolyte films characterized by a thickness of 10-30 nm. This unique functionality allows the ability to simultaneously correlate the electrocatalytic activity of electrodes to both the chemical modifications of the electrode surface, and the electrolyte.

This talk will provide details on *in-situ* and *operando* AP-XPS measurements on the chemical modifications of polycrystalline Pd surface studied at different electrochemical potentials. Pd is a cost-effective materials alternative to Pt showing similar electrocatalytic property of Pt in various reactions, such as oxygen reduction and electrooxidation of hydrogen and formic acid. On the other hand, it is well known that the Pd activity decreases faster than that of Pt especially in formic acid oxidation [2]. This phenomenology could be understood by the direct observation of

the Pd surface chemistry evolution at electrified solid/liquid interface. We will discuss the performance of the Pd electrode in two different aqueous electrolytes, in particular in an alkaline medium and in a formic acid solution, an electroactive liquid organic molecule. We believe that our findings represent a step forward in the rationalization of the electrocatalytic behavior of Pd.

[1] S. Axnanda, E.J. Crumlin *et al.*, *Sci. Rep.* 5 (2015) 9788.; b. E.J. Crumlin *et al.*, in preparation.

[2] H. Jeon, S. Uhm, B. Jeong, J. Lee, *Phys. Chem. Chem. Phys.* 13 (2011) 6192.

12:00pm **IS+AS+SA+SS-TuM13 In situ Characterization of Switchable Ionic Liquids by Liquid ToF-SIMS and SALVI**, *Juan Yao, X. Sui, D. Lao, Y. Zhou, S. Nune, D. Heldebrant, Z. Zhu, X.-Y. Yu*, Pacific Northwest National Laboratory

A vacuum compatible microfluidic reactor, SALVI (System for Analysis at the Liquid Vacuum Interface) was employed for *in situ* chemical imaging of switchable ionic liquids (SWILs) using time-of-flight secondary ion mass spectrometry (ToF-SIMS). A model SWIL system consisting of 1,8-diazabicycloundec-7-ene (DBU) and 1-hexanol with CO₂ gas to change solvent polarity was selected. A series of ionic liquids with different CO₂ loading was analyzed. Spatial chemical differences were observed within the same ionic liquid, indicating inhomogeneity of the ionic liquid. Spectral principal component analysis (PCA) was conducted using both positive and negative ToF-SIMS data. Clear distinctions were observed among SWILs of different CO₂ loadings. The loading plots strongly indicate that fully loaded SWILs share similar spectral components as those of the non-loaded ILs. This finding confirms the hypothesis of the biphasic structure in the fully loaded IL predicated by molecular dynamic simulation and presents the first physical evidence of the liquid microenvironment of IL determined by liquid ToF-SIMS. Various ion pairs were also observed in addition to the known SWIL chemistry of the DBU and 1-hexanol system, indicating the complexity of the ionic liquid previously unknown. The vacuum compatible microchannel in SALVI provides a new way to study ionic liquids in vacuum by sensitive surface techniques. Our approach directly visualized spatial and chemical heterogeneity within the SWILs by dynamic liquid ToF-SIMS for the first time.

Surface Science

Room: 112 - Session SS+AS+EN+NS-TuM

Nanostructures, Nanoplasmonics and Surface Reactions

Moderator: Bruce Koel, Princeton University

8:20am **SS+AS+EN+NS-TuM2 ENDOM: A Simple Method to Deposit Nanostructures from Nanowires to Nanopores**, *Ashley Ellsworth, A.V. Walker*, University of Texas at Dallas

A key challenge in the practical application of nanostructures is their effective integration through assembly, patterning and alignment on technologically relevant substrates. We have recently demonstrated a new technique, electroless nanowire deposition on micropatterned substrates (ENDOM), by which to simultaneously synthesize and place nanowires on chemically patterned substrates. The nanowires can be precisely oriented on the surface in arbitrary shapes, such as an arch and around a right angle bend. In ENDOM, the shape of the deposit is controlled by the substrate pattern while its width is controlled by the reaction conditions. By employing longer deposition times and the appropriate substrate patterns, nanopores and nanochannels can be produced. However for sensing and nanoelectronic applications, free standing nanopores and nanochannels are generally employed. We have observed that the nanostructure adhesion to the surface is dependent upon the reagent concentrations. For example in Cu ENDOM, upon reduction of triethanolamine (complexing agent and buffer) concentration, nanowires no longer adhere strongly to the substrate and can be transferred to another substrate. In this presentation, we shall discuss the mechanisms of adhesion, transfer of these nanostructures to other substrates and proof-of-concept studies to synthesize free-standing nanostructures.

8:40am **SS+AS+EN+NS-TuM3 Chemical Reaction on Photo-excited Plasmonic Nanostructures**, *Sulio Linic*, University of Michigan **INVITED**
We will also show that plasmonic silver nanoparticles, optically excited with low intensity visible light, exhibit direct photo-catalytic activity in a number of oxidation reactions.¹ We will discuss underlying mechanisms associated with these phenomena and predictive models that can capture the outcome of chemical transformations on these materials.^{2,3,4} We propose that this new family of plasmonic metal photo-catalysts could prove useful

for many heterogeneous catalytic processes that cannot be activated using conventional thermal processes on metals or photo-catalytic processes on semiconductors. I will show an example of such a process.⁵

1. D. B. Ingram, S. Linic, *JACS*, 133, 5202, 2011

2. Suljo Linic, Phillip Christopher and David B., *Nature Materials*, 10, 911, 2011.

3. Ingram P. Christopher, H. Xin, S. Linic, *Nature Chemistry*, 3, 467, 2011.

4. P. Christopher, H. Xin, M. Andiappan, S. Linic, *Nature Materials*, 11, 1044, 2012.

5. M. Andiappan, J. Zhang, S. Linic, *Science*, 339, 1590, 2013

9:20am **SS+AS+EN+NS-TuM5 Structured Noble Metal Nanosurfaces for Biosensing and Bioanalysis (4): TLC-SERS and In Situ Monitoring of Surface-Adsorbed Target Molecules**, *Hiroyuki Takei, J. Saito, K. Watanabe*, Toyo University, Japan, *T. Okamoto*, Riken, Japan, *H. Vieker, A. Beyer, A. Götzhäuser*, Bielefeld University, Germany

Surface-enhanced Raman spectroscopy, SERS, is a powerful technique for in-situ characterization of chemical species. Requisite noble metal nanosurfaces can be prepared with a variety of techniques, ranging from simple vacuum deposition of a metal followed by annealing to intricate processing by electron beam lithography. Some commercial SERS plates are now available, and it is sometimes possible to detect signals from even single molecules if pure. However, in real-world applications, target molecules are often found in mixtures, either containing other Raman-active chemical species or a background material that can overwhelm the target molecule. It can also happen that one might be interested in directly obtaining SERS spectra of chemical species adsorbed on a solid surface.

When faced with a mixture sample, we can carry out separation before SERS measurement. To do so, we incorporated a SERS layer into a thin layer chromatographic plate. While a number of workers have reported applying noble metal nanoparticles after separation with a conventional TLC plate, we feel that such an additional step is cumbersome and does not guarantee uniformity in SERS signals. Our TLC-SERS is prepared with the following procedure; (1) adsorption of 100 nm diameter SiO₂ nanospheres as a dense monolayer on a glass slide, (2) evaporation of gold or silver with thicknesses up to 100 nm, and (3) spreading of chromatography silica gels. Steps (1) and (2) give rise to surface-adsorbed cap-shaped noble metal nanoparticles. We demonstrate that the TLC-SERS can actually separate mixture samples and provide in-situ SERS spectra. Two examples will be used to demonstrate the utility of our TLC-SERS plates. One deals with a mixture of roughly equal portions of Raman-active chemical species, rhodamine 6 G, crystal violet and BPE. The other is skim milk to which a trace amount of melamine has been added. We show that the three-component mixture could be separated and SERS spectra of all three components could be obtained separately and that melamine added to skim milk could be detected after separation but not before.

For detection of surface-adsorbed chemical species, we prepared silver nanoparticles on a PDMS sheet, using the same protocol as above. The PDMS sheet can be made less than 1 mm thick so that with an appropriate pressurization system, pressure can be applied to the PDMS sheet in order to press the silver nanoparticles against a near-by solid surface to which target molecules are adsorbed. Such a system can be utilized to detect, for example, residual pesticides on agricultural produces. We will demonstrate direct detection of ferbam on a grapefruit.

9:40am **SS+AS+EN+NS-TuM6 Growth and Intercalation of Cu and Dy on the Basal Plane of Graphite**, *Patricia A. Thiel, D. Appy, E.J. Kwolek, D. Shao, M. Wallingford, M.C. Tringides, J.W. Evans, Y. Han*, Iowa State University, *H. Lei*, Institute of Solid State Physics, CAS, China, *C.-Z. Wang*, Iowa State University

Graphite, and surface processes on graphite, serves as a valuable benchmark for carbon-based materials such as graphene. We have studied copper and dysprosium on graphite, deposited by an e-beam evaporator in UHV and imaged with STM, to determine the characteristic features of nucleation and growth of metal islands. One of the fundamental questions that arises naturally is whether metal nucleates homogeneously on the terraces or whether it nucleates heterogeneously at defect sites. To answer this question we employ several tools, especially a comparison between high-level van der Waals theory for single atom diffusion, and measured island density. We also present evidence for unexpected metal intercalation at the surface of graphite, after treatment at elevated temperature.

11:00am **SS+AS+EN+NS-TuM10 Surface-Mediated Self-assembly of a Flexible Nucleoside Analogue into Micron-sized Hydrogen-bonded Polymers**, *Jun Wang, P. Bonnesen*, Oak Ridge National Laboratory, *E. Rangel, E. Vallejo, A. Sanchez-Castillo*, Universidad Autónoma del Estado de Hidalgo, Mexico, *H.J. Cleaves*, Tokyo Institute of Technology, Japan, *A.P. Baddorf, B. Sumpter, M. Pan, P. Maksymovych, M. Fuentes-Cabrera*, Oak Ridge National Laboratory

We report on an extraordinary large-scale surface-mediated molecular self-assembly of a flexible nucleoside analogue into a well-organized hydrogen-bonded polymer on Au(111). The nucleoside analogue is (*R,S*)-*N*⁹-(2,3-Dihydroxypropyl)Adenine (*R,S*-DHPA), and it consists of the Adenine nucleobase and a tethered glycol group. Employing scanning tunneling microscopy and density functional theory calculations we show that the polymer primarily self-assembles along the Au(111) herringbone reconstruction pattern and extends to the micrometer scale and beyond. The profound propensity toward self-assembly in this case arises from the properties of the glycol moiety of the *R,S*-DHPA molecule: it is linear and flexible, and these features, together with the specific ways in which the glycol and the Adenine moieties can hydrogen bond, confer *R,S*-DHPA with a superior self-assembly ability. Our results suggest that nucleoside analogues with flexible acyclic groups could provide the means for synthesizing substrate-supported mesoscale hydrogen-bonded polymers.

ACKNOWLEDGEMENTS

This research was conducted at the Center for Nanophase Materials Sciences (CNMS), which is a DOE Office of Science User Facility.

11:20am **SS+AS+EN+NS-TuM11 Nanowire Kinking during Vapor-liquid-solid Growth: Experiments and Simulations**, *Yanning Wang, Y. Li*, Stanford University, *S. Ryu*, Korea Advanced Institute of Science and Technology, *P.C. McIntyre, W. Cai*, Stanford University

Nanowires (NWs) are promising components for next-generation electronic and optical devices, and the vapor-liquid-solid (VLS) growth is a widely studied method for NW fabrication. However, many fundamental questions regarding the VLS mechanism are still not understood, such as NW kinking during growth. Kinking, a sudden change in axial orientation of nanowires during growth, is a common defect that complicates the directed synthesis of these nanocrystals. Understanding such defects is important for better control of the NW orientation, yield and quality required for applications.

Experimental studies of coherent kinking of germanium nanowires detect two different kinking structures. One structure, which is most pronounced for Ge NW's of diameter close to 20 nm, involves kinking from a vertical $\langle 111 \rangle$ to $\langle 110 \rangle$ growth axis on Ge (111) single crystal substrates. The other involves kinking from the vertical [111] axis to an inclined $\langle 111 \rangle$ growth direction for NWs of > 30 nm diameter.

The balance of capillary forces driving these two modes of kinking are analyzed quantitatively. We developed a 3D multi-phase field model for VLS NW growth. The model captures the NW tapering and sidewall facets in good agreement with experimental observations. The model predicts the steady-state NW growth velocity is a linear function of the vapor chemical potential and the inverse of catalyst diameter, providing a confirmation of the Gibbs-Thomson effect in nanowire growth. With anisotropic interfacial energies, the model shows the NW growth orientation dependence on catalyst diameter and hence it provides an explanation of the NW kinking in the steady-state growth regime. In this model, we introduce a perturbation force to induce the NW structural transition and the free energies are evaluated at different stages during the droplet movement. It enables us to discuss the instability of the catalyst droplet for different pedestal structures, which is important for understanding the onset of the kinking at the NW base.

11:40am **SS+AS+EN+NS-TuM12 Adsorption of Water and Bromine on Gold Nanoclusters Investigated by Neutralization in Low Energy Alkali Ion Scattering**, *Christopher Salvo, J. Keagy, J.A. Yarmoff*, UC Riverside

Small gold (Au) nanoclusters have been heavily studied because of their intriguingly high catalytic activity, especially when compared to bulk gold. We employ a specialized method of Low Energy Ion Scattering (LEIS) to probe the electronic properties of nanoclusters prepared with a variety of methods. The experiments measure the neutralization probability of singly scattered alkali ions, which is acutely sensitive to the local electrostatic potential a few Å's above the surface. Because the Au atoms are much more massive than the substrate atoms, this method allows the signal from the nanoclusters to be separated from that of the substrate so that the neutralization reflects the local properties of the cluster surfaces. Earlier work had demonstrated that the neutralization is a function of cluster size, and that it is enhanced for the smallest clusters presumably because they are negatively charged [1]. The work presented here investigates the adsorption of water and Br on Au nanoclusters grown on TiO₂ or SiO₂. There are multiple factors that can contribute to a change in the neutralization of the

scattered ions, such as the cluster size, shape, or charge state. When Br attaches to a nanocluster, the neutralization decreases presumably due to charge transfer from the cluster to the electronegative Br atom. Surprisingly, it is found that the neutralization of scattered K⁺ ions increases in the presence of adsorbed water at liquid nitrogen temperatures. Furthermore, the increase of neutralization for adsorbed water is independent of whether the water or the Au is deposited first. Possible explanations for these observations will be discussed.

[1] G.F. Liu, Z. Sroubek and J.A. Yarmoff, Phys. Rev. Lett., **92**, 216801 (2004).

12:00pm **SS+AS+EN+NS-TuM13 Optical Constants Measured for Fe, Ni and Pd by Reflection Electron Energy-Loss Spectroscopy Spectra**, *H. Xu, B. Da, S.F. Mao*, University of Science and Technology of China, *J. Toth, K. Tokesi*, Institute for Nuclear Research, Hungarian Academy of Sciences (ATOMKI), *Zejun Ding*, University of Science and Technology of China

The energy loss function (ELF), which is directly related to optical constants of a solid, dominates the energy loss process of an electron moving inside or flying nearby a solid. It is therefore able to obtain optical constants by surface electron spectroscopy technique. Accurate measurement of optical data by optical methods in a photon energy range up to 10² eV is still insufficient; delicate experimental conditions are required when measuring data in vacuum ultraviolet region (20-50 eV). Fortunately, such information is essentially contained in and, therefore, can be extracted from a reflection electron energy loss spectroscopy (REELS) spectrum due to the shorter information depth of signal electrons compared with that of photons.

In the present work, reflection electron energy loss spectra of transition metals, Fe, Ni and Pd, were measured at several primary energies ranging from 0.5 keV up to 5 keV and in a wide energy-loss range. Prior to the measurements in situ cleaning of the sample surface was performed using Ar⁺ ion sputtering with proper current density and time. Vacuum was kept as 1.5×10⁻⁹ mbar in the measurement chamber during the REELS measurements. Surface cleanliness was checked by XPS in several cases after the REELS measurements. An improved reverse Monte Carlo simulation for determination of optical constants via accurate description of electron inelastic transport process was performed. ELF of those metals were extracted from experimental REELS spectra. The accuracy of the obtained optical data has been confirmed by f-sum and ps-sum rules. Comparisons of our data with other sources from either experimental measurements or density functional theory calculation are given.

Surface Science

Room: 113 - Session SS+AS+EN-TuM

Mechanistic Insight of Surface Reactions: Catalysis, ALD, etc. - I

Moderator: Ludwig Bartels, University of California - Riverside

8:00am **SS+AS+EN-TuM1 Active Sites of Nitrogen-Doped Carbon Materials for Oxygen Reduction Reaction**, *Takahiro Kondo, D. Guo, R. Shibuya, C. Akiba, S. Saji, J. Nakamura*, University of Tsukuba, Japan

Nitrogen-doped carbon materials have been found to demonstrate high electrocatalytic activity for oxygen reduction reaction (ORR) as the non-metal catalysts but the active site is still under debate. This is due to the complexity of the real catalysts, such as mixing of different type of N and inhomogeneity in both structure and conductance. Here we designed the nitrogen doped graphite (HOPG) model catalysts with different type of N dominance and its concentration to directly clarify the ORR active site. ORR measurements showed that active site was created by pyridinic N (N bonded to two carbon atoms). The ORR active site was ascribed to the carbon atom with Lewis base property created by neighbour pyridinic N based on the investigations of intermediate state of ORR, localized electronic states at carbon next to pyridinic N and CO₂ adsorption property by X-ray photoelectron spectroscopy (XPS), scanning tunneling spectroscopy (STS) and temperature programmed desorption (TPD), respectively. The ORR activity of model catalyst per pyridinic N concentration was then found to be in good agreement with that for real nitrogen-doped graphene catalyst.

8:20am **SS+AS+EN-TuM2 Cerium Oxide-Induced Intercalation of Oxygen on Supported Graphene**, *Zbynek Novotny*, Pacific Northwest National Laboratory, *F.P. Netzer*, Karl-Franzens University, Austria, *Z. Dohnalek*, Pacific Northwest National Laboratory

Cerium oxide is an important catalytic material known for its ability to store and release oxygen, and as such, it has been used in a range of applications, both as an active catalyst and as a catalyst support. Using scanning tunneling microscopy and Auger electron spectroscopy, we investigated oxygen interactions with CeO_x clusters on a complete graphene monolayer-covered Ru(0001) at elevated temperatures (550 – 700 K). Under oxidizing conditions (~10⁻⁷ Torr of O₂), oxygen intercalation under the graphene layer is observed. Time dependent studies demonstrate that the intercalation starts in the vicinity of the CeO_x clusters and extends until a completely intercalated layer is observed. Atomically resolved images further show that oxygen forms p(2×1) structure underneath the graphene monolayer. Temperature dependent studies yield an apparent kinetic barrier for the intercalation of 0.9 eV. This value correlates well with the theoretically determined value for the reduction of small CeO₂ clusters reported previously. At higher temperatures, the intercalation is followed by a slower etching of the intercalated graphene (apparent barrier of 1.1 eV). The intercalated oxygen can also be released through the CeO_x clusters by annealing in vacuum. In agreement with previous studies, no intercalation is observed on a complete graphene monolayer without CeO_x clusters, even in the presence of a large number of point defects. These studies demonstrate that the easily reducible CeO_x clusters act as intercalation gateways capable of efficiently delivering oxygen underneath the graphene layer.

8:40am **SS+AS+EN-TuM3 Dissociation Dynamics of Energetic Water Molecules on TiO₂(110): Combined Molecular Beam Scattering and Scanning Tunneling Microscopy Study**, *Z.-T. Wang, Y.-G. Wang, R.T. Mu, Y. Yoon, G.A. Schenter, R. Rousseau, I. Lyubnitsky, Zdenek Dohnalek*, Pacific Northwest National Laboratory

Molecular beam scattering techniques have proven extremely useful in determining the dynamics of energy flow in the course of chemical reactions. We have successfully designed and constructed a unique, state of the art instrument combining a molecular beam scattering source coupled with a low temperature scanning tunneling microscope (STM). The combination of these techniques allows us to follow the same area during adsorption and image surface species as a function of incident energy of reacting molecules. Our first study focuses on reversible water dissociation on Ti rows of TiO₂(110), which leads to the formation of pairs of terminal and bridging hydroxyl species, H₂O ↔ HO_t + HO_b. The results of our measurements show the onset of H₂O dissociation at 0.2-0.3 eV of incident energy, independent of whether the molecules impinge along or across the Ti rows at an incident angle of 60° relative to surface normal. Following the onset, the dissociation probability increases linearly with increasing incident energy. Ensembles of *ab initio* molecular dynamics (AIMD) simulations at several incident energies reproduce the product distribution seen in the STM. Additionally, these studies show that the dissociation occurs only for the impacts in the vicinity of surface Ti ions with an activation energy of 0.3 eV and that the O-H bond cleavage is accomplished within the time of a single vibration. The AIMD simulations were further used to construct a classical potential energy surface for water/TiO₂(110) interactions and execute non-equilibrium classical MD simulations that closely reproduce the onset and linear energy dependence of the dissociation probabilities.

9:00am **SS+AS+EN-TuM4 Tracking Site-Specific C-C Coupling of Formaldehyde Molecules on Rutile TiO₂(110)**, *Zhenrong Zhang, K. Zhu, Y. Xia*, Baylor University, *M. Tang*, Southern Illinois University Carbondale, *Z.-T. Wang, I. Lyubnitsky*, Pacific Northwest National Laboratory, *Q. Ge*, Southern Illinois University Carbondale, *Z. Dohnalek*, Pacific Northwest National Laboratory, *K. Park*, Baylor University

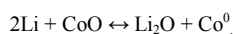
We report the direct visualization of molecular coupling of the smallest aldehyde, formaldehyde, on reduced rutile TiO₂(110) surfaces using scanning tunneling microscope (STM). Images from the same area at viable temperatures (75 ~ 170 K) show that formaldehyde preferably adsorbs to bridging-bonded oxygen vacancy (V_O) defect site. V_O-bound formaldehyde couples with Ti-bound CH₂O form a diolate species, which stays stable at room temperature. In addition, two V_O-bound formaldehyde molecules can couple and form Ti-bound species, which desorbs above ~215 K. This coupling reaction heals both the V_O sites indicating formation and desorption of ethylene. We also directly observed the diffusion of methylene groups to nearby empty V_O sites formed upon dissociation of the C-O bond in V_O-bound formaldehyde, which suggests that the ethylene formation is via coupling of the methylene groups.

9:20am **SS+AS+EN-TuM5 AVS 2014 Gaede-Langmuir Invited Talk: Models for Heterogeneous Catalysts: Complex Materials at the Atomic Level**, *Hajo Freund**, Fritz Haber Institute of the Max Planck Society, Germany **INVITED**

Our understanding of catalysis, and in particular heterogeneous catalysis, is to a large extent based on the investigation of model systems. The enormous success of metal single crystal model surface chemistry, pioneered by physical chemists, is an outstanding example. Increasing the complexity of the models towards supported nanoparticles, resembling a real disperse metal catalyst, allows one to catch in the model some of the important aspects that cannot be covered by single crystals alone. One of the more important aspects is the support particle interface. We have developed strategies to prepare such model systems based on single crystalline oxide films, which are used as supports for metal, and oxide nanoparticles, which may be studied at the atomic level using the tools developed in surface science. However, those oxide films may also serve as reaction partners themselves, as they are models for SMSI states of metal catalyst. Using such model systems, we are able to study a number of fundamental questions of potential interest, such as reactivity as a function of particle size and structure, influence of support modification, as well as of the environment, i.e. ultra-vacuum or ambient conditions, onto reactivity. The thin oxide film approach allows us to prepare and study amorphous silica as well as 2D-zeolites. Those systems, in spite of their complexity, do lend themselves to theoretical modelling as has been demonstrated.

11:00am **SS+AS+EN-TuM10 The Solid State Li-CoO Conversion Reaction Studied by ARXPS and STM**, *Ryan Thorpe, S. Rangan*, Rutgers, the State University of New Jersey, *A. Howansky*, Stony Brook University, *R.A. Bartynski*, Rutgers, the State University of New Jersey

Cobalt (II) oxide is a promising electrode material for Li-ion conversion batteries, undergoing the following reversible redox reaction upon exposure to lithium:



In order to characterize the phase progression and morphology of the Li-CoO reaction, epitaxial CoO(100) and (111) films were exposed to lithium in an ultra-high vacuum chamber. The early stages of the reaction were then characterized with scanning tunneling microscopy (STM), while the diffusion of Li into the films and resultant reduction of CoO was quantified using angle-resolved x-ray photoemission spectroscopy (ARXPS). From these measurements, a model of the Li-CoO reaction was constructed for each orientation.

For CoO(111) films, the conversion reaction initiated at step edges and defect sites before proceeding across the surface of the film. STM images of CoO(111) after 0.2 ML of Li exposure suggest that the conversion reaction products initially assumed a periodic structure which was in registry with the CoO(111) surface. For larger Li exposures, ARXPS measurements indicated that the reaction proceeded in a layer-by-layer fashion into the bulk, maintaining a planar interface between reacted and unreacted CoO.

The reaction of the CoO(100) surface with 0.1 ML of Li resulted in the formation of 2-3 nm Co metal nanoparticles which decorated the CoO step edges. Upon further lithiation, the conversion reaction proceeded into the film preferentially at step edges. ARXPS measurements suggested that the reaction penetrated deep into the CoO film from these nucleation points before spreading across the rest of the surface. These combined results show the importance of crystallographic orientation in determining the reaction kinetics in a Li-ion battery.

11:20am **SS+AS+EN-TuM11 Imaging Water Adsorption and Dissociation on RuO₂ (110) Surfaces**, *Rentao Mu, D.C. Cantu, X. Lin, V.A. Glezakou, Z.-T. Wang, I. Lyubnitsky, R. Rousseau, Z. Dohnalek*, Pacific Northwest National Laboratory

Understanding water/solid interactions is a current critical scientific challenge with important implications for a variety of fundamental and applied processes. Here we study the interactions of water with RuO₂, which has a wide range of applications in photocatalytic water splitting, heterogeneous catalysis, electrochemistry and many other energy-related areas. We prepared stoichiometric (*s*-), reduced (*r*-) and oxidized (*o*-) RuO₂(110) surfaces and studied water adsorption, dissociation, and diffusion using time-lapsed scanning tunneling microscopy and density functional theory calculations. On *s*-RuO₂(110) we show that water monomers become mobile above 238 K and form dimers which are immobile below 273 K. More importantly, we find that the mobile water dimers dissociate readily to form Ru-bound H₃O₂ and hydroxyl species (HO_b) on bridging oxygen (O_b) rows. The onset for diffusion of H₃O₂ on *s*-RuO₂(110) is observed at ~273 K, indicating a significantly higher diffusion barrier than that for water monomers. The experimentally determined

* Gaede Langmuir Award Winner

diffusion barriers are in agreement with those obtained from the DFT calculations. The observed behavior is compared and contrasted with that observed for water on isostructural rutile $\text{TiO}_2(110)$ where both molecularly-bound monomers and dimers are in equilibrium with their deprotonated states. In contrast with $\text{TiO}_2(110)$, the larger separation of Ru atoms induces the segmentation of water chains at high water coverages. On slightly oxidized $o\text{-RuO}_2(110)$, water molecules react with oxygen adatoms (O_a 's) on Ru rows and form pairs of terminal hydroxyl groups which can reversibly dissociate back to a water molecule and O_a . This process results in the displacement of O_a 's along the Ru rows. Along- and across-row diffusion of isolated water molecules is tracked at room temperature on both slightly, and heavily oxidized $o\text{-RuO}_2(110)$ by following the position of hydroxyl pairs. On $r\text{-RuO}_2(110)$, we find that water molecules readily dissociate at bridging oxygen vacancies and form bridging hydroxyl groups. The mechanism of along- and across-row diffusion of the bridging hydroxyl protons is also studied at room temperature. The atomically-detailed, quantitative assessment of binding and diffusion of the surface species formed upon water adsorption on $\text{RuO}_2(110)$ represent a critical step in achieving fundamental level understanding of the role RuO_2 plays as H_2 and O_2 evolution co-catalysts in photocatalytic water splitting reactions.

11:40am **SS+AS+EN-TuM12 Surface Reaction Kinetics during Low Temperature ALD of Al_2O_3 Studied by Broadband Sum-frequency Generation**, Vincent Vandalon, W.M.M. Kessels, Eindhoven University of Technology, Netherlands

The nonlinear optical technique of broadband sum-frequency generation (BB-SFG) has been used to study the surface reactions during atomic layer deposition (ALD). Vibrational BB-SFG spectroscopy is excellently suited for *in-situ* studies of the surface chemistry governing ALD because of its inherent interface selectivity, submonolayer sensitivity, and short acquisition times. In contrast to BB-SFG, conventional absorption spectroscopy, based on the so called "differential" measurements, monitors only changes on the surface. On the other hand, due to its surface selectivity, BB-SFG reveals information about both *persistent* and *changing* surface groups. Therefore, with this technique, open questions can be addressed such as the origin of the decrease in growth per cycle (GPC) at low temperatures of the ubiquitous process of thermal ALD of Al_2O_3 from $\text{Al}(\text{CH}_3)_3$ and H_2O . So far, a complete picture of the surface chemistry explaining the reduced GPC is missing and the exact cause of the limited growth at low temperatures remains unclear.

More particularly, the surface chemistry of thermal ALD Al_2O_3 was followed by monitoring the density of the $-\text{CH}_3$ surface groups. In contrast to ALD at high temperatures, below 200°C it was observed that a significant amount of $-\text{CH}_3$ could not be removed during the water half-cycle. The observed kinetics could not be explained by a thermally-activated first-order reaction with a constant cross section. We investigated the temperature dependence of the reaction kinetics further by measuring the $-\text{CH}_3$ coverage as a function of precursor and co-reactant exposure at different temperatures. It found that the absolute cross section obtained for the TMA half-cycle was independent of temperature, indicating that the chemisorption of TMA is not a thermally activated process. The behavior during the water half-cycle was found to be more complex showing a strong dependence on temperature; it cannot be described as a reaction simply obeying Arrhenius behavior. This is in line with the more complex behavior predicted by recent DFT work carried out by Shirazi and Elliott [Nanoscale 2015] where a so-called "cooperative" effect was observed leading to a coverage dependent reactivity. The observations presented in this work are direct experimental evidence of such a "cooperative" effect and were only possible due to the inherent surface selectivity of BB-SFG.

12:00pm **SS+AS+EN-TuM13 The Preparation and Redox Properties of $\text{Cu}/\text{Al}_2\text{O}_3/\text{ZnO}(0001)$ Model Surfaces**, J. Hu, J.J. Huang, H. Zhang, Mingshu Chen, Xiamen University, China

The $\text{Cu}/\text{Al}_2\text{O}_3/\text{ZnO}(0001)$ -Zn ternary model catalysts were prepared and characterized by XPS and LEISS. The $\text{Al}_2\text{O}_3/\text{ZnO}$ was prepared by depositing Al onto the ZnO surface in O_2 atmosphere at 523 K, and Cu/ZnO was prepared by depositing Cu onto ZnO surface at room temperature. It was found that Al_2O_3 grew on the ZnO surface by a layer-by-layer model, while Cu formed two-dimensional islands only at low coverage and three dimensional clusters at high coverage. For $\text{Cu}/\text{Al}_2\text{O}_3/\text{ZnO}(0001)$ -Zn, the XPS and LEIS spectra showed that the copper islands were preferred on the interfaces of $\text{Al}_2\text{O}_3/\text{ZnO}$. Comparing to the Cu/ZnO binary model catalyst, the addition of Al_2O_3 obviously slowed down the reduction of $\text{Cu}/\text{Al}_2\text{O}_3/\text{ZnO}$ by H_2 . More significantly, the existence of Al_2O_3 in the ternary model catalyst led to an increase of Cu^+ concentration. The enhancement of Al_2O_3 in $\text{Cu}/\text{Al}_2\text{O}_3/\text{ZnO}(0001)$ -Zn for methanol synthesis may origin from that the Al_2O_3 helps to stabilize the surface Cu^+ which has been proposed as one of the active sites.

Tuesday Afternoon, October 20, 2015

Applied Surface Science

Room: 212D - Session AS+BI-TuA

Challenges in the Characterization of Polymer/Organic/Biological Systems

Moderator: Bonnie Tyler, National Physical Laboratory (NPL), Jeffrey Fenton, Medtronic plc

2:20pm **AS+BI-TuA1 ASSD 30th Anniversary Lecture: 30 Years (ToF-)SIMS of Organic Materials: from Monolayer to 3D Microarea Analysis, Birgit Hagenhoff**, Tascon GmbH, Germany **INVITED**

The presentation will follow the development track and the learning curve of (ToF)-SIMS for the characterization of organic materials.

Starting in the early 70s of the last century, when Alfred Benninghoven, based on research results for Ag catalyst samples, started into what would later become the wide-spread field of Static SIMS, the talk will cover the following areas

- Static SIMS: early beginnings
- Static SIMS: the importance of noble metal substrates
- Static SIMS: from quadrupoles to Time-of-Flight Analyzers
- Charge compensation: the gateway to bulk analysis
- Organic Imaging: limits of lateral resolution
- Cluster ion guns: getting sub- μm using Au and Bi LMIGs
- The road to organic depth profiling: SF_5^+ and C_{60}^+ sputtering
- Organic depth profiling: the use of Ar cluster ion sputtering
- 3D Microarea Analysis: Status-quo and challenges for the future

3:00pm **AS+BI-TuA3 Characterization of the Buried Interface between a Bacterial-Biofilm Resistant Coating and a Silicon Catheter by using Gas Cluster ToF-SIMS and Raman Microscopy, Bonnie Tyler**, National Physical Laboratory (NPL), UK, *A.L. Hook, M.R. Alexander*, University of Nottingham, UK, *A. Giovannozzi*, INRIM, *A. Pelster, H.F. Arlinghaus*, University of Muenster, Germany

Thin film coatings are widely used in medical devices in order to improve the biological response to the device without compromising its mechanical performance. These coatings are frequently organic in nature and are applied to a wide range of substrate materials. The challenge of ensuring a stable linkage between the coating and the underlying substrate is common to all of these systems. Defects at the interface between the coating and the substrate can result in failure of the medical device with potentially serious consequences. The study of buried interfaces in organic systems, like those common in medical devices, has in the past been a nearly intractable problem because sputter depth profiling with monatomic ions destroys the relevant chemical information. Recent advances in Gas Cluster Ion Beam technology have opened up exciting possibilities to better understand these buried interfaces. In this work, we have studied adhesion between an bacterial-biofilm resistant polymer coating and an oxygen plasma-treated polymer surface using Argon Cluster 3D-imaging Time-of-Flight Secondary Ion Mass Spectrometry (ToF-SIMS) and Raman Microscopy. Analysis has been performed in both dry and hydrated state. The analysis provided several analytical challenges. Because the overlayer was not of uniform thickness, a depth scale correction was needed to reduce misleading artefacts at the interface. Analysis of the hydrated catheters required cryogenic analysis conditions. From the ToF-SIMS data we have been able to observe the presence of particles, cracks and water, and to monitor hydrophobic recovery at the interface between the coating and the catheter. Raman analysis has provided complementary information on the Van-Der-Waal interactions at the interface. The results have been compared to mechanical adhesion tests and help to provide a better understanding of the processes that influence adhesion between the coating and the catheter.

3:20pm **AS+BI-TuA4 How to Measure Reaction Rates on Surfaces?: Ambient Mass Spectrometry and XPS to Study the Rate of Organic Reactions on Functionalized Surfaces., R. Sen, J. Escorihuela, Han Zuilhof**, Wageningen University, Netherlands

Ultrathin coatings like self-assembled monolayers and polymer brushes have been used for a wide variety of studies and applications. Reactions within such monolayers or brushes are often difficult to follow, and their rates are typically not measurable: apart from a handful of cases in which electrochemical methods have been used, no rigorously measured kinetics on reactions within e.g. self-assembled monolayers are available. The

current presentation will outline a generic approach, combining ambient mass spectrometry and XPS, to fill this gap, and provide a truly generic method to measure the rate of intramonolayer or intrapolymer organic reactions. Examples will include a variety of so-called click reactions, as these display a very high potential in materials science.

4:20pm **AS+BI-TuA7 Surface versus Bulk Chemistry of Reverse Osmosis Membranes, Tamlin Matthews, R. Cieslinski, M. Paul, A. Roy**, The Dow Chemical Company

The polyamide layer of reverse osmosis (RO) thin-film composite membranes is ~ 100 nm thick. Separation of this thin layer from the supporting layers is a complex process and can only be done chemically, which results in a fragile polyamide layer and makes characterization challenging. X-ray photoelectron spectroscopy (XPS, near-surface) and Rutherford backscattering spectrometry (RBS, bulk) have been applied to characterize the polyamide layer, without the need to separate polyamide from the supporting layers. The combination of these methods allows the comparison of bulk vs. near-surface carboxylic acid content, which is a driver in RO performance. Additionally, elemental composition, thickness, and roughness of the RO membranes can be compared in systems with systematically changed monomers. This talk will focus on how the application of XPS and RBS can be used together for surface vs bulk chemical composition.

4:40pm **AS+BI-TuA8 Effect of Deep UV Irradiation on Polyester Family Polymers, Lopamudra Das, M.J. Kelley**, College of William and Mary

In films and fibers, desired attributes of these polymers are often surface-mediated. Radical chemistry launched by deep UV offers attractive opportunities for surface modification, free of the environmental burdens of wet chemistry. We report the effect of 172 nm irradiation in the absence of oxygen on PET, PTT, PBT and PEN films, observed by FTIR, XPS and ToF-SIMS. Initial findings include carboxylic acid production and a loss of carbonyl carbon. To better understand surface reactivity, samples of each polymer were treated with silver trifluoroacetate or with heavy water.

5:00pm **AS+BI-TuA9 Going beyond State of the Art in SIMS Imaging in the Life-Sciences and for Organic Devices, Ian Gilmore**, National Physical Laboratory, UK **INVITED**

In this celebratory 30th year of the Applied Surface Science Division, we can be sure that secondary ion mass spectrometry will feature strongly in the "Top-30" hit-parade. For example, SIMS, with its ability for high-sensitivity analysis has played an important role in the semiconductor industry measuring dopant profile concentrations. The rapid growth of the semiconductor industry is popularly summarised by Moore's law¹; which shows that over the last five decades the number of transistors in a chip doubles every two years. Recently, Scannell et al² show that the reverse is the case for the pharmaceutical industry and the number of drugs per billion dollars of investment has dropped from around 50 to less than 1 over a similar timescale. They call this "Eroom's" law, Moore's law in reverse.

Analogously to the semiconductor industry, SIMS could now provide important benefits to the pharmaceutical industry. The challenge here is to measure where drugs go at the cellular level, even within specific organelles, to answer long-standing questions about whether drug concentrations are sufficiently high in the right places to have a therapeutic effect, or if the medicine is lodging within cellular components and causing toxicity. If anomalies were spotted earlier it might help to explain toxicities or lack of efficacy of a medicine and reduce costly late-stage failures.^{3,4}

To meet this challenge, NPL in collaboration with GlaxoSmithKline, ION-TOF GmbH, Thermo Fisher Scientific and the University of Nottingham is building a revolutionary new instrument, the 3D nanoSIMS,⁴ which incorporates the powerful Thermo Scientific™ Orbitrap™ mass analyzer for high-performance identification of drugs and metabolites. The stunning capability of SIMS to study drugs in tissue and cells will be highlighted and the characteristics of the new instrument will be outlined. The benefits of combining SIMS with the new generation of ambient mass spectrometry techniques and the rapidly rising challenge of Big Data will also be discussed.

References:

- [1] Moore, Gordon E.. "Cramming more components onto integrated circuits" (PDF). Electronics Magazine. (1965)
- [2] Scanwell, J.W., Blanckley, A., Boldon, H., Warrington B., Nat. Rev. Drug Discovery., 11, 191-99 (2012)
- [3] C T Dollery, Clinical Pharmacology & Therapeutics, (2013); 93, 263–266.

[4] The 3D nanoSIMS project, <http://www.npl.co.uk/news/3d-nanosims-label-free-molecular-imaging> [2013 [<http://www.npl.co.uk/news/3d-nanosims-label-free-molecular-imaging%20%5b2013%5d>]]

5:40pm AS+BI-TuA11 **Can *In Situ* Liquid SIMS Provide Enough Signals for Biology and Environmental Research?**, *Zihua Zhu, Y. Zhou, X. Hua, J. Yu, J.E. Evans, D. Lao, X.-Y. Yu*, Pacific Northwest National Laboratory

In situ liquid SIMS is an R&D 100 award winner that was developed in PNNL since 2010. System for analysis at the liquid vacuum interface (SALVI) coupled with liquid SIMS has proven to be a promising new tool to provide molecular information at solid/liquid interfaces.[1,2] However, our initial data showed that signals of secondary positive ions were too low to be usable in some cases.[2,3] In addition, it was difficult to obtain strong negative molecular ion signals with $m/z > 100$. [2] These two drawbacks make SIMS community wonder the potential applications of this new analytical approach. In this presentation, we report that strong positive and negative molecular signals are achievable after we optimize the SIMS experimental conditions. Our results show that both beam current and primary ion species (e.g., Bi^+ , Bi_3^+ , Bi_5^{2+}) play important roles in achieving optimal molecular signals at the liquid interface. Data sets from three model systems, including an ionic liquid, water, and several liposome solutions, will be presented. In addition, beam damage at the liquid surface will also be discussed.

[1] B. Liu, X. Y. Yu, Z. Zhu, X. Hua, L. Yang, Z. Wang, *Lab Chip*, **2014**, *14*, 855.

[2] X. Hua, X. Y. Yu, Z. Wang, L. Yang, B. Liu, Z. Zhu, A. E. Tucker, W. B. Chrisler, E. A. Hill, S. Thevuthasan, Y. Lin, S. Liu, and M. J. Marshall, *Analyst*, **2014**, *139*, 1609.

[3] L. Yang, Z. Zhu, X. Y. Yu, S. Thevuthasan, J. P. Cowin, *Anal. Methods*, **2013**, *5*, 2515.

6:00pm AS+BI-TuA12 **Fundamental Metrology for Tissue Imaging by SIMS - A Study of Cholesterol and Determination of the Argon Cluster Sputtering Yield**, *P.D. Rakowska, M.P. Seah, Rasmus Havelund, I.S. Gilmore*, National Physical Laboratory, UK

Secondary Ion Mass Spectrometry (SIMS) has become an invaluable tool to study organic and biological samples. An important biological application is in the analysis of mammalian cellular membranes. Considerable contribution to the field comes with the use of large cluster ion beams, and in recent years the application of argon gas cluster ion beam has emerged as the prevailing method.

Cholesterol, as a key component of nearly all mammalian cell membranes, is of particular interest. It alters the physical properties of the membranes, interacts with neighbouring lipids and proteins and is involved in numerous biomolecular processes. Being able to detect, identify and characterise the distribution of cholesterol in biological samples has vast implications in medical sciences. To do this, we need to underpin the basic metrology involved. It is important to evaluate cholesterol sputtering yields for argon cluster sputtering over a range of energy and cluster sizes so that a general description of the molecule behaviour may be established.

In this study, we compared the use of C_{60}^{+} and Ar_n^+ as sputtering ions for depth profiling of cholesterol thin films. Films of different thicknesses were prepared by thermal evaporation and the sputtering yields of cholesterol were measured from depth profiles made using 2.5 to 20 keV Ar_{1000}^+ and Ar_{5000}^+ and 10 and 20 keV C_{60}^{+} sputtering beams. We show that, at room temperature, the C_{60}^{+} ions caused significant damage but gave a well-behaved depth profile whereas Ar_n^+ gas clusters left the material undamaged but the very clean layer readily restructured making the profiles much more complex. This restructuring does not occur at room temperature normally but results from the actions of the beams in the sputtering process for profiling in SIMS. The sputtering yields from these restructured films are up to twice that for material not so restructured. Good profiles may be made by reducing the sample temperature. This is likely to be necessary for many lower molecular weight materials (below 1000 Da) to avoid the movement of molecules. The yields for both C_{60}^{+} and Ar_n^+ fit the universal yield equation [1]. Our results show that considerable differences can occur between the measurements performed with the two ion clusters, affected, in addition, by factors such as sample temperature or exposure to light. These will be discussed.

[1] M.P. Seah, *J. Phys. Chem. C*, **2013**, *117* (24), pp 12622–12632

In-Situ Spectroscopy and Microscopy Focus Topic Room: 211C - Session IS+AS+SS-TuA

Environmental TEM Studies for Catalytic and Energy Materials

Moderator: Franklin (Feng) Tao, University of Kansas, Judith Yang, University of Pittsburgh

2:20pm IS+AS+SS-TuA1 ***In Situ* and *Operando* TEM of Thermal and Photocatalysts**, *Peter Crozier, B.K. Miller, L. Zhang, Q. Liu*, Arizona State University

INVITED

Heterogeneous catalysts play a vital role in the development of energy technologies. Understanding the fundamental relationships between catalyst activity and structure at the nanoscale will enable the improved design of catalyst nanostructures. *In-situ* and *operando* environmental transmission electron microscopy (ETEM) is a powerful technique for the investigation of structure-reactivity relationships in high surface area catalysts under reaction conditions. With current instruments, atomic resolution imaging and spectroscopy can be carried out in the presence of gas, liquid, light and thermal stimuli. The combination of mass spectrometry and electron energy-loss spectroscopy allow catalytic products to be detected and quantified directly in the electron microscope. Several specific applications of ETEM instrumentation and experiments to several heterogeneous catalysts will be presented.

Photocatalytic water splitting can be accomplished by a heterostructure of several materials, including a light absorbing semiconductor and one or more co-catalysts. Our group has focused on Ni-NiO co-catalysts on both TiO_2 and Ta_2O_5 . In the Ni-NiO/ TiO_2 system, deactivation occurs due to this Ni dissolution into water during illumination and H_2 is only produced by the oxidation of Ni metal[1]. For the Ta_2O_5 supported catalyst, H_2 was produced predominantly by a catalytic reaction [2] and the deactivation rate was found to be inversely proportional to the initial thickness of the NiO shell. In both systems, deactivation is observed only during light illumination, so that this deactivation is properly called photocorrosion.

Our group has also been pioneering the use of *operando* TEM to study CO oxidation over supported Ru nanoparticles [3]. There is uncertainty and debate in the literature regarding the most active form of this catalyst. Images of the Ru nanoparticles after reduction *in-situ* show a clean metal surface, but after only 0.5% O_2 is introduced into the cell, a thin oxide layer forms on the surface. Similar experiments are currently being performed under *operando* conditions.

References:

[1] L. Zhang, et al. *The Journal of Physical Chemistry C*, **119**, (2015), p. 7207–7214.

[2] Q. Liu, et al. *Applied Catalysis B: Environmental*, **172–173**, (2015), p. 58–64.

[3] B.K. Miller, P.A. Crozier *Microscopy and Microanalysis* **20**, (2014), p. 815–824.

[4] The support from the U.S. Department of Energy (DESC0004954), and the National Science Foundation (CBET-1134464), and the use of ETEM at John M. Cowley Center for HR Microscopy at Arizona State University is gratefully acknowledged.

3:00pm IS+AS+SS-TuA3 **Environmental TEM Study of Gold and Platinum Nanoparticulate Catalysts**, *H. Yoshida, Y. Kuwauchi, H. Omote, Seiji Takeda*, Osaka University, Japan

INVITED

The catalytic activity of metal nanoparticles depends on their size, shape, and surface structure. It is well-known that the adsorption of gases induces changes in the shape and surface structure of metal nanoparticles. Thus, it is important to obtain structural information about metal nanoparticles under reaction conditions to elucidate the correlation between the catalytic activity and the morphology of the nanoparticles. Environmental transmission electron microscopy (ETEM) is one of the powerful methods for the study of catalytic materials under reaction conditions at atomic scale [1]. In this study, we have investigated the shape and surface structure of Au and Pt nanoparticles that are supported on CeO_2 in reactant gases by a Cs-corrected ETEM.

We have found that the surface structure of a Au nanoparticle was reconstructed during CO oxidation at room temperature [2]. The {100} facets remain unreconstructed in vacuum. Under CO oxidation reaction conditions, the Au atomic columns on the topmost and second topmost {100} layers shift to peculiar positions. In the reconstructed surface the Au atoms on the topmost surface layer form an undulating hexagonal lattice, while those on the second topmost surface layer form a normal square lattice with slight distortion. This atomic-scale *in-situ* visualizing method

provides us with insights into reaction mechanisms in heterogeneous catalysis.

We have observed the oxidation and reduction processes of the surface of Pt nanoparticles by ETEM. Atomic layers of Pt oxide were formed gradually in O₂ at room temperature during ETEM observations. In situ atomic resolution ETEM, combined with in situ electron energy-loss spectroscopy, showed that atomic layers of Pt oxides, including α -PtO₂ and Pt oxides of other forms, first started forming on the preferential facets of Pt nanoparticles at the early stage, entire oxidation on the whole surface of Pt nanoparticles then followed. The oxides were reduced promptly to Pt by adding a small amount of CO or H₂O vapor to the dominant O₂ gas. It is concluded that electron irradiation during ETEM observation activates the gases non-thermally, therefore promoting or suppressing the processes at room temperature [3].

[1] S. Takeda, Y. Kuwauchi, H. Yoshida, *Ultramicroscopy*, **151** (2015) 178.

[2] H. Yoshida, Y. Kuwauchi, J. R. Jinschek, K. Sun, S. Tanaka, M. Kohyama, S. Shimada, M. Haruta, S. Takeda, *Science***335** (2012) 317.

[3] H. Yoshida, H. Omote, S. Takeda, *Nanoscale*, **6** (2014) 13113.

4:40pm IS+AS+SS-TuA8 Environmental Study of the Reaction-driven Restructuring of Ni-Co Bimetallic Nanoparticles. *C.S. Bonifacio*, University of Pittsburgh, *H.L. Xin*, Brookhaven National Laboratory, *Sophie Careno*, *M.B. Salmeron*, Lawrence Berkeley National Laboratory, *E. Stach*, Brookhaven National Laboratory, *J.C. Yang*, University of Pittsburgh

Bimetallic nanoparticles (NPs) possess novel catalytic, optical, and electronic properties compared to their monometallic counterparts. These catalytic properties can be controlled by fine-tuning the NP structure and dimension, surface oxidation, and chemical composition. For instance, bimetallic NPs with a core-shell structure can allow for fine tuning of reactivity, averting sintering issues in the core, and even increase tolerance to high temperature exposure. Above all, elemental segregation in the core-shell structure has been demonstrated as a potential route of modifying the NPs catalytic properties through *in situ* gas reaction studies. To confirm this hypothesis, we have used *in situ* imaging and spectroscopy techniques to study Ni-Co core-shell NPs under environmental conditions to provide direct evidence of elemental redistribution during reaction. Two pairs of oxidation and reduction reactions were performed in an environmental transmission electron microscope (ETEM) at 0.3 Torr in O₂ and H₂ gas at 220°C and 270°C, respectively. Electron diffraction patterns and electron energy loss spectroscopy (EELS) maps showed a reaction-driven restructuring of the core-shell NPs with Ni species migrating to the NP surface by the 2nd reduction cycle. These results are in agreement with previous ambient-pressure x-ray photoelectron spectroscopy (AP-XPS) studies of the same NPs under identical reaction conditions. Furthermore, the ETEM results confirm the NP structure without erroneous interpretations that may result from post-mortem analysis of the samples. Quantitative analysis of the EELS results is underway to identify the valence states during the oxidation-reduction reactions. Correlation of the reaction-driven restructuring of NPs with the electronic structure changes from ETEM and AP-XPS will provide insight into the optimum reaction conditions, i.e., catalytic properties, of the Ni-Co core-shell NPs in challenging reactions such as selective CO₂ reduction.

5:00pm IS+AS+SS-TuA9 In situ Vibrational Spectroscopy Investigation of the Surface Dependent Redox and Acid-base Properties of Ceria Nanocrystals. *Zili Wu*, Oak Ridge National Laboratory **INVITED**

Ceria is best known for its excellent redox property that makes it an important component in the three-way catalyst for auto exhaust cleanup. This is a result of its high oxygen storage capacity associated with the rich oxygen vacancy and low redox potential between Ce³⁺ and Ce⁴⁺ cations. Equally interesting yet less is known about ceria is its versatile acid-base properties. Either as a standalone catalyst, a modifier or a support, ceria and ceria-based catalysts can catalyze the transformation of a variety of organic molecules that makes use of the acid-base as well as the redox properties of ceria.

Recent advances in nanomaterials synthesis make it possible to achieve nanocrystals with crystallographically defined surface facets and high surface area, which can be considered as ideal model systems for catalytic studies under realistic conditions. In this work, I will showcase how we can make use of ceria nanoshapes as model systems to gain molecular level understanding of the shape effect on both redox and acid-base properties and catalysis of ceria nanocrystals *via in situ* IR and Raman spectroscopy. Insights have been gained into how the surface structure of ceria catalyst affects profoundly its redox and acid-base properties and consequently the catalytic behaviors. It is suggested that the surface structure of ceria controls the catalytic performance through the combination of various factors including structure-dependent surface sites geometry, lattice oxygen

reactivity, surface vacancy formation energy, defect sites, and acid-base property on ceria.

Acknowledgements: This work was supported by Division of Chemical Sciences, Geosciences, and Biosciences, Office of Basic Energy Sciences, U.S. Department of Energy. A portion of the work was supported by the Center for Understanding & Control of Acid Gas-Induced Evolution of Materials for Energy (UNCAGE-ME), an Energy Frontier Research Center funded by DOE, Office of Science, Basic Energy Sciences. The IR and Raman work were conducted at the Center for Nanophase Materials Sciences, which is a DOE Office of Science User Facility.

5:40pm IS+AS+SS-TuA11 Direct Writing of sub-10 nm Structures from Liquid with Helium Ions. *V. Iberi*, *R.R. Unocic*, *Nathan Phillip*, *A. Belianinov*, *A.J. Rondinone*, *D.C. Joy*, *O.S. Ovchinnikova*, Oak Ridge National Laboratory

In-situ direct writing by electron beam from solutions opens a pathway for resistless fabrication of nanostructures at high throughput. However, when using electrons to direct write in solution the minimal size of the created structures is limited to the micron scale due to fundamental physics of the interactions between the electron beam and the liquid, including the lateral transport of solvated electrons and ionic species. Use of the helium beam with the opposite charge and shorter mean free path offers the potential for the localization of the reaction zone on the single digit nanometer scale. Here we will present our results demonstrating writing of platinum structures from liquid (beam induced electroplating) in a platinum chloride solution using helium ions with sub-10 nm resolution. Using data analytics on acquired in-situ growth movies we are able to elucidate the main statistical descriptors for helium ion beam initiated platinum structure growth. The possible mechanisms of beam induced growth and ultrahigh localization of reaction zone are discussed. Furthermore, we will discuss optimization of solution chemistry and instrumental parameters as they relate to the quality and thickness of structures and the extension to device fabrication on a single digit nanometer level.

This work was conducted at the Center for Nanophase Materials Sciences, which is a Department of Energy (DOE) Office of Science User Facility.

Surface Science

Room: 113 - Session SS+AS+EN-TuA

Mechanistic Insight of Surface Reactions: Catalysis, ALD, etc. - II

Moderator: Bruce D. Kay, Pacific Northwest National Laboratory

2:20pm SS+AS+EN-TuA1 How does Absorbed Hydrogen Drive Olefin Hydrogenation on Pd? *Satoshi Ohno*, *M. Wilde*, *K. Fukutani*, The University of Tokyo, Japan

Pd-dissolved hydrogen is an essential ingredient in the highly selective hydrogenation of olefinic C=C double bonds catalyzed by Pd, yet the particular role played by H below the surface has long been debated controversially. Some proposed that absorbed H atoms become directly involved in hydrogenation reactions after they emerge from the metal interior onto the catalyst surface in an energetic state. Others considered that sizeable populations of subsurface sites by absorbed hydrogen indirectly activate surface-adsorbed hydrogen by altering the electronic structure of the catalyst.

To resolve this dispute we have studied the hydrogenation reaction of cis-2-butene to butane on a Pd(110) model catalyst surface with temperature-programmed desorption (TPD) and ¹H(¹⁵N, ag)¹²C nuclear reaction analysis (NRA) that reveals the hydrogen distribution on and beneath the surface. TPD demonstrates that the catalytic hydrogenation reaction proceeds efficiently between 160 and 250 K. NRA under the hydrogenation reaction condition, on the other hand, shows that the H concentration in the Pd subsurface region is as small as 0.5 at. %. Thus, the scenario of indirect surface-hydrogen activation through large quantities of H in the subsurface sites appears rather unrealistic for our experimental conditions. We furthermore elucidate that the butane reaction yield scales linearly with the number of Pd-dissolved H atoms that reach the surface after diffusion from the Pd bulk. This observation clarifies that the Pd-catalyzed olefin hydrogenation is triggered by the emergence of bulk-dissolved hydrogen onto the Pd surface. Our NRA H profiles also demonstrate that the catalytic reaction proceeds on the Pd surface fully saturated with chemisorbed hydrogen. This surface hydrogen is considered important, as it possibly prevents deactivation of reactive surface hydrogen species in vacant chemisorption sites.

Finally, the TPD spectrum of butene shows four peaks at 140, 165, 190, and 225 K, suggesting multiple butene-adsorption modes onto Pd(110) surfaces. Reactive TPD experiments in presence of absorbed hydrogen exhibit a significant decrease in the 165 K peak, identifying this feature as the reactive butene species in the catalytic hydrogenation reaction.

2:40pm SS+AS+EN-TuA2 CO Oxidation over Pd Catalysts Supported on Different Low-Index Surfaces of CeO₂: A Combined Experimental and Computational Study, Xiao Liu, Y.W. Wen, Z.Z. Chen, B. Shan, R. Chen, Huazhong University of Science and Technology, China

Pd/CeO₂ has attracted much attention on the low temperature CO oxidation due to the strong metal-support interactions. In this study, we have systematically investigated the interface properties and CO oxidation activities of Pd catalysts supported on different low-index surfaces of CeO₂. The Pd/CeO₂ nanorods have been prepared by incipient wetness impregnation method and the exposed surfaces of CeO₂ nanorods have been controlled by changing the calcination temperature after their successful synthesis by hydrothermal method. Their catalytic activities in CO oxidation have been tested and the results show that Pd catalysts supported on CeO₂ nanorods exposed by (100) and (110) (calcined at 500 °C) are more activated than that exposed by (111) (calcined at 700 °C), which is related to the surface oxygen vacancies concentration and the strength of interface interaction. By performing density functional calculations, the surface oxygen activities and the binding strength of Pd clusters on these low-index surfaces of CeO₂ have been investigated. The results show that the oxygen vacancy formation energies of (100) and (110) are smaller than that of (111). The binding strength of Pd clusters on these surfaces follows the sequence: (100) > (110) > (111). Furthermore, CO oxidation routes on these surfaces proceeding through the LH, ER and MvK mechanism have been studied. Our studies not only reveal that the catalytic performance of Pd/CeO₂ can be tuned by controlling the exposed surface of oxide but also shed light on the interface structures and CO oxidation mechanism of Pd/CeO₂ system.

3:00pm SS+AS+EN-TuA3 In Situ Adsorption and Decomposition Studies of Dimethyl Methyl Phosphonate on Molybdenum Oxide Surfaces and Nanoparticles, Ashley Head, L. Trotochaud, Y. Yu, Lawrence Berkeley National Laboratory (LBNL), Z. Hicks, X. Tang, K. Bowen, Johns Hopkins University, B. Eichhorn, University of Maryland, College Park, H. Bluhm, LBNL

There is great interest in understanding the interaction between the nerve agent simulant dimethyl methyl phosphonate (DMMP) and metal oxide surfaces to further nerve agent filtration technology and decomposition methods. To this end, we have studied the room temperature adsorption of DMMP on MoO₂ and MoO₃ surfaces up to 30 mTorr using ambient pressure x-ray photoelectron spectroscopy (APXPS). On both surfaces, the majority of DMMP adsorbs intact, but differences in the behavior of DMMP on the two substrates are found upon heating. Two phosphorus species are seen on the MoO₂ surface and three are seen on the MoO₃; these species remain on both surfaces up to 450 °C. Additionally, carbon remains on the MoO₂ at high temperatures but is removed from MoO₃ by 420 °C. The APXPS data were correlated with TPD measurements of DMMP adsorbed on MoO₃ clusters on HOPG, a model system closer to real filtration materials. Methanol was found as the major decomposition product in addition to trace amounts of dimethyl ether. The easily reducible MoO₃ is likely responsible for an oxidative cleavage of the P-CH₃ bond on both the surface and nanoparticles. These studies highlight how APXPS coupled with TPD yields chemical information relevant to real-world applications.

3:20pm SS+AS+EN-TuA4 Adsorption of Sterically Hindered Sulfur Containing Molecules on a Heterogeneous Model Catalyst, Signe Sørensen, J.V. Lauritsen, Aarhus University, Denmark

Cobalt promoted MoS₂ nanoclusters (CoMoS) are the active phase of the hydrodesulfurization catalyst which enables sulfur removal from crude oil. New legislations on sulfur impurity levels in diesel in EU and US demands still lower sulfur content which increases the requirements for even more effective catalysts.

Previously catalysts were improved by costly trial-and-error experiments. To target the improvements attempts, understanding of the catalytic mechanism is crucial. In the hydrodesulfurization catalysis the main source to residual sulfur content is the sterically hindered sulfur containing molecules, as the reactivity towards these is very low. To targeted enhance the catalytic activity, atomic scale understanding of this catalytic mechanism is essential.

Scanning tunneling microscopy (STM) is an outstanding tool for real space, atomic-scale imaging of supported nano-scale systems. This makes it the optimal tool for investigating the interaction between the sulfur containing molecules and metal-supported CoMoS, as it offers the unique and powerful

ability to directly observe the catalytic active site by imaging single molecules adsorbing on the nanoparticles.

In this study STM is used on a model system of Co-promoted MoS₂ on a gold substrate under ultrahigh vacuum conditions. To study the adsorption of the strongly steric hindered sulfur containing molecule 4,6-dimethyl-dibenzothiophene the molecule is dosed directly onto the nanoparticles which means that their location, orientation and the dynamics of single molecules can successfully be revealed through atom-resolved STM images and films. All observed adsorption modes are either associated with a sulfur vacancy on the corner site of the nanoclusters or with the one-dimensional metallic edge state associate with the edge of the Co-promoted MoS₂ nanoclusters. These observations strongly indicate that these sites are important active sites of the catalyst and enable targeting the attempts for enhanced activity to optimization of the number of these apparent active sites in the industrial catalyst.

4:20pm SS+AS+EN-TuA7 Metal Nanoparticles on Thin Film Oxide Supports: Interaction and Reaction of Metals with Hydroxyls, Martin Sterrer, University of Graz, Austria

INVITED

Water-oxide interaction is of great importance in a number of technologically relevant fields, among them heterogeneous catalysis. Several studies report on the promoting effect of water in catalytic reactions, the participation of surface hydroxyls in catalytic reactions, and the influence of hydroxylation on the binding of metals to oxide surfaces. Achieving a fundamental atomic scale understanding of water-oxide interaction at environmentally and catalytically relevant conditions (e.g. ambient pressure) represents, therefore, a challenge for surface science studies related to heterogeneous catalysis. In this contribution, I will present results of our recent studies related to the interaction of water with thin, single crystalline oxide films (Fe-oxides, alkaline earth oxides) carried out in a wide range of water chemical potential (from UHV to mbar water pressures). Topics that will be discussed are the characterization of ordered water monolayers, the dewetting of ice on oxide surfaces, hydroxylation of oxide surfaces at elevated pressure, the influence of hydroxyls on metal nucleation and sintering, and metal deposition onto oxide surfaces from aqueous solutions.

5:00pm SS+AS+EN-TuA9 Dynamics of Isolated Surface Complexes Formed Between a Chemisorbed Chiral Molecule and a Prochiral Reactant, Jean-Christian Lemay, Y. Dong, P.H. McBreen, Laval University, Canada

Adsorbed chiral molecules (chiral modifiers) can interact stereoselectively with prochiral co-adsorbates on reactive metal surfaces (1). This is used in one of the most common methods to perform asymmetric heterogeneous catalysis. The chiral modifier provides stereoselection through non-covalent assembly with a substrate, forming isolated complexes with well-defined geometries. We will present a variable temperature STM study of individual bimolecular complexes formed by enantiopure 1-(1-naphthyl)ethylamine and three representative prochiral substrates on Pt(111). The results reveal sub-molecularly resolved and time-resolved stereospecific data for competing complexation geometries. Time-lapsed STM measurements of individual substrate molecules sampling a set of interaction geometries provide new insight on the dynamics of stereocontrol. The results reveal that a single prochiral substrate can probe various sites on the surface due to diffusion and prochiral switching. This shows the importance of considering interconversion between complexation geometries to fully understand the stereocontrol operated by the chiral modifier. The results will be discussed in the context of proposed mechanisms for enantioselective hydrogenation.

5:20pm SS+AS+EN-TuA10 Density Functional Theory Study of CO Assisted Water Dissociation, Liney Arnadottir, L. Halberstadt, Oregon State University

Previous computational studies of methanol oxidation reaction intermediates (H-C=O and C-OH) have shown significant effects of water on both adsorbate adsorption energy as well as activation energies of interconversion between the two. On a clean Pt(111) surface the interconversion between the two forms goes through a very stable COads and Hads intermediates and the activation barriers of CO + H to form HCO or COH are high or 1.3 and 1.8 eV respectively. In the presence of a single coadsorbed water molecule the activation barrier for this interconversion from HCO to COH was found to be much lower or 0.62 eV. These studies were motivated by experimental studies of methanol oxidation on Pt which found CO₂ formation at potentials lower than typically required for CO oxidation. Here we investigate Pt-water interactions and the effects of co-adsorbate CO on water dissociation as a possible CO assisted water dissection as an alternative reaction pathway on Pt surfaces.

6:00pm **SS+AS+EN-TuA12 Crystalline Growth of Ice - Studying the Transition from the First Wetting Layer to Multilayers with Scanning Tunneling Microscopy.** *Barbara Lechner, S. Maier, M.B. Salmeron,* Lawrence Berkeley National Laboratory

The growth of water layers on model substrates has been studied intensively, yet many questions still remain [1,2]. After many years of research, the structure of the first wetting layer on metal surfaces has been determined in comprehensive experimental and theoretical studies [3-5]. A surprisingly complex behavior was revealed, showing that the strain caused by the mismatch of the hexagonal planes in the ice crystal structure and the lattice of the substrate is released by forming structures that include rotated hexagons, pentagons and heptagons of molecules, in addition to strongly bound hexagonal rings commensurate with the substrate. A range of experimental and theoretical investigations showed that, on many substrates, the water monolayer does not expose any dangling hydrogen bonds as all water molecules adsorb either flat-lying or with a hydrogen atom pointing towards the surface [1,6]. Growth of multilayer water films that preserve the “down-pointing” average dipole orientation of water has been proposed to occur in some cases, resulting in the formation of “ferroelectric ice” [7]. However, the growth of the entropically more favorable, proton-disordered ice requires flipping some of the molecules in the first layer to expose dangling hydrogen bonds. Such molecular reorientation may be kinetically hindered, and has been invoked to be the reason for the hydrophobic character of many water monolayer films at low temperatures [6].

Here, we present high-resolution scanning tunneling microscopy (STM) measurements of water layers adsorbed on Pt(111) and Ru(0001) to study the transition from the first layer to multilayers. We observe that a second water layer initially grows in an amorphous structure when grown on the crystalline monolayer containing pentagons, hexagons and heptagons of water molecules. To facilitate the growth of ice in a bulk-like hexagonal arrangement, the first wetting layer needs to rearrange into a hexagonal structure commensurate with the surface.

[1] Hodgson, A.; Haq, S. *Surf. Sci. Rep.* **2009**, *64*, 381–451.

[2] Carrasco, J.; Hodgson, A.; Michaelides, A. *Nat. Mater.* **2012**, *11*, 667–674.

[3] Maier, S.; Stass, I.; Cerdá, J. I.; Salmeron, M. *Phys. Rev. Lett.* **2014**, *112*, 126101.

[4] Tatarkhanov, M.; Ogletree, D. F.; Rose, F.; Mitsui, T.; Fomin, E.; Maier, S.; Rose, M.; Cerdá, J. I. *J. Am. Chem. Soc.* **2009**, *131*, 18425–18434.

[5] Nie, S.; Feibelman, P. J.; Bartelt, N. C.; Thürmer, K. *Phys. Rev. Lett.* **2010**, *105*, 026102.

[6] Kimmel, G. A.; Petrik, N. G.; Dohnálek, Z.; Kay, B. D.; Kimmel, G. A.; Petrik, N. G.; Dohnálek, Z.; Kay, B. D. *J. Chem. Phys.* **2007**, *126*, 114702.

[7] Su, X.; Lianos, L.; Shen, Y. R.; Somorjai, G. A. **1998**, 1533–1536.

Wednesday Morning, October 21, 2015

Actinides and Rare Earths Focus Topic
Room: 230A - Session AC+AS+MI-WeM

Magnetism, Complexity and Superconductivity in the Actinides and Rare Earths

Moderator: Tomasz Durakiewicz, Los Alamos National Laboratory

8:00am **AC+AS+MI-WeM1 The Valence-Fluctuating Ground-State of δ -Pu**, *Marc Janaschek*, Los Alamos National Laboratory **INVITED**

Plutonium (Pu) is arguably the most complex elemental metal known because its 5f electrons are tenuously poised at the edge between localized and itinerant configurations. This complex electronic structure leads to emergent behavior—all a direct consequence of its 5f electrons—including six allotropic phases, large volumetric changes associated with these transitions of up to 25%, and mechanical properties ranging from brittle α -Pu to ductile δ -Pu. Pu also exhibits a Pauli-like magnetic susceptibility, electrical resistivity and a Sommerfeld coefficient of the specific heat that are an order of magnitude larger than in any other elemental metal. Finally, while experiments find no sign for static magnetism in Pu, most theories that use the correct volume predict a magnetically ordered state. This discrepancy might be reconciled by recent Dynamical Mean Field Theory (DMFT) calculations that suggest that the electronic ground state of δ -Pu is a quantum-mechanical admixture of localized and itinerant valence configurations. The question whether the ground state of δ -Pu is indeed a true quantum-mechanical superposition may only be answered via observation of the associated virtual valence (charge) fluctuations among the distinct $5f^6$, $5f^7$, and $5f^8$ configurations. The characteristic energy scale for the associated spin fluctuations is expected to $T_K \approx 800$ K ($E_{sf} \approx 70$ meV) that will result in a dynamical spectral response centered at this energy for $T < T_K$. We have performed high-energy inelastic neutron spectroscopy at room temperature using a large polycrystalline sample of δ - ^{242}Pu with a total mass of $m \approx 21$ g at the Lujan Center and at the Spallation Neutron Source. Our measurements demonstrate the existence of high energy magnetic fluctuations centered at $E_{sf} = 84$ meV, in good agreement with the DMFT calculations. In addition, they allow us to extract the magnetic form factor of δ -Pu, yielding critical information about its valence state. These unprecedented results place show that the magnetism in Pu is not "missing" but dynamic, but dynamic, and is driven by virtual valence fluctuations. Our measurements provide a straightforward interpretation of the microscopic origin of the large, Pauli-like magnetic susceptibility of δ -Pu and associated Sommerfeld coefficient. Furthermore, because the various valence configurations imply distinct sizes of the Pu ion, the valence-fluctuating ground state of Pu also provides a natural explanation for its complex structural properties and in particular the large sensitivity of its volume to small changes in temperature, pressure or doping.

8:40am **AC+AS+MI-WeM3 Exchange Bias in Heterostructures Based on UO_2** , *Evgeniya Tereshina*, Institute of Physics ASCR, Czech Republic, *Z. Bao*, PANalytical B.V., Netherlands, *L. Havela*, Charles University in Prague, Czech Republic, *R. Springell*, University of Bristol, UK, *S. Danis*, Charles University in Prague, Czech Republic, *A. Mackova*, Nuclear Physics Institute ASCR, Czech Republic, *T. Gouder*, *R. Caciuffo*, Institute for Transuranium Elements (ITU), Germany **INVITED**

Interfacial exchange interaction in bilayers consisting of two dissimilarly ordered magnetic materials (e.g. an antiferromagnet (AF) and a ferro- or ferrimagnet (F)) may give rise to a phenomenon called the magnetic exchange bias (EB) effect [1]. The EB manifests itself as a shift of a magnetic hysteresis loop along the field direction when the bilayer is field-cooled below the Néel temperature (T_N) of the AF. This property is of great value for magnetic recording applications. Despite the conceptual simplicity, a generally accepted theory that predicts the EB behavior for an apt pair of materials is still missing. The reason for that might be in poorly defined interface structure in both magnetic and crystallographic aspects.

Critical dependence of EB on magnetic anisotropy brings us the possibility to use actinides with strong spin-orbit interaction as the key ingredient. Here we report exchange bias studies in magnetic bilayers consisting of a stoichiometric UO_2 film grown epitaxially on different substrates and covered with polycrystalline metallic ($\text{Ni}_{180}\text{Fe}_{20}$ and Fe) and highly textured oxide (Fe_3O_4) layers of variable thickness. Large longitudinal exchange bias ~ 2.6 kOe is found in $\text{UO}_2/\text{Fe}_3\text{O}_4$ bilayers [3] while UO_2 combined with metallic ferromagnets displays perpendicular exchange coupling with an order of magnitude smaller EB. Interestingly, unusual effects in $\text{UO}_2/\text{Fe}_3\text{O}_4$ were observed, namely, exchange bias did not vanish at T_N of UO_2 . Apart from the fact that single layers of magnetite were showing some EB (not

more than 25 % of the total effect in $\text{UO}_2/\text{Fe}_3\text{O}_4$), the EB in $\text{UO}_2/\text{Fe}_3\text{O}_4$ bilayers exceeded notably that of the single Fe_3O_4 's to approx. 70 K that was attributed to possible proximity effects of Fe_3O_4 on T_N of UO_2 and/or to the magnetic anisotropy of UO_2 preserved locally above T_N . The effects were observed for the samples of quality controlled by different methods such as X-ray Photoelectron Spectroscopy, conventional X-ray Diffraction, Transmission Electron Microscopy and Rutherford Backscattering Spectroscopy. The work has been supported by the Czech Science Foundation, grant No. 13-25866P.

[1] W. H. Meiklejohn and C. P. Bean, "New magnetic anisotropy", Phys. Rev. B 102, 1413 (1956).

[2] V. Sechovsky, L. Havela, in: Magnetic Materials, K.H.J. Buschow (Ed.), Elsevier, Amsterdam, 1998, Vol. 11, p. 1.

[3] E. A. Tereshina et al., Appl. Phys. Lett. 105, 122405 (2014).

9:20am **AC+AS+MI-WeM5 Transport and Magnetism of 4f and 5f Systems: What we can Learn from Thermoelectric Power**, *Krzysztof Gofryk*, Idaho National Laboratory **INVITED**

The interplay between different electronic ground states, especially magnetism and superconductivity, has evolved in a climate of discovery in which many of the fundamental rules of condensed matter physics are questioned by materials with unexpected properties. These "emergent properties," such as complex magnetism, heavy-fermion superconductivity, the coexistence of magnetism and superconductivity, and/or Kondo physics emerge from complex materials in which quasiparticles develop different states of organization and correlation. The majorities of these bizarre electronic ground states are encountered in f -electron systems and are linked to the hybridization between the f -states and ligand electrons. How these properties evolve with the progressive filling of the f -shells remains an open question, but it is a key ingredient for their understanding. The 4f and 5f strongly correlated electron systems at the border of magnetism are of active current interest, particularly because the accompanying quantum criticality provides a route towards both strange-metal, non-Fermi-liquid behavior, and unconventional superconductivity. In spite of large theoretical and experimental efforts the nature of the electronic behaviors is still unclear. One way to address the electronic properties of these fascinating materials is to perform extensive transport studies such as Hall, Nernst, or Seebeck effects. In particular, the latter one has gained importance in recent years in thermoelectric materials as potential solutions for applications, such as spot cooling of electronic components, waste heat recovery system and/or remote power generation in space stations and satellites. In addition, the Seebeck coefficient is a sensitive probe of energy relative to the Fermi level, it can therefore be used as a tool to characterize the electronic structure of materials, especially in the vicinity of the narrow gap or pseudo-gap. During the talk I will provide a general introduction to the magnetic and transport characteristics of 4f and 5f electron systems. Then, I will present thermoelectric properties of selected 4f and 5f materials and give an overview on how the thermoelectric power studies can be used to probe electronic properties in this class of materials. I will discuss implications of the results, and their limitations.

11:00am **AC+AS+MI-WeM10 Magnetic Properties of 2-2-1 Rare-earth and Uranium Compounds and their Interaction with Hydrogen**, *Silvie Maskova*, Charles University, Prague, Czech Republic, *R.V. Denys*, Institute for Energy Technology, Kjeller, Norway, *I. Halevy*, Nuclear Research Center Negev, Beer-Sheva, Israel, *K. Miliyanchuk*, *L. Akselrud*, Ivan Franko National University of Lviv, Lviv, Ukraine, *A. Kolomiets*, Lviv Polytechnic National University, Lviv, Ukraine, *V. Yartys*, Institute for Energy Technology, Kjeller, Norway, *M. Giovannini*, University of Genova, Genova, Italy, *L. Havela*, Charles University, Czech Republic

We have been studying some members of large family of $\text{A}_2\text{T}_2\text{X}$ (A = Rare-Earth (RE) or actinide, T = transition metal, X = p -metal) compounds crystallizing in the Mo_2FeB_2 structure type (space group $P4/mbm$). $\text{U}_2\text{T}_2\text{X}$ interact with H_2 only at high pressure (≈ 100 bar) reaching 2 H/f.u. The H absorption produces a lattice expansion, while the tetragonal structure is preserved. The H atoms presumably enter the 8k position inside the U_3T tetrahedra occupied randomly up to 50%. On the other hand, it was found that some $\text{RE}_2\text{T}_2\text{X}$ compounds can absorb more hydrogen compared to their U-counterparts in much lower H pressures. The amorphization of the structure upon hydrogenation (4 H/f.u.) was found for $\text{RE}_2\text{Pd}_2\text{In}(\text{Sn})$ with light RE (La, Nd). $\text{RE}_2\text{Pd}_2\text{In}(\text{Sn})$ with heavy RE behave similar way as $\text{U}_2\text{T}_2\text{X}$ compounds (2 H/f.u., crystal structure type not changed). For the isostructural indide $\text{Nd}_2\text{Ni}_2\text{In}$ the hydrogen absorption of 7 H/f.u. leads to the orthorhombic distortion of the crystal structure.

Recently, we have been studying several isostructural $\text{RE}_2\text{T}_2\text{Mg}$ (T = Ni, Pd). The H absorption in these compounds depends on the type of transition

metal. The compounds with Ni tend to absorb up to 8 H/f.u. The crystal structure is changed to monoclinic (space group $P2_1/c$). If the transition metal is Pd, the hydrogen absorption is lower, reaching approx. 6 H/f.u. and the crystal structure is modified in different way. The Tb_2Pd_2Mg -hydride crystallizes in a new ternary structure type ($Fmmm$). In the case of Mg-compounds, the hydrogen absorption is not reversible. Upon desorption of H the initial crystal structure is not restored.

We have found that in U-compounds the ordering temperatures increase upon hydrogenation contrary to the RE-compounds where the ordering temperatures are dramatically reduced. Magnetic properties of U-compounds strongly depend on the inter-U distances. Hydrogen intrusion modifies the lattice by expanding it without changing the crystal-structure type leading to a band narrowing. As a consequence doping of U intermetallics by interstitial hydrogen leads to stronger magnetic properties. On the other hand, the hydrogen absorption has opposite effect on magnetic properties of RE_2T_2X compounds. For RE compounds, hydrogenation affects mainly the $4f$ -magnetic moments and their ordering. The exchange coupling is reduced presumably by reducing the concentration of conduction electrons.

11:20am **AC+AS+MI-WeM11 Structural, Electronic, and Magnetic Characteristics of Np_2Co_{17} and Analogue Compounds Under Pressure.** *Izhak Halevy*, Nuclear Research Center Negev, Israel, *A. Hen*, Institute for Transuranium Elements (ITU), Germany, *I. Orion*, Ben Gurion University, Israel, *E. Colineau*, *R. Eloidri*, *J.C. Griveau*, ITU, Germany, *F. Wilhelm*, *A. Rogalev*, ESRF, France, *N. Magnani*, *A.B. Shick*, *R. Caciuffo*, ITU, Germany

A previously unknown neptunium-transition-metal binary compound Np_2Co_{17} has been synthesized and

characterized by means of powder x-ray diffraction, ^{237}Np Mössbauer spectroscopy, superconducting-quantum-interference-device magnetometry, and x-ray magnetic circular dichroism. The compound crystallizes

in a Th_2Ni_{17} -type hexagonal structure with room-temperature lattice parameters $a=8.3107\text{\AA}$ and $c=$

8.1058\AA . Magnetization curves indicate the occurrence of ferromagnetic order below $T_C>350\text{ K}$. Mössbauer

spectra suggest a Np^{3+} oxidation state and give an ordered moment of $\mu_{Np}=1.57\mu_B$ and $\mu_{Co}=1.63\mu_B$

for the Np atoms located, respectively, at the $2b$ and $2d$ crystallographic positions of the $P6_3/mmc$ space group.

Combining these values with a sum-rule analysis of the XMCD spectra measured at the neptunium $M_{4,5}$ absorption

edges, one obtains the spin and orbital contributions to the site-averaged Np moment [$\mu_S=-1.88\mu_B$,

$\mu_L=3.48\mu_B$]. The ratio between the expectation value of the magnetic-dipole moment and the spin magnetic

moment ($m_{md}/\mu_S=1.36$) is positive as predicted for localized $5f$ electrons and lies between the values

calculated in intermediate-coupling (IC) and jj approximations. The expectation value of the angular part of

the spin-orbit-interaction operator is in excellent agreement with the IC estimate. The ordered moment averaged

over the four inequivalent Co sites, as obtained from the saturation value of the magnetization, is $\mu_{Co}\sim 1.6\mu_B$.

The experimental results are discussed against the predictions of first-principles electronic-structure calculations

based on the spin-polarized local-spin-density approximation plus the Hubbard interaction. The structural behavior of Np_2Co_{17} is investigated by means of high pressure diamond-anvil compression measurements and is compared with that of the isostructural compounds Lu_2Co_{17} and Lu_2Ni_{17} . The Th_2Ni_{17} -type hexagonal crystal structure is preserved with no measurable discontinuous volume collapses up to the highest achieved pressure, $p=43\text{ GPa}$. For Np_2Co_{17} , fits to the Birch-Murnaghan and Vinet equations of state give values of the isothermal bulk modulus and

its pressure derivative of $B_0=286\text{ GPa}$ and $B_0=3$, revealing that this Np compound is a highly incompressible solid with stiffness comparable to that of superhard covalently bonded materials. The isothermal equation of state for the studied compounds are in excellent agreement with the results of *ab initio* fully-relativistic, full potential local spin-density functional calculations. Theoretical estimates of the bulk modulus are given also for Np_2Ni_{17} , for which B_0 is predicted to assume values intermediate between those measured for Lu_2Ni_{17} and Np_2Co_{17} .

11:40am **AC+AS+MI-WeM12 Alloying UH_3 as a Probe into the $5f$ Magnetism.** *Ladislav Havela*, *M. Paukov*, *I. Tkach*, *M. Cieslar*, *Z. Matej*, *D. Kriegner*, *D. Drozdenko*, *I. Turek*, *M. Divis*, Charles University, Czech Republic, *N.-T.H. Kim-Ngan*, Pedagogical University, Poland

Several routes of preparation of alloyed U trihydrides, UH_3 , were discovered. Starting from the U_6T compounds, hydrogenation leads to T atoms embedded in the $\beta-UH_3$ structure, with transition-metal atoms T occupying one of the U sites. We have been hydrogenating $\gamma-U$ alloys, using various transition metals helping (together with ultrafast cooling) to retain the bcc U structure down to low temperatures. As such alloys are much more resistant to hydrogen attack, high pressures of H_2 gas had to be applied. The H absorption corresponds to approx. $3H/\text{atoms per } 1\text{ U atom}$. In none of the cases the alloying metals segregate and two different structures were obtained. The hydrides $(UH_3)_{1-x}Zr_x$ form the $\alpha-UH_3$ structure, i.e. the bcc structure expands and fills by H. Hence basic electronic properties of $\alpha-UH_3$ could be established. Starting from $U_{1-x}Mo_x$, we obtained $(UH_3)_{1-x}Mo_x$, which tends to be $\beta-UH_3$ like, but has the grain size is 1 nm only, i.e. practically amorphous. This amorphous phase also easily accepts additional dopants, as Zr, Fe, Ti, V...however magnetic properties remain only weakly affected. It is quite remarkable that all such materials are ferromagnets with the Curie temperature in the range 160-205 K, even if the active U sublattice is diluted by more than 30% of other metals. In this respect the hydrides are different than conventional band ferromagnets, sensitive to inter-atomic spacings and alloying. Albeit all are metallic, the U-H interaction, which can have a partly ionic character, plays clearly important role. Electronic structure calculations (performed for the $\alpha-UH_3$ structure and in ferromagnetic or Disordered Local Moment state, with possible random Zr occupancy) suggest a transfer of U-6d and 7s electrons into H-1s states, reducing the hybridization of 5f and non-f states, supporting thus magnetism even if the U-U spacing is below the Hill limit [1].

[1] I. Tkach et al. Phys.Rev. B 91, 115116 (2015).

Applied Surface Science

Room: 212D - Session AS-WeM

Practical Surface Analysis II: Influence of Sample Preparation and Novel Sample Prep Techniques

Moderator: Gregory Herman, Oregon State University, Kathryn Lloyd, DuPont Corporate Center for Analytical Sciences

8:00am **AS-WeM1 ASSD 30th Anniversary Lecture: A Historical Perspective of the Materials Challenges and Instrumentation Solutions Available for Practical X-ray Photoelectron and Auger Electron Spectroscopy.** *John Moulder*, Physical Electronics USA **INVITED**

During the first 30 years of the Applied Surface Science Division's (ASSD) existence the changing world around us has driven the need for new materials for a wide range of applications including: higher performance coatings, structural materials, electronics, data storage devices, display and printing technology, energy storage devices, and many more. For most of these materials systems the composition of a surface, interface, thin film or nanostructure plays a critical role in the performance of the material. During the same period of time, analysts have endeavored to characterize these new materials and instrument manufacturers have endeavored to provide the analytical capabilities required by the analyst to answer critical questions about the materials being studied.

When the ASSD was formed in the 1985 the second generation of XPS and AES based surface analysis instrumentation was emerging and surface analysts were characterizing structural materials, catalysts, thin film coatings, semiconductor devices, magnetic storage media, and more. Common challenges faced by the analyst included quantification, insulator analysis, micro area analysis, the desire for more chemical information, the desire for 2D and 3D information, and keeping up with the demand for more data.

This presentation will provide a historical perspective on the evolution of both the materials challenges faced by surface analysts and the XPS and AES instrumentation that became commercially available to address these challenges. Finally we will comment on where we are today and possible future directions.

8:40am **AS-WeM3 Using Argon clusters for Improved XPS Information**, Jonathan Counsell, S.J. Coultas, C.J. Blomfield, D. Surman, C. Moffitt, Kratos Analytical Limited, UK

A thin layer of carbonaceous material is commonly found on the surface of air exposed samples - this layer is generally known as adventitious carbon. Adventitious carbon is generally comprised of a variety of relatively short chain, perhaps polymeric hydrocarbons species with small amounts of both singly and doubly bound oxygen functionality. Even brief exposures to atmosphere will produce a thin overlayer. During XPS analysis this overlayer has the unfortunate effect of attenuating the signal from the material underneath decreasing the signal strength and intensity. Furthermore, the presence of Carbon and Oxygen also add complexity to the peak fitting and assignment of high resolution spectra of these elements. For analysts it is seen as a hindrance when wanting to know the "real" surface chemistry

In recent times Argon cluster ions have been used to depth profile soft materials. The cluster ion sputters away sample material however the collision mechanism limits the propagation of damage into the sample bulk. This new method has been widely exploited with polymeric thin-films and biomaterials¹. Here we will discuss the use of Argon cluster ions as a novel way to remove adventitious carbon to improve the information obtainable through analysis. Improvements in both sensitivity and detection limit will be discussed as well as improved spectral resolution. We will also demonstrate how Argon cluster cleaning can improve the spatial resolution of XP imaging. A variety of systems will be discussed to demonstrate the broadness of the application. A comparison with low energy monatomic Argon cleaning is also made including discussion ion incorporation and lattice damage.

[1] P. Cumpson, J. F. Portoles, N. Sano, and A. J. Barlow, *J. Vac. Sci. Technol. B* 31(2), 2013.

9:00am **AS-WeM4 In Situ Chemical Imaging of Environmental Liquid Surfaces and Interfaces Using Microfluidics and Dynamic ToF-SIMS: Toward Multimodal and Mesoscale Imaging**, Xiao-Ying Yu, Z. Zhu, Pacific Northwest National Laboratory

The surfaces of aqueous phases and films have unique kinetics and thermodynamics, distinct from the bulk. However, major surface analytical techniques are mostly vacuum-based and direct applications for volatile liquid studies are difficult. We developed a vacuum compatible microfluidic interface, System for Analysis at the Liquid Vacuum Interface (SALVI), to enable direct observations of liquid surfaces and liquid-solid interactions using time-of-flight secondary ion mass spectrometry (ToF-SIMS). The unique aspects of this R&D 100 award winner include the following: 1) the detection window is an aperture of 2-3 mm in diameter allowing direct imaging of the liquid surface, 2) surface tension is used to hold the liquid within the aperture, and 3) SALVI is portable among multiple analytical platforms. SALVI is composed of a silicon nitride (SiN) membrane as the detection area and a microchannel made of polydimethylsiloxane (PDMS). Its applications ToF-SIMS as an analytical tool were evaluated using a variety of aqueous solutions and complex liquid mixtures, some of which contain nanoparticles. SALVI was also used to investigate the solvent structure of switchable ionic liquids. Recently, we demonstrated *in situ* probing of the electrode-electrolyte solution interface (or solid-electrolyte interface, SEI) using a new electrochemical SALVI. It provides the first direct observation of the surface and diffused layer of SEI in a liquid with chemical speciation using dynamic ToF-SIMS. Moreover, SALVI was extended for studying biofilm growth and single mammalian cells using correlative imaging by more than one spectroscopy and microscopy technique, each offering different spatial and temporal scales. That is, collecting data on different information level from an identical area in the same sample ideally could lead to a more holistic view of the hierarchical structural organization of complex systems in the real world. Selected results from our latest development will be presented, showcasing new directions and applications of multimodal imaging of environmental surfaces and interfaces and studying chemistry from the bottom up, all based on microfluidics. SALVI, a portable microfluidic reactor, sets the analytical foundation toward chemical imaging of complex phenomena occurring in multiple time and length scales, or the mesoscale, underpinning chemical changes at the molecular level.

9:20am **AS-WeM5 A VAMAS Inter-laboratory Study of the Measurement of Chemistry and Thickness of Nanoparticle Coatings**, David Cant, N.A. Belsey, C. Minelli, A. Shard, National Physical Laboratory, UK

Nanoparticles with a coating or shell are widely studied in both academic and industrial research. X-ray Photoelectron Spectroscopy (XPS) and Low/Medium Energy Ion Scattering (LEIS/MEIS) have potential for accurate measurement of chemistry and thickness of nanoparticle coatings, but the accuracy of these measurements is dependent upon correct

modelling for analysis and reproducibility of sample preparation. There is as yet no uniform approach to these issues; to address this, VAMAS project A19 – an interlaboratory study involving 24 participants in 12 countries – has been undertaken with the following objectives:

- Assessment of inter-laboratory variability in measuring nanoparticle coating thickness
- Comparison of sample preparation techniques.
- Testing variability of procedures for quantitative analysis.

Samples were prepared from commercial gold colloid and incubated with a short peptide. Each participant received one pre-deposited sample on Si wafer, and one solution (and Si wafer) for their own in-house deposition. Participants were requested to return their samples to help identify the effect of differences in sample deposition between pre-deposited and in-house samples.

Thickness values reported by participants performing XPS were compared to values calculated from reported atomic concentrations using the $T(NP)$ method [1,2]. A significant difference was observed between thicknesses determined for the pre-prepared sample and those determined for samples deposited by the participants in-house. Thicknesses determined for the in-house samples were larger than those determined for the pre-deposited samples. This was attributed to increased hydrocarbon presence observed in the C 1s spectra – likely caused by uneven sample deposition allowing detection of substrate contamination. In some cases, both pre-deposited and in-house samples exhibited abnormally low calculated thicknesses, potentially due to damaging of the coating by the x-ray beam.

The results of this study will assist in the development of a new ISO standard on the measurement of surface chemistry and thickness of nanoparticle coatings. The study will also provide information relevant to the ISO standard for reporting information related to the history, preparation, handling and mounting of nanomaterials prior to analysis, currently in development under ISO TC201. The production of guidelines for the measurement of nanoparticle coatings and sample preparation will be of great use in commercial applications of coated nanoparticles.

References

[1] Shard, A.G., *Journal of Physical Chemistry C*, 2012. 116(31): 16806-16813

[2] Belsey, N. A., Shard, A. G., Minelli, C. *Biointerphases*, 2015. 10, 019012

11:00am **AS-WeM10 A Quantitative Quest: Single Cell Analysis by LG-SIMS**, Christopher Szakal, National Institute of Standards and Technology (NIST)

Large geometry secondary ion mass spectrometry (LG-SIMS) has been used extensively for particle analyses and geochemical analyses, owing to its ability to maintain adequate mass resolution while operating at high secondary ion transmission. Efforts will be presented that extend the knowledge acquired in these application areas to single cell analyses of elemental species. To be useful, LG-SIMS results likely need to be quantitative for the amounts of a given element per cell and/or in ratios of different elements within each cell. Approaching this level of detail requires the establishment of the natural variability of such data from cell-to-cell, the reproducibility of the measurement technique, and whether the data is relevant to pertinent questions about the cellular population. Progress will be shown towards achieving these aims for single bacterial cells, including sample preparation necessary for such measurements, technique-specific considerations, and analytical figures of merit for LG-SIMS elemental ratios. Prospective application areas will be presented, along with potential pitfalls of such an approach.

11:20am **AS-WeM11 Ambient Mass Spectrometry Imaging of Live Cells and Tissues**, J.K. Kim, DaeWon Moon, DGIST, Republic of Korea

Currently, mass spectrometry imaging is based on Secondary Ion Mass Spectrometry (SIMS) and Matrix-Assisted Laser Desorption and Ionization (MALDI). Generally specimens for SIMS and MALDI are prepared by cryo-section and drying, which modifies the intrinsic biology due to sample preparations and subsequently does not allow dynamic response studies of biosystems to various chemical and physical stimuli. Most of recently developed ambient mass spectrometry have the spatial resolution in the range of ~50 μm , lacking in cellular and subcellular imaging of cells and tissues.

To investigate the intrinsic biology and dynamic responses of live cells and tissues in the cellular level, we developed an ambient imaging mass spectrometry system with ~5 μm spatial resolution. The ambient imaging mass spectrometry is based on low temperature plasma-surface reaction and desorption and ionization of surface products using near IR (808 nm) laser. Mass imaging is based on the movement of the sample stage. To enhance the laser desorption and ionization, Au nanorods of 10 nm diameter and 40

nm length were used. To further enhancement of sensitivity and possibly membrane specificity, liposome conjugated Au nanorods were used. An orbitrap mass spectrometer with a differential pumping and a pumping load adjustment is used as a mass analyzer.

Colonies of HCT-8 cells and hypothalamus tissues were mass imaged. Hypothalamus tissues were prepared with vibrotome, which allow sectioning of a hypothalamus tissue without freezing. Approximately 40 mass peaks from ~80 amu upto ~ 350 amu were observed with mass imaging. Single cells were observed clearly form a colony of HCT-8 cells and a hypothalamus tissue. Identification of imaged mass peaks are in progress with mass reference data and mass-mass analysis.

11:40am **AS-WeM12 Intricacies of Sample Preparation for ToF-SIMS Analysis of Biological Specimens, John Fletcher**, Chalmers University of Technology, Sweden **INVITED**

Biological and medical research is a popular and expanding area of application for time-of-flight secondary ion mass spectrometry (ToF-SIMS). The ability to perform such analyses has greatly benefited in recent years from the introduction of new ion beams that generate more signal from intact molecular ions that are generally more chemically characteristic and so aid in the interpretation of the complex spectra generated from biological specimen. The introduction of polyatomic ion beams such as C₆₀ heralded the dawn 3D molecular imaging with ToF-SIMS and most recently gas cluster ion beams such as Ar₄₀₀₀ have shown dramatic improvements for the detection of intact lipid species from tissue.

However, such advances are meaningless if the information from the analysis is erroneous due to artefacts introduced during the preparation of chemically complex, and delicate, biological samples such as cells and tissue sections. Analysis of samples in a frozen hydrated state is often considered to be the best approach for maintaining the integrity of the sample but is not always possible or practical. In this presentation the implications of different preparation approaches are presented and discussed and methods for removing artefacts due to imperfect sample preparation are presented.

In-Situ Spectroscopy and Microscopy Focus Topic Room: 211C - Session IS+AS+SA+SS-WeM

In-situ Studies Using X-ray Absorption Spectroscopy and Vibrational Spectroscopy for Catalytic and Energy Materials

Moderator: Franklin (Feng) Tao, University of Kansas, Zili Wu, Oak Ridge National Laboratory

8:00am **IS+AS+SA+SS-WeM1 In Situ X-ray Absorption Spectroscopy Technique for Metal/Water Interface Characterization, Chenghao Wu***, University of California, Berkeley and Lawrence Berkeley National Laboratory, *J.-H. Guo, M.B. Salmeron*, Lawrence Berkeley National Laboratory

Most of the electrochemistry processes occur within the thin layer of electrolyte at the electrolyte/electrode interfaces, commonly denoted as the electrical double layer (EDL). Although some classic continuum theories about EDL have been established and widely accepted over the past century, very little experimental information is available regarding the molecular-level details at such solid/liquid interfaces. We have developed in-situ liquid cells to study such solid/liquid interfaces by means of soft x-ray absorption spectroscopy [1]. Because the fluorescence x-ray photon has much larger mean free path in condensed matters than the secondary electrons, by comparing the total fluorescence yield (TFY) and total electron yield (TEY) spectra, we can extract useful information about the compositional, structural or chemical difference between the bulk and the interfacial electrolyte. Under different bias, by modulating the incident x-ray, the TEY signal current becomes alternating and can be separated from the dominant faradaic current so that we can obtain surface-sensitive TEY signal under electrochemical conditions.

With this *in-situ* and *operando* XAS technique, we investigated the gold/water interface [1] and platinum/sulfuric acid solution interface. It was found that at gold/water interface, the interfacial water layer has significantly different hydrogen-bonding network structure compared to the bulk water. Under different bias, the polar water molecules respond to the external electrical field and reorient at the gold electrode surface, which significantly changes the amount of distorted or broken hydrogen bonds.

* ASSD Student Award Finalist

First-principle simulations were able to corroborate the experimental results and qualitatively reproduce the change in the x-ray absorption spectra at different bias. In the platinum/sulfuric acid system, the charged solute species, such as SO₄²⁻ ions, hydronium ions, introduce extra complexity at the surface under different bias. Using the same *in-situ* technique, we were also able to identify some intermediate surface species in the potential window of OER reaction.

[1]. J.J. Velasco-Velez, C.H. Wu, T.A. Pascal, L.F. Wan, J.-H. Guo, D. Prendergast, and M. B. Salmeron, *Science*, **346**, 831-834 (2014).

8:20am **IS+AS+SA+SS-WeM2 Tip Enhanced Raman Spectroscopy (TERS) of Graphene Nano-Ribbons and Graphene on Au Surfaces: Imaging and Vibrational Spectroscopy of Surface Reaction Products, Delroy Baugh, S. Liu, T. Kumagai, M. Wolf**, Fritz-Haber-Institut der Max-Planck-Gesellschaft, Germany

Tip Enhanced Raman Spectroscopy (TERS) is currently one of the most powerful probe techniques available and could be used to study reactions on surfaces at the single molecule level. TERS combines two very well developed techniques scanning probe microscopy (SPM), used to image single molecules on surfaces, and surface enhanced Raman spectroscopy (SERS), used to characterize vibrational spectra also of single molecules on surfaces. TERS could therefore provide unique and heretofore unprecedented insight on adsorbate reactions at the single-molecule level, e.g., image a molecule while it evolves from reactant to product at well defined surface sites as well as monitor vibrational spectra to provide bond specific information about the reaction. However, in order to clarify the vibrational structure in TERS, the details of the enhancement mechanism and the issues regarding the plasmonic background that is almost always observed in TER spectra as well the “blinking” that occurs in the SERS part of TERS must be resolved. Towards this end here we will report studies of Graphene and Graphene Nanoribbons (GNR’s) on Au surfaces as a model systems because their electronic and vibrational structure are clearly defined. Specifically, Near and Far-field Raman spectra will be reported for these systems and the above issues will be addressed experimentally and a simple theoretical model will be presented for the TERS observations.

8:40am **IS+AS+SA+SS-WeM3 Isomerization of One Molecule Observed through Tip-Enhanced Raman Spectroscopy: Azobenzene Thiol on Au(111), Joonhee Lee, N. Tallarida, L. Rios, V.A. Apkarian**, University of California, Irvine

The reversible *cis-trans* isomerization of a single azobenzene thiol (ABT) molecule is captured in tip-enhanced Raman trajectories in which the anti-correlated flip-flop between discrete, on and off-states of the two structural isomers is seen. The strongly blue-shifted spectra are recorded from a molecule that appears at the junction plasmon of a scanning tunneling microscope (STM), consisting of an atomically flat Au(111) surface and a silver tip. The variation in frequencies of switching events identifies heterogeneously photocatalyzed chemistry. The chemisorbed ensemble of ABT molecules lie flat on Au(111) surface with azobenzene headgroup strongly coupled to the surface. Nevertheless, we establish through STM imaging that the ABT molecules undergo both current driven and photoinduced *cis-trans* isomerization. Rather than decoupling from the surface, we suggest that strong coupling of the reaction coordinate to a vibrational energy sink is required for *cis-trans* isomerization of azobenzenes on metal surfaces.

9:00am **IS+AS+SA+SS-WeM4 In Situ Characterization and Reaction Studies of MnO_x/Co₃O₄ Catalyst for CO and CO₂ Conversion, Walter Ralston, G. Melaet**, University of California, Berkeley, *S. Alayoglu*, Lawrence Berkeley National Laboratory (LBNL), *G.A. Somorjai*, University of California, Berkeley

As the energy and fuel demands of our growing world continue to increase, non-fossil fuel carbon sources are increasingly attractive – especially if these carbon sources can be easily converted to transportable fuels and higher-value chemicals. Much attention has been focused on carbon dioxide, as capture and storage technology has emerged to mitigate emissions and CO₂ can be used to produce methanol.

Recently, we reported a catalyst for the low-pressure conversion of CO₂ to methanol¹. Manganese oxide nanoparticles supported in mesoporous Co₃O₄ produced methanol in high yields and at significantly lower pressure conditions than typical Cu/ZnO catalysts used industrially. The advantage of this catalyst is in its lower pressure requirement, its high yield of methanol, and its evidence of carbon-carbon bond formation (10% ethylene production).

Catalytic testing of the material has shown the catalyst to be more than the sum of its parts; when each component is tested separately (MnO_x nanoparticles supported in SiO₂; mesoporous Co₃O₄ alone) CH₄ and CO are the major products. Preparation and testing of an inverse catalyst – CoO_x nanoparticles on a mesoporous MnO₂ support – proves the importance of

the hybrid architecture in determining the selectivity of the catalyst, as the inverse catalyst is dominated by the selectivity of the support (>80% selective to CO).

Towards understanding this catalyst, in-situ X-ray Absorption Spectroscopy (XAS) utilizing both soft and hard x-ray energies has allowed for a detailed characterization of the catalyst under oxidation, reduction, and reaction conditions. In addition to CO₂, in-situ characterization under CO hydrogenation conditions was used to understand the Fischer-Tropsch activity of the catalyst for making longer chain hydrocarbons. The results of these in-situ studies are correlated with catalytic reaction data to help understand the nature of the active site/interface and guide future catalyst design.

References

(1) C. S. Li, G. Melaet, W. T. Ralston, *et al.* High-performance hybrid oxide catalyst of manganese and cobalt for low-pressure methanol synthesis. *Nature Communications*, 6:6538, 2015.

9:20am **IS+AS+SA+SS-WeM5 In Situ and Operando Raman Methodology to Understand the States of Oxide Catalysts and Alkane Oxidative Dehydrogenation and Ammoxidation Reactions, Miguel A. Bañares**, Instituto de Catálisis y Petroleoquímica, Madrid **INVITED**

Operando methodology combines in situ spectroscopy during reaction with simultaneous performance measurement in a cell that behaves like a catalytic reactor. *Operando* methodology connects changes in the performance and in the structure in a simultaneous manner; this is fundamental to assess the structure-performance relationships at a molecular level.

Molecularly dispersed vanadia on oxide carriers is a key component in many catalytic formulations in environmental and selective oxidation and ammoxidation catalysis. The actual state of vanadia catalysts in specific environments depends on its surface density, the nature of the support and the presence of additives. We will summarize our experience on the state of supported vanadia paying particular attention to how the environment and reaction conditions finally shape the structure of vanadia catalysts. *Operando* Raman spectroscopy is an invaluable approach to fully understand the actual state of the catalyst, its transformations during reaction and how these correlate with changes in catalytic performance.

A single technique, may not deliver the complete vista, thus collaboration with complementary talents and techniques is critical. We show the outcome of collaborations with theoretical chemistry approaches to bring the rationale behind structure-activity relationships inferred through *operando* Raman methodology. We also show the interaction with engineering approaches.

11:00am **IS+AS+SA+SS-WeM10 Operando Studies of Dynamic Restructuring of Working Catalysts by Correlated Imaging and Spectroscopy Probes, Anatoly Frenkel**, Yeshiva University **INVITED**

Understanding mechanisms of reactivity is often hindered by complexity of nanoscale supported metal catalysts. In the size range of 1-5nm, they feature a variety of structural motifs, sizes, shapes, compositions, degrees of crystalline order as well as multiple temporal scales. Hence, new experimental methodologies are called for, ones that are capable to capture not only the details of kinetic, dynamic and catalytic properties of metal clusters, but also their statistical distributions over ensemble of such clusters in a particular working catalyst, i.e., in reaction conditions. I will present our recent results obtained at the National Synchrotron Light Source, Advanced Light Source and Center for Functional Nanomaterials, where we combined x-ray absorption spectroscopy, high resolution transmission electron microscopy and micro-IR spectroscopy studies of a complex catalytic system *in operando*, using the same portable micro-reactor. This method will be illustrated on the example of supported Pt and Pd catalysts undergoing dynamic restructuring during ethylene hydrogenation reaction. Our results demonstrate a complexity of structures exhibited in this system and their dynamic, responsive transformations throughout changing reaction conditions. The new method is both general and generalizable to quantitative *operando* studies of complex material systems of broad interest to areas as diverse as catalysis science, applied physics and materials science, using a wide variety of x-ray and electron based experimental probes.

11:40am **IS+AS+SA+SS-WeM12 A Correlation of Raman and Single and Multiple Layer Graphene Conductivity as Detected with a Cryogenic Multiprobe AFM with On-line Raman, NSOM and Other SPM Modalities, Aaron Lewis**, The Hebrew University of Jerusalem and Nanonics Imaging Ltd, Israel, *O. Zinoviev, A. Komissar, E. Maayan, D. Lewis*, Nanonics Imaging Ltd, Jerusalem, Israel

It is a challenge to study 2D materials, such as Graphene, MoS₂, WSe₂, etc. at temperatures down to 10°K when one considers the wide variety of

physical phenomena that have to be applied to get a full picture of the functionality of these materials. This involves questions of structure, nanometric photoconductivity, electrical properties, thermal properties, near-field optical in the apertured and scattering modes, Kelvin probe, and of course Raman. All of these phenomena are common not only to 2D materials but also to carbon nanotubes and related nanomaterials. This presentation will describe both the instrumental development of such a multiprobe cryogenic system that allows for state of the art on-line optical measurements and will also include a review of the probe developments that permit such multifunctional multiprobe operation with on-line full optical access. The system that will be described has a completely free optical axis from above and below that is not obscured by electrical or other probes that have been developed for this system for multiprobe operation. This permits on-line Raman and Tip Enhanced NanoRaman Scattering. With such a system we have investigated graphene and HfO₂ using multiprobe electrical, Kelvin probe, NSOM and on-line Raman. The results have yielded new insights into the chemical changes that are correlated to the electrical conductivity.

12:00pm **IS+AS+SA+SS-WeM13 Surface Structure and Chemistry of Rh(110)-1×2 Under Reaction Condition and During Catalysis explored with AP-XPS and HP-STM, Franklin (Feng) Tao, L. Nguyen**, University of Kansas

High pressure scanning tunneling microscopy (HP-STM), ambient pressure X-ray photoelectron spectroscopy (AP-XPS), and computational studies were used to study the surface chemistry and structure of Rh(110)-1×2 and Rh(110)-1×1 at atomic scale in CO at different pressure and different temperature, and during CO oxidation at different pressure and different temperature. In gas of CO at a low pressure of 8×10⁻⁸ Torr, a Rh(110)-1×2 covered with CO is formed at 25C by replacing the adsorbed oxygen atoms adsorbed on Rh(110)-1×2 by CO molecules of gas phase. A pressure dependent structure of adsorbate layer of CO on Rh(110)-1×2 was revealed. In gas of CO at a high pressure of 0.08 Torr, the portion of CO molecules bound in atop configuration in the adsorbed layer increases along with the increase of pressure of CO gas though there is no restructuring of Rh(110)-1×2 at 25C in the pressure range of 8×10⁻⁸ to 0.8 Torr. This is supported by the calculated coverage-dependent binding energy of CO on this surface. At a relatively high temperature of 55C, Rh(110)-1×2 in 0.08 Torr CO is restructured to Rh(110)-1×1 (Figure 1b). This temperature of surface restructuring is much lower than 153C for Rh(110)-1×2 in UHV. Theoretical simulation suggests that adsorbed CO molecules promote this restructuring compared to the restructuring in UHV since adsorption of CO on the intermediate structures of this restructuring in gas of CO lower the activation barrier of these intermediate structures. Rh(110)-1×2 is restructured to Rh(110)-1×1 during catalysis in the mixture of CO (0.08 Torr) and O₂ (0.02 Torr) even at 25C. Compared to the lack of restructuring in pure CO of 0.08 Torr at 25C, this restructuring during catalysis could result from a local heating of the catalyst surface by the exothermic reaction of CO oxidation. During CO oxidation, certain number of CO molecules are still remained on the catalyst surface. In the temperature range of 50-130C the active phase of catalysis is metallic Rh(110)-1×1. However, at 200C the active phase is surface rhodium oxide. These in-situ studies of surface structure and chemistry integrated with computational studies of Rh(110) in pure CO and in mixture of CO and O₂ clearly demonstrate the complexity of surface structure of a catalyst under reaction condition and during catalysis. The pressure-dependent structure of adsorbate layer, temperature-driven surface restructurings, generation of a new active surface phase of catalyst during catalysis, suggest the significance of in-situ studies of structure and chemistry of surface of a catalyst during catalysis.

**Scanning Probe Microscopy Focus Topic
Room: 212A - Session SP+AS+NS+SS-WeM**

Advances in Scanning Probe Microscopy

Moderator: An-Ping Li, Oak Ridge National Lab, Saban Hus, Oak Ridge National Laboratory

8:00am **SP+AS+NS+SS-WeM1 Designer Electrons: Quantum Information and New Particles in Atomically Assembled Matter, Hari Manoharan**, Stanford University **INVITED**

The observation of massless Dirac fermions in monolayer graphene has propelled a new area of science and technology seeking to harness charge carriers that behave relativistically within solid-state materials. Using low-temperature scanning tunneling microscopy and spectroscopy, we show the emergence of Dirac fermions in a fully tunable condensed-matter system—molecular graphene— assembled via atomic manipulation of a conventional two-dimensional electron system in a surface state. We embed, image, and

tune the symmetries underlying the two-dimensional Dirac equation into these electrons by sculpting the surface potential with manipulated molecules. By distorting the effective electron hopping parameters into a Kekulé pattern, we find that these natively massless Dirac particles can be endowed with a tunable mass engendered by the associated scalar gauge field, in analogy to the Higgs field. With altered symmetry and texturing of the assembled lattices, the Dirac fermions can be dressed with gauge electric or magnetic fields such that the carriers believe they are in real fields and condense into the corresponding ground state, as confirmed by tunneling spectroscopy. Using these techniques we ultimately fabricate a quantum Hall state without breaking time-reversal symmetry, in which electrons quantize in a gauge magnetic field ramped to 60 Tesla with zero applied laboratory field. We show that these and other chiral states now possible to realize have direct analogues in topological insulators, and can be used to guide or confine charge in nontrivial ways or to synthesize new particles [1,2].

[1] K. K. Gomes, W. Mar, W. Ko, F. Guinea, H. C. Manoharan, "Designer Dirac Fermions and Topological Phases in Molecular Graphene," *Nature* **483**, 306–310 (2012).

[2] M. Polini, F. Guinea, M. Lewenstein, H. C. Manoharan, V. Pellegrini, "Artificial Honeycomb Lattices for Electrons, Atoms, and Photons," *Nature Nanotechnology* **8**, 625–633 (2013).

8:40am **SP+AS+NS+SS-WeM3 Scanning Quantum Dot Microscopy**, *Ruslan Temirov, C.W. Wagner, M.F.B.G. Green, P.L. Leinen*, Forschungszentrum Juelich GmbH, Germany, *T.D. Deilmann, P. Krueger, M.R. Rohlfiing*, Muenster University, Germany, *F.S.T. Tautz*, Forschungszentrum Juelich GmbH, Germany

Interactions between atomic and molecular objects are to a large extent defined by the nanoscale electrostatic

potentials which these objects produce. Consequently, a tool for nanometre scale imaging and quantification of

local electrostatic fields could help in many areas of nanoscience research. In this contribution we introduce a

scanning probe technique that for the first time enables truly three-dimensional imaging of local electrostatic

potential fields with sub-nanometre resolution. Registering single electron charging events of a molecular

quantum dot attached to the tip of a tuning fork atomic force microscope operated at 5 K, we image the

quadrupole field of a single molecule adsorbed on a metal surface. To demonstrate quantitative measurements,

we investigate the Smoluchowski dipole field created by a single metal adatom adsorbed on a metal surface. We

show that because of its high sensitivity the technique can probe electrostatic potentials at large distances from

their sources, which should allow for the imaging of samples with increased surface roughness.

Reference

[1] C. Wagner, M. F. B. Green, P. Leinen, T. Deilmann, P. Krüger, M. Rohlfiing, R. Temirov, F. S. Tautz

arXiv:1503.07738 (2015)

9:00am **SP+AS+NS+SS-WeM4 Local Probing of the Photo-carrier Lifetime by Kelvin Probe Force Microscopy**, *Nicolas Chevalier, S. Pouch, D. Mariolle*, Univ. Grenoble Alpes/ CEA, LETI, MINATEC Campus, France, *B. Grevin*, Univ. Grenoble Alpes/ CEA, INAC, SPrAM, LEMOH, France, *L. Borowik*, Univ. Grenoble Alpes/ CEA, LETI, MINATEC Campus, France

The photo-carrier lifetime plays a major role in the overall efficiency of a solar cell because it limits the proportion of photo-generated charges collected at the electrodes. This lifetime, which should be ideally as large as possible in an organic or inorganic solar cell, is rather difficult to measure in nanostructured materials or in more complex hybrid systems, indirect band-gap semiconductors, and ultra-thin layers. Identifying the losses mechanisms is one of the main objectives for increasing the performances of solar cells. Most of the experimental approaches developed so far consist in studying recombination by techniques such as transient photovoltage measurements or charge extraction. All these techniques average sample properties over macroscopic scales, making them unsuitable for directly assessing the impact of local heterogeneity on the recombination process. In this paper, we propose a steady method to measure the photo carrier lifetime by photo-modulated techniques based on Kelvin probe force microscopy (KPFM). [1] Additionally, KPFM technique provides a spatially resolved measurement, which is applicable on the overall of solar cells.

We will present the principle of this original method based on the measurement of the surface potential by KPFM under an illumination with a rectangular waveform light modulation. Photo-carrier lifetime down to μs scale is reachable with our experimental setup. The modulation-dependent surface potential is plotted as a function of the frequency. Assuming an immediate generation time under illumination and an exponential decay of the surface potential during the dark condition, the averaged surface potential over a cycle can be fitted as a function of the frequency by simple equation where the only fit parameter is the photocarrier-lifetime. [2] Instrumental aspects as well as data treatment will be reviewed. Measurements obtained on silicon nanocrystals embedded in 30 nm film of silicon dioxide [3] and on organic donor-acceptor blend (PBTFB and PCBM) [4] will be presented to illustrate the potential of the technique.

This work was supported by the French "Recherche Technologique de Base" Program and performed in the frame of the trSPV Nanoscience project. The measurements were performed on the CEA Minatéc Nanocharacterization Platform (PFNC).

1. L. Borowik *et al.* Phys. Rev. B **82**, 073302 (2010).
2. L. Borowik *et al.* Nanotechnology **25**, 265703 (2014).
3. D. Asakura *et al.* Phys. Rev. Lett. **93**, 247006 (2004).
4. N. Delbosch *et al.* RSC Adv **4**, 15236 (2014).

9:20am **SP+AS+NS+SS-WeM5 Nanoscale Capacitance-Voltage (C-V) Curves: Using Scanning Microwave Impedance Microscopy (sMIM) to Characterize Local Electrical Properties of Linear and Non-Linear Materials**, *Stuart Friedman, Y. Yang, O. Amster*, PrimeNano, Inc.

Understanding and optimizing advanced materials frequently requires detailed knowledge of nanoscale electrical properties. Scanning probe techniques such as scanning tunneling microscopy (STM), conductive AFM (cAFM), scanning capacitance microscopy (SCM), and Kelvin probe force microscopy (KPFM) provide such nano-electrical measurements, but are generally limited in the classes of materials they can characterize or the properties they can measure. Scanning microwave impedance microscopy (sMIM) uses GHz frequency microwaves and shielded AFM probes to directly measure the impedance (capacitance and conductance) of the tip sample interface. As such sMIM is sensitive to the permittivity and conductivity of a wide variety of samples including dielectrics, conductors, and semiconductors.

When sMIM is applied to non-linear materials, changing the tip sample bias changes the local electric field thereby changing the local electrical properties of the sample just under the AFM tip. The electric field induced changes in the sample create changes in the tip-sample impedance that can be measured by sMIM. For example, when imaging doped semiconductor samples, the tip sample interface forms either a metal-semiconductor junction or a metal-insulator-semiconductor junction. Plotting the sMIM measured capacitance as a function of the tip sample bias voltage produces the equivalent of a typical capacitance-voltage curve, but from nanoscale regions selected from an AFM image. C vs V results from doped silicon samples that closely match theoretical calculations will be discussed. The talk will also present results from advanced and novel materials and devices, such as III-V semiconductors, 2D materials and 1D structures where sMIM data has been used to assess non-linear behavior and characterize dopant type and distribution.

9:40am **SP+AS+NS+SS-WeM6 STM Study of the Correlation between Structural, Magnetic, and Electronic Properties of Co Nano-Islands on Cu(111)**, *Jewook Park, C. Park, M. Yoon, Z. Gai, A.P. Baddorf, A.-P. Li*, Oak Ridge National Laboratory

An epitaxially grown Co nano-island on Cu(111) surface is a model system to study the correlation between structural, magnetic, and electrical properties of nanophase materials. We carried out an extensive study on Co islands by using spin-polarized scanning tunneling microscopy and spectroscopy (SP-STM/S) at low temperatures (130 K and 38 K). Two structurally different island types are clearly distinguished, rotated by 180° about the surface normal due to a stacking fault in one type of the islands. The triangular Co islands are 5-20 nm wide and 4 Å high. Regardless of the structural asymmetry, both faulted and un-faulted Co islands possess two distinctive spin orientations. With Cr-coated W-tip as a spin-polarized probe, bias-dependent tunneling conductance maps are measured on Co islands. An antiparallel spin-orientation between magnetized tip and Co islands display higher conductance compared to a parallel relation at -400 meV and *vice versa* at around Fermi-level, which is verified by density functional theory calculations. Furthermore, by recording 23 hours of time-lapse images from the same Co islands, we demonstrate a time-dependent correlation between structural, magnetic, and electrical behaviors. We find that a contamination-induced structural change modifies the magnetic properties of Co islands and is confirmed by theoretical calculations.

This research was conducted at the Center for Nanophase Materials Sciences, which is a DOE Office of Science User Facility, and supported by the Laboratory Directed Research and Development Program of Oak Ridge National Laboratory, managed by UT-Battelle, LLC, for the US DOE.

11:00am SP+AS+NS+SS-WeM10 Probing Electrostatic Field Effect in Quantum Materials by Microwave Impedance Microscopy, Keji Lai, University of Texas at Austin
INVITED

The research of complex quantum materials, in which a dazzling number of emergent phenomena take place in the nanoscale, is a major theme in modern condensed matter physics. For real-space imaging of complex systems, electrical impedance microscopy fills an important void that is not well represented by the existing local probes. Using shielded cantilever probes and sensitive microwave electronics, we can now perform non-invasive electrical imaging with sub-100nm resolution and sub-aF sensitivity.

Combining the cryogenic microwave impedance microscopy (MIM) and a spin-coated thin ionic gel layer, we are able to visualize the metal-insulator transition of functional materials in electrolyte-gated electric double-layer transistors. The microwave images acquired at different gate voltages clearly show the spatial evolution of channel conductivity and its local fluctuations through the transition. By applying a large source-drain bias above the glass transition temperature of the gel, an uneven conductance profile is established across the EDLT channel, which can be visualized by the MIM and further investigated by transport measurements and numerical simulations. The combination of ultra-thin ion-gel gating and microwave microscopy paves the way for studying the microscopic evolution of phase transitions in complex materials induced by electrostatic field effects.

11:40am SP+AS+NS+SS-WeM12 Subsurface Visualization of Soft Matrix using 3D-Spectroscopic Atomic Force Acoustic Microscopy, Kuniko Kimura, K. Kobayashi, A. Yao, H. Yamada, Kyoto University, Japan

Nondestructive visualization of subsurface features of various materials with nanometer-scale spatial resolution is strongly demanded in a wide variety of scientific research fields such as nanoelectronics, nanomechanics and life science. Recently, many research groups have demonstrated the visualization of nanometer-scale subsurface features using various techniques based on atomic force microscopy (AFM) [1-4]. (All references and figures are given in Supplement.) We recently demonstrated the imaging of Au nanoparticles buried under 900 nm from the surface of a polymer matrix by atomic force acoustic microscopy (AFAM), as shown in Fig. 1 [5]. In AFAM, the amplitude and phase of the cantilever vibration at the contact resonance frequency induced by the sample excitation are measured, which allows us the quantitative evaluation of surface stiffness [6]. The AFAM images in Fig. 1 show that the surface viscoelasticity of the soft matrix is affected by subsurface hard objects such as the Au nanoparticles buried even roughly 1 micro-meter below the surface. However, only from AFAM images, it is difficult to determine which the dominant mechanism for the subsurface imaging is viscosity variation or elasticity variation, because AFAM images were taken at a single excitation frequency near contact resonance.

In this presentation, we discuss the origin of the visualization of subsurface features in soft matrix based on spectroscopy of AFAM [7]. We recorded the amplitude and phase spectra at every pixel of the AFAM image as represented in Fig. 2, which we call 3-dimensional spectroscopic atomic force acoustic microscopy (3D-spectroscopic AFAM). A schematic diagram of the 3D-spectroscopic AFAM is shown in Fig. 3. After the tip was brought into contact with the surface, we first measured the contact resonance frequency (f_c). Then we recorded the amplitude and phase spectra measured by a lock-in amplifier, while the tip was raster-scanned with the contact mode. At each scanning pixel, the excitation frequency was swept with the span of 25 kHz which was centering around f_c , whose sweep time was 35 msec. The total acquisition time for 128 x 128 pixels took about 20 min.

Using this method, we can compare the frequency spectrum measured on the subsurface Au nanoparticle with that on another position having no subsurface particle, as shown in Fig. 4. We can also reconstruct AFAM images of arbitrary frequencies within the sweep frequency range, which is the meaning of "3-dimensional". Moreover, the 3D-spectroscopic AFAM enables us to characterize the amplitude and phase spectra and to detect the variation that may be caused by the nonlinear tip-sample interactions.

12:00pm SP+AS+NS+SS-WeM13 Quantifying the Effects of Cantilever Modes Shapes on Studies of the Liquid-Solid Interface, Aleks Labuda, M. Viani, D. Walters, R. Proksch, Asylum Research, an Oxford Instruments company

At the core of most AFM measurements is the assumption that the motion of the cantilever probe can be well quantified. However, most AFM systems

use a "beam bounce" optical beam deflection (OBD) method which, because it is fundamentally an angular measurement, only provides accurate tip position information when the mode shape of the cantilever matches the calibration conditions. For example, if the OBD sensitivity is calibrated with a force curve, the calibration holds true only for experiments where the mode shape is similar to an end-loaded cantilever. This assumption is quickly violated when the cantilever is oscillated at frequencies different from the calibration. This is especially true in liquids, where $Q \sim 1$ and the combination of significant base motion and hydrodynamic effects lead to a variety of different mode shapes that are strongly frequency dependent (see Figure). This clearly demonstrates that the sensitivity (nm/V) is actually a frequency dependent quantity. Worse, it may also drift with time. Another consequence is that the effective stiffness of the cantilever, which depends on mode shape, is also highly frequency dependent. Both of these effects cause quantitative misinterpretation of the tip-sample interaction and artifacts in imaging contrast. These problems affect both dynamic AFM modes (such as AM-AFM and FM-AFM) as well as sub-resonance modes such as fast force mapping and force modulation.

To quantify this effect, we present measurements based on Ref [1-2] using a modified commercial AFM that combines a standard OBD detector with an integrated laser Doppler vibrometer (LDV) system that directly measures displacement. As shown in the Figure, the OBD and LDV can be used simultaneously, such that the cantilever base motion or tip motion can be accurately monitored with the LDV during an AFM experiment – independent of the OBD and any feedback loops. In the Figure, the $\sim 2 \mu\text{m}$ LDV laser spot was scanned along the cantilever for high-resolution in situ mapping of its dynamics across a wide spectrum of frequencies and showing significant deviations from ideal mode shapes over the entire frequency range.

The effects of these frequency-dependent mode shapes are then quantified by appropriate modeling for a variety of experimental conditions, and demonstrated experimentally using stiff levers for AM-AFM at the calcite-water interface and soft levers for fast force mapping of polymeric materials.

Surface Science

Room: 113 - Session SS+AS+NS-WeM

Metals, Alloys & Oxides: Reactivity and Catalysis

Moderator: John Russell, Jr., Naval Research Laboratory

8:00am SS+AS+NS-WeM1 Surface Chemistry of Single-Layer MoS₂, Koichi Yamaguchi, E. Li, L. Bartels, University of California - Riverside

Molybdenum disulfide (MoS₂) is a semiconducting transition metal dichalcogenide (TMD) that forms a stable monolayer 2D crystal structure similar to graphene. It is the key material for industrial hydrodesulfurization (alloyed with cobalt) and has shown promise in electrocatalytic water splitting. We present a study of MoS₂'s ability to bind small reactants and its stability when exposed to them at elevated temperature. We utilize a combination of thermally programmed desorption measurements and in-situ PL imaging. The latter permits us to study the film activity over a wide pressure range (high-vacuum to ambient).

8:20am SS+AS+NS-WeM2 On the Adsorption Behavior of a Porphyrin on Different Cu Surfaces: A Comparative Scanning Tunneling Microscopy Study, Liang Zhang, Universität Erlangen-Nürnberg, Germany, M. Lepper, Universität Erlangen-Nürnberg, Germany, M. Stark, S. Ditze, H.-P. Steinrück, H. Marbach, Universität Erlangen-Nürnberg, Germany

Self-assembly of functional molecular building blocks on well-defined surfaces is a promising approach for the bottom-up fabrication of two-dimensional nanostructures with outstanding properties. In this respect, porphyrins are particularly attractive because of their distinct chemical and physical properties.^{1,2}

In this presentation, we investigate and compare the adsorption behaviour of 2H-5,10,15,20-Tetrakis-(3,5-di-tert-butyl)-phenylporphyrin (2HTTBPP) on different substrates, i.e., Cu(111),^{3,5} Cu(110) and Cu(110)-(2X1)O, under ultra-high vacuum conditions by scanning tunneling microscopy (STM). At room temperature, supramolecular arrangements of 2HTTBPP are observed on Cu(111) and Cu(110)-(2X1)O, while on Cu(110) individual 2HTTBPP molecules are observed in a disordered layer. Interestingly, the intramolecular conformations of the molecules are quite different on the investigated substrates, as determined by STM.⁴ The corresponding findings are interpreted by accounting for specific molecule-molecule and molecule-substrate interactions. In addition, the so-called self-metalation of 2HTTBPP with Cu atoms will be reported and discussed.^{4,5}

References:

1. Auwärter, *et al.*, Nat. Chem., 2015, 7, 105.
2. Gottfried, Surf. Sci. Rep., 2015, doi:10.1016/j.surfrep.2015.04.001.
3. Ditze *et al.*, J. Am. Chem. Soc., 2014, 136, 1609.
4. Stark *et al.*, Chem. Commun., 2014, 50, 10225.
5. Marbach *et al.*, Chem. Commun., 2014, 50, 9034.

8:40am **SS+AS+NS-WeM3 Redox-Active On-Surface Assembly of Metal-Organic Chains with Single-Site Transition Metals, Steven Tait, Indiana University**
INVITED

Programming the specific chemistry of single-site transition metal centers at surfaces by organic ligand design is a promising route to improve selectivity in surface catalysts. The chemical behavior of the surface and redox chemistry happening at the surface need to be further developed and understood. These studies benefit from interdisciplinary research into the programming of the growth, reactivity, and functionality of nano-scale systems in general and metal-organic complexes as surface catalysts in particular. Our group has recently demonstrated the formation of structurally ordered and chemically uniform single-site centers at surfaces by on-surface redox chemistry of metallic precursors including platinum, chromium, iron, and vanadium with organic ligands on a gold surface (*J. Am. Chem. Soc.* 2014, **136**, 9862-9865; *J. Chem. Phys.* 2015, **142**, 101913; and newly submitted work). The on-surface redox process relies on straightforward vapor deposition protocols and takes advantage of the catalytic role of the surface to show promise as an approach for the growth of inorganic complexes at surfaces. The ability to tune the reactivity and catalysis of these systems is a central question in this field. We report new results here that probe the extent of oxidation state control in these systems using tailored tetrazine-based ligands and vanadium metal; vanadium is an excellent candidate for probing access to a variety of oxidation states. The oxidizing power of the tetrazine species is tuned by peripheral functional groups to access two and three electron oxidation processes, as determined by X-ray photoelectron spectroscopy (XPS). Platinum(II) centers have also been formed with these ligands. In each of these cases, the metal-ligand complexes take the form of nearly identical one-dimensional polymeric chains, resolved by molecular-resolution scanning tunneling microscopy (STM). These structures provide highly uniform quasi-square-planar coordination sites for the metal, which contributes to the well-defined chemical state of the metal. This strategy is also applied to earth-abundant metals such as iron and chromium using commonly available phenanthroline ligands and is allowing us to develop understanding of how to control and program single-site metal centers on surfaces for next-generation catalysis.

9:20am **SS+AS+NS-WeM5 Ultra-thin Bi(110) Films on Si(111) $\sqrt{3}\times\sqrt{3}$ -B Substrates, I. Kokubo, Y. Yoshiike, K. Shishikura, K. Nakatsuji, Hiroyuki Hirayama, Tokyo Institute of Technology, Japan**

Bismuth (Bi) takes the rhombohedral (A7) crystalline structure in bulk. However, it also takes the black phosphorous (BP) structure in ultrathin films. Theoretically, a few bilayer thick Bi(110) films with the BP structure were predicted to be a nontrivial two-dimensional topological insulator by removing the buckling at the surfaces [1]. In the meantime, ultrathin Bi(110) films with the A7 structure was suggested to realize the Dirac electron system at the surfaces [2]. From these viewpoints, the growth, structure, and electronic states of the Bi(110) ultra-thin films are of great interest. In this study, we investigated the details of the atomic arrangements and electronic states at the Bi(110) islands on the Si(111) $\sqrt{3}\times\sqrt{3}$ -B substrate experimentally using scanning tunneling microscope (STM) [3] and angle-resolved photoelectron spectroscopy (ARPES) in a synchrotron radiation facility.

In the study, we found that atomically flat, long, narrow Bi(110) islands grew along specific orientations on the Si(111) $\sqrt{3}\times\sqrt{3}$ -B substrate. The orientations belonged to one of the two sets of three-fold rotational axes, which differed by 26° each other. The preference of the specific orientations were reasonably attributed to the commensuration of the diagonal of the rectangular Bi(110) lattice to the $\sqrt{3}\times\sqrt{3}$ substrate unit cell. The islands grew as to make their edges parallel to the short side of the Bi(110) rectangular unit cell. The combination of the Bi domains of different orientations caused various types of boundaries on the wide terraces of the Bi(110) islands. In particular, the domains along $\pm 87^\circ$ from the $\{1-10\}$ direction were found to be connected perfectly on the atomic scale at the straight boundary by inserting a local switching of the bond direction to the zigzag chains of the in-plane bonds. On the Si(111) $\sqrt{3}\times\sqrt{3}$ -B substrate, both the odd layer thick A7 and even layer thick BP Bi(110) islands appeared. The dispersive surface bands and their Fermi surface mapping with characteristic electron and hole pockets were observed in ARPES spectra. Details will be reported in the presentation.

[1] Y. Lu, W. Xu, M. Zeng, G. Yao, L. Shen, M. Yang, Z. Luo, F. Pan, K. Wu, T. Das, P. He, J. Jiang, J. Martin, Y. P. Feng, H. Lin, X. Wang, Nano Lett. 15, 80 (2015).

[2] G. Bian, X. Wang, T. Miller, T. -C. Chiang, P. J. Kowalczyk, O. Mahapatra, S. A. Brown, Phys. Rev. B 90, 195409 (2014).

[3] I. Kokubo, Y. Yoshiike, K. Nakatsuji, H. Hirayama, Phys. Rev. B 91, 075429 (2015).

}

9:40am **SS+AS+NS-WeM6 STM Study of Growth Processes for Ir/Ge(111), M.S. van Zijll, B.H. Stenger, C.H. Mullet, E.S. Huffman, D. Lovinger, W.F. Mann, Shirley Chiang, University of California, Davis**

Using scanning tunneling microscopy (STM), we have characterized the surface of clean Ge(111) dosed with 0.66 to 2.0 monolayers (ML) of Ir and then annealed to temperatures between 550 K and 800 K. We observed a broad range of surface formations, including Ir adatom clusters and various stages of island formation. Islands with winding, wormy shapes formed around 580K. As the annealing temperature increased above 650K, round islands formed. In addition, a new type of growth is observed in which the Ir gathers along the antiphase domain boundaries between competing surface domains of the Ge surface reconstruction; this gives the appearance of the Ir forming pathways interconnecting different Ir islands. The low energy electron diffraction (LEED) pattern for this surface shows domains with $(\sqrt{3}\times\sqrt{3})R30^\circ$ reconstruction and becomes sharper as the temperature is increased. In the STM images, the Ge top layer reconstruction, the Ir adatom clusters, the pathways, and the Ir round islands all have $\sqrt{3}$ -spacing between features. X-ray photoemission spectroscopy (XPS) was used to determine that the Ir coverage was ~ 2.0 monolayers when low energy electron microscopy (LEEM) images showed completion of 1 overlayer of Ir grown on Ge(111) at 600C. We present a model consistent with our XPS and LEEM data that suggests that each Ir adatom cluster observed in STM images corresponds to three Ir adatoms. To model the surface-adsorption processes for the Ir/Ge(111) system, we used simple Monte Carlo simulations with pair-wise surface potentials and random walks of atoms to imitate surface diffusion. Particular parameter choices yielded growth along pathways between domain boundaries of the substrate, in agreement with the experimental data.

11:00am **SS+AS+NS-WeM10 Gas Sensor Resistance Changes for Ar/O₂ and H₂O Plasma Modified SnO₂ Nanomaterials, Erin Stuckert, C.J. Miller, E.R. Fisher, Colorado State University**

Although steps have been made to decrease toxic gas emissions globally, these emissions persistently cause detrimental health effects worldwide. Current household gas sensors are limited in their abilities to detect sensitively and selectively at or below relevant toxicity levels for many gases. Tin(IV) oxide (SnO₂) nanomaterials are well-equipped to address some of these limitations as a result of dual valency (Sn²⁺ and Sn⁴⁺) and high surface area, thus creating diverse surface chemistry. These properties are advantageous for gas sensing devices because SnO₂ functions as a sensor via gas-surface interactions, facilitated by adsorbed oxygen species. By measuring changes in resistance upon gas exposure, sensitivity and selectivity are observed. To increase sensitivity through maximizing gas surface interactions, chemical vapor deposition-grown SnO₂ nanowires and commercial nanoparticles were treated with an Ar/O₂ and H₂O_(v) plasma resulting in increased oxygen adsorption. Surface and bulk characterization throughout the plasma treatment process demonstrate an increase in adsorbed oxygen content over a 30 - 150 W applied power range regardless of plasma precursor, in addition to showing that tin reduction occurs upon H₂O_(v) plasma treatment. Gas sensing performance was initially explored by exposing SnO₂ sensors to air at temperatures of 25-300° C to determine base resistance of the materials in an ambient atmosphere. The data show changes in resistance that are dependent upon nanomaterial architecture, plasma treatment conditions, and sensor temperature. Base resistance changes for specific plasma and sensor conditions will be discussed as well as sensor responses and selectivity upon exposure to toxic gases including benzene and carbon monoxide. By combining materials characterization with gas sensor responses, we can optimize sensor sensitivity and selectivity by tuning plasma modification conditions with aims for targeted gas sensing applications.

11:20am **SS+AS+NS-WeM11 Enhanced Adsorption of CO₂ at Steps of Planar ZnO(0001) Grown on Au(111), Xingyi Deng, D. Sorescu, J. Lee, National Energy Technology Laboratory**

In this work, we study the energetics of CO₂ adsorbed on the bi- and tri-layer ZnO(0001) grown on Au(111) using temperature programmed desorption (TPD) and calculations based on density functional theory (DFT). Both bi- and tri-layer ZnO(0001) on Au(111) adopt a planar, graphite-like structure via an inter-layer relaxation to minimize the surface dipole arising from alternating Zn²⁺ and O²⁻ layers. CO₂ is adsorbed weakly

on these planar ZnO(0001) surfaces, desorbing between 125-130 K in TPD. Two other desorption peaks were also observed in TPD at ~ 150 and 280-320 K and are attributed to the CO₂ adsorption at the steps between the bi- and tri-layer ZnO(0001) surfaces. This enhanced adsorption of CO₂ at the steps is supported by DFT calculations: the computed energetics of CO₂ adsorbed on surfaces and at steps is indeed consistent with that estimated from the TPD experiments via the Redhead method. Implications of our fundamental results for ZnO based catalysts will be discussed.

11:40am **SS+AS+NS-WeM12 Characterization of Band Gap and Lattice Constant of Ultrathin ZnO Layers on Au(111)**, *Junseok Lee, D. Sorescu, X. Deng*, National Energy Technology Laboratory

Ultrathin layers of ZnO grown on the Au(111) substrate have been characterized using low-temperature scanning tunneling microscopy (STM). Under reactive deposition condition, the ZnO layers have been found to grow by forming islands. Detailed analysis of electronic structure have been conducted using scanning tunneling spectroscopy (STS) and the density functional theory (DFT) calculations. The band gap of ultrathin layers of ZnO is found to be larger compared to the bulk ZnO wurtzite structure. The density functional theory calculations provides understanding of the increased band gaps of thin ZnO layers. The lattice constants of ultrathin ZnO layers on Au(111) are also found to be larger than that of the bulk lattice constant, which could be explained by the formation of graphitic-like ZnO layers.

12:00pm **SS+AS+NS-WeM13 Submonolayer Water Adsorption on Stepped and Planar Pt Surfaces**, *Rachael Farber*, Loyola University Chicago, *M.J. Kolb*, Leiden Institute of Chemistry, *J. Derouin*, Loyola University Chicago, *M.T.M. Koper*, *L.B.F. Juurlink*, Leiden Institute of Chemistry, *D.R. Killelea*, Loyola University Chicago

The adsorption of water onto metal surfaces yields a host of intricate adsorbate structures at

coverages less than a single layer. Complex adsorption structures arise due to the delicate balance

of hydrogen bonding between water molecules as well as attractive forces between water molecules

and the metal surface. Therefore, the complexity of the system provides an excellent opportunity to

refine models of water-water and water-surface interactions. Water molecules are largely confined

to a single plane and, as a result, the geometry of aligned water molecules gives rise to frustrated

hydrogen bonding. At low coverages of water on metal surfaces, these frustrated intermolecular

interactions result in the formation of structures other than the classic hexagons of bulk water. We

will report the results of a combined theory-experiment study of water adsorption on planar Pt(111)

and stepped Pt(553). Experimentally, temperature programmed desorption (TPD) and ultra-high

vacuum scanning tunneling microscopy (UHV-STM) were used to quantify water coverage and to

image the resultant surface structures. On Pt(111), 5, 6, and 7-membered rings were found to form

across the Pt surface, in agreement with previously reported experimental results and electronic

structure calculations. On Pt(553), however, tetragonal structures that have not been previously

observed were found to form across monatomic steps. These observations confirm DFT

calculations for submonolayer water coverage on Pt(553) and provide fine details as to how water-

water and water-surface interactions are balanced on active metal surfaces.

Wednesday Afternoon, October 21, 2015

Actinides and Rare Earths Focus Topic
Room: 230A - Session AC+AS+MI-WeA

Chemistry and Physics of the Actinides and Rare Earths

Moderator: Ladislav Havela, Charles University, Prague, Czech Republic

2:20pm **AC+AS+MI-WeA1 High Resolution X-ray Absorption Spectroscopy as an Advanced Tool for Structural Investigations of Actinides, Tonya Vitova, Karlsruhe Institute of Technology, Germany**
INVITED

Advanced spectroscopy methods, which provide precise speciation, redox state, and electronic structure information, are needed to benchmark and drive improvement of geochemical/thermodynamic modeling and quantum chemical computational methods. The high energy resolution X-ray absorption near edge structure (HR-XANES) spectra contain additional information compared to the conventional XANES spectra, as they are rich in resolved resonant spectral features for specific An oxidation states.^[1]The An $M_{4,5}$ edge HR-XANES probes directly the An valence unoccupied 5f states ($3d \rightarrow 5f$) and thus yields insight to the role these frontier orbitals play in hybridization with ligands and bond formation.

The characterization capabilities of the An $M_{4,5}$ and L_3 edge HR-XANES technique will be highlighted by recent results obtained for both model and complex U, Np and Pu materials. In one example, a single crystal of dicesium uranyl tetrachloride ($Cs_2UO_2Cl_4$) as a model UO_2^{2+} (uranyl ion) compound was investigated using U M_4 ($3d_{3/2} \rightarrow 5f$) and L_3 ($2p_{3/2} \rightarrow 5f/6d$) edge polarization dependent HR-XANES (PD-HR-XANES) with remarkable energy resolution. Comparison of experimentally determined relative energies of U $5f\delta$, $5f\phi$, $5f\pi$, and $5f\sigma$ orbitals, as well as 5f and 6d orbitals obtained from the spectra, to predictions from quantum chemical Amsterdam density functional theory (ADF) and FEFF codes and show excellent results.^[2] A number of examples for determination of An redox states in liquids and solid systems will be discussed. Comparison of U/Pu/Np M_4/M_5 HR-XANES spectra of UO_2^{2+} , NO_2^{2+} and PuO_2^{2+} as well as Pu M_5 HR-XANES and L_3 XANES of various Pu oxidation states in aqueous solution will be presented. In addition, recent results unambiguously demonstrate that U(V) can exist alongside U(IV) and U(VI) in magnetite nanoparticles under anoxic conditions; this underpins the utility of HR-XANES for understanding U retention mechanisms on corrosion products.

[1] At. Vitova, M. A. Denecke, J. Göttlicher, K. Jorissen, J. J. Kas, K. Kvashnina, T. Prüßmann, J. J. Rehr, J. Rothe, Journal of Physics: Conference Series, 430, Bk. O. Kvashnina, S. M. Butorin, P. Martin, P. Glatzel, Phys Rev Lett, 111; Ct. Vitova, K. O. Kvashnina, G. Nocton, G. Sukharina, M. A. Denecke, S. M. Butorin, M. Mazzanti, R. Caciuffo, A. Soldatov, T. Behrends, H. Geckeis, Phys Rev B, 82.

[2] T. Vitova, J. C. Green, R. G. Denning, M. Löble, K. Kvashnina, J. J. Kas, K. Jorissen, J. J. Rehr, T. Malcherek, M. A. Denecke, Inorganic Chemistry, 54, 174-182.

3:00pm **AC+AS+MI-WeA3 Soft X-ray Spectromicroscopy of Actinide Materials, David Shuh, Lawrence Berkeley National Laboratory**
INVITED
Soft X-ray synchrotron radiation methodologies are being developed and employed at the Advanced Light Source (ALS) of Lawrence Berkeley National Laboratory to elucidate the electronic structure of actinide materials. Results from these investigations have begun to provide improved fundamental knowledge that can be used as a scientific basis for the enhanced design of special-purpose actinide materials and the overall understanding of actinide materials. The experimental developments at the ALS have centered on the use of the Molecular Environmental Science (MES) scanning transmission X-ray microscope (STXM) at Beamline 11.0.2 for near-edge X-ray absorption spectroscopy (XAS), and on X-ray emission spectroscopy (XES) at several beamlines, focusing primarily on light atom constituents (C, N, O, F) for ligand K-edge XAS, and on metal-ion centers plus light-atom signals for XES. The spectromicroscopy capabilities of the STXM provide the means to investigate and determine the speciation in actinide materials and environmentally-relevant systems with spatial resolution that reaches to the true nanoscale.

An absolutely critical and key enabling component for all of the soft X-ray investigations is the contribution of theory, that when combined with experiment, has firmly provided more detailed knowledge of electronic structure in actinide materials in terms of orbital composition and mixing, and oxidation state. The highlights of recent investigations of metallocenes at the carbon K-edge and uranyl complexes at the nitrogen K-edge will be

highlighted in this respect. The spectromicroscopy attributes of the STXM have enabled the investigation of contaminant speciation in a range of model and real environmental systems. The results of the most recent environmentally-related studies, cesium in clay materials relevant to clean up efforts in Japan, will be presented.

Acknowledgement: Supported by the Director, Office of Science, Office of Basic Energy Sciences, Division of Chemical Sciences, Geosciences, and Biosciences Heavy Element Chemistry Program of the U.S. DOE at LBNL under Contract No. DE-AC02-05CH11231.

4:20pm **AC+AS+MI-WeA7 Resonant Ultrasound Spectroscopy Detects 100 Part-per-billion Effects in Plutonium, Albert Migliori, Los Alamos National Laboratory**
INVITED

The speeds of sound, or, equivalently, the elastic moduli are some of the most fundamental attributes of a solid, connecting to fundamental physics, metallurgy, non-destructive testing, and more. With modern advances in electronics and analysis, changes in elastic moduli are detectable at 100 parts per billion, providing new and important insight into grand challenges in plutonium science. Applied to ^{239}Pu , the effects of aging are measured in real time as a function of temperature, and the temperature dependence of the elastic moduli of gallium stabilized delta plutonium leads to important questions about the validity of electronic structure theory, and points towards inescapable constraints on any theory of this metal.

This work was supported as part of the Materials Science of Actinides, an Energy Frontier Research Center funded by the U.S. Department of Energy, Office of Science, Basic Energy Sciences under Award # DE-SC0001089.

5:00pm **AC+AS+MI-WeA9 Spectroscopic Studies of the Oxide Layer formed on Plutonium under Ambient Conditions, Alison Pugmire, Los Alamos National Laboratory, C.H. Booth, Lawrence Berkeley National Laboratory, J. Venhaus, L. Pugmire, Los Alamos National Laboratory**

One of the fundamental challenges of modern science lies in understanding the chemistry and physics of the actinides, and in particular, plutonium. It's unpredictable behavior and reactivity has led to a very poor understanding of its metallurgy and corrosion process. This not only poses a basic scientific challenge, but directly affects the safe, long term storage of this material. In an effort to understand the surface chemistry and corrosion of plutonium, knowledge of the surface oxide composition is paramount. The currently accepted description of the oxide layer formed under ambient temperatures and pressures consists of a thick PuO_2 surface layer over a thin Pu_2O_3 layer at the metal interface. However, recent studies by our group indicate this description is inadequate, and the oxide layer formed in the initial stages, in particular, is much more complex. We have recently focused on studying the oxide layer formed on gallium stabilized δ -plutonium in ambient conditions (pressure, temperature). We have characterized this layer using multiple spectroscopic techniques, including spectroscopic ellipsometry (SE), x-ray photoelectron spectroscopy (XPS), and x-ray absorption spectroscopy (XAS). This diverse and complimentary suite of experimental techniques will address many long-standing issues regarding the nature of the oxide layer and the corrosion mechanism.

5:20pm **AC+AS+MI-WeA10 Covalent Mixing In Actinide and Lanthanide Compounds: Reliable Assignment of Cation Charges, Paul Bagus, University of North Texas, C.J. Nelin, Consultant**

The importance of covalent and ionic interaction and bonding in heavy metal oxides, for example for the actinide dioxides, AnO_2 , is controversial with some claiming that the interactions are nearly purely ionic and with others arguing that there is important covalent character. Similar questions also exist for halides and for lanthanide compounds. One way to view this is to consider how close the actual charge state of the cation is to the nominal oxidation state. Our analysis is based on using wavefunctions for embedded clusters which model the bulk oxides. With these wavefunctions, we show that considerable departures of the cation charge from the nominal value are a common occurrence. We also show how the departure from the nominal charge state depends on several factors including: (1) nominal oxidation state, (2) ligand, and (3) position in the row of the periodic table. It is also necessary to determine which metal orbitals are involved in the covalent mixing. For actinides, the natural choice is the open cation 5f shell but the normally empty 6d shell may also contribute to the covalent mixing and, in fact, may even have a larger contribution than the 5f. In order to characterize the extent and importance of the covalent mixing, two factors need to be taken into account: (1) the estimate of the actual charge state of the cations and (2), perhaps even more important, the contribution of the covalent mixing of the cation and anion frontier orbitals to the total energy of the compound. Our approach to address both of these aspects is to limit the variational freedom when we self-consistently optimize the orbitals of

the models used to represent the compounds studied. By restricting the variational space, the importance of the mixing of ligand and metal frontier orbitals can be explicitly measured by determining the difference between a wavefunction where these frontier orbitals are excluded from the variational process and a wavefunction where they are allowed to mix with other orbitals. With this approach, it is possible to make quantitative estimates of energies associated with the covalent mixing as well as the effective charges that can be associated with the cations and ligands. Furthermore, it is possible to visualize the changes in the charge distribution for different degrees of variational freedom with suitable contour plots. We acknowledge support for this work by the Geosciences Research Program, Office of Basic Energy Sciences, U.S. DOE.

5:40pm **AC+AS+MI-WeA11 An XPS and ToF SIMS Investigation of Cerium Oxidation**, Paul Roussel, AWE, United Kingdom of Great Britain and Northern Ireland

In this study fcc γ -cerium has been used as a non radioactive surrogate material for fcc δ -plutonium. The common cerium oxides are the trivalent sesquioxide and the tetravalent dioxide both of which are iso-structural with the oxides formed on plutonium metal. Similarly, cerium (I) like plutonium (2) displays parabolic oxidation kinetics at low temperatures and linear kinetics elevated temperatures. This makes cerium an ideal surrogate material to study the kinetics and mechanism of plutonium oxidation. The initial oxidation of cerium at 274 K was studied using X-ray Photoelectron Spectroscopy. On exposure to Langmuir quantities of oxygen cerium rapidly oxidizes to the trivalent oxide followed by the slower growth of the tetravalent oxide. The growth modes of both oxides have been determined. It was found the surface formed tetravalent oxide was unstable in ultra high vacuum and reduced to the trivalent oxide by an apparent solid state diffusion reaction with cerium metal. This reduction reaction can be explained by the thermodynamic instability of the tetravalent dioxide with respect to cerium metal. The complexity of this reduction reaction appears to be enhanced by the formation of surface hydroxyl species as a function of time. Time of Flight Secondary Ion Mass Spectrometry was used to support characterization of the surface hydroxyl species.

(1) D. Cubicciotti, J. Am. Chem. Soc., 74 (1952) 1200.

(2) J. L. Stakebake, J. Less Common Met., 123 (1986) 185.

© British Crown Copyright 2015/AWE

Applied Surface Science

Room: 212D - Session AS+SS-WeA

Characterization of Buried Interfaces

Moderator: Xia Dong, Eli Lilly and Company, James Ohlhausen, Sandia National Laboratories

2:20pm **AS+SS-WeA1 ASSD 30th Anniversary Speaker: Characterization of Sub-surface Interfaces using SIMS, TEM, and FIB or: How Much will it Cost me to Fix that Interface?**, Fred Stevie, North Carolina State University **INVITED**

Characterization of interfaces between layers or between layer and substrate has always been of interest. Interface issues include visible problems, such as delamination or corrosion, and contamination that can affect product quality, such as electrical properties in semiconductors. The information desired includes the physical quality of the interface and identification and quantification of contaminants. This presentation summarizes multiple approaches to interface analysis, particularly with use of SIMS, FIB, and TEM.

Common approaches for analysis of a buried interface involve a depth profile or cross section. Depth profiling by SIMS is often used because of good sensitivity and depth resolution. Matrix, dopant and contaminant species in the structure can be characterized with a single SIMS depth profile. Quantification of contamination at an interface is highly desired but can be difficult to obtain. Once an element has been identified as a contaminant, quantification at interfaces may be possible with ion implantation. Significant improvements have been made with the species used for depth profiling. C_{60} and argon cluster beams are used to depth profile organic materials. These high mass ion beams provide better sensitivity for high mass species and do not affect the chemical composition, so it is possible to obtain interfacial chemistry.

The FIB has revolutionized sample preparation and lift-out methods can routinely prepare cross section specimens for TEM analysis. A sample polished to provide an edge can rapidly be trimmed with FIB to provide a surface 50 to 100 μ m in height that is suitable for high resolution analysis. Optimization of beam conditions such as dwell and overlap can increase

removal rate by several times. Plasma ion sources dramatically increase material removal rates and make possible the study of 100 μ m deep interfaces which will cover most layers of interest. Plating coatings are commonly less than 5 μ m thick and paint coatings 100 to 150 μ m.

3:00pm **AS+SS-WeA3 FIB-TOF Tomography Characterization of Organic Structures**, David Carr, G.L. Fisher, Physical Electronics USA, S. Iida, T. Miyayama, ULVAC-PHI

1. Introduction

There are practical limitations to the use of ion beam sputtering for probing the sample chemistry beyond the surface region which include preferential sputtering and accumulated sputter beam damage. Both effects result in a distortion or complete loss of the true 3D chemical distribution as a function of depth

An alternative approach to achieve 3D chemical imaging of complex matrix chemistries is to utilize *in situ* FIB milling and sectioning in conjunction with TOF-SIMS chemical imaging, or 3D FIB-TOF tomography [1]. This can minimize or eliminate artifacts caused by sputter depth profiling such as differential sputtering and accumulated ion beam damage.

However, even with FIB polishing there remains some FIB beam-induced chemical or molecular damage that may or may not limit the detection of characteristic molecular signals. For certain specimens, it is an advantage to follow FIB polishing with cluster ion polishing to recover the characteristic molecular signals.

2. Method

The 3D chemical characterization of pure organic and metal-organic mixed composition structures was achieved utilizing 3D FIB-TOF tomography on a PHI TRIFT *nanoTOF* II (Physical Electronics, USA) imaging mass spectrometer. The spectrometer's large angular acceptance and depth-of-field maintain high mass resolution and high mass scale linearity even in this challenging geometry. This provides the highly desirable ability to perform artifact-free chemical imaging of high aspect ratio features.

3. Results

The present study investigated samples from two classes of materials: one metal-organic mixed matrix composition and one mixed organic phase comprised of two polymer moieties. Since there was no preferential sputtering, an immediate result of the FIB-TOF imaging was the accurate determination of the depth scale. We have collected characteristic molecular information from each sample for the purposes of 2D and 3D imaging. Cluster ion beam polishing (e.g. C_{60}^+ or $Ar_{2,500}^+$) was necessary to remove the FIB beam-induced damage, and the new instrument configuration allows cluster ion polishing to be accomplished with ease. We will highlight certain aspects of the studies for presentation.

4. References

[1] A. Wucher, G.L. Fisher and C.M. Mahoney, Three-Dimensional Imaging with Cluster Ion Beams (p. 207-246) in *Cluster Secondary Ion Mass Spectrometry: Principles and Applications*, C.M. Mahoney (Ed.), Wiley & Sons, N.J. (2013).

4:20pm **AS+SS-WeA7 Interface Characterization using Ballistic Electron Emission Microscopy and Spectroscopy: Recent Results and Related Techniques**, Douglas Bell, Jet Propulsion Laboratory, California Institute of Technology **INVITED**

Ballistic electron emission microscopy (BEEM) is a microscopy and spectroscopy based on scanning tunneling microscopy (STM), developed as a scanning probe of subsurface interface properties. By monitoring the fraction of tunneling current between STM tip and sample that traverses a subsurface heterostructure, BEEM can probe hot-carrier transport as well as heterostructure and material properties. Because BEEM uses an STM tip to inject a highly localized carrier distribution, high-resolution imaging of interface electronic structure can be performed. Control of tunnel voltage polarity allows injection of either holes or electrons into the sample structure, thus enabling characterization of electronic structure both above and below the Fermi level.

Since its inception, BEEM has found many applications such as studies of interface heterogeneity, carrier scattering, band structure, transport in oxides, and interface chemistry. A wide range of structures have been probed, including metal/semiconductor, metal/oxide/semiconductor, quantum wells, and quantum dots. Researchers have measured quantized energy levels and spatial variations of Schottky barrier height. BEEM has also provided a new means for studying fundamental characteristics of interface transport such as conservation of momentum parallel to an interface.

More recently, BEEM has been applied to the investigation of other novel materials and structures. Organic materials, graphene layers, and nanowires have received attention, and research has been done on molecular vibrational spectroscopy. Related techniques for magnetic materials, and

measurements of BEEM-induced luminescence, have been further developed and demonstrated.

This talk will discuss some of these recent advances and extensions, as well as further developments in more traditional areas. Some comparisons with results from other characterization techniques will also be presented.

5:00pm **AS+SS-WeA9 Using XPS to Study Electrochemical Solid-Liquid Interfaces In-Operando: Standing-Wave Ambient-Pressure XPS (SWAPPS)**, *Osman Karstlioglu*, Lawrence Berkeley National Laboratory, *S. Nemsak*, Forschungszentrum Juelich GmbH, Germany, *I. Zegkinoglou*, *A. Shavorskiy*, *M. Hartl*, *C.S. Fadley*, *H. Bluhm*, Lawrence Berkeley National Laboratory

Accessing the chemical and electrical potential information at a solid/liquid interface is an important capability for investigating a process like corrosion where electrochemical transformations are at work. Here we report the first results of a combination of techniques, where we use X-ray standing waves to enhance the photoemission signal from the solid-liquid interface during an ambient-pressure XPS experiment, investigating the oxidation of Ni. X-ray standing waves were generated by a Si/Mo multilayer mirror, on which the sample is prepared as a thin layer (~8 nm Ni in this case). A thin liquid layer was formed on the surface by dipping the sample into an electrolyte (KOH(aq), 0.1 mol/L) and pulling back partially. The solid-liquid interface was probed through this thin liquid layer using hard X-rays (3100 eV). The sample was the working electrode in a 3-electrode cell, and it was oxidized by applying a positive potential using the potentiostat. Comparing the experimental rocking curves for Ni 3p and O 1s with theory provided thickness and roughness information for solid and liquid layers with ~1 nm resolution.

5:20pm **AS+SS-WeA10 Exploring the Usefulness of Monochromatic Ag La X-rays for XPS**, *Sarah Coultas*, *J.D.P. Counsell*, *S.J. Hutton*, *A.J. Roberts*, *C.J. Blomfield*, Kratos Analytical Limited, UK

High energy X-ray sources have been used in XPS analysis for some time to access more core-levels and probe deeper into the sample surface. Lab based sources such as Zr and Ti have been offered in the past but the broad X-ray line widths produced by such sources limit their applications for chemical analysis. This problem is mitigated by the use of an Ag La X-ray source. The source energy is 2984 eV, conveniently approximately twice that of Al K α , hence the same quartz crystal mirror may be used to monochromate the Ag La X-ray line producing a narrow, high energy source of X-rays for XPS. Modern X-ray photoelectron spectrometers may be fitted with automated Al / Ag X-ray monochromators which greatly improve the usability of Ag La X-rays allowing Al and Ag X-ray generated spectra to be recorded from the same sample as part of automated data acquisition. Highlights of the source's characteristics include:

- Good sensitivity and energy resolution provide useful chemical information
- Enhanced surface compositional information from approximately twice the analytical depth as Al K α radiation for same core line
- Higher excitation energy allows deeper core levels and additional Auger lines to be explored
- Large energy range of Ag La allows exploitation of "depth dimension" for surface segregation studies

Here we investigate the practical uses of these characteristics. This includes using the Auger parameter for aluminium and silicon containing compounds where the higher energy radiation can excite the 1s core lines and the KLL Auger series. Earlier studies [1] have shown the usefulness of higher excitation energies in elucidating structure via Auger parameters.

We also illustrate the usefulness of Ag La as an additional tool for the surface analyst by way of examples of spectroscopy, ARXPS, depth profiling and imaging.

1. References

[1] J.E. Castle, L.B. Hazell & RH West, *J. Electron Spectrosc. Relat. Phenom.*, 1979, **16**, 97

5:40pm **AS+SS-WeA11 Optimizing the TOF-SIMS CsM⁺ Depth Profile of a Tunnel Magneto Resistance (TMR) Structure**, *Alan Spool*, HGST, a Western Digital Company

Used now for many years in modern magnetic recording devices, TMR sensors consist at their heart of a complicated series of layers, mostly metallic, ranging in thickness from less than a nm to several nm. In order to use the potentially better depth resolution and sensitivity of a SIMS depth profile over other surface analytical techniques, CsM⁺ profiles were obtained using a variety of conditions. The ratio of the sputter ion to primary ion fluences, the sputter ion beam energy, and the % of Cs in a combined Cs/Xe sputter ion beam were all varied, and the results for a single wafer compared. In addition to changes in various CsM⁺ ion

intensities and therefore their signal to noise, the Cs/Xe ratio sometimes had unexpected effects on the profile shapes. The primary ion beam fluence was lessened by increasing its raster size over more than the crater bottom. Depth profiles were then created retrospectively from the raw data, using the results themselves to select the flattest portion of the crater bottom.

6:00pm **AS+SS-WeA12 Interface and Composition Analyses versus Performances: How to Improve Perovskite Solar Cells**, *Y. Busby*, University of Namur, B-5000 Namur, Belgium, *F. Matteocci*, University of Rome "Tor Vergata", Italy, *G. Divitini*, *S. Cacovich*, University of Cambridge, UK, *C. Ducati*, University of Cambridge, *A. di Carlo*, University of Rome "Tor Vergata", Italy, *Jean-Jacques Pireaux*, University of Namur, Belgium

Hybrid halide perovskite solar cells (PSCs) have received much attention during the very last years because of their very promising cost/performance ratio. Different architectures and preparation methods have been tested, but still some general guidelines for their optimization are missing. In particular, the interfaces are now well known to play a dominant role in the device performances but have been so far poorly studied.

In this work, we correlated the solar cell characteristics to their interface composition and morphology in PSCs deposited by different procedures (single-step, double-step by dipping, double-step by a vacuum assisted technique) and different conversion environments (air, vacuum and nitrogen atmosphere). The interface quality is found to be affected by the perovskite conversion method and in particular from the environment where the conversion is performed. Power conversion efficiencies between 7 and 14.5% have been measured from the characteristics of the differently prepared cells. The morphology, crystal size and interdiffusion have been fully characterized by scanning transmission electron microscopy (STEM), equipped with high resolution energy-dispersive X-ray spectroscopy (EDX). Interfaces have been further characterized by depth profile techniques by combining ion beam sputtering with atomic and molecular composition analysis with X-Ray photoelectron spectroscopy (XPS) and Time of Flight Secondary Ion Mass Spectroscopy (ToF-SIMS). In particular these techniques allowed detecting and evaluating the diffusion of metals into the hole transport material (SpiroOMeTAD) and iodine and chlorine diffusion in the TiO₂ back contact. Interestingly, the higher oxygen content perovskite formed in air is not associated to a sensibly lower (short term) efficiency of the solar cell.

Electronic Materials and Processing

Room: 211C - Session EM+AS+MS+SS-WeA

Surface and Interface Challenges in Wide Bandgap Materials

Moderator: Aubrey Hanbicki, U.S. Naval Research Laboratory, Rachael Myers-Ward, U.S. Naval Research Laboratory

2:20pm **EM+AS+MS+SS-WeA1 Effects of Nitrogen and Antimony Impurities at SiO₂/SiC Interfaces**, *Patricia Mooney*, Simon Fraser University, Canada **INVITED**

4H-SiC is an attractive material for devices operating at high power and high temperatures because of the large bandgap energy, 3.23 eV, the high critical breakdown field, 2.0 MVcm⁻¹, and high electron mobility,

850 cm²V⁻¹s⁻¹. Commercialization of 4H-SiC MOSFET technology was long delayed due to the high density of defects near the SiO₂/SiC interface. Post oxidation annealing in NO ambient, the process that enabled the commercialization of SiC Power ICs in 2011, significantly reduces the density of near-interface traps and results in typical effective MOSFET channel electron mobility (μ_{FE}) values of ~20 cm²V⁻¹s⁻¹ [1]. The relatively high density of near-interface traps having energy levels within 0.5 eV of the SiC conduction band was investigated using constant capacitance transient spectroscopy (CCDLTS). These measurements showed that NO annealing reduced the density of the two near-interface oxide trap distributions, attributed to Si interstitials and substitutional C pairs in SiO₂, by as much as a factor of 10 [1,2].

It has also been shown that introducing impurities such as Na, P, or Sb near the SiO₂/SiC interface further increases μ_{FE} , to peak values of 104 cm²V⁻¹s⁻¹ and to 50 cm²V⁻¹s⁻¹ at high electric field for Sb [3]. The much higher value of μ_{FE} in Sb-implanted MOSFETs was attributed to counter-doping by Sb in SiC near the interface. To investigate the effects of Sb at SiO₂/SiC interfaces, Sb ions were implanted near the surface of the 4H-SiC epitaxial layer and the wafer was annealed at 1550 °C in Ar to activate the Sb donors. Dry thermal oxidation was done at 1150 °C and the sample was then NO-

annealed at 1175 °C for 30 or 120 min. CCDLTS results of Sb-implanted MOS capacitors were compared with those having no Sb implant but with similar dry oxidation and NO-annealing processes. The density of near-interface oxide traps was similar in samples with and without Sb, indicating that Sb has little effect on those defects. However, CCDLTS spectra taken at bias and filling pulse conditions that reveal defects in the SiC depletion region, show both the deeper of the two N donor levels at $E_c - (0.10 \pm 0.01)$ eV and a second energy level only in Sb-implanted samples at $E_c - (0.12 \pm 0.01)$ eV. To our knowledge this is the first measurement of Sb donors in SiC and it confirms counter doping of SiC by Sb near the SiO₂/SiC interface.

[1] P.M. Mooney and A.F. Basile, in *Micro and Nano-Electronics: Emerging Device Challenges and Solutions*, Ed. T. Brozek (CRC Press, Taylor and Francis, 2014) p. 51.

[2] A.F. Basile, et al., *J. Appl. Phys.* **109**, 064514 (2011).

[3] A. Modic, et al., *IEEE Electron Device Lett.* **35**, 894 (2014).

3:00pm EM+AS+MS+SS-WeA3 Hydrogen Desorption from 6H-SiC (0001) Surfaces, Sean King, Intel Corporation, R. Nemanich, R. Davis, North Carolina State University

Due to the extreme chemical inertness of silicon carbide (SiC), *in-situ* thermal desorption is commonly utilized as a means to remove surface contamination prior to initiating critical semiconductor processing steps such as epitaxy, gate dielectric formation, and contact metallization. *In-situ* thermal desorption and silicon sublimation has also recently become a popular method for epitaxial growth of mono and few layer graphene. Accordingly, numerous thermal desorption experiments of various processed silicon carbide surfaces have been performed, but have ignored the presence of hydrogen which is ubiquitous throughout semiconductor processing. In this regard, we have performed a combined temperature programmed desorption (TPD) and x-ray photoelectron spectroscopy (XPS) investigation of the desorption of molecular hydrogen (H₂) and various other oxygen, carbon, and fluorine related species from *ex-situ* aqueous hydrogen fluoride (HF) and *in-situ* thermal and remote hydrogen plasma cleaned 6H-SiC (0001) surfaces. Using XPS, we observed that temperatures on the order of 700 - 1000 °C are needed to fully desorb C-H, C-O and Si-O species from these surfaces. However, using TPD, we observed H₂ desorption at both lower temperatures (200 - 550 °C) as well as higher temperatures (> 700 °C). The low temperature H₂ desorption was deconvoluted into multiple desorption states that, based on similarities to H₂ desorption from Si (111), were attributed to silicon mono, di, and trihydride surface species as well as hydrogen trapped by sub-surface defects, steps or dopants. The higher temperature H₂ desorption was similarly attributed to H₂ evolved from surface O-H groups at ~ 750 °C as well as the liberation of H₂ during Si-O desorption at temperatures > 800 °C. These results indicate that while *ex-situ* aqueous HF processed 6H-SiC (0001) surfaces annealed at < 700 °C remain terminated by some surface C-O and Si-O bonding, they may still exhibit significant chemical reactivity due to the creation of surface dangling bonds resulting from H₂ desorption due from previously undetected silicon hydride and surface hydroxide species.

3:20pm EM+AS+MS+SS-WeA4 Chemical and Microstructural Characterization of Interfaces between Metal Contacts and β -Ga₂O₃, Lisa M. Porter, Y. Yao, J.A. Rokholt, R.F. Davis, Carnegie Mellon University, G.S. Tompa, N.M. Sbrockey, T. Salagaj, Structured Materials Industries, Inc.

β -Ga₂O₃ is a promising alternative to traditional wide bandgap semiconductors, as it has a wider bandgap (~4.9 eV) and a superior figure-of-merit for power electronics and other devices; moreover, β -Ga₂O₃ bulk single crystals have recently been grown commercially using melt-growth methods. While several groups have demonstrated Ga₂O₃-based devices such as Schottky diodes and MOSFETs, understanding of contacts to this material is limited. In this study, we investigated a variety of metal contacts (Ti, In, Mo, W, Ag, Au, and Sn) to both (-201) β -Ga₂O₃ single crystal substrates (from Tamura Corp.) and β -Ga₂O₃ epitaxial layers grown by MOCVD on various substrates (sapphire and single crystal β -Ga₂O₃) by co-authors at Structured Materials Industries. We have characterized these substrates and epilayers using techniques such as X-ray diffraction and transmission electron microscopy (TEM), which show that the epitaxial layers are oriented (-201) with respect to the substrates. We found that the electrical characteristics of the metal contacts to the Ga₂O₃ epilayers and substrates are highly dependent on the nature of the starting surface and the resulting interface, and less dependent on the work function of the metal than expected. For example, both Ti and bulk In readily form ohmic contacts to Ga₂O₃, whereas other low-workfunction metals, such as Sn, did not form ohmic contacts even after annealing to 800 °C. For Ti ohmic contacts on Sn-doped Ga₂O₃ substrates the optimal annealing temperature was ~400 °C: the electrical characteristics continually degraded for annealing temperatures above ~500 °C. Thermodynamics predicts that Ti

will reduce Ga₂O₃ to produce Ti oxide, therefore indicating that the Ti/Ga₂O₃ interface is unstable. In correspondence with this prediction, high-resolution cross-sectional TEM images of 400 °C-annealed samples show the formation of an ultra-thin (~2 nm) interfacial amorphous layer. TEM samples at higher annealing temperature have also been prepared for analysis; electron energy loss spectroscopy will be used to characterize the interfacial composition profiles in these samples to determine the relationship between composition and thickness of the interfacial layer and the electrical degradation of the contacts. Schottky diodes with Au, Mo, W and Sn as the Schottky metal were also fabricated. The Schottky barrier heights (SBHs) showed a weak dependence on the metal workfunction. An overview of the electrical behavior of different metals as ohmic or Schottky contacts to Ga₂O₃ and the interfacial chemistry and microstructure will be presented.

4:20pm EM+AS+MS+SS-WeA7 Regrown InN Ohmic Contacts by Atomic Layer Epitaxy, Charles Eddy, Jr., U.S. Naval Research Laboratory, N. Nepal, Sotera Defense Solutions, M.J. Tadjer, T.J. Anderson, A.D. Koehler, J.K. Hite, K.D. Hobart, U.S. Naval Research Laboratory

For the past 25 years, compound semiconductors comprised of elements from group III-B of the periodic table and nitrogen have attracted a sustained, high-level of research focus. More recently they have found growing application to rf and power electronics in the form of advanced transistor structures such as the high electron mobility transistor (HEMT) with and without insulated gates. Key performance parameters for such devices (cut-off frequency for rf transistors and on-resistance for power transistors) are often dominated by the contact resistance. The current best approach to contact resistance minimization involves aggressive processing requirements that challenge device fabrication, especially when insulated gates are required. A potential solution is the regrowth of highly conducting semiconductor contact layers where ohmic contacts are needed.

Here we report on initial efforts to employ regrown indium nitride (InN) contact layers by atomic layer epitaxy (ALE) as a low temperature solution to the ohmic contact challenge for III-N transistors. Recently, we have reported that good crystalline quality InN can be grown at less than 250 °C by ALE [1]. Here we employ such conditions to grow very thin layers and assess them morphologically and electrically.

InN regrown contact layers of 5nm thickness grown on sapphire are very smooth (rms roughness < 0.17nm) and possess sheet resistances as low as 3.6 k Ω /sq, corresponding to electron sheet carrier densities of 2-3 x 10¹³ cm⁻² and mobilities of 50 cm²/V-s. These electron mobilities are higher than previously reported (30 cm²/V-s) for much thicker films (1.3 μ m) [2]. Similarly grown 22.5 nm thick InN layers on highly resistive silicon were processed with mesa isolation regions and 20/200 nm thick titanium/gold contact metals. Without any contact annealing, an ohmic contact resistance of 9.7x10⁻⁷ Ω -cm² (1.2 Ω -mm) was measured, comparable to the best high temperature alloyed contact to an AlGaIn/GaN HEMT.

In our initial non-alloyed ohmic contact process, contact regions were recessed down to the GaN buffer layer to establish physical contact between the highly-conductive InN layer and electrons in the HEMT channel. A 25 nm thick InN layer was then grown by ALE, and the InN-filled ohmic regions were then capped with a Ti/Al/Ti/Au layers. Using the metals as an etch mask, the InN outside of the ohmic regions was etched away. We will report on initial results of application of ALE InN regrown contact layers and the modified fabrication approaches to AlGaIn/GaN HEMTs.

1. N. Nepal, et al., *J Cryst. Growth and Design*, **13**, 1485-1490 (2013).

2. Kuo et al., *Diamond & Related Materials*, **20**, 1188 (2011).

4:40pm EM+AS+MS+SS-WeA8 High-Temperature Characteristics of Ti/Al/Pt/Au Contacts to GaN at 600 °C in Air, Minmin Hou, D.G. Senesky, Stanford University

The high-temperature characteristics (at 600 °C) of Ti/Al/Pt/Au contacts to gallium nitride (GaN) in air are reported. GaN is a wide bandgap semiconductor material being developed for high-temperature electronics and micro-scale sensors. Ti/Al/Pt/Au metallization is frequently used for forming ohmic contacts to GaN. However, few studies have been devoted to studying the electrical characteristics of the Ti/Al/Pt/Au metallization at elevated temperatures and even fewer in oxidizing environments. It is not practical to obtain a hermetic sealing at elevated temperatures and a number of sensing applications may require non-hermetic packages. Therefore, the electrical characteristics of Ti/Al/Pt/Au contacts in a hot oxidizing ambient instead of an inert ambient or vacuum can provide new insights. In this work, the electrical and microstructural properties of Ti/Al/Pt/Au contacts to GaN upon exposure to 600 °C in air are presented.

In this work, microfabricated circular-transfer-line-method (CTLTM) patterns were used as the primary test structure. Ti/Al/Pt/Au were patterned through a standard lift-off process on unintentionally-doped GaN epitaxial

layer grown by metal organic chemical vapor deposition (MOCVD) on sapphire. After lift-off, the samples were subject to a rapid thermal annealing (RTA) process at 850°C for 35 seconds in a nitrogen ambient.

To observe the impact of thermal exposure on the electrical and microstructural properties, the test structures were subject to a 10-hour thermal storage test in a furnace (air ambient), during which time the test structures were taken out of the furnace every two hours and their I-V characteristics were measured at room temperature. After the initial 2-hour “burn-in” period, the contact resistance remained stable over the entire remainder thermal storage test, with the variance within less than 3% and the specific contact resistivity remained on the order of $10^{-5} \Omega\text{-cm}^2$.

In addition, the samples were subject to in-situ high-temperature I-V tests at 600°C in air both before and after the thermal storage using a high-temperature probe station. The linear I-V response confirms that the contacts remained ohmic after the thermal storage. The contact resistance at 600°C showed minimal change (approximately 9%) for a 20- μm -wide gap CTLM test structure, before and after thermal storage.

The microstructural analysis with atomic force microscopy (AFM) showed minimal changes (less than 0.1%) in surface roughness after thermal storage. The results support the use of Ti/Al/Pt/Au metallization for GaN-based sensors and electronic devices that will operate within a high-temperature and oxidizing ambient.

5:00pm **EM+AS+MS+SS-WeA9 Schottky Contacts and Dielectrics in GaN HEMTs for Millimeter-Wavelength Power Amplifiers, Brian Downey**, Naval Research Laboratory **INVITED**

Although GaN RF transistor technology has begun to enter commercial markets, there are still several active research efforts aimed at extending the operating frequency of GaN devices to the millimeter-wavelength (MMW) frequency range of 30 – 300 GHz. In order to facilitate power gain at MMW frequencies, both geometric device scaling and novel heterostructure/device design are required, which present interesting materials and processing challenges. In this talk, an overview of NRL’s approaches to MMW GaN high-electron-mobility transistor (HEMT) technology will be presented. In one approach, N-polar GaN inverted HEMT structures are employed, which places the GaN channel at the surface of the device. In this case, Schottky gate contacts are made directly to the N-polar GaN channel. The effect of GaN crystal polarity on Schottky barrier height will be discussed along with strategies to increase the Schottky barrier height of metals to N-polar GaN. In a second approach, Ga-polar GaN HEMTs with vertically-scaled barrier layers are utilized to reduce the surface-to-channel distance in order to maintain electrostatic control of the channel in short gate length devices. The high electric fields in these vertically-scaled barrier devices can create large tunneling-related gate leakage currents, leading to high off-state power dissipation and soft breakdown characteristics. The use of gate dielectrics in these scaled structures will be discussed including their effect on device electrical performance.

5:40pm **EM+AS+MS+SS-WeA11 Nitrogen as a Source of Negative Fixed Charge for Enhancement Mode Al₂O₃/GaN Device Operation, MuhammadAdi Negara, R. Long, D. Zhernokletov, P.C. McIntyre**, Stanford University

In recent years, significant research efforts have focused on developing enhancement mode (E-mode) GaN-based devices fueled by many potential applications. Simpler power amplifier circuits using a single polarity voltage supply and increased safety using a normally-off device can be achieved using E-mode devices leading to lower cost and an improvement of system reliability. Using the combination of E-mode and depletion mode (D-mode) devices in direct coupled logic open up also new applications for nitride semiconductors. To realize normally-off operation of GaN transistors, several approaches have been reported in the past including recessed gate structures [1], p-type gate injection [2], fluorine plasma treatment [3], surface channel GaN [4], thermally oxidized gate insulator [5] and oxide charge engineering [6]. In this report, nitrogen impurities introduced during atomic layer deposition of an Al₂O₃ gate dielectric are investigated as a means of modifying the threshold voltage (V_{th})/flat band voltage (V_{fb}) of GaN MOS devices. As reported in reference [7], nitrogen may incorporate on either cation or anion substitutional sites or on interstitial sites in Al₂O₃ and become a source of negative fixed charge within Al₂O₃. The effectiveness of this approach for fixed charge modification of ALD-grown Al₂O₃ compared to several alternative approaches will be presented.

References:

- [1] W. B. Lanford, et al., Electron. Lett. 41, no. 7, 449 (2005).
- [2] Y. Uemoto, et al., IEEE Trans. Elect. Dev. 54, no. 12, 3393 (2007).
- [3] Zhang et al., Appl. Phys. Lett. 103, 033524 (2013).
- [4] W. Huang, et al., IEEE Elect. Dev. Lett. 27, no. 10, 796 (2006).

[5] K. Inoue et al., Elect. Dev. Meet., IEDM Technical Digest. International, pp. 25.2.1 (2001).

[6] B. Lu, et al., in Proc. Int. Workshop Nitride Semicond. Abstr.,536 (2008)..

[7] Choi et al., Appl. Phys. Lett. 102, 142902 (2013).

6:00pm **EM+AS+MS+SS-WeA12 Activation of Mg-Implanted GaN Facilitated by an Optimized Capping Structure, Jordan Greenlee, B.N. Feigelson, T.J. Anderson, K.D. Hobart, F.J. Kub**, Naval Research Laboratory

For a broad range of devices, the activation of p and n-type implanted dopants in GaN is needed. The activation of implanted ions by annealing requires post-implantation damage removal and the arrangement of implanted ions in their proper lattice sites. Post-implantation activation of Mg via annealing requires high temperatures (>1300 °C). At these high annealing temperatures, GaN decomposes, leaving behind a roughened surface morphology and a defective crystalline lattice, both of which are detrimental for GaN device applications. To combat decomposition, either a high pressure environment, which is prohibitively expensive and not easily scalable, or a capping structure combined with short exposure to T >1300°C is required to preserve the GaN. In this work, we explore the effects of different capping structures and their ability to protect the GaN surface during a high temperature pulse, similar to those used in the Multicycle Rapid Thermal Annealing (MRTA) process.

It was determined that the sputtered cap provides sufficient protection for the underlying GaN during a rapid heat pulse. The in situ MOCVD-grown AlN cap, although it should have a better interface and thus provide more protection for the GaN layer, is inferior to the sputtered cap as determined by Nomarski images. After etching the surface with AZ400k developer, it was determined that the GaN underneath the MOCVD-grown cap has pits as-grown. Since both GaN layers were grown with the same recipe, we attribute these pits to the HT MOCVD AlN growth process. Atomic force microscopy was used to determine the as-grown and post annealing surface morphologies of the samples. The as-grown sample covered with MOCVD AlN does not exhibit the same smooth step flow growth as the as-grown sample without the MOCVD AlN cap. After annealing and etching off the AlN caps, the surface that was capped with MOCVD AlN shows evidence of pitting while the sample that was protected with only sputtered AlN no longer exhibits step flow growth like the as-grown sample. Since we are above 2/3 of the melting point of GaN, we expect that bulk diffusion is occurring and causing this rearrangement at the surface. This implies that sputtered AlN can provide sufficient protection of the underlying GaN surface, which will facilitate mid-process implantation and activation of Mg in GaN.

In-Situ Spectroscopy and Microscopy Focus Topic Room: 211B - Session IS+SS+NS+BI+VT+MN+AS-WeA

In situ Imaging of Liquids using Microfluidics

Moderator: Xiao-Ying Yu, Pacific Northwest National Laboratory, Stephen Nonnenmann, University of Massachusetts - Amherst

2:20pm **IS+SS+NS+BI+VT+MN+AS-WeA1 In Situ Multimodal Biological Imaging using Micro- and Nanofluidic Chambers, James Evans, C. Smallwood**, Pacific Northwest National Laboratory **INVITED**

Biological organisms have evolved a number of spatially localized and highly orchestrated mechanisms for interacting with their environment. Since no single instrument is capable of probing the entire multidimensional landscape, it is not surprising that one of the grand challenges in biology remains the determination of how dynamics across these scales lead to observed phenotypes.

Therefore, there is a need for in-situ correlative multimodal and multiscale imaging to fully understand biological phenomena and how chemical or structural changes at the molecular level impact the whole organism. We have been advancing new methods for both cryogenic and in-situ correlative analysis of biological samples using electron, ion, optical and x-ray modalities. Central to this work is the development of new micro- and nanofluidic chambers that enable in-situ observations within precisely controlled liquid-flow environments. In this talk I will review the design of these new chambers, highlight current science applications and outline our future goals for adding additional functionality and expanding the versatility of the devices to other disciplines.

3:00pm **IS+SS+NS+BI+VT+MN+AS-WeA3 Glyoxal Aqueous Surface Chemistry by SALVI and Liquid ToF-SIMS**, *Xiao Sui, Y. Zhou, Z. Zhu*, Pacific Northwest National Laboratory, *J. Chen*, Shandong University, China, *X.-Y. Yu*, Pacific Northwest National Laboratory

Glyoxal, a ubiquitous water-soluble gas-phase oxidation product in the atmosphere, is an important source of oxalic acid, a precursor to aqueous secondary organic aerosol (SOA) formation. Many recent laboratory experiments and field observations suggest that more complex chemical reactions can occur in the aqueous aerosol surface; however, direct probing of aqueous surface changes is a challenging task using surface sensitive techniques. The ability to map the molecular distribution of reactants, reaction intermediates, and products at the aqueous surface are highly important to investigate surface chemistry driven by photochemical aging. In this study, photochemical reactions of glyoxal and hydrogen peroxide (H_2O_2) were studied by a microfluidic reactor, System for Analysis at the Liquid Vacuum Interface (SALVI), coupled with Time-of-Flight Secondary Ion Mass Spectrometry (ToF-SIMS). Aqueous surfaces containing glyoxal and hydrogen peroxide were exposed to UV light at variable lengths of time and were immediately analyzed in the SALVI microchannel by in situ liquid ToF-SIMS. In addition, various control samples were conducted to ensure that our findings were reliable. Compared with previous results of bulk solutions using ESI-MS, our unique liquid surface molecular imaging approach provided observations of glyoxal hydrolysis (i.e., first and secondary products, dimers, trimers, and other oligomers) and oxidation products (i.e., glyoxylic acid, oxalic acid and formic acid) with sub-micrometer spatial resolution. We potentially provide a new perspective and solution to study aqueous surface chemistry as an important source of aqueous SOA formation of relevance to atmospheric chemistry known to the community.

3:20pm **IS+SS+NS+BI+VT+MN+AS-WeA4 Investigating *Shewanella Oneidensis* Biofilm Matrix in a Microchannel by In Situ Liquid ToF-SIMS**, *Yuanzhao Ding*, Nanyang Technological University, Singapore, *X. Hua, Y. Zhou, J. Yu, X. Sui, J. Zhang, Z. Zhu*, Pacific Northwest National Laboratory, *B. Cao*, Nanyang Technological University, Singapore, *X.-Y. Yu*, Pacific Northwest National Laboratory

Biofilms consist of a group of micro-organisms attached onto surfaces or interfaces and embedded with a self-produced extracellular polymeric substance (EPS) in natural environments. The EPS matrix, like the "house of the cells", provides bacteria cells with a more stable environment and makes them physiologically different from planktonic cells. *Shewanella oneidensis* MR-1 is a metal-reducing bacterium, forming biofilms that can reduce toxic heavy metals. This capability makes *S. oneidensis* biofilms very attractive in environmental applications. To better understand the biofilm EPS matrix composition at the interface, in situ chemical imaging with higher spatial resolution and more molecular level chemical information is strongly needed. Traditionally, electron microscopy and fluorescence microscopy are common imaging tools in biofilm research. However, the bottlenecks in these imaging technologies face the limitations that it is difficult for them to provide chemical information of small molecules (e.g., molecule weight <200). In this study, we use an emerging technology liquid Time-of-Flight Secondary Ion Mass Spectrometry (ToF-SIMS) to observe *S. oneidensis* biofilm cultured in a vacuum compatible microchannel of the System for Analysis at the Liquid Vacuum Interface (SALVI) device. Chemical spatial distributions of small organic molecules that are considered to be the main building components of EPS in live biofilms are obtained. Principal component analysis is used to determine differences among biofilms sampled along the microchannel. This new approach overcomes previous limitations in live biofilm analysis and provides more chemical information of the EPS relevant to biofilm formation. Better understanding of the biofilm matrix will potentially fill in the knowledge gap in biofilm surface attachment and detachment processes and improve the engineering and design of *S. oneidensis* biofilms with high efficiencies in heavy metal reduction.

4:20pm **IS+SS+NS+BI+VT+MN+AS-WeA7 Ultrafast Proton and Electron Dynamics in Core-Level Ionized Aqueous Solution**, *Bernd Winter*, Helmholtz-Zentrum Berlin für Materialien und Energie/Elektronenspeicherring BESSY II, Germany **INVITED**

Photo- and Auger electron spectroscopy from liquid water reveals a novel electronic de-excitation process of core-level ionized water in which a pair of two cations forms, either $H_2O^+-H_2O^+$ or $OH^+-H_3O^+$. These reactive species are the delocalized analogue to H_2O^{2+} , formed in a localized on-site Auger decay, and are expected to play a considerable role in water radiation chemistry. Both cationic pairs form upon autoionization of the initial ionized water molecule, and we are particularly interested in the situation where autoionization occurs from a structure that evolves from proton transfer, from the ionized water molecule to a neighbor molecule, within a few femtoseconds. The actual autoionization is either through intermolecular Coulombic decay (ICD) or Auger decay. Experimental

identification of the proton dynamics is through isotope effects. A question that arises is whether such so-called proton-transfer mediated charge separation (PTM-CS) processes occur in other and similarly hydrogen-bonded solute molecules as well. This is indeed the case, and is illustrated here for ammonia and glycine in water, as well as for hydrogen peroxide in water, where characteristic differences are detected in the Auger-electron spectra from the light versus heavy species, i.e., NH_3 in H_2O versus ND_3 in D_2O , glycine(H) in H_2O versus glycine(D) in D_2O , and H_2O_2 in H_2O versus D_2O_2 in D_2O . The important spectral feature here is the high-kinetic energy tail of the Auger spectrum, which has no gas-phase analogue, and hence reflects the participation of solvent water in the relaxation process. The probability of the proton dynamics, judged from the intensities of the electron signal and inferred from methods of quantum chemistry and molecular dynamics, is found to depend on hydrogen-bond strength and hence on the specific hydration configuration. Favorable configurations for hydrogen peroxide(aq) occur due to the molecule's flexible structure. In ammonia(aq) the PTM processes are found to be less probable than for water(aq), which is attributed to the planarization of the ammonia molecule upon core-level ionization. The effect is smaller for the neutral $-NH_2$ (aq) group of glycine at basic pH, where intramolecular dynamics is less likely. Nature and chemical reactivity of the initial transient species and their role for radiation chemistry and for local reactions relevant for biological molecules in an aqueous environment are discussed for the different molecular hydrogen-bonded systems.

5:00pm **IS+SS+NS+BI+VT+MN+AS-WeA9 Water Dissociation in Metal Organic Frameworks with Coordinatively Unsaturated Metal Ions: MOF-74**, *Kui Tan*, The University of Texas at Dallas, *S. Zuluaga*, Wake Forest University, *E. Fuentesf*, The University of Texas at Dallas, *H. Wang*, Rutgers University, *P. Canepa*, Wake Forest University, *J. Li*, Rutgers University, *T. Thonhauser*, Wake Forest University, *Y.J. Chabal*, The University of Texas at Dallas

Water dissociation represents one of the most important reactions in catalysis, essential to the surface and nano sciences. However, the dissociation mechanism on most oxide surfaces is not well understood due to the experimental challenges of preparing surface structures and characterizing reaction pathways. To remedy this problem, we propose the metal organic framework MOF-74 as an ideal model system to study water reactions. Its crystalline structure is well characterized; the metal oxide node mimics surfaces with exposed cations; and it degrades in water. Combining *in situ* IR spectroscopy and first-principles calculations, we explored the MOF-74/water interaction as a function of vapor pressure and temperature. Here, we show that, while adsorption is reversible below the water condensation pressure (~19.7 Torr) at room temperature, a reaction takes place at ~150 °C even at low water vapor pressures. This important finding is unambiguously demonstrated by a clear spectroscopic signature for the direct reaction using D_2O , which is not present using H_2O due to strong phonon coupling. Specifically, a sharp absorption band appears at 970 cm^{-1} when D_2O is introduced at above 150 °C, which we attribute to an O-D bending vibration on the phenolate linker. Although H_2O undergoes a similar dissociation reaction, the corresponding O-H mode is too strongly coupled to MOF vibrations to detect. In contrast, the O-D mode falls in the phonon gap of the MOF and remains localized. First-principles calculations not only positively identify the O-D mode at 970 cm^{-1} but derive a pathway and kinetic barrier for the reaction and the final configuration: the D (H) atom is transferred to the oxygen of the linker phenolate group, producing the notable O-D absorption band at 970 cm^{-1} , while the OD (or OH) binds to the open metal sites. Experimental data and theoretical modeling further shows that the reaction is facilitated by a cooperative effect of several H_2O molecules. This finding explains water dissociation in this case and provides insight into the long-lasting question of MOF-74 degradation. Overall, it adds to the understanding of molecular water interaction with cation-exposed surfaces to enable development of more efficient catalysts for water dissociation.

Ref: K. Tan, S. Zuluaga, Q. Gong, P. Canepa, H. Wang, J. Li, Y. J. Chabal and T. Thonhauser, *Chem. Mater.*, 2014, **26**, 6886-6895.

5:20pm **IS+SS+NS+BI+VT+MN+AS-WeA10 Competitive Co-Adsorption of CO_2 with H_2O , NH_3 , SO_2 , NO , NO_2 , N_2 , O_2 , and CH_4 in M-MOF-74 (M= Mg, Co, Ni): The Role of Hydrogen Bonding**, *K. Tan*, The University of Texas at Dallas, *Sebastian Zuluaga*, Wake Forest University, *H. Wang*, Rutgers University, *Y. Gao*, The University of Texas at Dallas, *J. Li*, Rutgers University, *T. Thonhauser*, Wake Forest University, *Y.J. Chabal*, The University of Texas at Dallas

The importance of co-adsorption for applications of porous materials in gas separation has motivated fundamental studies, which have initially focused on the comparison of the binding energies of different gas molecules in the pores (i.e. energetics) and their overall transport. By examining the competitive co-adsorption of several small molecules in M-MOF-74 (M= Mg, Co, Ni) with *in-situ* infrared spectroscopy and *ab initio* simulations, we

find that the binding energy at the most favorable (metal) site is not a sufficient indicator for prediction of molecular adsorption and stability in MOFs. Instead, the occupation of the open metal sites is governed by kinetics, whereby the interaction of the guest molecules with the MOF organic linkers controls the reaction barrier for molecular exchange. Specifically, the displacement of CO₂ adsorbed at the metal center by other molecules such as H₂O, NH₃, SO₂, NO, NO₂, N₂, O₂, and CH₄ is mainly observed for H₂O and NH₃, even though SO₂, NO, and NO₂ have higher binding energies (~70-90 kJ/mol) to metal sites than that of CO₂ (38 to 48 kJ/mol) and slightly higher than water (~60-80 kJ/mol). DFT simulations evaluate the barriers for H₂O↔CO₂ and SO₂↔CO₂ exchange to be ~13 and 20 kJ/mol, respectively, explaining the slow exchange of CO₂ by SO₂, compared to water. Furthermore, the calculations reveal that the kinetic barrier for this exchange is determined by the specifics of the interaction of the second guest molecule (e.g., H₂O or SO₂) with the MOF ligands. Hydrogen bonding of H₂O molecules with the nearby oxygen of the organic linker is found to facilitate the positioning of the H₂O oxygen atom towards the metal center, thus reducing the exchange barrier. In contrast, SO₂ molecules interact with the distant benzene site, away from the metal center, hindering the exchange process. Similar considerations apply to the other molecules, accounting for much easier CO₂ exchange for NH₃ than for NO, NO₂, CH₄, O₂, and N₂ molecules. In this work, critical parameters such as kinetic barrier and exchange pathway are first unveiled and provide insight into the mechanism of competitive co-adsorption, underscoring the need of combined studies, using spectroscopic methods and *ab initio* simulations to uncover the atomistic interactions of small molecules in MOFs that directly influence co-adsorption.

Ref: K. Tan, S. Zuluaga, Q. Gong, Y. Gao, N. Nijem, J. Li, T. Thonhauser and Y. J. Chabal, *Chem. Mater.*, 2015, **27**, 2203-2217.

6:00pm **IS+SS+NS+BI+VT+MN+AS-WeA12 In Situ STM Observation of Pd(110) Under the Hydrogen Pressure Between 10⁻⁶ Pa and 10⁻³ Pa**, Jun Yoshinobu, H. Kikuchi, T. Koitaya, K. Mukai, S. Yoshimoto, University of Tokyo, Japan

Hydrogen adsorption and absorption on/in Pd and Pd alloys are vital processes for the hydrogen storage and hydrogen permeation materials. We investigated the Pd(110) surface under the hydrogen pressures between 10⁻⁶ Pa and 10⁻³ Pa at room temperature using in-situ atom-resolved scanning tunneling microscopy (STM). We observed missing-atom, missing-row and added-row structures and the number of atoms in these structures were quantitatively analyzed as a function of exposure time. Note that adatoms were not detected probably because they were mobile in the present experimental conditions. At 10⁻⁶ Pa, the numbers of missing-row and added-row atoms increased up to ~20 L (langmuir) and after that they were gradually reaching the saturation (steady-state). On the other hand, the number of missing-atoms decreased gradually from the initial stage. With increasing the hydrogen pressures the number of missing-row atoms and added-row atoms increased, and the whole surface was covered with these reconstructed structures after large exposures (>1000 L). It has been known that not only hydrogen adsorption but also hydrogen absorption occur in such conditions. Thus, the missing-row and added-row reconstructed structures are inevitable for hydrogen absorption on Pd(110).

Plasma Science and Technology

Room: 210B - Session PS+AS+SS-WeA

Plasma Surface Interactions

Moderator: Steven Vitale, MIT Lincoln Laboratory

2:20pm **PS+AS+SS-WeA1 In Situ FTIR Diagnostics and Characterization of Etch By-Product Deposition on Chamber Walls and Wafer Surface during Halogen Etching of Silicon**, Neema Rastgar, S. Sriraman, R. Marsh, A. Paterson, Lam Research Corporation

Plasma etching is a critical technology for nanoelectronics fabrication, but the use of a vacuum chamber limits the number of in situ, real-time diagnostics measurements that can be performed during an etch process. Byproduct deposition on chamber walls during etching can affect the run-to-run performance of an etch process if there is build-up or change of wall characteristics with time. Knowledge of chamber wall evolution and the composition of wall-deposited films are critical to understanding the performance of plasma etch processes, and an in situ diagnostics measurement is useful for monitoring the chamber walls in real time.

In this talk, we report the use of attenuated total reflectance Fourier transform infrared spectroscopy (ATR-FTIR) to perform in situ diagnostics of a vacuum chamber's walls during plasma etching. Using ATR-FTIR, the relative thickness and makeup of chamber wall deposits in real time is monitored. This information is then used to develop a chamber wall

cleaning process in order to maintain reproducible etching conditions from wafer to wafer. In particular, we report mid-IR (4000-650 cm⁻¹) absorption spectra of chamber wall-deposited silicon byproducts formed during halogen etching of silicon wafers. Preliminary results demonstrating measurements of on-wafer etch byproduct evolution as well as its correlation to chamber wall deposits will be discussed.

2:40pm **PS+AS+SS-WeA2 Particle as a Temperature Probe: Thermal Effects in Non-Thermal Plasmas**, Thomas Lopez, L. Mangolini, University of California Riverside

Silicon nanocrystals are currently under investigation for several applications including nanoelectronics, light emitting devices, photovoltaics, thermal electric devices, and energy recovery and storage. Continuous flow nonthermal plasmas reactors are ideal for silicon nanoparticle production for many reasons; continuous flow non thermal plasma reactors are a scalable system, they readily produce completely amorphous to completely crystalline samples, and they have the ability to control size and size distributions of produced particles [1]. Extensive *in-situ* and *ex-situ* characterization on continuous flow non-thermal plasma reactors has been carried out characterizing nucleation, growth, and structural evolution [2]. Particle size, structure, and surface termination are all particle properties that are directly correlated to the particles' interactions with ions and other plasma produced radicals during their creation [2]. It has been shown that the interactions between particles, ions and other radicals in non-thermal plasmas leads to a thermal annealing process [3], meaning particles in non-thermal plasmas are heated well above the temperatures of their respective carrier gases. We probe the temperature of silicon nanoparticles produced via continuous flow non-thermal plasma reactors by monitoring their surface termination. *In-situ* FTIR has been utilized to track changes in the surface chemistry of particles, which have then been correlated to the particle temperature as a function of plasma power. FTIR data shows that hydrogen termination of silicon nanoparticles as they flow through a plasma is power dependent, with higher power leading to a decrease in hydrogen surface termination. We attribute this behaviour to thermally induced desorption from the particle surface. A discussion on the characterization of nanoparticle interactions with the plasma based on *in-situ* FTIR, optical emission spectroscopy and ion density measurements will be presented.

1. Lopez, T. and L. Mangolini, *Low activation energy for the crystallization of amorphous silicon nanoparticles*, *Nanoscale*, 2014. **6**(3): p. 1286-1294

2. Lopez, Thomas, and Lorenzo Mangolini. *Journal of Vacuum Science & Technology B* 32.6 (2014): 061802.

3. Kramer, N.J., R.J. Anthony, M. Mamunuru, E.S. Aydil, and U.R. Kortshagen, *Plasma-induced crystallization of silicon nanoparticles*, *Journal of Physics D: Applied Physics*, 2014. **47**(7): p. 075202.

3:00pm **PS+AS+SS-WeA3 Plasma-Surface Interactions at Low and High Pressure**, Vincent Donnelly, University of Houston **INVITED**

This talk will review studied of the interactions of low pressure Cl₂, HBr, and O₂ inductively-coupled plasmas with reactor chamber walls, with and without Si etching, using the "spinning wall" technique. The spinning wall is part of the reactor chamber walls, allowing near-real-time analysis of the composition of surface layers via Auger electron spectrometry, and determination of species desorbing off the walls by mass spectrometry. Langmuir-Hinshelwood (L-H) reactions, with surface residence times > 0.5 ms can be studied by this technique. Many commonalities were found for the different source gas plasmas. For example, when the walls were coated with SiO_x or AlO_x layers, A + B recombination reactions including O + O, O + Cl, Cl + Cl and H + Br are detected, provided that the surface contains a level of oxygen above some critical value. During Si etching, surfaces coated with Si-halide products tend to be less catalytic toward L-H recombination reactions, while Si-oxyhalides films formed on chamber walls when oxygen is present in the plasma are much more active in promoting L-H recombination, as well as adsorption and delayed desorption of Cl₂. At most sites, O is believed to be in the inactive form of Si-O-Si. In relatively few cases, O cannot coordinate to a second Si and the active Si-O- forms. This quickly forms Si-O-A and then mobile B on the surface forms Si-O-AB, followed by desorption of AB, which could also be delayed. For all of the products observed, formation and desorption of AB is exothermic. Si etching with small oxygen addition leads to "sticky" products with a range of masses up to at least the limit of our mass spectrometer (m/e = 500) that desorb from chamber wall surfaces in ms to min after plasma exposure. Gaseous products contain -O-Si-O- linkages are prominent, in addition to Si-mono and tri-halides. In HBr-containing plasmas, products contain little or no H. Experiments have also begun to study plasma-surface interactions at atmospheric pressure. Species present within one mean free path of a quartz substrate exposed to a He jet plasma in ambient air and in a sealed chamber with gas additives are spatially resolved using a new near-field optical emission spectroscopy method.

4:20pm **PS+AS+SS-WeA7 Measurements of IIEE Emitted Electrons from Chemically-Cleaned and Sputtered-Cleaned Semiconductor Surfaces**, *D. Urrabazo, Lawrence Overzet*, University of Texas at Dallas

Plasma-surface interactions with semiconductors comprise a variety of interesting phenomena in addition to etching and deposition. One such phenomenon is ion induced electron emission (IIEE). IIEE has historically been viewed as extremely surface sensitive; but recent measurements have suggested that the IIEE yield from semiconductors, unlike metals, may in fact depend on the sub-surface properties as well. We investigated the effects of the surface and sub-surface properties (doping type, Fermi level, cleanliness level) on the relative IIEE yields from Si and Ge. Our measurements indicate that the relative IIEE yields did not depend on the doping type to a significant degree independent of the level of cleanliness. This result is consistent with IIEE theory. We further explored the sensitivity of the IIEE yield to surface cleanliness by making XPS and UPS measurements on the surface chemistry and approximate surface density of states (sDOS) of the semiconductors. By combining the theoretical IIEE model with the sDOS, we were able to replicate the changes in the IIEE emitted electron distribution functions due to surface cleanliness changes. Thus, we confirmed that the IIEE yield is affected by the cleanliness of the surface primarily through the change in the surface density of states.

Acknowledgement: This material is based upon work supported by the Department of Energy under Award Number DE-SC-0009308.

4:40pm **PS+AS+SS-WeA8 Effects of Hydrogen on Etching Processes for Transparent Conducting Films**, *Hu Li*, K. Karahashi*, Osaka University, Japan, *M. Fukasawa, K. Nagahata, T. Tatsumi*, Sony Corporation, Japan, *S. Hamaguchi*, Osaka University, Japan

The market demand for high-resolution optoelectronic devices such as head-mounted displays has accelerated the development of micro pattern formation technologies for transparent conducting oxides (TCOs) with a pattern resolution of sub-microns or even nanometers. Reactive ion etching (RIE), which has been widely used in the fabrication of semiconductors, is also a promising technology for patterning of TCOs. Tin-doped indium oxide (ITO) and Zinc oxide (ZnO) are widely used TCOs in the industry. The goal of this study is therefore to establish RIE technologies for ITO and ZnO for high-resolution patterning.

Typical RIE processes for ITO and ZnO use plasmas based on organic gases such as CH₄ and CH₃OH. CH₄ and CH₃OH are non-corrosive gases and RIE processes with such gases are expected to achieve high etching rates with less process damages. In this study, we have mostly focused on ZnO etching processes and evaluated sputtering yields and analyzed surface reaction characteristics of ZnO by various chemically reactive species such as CH_x⁺, H⁺, and H*, using a mass-selected ion beam system. The mass-selected ion beam system allows one to examine surface reactions caused by specific ion species with a given incident energy incident upon the sample substrate set in an ultra-high vacuum (UHV) reaction chamber. Simultaneous injection of hydrogen radicals have been also performed with a hydrogen radical source. Surface chemical composition after such beam injections have been analyzed by *in-situ* X-ray Photoelectron Spectroscopy (XPS) installed in the reaction chamber.

Our previous study [1] found that the sputtering yield of ZnO strongly depends on the number of hydrogen atoms contained in each incident molecular ions. In this study, we have clarified the effects of incident hydrogen ions and radicals. When ZnO is etched by simultaneous injection of energetic CH⁺ ions and abundant hydrogen radicals, it has been found that etching proceeds with no carbon deposition and the sputtering yield of ZnO is closed to that of the corresponding physical sputtering. This result suggests that hydrogen radicals prevent carbon accumulation on ZnO and energetic hydrogen ion incidence leads to the formation of a surface damage layer, which is more easily sputtered by incident energetic ions. Therefore the presence of CH₃⁺ ions is not indispensable in such a RIE process and the embrittlement of ZnO by hydrogen is more crucial to the achievement of efficient etching processes for ZnO.

[1] H. Li, K. Karahashi, M. Fukasawa, K. Nagahata, T. Tatsumi, and S. Hamaguchi, AVS61st Int. Symp. Exh. Abst. 4892, PS-TuM11.

5:00pm **PS+AS+SS-WeA9 Mechanisms of Hydrocarbon Based Polymer Etch using Pulsed Plasmas**, *Barton Lane, P. Ventzek, M. Matsukuma, A. Suzuki, A. Koshiishi*, Tokyo Electron Limited

Dry etch of hydrocarbon based polymers is important for semiconductor device manufacturing. The etch mechanisms for oxygen rich plasma etch of hydrocarbon based polymers has been studied but the mechanism for lean chemistries has received little attention. We report on an experimental and analytic study of the mechanism for etching of a hydrocarbon based polymer using an Ar/O₂ chemistry in a single frequency 13.56 MHz test bed. The experimental study employs an analysis of transients from sequential oxidation and Ar sputtering steps using OES and surface analytics to constrain conceptual models for the etch mechanism. The conceptual model is consistent with observations from MD studies and surface analysis performed by Vegh, et al. and Oehrlein, et al. [1,2] and other similar studies. Parameters of the model are fit using published data and the experimentally observed time scales. [1] J.J. Vegh, D. Nest, D. B. Graves, R. Bruce, S. Englemann, T. Kwon, R. J. Phaneuf, G. S. Oehrlein, B. K. Long, and C. G. Willson, *Jour. of Applied Physics* **104**, 034308 (2008), [2] G.S. Oehrlein, R. J. Phaneuf, D. G. Graves, *J. Vac. Sci. Tech. B* **29**, 010801-1 (2011).

5:20pm **PS+AS+SS-WeA10 Role of Plasma Density in Damage Characterization and its Impact on Low-Damage Plasma Process Design**, *Koji Eriguchi, M. Kamei, Y. Nakakubo, K. Ono*, Kyoto University, Japan

Plasma process-induced damage (PID) is one of critical issues in designing metal-oxide-semiconductor field-effect transistors (MOSFETs) with higher performance and reliability. The damage creation mechanisms—plasma-induced physical damage (PPD) and charging damage (PCD) [1]—have been characterized by various techniques so far [2] to design low plasma processes. In this study, conflicting results leading to erroneous conclusions in designing future plasma processes are presented, where ion flux and charge injection from plasma (~ plasma density) play a key role in these conventional characterizations. Firstly, regarding PPD, n-type (100) Si wafers were exposed to Ar-based ICP and CCP discharges [3] and the localized defects were created in the Si substrates by ion bombardment. It is found that, although the average energy of incident ions (E_{ion}) is larger for the case of CCP, the latent defect density (n_{dam}) of CCP-damaged samples is smaller than that of ICP, even after the damaged-layer removal. This observation is in sharp contrast to previous pictures, i.e., the larger E_{ion} leads to the larger PPD. Secondary, MOSFETs with "high-k" (HfSiO₂) gate dielectric were damaged by the Ar-based ICP plasma and the high-k damage (~ carrier trap site generation) by PCD is evaluated by time-dependent dielectric breakdown (TDDB) measurement [4]. We identify that the TDDB lifetime becomes longer under a certain amount of charge injection by plasma-induced current. This finding implies that one might be misled to an erroneous design rule of future LSIs. We propose a model explaining these conflicting results, where both ion flux and charge injection from plasma and the nature of the analysis techniques are taken into account. Since modern FinFETs with high-k dielectrics [5] are susceptible to PPD and PCD, the present model should be intensively implemented in designing future "low-damage" plasma processes.

This work was supported in part by a Grant-in-Aid for Scientific Research (B) 25630293 from the Japan Society for the Promotion of Science.

[1] For example, K. Eriguchi and K. Ono, *J. Phys. D* **41**, 024002 (2008).

[2] M. Fukasawa et al., *Dry Process Symposium*, 183, (2013).

[3] Y. Nakakubo et al., *ECS J. Solid State Sci. Technol.*, **4** N5077 (2015).

[4] M. Kamei et al., *IEEE Int. Integrated Reliability Workshop Final Report*, 43 (2014).

[5] For example, I. Ferain et al., *Nature* **479**, 310 (2011).

5:40pm **PS+AS+SS-WeA11 Dry Deep Etching Of Bulk Titanium By Plasma Processes**, *Edouard Laudrel, T. Tillocher, P. Lefauchaux*, GREMI CNRS/Université d'Orléans, France, *B. Boutaud*, Sorin Crm, France, *R. Dussart*, GREMI CNRS/Université d'Orléans, France

Bio-MEMS have emerged these last years with applications for biosensors, drug delivery, etc. The biocompatibility, the mechanical strength and the hydrophilicity properties have made titanium a widely used material with a great interest in the biomedical field. This element was chosen to fabricate body implantable devices with the help of microfabrication methods from microelectronics technologies in order to pattern structures with vertical sidewalls and smooth surfaces. Most of the literature with an interest in titanium deep etching relies on chlorine plasma processes. They are performed at room temperature of the substrate with typical etch rates close to 1 $\mu\text{m}\cdot\text{min}^{-1}$ and provide rather smooth surfaces. TiO₂ or Ni are typically used as hard mask. However, a thick (several 10s of microns) SU8 layer, which is a negative photoresist, has also been reported as an alternative mask because it can be easily patterned and stripped.

Samples used in our experiments consist of coupons of a patterned titanium wafer glued on a silicon carrier wafer. The titanium wafer is 300 μm thick with a 15 μm thick backside thermal TiO_2 layer and the mask is a 15 μm electrochemically deposited thick nickel layer. The samples were processed in two different ICP reactors. Two different chemistries can be used to etch titanium. A chlorine-based chemistry at low pressure can be used to obtain anisotropic profiles but with reduced etch rates at room temperature. With the first reactor, equipped with a diffusion chamber, titanium etch rate was 1 $\mu\text{m}\cdot\text{min}^{-1}$. A fluorine-based chemistry admits higher etch rate (as 4 $\mu\text{m}\cdot\text{min}^{-1}$) at higher pressure (few Pa) with isotropic profiles if the sample temperature is sufficient to form volatile etch by-products. Both chemistries, as well as $\text{Cl}_2/\text{Ar}/\text{SF}_6$ mixture, produced non-reproducible results and a high roughness. These observations were attributed to the redeposition of etch by-products (like SiOCl_x) on the sample surface. It induces a micro-masking effect which generates a high roughness and leads to reproducibility issues. The so-called APETi (Alternated Process for the deep Etching of Titanium) process has been developed to prevent this roughness and increase the reproducibility. An average etch rate of 1.4 $\mu\text{m}\cdot\text{min}^{-1}$ has been achieved with reproducible features.

Comparative experiments have started on a second ICP reactor which enables higher etch rates due to a higher self-bias voltage and higher density species. The substrate holder temperature can also be higher, which should help to enhance chemical etching processes with a fluorine chemistry.

6:00pm **PS+AS+SS-WeA12 Particle Transport with Wafer Potential Controlled by Dipole Electrostatic Chuck Electrodes, Masaki Ishiguro, M. Sumiya**, Hitachi High-Technologies Corp., Japan

In plasma etching for semiconductor manufacturing, it is important to prevent particle attachment on the wafer during processing to maintain high yield rate. As the device size continues to be scaled down, smaller particles should be taken care not to attach onto the wafer. It is said that 10 nm particles will be critical for semiconductor manufacturing in 2019 [1]. One important approach to prevent particle attachment on the wafer is controlling particle transport. Electrostatic force is one of the suitable forces to control particle transport. In the case that particle charge and wafer potential polarity is opposite, large number of small particles can be attracted onto the wafer. In plasma etching process, plasma on and off periods are periodically repeated. Kobayashi *et al.* revealed that in plasma on period, the particles are trapped at the plasma sheath boundary and there is a less-risk of particle attachment to the wafer [2]. It suggested that, in plasma off period, there is a large-risk of particle attachment to the wafer if the wafer and the particles have opposite charge respectively.

In this study, the relationship between particle attachment to the wafer and wafer potential in plasma off period was investigated. Particle count on the wafer was measured at different wafer potential during plasma-off period by changing voltage settings of dipole electrostatic chuck electrodes (ESC) in Ar, O_2 and N_2 plasma. In the case of negative wafer potential, particle counts increased as the plasma off time was prolonged. On the other hand, in the case of positive or 0 wafer potential, particle count was relatively low level and it did not increase even if plasma off time was prolonged. This result suggests that, in our experimental condition, the particles charge positive during plasma off period and they are continuously generated from inner chamber wall. If the wafer has negative potential, the particles are attracted by electrostatic force. The numerical simulation result will also be shown to understand the effect of electrostatic force on small particle attachment.

In plasma on period, wafer has plasma floating potential and the potential remains on the wafer even after plasma discharge is finished. It leads to increase of particle attachment risk as mentioned above. In this time, newly developed wafer potential control sequence with ESC electrodes to reduce wafer potential during plasma off period will be reported. This sequence enables to reduce particle attachment during plasma off period.

[1] International Technology Roadmap for Semiconductors 2013.

[2] H. Kobayashi, *et al.*, IEEE trans. Semicond. Manuf., **22**, 462 (2009).

Scanning Probe Microscopy Focus Topic Room: 212A - Session SP+2D+AS+NS+SS-WeA

Probing Electronic and Transport Properties

Moderator: Tae-Hwan Kim, Pohang University of Science and Technology, Jewook Park, Oak Ridge National Laboratory

2:20pm **SP+2D+AS+NS+SS-WeA1 Geometric and Electronic Structures of Epitaxially Grown Pnictide 122, 111 and $\text{Cu}_x\text{Bi}_2\text{Se}_3$ Samples, Young Kuk**, Seoul National University, Republic of Korea
INVITED

Order parameters were measured mainly on low-temperature cleaved, superconductor surfaces from their measured topographic images (constant current maps) and Fourier-transformed, measured density of states (energy dependent dI/dV map) in previous scanning tunneling microscopy (STM) studies. However, no direct evidence of coupling mechanisms has been given for these *high temperature* superconductors by these STM studies. We intend to study how homogeneity of a doped sample influences the superconducting property in an STM study. We were able to grow pnictide 111, 122, and $\text{Cu}_x\text{Bi}_2\text{Se}_3$ samples by molecular beam epitaxy. We found that surfaces of these grown samples are often terminated by alkali or alkaline atomic plane or non-superconducting metallic planes. These surfaces reveal distorted superconducting or non-superconducting properties. We adopted various ways to expose the superconducting planes in these samples. At the same time, we tried to grow samples homogeneously doped over the coherence lengths. Nodal structures were observed on these samples in their quasiparticle interference patterns. In this talk we will discuss the properties of the s_{\pm} , s , d states as likely candidates pairing states for these materials.

3:00pm **SP+2D+AS+NS+SS-WeA3 Direct Measurement of Conductance from Topological Surface States in Topological Insulators, Corentin Durand, X. Zhang, S. Hus, M. McGuire, I. Vlassiouk, A.-P. Li**, Oak Ridge National Laboratory

Topological insulators (TI) with characteristic topological surface states (TSS) attract great interest for both fundamental physics and device applications. However, the unavoidable presence of defects in bulk single crystals usually dopes the material leading to a metallic behavior. Thus, the direct measurement of the TSS electronic transport properties is hard to achieve due to the dominant contribution from the bulk states. Here, we measure the transport properties of Bi_2Se_3 crystals by Four Probe Scanning Tunneling Microscopy (4P-STM) technique at different temperatures on fresh surfaces obtained by cleavage in Ultra-High Vacuum (UHV) (base pressure = 2×10^{-10} Torr). In contrast to conventional models that assume two resistors in parallel to count for both the TSS and bulk conductance channels, we show that this technique can be used to differentiate the 2D contribution of TSS to the transport from the 3D contribution (bulk) by considering the potential profiles across the interface. Our method allows quantitative determination of conductivities from both channels. We also compare our results with samples exhibiting pure 2D and 3D transport behaviors. Our results shows that our approach enables direct distinguishing and accessing electronic transport of TI surfaces surface states, which can be applied to the studies of 2D to 3D crossover of conductance in other complex systems.

This research was conducted at the Center for Nanophase Materials Sciences, which is a DOE Office of Science User Facility.

3:20pm **SP+2D+AS+NS+SS-WeA4 Chiral Edge States of Topological Insulator in 1D, Tae-Hwan Kim**, Pohang University of Science and Technology, Republic of Korea, S. Cheon, S.-H. Lee, Institute for Basic Science, Republic of Korea, H.W. Yeom, Pohang University of Science and Technology and Institute for Basic Science, Republic of Korea

Chiral edge states are one of the most fascinating hallmark of topological insulators [1-4]. While chiral edge states are the vitally important feature of 2D and 3D topological insulators, no correspondence has yet been found in 1D. On the other hand, in 1D, a Peierls-distorted atomic chain such as polyacetylene has two topologically different ground states and a topological edge state or so-called a topological soliton connecting between them [5,6]. The topological edge states in 1D show many interesting properties such as charge-spin separation, fractional charge, and so on [7,8]. However, they do not exhibit chirality as 2D or 3D topological insulators do. In this talk, we report that the 1D topological edge states, solitons, of the charge-density wave (CDW) system of indium atomic wires self-assembled on a silicon surface have the chiral property [9,10]. Our system can be well described by a coupled double Peierls-distorted atomic chain with zigzag interchain coupling, which induces dynamical sublattice symmetry breaking. This subtle change ensures a dynamically generated topological

structure with four-fold symmetric ground states and has topological edge states with a new degree of freedom, chirality, which is absent in the case of a single Peierls atomic chain. We have performed scanning tunneling microscopy and spectroscopy in order to obtain experimental evidences of the chiral edge states in the 1D CDW. Individual right- and left-chiral edge states are directly identified from non-chiral ones, which are similar to the topological solitons found in a single Peierls atomic chain. Furthermore, we found that chiral edge states can produce quantized charge pumping across the chain that is topologically protected and controllable by their chirality. Thus, these topological chiral edge states or solitons can be utilized for future single-electron-level data storage devices or logic circuits, which are topologically protected.

- B. A. Bernevig, T. L. Hughes, and S.-C. Zhang, *Science* **314**, 1757 (2006).
 M. König, S. Wiedmann, C. Brüne, A. Roth, H. Buhmann, L. W. Molenkamp, X.-L. Qi, and S.-C. Zhang, *Science* **318**, 766 (2007).
 M. Z. Hasan, C. L. Kane, *Rev. Mod. Phys.* **82**, 3045 (2010).
 X.-L. Qi, S.-C. Zhang, *Rev. Mod. Phys.* **83**, 1057 (2011).
 W. P. Su, J. R. Schrieffer, A. J. Heeger, *Phys. Rev. Lett.* **42**, 1698 (1979).
 R. Jackiw, C. Rebbi, *Phys. Rev. D* **13**, 3398 (1976).
 T. Giamarchi, *Quantum Physics in One Dimension* (Oxford University Press, Oxford : New York, 2004).
 T. Dauxois, M. Peyrard, *Physics of Solitons* (Cambridge University Press, 2006).
 T.-H. Kim, H. W. Yeom, *Phys. Rev. Lett.* **109**, 246802 (2012).
 S. Cheon, T.-H. Kim, S.-H. Lee, H. W. Yeom, under review.

4:20pm SP+2D+AS+NS+SS-WeA7 Electronic Properties of Quasi-one-dimensional Defects in Monolayer h-BN, Chuanxu Ma, J. Park, Oak Ridge National Laboratory, L. Liu, G. Gu, The University of Tennessee, A.P. Baddorf, A.-P. Li, Oak Ridge National Laboratory

Two-dimensional (2D) hexagonal boron nitride (h-BN) monolayers have wide promising applications in nanoelectronics. The presence of defects could greatly impact its electronic properties. Here, we present experimental results about two types of line defects in h-BN monolayers, prepared on Cu foils by chemical vapor deposition (CVD) method.

Using scanning tunneling microscopy/spectroscopy (STM/STS), the structural and electronic properties of two types of quasi-1D defects are characterized in monolayer h-BN. An energy gap ~ 4 eV is observed for h-BN monolayers on Cu foils. The first type of quasi-1D defects is the worm-like defects with length 3–30 nm, and width ~ 1.5 nm. Nano-ripples with modulation $\lambda \sim 5.2$ Å, which is about double the size of h-BN lattice, are observed both from the topographic images and Di/Dv mappings along the worm-like defects. The modulation is in phase at negative bias and out of phase at positive bias between the topographic images and Di/Dv mappings. The defects also show higher tunneling conductance than the h-BN sheet in the Di/Dv mappings. The observed nano-ripples in the defects might indicate interesting electronic properties, such as charge density wave (CDW).

The other type of defects are the linear boundaries of h-BN. The tilting angle between the two domains at the both sides of the boundary is about 90° , which is well in line with our simulations. From the Di/Dv mapping, the boundary shows lower tunneling conductance than the h-BN sheet, which is different from the first type of quasi-1D defects.

Our experimental results demonstrate that the existence of quasi-1D defects tremendously affect the structure and electronic properties of h-BN, thus could be used to tune the transport properties in h-BN-based nanodevices.

This research was conducted at the Center for Nanophase Materials Sciences, which is a DOE Office of Science User Facility, and supported by the Laboratory Directed Research and Development Program of Oak Ridge National Laboratory, managed by UT-Battelle, LLC, for the US DOE.

4:40pm SP+2D+AS+NS+SS-WeA8 Real-Space Imaging of the Multiple Scattering in Single Layer Graphene: FT-STM/STS Studies, M. Jung, S.-D. Sohn, J. Park, K. Lee, Hyung-Joon Shin, Ulsan National Institute of Science and Technology, Republic of Korea

The electrons in graphene exhibit unusual two-dimensional behaviors, which can be described by massless Dirac quasiparticles. In order to understand the fundamental electronic properties of graphene, extensive studies have been focused on graphene both experimentally and theoretically. Undoubtedly, however, not only the electronic property of graphene itself but also that of graphene on metallic substrates is of great importance for the further applications. In this study we investigated the scattering behaviors of electrons in single layer graphene (SLG) on a Cu(111) substrate by means of low-temperature scanning tunneling microscopy (LT-STM) and scanning tunneling spectroscopy (STS). When there is a defect in graphene, we can observe the scattering of electrons in

the form of interference pattern by STM. In previous STM studies, the energy level of Dirac point has been assigned by the position of a dip in dI/dV curve. It is very difficult, however, to determine the exact position of Dirac point from STS for the graphene on metallic substrates, because surface states of the substrate is too close to Dirac point of graphene in energy level. Here, we could successfully deconvolute and identify the electronic dispersion relations in graphene and in Cu(111) by applying Fourier transformation to one-dimensional and two-dimensional STS maps, which enables us to resolve surface states of Cu(111) and Dirac point of graphene respectively. We will also present our first observation of the defect-induced intravalley scattering, which has not been observed experimentally to date for SLG. Our results show that the careful examination of interference pattern can provide valuable information regarding intravalley, intervalley, and interband scatterings of electrons in graphene/Cu(111).

5:00pm SP+2D+AS+NS+SS-WeA9 Tunability of Single-Atom Electron Spin Relaxation Times and Their Characterization by Pump-Probe STM, William Paul, S. Baumann, IBM Research - Almaden, K. Yang, Chinese Academy of Sciences, N. Romming, University of Hamburg, Germany, T. Choi, C.P. Lutz, A. Heinrich, IBM Research - Almaden

A single atomic spin constitutes the ultimate limit to the miniaturization of magnetic bits. Can the state of such a spin be made stable against the quantum mechanical tunneling of magnetization? The energy relaxation time, T_1 , of single spins on surfaces can be measured by spin-polarized pump-probe STM [1]. To date, the relaxation times reported for Fe-Cu dimers on Cu_2N insulating films have been of the order ~ 100 ns [1]. A three-order-of-magnitude enhancement of lifetime, to ~ 200 μs , was recently demonstrated for Co on a single-monolayer of MgO [2]. This was accomplished by choosing a less conductive decoupling layer to electronically separate the atom from a metal substrate, along with the careful design of the symmetry of orbital states. Here, we report on the tailoring of the T_1 lifetime of single Fe atoms on single- and multi-layer MgO films grown on Ag(001). We focus on the characterization of intrinsic lifetimes for the atom-substrate system which are independent of the STM tip used to probe them, that is, without influence of the nearby STM tip which can be a strong source of electronic de-excitation. We also report on new advances in pump-probe techniques which were necessary to carry out these measurements. These advances extend lifetime detection to the femto-ampere and many-millisecond regimes demanded by the Fe on MgO system.

- [1] Loth *et al.*, *Science* **329**, 1628 (2010)
 [2] Rau *et al.*, *Science* **344**, 988 (2014).

5:20pm SP+2D+AS+NS+SS-WeA10 Imaging and Spectroscopy of Graphene Heterostructures, Brian LeRoy, University of Arizona
INVITED

The ability to create arbitrary stacking configurations of layered two-dimensional materials opens the way to the creation of designer band structures in these materials. Graphene on hexagonal boron nitride is an example of such a van der Waals heterostructure where the electronic properties of the composite material can be different from either individual material [1]. These van der Waals heterostructures can be formed using a wide variety of layered materials including from transition metal dichalcogenides, graphene and topological insulators. This talk will focus on devices consisting of graphene coupled to other layered materials. The lattice mismatch and twist angle between the layers produces a moiré pattern and affects their electronic properties. In double layer graphene systems, we find a van Hove singularity whose energy depends on the rotation angle [2]. This singularity in the density of states leads to a strong enhancement of the absorption at a particular wavelength. In graphene on transition metal dichalcogenides, the interaction between the materials leads to the possibility of commensurate stackings and the presence of new states in graphene [3].

- [1] M. Yankowitz *et al.*, *Nature Physics* **8**, 382 (2012).
 [2] S. Huang *et al.*, arXiv:1504.08357 (2015).
 [3] M. Yankowitz *et al.*, *Nano Letters* **15**, 1925 (2015).

6:00pm SP+2D+AS+NS+SS-WeA12 Correlated STM and Electron Transport Study of Individual Nanowires down to Atomic Scale, Shengyong Qin, University of Science and Technology of China, T.H. Kim, Oak Ridge National Laboratory, Y. Zhang, R. Wu, University of California, Irvine, H.H. Weitering, The University of Tennessee, Knoxville, C.K. Shih, The University of Texas at Austin, A.-P. Li, Oak Ridge National Laboratory
 The electronic conductance in quantum wires is often dictated by quantum instabilities and strong localization at the atomic scale. We present a novel nano-transport technique which combines local nano-contacts and four-probe STM. The approach allows for correlated study of electron transport

and scanning tunneling spectroscopy in individual nanowires. We first apply it to the GdSi₂ quantum wires, which show that isolated nanowires exhibit a metal-insulator transition upon cooling, driven by the defect-induced localizations, while wire bundles maintain a robust metallic state, stabilized by interwire electronic coupling. We then demonstrate applications of this transport technique with carbon nanotubes and copper wires in situ. The method bridges the gap between the transport and the local electronic and structural properties down to the atomic scale.

Surface Science

Room: 113 - Session SS+AS+EN-WeA

Metals, Alloys & Oxides: Reactivity and Catalysis

Moderator: Daniel Killelea, Loyola University Chicago

2:20pm SS+AS+EN-WeA1 **Understanding Chemical Activity in Pt-Re Bimetallic Systems**, Donna Chen, R.P. Galhenage, K. Xie, A.S. Duke, University of South Carolina, H. Yan, Brookhaven National Laboratory
INVITED

The nucleation, growth and chemical activity of bimetallic Pt-Re clusters on titania have been investigated as model systems for understanding Pt-Re catalysts for oxidation reactions. Scanning tunneling microscopy studies demonstrate that exclusively bimetallic clusters can be grown from the sequential deposition of Pt on Re or Re on Pt, provided that the deposition of the first metal creates a high enough cluster density for the nucleation of the second metal. Low energy ion scattering experiments indicate that the bimetallic clusters are Pt-rich regardless of the order of deposition. However, X-ray photoelectron spectroscopy (XPS) suggest that a Pt-Re alloy is formed from deposition of Re on Pt but not from Pt on Re. Furthermore, Re interacts more strongly with the titania support than Pt, resulting in reduction of titania. Temperature programmed desorption studies for CO desorption and methanol reaction confirm that the Re clusters have lower activity than Pt despite their higher surface area, and this behavior is attributed to oxidation of Re by the titania support. The alloyed clusters exhibit new activity for CO and H₂ evolution that is not observed for the pure or unalloyed clusters. Methanol oxidation activity of these model surfaces are studied in a microreactor attached to an ultrahigh vacuum chamber so that the surfaces can be characterized by XPS before and after reaction. Specifically, changes in the oxidation states of Re in the bimetallic and pure Re clusters are investigated.

3:00pm SS+AS+EN-WeA3 **Removal of Surface Carbon from Pt(111) by Hydrogenation via an Ethylidyne Intermediate**, J.D. Krooswyk, C.M. Kruppe, Michael Trenary, University of Illinois at Chicago

Transition metals that are used to catalyze reactions of hydrocarbons are often deactivated by the deposition of unreactive carbon on the catalyst surface. The structure and properties of the deposited carbon are often poorly defined. We have investigated the reactivity of carbon deposited onto a Pt(111) surface through exposure to acetylene at 750 K. At this temperature the acetylene is completely dehydrogenated leaving only carbon on the surface. Earlier work had shown that the carbon deposited in this way largely consists of C₂ molecules. We have used reflection absorption infrared spectroscopy (RAIRS) to characterize the reactivity of the deposited carbon under ambient pressures of H₂(g) up to 10 torr. The results show that C₂ can be hydrogenated to ethylidyne (CCH₃) and that the ethylidyne is slowly hydrogenated to ethane, which desorbs thus removing carbon from the surface. The maximum coverage of the C₂ molecules can be deduced from comparison with the peak areas measured with RAIRS for ethylidyne formed from ethylene exposure, which is known to give an ethylidyne coverage of 0.25 monolayer. Auger electron spectroscopy confirms that surface carbon is removed by hydrogenation under these conditions. In separate experiments based on comparisons of s- and p-polarized RAIR spectra in which both surface and gas phase species can be simultaneously monitored, we have shown that surface ethylidyne is a spectator species as gas phase acetylene is converted first to gas phase ethylene and then to gas phase ethane. Although ethylidyne is a spectator species in the hydrogenation of ethylene and acetylene to ethane over Pt(111), in the case of C₂ hydrogenation, ethylidyne plays the role of a reaction intermediate.

3:20pm SS+AS+EN-WeA4 **Density Functional Study of the Oxygen Chemistry and NO Oxidation Mechanism on Low-index Surfaces of SmMn₂O₅ mullite**, X. Liu, Z.Z. Chen, Huazhong University of Science and Technology, China, K.J. Cho, The University of Texas at Dallas, R. Chen, Bin Shan, Huazhong University of Science and Technology, China
SmMn₂O₅ mullite has recently been reported to be a promising alternative to traditional Pt-based catalysts for environmental and energy applications.

By performing density functional calculations, we systematically investigated lattice oxygen reactivity and oxygen adsorption/dissociation/migration behaviors on low index surfaces of SmMn₂O₅ mullite with different terminations. The (001), (010) and (100) surfaces have lowest barriers against exchanging O species with environments and thus are expected to be active surfaces. Furthermore, we have calculated the reaction routes along different channels on these three surfaces. Our results show that both ER and MvK mechanisms co-exist in NO oxidation by SmMn₂O₅. The most active surface is the (010) facet with Mn⁴⁺ ions in the surface layer where oxidation can be realized by a synergetic mechanism involving ER processes along bridge-MnO channels. The (001) surface with Mn⁴⁺ ions in the surface layer is also expected to be active for oxidation via the MvK mechanism. On the other hand, despite the low oxygen vacancy formation energy, the (110) surface could easily undergo surface reconstruction and quickly lose active sites. Our calculations also suggest that the rate determining step of oxidation reaction on SmMn₂O₅ surfaces is the desorption of NO₂ on both (010) and (001) facets. Our study presents systematic pictures on catalytic activities of SmMn₂O₅, which are important to the full understanding and improvement of SmMn₂O₅ performance. The comprehensive micro-kinetic model on the reaction dynamics of SmMn₂O₅ is under construction.

4:20pm SS+AS+EN-WeA7 **Medard W. Welch Award Lecture - Thermodynamics and Kinetics of Elementary Reaction Steps on Late Transition Metal Catalysts**, Charles Campbell*, University of Washington
INVITED

Experimental and theoretical results concerning the thermodynamics and kinetics of surface chemical reactions of importance in late transition metal catalysis will be reviewed. Topics include: (1) calorimetric measurements of the adsorption energies of small molecules and molecular fragments on single crystal surfaces, and their comparison to different DFT methods; (2) measurements of the entropies of adsorbates and their trends, (3) using these together with elementary-step rate measurements to build microkinetic models for multi-step catalytic reactions, and a method for analyzing these that quantifies the extent to which each elementary step and intermediate controls the net rate; and, (4) measurements of the energies of transition metal atoms in nanoparticle catalysts as a function of particle size and support, which correlate with catalytic activity and sintering rates.

· Work supported by NSF and DOE-OBES Chemical Sciences Division.

5:00pm SS+AS+EN-WeA9 **Bridging Hydroxyl Formation from Water on Reduced TiO₂(110)**, Nikolay Petrik, G.A. Kimmel, Pacific Northwest National Laboratory

TiO₂ is an important photocatalyst with many practical applications. It is also a good model system for fundamental studies of thermal and non-thermal reactions, including photocatalytic water splitting. Our understanding of water's reactions on TiO₂ surface is limited. In this paper, we have investigated temperature-dependent reaction of water molecules with bridging oxygen vacancy (V_O) on rutile TiO₂(110) surface using three independent methods: i) infrared reflection absorption spectroscopy (IRAS) to monitor the bridging hydroxyl (OH_B or OD_B) formation, ii) electron-stimulated desorption (ESD) of molecular water to monitor the water coverage,¹ and iii) photon-stimulated desorption (PSD) of CO₂ – which is a product of CO photooxidation – to monitor the unoccupied V_O coverage.² Narrow, distinct peaks for isolated OD_B and OH_B at ~2736.5 cm⁻¹ and ~3711.5 cm⁻¹ are detected in P-polarized mode for the samples exposed to D₂O and H₂O, respectively. If water is dosed at low temperature and annealed, bridging hydroxyl peaks appear above 150 K, growing with temperature until ~250 K, then saturate. In the same temperature range, molecular water and V_O coverages from the ESD and PSD data decrease in correlated fashion according to the reaction H₂O_{ti} + V_O → 2OH_B. The temperature range for this conversion appears to be too broad to be fitted with a single Arrhenius term and a reasonable pre-factor. On the other hand, the data can be fitted well using a “normal” prefactor (ν = 10¹² s⁻¹) and a distribution of activation energy (E_a) centered at 0.545 eV with ΔE_a(FWHM) = 0.125 eV. These parameters are close to those obtained from STM data³ and theory⁴ for the water monomer diffusivity on Ti sites, which most likely controls the water – vacancy reaction. This work was supported by the US Department of Energy, Office of Science, Office of Basic Energy Sciences, Division of Chemical Sciences, Geosciences & Biosciences.

(1) Zhang, Z.; Du, Y.; Petrik, N. G.; Kimmel, G. A.; Lyubintsky, I.; Dohnalek, Z. Water as a Catalyst: Imaging Reactions of O₂ with Partially and Fully Hydroxylated TiO₂(110) Surfaces. *J. Phys. Chem. C* 2009, 113, 1908-1916.

* Medard W. Welch Award Winner

(2) Petrik, N. G.; Kimmel, G. A. Off-Normal CO₂ Desorption from the Photooxidation of CO on Reduced TiO₂(110). *J. Phys. Chem. Lett.* 2010, 1, 2508-2513.

(3) Matthiesen, J.; Hansen, J. O.; Wendt, S.; Lira, E.; Schaub, R.; Laegsgaard, E.; Besenbacher, F.; Hammer, B. Formation and Diffusion of Water Dimers on Rutile TiO₂(110). *Phys. Rev. Lett.* 2009, 102, 226101.

(4) Hammer, B.; Wendt, S.; Besenbacher, F. Water Adsorption on TiO₂. *Top. Catal.* 2010, 53, 423-430.

5:20pm **SS+AS+EN-WeA10 The Adsorption and Desorption of Small Hydrocarbons on Rutile TiO₂(110).** *Long Chen, R.S. Smith, B.D. Kay, Z. Dohnalek*, Pacific Northwest National Laboratory

The interaction of small hydrocarbons with metal and metal oxide surfaces is important for a wide range of applications including heterogeneous catalysis, atmospheric chemistry, geochemistry and chemical sensing. In this work, temperature programmed desorption (TPD) and molecular beam techniques are used to study the adsorption and desorption kinetics of small hydrocarbons (C₁ - C₄) on rutile TiO₂(110) surface. In addition to n-alkanes, 1-alkenes (ethylene, propylene and 1-butylene) and 1-alkynes (acetylene, propyne and 1-butyne) were included to follow the effect of the nature of the carbon-carbon bond on hydrocarbon binding. We show that the sticking coefficients for all the hydrocarbons studied here are close to unity (> 0.95) at an adsorption temperature of 60 K. Similar to previous studies on metal and metal oxide surfaces, for n-alkanes on TiO₂(110) we find a linear increase in desorption energy with chain length. In contrast, for 1-alkenes and 1-alkynes, a roughly linear relationship between desorption energy and chain length is also observed at low coverages, but with a much smaller slope, suggesting that the additional CH₂ segments either interact less efficiently with the substrate or destabilize the bonding of the unsaturated carbon-carbon bond. Further, we also determined the absolute saturation coverages of each hydrocarbon on the five-fold coordinated titanium sites (Ti_{5c}). We show that except for CH₄, the saturation coverages of the same type of hydrocarbons on Ti_{5c} sites are nearly independent of the chain length, and that the saturation coverages of 1-alkynes consistently exceed those of n-alkanes and 1-alkenes, contrary to what one would expect based on their sizes.

5:40pm **SS+AS+EN-WeA11 Pd-Au Single Atom Alloys for the Activation of Diatomic Molecules.** *Felicia Lucci, E.C.H. Sykes*, Tufts University Department of Chemistry

Pd-Au alloys are known to catalyze a wide range of hydrogenation and oxidation reactions; however, the size of Pd ensembles in Au required for small molecule activation is not well understood. On the atomic scale, we investigate size effects of Pd atoms in Au for the catalytic activation of H₂ and O₂. We show that isolated Pd atoms are capable of catalyzing the dissociative adsorption of H₂, a process which was previously thought to require contiguous Pd sites. H spillover from active Pd sites to the Au surface can be induced the adsorption of CO. Conversely, single Pd atoms are not capable of O₂ dissociation. Small Pd clusters on Au enable O₂ activation and adsorption at Pd-Au interface sites. Since weakly bound H and O atoms are capable of enhancing reaction selectivity on Au substrates, this Pd-Au system serves as an ideal model system with which to probe selective hydrogenation and oxidation reactions at both single and ensemble active sites.

6:00pm **SS+AS+EN-WeA12 Pt/Cu Single Atom Alloys for Highly Selective Formic Acid Dehydrogenation.** *Matthew Marcinkowski, C.J. Murphy, M.L. Liriano, N.A. Wasio, F.R. Lucci, E.C.H. Sykes*, Tufts University Department of Chemistry

Selective decomposition on metal catalysts is a critical step in formic acid's application as a hydrogen storage molecule and for its use in direct formic acid fuel cells. Depending on the metal, formic acid can decompose via a dehydrogenation pathway to produce CO₂ and H₂, or a dehydration pathway to produce CO and H₂O. For most applications, very high selectivity to dehydrogenation is preferred as reactively formed CO from dehydration can poison the catalyst. The Cu(110) surface is known to selectively decompose formic acid via dehydrogenation, however, despite being the most dominate facet of nanoparticles, Cu(111) has received little study. Pt surfaces exhibit greater reactivity to decomposition, but are not as selective resulting in increased catalyst poisoning. We report that formic acid on Cu(111) and Pt/Cu(111) selectively decomposes via dehydrogenation. We find the bare Cu(111) surface to be 100% selective towards dehydrogenation, but not very active. Substitution of 1% of a monolayer of Pt into the Cu(111) surface results in a single atom alloy (SAA) that maintains this high selectivity and is ~six times more reactive than Cu(111). Higher coverages of Pt improve reactivity further, but beyond the single atom regime the selectivity towards dehydrogenation decreases and dehydration is observed. Our results show that Pt/Cu SAAs significantly improve the reactivity of Cu, while also maintaining high selectivity towards dehydrogenation,

therefore avoiding catalyst poisoning by CO. Based on our results, real nanoparticle catalysts designed on the SAA principle are expected to be promising candidates for formic acid dehydrogenation.

Surface Science

Room: 112 - Session SS+AS-WeA

Surface Dynamics, Non-Adiabaticity, and Single Molecule Phenomena

Moderator: Eddy Tysøe, University of Wisconsin-Milwaukee

2:20pm **SS+AS-WeA1 Benchmarking Theory with Vibrational State Resolved Reactivity Measurements.** *Arthur Utz, E. Peterson, E. Dombrowski, E. Nicotera, E. High*, Tufts University

Electronic structure calculations provide predictions of energy thresholds for a wide range of surface chemical reactions, and they are the basis for significant advances in our understanding of surface reactivity. Despite the central role these calculations and their predictions play, testing the absolute accuracy of these calculations with direct experimental measurements has proven to be challenging.

The presentation will focus on using the results of state-resolved beam-surface scattering measurements to benchmark theoretical predictions. We find that when these measurements are performed on a cold surface, we observe sharp energetic thresholds for reaction. These observations result from our ability to control and vary precisely all energetic degrees of the system. These experimentally measured threshold energies can be compared directly with both electronic structure calculations, as well as with quantum dynamics predictions of chemical reactivity. We will compare experimental results for methane dissociation on Ni(111) with recent computational predictions from the Jackson group to illustrate this approach. We will also provide an update on our work extending this approach to other molecule-surface systems.

2:40pm **SS+AS-WeA2 Confirming the role of Hydrogen Bonding in Electron-promoted Desorption at Water Ice Surfaces.** *D. Marchione, A.G.M. Abdulgalil, M.P. Collings, Martin McCoustra*, Heriot-Watt University, UK

We have previously reported observations of large (>10⁻¹⁶ cm²), low-energy (<500 eV), electron-promoted desorption cross-sections for benzene (C₆H₆) molecules adsorbed on the surface of amorphous solid water [1]. We will now report on the extension of this work to other molecular solids exhibiting varying degrees of hydrogen bonding within the molecular solid itself and between the solid surface and adsorbed benzene; specifically we have repeated our measurements employing substrates comprised of solid methanol (CH₃OH) and diethyl ether (CH₃CH₂OCH₂CH₃). Our report will detail our studies of the structure of adsorbed layers of C₆H₆ on the molecular solids and demonstrate the crucial role of hydrogen bonding in propagating electronic excitation to the solid-vacuum interface where C₆H₆ desorption can occur. Competitive electron-promoted chemistry in the form of H₂ formation will also be reported. Conclusions related to the impact of these observations on the early phase of icy interstellar grain chemistry will be discussed.

[1] Highly efficient electron-stimulated desorption of benzene from amorphous solid water ice, J. D. Thrower, M. P. Collings, F. J. M. Rutten, and M. R. S. McCoustra, *Chem. Phys. Lett.*, 2011, **505**, 106-111.

3:00pm **SS+AS-WeA3 Strategic Applications of the Vibrational Dynamics of the Outer Layer of Metal Nanoparticles.** *Marisol Alcántara Ortigoza*, University of Central Florida **INVITED**

The structure characterization, stability and thermal properties of nanoparticles (NPs) are topics of fundamental and technological significance. This information, however, is not always readily available from experiment. Moreover, the vibrational density of states VDOS of small (<2 nm) metal NPs definitely does not have a quadratic decay at the low-frequency end, for which the thermal properties cannot be obtained from the VDOS as Debye proposed in 1912. The features particular to the VDOS of NPs will be rationalized in terms of the charge density distribution around low-coordinated atoms, the quasi-radial geometric distribution of NPs, force constant variations, degree of symmetry of the nanoparticle, discreteness of the spectrum, and the confinement of the eigenmodes. I will present an explanation and application of the enhanced low- and high energy tails of the vibrational density of states (VDOS) of nanoparticles with respect to their bulk counterparts, as well as show that the eigenmodes defining the two extremes of the VDOS are not that alien to widely studied surface phonons. I will show that the high- and low-energy

tails of the VDOS of NPs may be a powerful tool to reveal information about their chemical composition and geometric structure of small NPs. For example, the size of the confinement gap at the low-frequency end of the VDOS and the extent by which the high-frequency end surpasses the bulk limit may indicate whether a NP is bulk-like or non-bulk-like and the extent to which it is disordered or segregated. Regarding thermal properties, I will also show that for NPs with a largely discrete VDOS, the frequency of their fundamental mode may largely determine their thermal properties.

4:20pm **SS+AS-WeA7 An Accurate Full-Dimensional Potential Energy Surface for H at Au(111): The Importance of Nonadiabatic Electronic Excitation in Energy Transfer and Adsorption**, *S.M. Janke, A. Kandratsenka, Daniel Auerbach, A.M. Wodtke*, Max Planck Institute for Biophysical Chemistry, Germany

We have constructed a potential energy surface (PES) for H atoms interacting with *fcc* gold based on the form of the PES in Effective Medium Theory. The PES was adjusted to match energies calculated by DFT in many configurations, including many with the Au atoms displaced from their lattice positions. It describes both the interatomic forces and electron densities in *full dimension* with the accuracy of the *ab initio* energies used in its construction. Calculations describing the motion of H and Au atoms using this full dimensional adiabatic PES agree with results obtained previously using *Ab Initio* Molecular Dynamics, demonstrating the accuracy of the PES for configurations occurring in the scattering of H atoms from a surface at finite temperature.

The analytic expression for the total energy contains the embedded electron density leading to a self-consistent approach to simulating nonadiabatic trajectories. We find that nonadiabatic electron-hole pair excitation is the most important energy loss pathway for the H atom. The calculated energy distributions for scattered H atoms are in reasonable agreement with experimental results that are just becoming available, and determines the probability and mechanism for its adsorption. Analysis of trajectories calculated with and without nonadiabatic energy dissipation shows the adsorption or sticking probability as well as the mechanism of H atom adsorption is changed dramatically by nonadiabatic energy transfer

4:40pm **SS+AS-WeA8 STM Characterization of Quasi-one Dimensional C₆₀ Nanostructures on Rippled Graphene**, *C. Chen, H. Zheng, A. Mills, Chenggang Tao*, Virginia Tech

Highly ordered one-dimensional (1D) molecular configurations are excellent model systems and prototypes of 1D quantum confinement of electronic states, and thus have potential importance in electronic nanodevices, spintronics and solid-state quantum computation. Due to the spherical geometry of C₆₀ molecules, it has been challenging to experimentally realize quasi-1D C₆₀ nanostructures, a highly anisotropic configuration. We will present our recent scanning tunneling microscopy (STM) characterization of novel quasi-1D C₆₀ nanostructures on rippled graphene. Through careful control of the subtle balance between the linear periodic potential of rippled graphene and the C₆₀ surface mobility, C₆₀ molecules can be arranged into a 1D C₆₀ chain structure with widths of two to three molecules. At a higher annealing temperature, the chain structure transitions to a more compact hexagonal close packed quasi-1D stripe structure. We will also discuss our scanning tunneling spectroscopy (STS) measurements on this hybrid system.

5:00pm **SS+AS-WeA9 Classical and Quantum Description of Ion Desorption from Ionic Crystals**, *Leszek Markowski*, University of Wrocław, Poland

It is well known that irradiation of the solid with electrons or photons can cause its decomposition. This process, or, more adequately processes, is very fast (typically finalized within a time shorter than 10⁻¹⁴ s) and is realized mainly by desorption of atoms or ions. Unfortunately, until now, existing models still do not give a proper value of the desorption yield and, simultaneously, a correct kinetic-energy distribution of emitted particles, as compared to the experimental observations.

In this talk a classical, quasi-quantum and quantum description of the positive ion desorption from ionic crystal surface, in which three potentials are involved, will be discussed and compared. It will be shown that the quantum description allows to explain some effects observed experimentally, such as a periodicity of small oscillations on the kinetic energy distribution (KED) curves (predicted by Wave-Packet Squeezing model) and emission through a temporarily existing potential barrier from the temporary bounded states located above the vacuum level. Moreover, analysis method of the ion KED oscillation and the fitting procedure which allows to determined a final effective desorption potential will be presented.

For two examples discussed, Li⁺ desorption from LiF and Na⁺ desorption from NaCl, desorption from two desorption sites can be distinguished – dominating ion desorption channel from adatom sites (more than 95%) and marginal one from the sites in the first surface layer. For the second

desorption channel neighboring negative ions, due to surface relaxation lying in the first surface layer slightly above positive one, can act as a two-dimensional array of rosette-like apertures. In consequence, positive ions after passing through them may form diffraction pattern.

Finally, it appears that when desorption process is described using three potentials both the ions desorption efficiency and their kinetic-energy distribution are in agreement with the experimental results.

5:20pm **SS+AS-WeA10 Spin and Isotope Effects on Molecular-Hydrogen Adsorption on Pd(210)**, *H. Kobayashi, S. Ohno, M. Wilde*, University of Tokyo, Japan, *M. Matsumoto*, Tokyo Gakugei University, Japan, *S. Ogura, Katsuyuki Fukutani*, University of Tokyo, Japan

Molecular hydrogen is physisorbed on flat metal surfaces via van der Waals interaction. By taking advantage of the fact that molecular hydrogen exists in nuclear-spin isomers of ortho and para species [1], we have shown the interaction potential on Ag(111) is anisotropic with a slight perpendicular preference [2]. The Pd(210) surface has a step-like structure consisting of alternately aligned (100) and (110) terraces, and it has been shown that H₂ is rather strongly adsorbed on H-covered Pd(210) with a significant contribution of orbital hybridization [3]. On the other hand, it has been suggested that molecularly adsorbed species could be important for hydrogen absorption into the interior of Pd surfaces [4]. In the present study, we have investigated the adsorption of H₂ and D₂ on the Pd(210) with temperature-programmed desorption (TPD) combined with resonance-enhanced multi-photon ionization (REMPI).

When Pd(210) was exposed to H₂ at 115 K, TPD revealed a desorption peak at 180 K (α -peak) originating from the adsorbed state as well as a peak at 280-320 K (β -peak) due to chemisorbed H. From the uptake rate of the α -peak, the absorption probability of H on Pd(210) was estimated to be 3×10^{-3} . When the surface was exposed to either H₂ or D₂ at 45 K, on the other hand, an additional TPD peak was observed at about 70 K (γ -peak), which was attributed to molecular adsorption. While a small difference between H₂ and D₂ was observed for the β -peak, the γ -peak temperature of D₂ was found to be higher than that of H₂ by 9 K, which corresponds to the difference in the adsorption energy of about 20 meV. Assuming that this difference is due to the zero-point energy difference in the adsorption potential, the adsorption potential was analyzed in terms of the Morse potential. By applying REMPI-TPD, furthermore, the TPD spectra of ortho-H₂ in the rotational state of $J=1$ and para-H₂ in $J=0$ were state-selectively measured. The desorption temperature of ortho-H₂ was found to be higher than that of para-H₂ by about 4 K, which corresponds to a difference in the adsorption energy of about 10 meV. We discuss that this large energy difference between the ortho and para species originates from the potential anisotropy on the basis of the first-order perturbation.

[1] K. Fukutani, T. Sugimoto, *Prog. Surf. Sci.* 88, 279 (2013).

[2] T. Sugimoto, K. Fukutani, *Phys. Rev. Lett.* 112, 146101 (2014).

[3] P. K. Schmidt et al., *Phys. Rev. Lett.* 24 87, 096103 (2001).

[4] S. Ohno et al., *J. Chem. Phys.* 140, 134705 (2014).

5:40pm **SS+AS-WeA11 Eley-Rideal Typed Mechanism of Formate Synthesis by Hydrogenation of Carbon Dioxide on Cu Surfaces**, *J. Qian*, University of Tsukuba, Japan, *T. Ogawa*, University of Tsukuba, Japan, *T. Kondo*, University of Tsukuba, Japan, *G. Wang*, Nankai University, China, *Junji Nakamura*, University of Tsukuba and ACT-C, Japan

Methanol synthesis by hydrogenation of CO₂ using Cu catalysts is one of the promising reactions to convert CO₂ into useful chemicals. Formate species is the pivotal intermediates formed as the initial step of CO₂ hydrogenation (CO₂ + H_a → HCOO_a). The reaction rate of formate synthesis is very low and the reaction probabilities are about 10⁻¹² at 340K. Our previous kinetic measurements have suggested that formate is synthesized via Eley-Rideal typed mechanism, in which CO₂ molecules directly attack adsorbed hydrogen atoms on Cu surfaces. The structure insensitivity observed for formate synthesis experiments on Cu(111), Cu(100), and Cu(110) were well explained by the Eley-Rideal mechanism based on DFT calculations. In addition, sharp angular desorptions of CO₂ have been observed for formate decomposition as the reverse reaction of formate synthesis, indicating thermal non-equilibrium reaction. In the present study, we performed molecular beam experiments to prove the Eley-Rideal typed mechanism, in which CO₂ molecules with controlling vibrational and translational energies were reacted with adsorbed hydrogen on cold Cu(111) and Cu(110) surfaces (T_s = 150-215 K). We confirmed the formation of formate species on Cu(111) and Cu(110) with reaction probabilities of 10⁻⁵ by heating nozzle above 1000 K, while no formate is formed at nozzle temperatures below 1000 K. The results indicate the Eley-Rideal typed mechanism with thermal non-equilibrium character. DFT calculations also reproduce the Eley-Rideal typed mechanism, in which

vibrational excitations of CO₂ are required to overcome the barrier of formate synthesis.

Thin Film

Room: 114 - Session TF+AS+BI-WeA

Thin Films for Biological and Biomedical Applications

Moderator: Christophe Vallee, LTM, Univ. Grenoble Alpes, CEA-LETI, Angel Yanguas-Gil, Argonne National Lab

2:20pm **TF+AS+BI-WeA1 On-chip Characterization of Engineered Nanomaterial Surface Properties by Real-time Affinity Monitoring.** C. Desmet, A. Valsesia, P. Colpo, European Commission, Joint Research Centre (JRC), **Francois Rossi**, European Commission, Joint Research Centre (JRC), Italy **INVITED**

The exhaustive characterization of the physico-chemical properties of engineered nanomaterials (ENMs) is essential to understand their mode of action and potential impact on health and environment. The development of characterization methods has been the object of important work in the past years, and has led to a better understanding on the ENM interaction with cellular systems and living organisms. One of the important surface properties of ENMs is the surface energy, for which there is no standard characterization technique established. Here, we demonstrate the feasibility of a characterization method based on a disposable microfluidic chip connected to an optical reader. The detection platform is based on the use of a micropatterned surface with tuned surface properties to bind ENMs selectively by hydrophobic forces and electrostatic interactions. The real-time absorption of ENMs on the differently functionalized micro domains is monitored by a microscope-coupled camera and gives information on the kinetics of adsorption, related to the affinity of the ENMs for the different surfaces as a function of their sizes and shapes. Interpretation of the results within the extended DLVO theory allows retrieving the surface energy characteristics of the ENMs surfaces. The key advantage of the device is the increase of the characterization throughput thanks to the all-in-one characterization process and the multiplexing that is able to replace the use of different methods and expensive equipment. In this way, the full characterization of ENMs could be expanded in all the areas covering nanomaterial-related applications.

4:20pm **TF+AS+BI-WeA7 Titanium-Niobium Thin Films Deposited by Magnetron Sputtering on AISI 316L Stainless Steel Substrate.** D. Gonzalez, T.C. Niemeyer, C.R.M. Afonso, **Pedro Nascente**, Federal University of Sao Carlos, Brazil

Metallic biomaterials such as AISI 316L stainless steel (SS), chromium-cobalt alloys, titanium and its alloys are commonly used in medical implants due to their interesting mechanical properties and thermal stability. However, 316L SS and Cr-Co alloys have much higher elastic modulus than bone, causing the loss after some years of implantation [1]. The elastic modulus of Ti-based alloys ranges from 55 to 110 GPa, being significantly lower than those for 316L SS (210 GPa) and Cr-Co alloys (240 GPa), making them more suitable for use in dental and orthopedic applications. Also Ti alloys present high strength, low density, high corrosion resistance, and good biocompatibility [1]. Pure Ti has two allotropic forms: hexagonal closest-packed (hcp), known as α phase, and body centered cubic (bcc), known as β phase, structures. Studies have shown that the addition of alloying β -stabilizing elements such as V, Mo, Nb, Zr, Mo, and Ta causes the decreasing of the modulus of elasticity of the β -Ti alloys without compromising the strength [1]. In this study, thin films of Ti-Nb alloys were deposited on AISI 316L stainless steel substrate by magnetron sputtering, and the structure, morphology, and composition of the films were analyzed by means of X-ray diffraction (XRD), X-ray photoelectron spectroscopy (XPS), and transmission electron microscopy (TEM). Thin films of three compositions were produced: Ti₈₅Nb₁₅ (Ti-26wt% Nb), Ti₈₀Nb₂₀ (Ti-33wt% Nb), and Ti₇₀Nb₃₀ (Ti-45wt% Nb). Structural characterization by XRD indicated that only the β phase was present in the thin films. XPS analysis showed a predominance of oxidized Ti and Nb on the film surfaces. TEM analyses were carried out in the following image modes: bright field (BF) images, selected area diffraction (SAD), scanning mode (STEM) BF and in annular dark field (ADF), and X-ray mapping using energy dispersive spectroscopy (EDS). For the Ti₈₀Nb₂₀ alloy film, TEM analysis showed columnar grains (~100 nm width) of β -Ti phase, with a Nb-rich transition layer ranging from finer grains (in contact with SS substrate) to a coarser columnar grains. For the Ti₇₅Nb₂₅ alloy film, TEM analysis showed columnar grains (~50 nm width) of β -Ti phase, with a transition layer away from the SS substrate.

Acknowledgements: A.L. Gobbi, C.A. Silva, S.R. Araujo, and J. Bettini from the Brazilian Nanotechnology National Laboratory, for their assistance in the growth and characterization of the thin films; and CNPq and CNPEM (Brazil), for support.

[1] M. Geetha *et al.*, Prog. Mater. Sci. 54 (2009) 397-425.

4:40pm **TF+AS+BI-WeA8 SAM-based Models of Cell Surfaces to Study the Interactions with Lectins and Bacterial Fimbriae.** **Andreas Terfort**, University of Frankfurt, Germany, **K. Lindhorst**, University of Kiel, Germany

Biologically important events such as cell-cell adhesion or infection typically start by directed and selective interactions with the highly glycosylated layer surrounding most eukaryotic cells. This layer, called the glycocalyx, consists of intricate glycopolymers, which – although in apparent disorder – clearly identify the cells. It is therefore of paramount interest to understand, which structural elements are important for the cell identification.

Self-assembled monolayers (SAM) can be used to simulate the chemical and sterical environment within such a glycocalyx. For this, glycosides are attached to oligoethyleneglycol (OEG) chains, which simulate the hydrogel matrix for the respective receptor. In this talk, we will focus on mannose-derivatives, which can be selectively recognized either by a lectin, concanavalin A, or by the adhesive fimbriae (tiny protein extrusions) of *E. coli* cells.

We would like to present different strategies for the construction of such SAMs [1,2] and discuss the advantages and disadvantages of these approaches. In extension of the mostly static systems, we will also present an approach to dynamically reorient the glycoside at the interface to determine the influence of steric factors on surface recognition [3].

References

- [1] Kleinert, M.; Winkler, T.; Terfort, A.; Lindhorst, T.K. *Org. Biomol. Chem.* **6**, 2118-2132 (2008)
- [2] Grabosch, C.; Kind, M.; Gies, Y.; Schweighöfer, F.; Terfort, A.; Lindhorst, T. K. *Org. Biomol. Chem.* **11**, 4006-4015 (2013).
- [3] Weber, T.; Chandrasekaran, V.; Stamer, I.; Thygesen, M.B.; Terfort, A.; Lindhorst, T.K. *Angew. Chemie Int. Ed.* **53**, 14583–14586 (2014).

5:00pm **TF+AS+BI-WeA9 Improving the Long-Term Stability of Thin-Film Contact and Electrode Metallizations for Implantable Silicon Neural Interfaces.** **Brian Baker**, R. Caldwell, University of Utah, **H. Mandal**, Blackrock Microsystems, **R. Sharma**, **P. Tathireddy**, **L.W. Rieth**, University of Utah

The Utah Electrode Array (UEA) is a penetrating multi-electrode interface designed to be implanted and communicate directly with the brain and peripheral nerves through recording and stimulation. These devices are used for treating neural disorders and controlling prosthetics.

The UEA is micromachined out of single crystal silicon and uses a Pt/Ir/IrOx thin film metallization stack as an electrical interface on the electrode tip and a Pt/Ir/Pt stack on the backside contacts. Delamination of these thin metal layers has been observed during fabrication processes, soak testing, and in vivo operation, and is the critical failure mode examined in this study.

Db-FIB and Cross-sectional STEM analysis were used to identify Kirkendall voids as the root cause of the adhesion failures. This investigation showed that these voids form during the platinum silicide annealing process at the interface between the PtSi and the Ir layers.

Typical thicknesses of the UEA metallization are 200 nm/500 nm/520 nm Pt/Ir/IrOx, and 200 nm/200 nm/325 nm Pt/Ir/Pt. We report the results of replacing the 200 nm base layer with 1) a 25 nm Pt base layer or 2) a 50 nm co-sputtered PtSi base layer. These layers were subjected to typical UEA annealing conditions of 375 °C in forming gas for 45 minutes, followed by a 475 °C, 30 minute oxygen anneal.

Cross-sectional STEM elemental mapping of each film stack showed complete transformation of the platinum layer to PtSi, with a 40 nm layer of iridium silicide formed at the PtSi/Ir interface. In addition, a reduction in the nanogaps caused by Kirkendall voiding was demonstrated by STEM analysis in the two new film stacks.

Both the 25 nm Pt base layer stack and the 50 nm co-sputtered PtSi base layer stack demonstrate low-resistance Ohmic contacts and wire bondability after annealing. Further electrical characterization of these thinner base layer stacks used on tip metal demonstrated impedances of 5-10 kOhms and charge injection capacities of 1-2 mC/cm² for typical electrode tip surface areas. Cross-sectional STEM analysis of the reactively sputtered iridium oxide film reveals a three dimensional morphology whose nanostructures provide a large augmentation of electrode surface area and a corresponding increase in charge injection capacity. In vitro stimulation and accelerated

lifetime tests are ongoing and electrical measurements and thin film adhesion stability will be reported.

5:20pm **TF+AS+BI-WeA10 On-Surface Synthesis of Organic Nanostructures on Copper Surfaces**, *Q.T. Fan*, University of Science and Technology of China, *J.M. Gottfried*, Philipps-Universität Marburg, Germany, *Junfa Zhu*, University of Science and Technology of China

The on-surface synthesis of organic nanostructures known as bottom-up approach paves a new way for surface structuring, which plays a vital role in catalysis, sensor systems, or organic electronics. In this presentation, we will report our recent studies on the on-surface synthesis of 2D organic nanostructures on Cu(111) and Cu(110) surfaces using a specially designed bromo-terphenyl precursor, namely 4,4'-dibromo-*meta*-terphenyl (DMTP). The study was performed under ultra-high vacuum conditions using a combination of scanning tunneling microscopy (STM) and X-ray photoelectron spectroscopy (XPS). The results indicate that the two different surface structures of Cu drive the precursor molecule to form different nanostructures on the surface. We will show temperature-dependent organic nanostructures formed after DMTP adsorbed on Cu(111) and Cu(110). These organic nanostructures include large-area, defect-free 2D ordered nanostructures of intact DMTP on Cu(111), 1- or 2D polymeric zigzag organometallic intermediates formed on Cu(111) and Cu(110), and the macromolecular nanostructures including hexagonal close-packed arrays of cyclo-octadecaphenylene (hyperbenzene), oligophenylene nanowires formed through Ullmann reaction mechanism. *This work is supported by the National Natural Science Foundation of China (21173200, 21473178) and National Basic Research Program of China (2013CB834605)*

5:40pm **TF+AS+BI-WeA11 Carbon Nanotube-Templated, Porous Films for Thermal Isolation**, *J.M. Lund*, *D.B. Syme*, *R. Vanfleet*, *R.C. Davis*, *B.D. Jensen*, **Brian Iverson**, Brigham Young University

Sensor usage has increased dramatically in detection applications due to miniaturization of components through micro and nanofabrication. These fabrication methods have also greatly increased production rates, as several sensors can be constructed in parallel. Reduction in feature size of sensors has resulted in an increase in sensor component proximity, making thermal diffusion or cross talk detrimental to proper function. This work investigates the use of carbon nanotube-templated manufacturing (CNT-M) to create thin-film, isolation layers for use in thermal sensors. CNT-M is a process wherein carbon nanotubes are used as a scaffold and coated with insulating materials (e.g. SiO₂) to create porous insulating films. Carbon nanotubes are removed in a post-deposition, burn out process rendering a porous matrix of insulating material. Thin-films are characterized using scanning electron microscopy, nanoindentation and the 3-omega method to determine mechanical and thermal properties. Thermal conductivity on the order of air has been observed while still maintaining a rigid structure that is compatible with subsequent MEMS processing.

Thin Film

Room: 111 - Session TF+AS+EM+EN+MN-WeA

CV Infiltration Methods and Energetic and Thermal Properties of Thin Films

Moderator: Richard Vanfleet, Brigham Young University, David Allred, Brigham Young University

2:20pm **TF+AS+EM+EN+MN-WeA1 The Many Avatars of PVD**, *Murali Narasimhan*, Applied Materials, Inc. **INVITED**

Physical Vapor Deposition has been used for many years for depositing thin film coatings for diverse uses ranging from jewelry to industrial cutting tools. PVD has found usage in the manufacture of advanced semiconductor manufacturing for depositing various metals and some specialty dielectrics as well. The majority of high purity metal deposition for semiconductor use has been done using PVD although the use of CVD and ALD has increased over the years because of requirements of conformality and gap fill where conventional planar PVD has not been adequate. However, breakthroughs in PVD technology have been successful in extending the use of PVD to advanced semiconductor manufacturing nodes by changing the geometry of PVD sources and reactors and the nature of the plasma involved. Collimated and long-throw sources developed by the semiconductor equipment industry in the early '90s enabled the deposition of high-purity Ti to lower contact resistance for transistors. Reactive sputtering of TiN enabled a robust barrier for CVD W plugs used at the 0.5um node. Further, use of electromagnetic fields to ionize and then guide the plasma and sputtered ionized atoms has been successful in improving the conformality

of PVD Ti films. Ionized Metal Plasma (IMP), Hollow-Cathode Magnetron (HCM) and Self-Ionized Plasma (SIP) were innovations in ionized PVD reactor design that led to widespread adoption of PVD TaN and PVD Cu for Cu interconnect barrier and seed layer production from the 90nm node to the present. The application of thermal energy on the substrate during PVD Al and Cu has been useful in improving the flow of deposited material and subsequent gap-fill of sub-micron features. The use of Radio Frequency (RF) energy to power the target has allowed for more efficient ionization at lower power levels. The application of a capacitive tuner to modulate the ion bombardment on the wafer and tailor the film properties of TiN for hard mask applications has enabled the realization of etched features at the 22nm node. Pulsed DC magnetrons enable sputtering of dielectric materials, thus opening up the controlled deposition of thin films of insulating films for various applications such as improving the brightness of high-efficiency LEDs. Multi-cathode off-axis PVD magnetrons have enabled the deposition of multi-layers of ultra-thin films for magnetic devices such as advanced in-plane and out-of plane MRAM and the manufacture of EUV mask blanks for sub 10nm manufacturing. This talk will present the above listed progression of PVD technology over the years and its use for many applications in semiconductor manufacturing.

3:00pm **TF+AS+EM+EN+MN-WeA3 Reactive Foil Ignition by Laser Irradiation: Experimental and Modeling Results**, *Ryan Murphy*, *C.D. Yarrington*, Sandia National Laboratories, *R.V. Reeves*, Lawrence Livermore National Laboratory, *D.P. Adams*, Sandia National Laboratories

It has been shown that forced mixing of reactive layers (foils) leads to an exothermic release of energy after initiation by pulsed laser irradiation. In order to understand the ignition of foils initiated by laser irradiation, we study the interaction of laser pulses with Al/Pt multilayer reactive foils prepared by sputter deposition. It will be shown that the single-pulse ignition threshold and dynamics are dependent on the length of the laser pulse as the pulse length is varied from 150 fs to 100 ms. The dependence of the ignition threshold on pulse length is a combination of laser-material interactions such as the size of the heat affected zone and the onset of ablation for ultrafast irradiation. Simulations of single-pulse laser heating were performed with Aria, the thermal package of the SIERRA finite element computational framework. Three-dimensional geometries were subjected to laser flux boundary conditions equal to those measured from the experimental conditions. Modeling and experimental results are correlated to show the effects of the heat affected zone size and shape on ignition thresholds and onset times.

Sandia National Laboratories is a multi-program laboratory managed and operated by Sandia Corporation, a wholly owned subsidiary of Lockheed Martin Company, for the United States Department of Energy's National Nuclear Security Administration under Contract DE-AC04-94AL85000.

3:20pm **TF+AS+EM+EN+MN-WeA4 The Effects of a Heat Sink on Self-Sustained Propagating Reactions in Sputter-Deposited Bimetallic Multilayers**, *David Adams*, *R.V. Reeves*, *M. Hobbs*, Sandia National Laboratories

Reactive multilayers grown by sputter deposition have recently attracted interest for applications including material joining (soldering, brazing) and energy sources. For these applications, a metal-metal multilayer is typically designed to have many discrete reactant layers and a composition that corresponds to the peak enthalpy for a given material system. A thickness of reactive multilayers as small as 1.6 microns has recently been demonstrated for microelectronics joining (Braeuer et al. ECS Transactions, 2012). However, little is known about the minimal multilayer thickness required for ensuring a self-sustained, high temperature synthesis (SHS) reaction.

With this presentation, we describe the behavior of thin reactive Al/Pt multilayers tested as freestanding foils and as adhered films. For multilayers having a total thickness of 1.6 microns, self-sustained, high temperature reactions readily occur when the multilayer is tested as a freestanding foil. When coupled to a semi-infinite substrate, the likelihood of reaction is reduced depending on the multilayer design.

Sandia National Laboratories is a multi-program laboratory managed and operated by Sandia Corporation, a wholly owned subsidiary of Lockheed Martin Corporation, for the U.S. Department of Energy's National Nuclear Security Administration undercontract DE-AC04-94AL85000.

5:00pm **TF+AS+EM+EN+MN-WeA9 Beyond Deep Silicon Etching – Generating High Aspect Ratio Microstructures by Infiltration of Carbon Nanotube Frameworks**, *Robert Davis*, Brigham Young University **INVITED**

In addition to being the anchor material for microelectronics, silicon is widely used as the basis of high aspect ratio microfabrication for MEMS with applications ranging from inertial sensors to neural probe arrays. Carbon nanotube templated microfabrication (CNT-M), extends the palette of materials and structures for high aspect ratio microfabrication beyond

those achievable with vertically etched bulk silicon. In CNT-M, 3-D forests of patterned vertically-aligned carbon nanotubes are grown as a high aspect ratio framework and then the “forests” are infiltrated with a secondary material by chemical vapor deposition. Precision structures (including nanoporous structures) with very high aspect ratios (greater than 400:1) can be generated with CNT-M. The infiltration materials range from ceramics to metals and include silicon dioxide, silicon nitride, carbon, nickel, and yes silicon. We are using CNT-M to fabricate functional structures for applications including mechanical actuation, chemical separations and detection, and electrochemical energy storage.

5:40pm **TF+AS+EM+EN+MN-WeA11 The Influence of Thin Binder Films on Reaction Behavior in Reactive Powder Complexes, Robert Reeves, K.T. Sullivan, A.E. Gash**, Lawrence Livermore National Laboratory

With the recently renewed interest in additive manufacturing (AM), there has been a recent upswell in the number of AM processes available. One such process that could be useful for reactive materials utilizes a curable liquid binder to adhere loose powders into coherent solid forms. In this process, tap-density powders are nearly saturated with binder, so the resulting film of binder present on each particle can represent a significant contaminant to the reaction system. In this work, the effect of the binder on reaction behavior in the Ni-Al system is explored. First, the distribution of binder and its elemental constituents are studied by electron microscopy and energy dispersive spectroscopy for powders with varying levels of binder saturation. Then, the effect of binder on the reaction kinetics and overall behavior is investigated. The change in overall heat release and apparent activation energy are quantified through differential scanning calorimetry, and the bulk reaction propagation rate is measured by high speed photography as a function of the weight fraction of binder in the compact. Finally, the reaction products are identified through x-ray diffraction. In all tests, comparisons are made to the neat Ni-Al system.

This work performed under the auspices of the U.S. Department of Energy by Lawrence Livermore National Laboratory under Contract DE-AC52-07NA27344.

6:00pm **TF+AS+EM+EN+MN-WeA12 Carbon Nanotube Sheets from Horizontally Aligned Carbon Nanotubes, Nathan Boyer, D.B. Syme, J.T. Rowley**, Brigham Young University, *M. Harker, R. Creighton, S. Cornaby*, Moxtek Inc., *R. Vanfleet, B.D. Iverson*, Brigham Young University, *L. Pei*, Johns Hopkins University, *R.C. Davis*, Brigham Young University

Carbon sheets comprised of horizontally aligned carbon nanotubes (CNT) were prepared by rolling vertically aligned CNTs into a thin-film. A subsequent infiltration step to coat the rolled CNTs with amorphous carbon or polymer has also been performed to improve adhesion of neighboring CNTs. Amorphous carbon infiltration was achieved using chemical vapor deposition and polymer infiltration was performed by dipping the sheet into a solvent-mediated, polymer solution. The typical failure mode of the CNT thin-films is to tear parallel to the alignment of the CNTs. Infiltration of the aligned CNT film with additional materials strengthens the film against tearing and increases burst pressure. Non-infiltrated CNT thin-films have sustained a differential pressure of 1.4 atm over a circular area of 7 mm² on a bulge test apparatus. Both carbon and polymer infiltrated sheets could be used in many applications including micromechanical sensing and actuation.

Thursday Morning, October 22, 2015

Actinides and Rare Earths Focus Topic
Room: 230A - Session AC+AS+MI-ThM

Nuclear Power and Waste Remediation

Moderator: David Shuh, Lawrence Berkeley National Laboratory

8:00am **AC+AS+MI-ThM1 Applications of Synchrotron Methods to f-Element Research in the Nuclear Fuel Cycle, Melissa Denecke**, The University of Manchester, UK

INVITED

Celebrating 60 years of civil nuclear power generation offers an excellent opportunity to review synchrotron radiation (SR)-based techniques to characterize nuclear materials and elucidate processes relevant to the nuclear fuel cycle. The penetration capability of intense SR X-ray sources allows in situ investigations, including samples within radiological containments or specialized environments. The presentation will concentrate on application of X-ray spectroscopic techniques in studies related to the nuclear fuel cycle (fuel, cladding, recycle, waste disposal).

8:40am **AC+AS+MI-ThM3 Ab Initio Study of Advanced Metallic Nuclear Fuels for Fast Breeder Reactors, Alexander I. Landa**, Lawrence Livermore National Laboratory

INVITED

The U-TRU-Zr and U-TRU-Mo alloys proved to be very promising fuels for TRU-burning liquid metal fast breeder reactors. The optimal composition of these alloys is determined from the condition that the fuel could remain stable in the bcc phase (γ -U) in the temperature range of stability of α -U phase. In other words, both Zr and Mo play a role of ' γ -stabilizers' helping to keep U in the metastable bcc phase upon cooling. The main advantage of U-Pu-Mo fuels over U-Pu-Zr fuels lies in much lower constituent redistribution due to the existence of a single γ -phase with bcc structure over typical fuel operation temperatures. The nucleation time for the decomposition of the metastable alloys, which controls the constituent redistribution process, is directly connected with the excess enthalpy of solution of these alloys. In the present study we perform KKR-ASA-CPA and EMTO-CPA calculations of the ground state properties of γ -U-Zr and γ -U-Mo alloys and compare their heats of formation with CALPHAD assessments. We discuss how the heat of formation in both alloys correlates with the charge transfer between the alloy components, and how the specific behavior of the density of states in the vicinity of the Fermi level promotes the stabilization of the U₂Mo compound. Our calculations prove that, due to the existence of a single γ -phase over the typical fuel operation temperatures, γ -U-Mo alloys should indeed have much lower constituent redistribution than γ -U-Zr alloys where a high degree of constituent redistribution takes place. The binodal decomposition curves for γ -based U-Zr and U-Mo solid solutions are derived from Ising-type Monte Carlo simulations incorporating effective cluster interactions obtained from the Screened Generalized Perturbation and Connolly-Williams methods. We also explore the idea of stabilization of the δ -UZr₂ compound against the α -Zr (hcp) structure due to increase of Zr d-band occupancy by the addition of U to Zr. Analogy with stabilization of the ω phase in Zr under compression is made. Though the U-Pu-Zr and U-Pu-Mo alloys can be used as nuclear fuels, a fast reactor operation on a closed fuel cycle will, due to the nuclear reactions, contain significant amount of MA (Np, Am, Cm). Calculated heats of formation of bcc Pu-U, Pu-Np, Pu-Am, Pu-Cm, Pu-Zr, Pu-Mo, Np-Zr, Np-Mo, U-Am, Np-Am, Am-Zr and Am-Mo alloys are also presented and compared with CALPHAD assessments. This work was performed under the auspices of the US Department of Energy by Lawrence Livermore National Laboratory under Contract DE-AC52-07NA27344 and was funded by the Laboratory Directed Research and Development Program at LLNL under project tracking code 12-SI-008.

9:20am **AC+AS+MI-ThM5 Shedding Light on Uranium Corrosion in Nuclear Waste Packages, Charilaos Paraskevoulakos**, University of Bristol, UK

Intermediate level waste (ILW) is encapsulated in grout and stored in stainless steel drums. A proportion of these have become a concern for the UK nuclear community, as significant distortion around the circumference of these drums has been observed. Distortion is ascribed to the generation of voluminous and potentially flammable corrosion products forming on uranium metal, e.g. uranium hydride. Thus potential oxygen influx caused by fracturing of canisters will threaten their suitability for waste disposal, potentially causing release of the encapsulated radioactive material or even ignition of the hydride. The association of the uranium corrosion mechanisms with the mechanical degradation of the encapsulants (stainless steel and grout), is the focus of the current project. Finite Element (FE)

Modelling, accelerated uranium corrosion tests as well as diffraction and tomography using synchrotron X-Rays/gamma rays could be employed to investigate the durability of the ILW packages.

9:40am **AC+AS+MI-ThM6 The Optical Properties of Uranium Carbide Measured by Spectroscopic Ellipsometry, Wigbert Siekhaus, A.J. Nelson, C.K. Saw**, Lawrence Livermore National Laboratory

Uranium carbide inclusions are common in metallic uranium, and uranium carbide itself is being used or being considered as a fuel in both gas-cooled, liquid metal cooled, and supercritical water-cooled reactors. To the best of our knowledge the only study of optical properties deals with high temperature radiance. [1] Here we first characterized a uranium carbide cube (supplied by Oak Ridge National Laboratory) with sides of approximately 3 mm length by X-ray diffraction and X-ray photo-electron spectroscopy and then measured its optical properties with an ellipsometer at angles of incidence between 65 and 75 degrees, and over an energy range from 1.26 to 3.2eV. The signal strength was low over that energy range, and too low to be useful above 3.2eV. The measured Δ and Ψ were converted to the dielectric constants ϵ_1 and ϵ_2 shown in the table below using a general oscillator model [2].

E, eV	ϵ_1	ϵ_2	E, eV	ϵ_1	ϵ_2	E, eV	ϵ_1	ϵ_2
1.26	-1.96	5.07	1.95	-0.30	2.73	2.61	2.61	1.32
1.33	-1.69	4.77	2.02	-0.21	2.55	2.68	2.68	1.21
1.40	-1.47	4.45	2.10	-0.12	2.34	2.75	2.75	1.07
1.47	-1.25	4.14	2.18	-0.03	2.18	2.83	2.83	0.94
1.54	-1.06	3.87	2.25	0.04	2.02	2.91	2.91	0.85
1.61	-0.89	3.63	2.32	0.12	1.87	2.98	2.98	0.76
1.69	-0.73	3.44	2.40	0.20	1.73	3.05	3.05	0.67
1.76	-0.60	3.23	2.47	0.28	1.59	3.12	3.12	0.58
1.84	-0.48	2.95	2.54	0.35	1.43	3.20	3.20	0.51

Prepared by LLNL under Contract DE-AC52-07NA27344, LLNL-ABS-670149

[1] D. Manara, F. De Bruycker, K. Boboridis, O. Tougait, R. Eloiardi, M. Malki, High temperature radiance spectroscopy measurements of solid and liquid uranium and plutonium carbides, J Nucl Mater, 426 (2012) 126-138.

[2] R. Synowicki, J.A. Woollam CO. Inc. 645 M Street, Suite 102, Lincoln, NE 68508-2243, USA

11:00am **AC+AS+MI-ThM10 Uranium Wet Oxidation in the Presence of Hydrogen Overpressure, Antonios Banos**, University of Bristol, UK

The radioactive intermediate level (IL) and high level (HL) waste have been accumulated in the UK's legacy ponds and silos for over 60 years. There is a great need for these wastes to be retrieved to follow long term storage. Uranium hydride (UH₃) has been identified as a reaction product of the corrosion process. Hydride formation occurs due to the increasing concentration of hydrogen gas, generated from the reaction of uranium, Magnox (MagnoxAl80) and other metals. The highly pyrophoric and unstable nature of UH₃ in air poses considerable environmental risks, due to potential radionuclide release. In this work we will try to simulate the corroding conditions by immersing an initially polished uranium sample in water under vacuum and introducing hydrogen gas overpressure to the system. The ternary system will be investigated in different temperatures and pressures with two main questions awaiting to be answered: 1. Is UH₃ identified? For this reason post-examination of the reacted surface will be conducted using Secondary Ion Mass Spectrometry (SIMS), Focus Ion Beam (FIB) milling. 2. If UH₃ is identified, on which part of the reaction is it produced and how this affects the overall reaction? The kinetics will be monitored using a specifically designed set-up comprised from a stainless steel pot and a pressure controller attached on one end and logged to a computer in order for the whole reaction to be recorded and the rate of corrosion through gas generation to be evaluated.

11:40am **AC+AS+MI-ThM12 Resolving the Issues of 5f Covalency and Ionicity in UO₂ and UF₄, James Tobin**, Lawrence Livermore National Laboratory

Building upon our recent work, a concerted effort to isolate and understand covalency and ionicity in uranium compounds has been pursued. Specifically, the isoelectronic formal charge systems, uranium dioxide and uranium tetrafluoride, have been investigated with a novel mixture of both soft and hard-x-ray spectroscopies. The results to be discussed will include the following: (1) the use of soft X-ray O1s/F1s X-ray absorption spectroscopy (XAS) and U4d X-ray emission spectroscopy (XES) to follow

the 2p/5f bonding via the unoccupied density of states; (2) the utilization of hard X-ray U L3 extended X-ray absorption fine structure (EXAFS) to trivially distinguish the ordering in each; and (3) the use of hard X-ray L3 resonant X-ray emission spectroscopy (RXES) to distinguish 5f occupation/covalency effects in UO₂ and UF₄. Collaborators include CH Booth, DK Shuh, T. Tyliczszak, G. van der Laan, D. Sokaras, T.-C. Weng, D. Nordlund, S.-W. Yu, W. Siekhaus and P.S. Bagus.

Applied Surface Science

Room: 212D - Session AS-ThM

Practical Surface Analysis III: Multiple-technique Problem-solving and Structure-property Correlations

Moderator: Michaelen Pacholski, The Dow Chemical Company, Daniel Gaspar, Pacific Northwest National Laboratory

8:00am **AS-ThM1 Correlation of Substrate Surface Chemistry and Roughness to Adhesion of Pressure Sensitive Adhesives**, *Michaelen Pacholski, T. Powell, D. Keely, W.B. Griffith*, The Dow Chemical Company
This investigation focuses on the surface chemistry and roughness of substrates and the relationship to adhesion. We discuss the variability in surface chemistry and roughness of materials all nominally identified as the same material. For example, high density polyethylene (HDPE) is a common material used for bottles as well as a preferred low energy substrate for adhesion testing. However, there are several types of surface treatments used to increase adhesion. Surface roughness can also affect adhesion. We have compared corrugated cardboard surfaces and the influence of surface roughness on adhesion.

8:20am **AS-ThM2 Surface and Interface Studies of Ultra-Low Wear (ULW) PTFE/Alumina Polymer Composites**, *Lei Zhang, G.S. Blackman, C.P. Junk, L. Ampacher, K.G. Lloyd, J.R. Marsh, D.J. Kasprzak*, DuPont Central Research and Development

In the past few years, polymer composites of polytetrafluoroethylene (PTFE) and alumina particles have attracted a lot of interest as a promising Ultra-Low Wear (ULW) material. It has been discovered that by adding a small amount of alumina additive (<5wt%) to PTFE, the wear rate of the PTFE is enhanced dramatically by over four orders of magnitude. Although this polymer composite system has shown its uniqueness and importance in the tribological research, the tribochemical mechanism has not been well understood.

To fully understand the chemistry that occurs during the tribology/wearing, it requires the precise design of experiments as well as applying integrated techniques to study the tribochemical process. In our studies, we investigated the tribochemical products by studying the unique chemistry of the transfer film formed at the composite and stainless steel interfaces during wearing. XPS, FTIR, and ToF-SIMS techniques have been applied to determine the chemistry of these tribochemical products as a function of number of sliding cycles. These characterization techniques have allowed us to understand the ultralow wear behavior and help to develop a conceptual framework for the ultralow wear material system.

8:40am **AS-ThM3 Investigation of Increased Glide Force of Prefilled Syringes Using Multiple Analytical Techniques**, *Xia Dong, Z. Xiao, C.A.J. Kemp, G.H. Shi*, Eli Lilly and Company

Time-based glide-force changes in pre-filled syringes built into autoinjector systems can lead to negative patient experience issues and dose accuracy problems. The long term performance of prefilled syringe systems is examined during stability testing study when monoclonal antibody solutions are stored at various temperatures for given time periods. Multiple parameters including lubricant amount, lubricant distribution, and surface chemistry contribute to friction between the plunger and barrel and consequently the glide force. Therefore, it is important to understand the impact of storage conditions on lubricant characteristics and surface properties so that the desirable long term performance can be achieved.

In the current study, a monoclonal antibody solution was filled in glass syringes coated with silicone lubricant. Increased glide forces were observed from syringes stored at 25 °C, comparing to those stored at 5 °C. Multiple analytical techniques, including ellipsometry, ICP-OES, contact angle, XPS and TOF-SIMS were utilized to characterize lubricant and surface properties of syringe interior surfaces to understand the root cause of undesirable glide force changes.

9:00am **AS-ThM4 Degradation of Polypropylene Surgical Mesh: An XPS, FTIR, and SEM Study**, *Bridget Rogers*, Vanderbilt University, *R.F. Dunn*, Polymer & Chemical Technologies, LLC., *S.A. Guelcher*, Vanderbilt University

Polypropylene mesh has been used to surgically treat stress urinary incontinence and has shown promising short-term results. However, serious complications have been associated with longer term implanted meshes. We hypothesize that these complications are due to oxidative degradation of the mesh brought about by reactive oxygen species that are released by adherent macrophages on the surface of the polypropylene.

Polypropylene is known to oxidize through a stable hydroperoxide (-COOH) intermediate, followed by chain scission and formation of a carbonyl (-C=O) end group. Oxidation of polypropylene leads to a reduction in molecular weight, embrittlement, cracking, and eventually fracture and fragmentation. An *in vitro* study was performed to study the oxidation of polypropylene surgical mesh in a model environment that simulates conditions the mesh would experience in the body. Samples cut from three commercially available surgical devices produced by two manufacturers and polypropylene control samples were placed in an oxidizing medium consisting of 20% H₂O₂ and 0.1 M CoCl₂.

Samples were placed in the oxidizing medium and were incubated at 37 °C on a shaker for up to 6 weeks. The oxidizing medium was replaced every 3 to 4 days. Six samples were removed every week, washed in DI water, and dried. XPS and FTIR were used to analyze the samples for the presence of hydroperoxide and carbonyl species. SEM micrographs were acquired at 0, 4, and 5 weeks of oxidation.

We will present the XPS, FTIR, and SEM analytical results of the samples from this *in vitro* study. These results show that the anti-oxidants in the polypropylene mesh delay, but do not inhibit oxidation. SEM micrographs show surface pitting and flaking of samples exposed to the oxidizing medium.

9:20am **AS-ThM5 ASSD 30th Anniversary Lecture: Evolution of the Nature and Application of Surface Analysis: Challenges, Pitfalls, and Opportunities Past, Present and Future**, *Donald Baer*, Pacific Northwest National Laboratory

INVITED

Over the past 30 years there has been a remarkable range of advances in the ability to understand the nature of many types of important surfaces and interfaces. X-ray photoelectron spectroscopy (XPS) has become nearly essential for characterizing many types of materials, verifying the quality of synthesis methods and understanding interactions of these materials in many environments and applications. This has become possible because of major improvements in instrumentation including stability, reproducibility, increases in spatial resolution, increases in count rate, major improvements in the ability to analyze insulating samples, digital control of instruments and advances in the ability to process, model and analyze the data. For Auger electron spectroscopy (AES) similar advances have occurred, with spatial resolution being an obvious differentiator. In the area of Secondary Ion Mass Spectrometry, the major excitement has been related to the evolution of new primary and sputter beams with Bucky ball and cluster sources. Thirty years ago scanning probe methods were just beginning to appear; now they serve as critical tools for many types of studies.

In spite of the significant progress, many important materials information needs remain, providing opportunities for continued evolution of traditional surface analysis tools and the development and applications of other methods. These might be framed in the context of some "what if" questions that are not out of the range of the possible. What if we could monitor in real-time the evolution of surfaces and buried interfaces (and the actual compositional and chemical information at those interfaces) in "operational" environments? What if we could obtain quantitative compositional and chemical information at the resolution of an AFM? What if micro-technology could be used to create an XPS unit that produced quality data and operated without or with only trivial need for vacuum? What would be possible if NMR could be easily used to quantitatively characterize surfaces, interfaces or individual particles? Examples of progress along these directions will be described. All indications are that the next 30 years will be as dynamic and productive as the past 30 years, if not more so.

11:00am **AS-ThM10 Unraveling the Dynamic Nature of Mixed-Metal Oxides Nanocatalysts: An *In Situ* Multiple-Technique Approach**, *Dario Stacchiola*, Brookhaven National Laboratory

INVITED

Catalysts have traditionally been characterized before or after reactions and analyzed based on static representations of surface structures. It is shown here how dynamic changes on a catalyst's chemical state and morphology can be followed during a reaction by a combination of *in situ* microscopy (AP-STM) and spectroscopy (AP-XPS and AP-IRRAS). In addition to determining the active phase of the catalyst by *in situ* methods, the presence of weakly adsorbed surface species or intermediates generated only in the

presence of reactants can be determined, allowing in turn the comparison of experimental results with first principle modeling of specific reaction mechanisms. Three reactions are used to exemplify the approach: CO oxidation ($\text{CO} + 1/2\text{O}_2 \rightarrow \text{CO}_2$), water gas shift reaction ($\text{CO} + \text{H}_2\text{O} \rightarrow \text{CO}_2 + \text{H}_2$) and methanol synthesis ($\text{CO}_2 + 3\text{H}_2 \rightarrow \text{CH}_3\text{OH} + \text{H}_2\text{O}$). During CO oxidation, the full conversion of Cu^0 to Cu^{+2} deactivates an initially outstanding catalyst. This can be remedied by the formation of a TiCuO_x mixed-oxide that protects the presence of active partially oxidized Cu^+ cations. We also show the switch from a redox mechanism on $\text{Cu}(111)$ to a more efficient associative mechanism pathway for the WGS at the interface of ceria nanoparticles deposited on $\text{Cu}(111)$ [1]. Similarly, the activation of CO_2 at the ceria/ $\text{Cu}(111)$ interface allows its facile hydrogenation to methanol [2]. Our combined studies emphasize the need of searching for optimal metal/oxide interfaces, where multifunctional sites can lead to new efficient reaction pathways.

[1] *Angew. Chem. Int. Ed.* **52**, 5101–5105 (2013)

[2] *Science*, **345**, 546-550 (2014)

11:40am **AS-ThM12 Correlation between Chemistry, Optical Properties, and Environmental Stability of DC Sputtered Rhenium Oxides**, Neil Murphy, Air Force Research Laboratory, L. Sun, General Dynamics Information Technology, J.G. Jones, Air Force Research Laboratory, J.T. Grant, General Dynamics Information Technology

Thin films of rhenium oxide (<150 nm) are deposited using magnetron sputtering employing a rhenium cathode within an argon-oxygen atmosphere. Throughout the deposition process, the working pressure is maintained at a constant level of 1.33 Pa as the oxygen content is varied from 0% to 80% in increments of 10%. As the oxygen content is varied, the extinction coefficient, k , of the deposited layers is monitored via *in situ* ellipsometry. *In situ* ellipsometry is used to identify absorption features specific to ReO_3 , including the characteristic reduction of k brought on by the optical band gap at 310 nm as well as the onset of intraband absorption above 540 nm. *In situ* ellipsometry results indicate that films deposited at oxygen levels of 50% and 60% have respective k_{450} values of 0.6 and 0.25, characteristic of ReO_3 . Chemical analysis via x-ray photoelectron spectroscopy confirmed that films individually deposited at oxygen levels of 50% and 60% are mixed-valent, consisting largely of ReO_3 (Re^{6+}), with contributions from ReO_2 (Re^{4+}) and Re_2O_7 (Re^{7+}). Note that films deposited at 50% oxygen content also contained up to 15% Re_2O_3 (Re^{3+}). Further monitoring of the films' valence states, after an environmental exposure time of 30 days, indicates a correlation between structural instability and the presence of both Re_2O_3 and Re_2O_7 . Analyses via XPS and *ex situ* spectroscopic ellipsometry indicate that films deposited within an atmosphere of 60% oxygen do not contain Re^{3+} and demonstrate stable surface chemistry and optical behavior throughout the 30 day period, while those deposited at 50% oxygen experience significant degradation. Increasing the stability of mixed-valent Re-O films could give rise to more widespread use of rhenium in optics and catalysis, especially in applications where mild moisture exposure is unavoidable.

12:00pm **AS-ThM13 Multi-Technique Surface Analysis of Geological Samples, Including sub-10 Micron Spectroscopic XPS Imaging**, Paul Mack, Thermo Fisher Scientific, UK

A single geological sample may have multiple phases, each with different chemical bonding environments. Geologists will typically have access to SEM-EDS, giving them elemental information from the different grains (from bulk depths). When it comes to chemical information, however, XPS provides a unique ability to easily acquire data from these small grains. It offers quantitative chemical bonding data with a probe size small enough to acquire data from individual phases.

In this work, rock cross-sections were analysed with XPS to quantify the elements in different phases and to identify and quantify the oxidation states of elements in these regions. The analysis can be divided into four main sections: 1) Finding the features of interest, 2) Aligning the X-ray spot on the features, 3) Acquiring the XPS data and 4) Processing the XPS data to answer the key questions about chemical bonding states.

Any XPS tool used for this analysis needs to have a high quality optical system, enabling to geologist to rapidly find the features of interest, with a live optical feedback system. The grains were typically 10s of microns in size, so a small X-ray analysis area is required. This small area analysis was achieved in two different ways: shrinking the

X-ray spot to match the feature size or collecting spectroscopic parallel imaging data. In the latter case, every pixel in the image has full XPS data allowing the analyst to perform sub-10mm area analysis directly from the X-ray image.

Techniques complementary to XPS can also help provide a more complete characterization of geological samples. SEM/Auger can offer analysis with a much smaller probe size than XPS, but it is necessary to charge

compensate during the experiment. Charge compensation methodology will be discussed in this work.

Helium Ion Microscopy Focus Topic

Room: 211B - Session HI+AS+SS+NS-ThM

Focused Ion Beam Technology (08:00-10:00)/Fundamentals of Helium Ion Microscopy (11:00-12:20)

Moderator: Gregor Hlawacek, Helmholtz-Zentrum Dresden - Rossendorf, Leonidas Ocola, Argonne National Laboratory

8:00am **HI+AS+SS+NS-ThM1 Ga+ Ion Beam Nanofabrication Techniques of 3D Micro- and Nano- Fluidic Devices**, Leonidas Ocola, Argonne National Laboratory

Three-dimensional (3D) fluidic geometries have been fabricated in the past by using several layers of Polydimethylsiloxane (PDMS) molds or double-sided Si etch steps [1], which require highly accurate chip bonding to complete the fluid path and multiple process steps. An alternative to this method is the use of direct write ion beam micromachining as a means to fabricate key components of a microfluidic device that require variations in depth as well as variations in width. 3-D microfabrication currently is mainly constrained to excimer lasers [2-3] and therefore is inherently diffraction limited. Grey scale lithography is also used for 3D structures but has limited capability. On the other hand, ion beam micromachining can scale down below the diffraction limit with no change in the technique and almost unlimited depth bandwidth. The focused ion beam / scanning electron microscope (FIB/SEM) is a powerful tool used for sample analysis and characterization. When equipped with a sophisticated pattern generator and lithography technology it can expand its use to new applications in nano- and micro-fabrication. Ion beam micromachining is akin to electron beam lithography, where a beam of charged particles are steered to draw structures contained in a computer aid design (CAD) file. Unlike electron beam lithography, one can program arbitrary depths by manipulating the dwell time, or dose, of a particular structure. In this paper the work reported previously [4-5] has been expanded to large and complex geometries to place emphasis on the applicability of ion beam micromachining to practical microfluidic applications, such as straight 3D mixers and serpentine 3D mixers with sections as deep as 70 microns and channel widths as large as 30 microns. We have found that these devices can achieve full mixing of aqueous solutions in about an order of magnitude faster than traditional devices. The challenges encountered and overcome to fabricate these mixers will be described and the scalability of different fabrication techniques to nano-fluidics will be revisited.

References:

1. R. H. Liu et al., *J. MEMS* **9** (2000) 190
2. Y. Liao et al., *Lab Chip*, **12** (2012) 746
3. A. Ródenas et al., *Proc. SPIE* **8542** (2012) 854217
4. A. Imre et al., *J. Vac. Sci. & Technol. B* **28** (2010) 304
5. E. Palacios et al., *J. Vac. Sci. Technol. B* **28** (2010) C611

Use of the Center for Nanoscale Materials, Argonne National Laboratory was supported by the U. S. Department of Energy, Office of Science, Office of Basic Energy Sciences, under Contract No. DE-AC02-06CH11357.

8:20am **HI+AS+SS+NS-ThM2 Adding 3D to Conventional SEM or FIB Surface Imaging Information - In situ Surface Sensing and Nanoprofilometry for Focused Electron and Ion Beam Induced Processes Verification**, Andre Linden, Raith America, Inc., A. Rudzinski, M. Levermann, T. Michael, Raith GmbH, E. Maynicke, RWTH Aachen
Nanopatterning processes and corresponding parameters are typically well understood for standard nanofabrication applications using resist based electron beam lithography (EBL) or FIB milling processes (e.g. for TEM lamella preparation).

Recently however, the bandwidth of nanofabrication applications for dedicated nanopatterning tools has significantly broadened and is no more limited to resist based EBL and mere, standard FIB milling tasks. Some latest generation multi-technique electron and ion beam nanolithography tools even facilitate additional *in situ* processes such as resistless focused electron or ion beam induced processes - e.g. material deposition or gas enhanced etching. The number of variable parameters for such complex processes involving e.g. new gas chemistry or ion species is nearly "infinite". Moreover, smart and flexible patterning strategies, e.g. by using loops in conjunction with various multi-directional patterning modes, have significant impact on the final nanostructure's definition and performance,

so that a straight *in situ* characterization of e.g. material deposition, milling or etching rates becomes crucial for most efficient understanding and subsequent optimization of such processes.

In contrast to elaborately using additional analytical equipment outside the vacuum and subsequently re-introducing the sample for further processing and optimization, we have implemented a distance sensitive nanomanipulator with nanoprofilometric capabilities into our professional multi-technique nanofabrication tools, which allows *in situ* characterization of nanostructures in 3D with ~10nm resolution by collecting topographic sample surface information.

First results of direct *in situ* growth rate determination of focused electron beam induced material deposition (FEBID) for process calibration as well as 3D surface topographic information of challenging milling applications will be presented.

8:40am HI+AS+SS+NS-ThM3 Nanofabrication Using Gas-Assisted Focused Ion Beams, Chad Rue, FEI Company INVITED

A brief introduction to gas-assisted etching for Focused Ion Beams (FIBs) is given, including typical chemical precursors for various applications, and appropriate beam control parameters such as pixel overlap, dwell time, and refresh time. These factors are reasonably well-understood for pattern dimensions that are large compared to the size of the ion beam. However, for applications such as nanofabrication, which require high milling precision over small areas, the limiting size of the ion beam and its associated activated volume begin to influence the milling performance. The remainder of the discussion will focus on the relatively-unexplored regime in which the size of the pattern dimension is comparable to the size of the ion beam itself. The influence of various beam control parameters, particularly refresh time, becomes critically important to the milled profile of the desired structure. Redeposition effects, peripheral erosion, and mill rate trends are discussed. Operating tips and tricks are described, including the use of drift compensation strategies. The minimum physically achievable via size is examined. For a 10 pA Ga⁺ beam at 30 keV, used to mill a via in a SiO₂ substrate with XeF₂-assist, the minimum achievable via size (FWHM) is found to be 50 ± 10 nm, and is relatively independent of depth or aspect ratio. Implications for nanofabrication are discussed and examples are shown.

9:20am HI+AS+SS+NS-ThM5 The Psychology and Applications of a Bipolar Plasma Focused Ion Beam, Rod Boswell, ANU, Australia, N. Smith, P. Tesch, N. Martin, Oregon Physics

A new high brightness ion source has been developed using bi-polar power supplies that can be used with either positive or negative ions. This has involved a redesign of the plasma source and the acceleration optics to allow high currents to be focused with an energy of up to 30keV. We expect to make significant advances in Ultra High Resolution SIMS with a negative oxygen beam; a second application is the milling of structures in glass with a O⁻ beam, such as a microfluidic set of channels. At the higher voltages mentioned above, it should be possible to cut cross sections of Through Silicon Vias in glass substrates. The challenges encountered in creating and extracting the negative ions will be discussed along with some performance and application data.

9:40am HI+AS+SS+NS-ThM6 Advanced FIB Applications with New Ion Species and Large Area Capabilities, Sven Bauerdick, L. Bruchhaus, Raith GmbH, Germany, J. Fridmann, Raith America, Inc., P. Mazarov, A. Nadzeyka, R. Jede, Raith GmbH, Germany

Focused ion beam (FIB) systems are applied to a wide range of applications in R&D nanofabrication, both for creating functional devices as well as for preparing sample imaging and analysis. With different ion species on one hand and very sophisticated patterning approaches on the other hand it is possible to improve results and provide solutions for more advanced applications. Here we show and discuss the capabilities of Ga and new ion species like Au or Si with high resolution, long-term stability and easy handling, which is combined with an instrument design enabling large area or elongated patterns by write field stitching or truly continuous writing, respectively.

The type of ion defines the nature of the interaction mechanism with the sample and has significant consequences on the resulting nanostructures or samples. Therefore, we have extended the FIB technology towards the delivery of multiple ion species selectable into a nanometer-scale focused ion beam by employing a liquid metal alloy ion source (LMAIS). A mass separation filter is incorporated into the column to allow for fast and easy switching between different ions. The respective capabilities of mainly Ga, Au and Si have been investigated (resolution, milling rate, imaging, implantation) and according results and applications will be presented.

Moreover we investigated, optimized and tested milling approaches for pattern (write field) stitching and for truly continuous patterning based on

precise stage movement while milling/ cutting with the ion beam. An improved beam pattern needs to mimic the looping strategy of conventional milling, so that grooves with defined depth, steep sidewalls and minimum re-deposition can be achieved. This combination of functionality enables applications like nanofabrication of micro-fluidic mixers, zone plates, large area gratings, or wafer-level nanopore devices as well as sample investigation e.g. imaging, X-sectioning and preparation in an automated way. Examples for new nanofabrication techniques like large area hard masking by implantation, both for reducing and increasing the rate in standard etching processes, or seamless direct milling of nano-fluidic channels over cm²'s will be discussed.

11:00am HI+AS+SS+NS-ThM10 SIMS on the Helium Ion Microscope : a Powerful Tool for High-resolution High-sensitivity Nano-Analytics, Tom Wirtz, D. Dowsett, Luxembourg Institute of Science and Technology (LIST), Luxembourg, S. Stjbrandij, Carl Zeiss Microscopy INVITED

While the ORION Helium Ion Microscope NanoFab has become an ideal high resolution imaging and nanofabrication tool, its analysis capability is currently limited. By contrast, Secondary Ion Mass Spectrometry (SIMS) is an extremely powerful technique for analysing surfaces owing in particular to its excellent sensitivity, high dynamic range, very high mass resolution and ability to differentiate between isotopes. The combination of He/Ne microscopy and SIMS would not just offer the prospect of obtaining SIMS information limited only by the size of the probe-sample interaction (~10 nm) but also of directly correlating such SIMS images with high resolution (0.5 nm) secondary electron images of the same zone taken at the same time. We have therefore investigated the feasibility of combining SIMS with Helium Ion Microscopy from a fundamental and instrumental point of view.

In order to reach good detection limits when probing very small voxels in imaging applications, the ionization probability of the sputtered atoms and molecules needs to be maximized. When using He⁺ and Ne⁺ bombardment, the intrinsic yields are low compared to the ones found in conventional SIMS. However, the yields may be drastically increased by using reactive gas flooding during analysis, namely O₂ flooding for positive secondary ions and Cs flooding for negative secondary ions. Our results show that both negative and positive ion yields obtained with He⁺ and Ne⁺ bombardment may be increased by up to 4 orders of magnitude when using such reactive gas flooding. This optimization of secondary ion yields leads to detection limits varying from 10⁻³ to 10⁻⁶ for a lateral resolution between 10 nm and 100 nm.

The prototype instrument we developed during this feasibility study contains extraction optics allowing the emitted secondary ions to be extracted with a maximized efficiency and without negatively impacting the focusing of the incoming He⁺ or Ne⁺ ion beam (broadening or distortion of the ion beam due to the electric fields). These extraction optics are coupled to a specially designed compact high-performance magnetic sector double focusing mass spectrometer that we developed for the purpose of HIM-SIMS. The specifications of this mass spectrometer include high mass resolution with optimized transmission (M/ΔM > 1000 at 100% transmission or M/ΔM > 3000 at 50% transmission), full mass range (H-U) and parallel detection of several masses.

The results are very encouraging and the prospects of performing SIMS on the Helium Ion Microscope are very interesting. In this paper we will present the main findings of our feasibility study, including fundamental, instrumental and application aspects.

11:40am HI+AS+SS+NS-ThM12 Nanometer TOF-RBS and TOF-SIMS in a Helium/Neon Ion Microscope, Nico Klingner, R. Heller, G. Hlawacek, S. Facsko, J. von Borany, Helmholtz-Zentrum Dresden - Rossendorf, Germany

Helium ion microscopes (HIM) have become powerful imaging devices within the last decade. Their excellent lateral resolution down to 0.3 nm and their high field of depth make them a unique tool in surface imaging [1]. So far the analytical capabilities of a HIM are rather limited or need complex detection setups. In addition we will discuss major challenges and physical limitations of ion beam analysis in the HIM.

We will present a new and relatively easy to implement method for ion beam analysis in the HIM by means of time of flight spectrometry to obtain elemental information from the sample. We will demonstrate the flexibility and applicability of the method to image samples with target mass contrast, to analyze the target compositions, and to measure depth profiles of films with few tens of nm thickness.

Pulsing the primary helium or neon ion beam and measuring the time of flight of ejected particles allows to obtain the energy of the backscattered particles as well as the mass of the ionized, sputtered target atoms. This has been achieved by chopping the primary ion beam down to pulse widths of 18 ns by use of the built-in beam blaster and a customized plug-on beam

blanking electronics. The secondary particles are detected by means of a multi channel plate mounted on a flange of the HIM.

We will show TOF-RBS and TOF-SIMS measurements for different materials, which can give complementary information. Lateral resolved TOF-SIMS allows to quickly obtain qualitative elemental mapping while the TOF-RBS gives the standard-free quantitative sample composition of regions of interest. We will also show, that with TOF-RBS depth profiling of nm-thick layers is possible.

[1] G. Hlawacek, V. Veligura, R. van Gastel, and B. Poelsema, *J. Vac. Sci. Technol. B* 32(2), 2014

12:00pm **HI+AS+SS+NS-ThM13 Improving Pattern Fidelity in Helium Ion Beam Lithography using Pixel Dose Optimization**, *N. Kalthor*, TU Delft, Netherlands, *W. Mulckhuysse*, TNO Technical Sciences, Netherlands, *Paul Alkemade*, TU Delft, Netherlands, *D. Maas*, TNO Technical Sciences, Netherlands

Scanning Helium ion beam lithography (SHIBL) with a sub-nanometer beam probe size at the sample surface is a promising technology for high-resolution lithography with high pattern density.¹ The advantages of SHIBL compared to e-beam lithography are higher sensitivity and a lower proximity effect. Remarkably, there are unique similarities in the activation response of resists to He-ions and extreme-ultraviolet (EUV) photons in EUV lithography (EUVL). Both primary beams produce low energy secondary electrons (SEs) and are not hindered by proximity effect. Recently Maas et al. experimentally demonstrated these similarities and suggested SHIBL as a promising method for pre-screening chemically amplified resists (CARs) prior to their final performance evaluation in an EUV scanner.²

However, unlike an EUV photon which only interacts with one resist molecule, an He-ion scatters inelastically in the resist and causes a chain of collisions with resist molecules, producing one or more SEs per collision. Also, a small dose-to-clear of 0.085 ions/nm² for SHIBL in a CAR was measured.² Hence, Maas et al. hinted at ion shot noise as a limiting factor in pattern fidelity in SHIBL.²

Here, we present a heuristic resist activation model for single-pixel dose SHIBL. The model employs a point-spread function (PSF) to account for all contributing factors in the resist activation. Ion shot noise impact is modeled with Poisson statistics. We show a good agreement between the model and our experimental single-pixel dose SHIBL results for line-and-space (LS) and contact hole patterns. Our model indicates pattern fidelity in sensitive CAR is not only limited by ion shot noise; instability of the He-ion source emission and post-exposure resist processing can also play important roles. Moreover, we introduce optimized-pixel-dose SHIBL to improve critical dimension uniformity (CDU), line width roughness (LWR), exposure latitude and throughput gain. In this approach, we calculate an optimum ion dose map for a given binary pattern such that the pattern's edges are exposed at the steepest part of the PSF to improve resist-pattern contrast and to minimize ion shot noise effect. Pixel dose optimization is advantageous to single-pixel exposure when the feature size is larger than the FWHM of the PSF. We discuss this by comparing our modeling results for single-pixel and optimized-pixel-dose SHIBL exposure modes for a desired LS pattern. We show that pixel-dose optimization could reduce LWR by ~45% (~1.3 nm) with a concurrent 20% dose reduction.

¹V. Sidorkin et al., *J. Vac. Sci. Technol. B* 27, L18 (2009)

²Maas et al., *SPIE Proc.* 9048, 90482Z (2014)

Selective Deposition as an Enabler of Self-Alignment

Focus Topic

Room: 210F - Session SD+AS+EM-ThM

Fundamentals of Selective Deposition

Moderator: Scott Clendenning, Intel Corporation, Suvi Haukka, ASM Microchemistry Ltd., Finland

8:00am **SD+AS+EM-ThM1 Fundamental Examinations of Surface Chemistry-Driven Approaches to Selective Area Atomic Layer Deposition**, *W. Zhang, J.-R. Chen, James Engstrom*, Cornell University

Most approaches taken to date concerning selective area growth have involved the use of masking layers consisting of photoresists or self-assembled monolayers (SAMs). While some success has been achieved with this approach there are a number of disadvantages intrinsic to these methods. First, SAMs are very difficult to form defect free, and second, and perhaps more important, these masking layers themselves must be patterned

or deposited selectively. A second approach to selective area ALD relies on intrinsic reactivity differences between exposed surfaces, which, unfortunately, may be limited to a few special cases. Here we seek to develop a more general approach to achieving selective area growth. We initially focus on the first half-cycle of ALD, where demonstrating selectivity for this part of the ALD process is a necessary, but not sufficient condition for selective area growth. We are examining two specific approaches to the surface chemistry: (i) the use of adsorption reversal agents; and (ii) the use of molecular blocking agents. Here for a thin film precursor we examine transition metal complexes with the generic structure, $M(XR_m)_n$, where M is the transition metal and XR_m is the coordinating ligand. In pursuing strategy (i) we examine the introduction of a second species in the first half-cycle that can act as a coordinating ligand, e.g., HXR'_m , or $HXR'_m \cdot IR''$, etc. In pursuing strategy (ii) species (Y) are selected that can effectively compete for adsorption sites, dependent on the composition of the substrate. Concerning strategy (i) we are currently investigating reactions between transition metal amido compounds and a series of amines ($X = N$). We have found a somewhat unexpected result for this chemistry: the partial pressure of H_2NR' produces similar effects on both a metal (Cu) and a dielectric (SiO_2) surface, where a low partial pressure attenuates the irreversible adsorption of the thin film precursor, while a high partial pressure results in no adsorption of the precursor. An investigation of the reactions between the thin film precursor and a molecular blocking agent with the structure HSR'' , gave much more encouraging results. Here we found complete blockage of chemisorption of the thin film precursor on a Cu surface, whereas on SiO_2 the molecular blocking agent had no effect on the adsorption of the metal for the first half-cycle. We will conclude this presentation with a discussion of the mechanisms that are likely operative in both cases, making use of *in situ* measurements involving X-ray photoelectron spectroscopy, and also initial results concerning the effectiveness of this approach for multiple (5-20) cycles of ALD.

8:20am **SD+AS+EM-ThM2 Mechanistic Understanding of Surface-Selective Chemical Vapor Deposition of Copper Films Using a Molecular Inhibitor**, *Elham Mohimi, S. Babar, B. Trinh, G.S. Girolami, J.R. Abelson*, University of Illinois at Urbana Champaign

Surface-selective chemical vapor deposition of thin films can enable the fabrication of nanoscale devices by eliminating difficult patterning and etching steps. However, stray nucleation of film on the non-growth surface due to defect or impurity sites remains a challenging problem. We previously demonstrated the use of molecular growth inhibitors in copper CVD to control morphology, ranging from a smooth and continuous thin film to particles in a narrow size distribution. Here, we show that an inhibitor can also be used to afford essentially perfect selective growth. Addition of vinyltrimethylsilane (VTMS) molecules during copper CVD from the Cu(hfac)VTMS precursor reduces the growth rate of copper on copper by a factor of four, but reduces the Cu deposition on thermal SiO_2 or porous carbon doped SiO_2 to below one monolayer (area averaged). In-situ FTIR and mass spectroscopy show that the VTMS undergoes associative desorption with adsorbed Cu(hfac) intermediate on the non-growth surface, and is responsible for the surface selective deposition of copper only on the intended (metallic) substrate areas. The processing window for this method is wide in terms of VTMS pressures (> 1 mTorr), growth times (1-90 min), and substrate temperature (100-180°C).

8:40am **SD+AS+EM-ThM3 Selective Deposition of Copper-Manganese Alloy for Interconnects**, *Roy Gordon*, Harvard University **INVITED**

As copper interconnections are made smaller, they fail more easily by electromigration. The dominant pathway for motion of Cu atoms is along the interfaces between Cu and the surrounding insulator surfaces. In current technology, a tantalum nitride diffusion barrier and a Ta or Co adhesion layer are placed between Cu and the insulators. Because these layers are more resistive than Cu, the composite interconnect line has a higher resistance than one that would consist entirely of pure Cu. Here we describe how selective placement of manganese within the insulator surface can provide the necessary stabilization, adhesion and barrier properties for Cu lines without the resistance penalty of TaN/(Ta or Co) layers. After trenches and vias are etched into the insulator, CVD is first used to deposit a thin layer of manganese nitride conformally on all exposed surfaces of the insulator as well as on the Cu exposed at the bottoms of the vias. Then less than a monolayer of iodine is chemisorbed onto the MnN_x from ethyl iodide vapor. Next, this iodine catalyzes selective, bottom-up CVD of Cu-Mn alloy so that it fills even the narrowest trenches and vias without any voids or seams at the centerlines. The iodine "floats" on the growing surface of the Cu, and is finally removed by chemical-mechanical polishing along with the Cu-Mn overburden and the MnN_x on top of the insulator. During subsequent anneals, Mn rapidly diffuses out from the MnN_x and from the Cu-Mn alloy into the near-surface regions of the insulator to form an insulating layer of $MnSi_xO_yN_z$ surrounding the Cu. The necessary Cu

adhesion and barrier properties are provided by this insulating layer of $MnSi_xO_yN_z$ selectively placed just inside the surfaces of the insulators. During anneals, Mn and nitrogen originally located on the Cu surfaces at the bottoms of vias disappear as the Mn and N are re-distributed by diffusion to nearby insulator surfaces. The result is direct, low-resistance connection between Cu in vias with Cu in the metallization level below. This selective migration of Mn leaves pure, low-resistance Cu completely filling the entire volume of trenches and vias, providing the lowest possible line resistance. Thus Mn is placed selectively only where it is required to increase adhesion and lifetime before failure by electromigration, to prevent diffusion of Cu into the insulator and to avoid corrosion of Cu by water or oxygen. The same sequence of process steps can apply Cu to the walls of through-silicon-vias to conduct signals from one chip to another. This process can also form Cu seed layers for electrodeposition of Cu-filled vias for distributing power through silicon chips.

9:20am SD+AS+EM-ThM5 Selective Growth of First Row Transition Metal Films by Atomic Layer Deposition, Charles Winter, Wayne State University **INVITED**

Our laboratory seeks to develop the growth of metallic first row transition metal thin films using atomic layer deposition (ALD). The microelectronics industry is calling for the growth of metallic first row transition metal films by the ALD method for a variety of applications, including copper metallization, seed layers for copper metallization, copper/manganese alloys for self-forming copper diffusion barriers, and magnetic alloys. The ALD growth of noble metal thin films has been explored extensively in the past ten years, due to the positive electrochemical potentials of these metal ions and relative ease of reduction to the metallic state. The low temperature ALD of high purity, low resistivity Cu films has been described, but ALD routes to the other metallic first row transition metal films remain poorly developed, largely because of the negative electrochemical potentials of most of the ions and a corresponding lack of powerful reducing co-reagents that can convert precursors in positive oxidation states to the metals. We will describe the synthesis, structure, and properties of a large series of new first row transition metal ALD precursors containing alkoxide ligands that combine high volatilities, high thermal stabilities, and high reactivities toward reducing agents. We will also report borane reducing agents that can react with the metal precursors to afford metallic films. Additionally, we will overview the thermal growth of metallic copper, nickel, cobalt, iron, manganese, and chromium thin films from these new precursors. Importantly, the growth of these metals is highly selective for noble metal substrates, such as ruthenium, palladium, and platinum. The noble metal substrates appear to activate the borane reducing agents, thus enabling selective metal growth. Chemical insights into the selective growth will be presented.

11:00am SD+AS+EM-ThM10 Etching and Chemical Functionalization of Silicon Nitride Surfaces for Selective Deposition, L.-H. Liu, T. Peixoto, W. Cabrera, D. Dick, J.-F. Veyan, University of Texas at Dallas, D.J. Michalak, R. Hourani, Intel Corporation, M.D. Halls, Schrodinger, Inc., S.P. Pujar, H. Zuithof, Wageningen University, Netherlands, Yves J. Chabal, University of Texas at Dallas

The ability to process silicon nitride and oxide films and chemically functionalize their surfaces by wet chemical methods is critical for selective deposition. The nature of HF-etched silicon nitride surface is complex and somewhat controversial. We have therefore performed an extensive study of HF etching of both Si_3N_4 and SiO_2 surfaces, combining spectroscopic techniques (Infrared absorption, X-ray photoemission, Low energy ion scattering), imaging (atomic force microscopy) and contact angle measurements with first principles calculations, as a function of HF concentration. We have also performed post-treatment in cold and hot water, and chemical functionalization with a range of organic molecules to help determine the chemical nature of the HF-etched surfaces.

The nature of silicon nitride surfaces is complex. We find that immediate rinsing in deionized water after HF wet-chemical etching yields smooth silicon nitride surfaces with clear evidence for Si-F surface termination. Low energy ion scattering experiments and XPS measurement as a function of gentle sputtering with Gas cluster ion beams (GCIB) confirm that the F is all located at the surface (i.e. not distributed into the bulk), and in the form of Si-F with high temperature stability (up to 600 °C in ultra-high vacuum). Hydrolysis in water is very slow at room temperature, but can be achieved at high temperature (~90 % removal at 70 °C for 30 min). However, water is found to etch silicon nitride, as evidenced by a loss of Si_3N_4 phonon absorption, suggesting that the removal of the surface fluorine may not only be due to surface reaction through a direct exchange mechanism via pentavalent Si intermediate, but also to the hydrolyzation of Si_3N_4 itself through back-bond chemical attack by water. In addition to F, we find that there is also surface $-NH_2$ species, as evidenced by IR active $-NH_2$ bending modes at 1550 cm^{-1} , which we estimate to be only ~20 % monolayer from analysis of reaction with aldehyde molecules. However, this coverage

appears sufficient to protect the Si_3N_4 surface. Finally, LEIS and XPS indicate that there is oxygen at the surface, which could either be in the form of $-OH$ or $Si-O-Si$. Functionalization with alkylsiloxanes reveals that ~50 % of the surface contains $Si-OH$. In summary, the sum of the concentrations (50 %, 20 %, 50 % in ML), i.e. exceeding 1 ML, suggests that the etched surface may be atomically rough. Overall, these findings provide a method for selective deposition by using first aldehyde reaction for Si_3N_4 functionalization, followed by silane reaction for SiO_2 functionalization.

11:20am SD+AS+EM-ThM11 Area Selective Deposition of Ultrathin Magnetic Cobalt Films via Atomic Layer Deposition, John Ekerdt, H. Nallan, T. Ngo, S. Chopra, Z. Zhang, University of Texas at Austin

Ferromagnetic thin films find applications in a variety of fields, such as electronics, spintronics, RF technology, energy, etc. With ever-decreasing device feature sizes, film conformity and crystalline structure become very important to determining magnetic properties. As such, atomic layer deposition (ALD) is a very attractive technique for magnetic film deposition as it ensures atomic level conformity. Since ALD film growth necessarily involves a film nucleation step, it is possible to engineer the surface energy of the substrate to cause preferential wetting and nucleation in only desired areas, resulting in area selective ALD (AS-ALD). Unlike conventional photolithography-based fabrication, a bottom-up patterning approach could eliminate the need for etch steps, reducing the cost of fabrication and overcoming scaling limitations in manufacturing devices. This work investigates the selective deposition of cobalt oxide via ALD that is subsequently reduced to carbon-free cobalt metal for use as the free magnetic layer within the magnetic tunnel junction of spin-transfer torque random access memory.

Alkylchlorosilanes and poly(trimethylsilylstyrene) are utilized to block water and cobalt bis(N-tert butyl, N'-ethylpropionamidate) from an oxide substrate, such as silicon dioxide, hafnium dioxide and magnesium oxide, ensuring selective deposition of CoO films. Poly(trimethylsilylstyrene) is the half of a lamellar forming diblock copolymer that remains after self-assembly and feature development. The alkylchlorosilanes can be blanket deposited through the vapor phase or stamped onto the oxide surface using a poly(dimethylsiloxane) stamp. Cobalt oxide ALD proceeds on the exposed oxide surface. Strontium and Al are deposited atop the CoO films to scavenge oxygen during thermal annealing to yield cobalt metal films. Alternatively, reducing gases such as CO and H_2 can be employed as an oxygen sink during thermal reduction of CoO to Co metal. Finally, we demonstrate control over the tunability of the coercivity of the resultant films by controlling the reduction conditions.

11:40am SD+AS+EM-ThM12 Area-Selective Al_2O_3 Pattern Grown by Atomic Layer Deposition, Seunggi Seo, H. Jung, I.K. Oh, H. Kim, Yonsei University, Republic of Korea, J. Yoon, C. Yoo, H.-J. Kim, Y.-B. Lee, LG Display Co., Ltd., Republic of Korea

Over many past years, area-selective atomic layer deposition (AS-ALD) has been developed for fabricating 3D nanostructures. ALD is a method to deposit thin films by self-limiting surface reactions between supplied gaseous precursors. Since ALD is a surface sensitive deposition technique, surface modification of substrate renders the deposition of films to be area-selective. Most previous studies on AS-ALD have utilized self-assembled monolayer (SAM), which inhibits the chemical reaction between substrate and precursors, so that the film cannot grow on SAM-coated area. AS-ALD has been studied on various materials, such as TiO_2 , ZnO, and HfO_2 . Although Al_2O_3 has been widely used for ALD, there is no experimental report on AS-ALD Al_2O_3 by using SAM. Rather, a previous report on the calculation of surface reactions between TMA and SAM by density functional theory (DFT) has been presented[1]. That paper describes that CH₃-terminated SAM shows no thermodynamic driving force for the reaction between them, leading to AS-ALD Al_2O_3 by using TMA.

In this work, we systematically investigated AS-ALD of Al_2O_3 on SAM in various conditions, such as SAM coating methods, the kinds of SAM and substrate, and ALD process parameters. Addressing previous calculation report, Al_2O_3 was deposited on CH_3 -terminated SAM, octadecyltrichlorosilane (ODTS) and octadecylphosphonic acid (ODPA).

However, we observed Al_2O_3 layers were formed on SAM coated SiO_2 and Ti substrate, which is inconsistent with previous report. To clarify, we investigated ALD Al_2O_3 on SAM coated substrate by using various analytic techniques such as contact angle measurement, Fourier transform infrared spectroscopy, ellipsometry, X-ray photoelectron spectroscopy (XPS), X-ray-reflectometry (XRR), and α -scanning. We observed TMA was physisorbed on CH_3 -terminated SAM, leading to Al_2O_3 deposition. Alternatively, we moved to our research toward the change of SAM coating methods, dipping and stamping, to lift both Al_2O_3 and underneath SAM coating off. Since stamping method is a faster process than dipping one, so that SAM by stamping might remain randomly distributed as forming weak

bonding between SAMs and substrate. Moreover, we chose ODPAs as a SAM due to its poor adsorption on SiO₂. We observed that both Al₂O₃ and its underneath ODPAs stamped on SiO₂ were lifted-off from the substrate, resulting in area-selective Al₂O₃ pattern. This result opens a new way to patterning techniques for many areas of technology.

[1] Xu et al./ Chem. Mater. 2004, 16, 646-653

Surface Modification of Materials by Plasmas for Medical Purposes Focus Topic

Room: 211D - Session SM+AS+BI+PS-ThM

Plasma Processing of Biomaterials

Moderator: Deborah O'Connell, University of York, UK,

Satoshi Hamaguchi, Osaka University, Japan

8:00am SM+AS+BI+PS-ThM1 Potential of Low Temperature Plasma Sources in Cancer Treatment, *Jean-Michel Pouvesle*, GREMI CNRS/Université d'Orléans, France, *G. Collet*, CNRS, *E. Robert*, GREMI CNRS/Université d'Orléans, France, *L. Ridou*, CNRS-CBM, France, *S. Dozias*, *T. Darny*, GREMI CNRS/Université d'Orléans, France, *B. El Hafni-Rahbi*, *C. Kieda*, CNRS-CBM, France **INVITED**

The last decade has seen an impressive increase of the research dedicated to the biomedical applications of low temperature Non Thermal Plasmas (lNTP), especially with plasma sources working at atmospheric pressure. Medical applications of lNTP now concern a very wide range of domains including cancer treatment. The antitumor effect of lNTP has been clearly shown *in vivo* on murine models with various cancer types (bladder, colon, glioblastoma, melanoma, ovary, pancreas). Although the involved mechanisms are far from being fully understood, the therapeutic effect is now totally admitted and the first clinical study (head and neck) has been reported [1]. In case of plasma jet experiments, the observed effect are most of the time attributed to the very rich chemistry generated by the interaction of the rare gas plasma plume with the surrounding environment constituted either from the ambient air, or this latter in complex interaction with liquids at the interface with the targeted organ. Our recent experiments performed on tissue oxygenation [2] or breast cancer treatments on immunocompetent mice [3] lead to the conclusion that probably the involved chemistry couldn't, alone, completely allow describing the observed phenomena. This, especially under very soft treatment conditions, is suggesting possible triggering of some immune system chain processes and also possible modifications in the microenvironment of tissue and tumors. In this context, there is still an unknown role of the electric field associated with the ionization front or generated in the environment of the plasma plume tip. Taking into consideration the recent vessel normalization based-cancer treatment, the lNTP effect should be further investigated in view of blood vessels structure and function (blood flow) as well as tumor hypoxia compensation to confirm a possible lNTP-based adjuvant approach for cancer treatments. These results suggest new ways, especially combined therapy, to consider the plasma and its therapeutic delivery in lNTP-based tumor therapy. In this talk, after a presentation of the context and the plasma devices, we will go through the specific case of cancer treatment with what have been already demonstrated *in vitro* and *in vivo*, what can be directly linked with the produced discharges, including recent results on electric field measurements in plasma biological application conditions.

This work is supported by the APR Region Centre PLASMEDNORM.

References:

[1] H.R. Metelmann *et al* Clin. Plas Med. Doi.org/10.1016/j.cpme.2015.02.001

[2] G. Collet *et al* PSST **23** (2014) 012005

[3] G. Collet *et al* ICPM5, May 18-23, 2014, Nara (Japan)

8:40am SM+AS+BI+PS-ThM3 Plasma Polymerized Polypyrrole Thin Films and Their Use in Drug Release Control, *C. Li*, National Yang Ming University, Taiwan, Republic of China, *Yung Te Lee*, National Central University, Taiwan, Republic of China, *J.H. Hsieh*, Ming Chi University of Technology, Taiwan, Republic of China

Polypyrrole thin films were deposited using a plasma polymerization process. During deposition, power input (between 30W to 70W), monomer (pyrrole) flow rate (30 sccm to 50 sccm), and Ar flow rate were varied. Optical emission spectroscopy (OES) was used to study the plasma characteristics under each deposition condition. After deposition, these films were characterized using FTIR, AFM, ellipsometry, ultraviolet-visible (UV-vis) spectroscopy, and surface profilometer. Eventually, these films were applied to control drug release rate under different thickness and

structure. The results were correlated with the process parameters and plasma conditions.

9:00am SM+AS+BI+PS-ThM4 Thin Film Metallic Glass: A Novel Coating for Various Biomedical Applications, *Chia-Chi Yu*, *Y. Tanatsugu*, *S. Chyntara*, *C.M. Lee*, *W. Diyatmika*, *J.P. Chu*, National Taiwan University of Science and Technology, Taiwan, Republic of China, *M.J. Chen*, *S.H. Chang*, *W.C. Huang*, Mackay Memorial Hospital Tamsui Campus, Taiwan, Republic of China

Thin film metallic glasses (TFMGs) exhibit unique properties such as high strength, smooth surface as well as good wear- and corrosion-resistances due to their amorphous atomic structure. The biocompatibility and antibacterial property of TFMGs can also be obtained, which show great potential for biomedical applications. In addition, the low surface free energy of TFMGs in certain compositions can be achieved and leads to the relatively high hydrophobicity and the low friction coefficient.

In this presentation, various applications of TFMG are discussed, including the property enhancements of dermatome blade and syringe needle, thrombosis reduction for intravenous catheter, and the suppression of cancer cell attachments. A Zr-based TFMG is coated on substrates by using magnetron sputtering. The TFMG-coated dermatome blade show a great enhancement of durability and sharpness, compared with those of the bare one. For the syringe needle, significant reductions in insertion and retraction forces for TFMG-coated needle are achieved due to the non-sticky property and relatively low coefficient of friction. For thrombosis reduction, less platelet aggregations are observed on the TFMG than that on the bare glass in platelets adhesion test, suggesting TFMG-coated catheters is potentially useful to be placed into vessels for long periods of time with reduced numbers of the aggregation of blood platelets. For cancer cell attachment suppressions, TFMG exhibits the least cancer cell attachment among other control groups. Thus, anti-proliferation and anti-metastasis of medical tools can be achieved with TFMG coating.

9:20am SM+AS+BI+PS-ThM5 Plasma Surface Functionalization of Nano-structured Materials for Biomedical Applications, *Masaaki Nagatsu*, *H. Chou*, *A. Viswan*, *T. Abuzairi*, *M. Okada*, *M.A. Ciolan*, Shizuoka University, Japan, *N.R. Poespawati*, *R.W. Purnamaningsih*, University of Indonesia, *A. Sakudo*, University of the Ryukyus, Japan, *S. Bhattacharjee*, Indian Institute of Technology, Kanpur, India **INVITED**

In this study, we will present the recent experimental results on plasma surface functionalization of nano-structured materials for bio-medical applications.

First, with the graphite-encapsulated magnetic nanoparticles (MNPs), we studied the surface functionalization by using the Ar plasma pre-treatment followed by NH₃ plasma post-treatment, to introduce the amino groups onto the surface of the nanoparticles.¹⁾ The amino group population of each nanoparticle with a typical diameter of 20 nm was evaluated by using the conventional chemical technique using SPDP and DTT solutions and we obtained about 8 x 10⁴ amino groups per nanoparticle.²⁾ Immobilization of the antibody of influenza virus onto the surface of amino-modulated magnetic nanoparticles was then performed for aiming at studying the feasibility of collection and condensation of virus. After magnetic separation, we succeeded in a significant concentration of the influenza virus number compared with that of the initial sample.³⁾ Using the same method, we also demonstrated a higher concentration of Salmonella about 70 times higher than that of initial sample by the magnetic separation.⁴⁾ The present results suggest the feasibility of the proposed plasma surface functionalized MNPs for rapid concentration of influenza virus or various bacteria.

As the second topic, the selective ultrafine surface modification of functional groups onto the polymeric substrate or vertically aligned CNT dot-array with a dot size of several μm was investigated using the atmospheric pressure plasma jet with a nano/micro-sized capillary. The micro-sized surface modification of amino or carboxyl groups introduced onto the CNT dot-array were confirmed by the fluorescence labelling technique.⁵⁾ With fluorescence-labeled avidin molecules, we also confirmed efficient capturing of avidin molecules by the biotin-immobilized CNT dot array through strong biotin-avidin binding process. The present result supports the feasibility of future biochip sensor to detect specific protein, virus or bacteria. In addition to these results, the other experimental results will be presented and discussed at the conference.

References

1) T. E. Saraswati, A. Ogino, M. Nagatsu, Carbon, 50 (2012) pp.1253-1261.

2) T. E. Saraswati, S. Tsumura, and M. Nagatsu, Jpn. J. Appl. Phys. 53 (2014) 010205(5 pages).

3) A. Sakudo, H. Chou, K. Ikuta, and M. Nagatsu, Bioorg. Med. Chem. Lett. 25 (2015) pp.1876-1879.

4) A. Sakudo, H. Chou, and M. Nagatsu, *Bioorg. Med. Chem. Lett.*, 25 (2015) pp. 1012-1016

5) T. Abuzairi, M. Okada, Y. Mochizuki, N. R. Poespawati, R. Wigajatri and M. Nagatsu, *Carbon*, 89 (2015) pp. 208-216.

11:00am **SM+AS+BI+PS-ThM10 Tailoring Biomaterials-cell Interaction through Reactive Surface Modification, Salvador Borros**, Institut Quimic de Sarrià, Ramon Llull University, Barcelona, Spain
INVITED

The immobilization of biologically active species is crucial for the fabrication of smart bioactive surfaces. For this purpose, plasma polymerization is frequently used to modify the surface nature without affecting the bulk properties of the material. Thus, it is possible to create materials with surface functional groups that can promote the anchoring of all kinds of biomolecules. Different methodologies in protein immobilization have been developed in recent years, although some drawbacks are still not solved, such as the difficulties that some procedures involve and/or the denaturalization of the protein due to the immobilization process. However, along with the chemical signals, the mechanical forces are critical for many tissues, since they are constantly suffering tension, shear, loading, etc. Essentially, the cell signaling exerted by forces is transduced through receptors that are in intimate contact with the matrix. Therefore, the main consequence of this receptor-matrix interaction is that cells and matrix are mechanically coupled, so that matrix deformation is considered the main cause of the mechanical signaling. By mimicking these mechanical forces in the surface of a material, it would be possible to obtain more physiological environments and thus a more physiological cell response. Again, the use of plasma polymerization techniques can help to design surfaces that can be tailored in terms of mechanical properties and chemical compositions and thus have a high potential for cells signaling.

This paper reports the work that we have developed in the last 10 years in the design, synthesis and characterization of thin films that can be a platform for studying the interaction between cells and separate influences of physical and chemical cues of a matrix on the adhesion, growth and final phenotype of cells.

11:40am **SM+AS+BI+PS-ThM12 Analysis of Amino Group Formation on Polystyrene Surfaces by Nitrogen-Hydrogen-Based Plasma Irradiation, Kensaku Goto, D. Itsuki, M. Isobe, S. Sugimoto, S. Miyamoto, A. Myoui, H. Yoshikawa, S. Hamaguchi**, Osaka University, Japan

Polystyrene is a widely used cell-culture plate material. Currently cell culture plates on the market include those whose inner surfaces are covered with amino and/or carbonyl groups for a better control of cell adhesion to the plate surfaces. Such functional groups on a cell culture plate surface may immobilize glycoproteins or other biopolymers that function as extracellular matrices (ECM) and thus affect the environments where the cells are cultured. The goal of this research is to understand how such functional groups, especially amino groups, are formed on a polystyrene surface, depending on the deposition methods. Of particular interest are plasma-based methods of surface functionalization. In this study, we have observed experimentally how exposure of N_2/H_2 or N_2/CH_3OH plasmas to polystyrene surfaces form amino-group-like structures and also examined using molecular dynamics (MD) simulation how a polystyrene surface interacts with incident energetic ions such as NH_3^+ as well as abundant low-energy radicals such as NH_2 under conditions similar to our experiments. In the experiments, we used parallel-plate discharges with an inverter power supply whose peak-to-peak voltage was about 3kV and frequency was 20kHz at a relatively high gas pressure of 250 - 2,500 Pa. In MD simulation, we used a simulation code with interatomic potential functions that had been developed in-house based on quantum mechanical calculations of atomic interactions involved in this system. Results of MD simulations under the conditions similar to plasma enhanced chemical vapor deposition (PE-CVD) by ammonia plasmas or cyclopropylamine (CPA) [1] suggest that, with energetic ion bombardment, amino groups tend to be broken to form new covalent bonds by ion bombardment. Preliminary results of cell culture experiments with plasma-treated polystyrene cell plates will be also reported.

[1] A. Manakhov, L. Zajickova, *et al.* *Plasma Process. Polym.* 11, (2014) 532.

12:00pm **SM+AS+BI+PS-ThM13 Tailoring the Surface Properties of Three-Dimensional, Porous Polymeric Constructs for Biomedical Applications Using Plasma Processing, Morgan Hawker, A. Pegalajar-Jurado, E.R. Fisher**, Colorado State University

Utilizing bioresorbable polymers to fabricate constructs with three-dimensional (3D), porous architectures is desirable as these constructs mimic the extracellular matrix—a critical characteristic for many biomedical applications including tissue engineering, controlled-release drug delivery, and wound healing. Although the bioresorbability and architecture of these

materials are suitable for such applications, the surface properties (i.e., chemical functionality and wettability) must often be customized depending on the desired function. Plasma processing is an attractive tool for surface modification of these delicate polymeric materials as it provides a low-temperature, sterile environment with a variety of precursor choices. The presented work will highlight the plasma modification of a variety of 3D, porous polymeric constructs. Specifically, we fabricated scaffolds via electrospinning and porogen leaching techniques using both poly(ϵ -caprolactone) (PCL) and polylactic acid (PLA) to develop a repertoire of native polymer constructs with differing bulk properties. We evaluated the efficacy of plasma-modifying 3D constructs using contact angle goniometry, X-ray photoelectron spectroscopy, and scanning electron microscopy to assess changes in wettability, chemical functionality, and scaffold architecture. The interactions of plasma-modified scaffolds with different biological species, including human dermal fibroblasts and *Escherichia coli* were explored, specifically to assess scaffold bioactivity. Notably, we demonstrate that scaffold properties, and thus bioactivity, can be customized depending on the choice of plasma precursor. We show that plasma treatment using fluorocarbon and hydrocarbon precursors (i.e., octofluoropropane, hexafluoropropylene oxide, and 1,7-octadiene) results in hydrophobic and bio-non reactive scaffolds. Additionally, precursors with nitrogen and oxygen functionality (i.e., allylamine, allyl alcohol, water, and ammonia) can be used to fabricate scaffolds that are hydrophilic and bio-reactive. Altogether, this work illustrates the comprehensive tunability of biologically-relevant polymeric constructs in terms of their bulk properties, surface properties, and cell-surface interactions.

Scanning Probe Microscopy Focus Topic
Room: 212A - Session SP+AS+NS+SS-ThM

Probing Chemical Reactions at the Nanoscale

Moderator: Stephen Nonnenmann, University of Massachusetts - Amherst, Shengyong Qin, University of Science and Technology of China

8:40am **SP+AS+NS+SS-ThM3 Adsorption of Trimethyl Acetic Acid on (1x2) Reconstructed $TiO_2(110)$, Kenneth Park, K. Zhu, Y. Xia, Z. Zhang**, Baylor University

The adsorption of trimethyl acetic acid on (1x2) reconstructed $TiO_2(110)$ is investigated using scanning tunneling microscopy (STM) with the same area analysis. After de-protonation, trimethyl acetate (TMA) molecules preferentially adsorb in the troughs between two adjacent 1x2 strands. The nearest neighbor distance between TMA molecules is about 5.9 Å, twice the lattice constant along [001], corresponding to the bridging bidentate configuration over two 5-coordinated Ti^{4+} sites. With increasing coverage, they form linear chains, separated by (1x2) strands leading up to the nominal saturation coverage of 0.25 ML. Upon further adsorption, the second-layer of TMA molecules start clustering on top of 1x2 strands. The coverage-dependent TMA adsorption structures on (1x2) reconstructed $TiO_2(110)$ will be compared and discussed with the reported TMA adsorption on (1x1) $TiO_2(110)$, and relative reactivity of TMA with other defect sites including cross-links will be presented.

9:00am **SP+AS+NS+SS-ThM4 Anticorrelation between Surface and Subsurface Point-Defects and Influence on Redox Chemistry at $TiO_2(110)$, Igor Lyubinetzky, Y. Yoon, Y. Du**, Pacific Northwest National Laboratory, J.C. Garcia, Worcester Polytechnic Institute, Z. Zhu, Z.-T. Wang, N.G. Petrik, G.A. Kimmel, Z. Dohnalek, M.A. Henderson, R. Rousseau, Pacific Northwest National Laboratory, N.A. Deskins, Worcester Polytechnic Institute

The atoms at the surface that constitute reactive sites clearly govern surface chemistry. But subsurface atoms, particularly substitutional and/or interstitial defects, can also influence surface chemistry, though a detailed understanding is still emerging. Here we report the interplay and relative impact of surface vs. subsurface defects on the surface chemistry of rutile TiO_2 , a prototypical metal oxide. Importantly, it contains both surface and subsurface intrinsic point-defects in the reduced state (along with residual extrinsic defects). Our scanning tunneling microscopy results show that O vacancies (V_O 's), the dominant surface defects, are virtually absent in the vicinity of positively-charged subsurface point-defects. Such anticorrelation of defects is consistent with density functional theory (DFT) calculations of the impact of subsurface defect proximity on V_O formation energy, which narrows down the possible candidates to certain interstitial defects, of both intrinsic and extrinsic nature. To monitor the influence of such (electron-donor type) defects on surface redox chemistry, a test reaction of the electron-mediated dissociative adsorption of O_2 is employed, which is observed to be suppressed around these defects. DFT results attribute this to

a perceived absence of the intrinsic (Ti) (and likely extrinsic) interstitials in the nearest subsurface layer beneath “inhibited” areas, while the underlying energetic driver is largely repulsive electrostatics. Finally, we postulate that the entire subsurface region up to several atomic layers deep could be voided of any charged point-defects, whereas such defects are proposed to exist beyond the subsurface region. Subsequently, prevalent V_O 's are largely responsible for both the surface/subsurface reduction and mediation of the redox chemistry at reduced $TiO_2(110)$ surface. Overall, this work provides new fundamental insights into the relation between surface and subsurface defects. In a broader perspective, the uncovered effects may prove to be general for other reducible oxides, and thus have potential implications in such diverse research fields as environmental remediation or microelectronics.

9:20am SP+AS+NS+SS-ThM5 Dissociation of Water on Oxygen Pre-Covered Cu(110) Observed with Scanning Tunneling Microscopy, Zongqiang Pang, Lawrence Berkeley National Laboratory (LBNL)

The dissociation of water on the oxygen pre-covered Cu(110) surface has been studied with Scanning Tunneling Microscopy (STM). At low temperature (77K), water reacts with pre-covered oxygen to produce hydrogen atoms and hydroxyl groups. Non-dissociated water molecules and hydroxyl groups combine to form a hexagonal network on the top of Cu(110) where water donates one hydrogen to the hydroxyl, while uncoordinated hydroxyls bind to the second layer intact water molecules. Following excitation by tunneling electron or by heat, the water molecules in the hexagonal network gradually dissociate. The oxygen atoms involved in the reaction of water dissociation return to its original position, leaving ordered Cu-O and hydroxyl dimer chains on the Cu(110) surface which both align along $\langle 001 \rangle$ direction. Our results demonstrate that the oxygen atoms pre-adsorbed on the Cu(110) surface lower the energy barrier for water dissociation on the Cu(110) surface.

9:40am SP+AS+NS+SS-ThM6 Probing Local Electrochemical Activity within Yttria-Stabilized-Zirconia via In Situ High-Temperature Atomic Force Microscopy, Jiaxin Zhu, University of Massachusetts - Amherst, C. Perez, T. Oh, R. Kungas, J. Vohs, D. Bonnell, University of Pennsylvania, S.S. Nonnenmann, University of Massachusetts - Amherst

Considerable interest in understanding interfacial phenomena occurring across nanostructured solid oxide fuel cell (SOFC) membrane electrode assemblies has increased demand for *in situ* characterization techniques with higher resolution. We briefly outline recent advancements in atomic force microscopy (AFM) instrumentation and sub-systems in realizing real time imaging at high temperatures and ambient pressures, and the use of these *in situ*, multi-stimuli probes in collecting local information related to physical and fundamental processes. Here we demonstrate direct probing of local surface potential gradients related to the ionic conductivity of yttria-stabilized zirconia (YSZ) within symmetric SOFCs under intermediate operating temperatures (500 °C – 600 °C) via variable temperature scanning surface potential microscopy (VT-SSPM). The conductivity values obtained at different temperatures are then used to estimate the activation energy. These locally collected conductivity and activation energy values are subsequently compared to macroscopic electrochemical impedance results and bulk literature values, thus supporting the validity of the approach.

Surface Science

Room: 113 - Session SS+AS+EM+EN-ThM

Semiconductor Surfaces and Interfaces - I

Moderator: Yves J. Chabal, University of Texas at Dallas

8:00am SS+AS+EM+EN-ThM1 Reaction of 1,2,3-Benzenetriol with the Ge(100)-2x1 Surface, Tania Sandoval, S.F. Bent, Stanford University
Functionalization of semiconductor surfaces can provide tunable control of interfacial properties in organic-inorganic hybrid devices. In particular, multifunctional molecules have the potential to change the surface chemistry by leaving unreacted functional groups available after adsorption. Understanding the adsorption of these complex molecules could lead to various applications as sensors, selective film deposition, and molecular electronics.

In this work, the reaction of 1,2,3-benzenetriol on Ge(100)-2x1 surface was investigated. While the reaction of hydroxyl groups has been previously studied, differences in selectivity can be expected due to the position of the functional groups along the ring. The purpose of this study is to determine the extent of these differences and the effect on product distribution.

An analysis of the adsorption energetics was carried out by density functional theory. As expected, a proton transfer reaction was shown to be

the most stable adsorbate configuration. However, after the adsorbate reacts with the surface through its first OH group, the energetics of the second OH dissociation showed differences based on two factors: (i) surface configuration (cross or diagonal trench and end or cross bridge) and more interestingly (ii) which two of the OH groups (1 and 2 or 1 and 3) are reacting with Ge. The latter constraint affects the adsorption energy of the second dissociation, where adsorption regardless of the surface configuration is less stable when the OH groups are next to each other. Finally, transition states for dissociation of the third OH were found to be limited by the configuration of the second dissociation, and in some cases were not possible to find without unrealistic distortions of the molecule.

Chemisorbed and physisorbed O(1s) and C(1s) spectra were obtained by X-ray photoelectron spectra. Differences between these spectra can be used to identify the reaction products. No change in the C(1s) spectra was observed, suggesting that no carbon forms a bond directly with the Ge surface. On the other hand, clear differences between the chemisorbed and physisorbed O(1s) spectra are observed. The presence of a second peak with a lower binding energy only in the chemisorbed spectra, assigned to oxygen bonded to Ge, confirms that 1,2,3-benzenetriol reacts with the Ge surface through OH dissociation. Quantitative analysis of the chemisorbed O(1s) spectra provides information on the fraction of OH groups reacting with the surface. Interestingly, about 66% of the total hydroxyl groups in 1,2,3-benzenetriol are involved in reaction with Ge, indicating that there is a significant fraction of unreacted OH groups.

8:20am SS+AS+EM+EN-ThM2 Ethylenediamine Grafting on Oxide-free H-, F-, and Cl- terminated Si(111) Surfaces, Tattiana P. Chopra*, R.C. Longo, K.J. Cho, University of Texas at Dallas, M.D. Halls, Schrodinger, Inc., P. Thissen, Karlsruhe Institute of Technology, Germany, Y.J. Chabal, University of Texas at Dallas

Amine termination of surfaces constitutes a core platform for fields as diverse as microelectronics and bioengineering, and for nanotechnology in general. Diamines are particularly attractive for surface amination because, unlike ammonia or simple amine molecules, they have a metal chelating capability useful in fabricating heterostructures. They can act as a linker molecule between inorganic electronic materials and biomolecules or photoactive quantum dots for applications in microelectronic, photonics and biosensing. Most work in the field utilizes self-assembled monolayers (SAMs) on oxidized substrates to present an amine termination of the surface. However, grafting on oxides through silanes or phosphonates is not robust. Moreover, several applications require as short a distance between the substrate and the amine group, which is hindered by the thickness of the oxide. Therefore, diamine grafting directly on oxide-free substrates is important, yet remains unexplored.

In this work, the attachment of liquid and vapor-phase ethylenediamine on three types of oxide-free (H-, F- and Cl-terminated) Si(111) surfaces is examined by infrared absorption spectroscopy and X-ray photoelectron spectroscopy in conjunction with first-principles calculations. We find that chemisorption is only possible on F- and Cl-terminated Si surfaces, with H-terminated Si surfaces yielding only physisorbed diamine molecules. On Cl-terminated Si surfaces, diamines adsorb in a mixture of monodentate and bridging configurations (chemical reaction of both amine endgroups), while on partially F-terminated Si surfaces the adsorption occurs primarily at one end of the molecule. The reaction of ethylenediamine with Cl-terminated Si surfaces is also characterized by complete removal of Cl and partial Si-H (~25% ML) formation on the surface. This unexpected result suggests that a proton-chlorine exchange may take place, with the endothermic barrier possibly reduced via a silicon lattice assisted process after an initial attachment of ethylenediamine to the surface.

8:40am SS+AS+EM+EN-ThM3 Reaction of Phenylhydrazine with Cl-Si(111) Surface by Wet Chemistry and with Clean Silicon Surface in UHV, A.V. Tephyakov, Fei Gao, University of Delaware

The monolayer coatings with aromatic functional groups can be used to tune mechanical, electronic, and chemical properties of semiconductor surfaces. This work focuses on obtaining well-defined surface of silicon functionalized with phenylhydrazine to produce an oxygen-free platform for further functionalization. Single crystalline Si(111) surface has been prepared using modified RCA procedure to produce well-ordered H-Si(111) surface. Next, Cl-terminated Si(111) surface is prepared from H-terminated Si(111) surface using PCl_5 in chlorobenzene solvent with trace amount of benzoyl peroxide as a reaction initiator under nitrogen atmosphere following previously established procedures. Phenylhydrazine-functionalized Si(111) sample is obtained from Cl-Si(111) surface with phenylhydrazine at 38°C under N_2 atmosphere. To confirm the presence of Si-N bonds following this procedure, establish the structures of surface species produced and to investigate the oxidation mechanism, we followed

*** Morton S. Traum Award Finalist**

the reaction by Fourier-transform infrared spectroscopy, X-ray photoelectron spectroscopy, and time-of-flight secondary ion mass spectrometry. To study the formation of Si-NH_x groups, this result was compared with the results of phenylhydrazine reactions on clean silicon surface under ultra-high vacuum (UHV) conditions. Density functional theory (DFT) calculations were performed to infer the mechanisms of surface reactions and further oxidation steps, and to compare the predicted vibrational spectra and core-level energies with the results of experimental studies.

9:00am **SS+AS+EM+EN-ThM4 Anomalously Low Surface Recombination Velocity for Fluorine Terminated Nanopatterned Si Surfaces**, *W.N. Peng, Jonghan Park, L.-H. Liu, R.C. Longo, University of Texas at Dallas, D.J. Michalak, Intel Corporation, D.M. Pak, Y.J. Lee, J.X. Hsu, K.J. Cho, Y.J. Chabal*, University of Texas at Dallas

Recently, oxide-free and partially methoxy-terminated Si surfaces¹ have been developed as a novel platform for surface reactions because of their superior reactivity compared to hydrogen termination². As a result, strong polar bonds such as Si-F could be stabilized on these surfaces. Since the electrical quality is critical for many applications (i.e. surface defects can degrade the device performance), we performed contactless surface recombination velocity measurements to examine the electronic quality of partially covered surfaces. Interestingly, we found that the carrier lifetime is significantly increased after fluorine termination, with the carrier lifetime 10 times higher than that of hydrogen terminated Si surfaces, approaching 1.5 ms. This anomalously long carrier lifetime can be explained either by a better surface passivation or by surface band bending effects. We therefore performed UPS and kelvin probe measurements to investigate the band structure of these surfaces after fluorine termination and found evidence for band bending. A potential model of a surface dipole layer induced band bending is supported by DFT calculations. Regardless of the mechanism controlling the recombination time, this method is well suited to explore the fluorination mechanism of H-terminated surfaces.

[1] D. Michalak, S. Amy, D. Aureau, M. Dai, A. Esteve, and Y. J. Chabal, *Nature Materials*, **9**, (2010)

[2] P. Thissen, T. Peixoto, R. Longo, W. Peng, W. Schmidt, K. Cho, and Y.J. Chabal, *JACS*, **134** (2012)

9:20am **SS+AS+EM+EN-ThM5 Molecular Functionalization of Semiconductor Surfaces: From Single Crystals to Quantum Dots**, *Stacey Bent*, Stanford University

Because the surfaces of small structures can dominate their properties, implementing functional nanoscale materials depends to a large extent upon understanding and controlling the surface reactivity. This talk will focus on studies of the adsorption of organic molecules at semiconductor surfaces, toward the ultimate goal of controlling the chemical and electrical properties of the substrate. We will describe model studies of molecular functionalization on both flat and nanostructured surfaces. The presentation will begin by examining adsorption on the Ge(100)-2×1 surface. Using a combination of experimental (infrared spectroscopy, X-ray photoelectron spectroscopy) and theoretical (density functional theory calculation, Monte Carlo simulation) methods, we will show how the molecular structure as well as the identity of the reactive moieties of organic molecules can affect the product distribution upon adsorption. We will then present results of a study in which the organic ligands bonded to semiconductor quantum dots (QDs) are used to tune the electronic properties of the QDs. We will describe experimental and theoretical studies of the effects of such interface engineering on the band gap and relative band positions in lead sulfide (PbS) QDs. These ligand-exchanged quantum dots are tested in multilayer colloidal QD solar cells, and the results show that molecular functionalization can be used to achieve enhanced photogenerated carrier collection in the devices.

11:00am **SS+AS+EM+EN-ThM10 Periodic Trends in the Hydrogen Elimination Thermal Decomposition Reaction on Si(100)-2×1: Linear and Branched Alkyl Halides, Alcohols, and Amines**, *Andrew Pohlman, K.L. Romolino, N.J. Burgener, S.M. Casey*, University of Nevada

The hydrogen elimination thermal decomposition reaction was studied on the Si(100)-2×1 surface using temperature programmed desorption mass spectrometry (TPDMS) and electronic structure methods for a selection of linear and branched alkyl halides, alcohols, and primary amines. Desorption activation energies and pre-exponential factors were determined using several analysis techniques from TPDMS spectra and compared to calculations based on ab initio canonical transition state theory using density functional theory (DFT). Values for activation energies and pre-exponential factors for dissociative desorption are compared within an adsorbate class based on a varying ratio of available alpha:beta:gamma hydrogens for elimination. Kinetic parameters are also compared between classes of adsorbates for general structure-activity periodic trends. TPDMS

experiments reveal desorbing masses consistent with hydrogen elimination in all cases; however, the different elimination channels remain convoluted. Rate constants for each desorption channel were calculated using DFT and used to determine branching ratios for each dissociative desorption reaction. Reaction barrier trends are consistent with previous reports; however, numerical values were found to be much lower when considering inter-dimer reaction mechanisms.

11:20am **SS+AS+EM+EN-ThM11 Diffusion of Arsenic Oxides During the Atomic Layer Deposition of Metal Oxide Films on GaAs(100) Surfaces**, *Alex Henegar, T. Gougousi*, University of Maryland, Baltimore County

It is known that native oxides of III-V semiconductors are consumed during atomic layer deposition using certain subsets of precursors. It was believed these surface oxides were completely removed during the first few deposition cycles because once the surface was covered by a coalesced film the native oxides would be protected. It has been observed, however, that native oxide consumption in systems such as ALD TiO₂ on GaAs(100) and InAs(100) proceeds continuously well after the surface is completely covered. Therefore there must be a transport mechanism that continuously moves these oxides through the developing film in order to interact with the precursor at the surface and be removed.

The aim of this work was to find unequivocal evidence of the transport mechanism needed for continuous oxide removal during ALD at typical processing conditions. ALD processes using metal organics and H₂O were used to deposit TiO₂, Al₂O₃ and HfO₂ films on GaAs(100). The experiments were designed so as to decouple the native oxide consumption from the native oxide transport and provide convincing evidence for the existence of this unacknowledged thus far mechanism. We will provide results that solidify the hypothesis that native oxide diffusion is a critical component in the complete and continuous removal of the interfacial layer.

11:40am **SS+AS+EM+EN-ThM12 Ultrafast Non-Equilibrium Effects in Ti Overlayers on P-Type GaAs(100) Investigated by Femtosecond XUV Photoemission Spectroscopy**, *Mihai E. Vaida*, University of California, Berkeley, *S.R. Leone*, University of California, Berkeley and Lawrence Berkeley National Laboratory

Time resolution, surface sensitivity and element specificity are technical ingredients required to investigate ultrafast photoinduced processes and charge localization at semiconductor surfaces. All these requirements are fulfilled by a new experimental apparatus that consists of a tunable femtosecond high harmonics XUV source, a pump-probe setup, and an ultra-high vacuum surface science chamber for surface preparation and investigation.

The present contribution focuses on the charge carrier dynamics at the surface of a bare p-type GaAs(100) as well as Ti overlayers on p-type GaAs(100). The charge transfer between the bulk and the surface of the bare GaAs(100) is produced by the pump laser pulse at the central wavelength of 800 nm and is investigated by monitoring the surface photovoltage through the shift of the Ga 3d photoemission peak with the XUV probe laser pulse as a function of the pump-probe time delay. A transient shift of the Ga 3d photoemission peak to lower binding energy at early pump-probe time delay, with a magnitude of 0.3 eV, is observed and is attributed to transport of the electrons from the bulk to the surface. Upon increasing the pump-probe time delay, a restoration of the Ga 3d peak is observed, which corresponds to the recombination of the positive and negative carriers.

When a Ti overlayer is deposited on the p-type GaAs(100) surface, a Schottky diode is formed. If the 800 nm pump laser pulse has sufficient intensity to produce a photoemission process via multi-photon excitation, non-equilibrium effects occur at the Ti-GaAs interface independently from the presence of the surface photovoltage. In this case, positive charges accumulate at the surface and are not effectively screened by the electrons coming from the bulk, and the Schottky diode is transiently driven into a reversed bias mode. The formation of the reverse bias Schottky diode, which is studied in real time with the XUV probe laser pulse by monitoring the Ti Fermi level photoemission shift as a function of the pump-probe time delay will be presented and discussed.

12:00pm **SS+AS+EM+EN-ThM13 Improving the Quality of p-type AlGaN Layers by Reactive-ion Etching**, *Joy McNamara, K.L. Phumisithikul, A.A. Baski, M.A. Reshchikov*, Virginia Commonwealth University, *J. Marini, F. Shahedipour-Sandvik*, SUNY Polytechnic Institute
AlGaN layers prepared by metal-organic chemical vapor deposition, with varying composition of Al (6 – 17%), were studied using the surface photovoltage (SPV) technique. Previous SPV studies on both *n* and *p*-type GaN allowed us to calculate the value of the surface band bending, by applying a thermionic model to explain the transfer of charges over the near surface barrier in various conditions (air, vacuum, and for a wide range of

temperatures, $T = 80 - 600$ K). [1,2] The band bending was estimated to be 1.0 eV and -2.0 eV, for n -type GaN and p -type GaN, respectively. SPV measurements on p -type AlGaIn layers were expected to have similar behaviors to their p -type GaN counterparts. However, numerous measurements showed that this was not the case. The SPV transients (upon turning on or off the excitation source) showed significantly slower transients and smaller values than expected from the thermionic model. Moreover, the restoration of the band bending, as indicated by the restoration of the SPV signal to its dark value, did not occur within a reasonable amount of time. The data could not be fit by the thermionic model, and thus we were unable to calculate the band bending. We attribute the slow transients and lack of restoration to a defective surface region which interferes with thermionic processes. To verify this assumption, the top 40 nm of the AlGaIn layer was etched using a reactive-ion etch (RIE). After etching, the SPV behavior exhibited substantially different behavior. Fast transients and close-to-thermionic behavior was recovered. Additionally, the effect of annealing the samples after etching provided even closer values to what is predicted by the thermionic model. From this study, it can be concluded that a defective, near surface region is inhibiting the transfer of holes over the near surface barrier under illumination, and hole trapping may be occurring during restoration. In both cases, this behavior cannot be modeled by theory. Etching removes the defective layer, and reveals a surface of presumably higher quality as evidenced by the subsequent thermionic behavior.

[1] M. A. Reshchikov, M. Foussekis, and A. A. Baski. *J. Appl. Phys.* **107**, 113535 (2010).

[2] M. Foussekis, J. D. McNamara, A. A. Baski, and M. A. Reshchikov, *Appl. Phys. Lett.* **101**, 082104 (2012).

Thin Film

Room: 111 - Session TF+AS+NS+SA-ThM

Thin Film: Growth and Characterization, Optical and Synchrotron Characterization I

Moderator: Divine Kumah, North Carolina State University

8:00am **TF+AS+NS+SA-ThM1 Oxynitride Thin Films by Reactive Radiofrequency Magnetron Sputtering - Versatile Materials for Optical Applications**, *Angelique Bousquet, A. Farhaoui, F. Zoubian, C. Taviot-Gueho, J. Cellier, E. Tomasella*, Institut de Chimie de Clermont-Ferrand, France

INVITED

Transition metal oxynitrides are increasingly studied because of their high versatility. Indeed, by tailoring the material composition, their optical, mechanical or electrical properties are tuned. Among thin film deposition processes, reactive sputtering is particularly attractive for this purpose because of its robustness, its wide use in industry and its high versatility. For several years, our research group at ICCF is specialized in control of reactive sputtering process, especially by plasma analysis using Optical Emission Spectroscopy, to deposit thin films for optical applications.

In this presentation, we will show how by tuning the Ar/O₂/N₂ atmosphere during sputtering of elemental target, it is possible to control the film composition in a ternary diagram in metal-rich, oxide, nitride or oxynitride region. The potentiality of this technique will be illustrated by tantalum and silicon oxynitride deposition.

In order to investigate the nature of oxynitride films (Random Bond Model or Random Mixture Model), thin films were characterized by various techniques, such as IR spectroscopy, XPS, XRD/Pair Distribution Function technique and Rutherford Backscattering Spectroscopy. Hence, we obtained an accurate picture of the diversity and the complexity of our material, following the Random Mixture Model, where segregated oxide and nitride phases are randomly distributed at very short scale.

Moreover, the modification of material composition allows controlling their optical properties, characterized by UV-visible spectroscopy and spectroscopic ellipsometry. This latter technique appears as a powerful technique to discriminate metallic, semiconductor and/or insulator contributions into such complex films by using model combining Tauc-Lorentz law and additional Lorentz oscillator. Hence, in a one hand, optical band gap of TaO_xN_y can be changed from 0-4.3 eV. This E_g fine-tuning more particularly in the range of 1.7-2.7 eV is interesting for application in photocatalytic water splitting using visible light. In the other hand, the refractive index variation in the 1.56-3.7 range (at 1.96 eV) of Si_xO_yN_z films is used to realized antireflective multilayer system from only one target. Finally, oxynitride films present promising properties for applications in material for Energy.

8:40am **TF+AS+NS+SA-ThM3 Surface Science in The Wild: Using Synchrotron Radiation and Lab Grown Thin Films to Understand The Behavior Of SiC in Accident Tolerant Nuclear Fuels**, *Jeffery Terry*, Illinois Institute of Technology

INVITED

Out in the "real world," systems are typically much less clean and much more complex than what is seen in the laboratory. This is often the case in the extreme environment of the core of a nuclear reactors. However, complexity often makes it very difficult to understand the dynamics that are occurring in the "real world" systems. Often our understanding can be greatly improved by using measurements on the "real world" system in combination with fundamental surface science measurements on likely components. We have applied these combinations to study the behavior of irradiated accident tolerant nuclear fuels. Development of new accident tolerant nuclear fuels is important because the explosions at Fukushima were the direct result of interactions between water and the Zr cladding on the fuel. The high temperature chemistry of those interactions led to the production of hydrogen gas which eventually ignited. Our research group has looked at potential claddings such as ZrC, ZrN, and SiC. Specifically, we are using synchrotron radiation techniques to collect data on reactor irradiated materials. We compare the results of those measurements with well controlled laboratory grown systems. The data is then provided to modelers to evaluate the performance of reactor components in extreme environments (temperature, neutron flux, chemistry). This talk will focus on the carbides and nitrides that may be used in accident tolerant, TRISO fuel pellets for application in both conventional and advanced nuclear reactors.

9:20am **TF+AS+NS+SA-ThM5 iTF Modulus Solution with xProbe Applications for Ultra-thin Film Systems (<=10nm)**, *Anqi Qiu, A. Romano*, Hysitron, Inc.

Reliable measurements of the Elastic Modulus of thin films is particularly challenging due to substrate effect. The prevalent rule of limiting indentation depth to 10% of the coating thickness to avoid the substrate's influence on the mechanical properties is challenging to assure, especially when the film thickness goes below 200nm. The tip radius can be one of the many factors limiting the application of Oliver-Pharr model on the elastic modulus calculation, just as the surface roughness. With the newly developed ultra-low noise xProbe transducer combined with the **Intrinsic Thin Film Property Solution from Hysitron**, quantitative mechanical properties from nanoindentation tests on 10nm thin film systems become possible. Here a MEMS based transducer with a noise floor similar to that of a contact mode Atomic Force Microscope (AFM). The linear actuation allows for direct and fully quantitative measurements without the need of modeling, which leads to more precise mechanical properties estimation and higher analysis throughput. By combining the ultra-low noise xProbe transducer and analytical intrinsic thin film solution (Itf), we quantitatively estimate elastic properties of the ultra-thin film systems of 10nm or below.

9:40am **TF+AS+NS+SA-ThM6 Real-time Study of Plasma Enhanced Atomic Layer Epitaxy of InN Films by Synchrotron X-ray Methods**, *Neeraj Nepal, V. Anderson, S.D. Johnson, B. Downey, D. Meyer*, U.S. Naval Research Laboratory, *A. DeMasi, K.F. Ludwig*, Boston University, *C. Eddy*, U.S. Naval Research Laboratory

Atomic layer epitaxy (ALE) is a layer-by-layer materials growth method. Recently, plasma enhanced ALE (PA-ALE) has been used to grow epitaxial III-nitride films at temperatures $\leq 500^\circ\text{C}$ [1-2]. At these growth temperatures, the ad-atom mobility is low and the growth process is significantly influenced by the nature of the substrate surface. Thus, the mechanisms of nucleation and growth kinetics is very important to understand to improve material quality for technological applications. Synchrotron x-ray characterization is one of the best methods for this study.

The temporal evolution of high quality InN growth on a-plane sapphire at 200-250°C were probed by synchrotron x-rays. The growth was carried out in a thin film growth facility installed at beamline X21 of the National Synchrotron Light Source at Brookhaven National Laboratory and at Cornell High Energy Synchrotron Source, Cornell University. Real-time grazing incidence small angle x-ray scattering (GISAXS) measurements at the x-ray incidence angle of 0.8 degrees show that H₂ plasma cleaning roughens the sapphire substrate surface, but this same surface is recovered completely during subsequent N₂ plasma pretreatment. GISAXS also reveals InN growth steps for each PA-ALE cycle at the optimal growth conditions. During the initial cycles the specular peak broadens and the Yoneda Wing (YW) scattering has a correlated length scale (CLS) of 17.4 nm indicating roughening of the surface during homogenous nucleation. At about 1.3 nm of growth the intensity of YW is increased at the CLS of 10.1 nm indicating a decrease in the surface roughening CLS. Despite this scattering, *ex situ* atomic force microscopy-measured roughness is below instrument sensitivity limits, demonstrating the effectiveness of GISAXS compared to more conventional approaches. *In situ* x-ray reflectivity measurements suggest that the InN growth was self-limited with a growth rate of 0.35 nm/cycle between 200-250°C. Hall measurements show

electron sheet carrier density and resistance of $3.5 \times 10^{13} \text{ cm}^{-2}$ and $3.59 \text{ k}\Omega/\text{sq}$, respectively. An electron mobility of $50 \text{ cm}^2/\text{V}\cdot\text{s}$ is measured for a 5.6 nm thick InN film on a-plane sapphire, which is higher than the reported value of $30 \text{ cm}^2/\text{V}\cdot\text{s}$ for a 1300 nm thick InN grown by MBE directly on sapphire [3]. *In situ* synchrotron x-ray study of the epitaxial growth kinetics of InN films is one of the most powerful methods to understand nucleation and growth mechanisms to improve material quality and broaden material applications.

References:

- [1] Nepal et al., *Cryst. Growth and Des.* **13**, 1485 (2013).
- [2] Nepal et al., *Appl. Phys. Lett.* **103**, 082110 (2013).
- [3] Kuo et al., *Diamond & Related Materials* **20**, 1188 (2011).

11:00am **TF+AS+NS+SA-ThM10 Nucleation and Growth of Few-Layer ALD Films on Various Substrates Studied by Low Energy Ion Scattering (LEIS).** *Malcolm Hathaway*, Harvard University, *T. Grehl*, *P. Bruener*, ION-TOF GmbH, Germany, *M. Fartmann*, Tascon GmbH, Germany, *H. Brongersma*, ION-TOF GmbH, Germany

Atomic Layer Deposition has found applications in many semiconductor processes due to its several unique characteristics, including high purity, conformality, pin-hole-free character, and atomic level thickness controllability. It is these last two characteristics which are of particular interest in this present work. The thickness control of ALD films is precise down to the angstrom level, even when depositing layers as thin as a few atomic layers. Ideally, in layers only a few angstroms thick, the ALD process produces material which is completely continuous and free of pin-holes. One of the challenges of characterizing ALD processes is the difficulty of directly measuring such thin films and confirming their continuous nature.

Low Energy Ion Scattering (LEIS) spectroscopy is uniquely suited to exploring these questions, due to its extreme surface sensitivity, easy quantification and its ability to yield additional information about the sub-surface composition. Using LEIS, analytical questions like layer closure, surface composition, diffusion processes, or growth modes can be addressed. In this work, we explore the limits of this technique to characterize few-layer ALD films on a variety of substrates, to confirm the capabilities of LEIS in this arena, and to shed new light on the nature of few-layer ALD films.

In the LEIS process, a noble gas ion beam of (1 -10 keV) is directed at the sample, and the fraction of backscattered ions is measured as a function of kinetic energy. Two main mechanisms determine the spectral response: Firstly, scattering in the first monolayer of atoms creates elemental peaks, allowing quantitative determination of the elemental composition of the outermost atomic layer. The intensity of these peaks is directly proportional to the surface coverage. Secondly, scattering processes below the surface (with the ion penetrating the surface, scattering at deeper layers and returning to the surface before leaving it) provide information about sub-surface layers, sometimes as deep as 10 nm , in a non-destructive way. As the additional energy loss is proportional to penetration depth, these data can be evaluated to determine the layer sequence, layer composition and layer thickness in a single measurement and in addition to the top layer composition.

In this study a number of oxide films (e. g. HfO_2 , Al_2O_3) on Si and other substrates like glassy carbon are evaluated. We apply LEIS among other techniques to characterize the films, especially in the early phases of film growth. Using the unique information from LEIS, conclusions on the nucleation behavior and growth are drawn.

11:20am **TF+AS+NS+SA-ThM11 $\text{Ni}_{1-x}\text{Pt}_x\text{Si}$ Film Characterization for sub-32 nm CMOS Fabrication.** *Suraj Patil*, *R. Rai*, *S. Beasor*, *L. Zhou*, GLOBALFOUNDRIES, NY, USA

Aggressive scaling of CMOS devices demands silicide engineering for high performance in the sub-32nm technology node and beyond. Ni-silicide can satisfy many of the integration challenges but it is limited by morphological stability at elevated temperatures. On the other hand, incorporating Pt into Ni-silicide forms a more robust nickel platinum silicide ($\text{Ni}_{1-x}\text{Pt}_x\text{Si}$) and improves morphological stability. Advantages of Pt incorporation include extension of the temperature range over which the NiSi exists, delay in the agglomeration of NiSi phase, suppression of the high resistive NiSi_2 phase formation and retardation of the Ni diffusion at the interface and grain boundaries which could lead to encroachment or piping. This work discusses three important aspects of $\text{Ni}_{1-x}\text{Pt}_x\text{Si}$ formation: (1) understanding NiPt diffusion with two step RTA anneals – formation (RTA1) and transition (RTA2), which is very important for thickness uniformity across structures with varying CDs, encroachment control, device performance and yield; (2) understanding NiSi phase formation for thermal stability, and (3) understanding Pt distribution in the final film with low RTA1 temperatures. For this study $\text{Ni}_{1-x}\text{Pt}_x\text{Si}$ samples were fabricated from a simple n-

$\text{Si}/\text{Ni}_{0.85}\text{Pt}_{0.15}/\text{TiN}$ stacks, annealed at range of RTA1 temperatures from RTA-20°C to RTA+30°C for 20s followed by a standard RTA2 anneal for 30s. Characterization of final $\text{Ni}_{1-x}\text{Pt}_x\text{Si}$ films obtained at different RTAs based on XRD phase identification and XPS analysis will be presented. Pt distribution in the final silicide films will be discussed.

11:40am **TF+AS+NS+SA-ThM12 Growth of β -Tungsten Films Towards a Giant Spin Hall Effect Logic Device.** *Ayaya Narasimham*, University at Albany-SUNY, *R.J. Matyi*, State University of New York, *A. Green*, University at Albany-SUNY, *A.C. Diebold*, *V. LaBella*, State University of New York

Spin-orbit coupling in metastable β -W generates spin transfer torques strong enough to flip magnetic moment of an adjacent magnetic layer. In a MTJ stack these torques can be used to switch between high and low resistive states. This technique can be used in designing efficient magnetic memory and non-volatile spin logic devices. Deposition conditions selective to β -W need to be understood for the large scale fabrication of such devices. The transition from β to α phase of Tungsten is strongly governed by thickness of W layer, base pressure and oxygen availability for example, above 5 nm β film relaxes and forms an α phase. Resistivity measurements as well as x-ray photoelectron spectroscopy and x-ray diffraction and reflectivity analysis are performed to determine the phase and thickness of tungsten films. We show that β phase is influenced by ultrathin thermal oxide of Si layer and the amount of oxygen flow during the growth. These results demonstrate a reliable technique to fabricate β -W films up to 20 nm on bare Si and silicon dioxide, while providing insight to growing it anywhere in the device stack.

12:00pm **TF+AS+NS+SA-ThM13 Aluminum Nitride Grown by Atomic Layer Epitaxy Characterized with Real-Time Grazing Incidence Small Angle X-ray Scattering.** *Virginia Anderson*, *N. Nepal*, *S.D. Johnson*, US Naval Research Laboratory, *A. DeMasi*, Boston University, *J.K. Hite*, US Naval Research Laboratory, *K.F. Ludwig*, Boston University, *C.R. Eddy, Jr.*, US Naval Research Laboratory

Aluminum nitride, gallium nitride, and indium nitride have desirable qualities for many semiconductor applications, and have recently been studied intensely.¹ Because of their direct, tunable band gaps and capacity for high current density they are attractive for photovoltaics and high power transistors. The current methods of depositing high-quality III-nitride films, are metalorganic chemical vapor deposition (MOCVD) and molecular beam epitaxy (MBE). The temperatures for the depositions make ternaries challenging. Indium nitride, for example, is difficult to mix with aluminum nitride, as typical MOCVD temperatures for AlN and for InN are 1000°C and 450°C respectively. Aluminum nitride deposition with atomic layer epitaxy (ALE) is currently being explored by some groups as a fabrication friendly technique for thin films at lower temperatures.²

Crystalline AlN deposited with plasma assisted ALE (PA-ALE) in a Fiji reactor from Ultratech/Cambridge Nanotech at 500°C currently has lower material purity than the AlN deposited by MBE and MOCVD, and understanding the film deposition mechanism in order to improve quality is the subject of ongoing research.³ There is a need for a better understanding about the film evolution during nucleation. Grazing incidence small angle x-ray scattering (GISAXS) is sensitive to changing surface features and can be conducted at a wide range of pressures, making it useful for real time monitoring of deposition.⁴

AlN deposited by PA-ALE was grown using trimethylaluminum and hydrogen/nitrogen plasma pulses in a custom reactor at the Brookhaven National Synchrotron Light Source and the Cornell High Energy Synchrotron Source. In both instances, GISAXS was used to examine surface changes during the deposition.

GISAXS information collected during AlN growth at nominally 400°C , 450°C , and 500°C suggested that temperature influenced nucleation, with changes in roughening behavior observed. Post-growth examination of the AlN films with x-ray photoelectron spectroscopy and atomic force microscopy gave important information on the final film elemental composition and morphology. The GISAXS data also show that the surface continued to evolve during the cooling after growth completion while still in the reactor. This information only adds to the necessity of *in situ* growth monitoring to fully understand the mechanisms involved in the ALE growth process.

References:

- ¹ M. Mori et al., *Appl. Phys. Express* **5** 082301 (2012)
- ² M. Bosund et al., *Appl. Surf. Sci.* **17** 7827 (2011)
- ³ N. Nepal et al., *Appl. Phys. Lett.* **103** 0 82110 (2013)
- ⁴ K. Devloo-Casier et al., *Appl Phys. Lett.* **98** 231905 (2011)

Thursday Afternoon, October 22, 2015

Applied Surface Science

Room: 212D - Session AS+SS-ThA

Advances in 2D Chemical Mapping and Data Analysis

Moderator: Kathryn Lloyd, DuPont Corporate Center for Analytical Sciences, Svitlana Pylypenko, Colorado School of Mines

2:20pm **AS+SS-ThA1 ASSD 30th Anniversary Lecture: Why Do (or Don't) People use Chemical State XPS Imaging?**, *Julia Fulghum, K. Artyushkova*, University of New Mexico, *A. Barlow, P. Cumpson*, Newcastle University, UK **INVITED**

XPS imaging can be used to acquire chemical-state specific information with a spatial resolution of several microns. In response to perceived user interest, instrument manufacturers have put significant resources into developing chemical state XPS imaging and image processing capabilities. Current instrumentation allows for parallel image acquisition over a range of photoelectron energies, resulting in quantitative, lateral surface chemistry determinations. Although publications citing XPS continue to increase, XPS imaging contributes to only a small percentage of published work.

In this talk, we'll present an overview of laboratory XPS imaging capabilities using a variety of examples to demonstrate the practical (and not-so-practical) experiments that are possible. Recent multivariate and multitechnique analysis applications, including Multivariate Auger Feature Imaging (MAFI) and XPS-Raman image correlation will be used to highlight current research utilizing XPS imaging. Results from a survey of instrument manufacturers, directors of XPS user facilities, and expert users will be presented, including speculation as to why the use of XPS imaging has not met expectations, recommendations for using XPS imaging and hopes for future developments.

3:00pm **AS+SS-ThA3 X-ray Photoelectron Spectromicroscopy: Combining Spectral and Spatial Information for Materials Characterization**, *Adam Roberts*, Kratos Analytical Limited, UK, *N. Fairley*, Casa Software Ltd, UK, *J.R. Mora*, University of Durham, UK

X-ray photoelectron spectroscopy is widely used in determining surface chemistry of materials. Improvements in instrument sensitivity mean that spectra are routinely acquired from areas with diameters in the tens of microns, although most routine analysis is performed at much larger areas. The assumption is that the material and spectra are homogeneous over the area probed is often made although it may not be true. Information of the lateral distribution of elemental and chemical states on a surface can be probed using XPS imaging either at a single binding (kinetic) energy or over a narrow energy range corresponding to a core-level photoemission peak.

Multispectral XPS imaging, also referred to as spectromicroscopy, where a series of images incremented in energy such that each pixel contains a spectrum, is relatively new and under exploited for surface characterisation. An advantage of spectromicroscopy is that spectral information can be reconstructed from defined areas which are smaller than those possible with focused x-ray or virtual probe selected area XPS. This means that the reconstructed spectra are no longer averaged over the total area from which the image is acquired such that both sample and instrument dependent differences can be studied.

The 256 x 256 pixel multi-spectral image contains >65,500 spectra which is ideally suited to multivariate analysis. Development of data processing to support spectromicroscopy data reduction has been necessary and a number of approaches have been successfully applied in the characterisation of model and real-world samples[1-3]. Multivariate analysis can be used to classify regions of interest across the field of view and data can be partitioned such that chemical state, changes in peak position and background shape can be investigated. Here we detail the use of spectromicroscopy for the characterisation of complex materials including functionalised multiwall carbon nanotubes (MWCNT). This approach has allowed the considerable challenges of surface analysis of such materials to be addressed and has allowed the influence of signal from the substrate material to be removed from the MWCNT of interest.

References

[1] E.F. Smith, D. Briggs and N. Fairley Surf. Interface Anal. 2005, **38**, 69-75

[2] J. Walton, N. Fairley Surf. Interface Anal. 2008, **40**, 478 - 481

[3] A.J. Barlow, O. Scott, N. Sano and P.J. Cumpson Surf. Interface Anal. 2015, **47**, 173-175

3:20pm **AS+SS-ThA4 Optimizing XPS Imaging Acquisition**, *Jon Treacy, C. Deeks, P. Mack, T.S. Nunney*, Thermo Fisher Scientific, UK

Surface structure and chemistry are properties that are crucial to the successful production and operation of numerous devices, materials and coatings. X-ray photoelectron spectroscopy (XPS) is an ideal tool for investigating these properties due to its inherent surface sensitivity, and ability to quantify the chemical states detected.

Whilst XPS is most often used for point analysis and/or depth profiling, it is also able to produce compositional maps of multi-phase materials. This is of particular use in scenarios where other surface science techniques are unsuitable, for example especially rough surfaces that cannot be imaged using SPM or surfaces with multiple phases of similar elemental composition, which cannot be differentiated by SEM-EDS. However the widespread implementation of XPS as a mapping tool has been hindered by the long acquisition times required.

Here we shall present the effects of increased x-ray performance, increased spectrometer sensitivity and modifications in data processing, i.e. both instrumental and software improvements, on the required acquisition time for XPS mapping. This is demonstrated using data from several samples, where multi-phase maps were acquired up to an order of magnitude more quickly than previously possible through implementation of these improvements.

4:00pm **AS+SS-ThA6 Enhancing Chemical Contrast: Latest Trends in Hyperspectral Image Analysis**, *Barry Wise, W. Windig*, Eigenvector Research, Inc. **INVITED**

Many analytical techniques that were originally developed as single sample methods have been adapted to produce multivariate aka hyperspectral images where each pixel contains an entire spectrum. These imaging techniques are used to produce "chemical maps" which elucidate the arrangement and chemical makeup of areas on the surface. Imaging techniques produce an avalanche of data which is often underutilized. Multivariate statistical methods are increasingly being used to capture the information in these large data sets, condense it down to a manageable level, and improve the signal to noise ratio. This serves to enhance the chemical contrast in the images. This talk surveys methods for hyperspectral image analysis, discusses their pros and cons, and gives some examples demonstrating what can be accomplished. Methods considered include Principal Components Analysis (PCA), Multivariate Curve Resolution (MCR) with contrast constraints, Independent Components Analysis (ICA), Maximal Autocorrelation Factors (MAF) and sample clustering techniques.

4:40pm **AS+SS-ThA8 Unambiguous Molecular Identification with TOF-SIMS Imaging MS/MS**, *G.L. Fisher, J.S. Hammond*, Physical Electronics USA, *R.M.A. Heeren*, Maastricht University, The Netherlands, *Scott Bryan*, Physical Electronics USA

First results from a new tandem imaging mass spectrometer will be presented. The unique TOF-TOF design allows the simultaneous collection of standard TOF-SIMS spectra and collision induced dissociation (CID) spectra of specifically selected precursors [1]. This new analytical capability maximizes the information content from a single acquisition and provides all data from the same analytical volume. The ability to acquire MS/MS data at the same primary ion beam repetition rate as used in conventional TOF-SIMS allows high speed image acquisition. The ability to unambiguously identify and image peaks above m/z 200 was applied to polymer additives and to the study of lipid composition changes in mouse spleen specimens infected with *F. novicida*.

[1] P.E. Larson, J.S. Hammond, R.M.A. Heeren and G.L. Fisher, Method and Apparatus to Provide Parallel Acquisition of MS/MS Data, U.S. Patent 20150090874, 02 April 2015.

5:00pm **AS+SS-ThA9 Utilizing Chemical State Mapping to Reveal Spatially Distributed Dynamics in Model Nanostructured Battery Electrodes**, *Alexander Pearse**, *E. Gillette, S.B. Lee, G.W. Rubloff*, University of Maryland, College Park

The rate at which a battery can deliver energy is ultimately dominated by the ability or inability to effectively transport both ions and electrons throughout the electrodes. When charge transport is a limiting factor, material utilization within the battery becomes spatially inhomogeneous, reducing performance. Additionally, the material and architectural requirements for optimizing transport for both ions and electrons are not

* ASSD Student Award Finalist

always synergistic, which can lead to design challenges. The effects of architecture on device performance are generally characterized by externally measured scalar quantities, such as cell potential or current, but these quantities do not reveal where within the electrode any problem may lie. There is a growing need to develop models which can accurately predict spatially resolved dynamics within battery electrodes, as well as experimental techniques to verify them, particularly as nanoscience produces more and more sophisticated electrode designs.

Here we show that chemical state mapping with X-ray photoelectron spectroscopy (XPS) is a powerful tool for revealing transport-limit-induced dynamics within battery electrodes, and connect surface science with electrochemical modeling. We examine the specific problem of facile ion transport but limited electronic transport, which often occurs in high aspect ratio electrodes made of low conductivity semiconductors or insulators. While characterizing complex structures using XPS is normally very challenging, it is possible to gain much more useful and accurate information when a model device is designed from the ground up to exploit the strengths of XPS. By fabricating battery chips in which the anticipated gradients of material utilization (i.e. the spatially varying amount of lithium intercalated) are laid out laterally on a flat substrate, we can clearly map chemical changes in the electrode as a function of distance from a current collector. By using transition metal oxide (M_xO_y) cathode materials, we are able to track the state of charge through local quantification of the reaction $M^{n+} + e^- \rightarrow M^{(n-1)+}$. Our data clearly reveal that as the applied current density increases, ion insertion activity is dramatically contracted towards the current collector, which leads to performance limitations at high rates. Importantly, we also use our spatially resolved data to validate the predictions of a sophisticated finite element multiphysics battery model. The visualization and understanding of design induced performance limits, as well as the validation of a predictive model, allow us to optimize the design of future high performance nanostructured battery electrodes.

5:20pm AS+SS-ThA10 Microstructural and Chemical Mapping of Discharged Hybrid CF_x-SVO Cathodes from Primary Li Batteries, D. Reifsnnyder Hickey, University of Minnesota, Jeffrey Fenton, K. Chen, P. Yurek, J. Lesser, G. Jain, Medtronic plc

Primary lithium batteries with hybrid carbon monofluoride-silver vanadium oxide (CF_x-SVO) cathodes have become widely commercialized as power sources in implantable medical devices. Although CF_x and SVO have been used separately as cathode materials, CF_x-SVO hybrid cathodes have been developed to meet the increased energy-density, power, and longevity requirements specific to multiyear operation at physiological temperature. However, the microstructural basis for the performance characteristics has not been well understood, including chemical changes in the cathode materials as they discharge. This work presents a microstructural study of discharged cathode materials, aimed at identifying chemical and structural characteristics that can be related to the observed battery-performance characteristics. As a result, the relationships established can be used to improve the performance of future medical device technologies. Scanning electron microscopy with energy dispersive spectroscopy, X-ray photoelectron spectroscopy, and X-ray diffraction were used to probe the cathodes chemistry and structure. Although a single analytical method cannot give a full picture of the cathode chemistry and microstructure, the combination of these complementary techniques makes it possible to develop a clearer picture of the structural and chemical changes that occur within the cathode as the battery discharges. The discharged cathodes of SVO, CF_x, and SVO-CF_x hybrid are compared, which demonstrates that the relatively gradual transformation of SVO that occurs in SVO-only cathodes is accelerated in the hybrid cathodes. Several trends will be shown including: (1) SVO loses its crystalline structure and silver content (replaced by lithium) with discharge; (2) CF_x converts into carbon and LiF with discharge; (3) and the hybrid cathodes show steady conversion of CF_x, accelerated conversion of SVO (as soon as 5% depth of discharge), and the beginning of LiF formation (as early as 10% depth of discharge).

5:40pm AS+SS-ThA11 A Novel Test Sample for the Spatially Resolved Quantification of Illicit Drugs on Fingerprints using Imaging Mass Spectrometry, Shin Muramoto, T.P. Forbes, NIST, A.C. van Asten, Netherlands Forensic Institute, G. Gillen, NIST

A novel test sample for the spatially resolved quantification of illicit drugs on the surface of a fingerprint using time-of-flight secondary ion mass spectrometry (ToF-SIMS) and desorption electrospray ionization mass spectrometry (DESI-MS) was demonstrated. Calibration curves relating the signal intensity to the amount of drug deposited on the surface was generated from inkjet-printed arrays of cocaine, methamphetamine, and heroin with a deposited-mass ranging nominally from 10 pg to 50 ng per spot. These curves were used to construct concentration maps that visualized the spatial distribution of the drugs on top of a fingerprint, as well as being able to quantify the amount of drugs in a given area within the map. For the drugs on the fingerprint on silicon, ToF-SIMS showed great

success as it was able to generate concentration maps of all three drugs. On the fingerprint on paper, only the concentration map of cocaine could be constructed using ToF-SIMS and DESI-MS as the signals of methamphetamine and heroin were completely suppressed by matrix and substrate effects. Spatially resolved quantification of illicit drugs using imaging mass spectrometry is possible, but the choice of substrates could significantly affect the results.

Spectroscopic Ellipsometry Focus Topic Room: 112 - Session EL+AS+BI+EM-ThA

Optical Characterization of Nanostructures and Metamaterials

Moderator: Bernard Drevillon, LPICM-CNRS, Ecole Polytechnique, France, Mathias Schubert, University of Nebraska - Lincoln

2:20pm EL+AS+BI+EM-ThA1 Electrostatic Coating with Ligandless Copper Nanoparticles, Lance Hubbard, A.J. Muscat, University of Arizona

Electroless deposition (ELD) produces conformal coatings at low temperatures. ELD occurs by chemical reduction of metal ions without an externally applied potential or catalyst layer. In this paper, we report on a nonaqueous ELD process that uses a charge compensator, but not a ligand or complexing agent. The weak electrostatic attachment of the charge compensator to the ions and particles in solution and the high pH conditions improve the driving force for metal deposition. Si(100) native oxide was hydroxylated and terminated with a self-assembled amine layer (4 mM (3-aminopropyl)-trimethoxysilane in methanol). Metal films were deposited by suspending samples in a bath made by dissolving Cu(II) chloride in ethylene glycol (reducing agent), and adding 1-butyl-3-methylimidazolium tetrafluoroborate as a charge compensator. The Cu particle ion shell is attracted to the positively charged amine groups at high pH depositing a thin metal film that is both continuous and cohesive. Annealing the coupons at 200°C in nitrogen promoted electrically conductive film formation. Electron microscopy images of the coated substrates showed a 80-95 nm thick film of 3 nm diameter particles. Four-point probe measurements of the films yielded electrical conductivities in the range 10^6 - 10^7 S/m (10-80% of bulk conductivity). The surface plasmon resonance (SPR) peak of the Cu nanoparticles in the bath and film was at 585 nm. Light scattering measurements and transmission electron microscopy (TEM) images yielded a size distribution of 3.1 ± 1.56 nm. Scanning electron microscopy (SEM) images at various angles in relation to the films were taken to examine film morphology and thickness. Spectroscopic ellipsometry (SE) data were modelled with bulk, nanophase d-band transition, and SPR absorbances. The SE agreed well with UV-VIS results for the SPR and shows an increasing contribution from d-band transitions with increasing ionic liquid concentration. SEM and Fourier transform infrared (FTIR) spectroscopy were used to determine film thicknesses and chemistry.

2:40pm EL+AS+BI+EM-ThA2 Using Plasmonic Effects to Design Ellipsometric Targets with Sub-Angstrom Resolution, Samuel O'Mullane, SUNY Polytechnic Institute, J. Race, N. Keller, Nanometrics, A.C. Diebold, SUNY Polytechnic Institute

For traditional ellipsometric targets, slightly changing the thickness of a layer or the index of refraction of a material results in a similarly small change in the observed spectra. If structures are designed to allow for plasmonic coupling, a slight change in those same parameters results in wildly different spectra. Specifically, localized plasmonic resonances in metallic grating structures allow for extraordinary sensitivity to parameters such as CD, sidewall angle and pitch.

Existing metallic grating structures are arrays of long, thin lines of copper that can be described using one dimension. The typical resolution for ellipsometric CD measurements on these structures ranges from nanometers to Ångströms. Because there is no confining second dimension, localized plasmons cannot be produced.

In order to obtain sub-Ångström resolution, additional structural modifications are required. This is achieved by adding a second metallic grating perpendicular to the original grating forming a cross-grating structure. Note that the added pitch and linewidth are an order of magnitude larger than the original parameters. This results in fully localized plasmonic resonances so that parameter variation on the order of tens of picometers could be detected through ellipsometric measurements. Making use of conical diffraction further increases the sensitivity to structural changes due to increased anisotropy.

These conclusions are the result of rigorous coupled wave-analysis (RCWA) simulations which were confirmed via finite element method (FEM) simulations. With both RCWA and FEM agreement, experimental confirmation is expected.

3:00pm **EL+AS+BI+EM-ThA3 Enhanced Temperature Stability of Slanted Columnar Thin Films by ALD Overcoating.** *Alyssa Mock, D. Sekora, T. Hofmann, E. Schubert, M. Schubert*, University of Nebraska - Lincoln

The demand for thermally stable nanostructures continues to increase as nanotechnology becomes ever more prevalent in both commercial and research applications. The high surface area of nanostructured thin films is susceptible to degradation under extreme temperatures. Scanning electron microscopy (SEM) and Mueller Matrix Generalized Ellipsometry (MMGE) were used to observe optical and structural properties of a glancing angle deposited cobalt slanted columnar thin film (SCTF) over increased annealing temperature. We show that the use of atomic layer deposition (ALD) to conformally passivate the SCTF surface provides both physical scaffolding and thermal protection during the annealing process up to 475°C as no changes in the SEM or MMGE results were present.

3:20pm **EL+AS+BI+EM-ThA4 Vector Magneto-Optical Generalized Ellipsometry on Heat Treated Sculptured Thin Films: A Study of the Effects of Al₂O₃ Passivation Coatings on Magneto-Optical Properties.** *Chad Briley, A. Mock*, University of Nebraska-Lincoln, *D. Schmidt*, National University of Singapore, *T. Hofmann, E. Schubert, M. Schubert*, University of Nebraska-Lincoln

We present the vector magneto-optical generalized ellipsometric (VMOGE) response¹ and model dielectric function (MDF) anisotropic hysteresis calculations² of ferromagnetic slanted columnar thin films under the effects of heat treatment up to 475°C. Directional hysteresis magnetization scans were performed with an octu-pole vector magnet at room temperature on Cobalt slanted columnar thin film samples grown by glancing angle deposition with and without Al₂O₃ conformal passivation overcoating done by atomic layer deposition. Analysis of the measured Mueller matrix ellipsometric data through a point-by-point best match model process determine the magneto-optical (MO) dielectric tensor. Three dimensional rendering of the anti-symmetric off-diagonal elements of the MO dielectric tensor displays anisotropic magnetic response of the thin film with the hard axis along the long axis of the columns. Data analysis reveals the preservation of anisotropic magneto-optical properties of the thin film with the passivated coating as compared to the non-passivated coating due to oxidation effects from heat treatment.

¹ D. Schmidt, C. Briley, E. Schubert, and M. Schubert, *Appl. Phys. Lett.* **102**, 123109 (2013).

² C. Briley, D. Schmidt, T. Hofmann, E. Schubert, and M. Schubert, *Appl. Phys. Lett.* **106**, 133104 (2015).

4:00pm **EL+AS+BI+EM-ThA6 Spectroscopic Ellipsometry for Critical Dimensions Analysis.** *Vimal Kamini*, GLOBALFOUNDRIES, *D. Dixit, S. O'Mullane*, SUNY Polytechnic Institute, *G. Iddawela, A. Vaid*, GLOBALFOUNDRIES, *A.C. Diebold*, SUNY Polytechnic Institute

INVITED

In this talk an overview of the current applications of spectroscopic ellipsometry (SE) towards measuring the shape of nanostructures will be presented. The transition of the semiconductor industry from planar to 3D transistors has expanded the applications of ellipsometry. Ellipsometry measurements on the periodic nanoscale structures enable a diffraction based measurement technique referred to as scatterometry. The critical dimensions can be extracted by means of a regression on the diffracted light using rigorous coupled wave analysis (RCWA). RCWA is a Fourier-space method used to generate the optical response by slicing the periodic structure of interest and matching the boundary conditions to compute EM modes. This method is inherently dependent on *a priori* knowledge of the dielectric function of the materials that construct the nanostructures as well as the shape of the nanostructure obtained from reference metrology. Furthermore, time-to-solution is one of the main drawbacks of developing scatterometry applications due to the dependency on developing a robust model and for validating the model with reference metrology measurement. To address these challenges new methods such as signal response metrology (SRM) encompassing machine-based statistical learning and virtual reference metrology have been proposed. [1,2] These methods will be reviewed along with their benefits and limitations when applied to advanced 3D transistor structures. In addition, application of Mueller matrix ellipsometry measurements on strained grating structures (SiGe/Si) and block copolymer structures to determine the impact of strain and defectivity (bridging defects, wiggles, LER, etc.) on anisotropy coefficients will be presented, respectively. [3,4] Additionally, hybrid approaches will be

proposed in conjunction with complementary/supplementary metrology methods (CD-SEM, HRXRD and CD-SAXS). [5-7]

[1] S. Pandev et al., *SPIE Proc.* 9424 (2015).

[2] A. Vaid et al., *SPIE Proc.* 9424 (2015).

[3] G. R. Muthinti et al., *SPIE Proc.* 8681 (2013).

[4] D. J. Dixit et al., *Journal of Micro/Nanolithography, MEMS, and MOEMS* 14, 021102 (2015).

[5] A. Vaid et al., *SPIE Proc.* 8324 (2012).

[6] A. C. Diebold et al., *Proceedings of SPIE* 8681, 86810I (2013).

[7] Charles Setters et al., *Journal of Micro/Nanolithography, MEMS, and MOEMS* 13, 041408 (2014)

4:40pm **EL+AS+BI+EM-ThA8 Structural and Ellipsometric Analysis of the Topological Insulator Bi₂Se₃.** *Avery Green*, SUNY Polytechnic Institute

Topological Insulator (TI) materials have been the subjects of increasing scientific interest in the last decade. Their spin-momentum locked Dirac cone surfaces and insulating bulks have resulted in new directions in physics research and new spintronic devices. Though these materials have been thoroughly described in theory, the experimental realization and measurement of these surface states has been problematic, due to various crystalline defects. Theory predicts that TI surface states are protected against local defects, but it is essential to study the effects of global perturbations caused by surface oxidation, stoichiometric aberrations, and significant structural defect densities. The aim of this study is to measure the time-dependent dielectric function of the Bi₂Se₃ surface and bulk in air, using a dual rotating compensator spectroscopic ellipsometer. These data are backed up with various metrological measurements (AFM, cross-sectional TEM, EDS) to confirm surface topology and oxide thickness. This analysis of optical properties and oxide formation will, in the future, be used to optimize the Bi₂Se₃ flake thickness identification process, and provide a control for further necessary structural analysis, as stated above.

5:00pm **EL+AS+BI+EM-ThA9 Visible Luminescence in the VLS Grown Self Ga Doped ZnS Nanostructures.** *Arshad Bhatti, H. Hussain, M.A. Johar, S. Rehman, M.A. Shehzad, M.A. Hafeez*, COMSATS Institute of Information Technology, Pakistan

ZnS is a wide band gap semiconductor and thus offers fascinating opportunities for tailoring and tuning its bandgap states for photonic devices in visible region of the spectra. Ga introduced a strong red luminescence in ZnS. VLS mechanism was employed to synthesize ZnS nanowires using Ga as a catalyst and dopant simultaneously. The thickness of Ga ultrathin film was varied from 0.5 nm to 5 nm to observe the effect of Ga droplet size on the formation, lifetime and activation energies of defect states in the band gap. It was expected that Ga³⁺ would replace Zn²⁺ sites and dope ZnS, in addition, an impurity phase of Ga₂S₃ was also observed, whose content showed strong dependence of Ga thickness. It also shrunk the crystallinity of ZnS due to varied size of Ga³⁺ (76 pm) ions replacing Zn²⁺ (88 pm), which was observed in the shifts of major XRD reflections of ZnS. Incorporation of Ga introduced strong impurity states in the band gap of ZnS. It also affected the intrinsic defect states of ZnS, namely Zn and S vacancies (Please refer to Figure 1, which also shows the de-convoluted band gap broad band). In the PL spectra, blue (440 nm), yellow (560 nm), orange (600 nm) and red (680 nm) bands were attributed to S vacancies, Ga related defects, donor-acceptor recombination and Ga₂S₃, respectively. Photoluminescence excitation spectroscopy revealed strong absorbance at corresponding energies. A strong correlation of these states was observed in the temperature dependent PL measurements due to presence in their presence in the vicinity as the activation energies of these states matched the energy differences of corresponding states. The conductivity measurements also complimented the optical results. Time resolved PL demonstrated the lifetime of these states was between 0.5 ns to 1.5 ns and had somewhat significant effect of dopant concentration. Finally, Ga doped ZnS showed extremely efficient IR sensitivity.

Figure 1: The room temperature PL spectra of Ga doped ZnS nanowires synthesized with varied thickness of Ga: (a) 0.5 nm, (b) 1.0 nm, (c) 3.0 nm, and (d) 5.0 nm. The broad band between 450 nm to 750 nm has been de-convoluted to show contribution of various defect states (as mentioned in the Figure). These states were identified from the PLE spectrum.

5:40pm **EL+AS+BI+EM-ThA11 Can Front-Surface Metal Mirrors Be Protected from Oxidation by Vacuum Applied Polymer Films?** *David Allred, R.S. Turley*, Brigham Young University, *R.T. Perkins*, Utah Valley University

We have used variable-angle, spectroscopic ellipsometry to monitor secular changes in multilayers consisting of chemically active thin films, such as

aluminum, deposited on dielectric-coated silicon wafers and protected by various vacuum-applied barrier layers. Ultrathin barrier layers included polymers such as parylene and rarely, sputtered inorganic films, such as silicon. Applications include the measurements of the oxidation of evaporated aluminum for use as a mirror in the VUV (vacuum ultraviolet) and the determination of the optical constants of materials such as Y_2O_3 potentially useful in VUV and XUV (extreme ultraviolet) optics.

Helium Ion Microscopy Focus Topic

Room: 211B - Session HI+AS+NS-ThA

Imaging and Milling with He and Ne Ion Beams

Moderator: Richard Livengood, Intel Corporation, John A. Notte, Carl Zeiss Microscopy

2:20pm **HI+AS+NS-ThA1 Focused Ion Beam Circuit Edit in the Nano-Device Age: A Search for the Ultimate Nano-Ion Beam, Shida Tan**, Intel Corporation **INVITED**

Evolution of the IC process technology continues to increase the challenge of circuit edit with smaller critical device dimensions, thinner process layers, densely packed structures, and complex device routing and design architecture. In this paper, the general approach employed, challenges encountered, and results acquired in neon application development using Zeiss NanoFAB (noble GFIS) platform for circuit edit will be presented. The merits and limitations of applying a Ne^+ beam in high precision circuit edit applications will be shared with the audience.

3:00pm **HI+AS+NS-ThA3 Electrical Nano-Patterning of Graphene Film by Helium Ion Beam Irradiation, Shinichi Ogawa, T. Iijima, Y. Naitou**, AIST, Japan

The helium ion microscopy is a unique technology for observation of soft materials such as low-k materials and photo resist patterns for LSI fabrication [1] and for nm order etch patterning. Graphene, a two-dimensional sheet of carbon atoms [2], is a promising channel material for next-generation transistors, and we have shown an on-off gating of current through a graphene nano-ribbon which was etched down by the helium ion beam using the helium ion microscope [3] and by controlling electrical properties of the graphene films themselves by the nano-scale helium ion irradiations generating defects [4]. This study precisely shows a nano-scale direct electrical patterning of the graphene film from a point of view of the irradiation conditions.

Helium ion beams of 0.3 nm diameter were 500 X 500 nm² regions scanned on single-layer graphene films on Si/SiO₂ substrates at doses of 0.62 - 10 10¹⁶ cm⁻² at 30 kV. A spatial resolution of the helium ion microscope patterning on the single-layer graphene was investigated by fabricating nano-ribbons of lines of 100 - 5 nm width. Dynamic force microscopy and scanning capacitance microscopy measurements revealed that helium ion irradiated regions appeared as depressed about 1 nm in topography image at above conditions, while a darker image was acquired at 2.0 10¹⁶ cm⁻² than those at less dose conditions which means transition to dielectric from metal occurred at the higher dose. A spatial resolution of the helium ion microscope patterning non-monotonically depended on the dosage of the helium ions. Increasing the dose to 5.0 10¹⁶ cm⁻² improved the spatial resolution to several tens of nanometers. However, doses of more than 1.0 10¹⁷ cm⁻² degraded the patterning characteristics.

Those results are discussed precisely changing irradiated beam conditions followed by structural analyses by such as CS-TEM.

[1] S. Ogawa, et al., Jpn. J. Appl. Phys., 49 (2010) 04DB12, [2] K. Novoselov, et al., Science 306, 666 (2004), [3] S. Nakaharai, et al., Appl. Phys. Express 5 015101 (2012), [4] S. Nakaharai, et al., 2012 IEEE International Electron Devices Meeting (IEDM), Technical Digest p.72 (2012), [5] Y. Naitou, et al., Appl. Phys. Lett. 106, 033103 (2015)

3:20pm **HI+AS+NS-ThA4 Nanopores in Silicon Nitride Membranes, Graphene and CNM: Milling and Imaging Techniques at the Helium Ion Microscope, Daniel Emmrich, E. Marschewski**, Bielefeld University, Germany, *A. Nadzeyka, F. Nouvertné*, Raith GmbH, Germany, *A. Götzhäuser, A. Beyer*, Bielefeld University, Germany

The Helium Ion Microscope (HIM) is a focussed ion beam system which can be used for both imaging and milling. In the low dose regime, the HIM operates as a microscope; high doses enable material modification and sputtering. Compared to conventional focussed ion beams (FIB), the HIM offers a very small focal spot size down to 0.35 nm and a strongly localized sputter interaction with the material. We employ the HIM for milling nanopores in free standing membranes, such as 30 nm thick Silicon Nitride, Graphene and 1 nm thick carbon nanomembranes (CNM) made from

aromatic self-assembled monolayers by electron-induced cross-linking. HIM is also used for the inspection of pores. The smallest He⁺-milled nanopores have a diameter of about 3 nm in all investigated membranes. The He⁺ beam thus overcomes the resolution limit of conventional FIB tools as we show in a comparison with a high resolution Ga-FIB. Different strategies for the characterization of pores with the HIM will be discussed. In particular, we compare the feasibility of the ion generated secondary electron signal to the He⁺ transmission signal.

4:00pm **HI+AS+NS-ThA6 Application of Focused Helium Ion Beams for Direct-write Lithography of Superconducting Electronics, Shane Cybart**, University of California San Diego **INVITED**

The 1986 discovery of high transition temperature (high- T_C) superconductivity in copper-oxide materials set in motion an intense research effort to develop superconducting electronics functioning in the range of liquid nitrogen temperatures (77 K). Scientists and engineers soon after discovered that these materials were much more complicated than initially imagined. Anisotropic electrical properties and a very short superconducting coherence length seriously narrowed or eliminated the possibility of using classical superconducting electronic structures. These new materials demanded novel device architectures that proved very difficult to realize. Nearly three decades have passed and progress in high- T_C superconducting devices has been very slow because process control at the sub ten nanometer scale is required to make high quality, reproducible Josephson junctions: the basic building block of superconducting electronics. Recent advances in gas field focused helium ion beams provide a new and promising approach for direct-write lithography of high- T_C materials for the realization of predictable and scalable high- T_C electronics. In this work, we demonstrate fabrication of a - b plane superconducting Josephson tunnel junctions for YBa₂Cu₃O_{7- δ} (YBCO) by utilizing a focused helium ion beam to create a narrow (~nm) in-plane tunnel barrier between two superconducting electrodes. The key to this method is that YBCO is sensitive to point defects in the crystal lattice caused by ion irradiation. Increasing irradiation levels has the effects of increasing resistivity and reducing the superconducting transition temperature. At very high irradiation levels YBCO becomes insulating and no longer superconducts. Test samples were written with ion fluence ranging between 10¹⁴ and 10¹⁸ He⁺/cm². In between these two extremes we were able to determine doses that could create very high-quality Josephson junctions with both metallic and insulating barriers. The current-voltage (I-V) characteristics for lower doses show nearly ideal Josephson junction behavior with a zero voltage supercurrent that oscillated in magnetic field as expected for the Josephson effect. At much higher doses (I-V) exhibited insulator behavior. Using ac techniques we measured the differential conductance (dI/dV) in this regime which revealed the YBCO superconducting energy gap near 33 mV. This feature is a result of quasi particle tunneling which provides strong evidence that we have created an insulating barrier less than 2 nm wide. These results demonstrate the unique ability of focused helium ion beams for maskless direct write lithography of oxide tunnel barriers for electronic devices.

4:40pm **HI+AS+NS-ThA8 A Novel Efficient Approach for Investigating the Ion Implantation Effect on Small Volume Copper, Zhang-Jie Wang**, Xi'an Jiaotong University, China, *F.I. Allen*, University of California, Berkeley, *Z.W. Shan*, Xi'an Jiaotong University, China, *P. Hosemann*, University of California, Berkeley

Ion implantation has been used for decades to investigate the response of materials to radiation damage. Understanding the effect of He in materials is a key aspect in the optimization of fusion, fast reactor and spallation sources suffering from high He/dpa (displacements per atom) ratios. The traditional large-area He implantation techniques are rather materials-constrained and time consuming, thus limiting systematic studies. The work presented here utilizes the Zeiss ORION NanoFab instrument which deploys He and Ne ion beams in combination with a Ga ion source to quickly and efficiently manufacture nanostructures and then perform direct He implantation in selected areas of interest. Demonstrated in single crystal and copper nanotwinned structures, the systematic study of He bubble lattice distribution and twin structure evolution under different implanting doses and dose rates is achieved in a fast and efficient manner. We also utilize the combined Ga-He beam system to increase sample throughput to manufacture nanopillars and implant with He in the same chamber. Each pillar was subsequently tested using a JEOL 3010 TEM equipped with a Hysitron PI95 nanomechanical testing system. The results show that the resistance of deformation twinning in single crystal Cu and twin boundary migration in nanotwinned Cu are both significantly improved for increasing He doses up to 1x10¹⁸He⁺/cm². The novel technique presented here makes it feasible and efficient to evaluate He ion damage and its effect on small volume materials.

5:00pm **HI+AS+NS-ThA9 Helium Ion Microscopy Analysis of Itokawa Asteroid Particles Obtained from Hayabusa Mission, Vaithiyalingam Shuthanandan**, Pacific Northwest National Laboratory, *R.C. Ogliore, K. Nagashima*, University of Hawai'i at Manoa

Particles returned from the S-type asteroid Itokawa by JAXA's Hayabusa mission show evidence of space weathering features. These features can be very small (<1 μm in size) and very shallow (within a 100 nm of the surface). The smallest space-weathering surface features and textures are difficult to resolve by field-emission SEM (FEG-SEM). In order to see these effects, we have used Helium ion microscopy (HIM). Two Hayabusa particles: RB-QD04-0062 (“#62”: 40 μm , olivine and plagioclase) and RB-QD04-0091 (“#91”: 43 μm , olivine and plagioclase) were imaged using HIM. The particles were removed from their glass slides with a Sutter micromanipulator and tungsten needle and then stuck on a SEM stub with a thin layer of Post-It note glue. The stub was coated with ~6 nm of carbon for electrical conductivity. Helium ion microscopy images of the surfaces of two Hayabusa grains revealed diverse space-weathering features on scales from several nm to several μm . Both Hayabusa particles show variable surface textures, a variety of splash melt features, adhering grains, and small holes. Two porous particles, with structures reminiscent of chondritic-porous interplanetary dust particles, were found adhering to the surface of the Hayabusa grains (a 1.2 μm object on #91, a 350 nm object on #62). Much of the surface of #62 was covered with small bumps 25–100 nm in size, whereas other regions were free of small bumps. A large, 6 μm quenched melt splash feature was found on the surface of #62. On the other hand, faces of #91 showed multiple concoidal fractures and splash melt droplets and pancakes, but fewer and smaller surface bumps compared to #62. For comparison purposes a 30 μm grain of lunar soil, which had a much higher density of sub- μm splash melt features than the Hayabusa grains, was also imaged. No obvious impact craters (holes with raised rims) were found on this surface. The variations in surface textures indicate that the grains of Itokawa asteroid experienced a complex history of fracturing and exposure to space-weathering processes on the surface of asteroid Itokawa.

5:20pm **HI+AS+NS-ThA10 Multi-Beam Ion Microscopy and Nanofabrication at UC Berkeley, Frances Allen**, UC Berkeley, Lawrence Berkeley National Laboratory (LBNL), Biomolecular Nanotechnology Center/QB3, *P. Lum*, Biomolecular Nanotechnology Center/QB3, *T.C. Pekin*, UC Berkeley and LBNL, *Z.J. Wang*, UC Berkeley and Xi'an Jiaotong University, Republic of China, *R. Thayer*, UC Berkeley, *J. Hong*, UC Berkeley and LBNL, *A.A. Omrani*, UC Berkeley, *M.F. Crommie*, *J. Bokor*, UC Berkeley and LBNL, *N.H. Patel*, UC Berkeley, *A.M. Minor*, UC Berkeley and LBNL, *P. Hosemann*, UC Berkeley

A Zeiss Orion NanoFab Helium Ion Microscope (HIM) has recently been installed at UC Berkeley in the Biomolecular Nanotechnology Center. The specialized gas-field ion source is operated using He or Ne gas and a separate column with a liquid-metal ion source is used to generate a Ga^+ beam. Thus, the advanced imaging and nanofabrication capabilities of the HIM using He^+ and Ne^+ can be combined with the bulk milling capability of Ga^+ enabling a range of imaging and nanofabrication modalities all in one tool.

We will present a selection of initial results from the microscope, highlighting the versatility of this multi-beam instrument and a close collaboration with Transmission Electron Microscopy (TEM) facilities at the National Center for Electron Microscopy in the Molecular Foundry of Lawrence Berkeley National Laboratory for the characterization of NanoFab-fabricated electron-transparent specimens. For example, using Ne^+ and Ga^+ beams and subsequent TEM analysis we explore the effect of Ne^+ milling versus conventional Ga^+ milling of TEM specimens focusing on aluminum alloys and their nanomechanical properties. We use the He^+ beam to selectively implant Ga^+ -milled nanopillars for TEM investigation of He-bubble superlattices and *in situ* TEM nanomechanical testing for a range of implantation doses. Further applications combining fine milling with high-resolution HIM imaging include the fabrication of magnetic multilayer tunnel junction island structures down to a diameter of <10nm, fabrication of MoS_2 nanoribbons, and site-specific cross-sectioning of scales from the wing of the *Junonia coenia* butterfly species for investigations of the development of nanostructures responsible for structural color. In many applications the use of the electron flood-gun for charge compensation when imaging insulating specimens is a crucial component.

Selective Deposition as an Enabler of Self-Alignment
Focus Topic

Room: 210F - Session SD+AS+EM+PS-ThA

Process Development for Selective Deposition and Self-aligned Patterning

Moderator: John Ekerdt, The University of Texas at Austin, Chuck Winter, Wayne State University

2:20pm **SD+AS+EM+PS-ThA1 Surface Chemistry Related to Selective Deposition, Suvi Haukka**, ASM Microchemistry Ltd., Finland, *J.W. Maes*, ASM Belgium **INVITED**

The shrinking device dimensions in semiconductor manufacturing call for new innovative processing approaches. One of these considered is selective deposition which has gained increasing interest among semiconductor manufacturers today. Selective deposition would be highly beneficial in various ways, for instance, it would allow a decrease in lithography and etch steps reducing the cost of processing and enable enhanced scaling in narrow structures making bottom up fill possible. Chemical vapor deposition (CVD) and especially atomic layer deposition (ALD) as very surface sensitive techniques are considered enabling techniques.

Selective deposition typically deals with a selective deposition method where, for instance, a metal layer is selectively deposited on metal surface over dielectric surface, or a dielectric layer is selectively deposited on hydrophilic polymer over a more hydrophobic polymer. In most of the selective deposition schemes of today the passivation is used for the surface on which no deposition is desired. The most known method is to use SAM's (self-assembled monolayers) which are silicon compounds with long carbon chains. Besides the SAM passivation of surfaces also the clever selection of precursors with built-in selectivity in certain process conditions could be applied.

In this paper, the chemistry challenges in the various selective deposition approaches and passivation means are reviewed. In addition, results from the selective deposition of metal on metal over dielectric surface in a Cu capping application and from selective strengthening of DSA (direct self-assembly) layers are presented.

3:00pm **SD+AS+EM+PS-ThA3 Selective Deposition - The New Patterning Paradigm?, Florian Gstrein**, Intel Corporation **INVITED**

Top-down patterning techniques based on optical lithography have made consumer electronics ever more powerful, ubiquitous and affordable. This is largely due to the ability of lithographic techniques to transfer trillions of mask features to wafers at defect densities approaching virtually zero in high-volume manufacturing. While the resolution of optical lithography tools is typically considered to be the main challenge for continued device scaling, it is actually accurate pattern placement, which has emerged as the biggest concern. Novel bottom-up patterning approaches such as selective deposition are needed to overcome shortcomings in pattern placement accuracy.

The talk will first outline the challenges patterning processes based on 193i pitch division and EUV lithography face in terms of alignment accuracy and how complementary patterning techniques such as selective deposition can reduce pattern placement errors. One of the great challenges of selective deposition is defect mitigation, especially as the sensitivity to killer defects increases as device dimensions scale. Defect mitigation requires a fundamental understanding of the chemical selectivity of surfaces. While molecules can recognize chemical functionality on a surface, selective deposition processes based on atomic layer deposition (ALD) or chemical vapor deposition (CVD) are exceedingly rare and largely limited to specific precursors and substrates. For metal deposition, inherent selectivity was achieved through judicious precursor ligand design. Experimental results will be presented in the context of a theoretical investigations aimed at calculating the kinetic barriers that govern the selectivity of metal deposition. The use of self-assembled monolayers (SAMs) as passivants and/or blocking layers for subsequent deposition is an attractive way of overcoming the non-selectivity of many CVD or ALD processes. Here, the critical parameters for selective blocking are choice of the terminal group, surface termination, carbon chain length, and proper precursor choice. Using SAMs, selective deposition of dielectrics with respect to a variety of surfaces was achieved. The talk will conclude with our vision of how defects can be mitigated: It comprises a fundamental understanding of the chemical nature of the surface, precursors with high kinetic barriers for defect formation, passivation of defect nucleation sites, and the removal of defects post deposition. Selective deposition, if properly resourced and developed, can provide powerful means to future scaling and is one way of ensuring that patterning will continue to support Moore's Law in the foreseeable future.

4:00pm **SD+AS+EM+PS-ThA6 Area-Selective Molecular Layer Deposition: Enhanced Selectivity via Selective Etching**, *Richard Closser, D.S. Bergsman, F.H. Minaye Hashemi, S.F. Bent*, Stanford University

Recent developments in electronic devices are pushing toward smaller and smaller features of both metal and dielectric patterns, along with a desire to produce selectively deposited organic thin films on such patterns. Techniques that allow for a high degree of control over the thickness and conformality of organic thin films, such as molecular layer deposition (MLD), are ideal candidates to meet these selective deposition requirements. Using MLD, several types of thin film polymers can be deposited with angstrom-level control due to the sequential, self-limiting surface reactions resulting in monomer-by-monomer growth. Selectivity in the MLD polymer growth is then achieved by utilizing the chemical functionality between the solid substrate surface and the gas phase monomer precursors.

Previously, we have shown the ability to selectively deposit thin film polymers by MLD onto pre-patterned metal and dielectric substrates by utilizing a blocking layer of octadecylphosphonic acid (ODPA) self-assembled monolayers (SAMs) that deposits onto metals more readily than onto dielectric films. Although this process can prevent MLD for up to 6 nm of deposition, selectivity of polymer growth is lost for thicker films, and therefore we are exploring new methods for increasing the MLD selectivity. For the current studies, ODPA SAM is deposited onto a patterned metal/dielectric (Cu on SiO₂) substrate to act as the MLD blocking layer. Once the SAM is fully deposited, polyurea films are grown onto the substrate by MLD to a desired thickness which can be controlled by the number of monomer dose cycles used. An acid etchant is then used to remove the surface oxide of the metal along with the SAM layer while leaving intact the polymer film deposited onto the dielectric. X-ray photoelectron spectroscopy, Auger electron spectroscopy, and ellipsometry measurements show that this process removes undesired MLD film that was deposited on the metal. Studies on patterned substrates confirm selective polymer film growth onto the dielectric over the metal. The etchant removal technique thus increases the selectivity of MLD growth by more than an order of magnitude when compared to the SAM blocking layer alone. Due to the increased selectivity with the etching based process, selective deposition of MLD films as thick as 12 nm have been demonstrated. Atomic force microscopy results show slight surface roughening due to etching while the bulk of the metal/dielectric pattern remains intact. This increase in MLD selectivity should allow for novel applications of selective polymer film deposition.

4:20pm **SD+AS+EM+PS-ThA7 Nucleation and Steady State ALD of Metallic Tin Using SnCl₄ and a Silyl Pyrazine Reducing Agent**, *Eric Stevens, M.B. Mousa, G.N. Parsons*, North Carolina State University

Metal atomic layer deposition (ALD) processes are typically limited to noble, high work-function metals where uniform nucleation and conformal growth can be problematic. Recent work suggests that 1,4-bis(trimethylsilyl)-1,4-dihydropyrazine (DHP) could be an effective reducing agent for deposition of metals with highly negative electrochemical potentials. This work investigates DHP as a potential reducing agent for tin metal ALD using tin (IV) chloride (SnCl₄).

Experiments were carried out in a custom-built, hot-wall reactor using N₂ carrier gas, an operating pressure of 1.3 Torr, and temperatures between 130 and 170°C. The DHP source was heated to 70°C to maintain a vapor pressure ~1.2 Torr. Initial films were deposited at 130°C on silicon using a SnCl₄/N₂/DHP/N₂ exposure sequence of 4/50/10/50 seconds, then analyzed ex-situ by X-ray photoelectron spectroscopy (XPS) with Ar depth profiling. In sputtering deeper into the film, XPS exhibited both Sn-Sn and Sn-O peaks at 485 and 486.7 eV, respectively, where a decrease in Sn-O and an increase in Sn-Sn peak intensities suggests native oxidation of the film upon exposure to air. Furthermore, 7% Cl and 19% N were found in the films after sputtering, presumably from an incomplete reaction and/or incorporation of reaction byproducts.

To better understand surface reactions and growth mechanisms, we characterized the ALD process at 130, 150, and 170°C using *in situ* quadrupole mass spectrometry (QMS) and quartz crystal microbalance (QCM). QCM analysis at 130 and 150°C showed continued growth with extended exposures, consistent with non-ALD growth. Deposition at 170 °C was more repeatable and more closely approached surface saturation. At 170°C, QCM showed a clear mass increase during the SnCl₄ dose and a corresponding mass decrease during the DHP dose, consistent with DHP removing Cl and reducing the Sn-Cl surface. Moreover, the QMS results showed peaks exclusively during DHP doses at m/z values of 80 (pyrazine) and 65, 93, 95 (trimethylsilyl chloride), which are the most probable byproducts of DHP reacting with a chlorinated surface.

Using gold-coated QCM crystals at 170°C, Sn growth proceeds slowly for the first ~150 ALD cycles, whereas growth on QCM crystals previously coated with Sn show a more rapid transition to steady-state growth (<20

cycles). We are currently investigating the nucleation on different substrates and how process conditions can be tuned to achieve selective deposition. Understanding the surface reaction and growth mechanisms of tin metal deposition using DHP could provide a foundation for deposition of metal thin-films that were previously unattainable.

4:40pm **SD+AS+EM+PS-ThA8 Determination of the Minimum Saturating Dose during Atomic Layer Deposition of Alumina and Titania on Si(100) and Si(100)-H**, *D. Dick*, University of Texas at Dallas, *Joshua Ballard, J. Randall*, Zyvex Labs, *Y.J. Chabal*, University of Texas at Dallas

Atomic layer deposition (ALD) has become an important process step in semiconductor manufacturing, where the self-limiting nature of each step of the process permits atomic scale control over the ultimate layer thickness in addition to relatively fast processing with high pressure reactors. However, it has been shown that ALD can be used to selectively deposit material onto patterned surfaces, requiring not only saturation of each deposition cycle in desired areas but also suppression of deposition in those areas where it is undesirable. One mechanism for improving practical selectivity would be to find the minimum exposure that saturates the growth where desired in order to avoid excess overall reaction probability in areas where inhibited growth is preferred.

To investigate this, we have examined the deposition in vacuum ("UHV ALD") of Al₂O₃ and TiO₂ with TMA and TiCl₄, respectively, on both hydrophobic, H-terminated Si(100) surfaces and hydrophilic OH-terminated Si(100) surfaces prepared by H₂O exposure of clean Si(100)-(2x1) surfaces. Surface reactions and relative coverages are determined by in-situ IR spectroscopy, and ex-situ XPS. We find that good selectivity can be achieved at 150°C. Preliminary data and calculations also suggest that an initial wetting layer of TMA on clean Si(100) promotes subsequent growth of TiO₂ or other high-k dielectrics. Finally, we will discuss how these findings have made it possible to develop a full multi-cycle process for a custom low-pressure ALD system equipped with scanning tunneling microscopy and atomic force microscopy.

5:00pm **SD+AS+EM+PS-ThA9 Selective Growth of GeSbTe Phase-Changing Materials Utilizing Self-Aligned Confined Structure**, *ByungJoon Choi*, Seoul National University of Science and Technology, Republic of Korea, *T. Eom, C.S. Hwang*, Seoul National University, Republic of Korea

GST Phase changing material, typically GeTe-Sb₂Te₃ pseudo-binary solid solution, has been extensively studied for rewritable digital versatile optical disks or phase change random access memory (PcRAM), on account of the drastic change of its optical reflectivity or electrical resistivity between amorphous and crystalline phases. As the device size of PcRAM is scaled down, GST materials should be confined into the contact-plug for reducing its programming current, which cannot be achieved by any physical deposition method.

Among the various metal-organic (MO) precursors, the combination of Ge(iBu)₄, Sb(iPr)₃ and Te(iPr)₂ has been extensively studied for plasma enhanced chemical vapor deposition or its variant methods with plasma-activated H₂ gas as a reducing agent of the MO-precursors. Plasma-enhanced pulsed CVD was attempted using the precursor pulse sequence consisting of Sb-Te-Ge-Te cycles (each elemental cycle is composed of precursor injection and Ar + H₂ plasma reduction steps). The chemical composition of the films was appropriately controlled by the cycle ratio and sequence of each precursor pulse. The linear growth with the number of cycles was shown, and the GPC (growth-per-cycle, i. e. growth rate) was determined to be 0.73 nm/super-cycle from the slope at a wafer temperature of 200°C.

Strong substrate dependency can be utilized in the selective growth of GST material on a TiN contact-plug formed in the SiO₂ inter-layer dielectric (ILD). Higher selectivity (difference of GPC) between TiN contact-plug and SiO₂ ILD layer was achieved by pulsed CVD with increasing the amount of Te(iPr)₂ injection. The reason for the selective growth was believed to have originated from the adverse interference of the residual gas (unreacted Te(iPr)₂ or its derivatives) to the chemical adsorption of Sb nuclei on the SiO₂ surface, which functions as a nucleation site for further GST growth. It was reported that amide-based Ge precursors also showed strong selectivity at a particular temperature, enabling Sb and Te precursors to be chemisorbed on the Ge seed layer, which could be utilized for selective growth of GST.

The most feasible explanation for the substrate-dependent growth behavior of the GST film is the electron donation from the substrate, which would enhance the precursor decomposition and removal of ligands from the adsorbed precursor molecules. The nucleation and growth behaviors of the GST films were studied on Si substrates with various nucleation or buffer layers. It turned out that the types of substrates have a crucial impact on the nucleation behaviors and the chemical composition of the film.

5:20pm **SD+AS+EM+PS-ThA10** **Toward an All- Vapor Process for Area Selective Atomic Layer Deposition**, *FatemehSadat Hashemi, S.F. Bent*, Stanford University

Modern electronic devices containing planar and 3-D structures utilize a number of metal/dielectric patterns in both the front and back end. The scaling of next generation electronic devices makes achieving these patterns increasingly difficult and motivates the development of novel processing methods. One such method—area selective deposition—has the opportunity to play an important role in significantly reducing process complexities associated with current top-down fabrication of patterned structures by eliminating some of the deposition and etching steps that are time-consuming and expensive.

Atomic layer deposition (ALD) is a good choice for area selective deposition because its chemical specificity provides a means to achieve selectivity on a spatially patterned substrate. Area selective ALD, reported previously by several groups, requires improvements for the process to be compatible with current device fabrication goals. Most previous studies of area selective ALD have achieved deposited thicknesses on the order of only a few nanometers and the selectivity was generally obtained by passivation of the surface using self-assembled monolayers (SAMs) in the regions where ALD was not desired. Existing methods are usually performed by dipping the substrates into a solution containing the SAM-forming molecules for several hours. A more desirable all-vapor process would require vapor delivery of the SAMs. This method would provide better SAM coverage on porous or three-dimensional structures, potentially decreasing the required deposition time for the passivation layer, and allowing the SAM passivation step to be integrated with the rest of the ALD process.

In this work, we investigate area selective dielectric-on-dielectric deposition by selectively depositing organic alkanethiol SAM as the blocking layer on metal parts of a metal/dielectric (Cu/SiO₂) pattern. We compare area-selective ALD achieved by introduction of the thiolate SAM in both the solution and vapor phase. We show that while in both cases the SAM can prevent subsequent deposition of metal oxide dielectric films via ALD, vapor deposition provides stronger passivation in a shorter exposure process on the metal. We also report results on regenerating the thiol SAM protecting layer from the vapor phase between ALD cycles and show that this approach is effective in improving the blocking properties of the SAM on Cu. This strategy provides the ability to significantly improve selective deposition of dielectrics. Moreover, it is a significant step toward an all-vapor process for area selective deposition, opening up the possibility for new applications in next generation electronic devices.

5:40pm **SD+AS+EM+PS-ThA11** **Selective Deposition of ALD Metal oxides and Metal Thin Films by Fab-Friendly Surface Treatments**, *Kandabara Tapily, K.-H. Yu, S. Consiglio, R. Clark, D. O'Meara, C. Wajda, G. Leusink*, TEL Technology Center, America, LLC

For the last 5 decades, the semiconductor industry has relied on the continued scaling down of the device feature size in order to improve performance and increase bit density according to Moore's law. However, with the delay in implementation of extreme ultraviolet lithography (EUV) in high volume manufacturing,¹ patterning beyond the 14 nm technology node is getting extremely difficult to manage due to the overlay control and the increase in manufacturing cost due to multi-layer alignments. In order to keep reducing the device feature size, new patterning solutions are needed such as selective deposition and selective etching of materials. Atomic layer deposition (ALD) has emerged as one of the leading film deposition techniques as a result of the semiconductor device scaling.² ALD provides excellent film control, uniformity and high conformality. ALD is highly surface reaction driven and it is possible to modify the substrate surface to activate or deactivate growth on selected area hence selective-area ALD (SA-ALD). Selective-area ALD can simplify and reduce the high manufacturing cost associated with highly aggressive patterning schemes by eliminating certain lithography steps. Thin films can now be selectively deposited or removed from a desired area. Most selective-area ALD studies in the literature are conducted with the use of self-assembled monolayers (SAMs) in order to deactivate or activate growth on certain areas.³⁻⁵ SAMs are thin organic films that form spontaneously in tightly packed oriented molecules on solid surfaces. A key enabler of SAMs is the ability to turn these organic layers into patterned layers. However, thermal stability and the slow formation process into well packed layer are some of the major drawbacks of SAMs.⁵

In this study, a non SAMs based approach was used to inhibit ALD growth of metals and metal oxides. Using different surface treatments, it was observed the growth of the ALD thin films can be modulated, see Fig.1 and Fig.2 respectively. ALD Al₂O₃ growth was suppressed by a combination of the vapor HF and cyclical low temperature plasma hydrogen treatment and deposition. Additionally, ALD TaN growth was also inhibited by the use of a combination trimethylsilane (TMS) and dimethylamine (DMA) treatment of the surface prior to ALD deposition.

Reference

1. J. Beynet, et al, *Proc. SPIE*, 7520, 75201J (2009).
2. S. M. George, *Chem. Rev.***110**, 111 (2010).
3. ChaMarra K et al. *Nanotechnol.***3**, 114 (2012).
4. J. C. Love et al., *Chem. Rev.*,**105**, 1103 (2005).
5. A. J. M. Mackus et al, *Nanoscale*, **6**, 10941 (2014).

Surface Modification of Materials by Plasmas for Medical Purposes Focus Topic

Room: 211D - Session SM+AS+BI+PS-ThA

Plasma Processing of Biomaterials and Biological Systems

Moderator: David Graves, University of California, Berkeley, Jean-Michel Povesle, GREMI CNRS/Université d'Orléans

2:20pm **SM+AS+BI+PS-ThA1** **Matching Plasma Sources with Intended Biomedical Outcomes: Open Questions in Modeling of Plasma Surface Interactions**, *W. Tian*, University of Michigan, *S.A. Norberg*, US Military Academy - West Point, *A.M. Lietz*, University of Michigan, *N.Yu. Babaeva*, Joint Institute for High Temperatures, **Mark Kushner**, University of Michigan

INVITED
Plasma surface modification of materials for biomedical applications typically involves atmospheric pressure plasmas in the form of dielectric barrier discharges (DBDs) or atmospheric pressure plasma jets (APPJs). In many cases, APPJs operate similarly to DBDs with an ionization wave (IW) propagating through a rare-gas dominated gas channel. The intersection of the IW with the surface being treated, for example tissue, in both DBDs and APPJ produces locally large fluxes of ions, UV/VUV photons and electric fields onto the surface. These fluxes are collectively *hard fluxes* due to the higher levels of activation energy they represent. Remote DBDs and APPJs where the plasma plume does not intersect the surface produce *soft fluxes*, dominated by neutral reactants. The character and ratios of *hard-to-soft fluxes* and their compositions are functions of flow dynamics, ambient conditions (e.g., humidity) and pulse power waveforms. In many biomedical applications, the tissue is covered by a liquid (or the intended surface is liquid as in plasma activated water). In these cases, plasma produced activation energy, radicals and ions must penetrate through the plasma-liquid interface, where liquid phase mechanisms then determine the reactants to the tissue. From one perspective, significant advances have been made in modeling these processes and furthering our understanding. From another perspective, there are still significant open questions that models need to address, including the manner of coupling of the gas phase plasma and liquid, gas induced fluid dynamics, long term evolution of the liquid chemistry, reactions at the surface of the tissue and control schemes to minimize variability. A brief overview of progress in modeling plasma modification of biomaterials will be provided followed by examples of the authors' modeling works for APPJs and DBDs intersecting with model tissues and liquids.

3:00pm **SM+AS+BI+PS-ThA3** **Plasma Processing of Biomimetic and Sintered Calcium Phosphates for Bone Regeneration and Repair**, *Cristina Canal*, Technical University of Catalonia, Spain **INVITED**

Large bone defects caused by trauma, osteoporotic fractures, infection and tumour or cysts resection pose a great clinical and socio economic problem. Bone grafting materials respond to the need generated by over 2 million bone grafting procedures that are performed every year worldwide. As an alternative to autografts or xenografts, different biomaterials have been proposed, yet with partial success since different aspects remain yet to be improved.

In this context, the use of low pressure (LP) and atmospheric pressure (AP) plasmas opens new opportunities in the field of bone biomaterials. It is the aim of this talk to provide an overview on the strategies undertaken in our group to enhance diverse features of bone biomaterials and to enhance bone therapies.

The examples discussed here include biomimetic hydroxyapatite (HA) and β -tricalcium phosphate (β -TCP) as the most clinically used calcium phosphate (CaP) ceramics for bone regeneration. Some of the points of improvement include increasing their mechanical strength, or using them as local dosage forms for the delivery of drugs, to aid in different therapies, such as combating infection or fighting cancer.

For instance, we have investigated LP plasmas with the aim of expanding the use of biomimetic CaPs to load-bearing sites. Although composites have been defined, their performance is not yet optimal, possibly due to insufficient adhesion between the matrix and the reinforcing agent. Oxygen and argon plasmas have been employed in the surface modification of polylactide fibers to improve the adhesion at the interface between them and biomimetic CaPs with interesting results.

In a different approach we have focused on modulating drug delivery from bone biomaterials. Both AP and LP plasmas are of interest with views on different medical applications and in the design of advanced biomaterials with controlled drug release properties. Different strategies are considered with that aim, such as using either plasma functionalization with AP plasma jet to modulate the interactions of the drug with the CaP surface or employing LP plasma polymerization on CaP scaffolds as a strategy to control the drug release. Lastly, AP plasmas are in the limelight due to their wide potential in the medical field, and here we will discuss some recent findings for application in bone therapies and regeneration.

Acknowledgements

Spanish Government is acknowledged for support through Project MAT2012-38438-C03-01, co-funded by the EU through European Regional Development Funds, and Ramon y Cajal fellowship of CC. The European Commission is also acknowledged through funding in FP7/2007-2013 under the Reborne project (no. 241879).

4:00pm **SM+AS+BI+PS-ThA6 Plasma Processing of Biomaterials and Biomedical Devices**, *H.J. Griesser, T.D. Michl, S.S. Griesser, M. Jasieniak, H.H. Mon, Bryan Coad*, University of South Australia **INVITED**

Gas plasmas have attracted considerable attention over more than 40 years as a convenient method for changing the surface chemical composition of biomaterials and thereby alter and control the interfacial interactions between biomedical devices and contacting "biology" such as protein solutions, blood, cells and tissue, and bacterial biofilm growth. Plasma technologies are already in use on a large industrial scale in several biomedical device companies; for example 30-day contact lenses use a thin plasma coating to confer wettability and low fouling to silicone-based contact lens materials. Bio-interfacial interactions are very short range, and hence it is sufficient to apply ultrathin coatings (< 20 nm thick). Plasma techniques are ideally suited because process control is straightforward and the resultant surface modifications or coatings tend to have a high degree of uniformity and reproducibility compared with other, solution based coating methods. On the other hand, the complex chemical composition of plasma gas phases prevents fine control of chemistry to the extent achievable by conventional chemical approaches. Detailed surface analysis is essential.

Plasma approaches are useful to produce coatings designed to combat the problem of bacterial and fungal biofilm growth on biomedical devices, which leads to infections and delayed healing. One approach is the use of organochlorine plasma polymer coatings, which are highly effective at contact killing. Other, cytocompatible approaches comprise the use of plasma polymer coatings that release NO or available antibiotics such as levofloxacin. A different approach entails the covalent immobilization of a monolayer of antimicrobial molecules onto a thin plasma polymer interlayer whose function is to provide good adhesion and reactive surface chemical groups that can be used to attach antibiotics. Such covalently grafted monolayers have given excellent deterrence of attachment and biofilm formation of bacteria and pathogenic fungi.

4:40pm **SM+AS+BI+PS-ThA8 Organs on a Chip – Biointerfaces in Stem Cell Research**, *Kevin Healy*, University of California at Berkeley **INVITED**

Highly regulated signals in the stem cell microenvironment such as ligand adhesion density, matrix stiffness and architecture, and growth factor presentation and concentration have been implicated in modulating stem cell differentiation, maturation, tissue formation, and ultimately function. My group has developed a range of materials systems and devices to study and control stem cell function and their self-organization into three-dimensional microtissues (e.g., "organs on a chip"). These systems are being developed for screening molecular therapies and patient specific medicine via *in vitro* disease specific tissue models. Examples of how biointerface science is important in these applications will be highlighted. The benefits of our approach include: 1) robust and reproducible platform embodies precision microengineering to create better microtissue environments; 2) precise delivery of molecules (e.g., drugs) in a computationally predictable manner; 3) ability to model human cardiomyopathy; and, 4) cost efficient and high content characterization of cardiac tissue drug response.

5:20pm **SM+AS+BI+PS-ThA10 Effect of the Radical Species for Gene Transfection by Discharge Plasma Irradiation**, *Yoshihisa Ikeda, M. Jinno*, Ehime University, Japan

Gene transfection is a technique of deliberately introducing nucleic acids into cells in order to give them specific characteristics. In practice, this can be achieved in three different ways: chemical method, physical method and the viral vector method.

One of the physical methods that uses discharge plasma irradiation was invented by Satoh, who is one of the authors, and his group in 2002. Since this technique is free from adverse effect associated with viruses, there are no risks as the others mentioned above. The plasma irradiation on genes and cells induces the transfection process in which the genes and cells are exposed to discharge current, charged particles and chemically reactive species.

The authors investigated the factors for plasma gene transfection by changing protocols and looked at the time periods the factors become effective. The results is that transfection rate drops to 1/10 of the standard protocol when the charged particles and chemically reactive species genes are washed out from the wells by PBS solution 60s after plasma irradiation. Since the life times of the charged particles delivered from plasma to the plasmid solution is less than 60s, the direct effect of the charged particles causing transfection finishes before wash out process. This means that nearly 1/10 of transfections occur during plasma irradiation and that the last 9/10 of transfections occur after plasma irradiation is stopped. This second stage transfection is mainly caused by the residual chemically reactive species, however, plasma irradiation stress to cells and plasmids also induces transfection, i.e. possibly charging effect and oxidation stress induce bio-chemical process of the cells in addition to the chemical reactions on the cell membrane and plasmid induced by chemically reactive species such as radicals.

5:40pm **SM+AS+BI+PS-ThA11 Nonlinear Optical Spectroscopic Observation of Plasma-Treated Bio-Specimen**, *Kenji Ishikawa, R. Furuta, K. Takeda*, Nagoya University, Japan, *T. Nomura, T. Ohta*, Meijo University, Japan, *H. Hashizume, H. Kondo*, Nagoya University, Japan, *M. Ito*, Meijo University, Japan, *M. Sekine, M. Hori*, Nagoya University, Japan

Applications of nonequilibrium atmospheric pressure plasma (NEAPP) to the medical field have been reported in recent years. However, a mechanism of interactions between NEAPP and living cells has not been yet elucidated comprehensively. Our strategy for elucidation of plasma-biomaterial interactions is to observe reactions *in situ* at real time. By applying nonlinear optical spectroscopic techniques, the vibrational sum-frequency-generation (SFG) and multiplex coherent anti-Stokes Raman scattering (CARS) microscopy, which are a beneficial tool for addressing best sensitivity at surface and interface, have been used in this study. By using SFG, we have explored topmost surface modification after the interaction between plasma and biopolymeric materials. For the NEAPP-induced reactions on budding yeasts as an eukaryotic cell model, a two-dimensional mapping of budding yeasts treated by the plasma using the CARS microscopy was observed with fluorescence label-free contrasts of chemical vibrational nature. The biomedical imaging of cell membranes, intracellular organelles, nucleus and so forth, was revealed to decompose intracellular membrane by exposure of plasma-generated chemically reactive species, especially for induction of lipid peroxidation. These results will be useful for understanding the plasma induced reactions in the plasma medicine.

Surface Science

Room: 113 - Session SS+AS+EM+EN-ThA

Atomistic Modeling of Surface Phenomena & Semiconductor Surfaces and Interfaces - II

Moderator: Talat Rahman, University of Central Florida

2:20pm **SS+AS+EM+EN-ThA1 Ideas Old and New Applied to Non-Ideal Surface Adsorption and Reaction**, *William Schneider*, University of Notre Dame **INVITED**

Free energies of adsorption are arguably the most elementary quantities in heterogeneous catalysis. These free energies depend on the surface and adsorbate (reactant, intermediate, or product) of interest, system temperature and adsorbate coverage. The free energy represents a balance between the energetic driving force for creating bonds between an adsorbate and a surface and the entropic cost of moving an adsorbate from a fluid phase to a surface. Standard density functional theory (DFT) approaches generally begin by optimizing the location of an adsorbate on a surface, computing a binding energy, and approximating the internal, translational, and configurational contributions to the free energy. In this work we

examine the reliability of standard approximations and describe easily applied improvements that give reliable free energy estimates. We describe applications to adsorption at metal surfaces and in the pores of zeolites.

3:00pm SS+AS+EM+EN-ThA3 Insights into the Oxidation of Stepped Cu Surfaces using Multiscale Investigations, Q. Zhu, W.A. Saidi, Judith Yang, University of Pittsburgh

Surface defects can induce non-canonical oxidation channels on metal surfaces that may lead to the formation of novel nanostructures. Recently, in situ environmental transmission electron microscopy (ETEM) experiments showed that the oxidation of stepped Cu surfaces promotes the formation of a flat metal-oxide interface through Cu adatoms detachment from steps and diffusion across the terraces. To bridge the gap between experiments and theory, we are investigating Cu oxidation using a multiscale computational approach. Our previous MD simulations based on a reactive force field (ReaxFF) demonstrated that the oxidation of stepped Cu(100) takes place on the upper terrace at a faster rate than the lower terrace due to a preferable oxygen diffusion from the lower to upper terraces. We have extended this study using first-principles density functional theory (DFT) and kinetic Monte Carlo (KMC), and performed a systematic study of all stepped Cu surfaces with a low Miller index. The DFT results show that the oxygen diffusion trend varies with the surface type, where in most cases the oxygen ascending diffusion is more favored. This result is confirmed also with ReaxFF MD and KMC simulations. The MD simulations, with a fine-tuned ReaxFF force field parametrization, have also indicated that oxygen adatoms on the upper terrace can enhance the interlayer Cu atom mass transport. These theoretical simulations provide essential fundamental understanding of the experimentally observed smoothing of the Cu surface during in situ oxidation.

3:20pm SS+AS+EM+EN-ThA4 Reconciling Complimentary Analyses of Epitaxial Growth: Role of Transient Mobility for para-Hexaphenyl on Mica, Josue Morales-Cifuentes, T.L. Einstein, University of Maryland, College Park, A. Pimpinelli, Rice University

In studies of epitaxial growth, a major goal is to assess the size of the smallest stable cluster (with $i + 1$ monomers, where i is the critical nucleus size). This is accomplished by analyzing either the capture zone distribution (CZD), the scaling of incident flux F to the density of stable islands N or the island-size distribution (ISD). For CZD, generalized Wigner distributions (GWD) have proven useful, [1,2] with successful applications to, non-comprehensively: polar-conjugated molecule Alq₃ on passivated Si(100), self-assembled Ge/Si(001) nanoislands and para-Hexaphenyl (6P) films on amorphous mica. [3] We concentrate on the last, for which the Winkler group found that $i \approx 3$.

Scaling of N usually follows $N \propto F^\alpha$, where α is the growth exponent. For 6P films, a difference in scaling behaviors at small and large F is attributed to DLA and ALA dynamics (i.e. $i = 5 \pm 2$, and $i = 7 \pm 2$, respectively). [4] This discrepancy motivates our current work, where transient mobility effects modify scaling non-trivially. [5]

Consider that monomers begin in a (ballistic) hot precursor state before thermalizing (random walk). The competing times of ballistic monomers becoming thermalized vs. being captured by an island naturally define a “thermalization” scale for the system. We obtain an analytic solution and elaborate on the physical meaning behind the energies and dimensionless parameters used. Novel scaling regimes are retrieved for which power-law scaling applies, with non-monotonic crossovers between them and the growth exponent exclusively dependent on i . Applying the model to the 6P films results in good agreement for the scaling and the activation energies: experimental values of the activation energies of 0.26eV (high-T) and 0.04eV (low-T) match model predictions of 0.3eV (high-T) and 0.04eV (low-T). Furthermore, the high-flux regime is interpreted not as ALA (attachment-limited aggregation) or HMA (hot monomer aggregation) but rather as an intermediate scaling regime related to DLA (diffusion-limited aggregation). Lastly, we discuss a simplifying approximation for the model and connections to some capture zone distribution considerations of α . [6]

[1] T.L. Einstein, A. Pimpinelli, D. González, J. Cryst. Growth 401, 67 (2014)

[2] T.L. Einstein, A. Pimpinelli, D. González, and J. R. Morales-Cifuentes, Proc. CCP2014, J. Phys.: Conf. Series (2015), in press.

[3] T. Potocar, G. Lorbek, D. Nabok et al. 2011 Phys. Rev. B 83 075423

[4] L. Tumbek & A. Winkler, Surf. Sci. 606, L55 (2012)

[5] J. R. Morales-Cifuentes, T. L. Einstein, and A. Pimpinelli. Phys. Rev. Lett. 113, 246101(2014)

[6] J. R. Morales-Cifuentes, T. L. Einstein, and A. Pimpinelli (in preparation)

4:00pm SS+AS+EM+EN-ThA6 Probing 2-DEG at InN Surface by Electrolyte-Gated Raman Spectroscopy, E. Alarcon Llado, Ecole Polytechnique Fédérale de Lausanne (EPFL), Switzerland, Tommaso Brazzini, Lawrence Berkeley Lab, University of California, Berkeley, J.W. Ager, Lawrence Berkeley National Laboratory (LBNL)

Indium nitride has attracted much attention as its narrow bandgap (~0.67eV) expands the range of the direct gaps of the group III-N alloys into the visible and near-IR and thus offers an outstanding potential for solar energy conversion and optoelectronic applications. However, experimental demonstration of high efficiency In-rich III-V pn rectification junctions has been hampered by the existence of an intrinsic interface electron accumulation layer, which seems to persist regardless of surface treatment. The large capacitance of the Helmholtz double layer that forms on a surface of an object in contact with an electrolyte allows the 2-DEG at the surface of InN to be tuned and even depleted. Using this effect, we demonstrated the first pn rectification behavior in InN.¹

In addition, the 2-DEG accumulation layer affects not only the electrical properties, but also has brought many controversies in the interpretation of optical experiments. Raman spectroscopy probes not only the lattice dynamics in a crystal, but also the electronic structure and free carriers. In particular, the interaction between the free electrons at the surface and the longitudinal optical (LO) phonon in InN has been addressed by several studies. However some questions still remain.

In this work, we present an in-situ micro-Raman study that confirms the presence of a surface related Raman mode in InN and shows its interaction with accumulated electrons at the surface. Electrolyte gated Raman spectroscopy (EGRS) on InN layers was performed in order to modulate and in-situ probe the surface electron accumulation region in InN. A reversible shift of the LO phonon with the applied gate potential is found (see figure 1). The peak position and shift depends on the probing light energy, however it is independent of bulk doping. We explain these findings by Martin’s double scattering mechanism and bandgap narrowing at the surface tuned by the gate voltage. InN nanocolumns were also investigated by EGRS. The LO mode lies at higher frequencies in all nanocolumn samples. This fact corroborates the nature of the scattering mechanism, which is strongly dependent on the surface orientation. In summary, our results clearly demonstrate the surface origin of this feature and allow the fundamental study and understanding of the electronic structure of InN.

1. Alarcón-Lladó, E. et al. PN junction rectification in electrolyte gated Mg-doped InN. Appl. Phys. Lett. 99, 102106 (2011).

4:20pm SS+AS+EM+EN-ThA7 Surface Termination of Single Crystal Bi₂Se₃ Investigated by Low Energy Ion Scattering, Weimin Zhou, J.A. Yarmoff, UC Riverside

Bismuth Selenide (Bi₂Se₃) is a prototypical topological insulator (TI) with a two-dimensional layered structure that enables clean and well-ordered surfaces to be prepared by cleaving. Although some surface structure studies have concluded that the cleaved surface is terminated with Se, as is expected from the bulk crystal structure, there are other reports that show either a Bi- or mixed-termination [1]. Low Energy Ion Scattering (LEIS) and low energy electron diffraction (LEED) are used here to compare surfaces prepared by *ex-situ* cleaving, *in-situ* cleaving and Ar⁺ ion bombardment and annealing (IBA) in ultra-high vacuum. Surfaces prepared by *in-situ* cleaving always have a sharp 1x1 LEED patterns and are Se-terminated. Surfaces prepared by IBA show a transition from Bi- to Se-termination with increasing annealing temperature. Samples inserted into the vacuum chamber following *ex-situ* cleaving have much dimmer LEED patterns, show surface contamination with Auger electron spectroscopy, and could be terminated either with Se or Bi. The angular dependence of LEIS spectra, which is sensitive to the surface atomic structure, doesn’t indicate any substantial differences between surfaces prepared by IBA or *in-situ* cleaving. Ion scattering simulations using Kalypso are compared to experimental angular data to obtain more details about the structure. Exposure of clean surfaces to gaseous species will also be discussed in an effort to determine the surface chemical reactions responsible for the termination change.

[1] X. He, W. Zhou, Z. Y. Wang, Y.N. Zhang, J. Shi, R.Q. Wu and J.A. Yarmoff, Phys. Rev. Lett. 110, 156101 (2013).

4:40pm SS+AS+EM+EN-ThA8 Real-Time Imaging with Atomic-level Spatial Resolution of Silicon Oxidation, Bryan Wiggins, L.G. Avila-Bront, R. Edel, S.J. Sibener, University of Chicago

The investigation of the initial stages of molecular oxygen adsorption on Si(111)-7x7 with real-time and real-space visualization will be discussed in this presentation. We will present the first results from a newly built supersonic molecular beam paired with a scanning probe microscope instrument. The system is designed with an oil free differentially pumped supersonic beam and has a custom scanning probe microscope with the surface plane normal to the beam. This geometric arrangement allows us to

perform real-time and real-space *in-situ* experiments. This study consists of exploring the potential energy surface for molecular oxygen adsorption on Si(111)-7x7. The questions that are being addressed are fundamental for issues relating to semiconductor oxidation as well as being of direct relevance to semiconductor processing. The site-specific locations of molecular oxygen reactivity on Si(111)-7x7 surfaces are not clear and remains a topic of current discussion. Recent spectroscopic studies show that by controlling the molecular beam energy (E_k) one can activate different adsorption pathways for molecules on surfaces. However, the effect of collimated and energy-selected beams impacting the surface at different incident angles has not been observed *in-situ* at the local molecular level until now. We will show high-resolution spatial images of the initial stages of oxygen adsorption on Si(111)-7x7 at different beam energies. The comparison of Si(111)-7x7 oxidation *via* thermal oxygen versus the specific adsorption sites that arise at different beam energies will also be discussed. The results indicate that using supersonic beams in this matter may provide enhanced control of semiconductor oxidation chemistry.

5:00pm **SS+AS+EM+EN-ThA9 Surface Band-Bending Upon Oxidation of Wurtzite and Zincblende InAs Depending on Surface Orientation and atomic Structure, Rainer Timm, M. Hjort, J. Knutsson, O. Persson, A. Troian, S. Lehmann, K.A. Dick, A. Mikkelsen, Lund University, Sweden**

InAs is known to typically show n-type behavior with an electron accumulation layer at the surface. Many studies have been performed for evaluating to which extent this behavior is due to adsorbates such as a native oxide layer, or to specific surface orientations and reconstructions of clean InAs. InAs nanowires (NWs) add an extra degree of complexity, since they can exist both in zincblende and wurtzite crystal structure, typically exhibiting unintended switching between both stacking orders during epitaxial growth. During recent years, a strong debate has been going on about how far such crystal phase mixing influences the conductivity of InAs NWs and therewith their suitability for high-mobility device application [1]. A staggered band alignment with band offsets in the range of up to 0.1 eV between zincblende and wurtzite conduction band edges has been reported, based on transport measurements in ambient atmosphere [2]. In contrast, our recent study of clean and unreconstructed InAs NW surfaces based on scanning tunneling microscopy and spectroscopy (STM/S) in ultrahigh vacuum showed aligned conduction band edges for zincblende [11-20] and wurtzite [11-20] surfaces [3].

Here, we present a systematic study of surface band-bending upon cleaning and oxidation of various InAs surfaces, including purely zincblende or purely wurtzite NWs, obtained by synchrotron-based X-ray photoemission spectroscopy (XPS). We were able to clean all investigated InAs surfaces from their native oxide by annealing them in the presence of atomic hydrogen [3]. Different rates of cleaning and re-oxidation were observed for the different surfaces. Even more importantly, from the energy shifts of the investigated core-levels upon oxidation, varying between 0.1 and 0.3 eV for various surfaces, we obtained significant differences in oxide-induced surface band-bending for different surface orientations. We will compare our XPS results with the atomic and local electronic structure of the specific surfaces as obtained by STM/S [4]. Our results indicate that the band alignment along InAs heterostructures, and therewith the transport properties of InAs NWs, depend on the surface orientation, composition, and atomic structure rather than the crystal phase of the specific InAs segments.

[1] Thelander *et al.*, Nano Lett. **11**, 2424 (2011)

[2] Dayeh *et al.*, Adv. Funct. Mater. **19**, 2102 (2009)

[3] Hjort *et al.*, ACS Nano **12**, 12346 (2014)

[4] Knutsson *et al.*, ACS Appl. Mater. Interfaces **7**, 5748 (2015)

5:20pm **SS+AS+EM+EN-ThA10 Control of Oxygen Defect Surface Injection in ZnO via Sub-Monolayer Sulfur Adsorption, Ming Li, E. Seebauer, University of Illinois at Urbana-Champaign**

Native oxygen defects within metal oxide semiconductors such as ZnO affect the material's performance in applications for photovoltaics, nanoelectronics, gas sensing, and photocatalysis. Previous work in this laboratory has shown that the semiconducting metal oxides surfaces can be used to manipulate the concentrations and spatial distributions of bulk oxygen defects, particularly oxygen vacancies. The interaction chemistry between bulk point defects and reactive sites on semiconductor surfaces is comparable in richness to the reactions of surfaces with gases. The present work discusses a novel mechanism of controlling oxygen defect injection in c-plane ZnO(0001) through surface active sites blocking with sub-monolayer sulfur adsorption. Oxygen diffusion rates were measured by exposing single-crystal ZnO to isotopically labeled oxygen ($^{18}\text{O}_2$) gas. Sulfur was deposited controllably via an electrochemical cell and characterized *in situ* by Auger Electron Spectroscopy (AES). The resulting diffusion profiles were measured by secondary ion mass spectrometry

(SIMS). Kinetic parameters were extracted by fitting the diffusion profiles with a previously derived mass transport model. The preliminary data shows that sulfur adsorption decreases the oxygen defect injection rate by roughly three times through affecting the injection flux, which points to a site blocking model. Subsequent temperature and pressure dependence study will help us gain insights into detailed injection kinetic pathways.

5:40pm **SS+AS+EM+EN-ThA11 Investigation of the Role of Electronic Defects and Grain Boundaries in Sputter Deposited CdS/CdTe Junctions and Solar Cells, Mohit Tuteja, University of Illinois at Urbana Champaign, P. Koirala, University of Toledo, J. Soares, University of Illinois at Urbana Champaign, R. Collins, University of Toledo, A. Rockett, University of Illinois at Urbana Champaign**

Device quality CdS/CdTe heterostructures and completed solar cells (~12% efficient) have been studied using low-temperature photoluminescence (PL) as a function of temperature (82-295 K) and laser excitation power (0.02-2 mW). The CdS/CdTe junctions were grown on transparent conducting oxide covered soda lime glass using rf-sputter deposition. It was found that the luminescence shifts from being dominated by sub-gap defect-mediated emission at lower excitation powers to near band edge excitonic emission at higher excitation powers. The effect of copper (Cu) used in making back contacts was studied in connection with the CdS/CdTe junction PL. It was found that the presence of Cu suppresses the sub-band gap PL emissions. This effect was concluded to be due either to Cu occupying cadmium vacancies (V_{Cd}) or forming acceptor complexes with them. This points to a potential role of Cu in plugging sub-band gap recombination routes and hence increasing charge separation ability of the device. An energy band diagram is presented indicating various observed transitions and their possible origins.

Thin Film

Room: 111 - Session TF+AS+NS+SA-ThA

Thin Film: Growth and Characterization, Optical and Synchrotron Characterization II

Moderator: Jay Hendricks, National Institute of Standards and Technology

2:20pm **TF+AS+NS+SA-ThA1 Dynamic and Structural Stability of Cubic Vanadium Nitride, Antonio Mei*, University of Illinois at Urbana-Champaign, O. Hellman, California Institute of Technology, N. Wireklint, Chalmers University of Technology, Sweden, C.M. Schlepütz, Argonne National Laboratory, D.G. Sangiovanni, B. Alling, Linköping University, Sweden, A. Rockett, University of Illinois at Urbana-Champaign, L. Hultman, Linköping University, Sweden, I. Petrov, J.E. Greene, University of Illinois at Urbana-Champaign**

Structural phase transitions in epitaxial stoichiometric VN/MgO(011) thin films are investigated using temperature-dependent synchrotron x-ray diffraction (XRD), selected-area electron diffraction (SAED), and resistivity measurements combined with high-resolution cross-sectional transmission electron microscopy (HR-XTEM) and *ab-initio* molecular dynamics (AIMD). At room temperature, VN has the B1 NaCl structure. However, at temperatures below $T_c = 250$ K, XRD and SAED results reveal forbidden (00l) reflections of mixed parity associated with a non-centrosymmetric tetragonal structure. At $T \leq T_c$, forbidden reflections intensify continuously following the scaling behavior $I \propto (T_c - T)^{1/2}$. This suggests a transition of second-order character, but the incompatible symmetries of the parent cubic VN (space group) and product tetragonal VN () phases ultimately requires that the structural transition be first order. Resistivity $\rho(T)$ plots between 300 and 4 K consist of two linear regimes resulting from different electron/phonon coupling strengths in cubic and tetragonal VN.

The VN transport Eliashberg spectral function $\alpha^2_{\text{tr}}F(\hbar\omega)$, the product of the phonon density-of-states $F(\hbar\omega)$ and the transport electron/phonon coupling strength $\alpha^2_{\text{tr}}(\hbar\omega)$, is determined and used in combination with room-temperature inelastic neutron scattering results to establish that while entropy favors the higher-temperature cubic phase, as T is lowered below T_c , tetragonal VN becomes the thermodynamic ground state due to its lower enthalpy. AIMD renormalized phonon dispersion relations are in agreement, showing that the energy of (00l) X-point phonons in NaCl-structure VN decreases and eventually becomes imaginary at $T \leq 250$ K. We demonstrate that free energy contributions due to vibrational entropy, often-neglected in theoretical modeling, are essential in understanding the

*** TFD James Harper Award Finalist**

room-temperature stability of NaCl-structure VN, and of strongly anharmonic systems in general.

2:40pm TF+AS+NS+SA-ThA2 Comparison of Solution Based Aluminum Oxide Phosphate Thin Films Deposited via Spin Coating vs. a Novel Mist Deposition System, Nishit Murari, R.H. Mansergh, Y. Huang, G. Westerfield, D. Keszler, J.F. Conley, Oregon State University

Solution based spin coating techniques are well known for producing high quality organic as well as inorganic metal oxide thin films. However, spin coating is primarily suitable for planar substrates and lacks the ability to form uniform ultrathin films over large surface areas. In recent years, several alternative mist based deposition techniques have been introduced to enable solution based deposition over large areas and non-planar substrates. Mist deposition involves the creation of a precursor mist and its subsequent condensation on the substrate. Mist deposition techniques to date have been limited by disadvantages such as the requirement for highly volatile precursors and the non-homogeneous distribution of the mist, both of which lead to inferior film thickness uniformity. To address these limitations, we employ a new mist deposition system with a novel mist creation technique consisting of an atomizer with two opposing precursor jets. The unique opposing configuration of the atomizer enables the formation of a highly uniform mist even from low volatility precursors. In this work, we address the question of whether this new mist deposition technique can produce film quality comparable to spin coating technique.

Amorphous aluminum phosphate (AlPO) thin films were deposited via mist deposition using a BENEQ ACS 200-101 as well as standard spin coating. All films were deposited at room temperature and pressure using precursors based on aqueous suspensions of aluminum phosphate inorganic clusters. The inorganic ligands decompose at low temperature with minimal volume change presenting a route to high density films at low temperature. Both mist and spin coating achieve thickness uniformity of 5% across a 150 mm Si substrate. Both techniques result in ultra-smooth films with average surface roughness of less than 1 nm RMS. Variation in film density and roughness as a function of annealing temperature was identical for both techniques. Finally, similar charge transport behavior and dielectric constant were exhibited as a function of anneal temperature.

An aqueous precursor was used in a side by side comparison of spin coating and a novel mist deposition technique. High quality AlPO thin films of similar uniformity, density, roughness, and electrical properties were obtained using both techniques. Based on these results, this novel mist based deposition technique appears to be a promising candidate for the next generation of thin film deposition techniques for large area electronics.

3:00pm TF+AS+NS+SA-ThA3 Electro-Optic Studies of $\text{Pb}_{0.95}\text{La}_{0.05}\text{Zr}_{0.54}\text{Ti}_{0.46}\text{O}_3$ Thin Films Deposited by Chemical Solution Deposition Method, Vaishali Batra, S. Kotru, V.N. Harshan, The University of Alabama, M. Varagas, C.V. Ramana, University of Texas at El Paso

Lanthanum doped lead zirconate titanate (PLZT) of perovskite type crystalline structure is an interesting transparent ferroelectric material due to its large remnant polarization and electro-optic effects, near the morphotropic phase boundary. The excellent optical and electrical properties make it material of choice for applications in MEMS, optical modulators/transducers and smart sensors. Recent studies reveal that this material possesses great potential for use in future photovoltaic (PV) devices which involves combination of optical transparency and ferroelectric properties. The advantage of using this material for PV applications is that the effect can be realized without a need of p-n junction as in semiconductor devices. Additionally the material exhibits bulk PV effect due to internal electric field originating from electric polarization. However, the optimization of processing conditions of deposited films is important to design efficient devices, which require understanding of the structure, its behavior with light, and response to electric field.

Lanthanum-modified lead zirconate titanate (PLZT) thin films with a composition of $(\text{Pb}_{0.95}\text{La}_{0.05})(\text{Zr}_{0.54}\text{Ti}_{0.46})\text{O}_3$ were deposited on Pt/TiO₂/SiO₂/Si substrates. The films were rapidly annealed in the temperature range of 550 to 750 °C in oxygen ambient to study the effect of crystallization on the electric and optical properties. X-ray diffraction revealed that the post deposition temperature changes the preferential orientation of the films. Optical band gap values determined from UV-visible spectroscopy and spectroscopic ellipsometry for PLZT films were found to be in the range of 3.42-4.00 eV. The optical constants and their dispersion profiles for PLZT films were also determined from SE analyses. PLZT films exhibit an index of refraction ~2.5 ($\lambda=630$ nm). The electrical properties were studied using the model for metal-ferroelectric-metal (MFM) heterostructures with Schottky contacts using Au electrodes. High remnant polarization (41.85 $\mu\text{C}/\text{cm}^2$), low coercive voltage (1.19 V) and high free carrier concentration ($\sim 1.1 \times 10^{18} \text{ cm}^{-3}$) were obtained from films

annealed at 750 °C. Thus post deposition annealing temperature plays a major role in deciding the electrical and optical properties.

3:20pm TF+AS+NS+SA-ThA4 Electron Scattering at Surfaces of Epitaxial Metal Layers, Pengyuan Zheng, D. Gall, Rensselaer Polytechnic Institute

Epitaxial Cu(001) is grown on MgO(001) with different overlayers to demonstrate that electron surface/interface scattering can be engineered by surface doping, causing a decrease in the resistivity. For instance, the resistivity of 9.3-nm-thick epitaxial and polycrystalline Cu layers is reduced by 11-13% when coated with 0.75 nm Ni. This is due to partially specular surface scattering with specularly parameters $p = 0.3$ and 0.15 for the Ni-coated Cu in vacuum and air, respectively, while scattering is completely diffuse ($p = 0$) for a pure Cu surface in air. This is attributed to the suppression of Cu₂O formation, leading to a lower localized density of states (LDOS) at the surface, and therefore less diffuse electron scattering. The change of surface scattering by controlling the LDOS is further confirmed: the sheet resistance of 9.5-nm-thick epitaxial Cu(001) increases by 4-43% if a 0.1-4 monolayer thick Ti coating is added, but subsequent exposure to 37 Pa of O₂ causes a resistivity reduction of 3-24%. This reduction is due to a recovery of specular interface scattering associated with a reduction of the LDOS during Ti oxidation from 15-27.4 to 2.4-6.5 eV⁻¹nm⁻², as quantified by ab initio calculations. Furthermore the surface scattering effect is found to be orientation dependent. For example, the resistivity of 5-nm-thick epitaxial tungsten layers is two times higher for 001 vs 110 orientated layers. This is due to the anisotropy in the Fermi surface, as indicated by transport simulations based on first-principles band structure calculations, which suggest a 1.5 times smaller size effect for the 110 orientation. These epitaxial films were sputter deposited onto Al₂O₃(11-20) and MgO(001) at 1050 °C and 900 °C, respectively, followed by in situ annealing at 1050 °C for 2 hrs. X-ray diffraction θ -2 θ , ω , and ϕ -scans confirm epitaxy and X-ray reflectivity indicates atomically smooth film-substrate interfaces and smooth film surfaces with a root-mean-square roughness that increases from 0.32±0.05 to 0.81±0.05 nm for W(110) with $t = 5.7$ -39.2 nm, and from 0.21±0.05 to 0.40±0.05 nm for W(001) with $t = 4.8$ -50 nm. In summary, we have systematically shown that (1) surface scattering can be altered by carefully controlling the surface LDOS at the Cu surface or interface with the barrier and (2) the crystalline orientation of interconnect wires with non-spherical Fermi surfaces is a major factor when considering alternative metals to replace Cu interconnects.

4:00pm TF+AS+NS+SA-ThA6 Lattice Relaxation in Multilayered Si_xGe_{1-x}/Si (001) Metamorphic Heterostructures, Tedi Kujofsa, J.E. Ayers, University of Connecticut

The inclusion of compositionally-graded metamorphic buffer layers in multilayered heterostructures allows tremendous flexibility designing novel SiGe/Si microelectronic and optical semiconductor devices. For example, advanced CMOS transistors can be fabricated on strain relaxed buffers to obtain enhanced mobility in n-channel and p-channel devices using tensile and compressive strain, respectively. While it is necessary to control the strain in the device layers, it is also desirable to fabricate these structures with low threading dislocation densities and minimum buffer thickness. Thus, understanding lattice relaxation in multilayered and compositionally-graded heterostructures is desirable to provide guidance in designing SiGe/Si devices. This work focuses on the design of the multilayered heterostructures comprising a uniform layer of Si_{1-x}Ge_x (device layer) deposited on a Si (001) substrate with an intermediate compositionally-graded buffer layer of Si_{1-x}Ge_x. The objective of this work is to study the relaxation dynamics and misfit dislocations in the device and buffer layer. We present minimum energy calculations and show that for a given device layer with fixed germanium composition and layer thickness, there exists a combination of the buffer layer thickness and compositional grading to provide tight control of the strain in the device layer. Furthermore, we give a simple model describing the strain in the device layer.

4:40pm TF+AS+NS+SA-ThA8 Growth Stress Evolution in Low Adatom Mobility Fe(Cr) Thin Films, Xuyang Zhou, The University of Alabama, T. Kaub, R.L. Martens, The University of Alabama, G.B. Thompson, The University of Alabama

During the post coalescence portion of thin film deposition, thin film stress is related to the grain size and adatom mobility of the depositing material. This stress state can be regulated by the mobility of atoms into or out of these grain boundaries. Using Fe(Cr) alloy thin films as a case study, the stress evolution during growth was investigated as a function of Cr content up to 8 at.%. During the deposition of the elemental films, each film grew with a tensile stress state on a Si wafer because of their low adatom mobility. Upon alloying 4 at.% Cr to the Fe film, the as-deposited grains grew from ~40 nm (pure Fe) to ~65 nm (Fe-04Cr), resulting in a stress relaxation from ~200 GPa*nm to 50 GPa*nm at a thickness of 300 nm. As the Cr content increased further, the grains refined back towards ~50 nm in

size resulting in a recovery of the higher tensile stress condition. The reduction of the grain size is contributed to Cr solute segregation to the grain boundaries, clustering, and ultimately precipitation at the boundaries. The real-time stress evolution during growth will be discussed in terms of the inferred microstructural evolution of the film using post-mortem atom probe tomography and transmission electron microscopy characterization. The results of which address how segregating behavior can be used as a means of thin film stress engineering.

5:00pm **TF+AS+NS+SA-ThA9 Development of an Analytical Model for Langmuir-Blodgett Silica Microsphere Assembly and Investigation of Ge Back Filling of the Opal Template by Polymer-Assisted Deposition**, Sarun Atiganyanun, M. Zhou, S.E. Han, S.M. Han, University of New Mexico

Self-assembled photonic crystals find a wide variety of applications, including low-loss waveguides, high-efficiency solar cells, and thermal emission control. Here, we investigate a low-cost scalable fabrication of an opal structure via self-assembly of colloidal silica microspheres and propose a model describing a relationship between assembly parameters. To fabricate an opal structure, silica microspheres with a diameter of ~900 nm are first functionalized with allyltrimethoxysilane. Langmuir-Blodgett (LB) method is then used to self-assemble silica microspheres onto Si(100) substrates. By optimally adjusting the pulling speed of the substrate and surface pressure within the trough, a hexagonally closed-packed structure is achieved. By repeating LB coating processes for n number of times, an n -multilayer assembly is formed, creating an opal template structure. Scanning electron microscopy and light diffraction experiment are used to identify assembly parameters that give the largest domain size. An analytical model is also derived from material flux balance and a 2D van der Waals equation of state of silica spheres on water surface to describe the relationship between pulling speed, surface pressure, barrier speed, number of layers, and sphere's diameter for optimal assembly. In this presentation, we will also discuss a facile approach to back-fill opal templates via polymer-assisted deposition of Ge. After forming the template structure, a solution of polyethylenimine, ethylenediaminetetraacetic acid and germanium dioxide is used to back-fill the voids between microspheres. The sample is then annealed in a forming gas environment, forming Ge films around the microspheres. After the microspheres are removed, the Ge structure is characterized with SEM, XRD, and light transmission.

5:20pm **TF+AS+NS+SA-ThA10 The Determination of Porosity and Pore Size Distribution of The Al_2O_3 Antireflection Coating Deposited By Atomic Layer Deposition**, Chao Li, M. Goorsky, University of California at Los Angeles

The porosity and pore size distribution of coatings prepared by atomic layer deposition and by other deposition techniques is important to understand their optical and mechanical properties. Specular X-ray reflectivity (SXRR) is capable of extracting layer thickness with angstrom resolution as well as determining the layer density. This makes it a good candidate for the porosity characterization of the antireflection coatings. On the other hand, advances in the development of X-ray generators and optics have made in-house glancing incidence small angle X-ray scattering (GISAXS) experimentation suitable for the determination of the size and shape of pores (in the scale of sub-nanometer to 100 nm) existing in thin films. It can be realized through the simulation of pore scattering based on distorted wave Born approximation (DWBA). Unfortunately, previous GISAXS studies failed to exclude the scattering from the rough surface and interfaces of thin films from the total scattering that was used for the simulation. In this study, we propose a refined GISAXS method characterizing the pore size distribution with the scattering from the rough surface and interfaces excluded. The scattering from the surface and interfaces was determined by the simulation of X-ray reflectivity (XRR) longitudinal scan with the parameters of the surface roughness σ , the lateral correlation length ξ and the Hurst parameter h extracted from the atomic force microscopy measurement, and layer thicknesses, densities and compositional grading determined by the specular XRR simulation. This refined GISAXS method, together the SXRR technique, was applied to utilize to reveal the effect of deposition techniques on the nanostructures of single-layer Al_2O_3 -based antireflection coatings. They were deposited using atomic layer deposition (ALD) which is a good candidate for multilayer antireflection coatings, due to the self-limiting nature of chemical reactions resulting in the precise control of film thickness and large-area uniformity. Each of them has two amorphous structures on a Si substrate grown with different deposition parameters. It is indicated by the refined GISAXS method that the first Al_2O_3 single layer is porous with a mean pore (spherical shape) radius of 7.2 nm while there are no pores in the second Al_2O_3 single layer. This agrees well with the SXRR showing a lower density of the first Al_2O_3 single layer (2.93 g/cm^3) than that of the second Al_2O_3 single layer (3.04 g/cm^3).

5:40pm **TF+AS+NS+SA-ThA11 Tuning Static and Dynamic Magnetic Properties of FeGa/NiFe Multilayer Composites**, Colin Rementer, Q. Xu, K. Fitzell, Z. Yao, P. Nordeen, G. Carman, Y. Wang, J.P. Chang, University of California at Los Angeles

Traditionally, the use of magnetic materials in high frequency applications has been limited to oxides. This is because the materials' high resistivity, which reduces the formation of eddy currents by the incident electromagnetic waves. However, these oxides have limited applications in multiferroics, which are materials that possess more than one ferroic ordering in a single phase or strain-coupled composite systems, due to their low magnetomechanical coupling. Metallic materials are more desirable to this end, but their magnetic hardness and conductive losses have limited their use.

Rare-earth-free iron-gallium (FeGa) is one of the most promising magnetostrictive materials for use in composite multiferroics, due to its high piezomagnetic coefficient (3 ppm/Oe) and high stiffness (70 GPa). It has been integrated into several multiferroic systems, but generally in the MHz range or below¹. This is due to the fact that the material has a large ferromagnetic resonance (FMR) linewidth (>300 Oe) at X band (9.6 GHz), which will result in incident energy being converted to heat. Metalloid dopants have been used to soften magnetic materials and to tune frequency dependent properties, such as permeability and piezomagnetic behavior, but at the cost of saturation magnetization as well as magnetostriction². In this work, multilayer laminates containing alternating hard and soft ferromagnetic layers were fabricated to reduce loss at high frequencies.

FeGa (hard) and NiFe (soft) were sputtered via alloy targets into multilayers on Si [100] and piezoelectric substrates with total thicknesses ranging from 40-500 nm. The compositions of the films were verified via X-ray photoelectron spectroscopy (XPS) and were found to be Fe_xGa_{1-y} ($78 \leq y \leq 85$ at%) and Ni_xFe_{1-x} ($79 \leq x \leq 83$ at%). Static magnetic properties were evaluated via superconducting quantum interference device (SQUID) magnetometry, and it was found that the incorporation of NiFe layers was found to reduce the coercivity by up to 80%, while only reducing the saturation magnetization by 20%. FMR measurements revealed a narrowing of the linewidth by up to 90% at X band. Permeability extracted from the reflection coefficient (S11) obtained via stripline measurement was found to be affected by layer thickness and number of layers. FeGa showed strong magnetoelastic behavior and the multilayers are expected to exhibit an enhanced piezomagnetic effect due their reduced coercivity.

References:

- 1.M. Hamashima, C. Saito, M. Nakamura and H. Muro, *Electr Commun Jpn* 95 (5), 1-7 (2012).
- 2.J. Lou, R. E. Insignares, Z. Cai, K. S. Ziemer, M. Liu and N. X. Sun, *Appl Phys Lett* 91 (18) (2007).

Tribology Focus Topic

Room: 230B - Session TR+AS+NS+SS-ThA

Molecular Origins of Friction

Moderator: Nicolas Argibay, Sandia National Laboratories

2:20pm **TR+AS+NS+SS-ThA1 Atomic-Scale Mechanisms of Single Asperity Sliding**, Ashlie Martini, X. Hu, University of California Merced, M.V.P. Altoe, Lawrence Berkeley National Laboratory **INVITED**

Isolating a single asperity to characterize its response to sliding is a heuristic approach to understanding the fundamental mechanisms that underlie friction and wear. A single asperity can be realized experimentally as the tip of an atomic force microscope cantilever. When the tip slides across a surface, friction is measured with atomic lattice-scale resolution and wear can be quantified in terms of nano- or even atom-scale volumes of material removed. However, challenges remain in interpreting these measurements because the observed friction and wear are due to processes that take place in the interface buried between the tip and the substrate on which it slides. Further, the nanometer scale of the contact implies that discrete atomic events in the interface may determine sliding behavior. Together, these observations suggest that the experiments could be complemented by atomistic models of the apex of the tip, near-contact substrate material and, of course, the interface itself. Although the simulations are limited to relatively small size and time scales, they have the potential to provide detailed information about mechanisms underlying phenomena that occur over short periods of time and small sliding distances. Specifically, in this research, we focus on the initial stages of friction and wear, and the processes that occur during the first tens of nanometers of sliding. The simulations are carefully designed such that they faithfully capture the corresponding experiments, including matching the materials, crystallography and geometry of the contacting bodies as

observed through transmission electron microscope images of the tip and atomic force microscope images of the substrate taken at 10 nm intervals during the sliding process. The experiments offer an unprecedented view of wear occurring single atomic layers at a time, and the simulations provide detailed complementary information about the atomic-scale mechanisms underlying this process.

3:00pm TR+AS+NS+SS-ThA3 Investigation of Epitaxy and Friction in Model Boundary Films, Hongyu Gao, University of California Merced, W.T. Tysoe, University of Wisconsin-Milwaukee, A. Martini, University of California Merced

Sliding friction of boundary films is investigated using ultrahigh vacuum (UHV) tribometer measurements of model alkali halide films on metals with complementary molecular dynamics (MD) simulations. We focus on a model system consisting of thin potassium chloride (KCl) films on an iron (Fe) substrate. The interaction potential between KCl and Fe is tuned using activation energy obtained from temperature programmed desorption (TPD) data and structures inferred from low-energy electron diffraction (LEED) measurements. The simulation is then used to explore the effect of film thickness and pressure on the formation of an epitaxial KCl film. The nature of this film and its near surface structure is then correlated with sliding friction behavior.

3:20pm TR+AS+NS+SS-ThA4 Temperature Dependence of Atomic-scale Friction on Two-dimensional Materials, Zhijiang Ye, University of California Merced, X.Z. Liu, K. Hasz, R.W. Carpick, University of Pennsylvania, A. Martini, University of California Merced

Temperature plays an essential, yet complex role in determining atomic-scale friction. Recent studies of the temperature dependence of atomic-scale friction have reported different trends that suggest distinct and possibly contradictory underlying mechanisms. Specifically, friction is usually found to decrease with increasing temperature (due to thermolubricity), but this behavior is not always observed (attributed to adsorbates or meniscus effects). To understand the origins of these trends, we use molecular dynamics (MD) simulations and parallel replica dynamics (PRD) to study the temperature dependence of atomic friction on two-dimensional (2-D) materials, such as molybdenum disulfide. The MD simulations are designed to be closely-matched with corresponding atomic force microscope (AFM) measurements [1, 2]. Using the simulations and experiments, we explore how friction varies with temperature and how that variation is affected by other parameters, including sliding velocity, material, and environment. These studies provide new insights into how temperature affects friction on 2-D materials, and into the origins of atomic-scale friction generally.

References:

1. Xin-Z. Liu, Zhijiang Ye, Yalin Dong, Philip Egberts, Robert W. Carpick, and Ashlie Martini. Dynamics of Atomic Stick-Slip Friction Examined with Atomic Force Microscopy and Atomistic Simulations at Overlapping Speeds, *Phys. Rev. Lett.* **114**, 146102 (2015).
2. Qunyang Li, Yalin Dong, Danny Perez, Ashlie Martini, and Robert W. Carpick. Speed dependence of atomic stick-slip friction in optimally matched experiments and molecular dynamics simulations. *Physical Rev. Lett.* **106**, 126101 (2011).

4:20pm TR+AS+NS+SS-ThA7 Single Molecule Experiments to Explore Friction and Adhesion, Rémy Pawlak, S. Kawai, A. Baratoff, T. Meier, University of Basel, Switzerland, W. Ouyang, Tsinghua University, China, T. Glatzel, University of Basel, Switzerland, E. Gnecco, IMDEA-Nanociencia - Universidad Autónoma de Madrid, Spain, A. Filippov, Donetsk Institute of Physics and Engineering, Ukraine, M. Urbakh, Tel Aviv University, Israel, E. Meyer, University of Basel, Switzerland

INVITED

Controlled manipulation processes of single-molecules with an atomic force microscope (AFM) provide valuable information about their interactions with surfaces, leading to fundamental insights into adhesion and friction properties. To understand such phenomena at such scale, tuning-fork based AFM operated at low temperature is an appropriate tool since complex manipulations of single-molecules can be readily performed and detected via advanced force spectroscopic techniques [1]. With such approach however, the measured frequency shifts are related to normal force gradients, and thus the interpretation of friction phenomena is not fully straightforward. To overcome this issue, we developed analytical models to simulate the experimental AFM data which allow us to determine adhesive energy and nanoscale friction. In this presentation, a first example will be given by the vertical pulling of long polymeric chains on Au(111), where their detachment leads to oscillations of the normal and lateral forces [2]. As in Frenkel-Kontorova (FK) models of friction, the polymer is represented by a chain of units connected by springs of stiffness k , each one interacting with a 2D periodic substrate potential. Force and gradient variations are dominated by the sequential detachment of each molecular

units if k is large enough to cause superlubric sliding. A second example will show vertical and lateral manipulations over a Cu(111) surface of a single porphyrin molecule attached to the AFM tip apex. In the frequency shift traces, atomic sawtooth modulations are systematically observed while sliding over the surface and are related to the internal degree of freedom of the molecular structure [3].

References:

- [1] R. Pawlak, S. Kawai, T. Glatzel, E. Meyer. *Single Molecule Force Spectroscopy* (ncAFM, vol.3, Springer, Japan 2015).
- [2] S. Kawai et al., Quantifying the atomic-level mechanics of single long physisorbed molecular chains, *Proc. Nat. Acad. Sci.*, **111**, 3968–3972 (2014)
- [3] R. Pawlak et al. *Intramolecular response of a single porphyrin molecule during AFM manipulations*. Submitted.

5:00pm TR+AS+NS+SS-ThA9 Effects of Humidity on the Adhesion and Friction of Carbon-Based Materials, Judith Harrison, M. Fallet, K.E. Ryan, United States Naval Academy, T. Knippenberg, High Point University, S.H. Kim, A. Al-Azizi, Pennsylvania State University

Atomic-scale wear in nanoscale contacts is of particular importance for tip-based nanomanufacturing applications. As a result, wear resistant materials, such as diamond-like carbon (DLC), have been used to coat AFM tips to improve the lifespan and reliability of AFM probes and surfaces. Unfortunately, the tribological performance of these materials is known to depend on environmental conditions, such as humidity levels. We have performed macroscopic and atomic force microscopy friction experiments and molecular dynamics (MD) simulations aimed at examining adhesion and wear of DLC in humid environments.

Macro-scale friction tests showed friction and transfer film dependence on humid conditions. Low humidity suppresses transfer film formation while keeping the friction low. Intermediate humidity, however, does not reduce transfer film formation and increases the friction. The effect of humidity on friction was found to agree with the adhesion dependence on relative humidity as measured with atomic force microscopy.

Because it is difficult to elucidate atomic-scale mechanisms via experimental methods, molecular dynamics simulations have been employed to examine this behavior. Adhesion and sliding simulations of non-hydrogenated, ultrananocrystalline diamond (UNCD) and DLC surfaces with various levels of hydrogen in the presence of water using the qAIREBO and the ReaxFF potentials have been performed. Because both of these potentials are able to model chemical reactions, the atomic-scale mechanisms responsible for adhesion and wear can be identified. Results obtained with both potentials will be compared to the experimental results.

5:20pm TR+AS+NS+SS-ThA10 Single Asperity Tribochemical Wear of Silicon AFM Tips Sliding on Aluminum Oxide, Erin Flater, S. Sorenson, Luther College, N. Ansari, A. Poda, W.R. Ashurst, Auburn University, B.P. Borovsky, St. Olaf College

Understanding of tribological mechanisms at the submillimeter scale continues to be relevant since friction and wear limit the commercial viability of small-scale mechanical devices such as microelectromechanical systems (MEMS). For example, tribochemical processes play a significant role in many materials systems, including silicon oxide and aluminum oxide, which are relevant materials for MEMS devices. Our work focuses on understanding tribological processes at the interface of silicon AFM tips and amorphous aluminum oxide surfaces. We observe wear of silicon tips after repetitive sliding on the aluminum oxide surface, which occurs even at low contact pressures, implying that the wear process is chemical in nature. We quantify tip wear by intermittently interrupting the wear experiment to perform indirect *in-situ* tip imaging on a sharp-spiked sample. We use these tip images to quantify volume of material lost during scanning. Wear as a function of sliding distance is modeled using reaction rate theory and is compared to the Archard wear model. While some of our results appear to agree with an Archard model, these results may be more appropriately interpreted in light of the more fundamental reaction rate theory.

5:40pm TR+AS+NS+SS-ThA11 Molecular Simulation of Indentation as a Probe of Scanning Probe Tip Mechanical Properties, J. David Schall, K. Vummaneni, Oakland University, J.A. Harrison, United States Naval Academy

Scanning probe tips should be robust, have low adhesion, and low wear to ensure repeatability and long tip life. As new tip materials are developed these properties must be quantified and compared to existing tip materials. In this study, molecular simulation is used to measure the elastic modulus and work of adhesion of a variety of tips against a common substrate material, in this case H-terminated diamond (111). The tip materials investigated include Si, SiC, amorphous SiC, diamond, diamond like carbon and ultra-nanocrystalline diamond (UNCD). SiC was recently proposed as a

new high hardness, low wear tip material. In simulation the tip geometry can be controlled to enable direct comparisons between each tip material. Both dynamic simulations at 300K and quasi-static indentions using stepwise energy minimization with and with out adhesion between tip and substrate were used. Simulations of sliding friction and wear have also been conducted to investigate the correlation between tip materials properties and friction and wear.

Thursday Evening Poster Sessions

Applied Surface Science

Room: Hall 3 - Session AS-ThP

Applied Surface Science Poster Session

AS-ThP1 Applications of EMSL's Radiochemistry Annex (RadEMSL) in Understanding of the Chemical Fate and Transport of Radionuclides in Terrestrial and Subsurface Ecosystems, Mark Engelhard, Pacific Northwest National Laboratory

(RadEMSL) is a radiochemistry facility, which is part of EMSL, Environmental Molecular Sciences Laboratory, a Department of Energy Office of Science User Facility sponsored by the Office of Biological and Environmental Research and located at PNNL. This facility is designed to accelerate scientific discovery and deepen the understanding of the chemical fate and transport of radionuclides in terrestrial and subsurface ecosystems. In this poster we present results obtained from two different studies that have utilized the X-ray Photoelectron Spectroscopy (XPS) capability in this facility.

The first application involved XPS analysis of Uraninite (UO_2). UO_2 is the primary component of most nuclear fuels, and can be a major phase in bio-remediated uranium-contaminated soils and aquifers. Understanding the mechanisms of UO_2 surface oxidation and corrosion is essential to predicting its stability in the environment throughout the nuclear fuel cycle. XPS shows clear evidence of U(IV) and U(V) oxidation states consistent with computational results. This new mechanism may be relevant to other fluorite structures, including plutonium dioxide (PuO_2).

The second application involves XPS analysis of Np. Neptunium (Np) is a long-lived radionuclide environmental contaminant associated with weapons production and processing that is transported in the subsurface as actinyl NpO_2^+ . The radioactive metallic element Np is created when uranium-based nuclear fuel is burned up in electricity-producing commercial reactors and in plutonium-producing reactors operated for military purposes. Researchers examined factors that impact structural incorporation of Np(V) neptunyl and U(VI) uranyl ions into carbonate and sulfate minerals. Co-precipitation of Np(V) into mineral structures could reduce transport in the subsurface and shows promise as a groundwater remediation strategy.

Rad(EMSL) offers experimental and computational tools uniquely suited for actinide chemistry studies. The spectroscopic and imaging instruments at this facility are ideally designed for the study of contaminated environmental materials, examination of radionuclide speciation and detection of chemical signatures. The annex houses nuclear magnetic resonance instruments and surface science capabilities, such as X-ray photoelectron spectroscopy, electron microscopy, electron microprobe, transmission electron microscopy and scanning electron microscopy.

AS-ThP2 XPS and AES Characterization of Tribofilm Formation on Non-Metallic Coatings Using ZDDP and Ionic Liquid Lubricant Additives, Harry Meyer III, J. Qu, Z.B. Cai, C. Ma, H. Luo, Oak Ridge National Laboratory

Interactions between oil additives and non-metallic surfaces are less well understood than tribofilm formation on metallic surfaces. The most common anti-wear additive for metallic surfaces is zinc dialkyldithiophosphate (ZDDP). In this study, ZDDP and a phosphonium-organophosphate ionic liquid (IL) are used with three hard coatings (AlMgB₁₄-TiB₂, TiB₂, and diamond like carbon), to determine what, if any, tribofilms are formed when sliding against a steel ball. Systematic characterization was conducted on the coating wear scars including top surface morphology imaging and elemental mapping, layer-by-layer chemical analysis, and cross section nanostructural examination. For boride coatings, tribofilms formed by ZDDP+IL are up to 50-70 nm thick with 75-80% surface coverage. On the other hand, tribofilms on DLC were <25 nm thick and only covered 20-30% of the contact area. The presence of iron compounds in the tribofilms suggests a critical role for wear debris in tribofilm formation. In addition, oxidation products of TiB₂ were detected in the tribofilms. No involvement of the DLC surface in tribofilm formation was observed. Results suggest that wear debris digestion and contact surface reaction both are critical in tribofilm formation: the former process is responsible in forming the bulk of the tribofilm and the latter provides strong bonding of the tribofilm to the contact surface. In this poster, the emphasis will be how scanning Auger microanalysis and x-ray photoelectron spectroscopy were used for characterizing the ZDDP+IL-derived tribofilms.

AS-ThP3 XPS Sputter Depth Profiling of Organometallic Multilayer Materials using Massive Argon Cluster Ions, Simon Hutton, Kratos Analytical Limited, UK, T. Bendikov, Weizmann Institute of Science, Israel, W. Boxford, S.C. Page, J.D.P. Counsell, A.J. Roberts, C.J. Blomfield, S.J. Coultas, Kratos Analytical Limited, UK

Thin polymer films are found in an enormous range of devices and have many applications from use in semi-conductors, displays and solar cells to corrosion protection and packaging. New ion sources such as the multi-mode Ar gas cluster ion source (GCIS) have revolutionised the study of such organic thin films by depth profiling with techniques such as X-ray photoelectron spectroscopy (XPS). As reported elsewhere the chemical composition of organic thin films may now be determined as a function of depth by a combination of XPS analysis and etching using massive Ar ions.

In this study we present results from GCIS XPS depth profiling of multi-layer organometallic thin films. The films consist of two well defined and iso-structural osmium and ruthenium polypridyl complexes. These complexes are deposited from solution in a sequence-dependent assembly regime leading to self-propagating molecular assemblies with distinct internal interfaces and composition. [1] The layer-by-layer deposition approach used here allows multiple building blocks to be incorporated into the film.

Depth profiling through the films using the GCIS allowed the structure to be confirmed and relative layer thicknesses to be tentatively compared. The depth profiles were carried out using optimised conditions for cluster formation and X-ray exposure was limited to reduce detrimental effects, including modification of the etch rate, noted elsewhere. [2]

[1] G. de Ruiter, M. Lahav, G. Evmenenko, P. Dutta, D. A. Cristaldi, A. Gulino and M. E. van der Boom, *J. Am. Chem. Soc.* 2013, 135, 16533-16544.

[2] P. Cumpson, J. F. Portoles, N. Sano, and A. J. Barlow, *J. Vac. Sci. Technol. B* 31(2), 2013.

AS-ThP4 XPS Analysis and Sample Preparation for EBSD Analysis using Argon Gas Clusters, Adam Bushell, Thermo Fisher Scientific, UK, R. Simpson, University of Surrey, UK, C.J. Stephens, C. Deeks, T.S. Nunnery, J.P.W. Treacy, Thermo Fisher Scientific, UK

The use of noble gas ions for sputter cleaning and profiling materials in X-ray Photoelectron Spectroscopy (XPS) analyses is well established. Monatomic ions are generally used while analysing hard inorganic materials, providing efficient cleaning and a good sputter rate while profiling. More recently, argon ion clusters have been found to be very effective at cleaning and profiling organic materials. Cluster ion sputtering of these materials is suitable for cleaning the surface without inducing chemical modification, but it also has potential for preparing surfaces for analysis by techniques other than XPS.

In this presentation we will show the results of an investigation into using a range of cluster energies and sizes not only for XPS, but how they can be used for sample preparation in EBSD. We will illustrate the potential level of successful EBSD analysis that can be achieved when the appropriate etching criteria are used on a sample.

AS-ThP5 Comprehensive Characterization High-k Dielectric Films Deposited by ALD using Multi-Technique Surface Analysis, Richard White, Thermo Fisher Scientific, UK

It has been known for many years that XPS is the ideal technique for characterizing ultra thin layers encountered during semiconductor device fabrication. Standard XPS analysis allows the analyst to detect and quantify elements and chemical bonding states in the stack of layers within 5-10nm thickness. Extension of the analysis to angle resolved XPS (ARXPS) adds another dimension to the data, enabling non-destructive depth profiling of the stack and the measurement of buried layer thickness.

Modern XPS spectrometers, which also come pre-configured with additional surface analysis techniques, can measure several other parameters of interest to the semiconductor engineer/scientist. As well as measuring surface elemental and chemical state information, XPS can provide the analyst with electronic information such as band gap and valence band offset. The complementary technique of Reflection Electron Energy Loss Spectroscopy (REELS) can also give a measurement of band gap in those situations where XPS has trouble, e.g. when the stack contains hafnium oxide.

Finally, if an XPS spectrometer is also configured with Ion Scattering Spectroscopy (ISS) then a direct indication of film surface coverage can be made. This technique measures the kinetic energy of noble gas ions

scattered from a surface and can be used to investigate the growth mode of high-k films during atomic layer deposition.

AS-ThP6 XPS and ToF-SIMS Characterization Functionalized 3D Mesostructures fabricated by Direct Laser Writing. *Michael Bruns, A. Welle, A.S. Quick, T. Claus, G. Delaittre*, Karlsruhe Institute of Technology, Germany, *T.S. Nunney*, Thermo Fisher Scientific, UK, *M. Wegener, C. Barner-Kowollik*, Karlsruhe Institute of Technology, Germany

In recent years significant effort has been spent to develop strategies for the fabrication of structured (bio)polymer modified surfaces on various substrates to alter the properties or to introduce entities with specific functions. These still ongoing activities are mainly stimulated by the wide range of applications in various scientific fields, such as lab-on-a-chip technology, biointerfaces, and tissue engineering. The utilization of photo-triggered Diels-Alder reactions in combination with shadow masking is an established efficient tool to achieve precise chemically structured surfaces in 2D.[1, 2] However, when aiming at the fabrication of complex 3D structures equipped with different surface functionalities, direct laser writing (DLW) is the method of choice. Most recently developed photoresists comprising e.g. orthogonal thiol-yne chemistry and click chemistry for a subsequent dual surface modification open up a facile avenue to fabricate various structures with several tailored functionalities.[3] In all cases surface analytical methods are indispensable to prove the successful chemical modification in a non-destructive manner. Therefore, the present contribution focuses on the characterization of such 3D structures using the combination of X-ray photoelectron spectroscopy (XPS) and complementary time-of-flight secondary ion mass spectrometry (ToF-SIMS). For non-patterned samples XPS quantitatively evidences the successful functionalization of surfaces for every single reaction step, whereas ToF-SIMS allows for rapid investigation of the chemical 2D patterning at high spatial resolution. For selected samples advanced parallel XPS imaging is additionally applied to calibrate the ToF-SIMS findings, obtaining quantitative information. For the chemical surface characterization of the well-defined 3D structures, ToF-SIMS proves an efficient tool for non-destructive 3D characterization of excellent spatial resolution with the advantage to achieve chemical/molecular information simultaneously.

[1] T. Tischer, T. K. Claus, M. Bruns, V. Trouillet, K. Linkert, C. Rodriguez-Emmenegger, A. S. Goldmann, S. Perrier, H. G. Börner and C. Barner-Kowollik, *Biomacromolecules* 14 (2013) 4340–4350.

[2] T. Paulöhr, G. Delaittre, V. Winkler, A. Welle, M. Bruns, H.G. Börner, A. M. Greiner, M. Bastmeyer, C. Barner-Kowollik, *Angew. Chem. Int. Ed.*, 51 (2012) 1071–1074.

[3] A. S. Quick, A. de los Santos Pereira, M. Bruns, T. Bückmann, C. Rodriguez-Emmenegger, M. Wegener and C. Barner-Kowollik, *Adv. Funct. Mat.* 2015, in press.

This work was carried out with the support of the KNMF, a Helmholtz Research Infrastructure at KIT.

AS-ThP7 Structure, Surface Analysis, Photoluminescent Properties and Decay Characteristics of Tb³⁺-Eu³⁺ Co-Activated Sr₂MgSi₂O₇ Phosphor. *M.A. Tshabalala, O.M. Ntwaeaborwa*, University of the Free State, South Africa, *Simon Dhlamini*, University of South Africa

Strontium magnesium silicate (Sr₂MgSi₂O₇) is an alkaline earth silicate that belongs to a group of natural minerals of the melilites group called sorosilicates. Sorosilicates have the same basic crystal structure and they can be represented by a general formula A₂MT₂O₇ (A = Ca, Sr, Na; M = Mg; and T = Si, Al, B). They usually crystallize in a tetragonal structure with a space group P4₂/m. Due to their tetragonal crystal structure without an inversion center, lanthanides or transition metals can be incorporated easily as activators or dopants in melilite hosts². Due to this ease of incorporation, melilites are today widely used as host lattices for rare-earth dopant and transitional metal ions to prepare light emitting materials or phosphors that can be used in many practical applications such as flat panel displays, light emitting diodes, solar cells and many other types of light emitting devices. In this study, we investigated the structure, chemical and electronic states, ionic and atomic distribution and photoluminescent properties of Sr₂MgSi₂O₇ single doped with Eu³⁺ or Tb³⁺ or co-doped with Eu³⁺ and Tb³⁺ by a solid-state reaction method. It turned out that the emission color could be tuned from blue to green or white depending on the dopant concentrations and the excitation wavelength.

The structure, stretching vibrations, chemical and electronic states, and photoluminescent properties were studied using X-ray powder diffraction (XRD), Fourier transformed infrared spectroscopy (FT-IR), X-ray photoelectron spectroscopy (XPS), Time-of-flight secondary ion mass spectrometer (ToF-SIMS) and Photoluminescence (PL) spectroscopy respectively. The XRD pattern of the Sr₂MgSi₂O₇:Eu³⁺, Tb³⁺ phosphor resemble the standard tetragonal phase of Sr₂MgSi₂O₇. The fitted XPS data demonstrated that there were two different Sr²⁺ sites in the host lattice and a

site occupied by Mg²⁺ cations which connects the Sr²⁺ sites with the Si⁴⁺ ions. The TOF-SIMS results demonstrated localization and distribution of various ions within the host lattice (Sr₂MgSi₂O₇) including the Tb³⁺ and Eu³⁺ dopants. The photoluminescence data indicated that the emission colour could be tuned from blue-green depending on the concentration of Tb³⁺. The white photoluminescence was observed from the Tb³⁺-Eu³⁺ co-activated system. This tunable emission has potential application in solid state lighting like white and multicolor light emitting diodes (LEDs).

References

1. T. Endo, Y. Doi, M. Wakeshima, Y. Hinatsu, *Inorg. Chem.* 2010, 49, 10809 - 10814.

2. A.A. Kaminskii, L. Bohaty, P. Becker, J. Liebertz, P. Held, H.J. Eichler, H. Rhee, J. Hanuza, *Laser Phys. Lett.* 2008, 5, 845 - 868.

AS-ThP8 XPS Study of Many-Electron Interaction & Exchange Interaction of Local Moments in Ion Beam Synthesized Ternary Transition Metal Silicides. *Wickramaarachchige Lakshantha, M. Dhoubhadel, F. McDaniel, B. Rout*, University of North Texas

In recent years, the interest in ternary metal (iron) silicides system is triggered by its potential use in advanced silicon based opto-electronic devices. However the ternary silicides have been by far less studied than their binary counterparts despite the fact that they might be beneficial in decreasing the formation temperature of disilicides. The phase formation of ternary silicides is not well understood, because most often the ternary silicides are formed in metastable phases. Among the well-known synthesis techniques to form or modify the composition and physical properties of thin films, low energy ion implantation has shown to be a very powerful technique. The ternary metal silicides can be synthesized by sequentially implantation of two metals into a Si substrate. In this study, Fe-Co-Si & Fe-Ti-Si ternary phases were formed by sequentially implanting either Co or Ti, along with Fe into Si (100) at room temperature (RT). Dynamic ion implantation simulation was performed to determine the ion fluences for concentration saturation of implant ions in the Si matrix. Then the optimal saturation fluences of each ions were implanted at 50 keV into Si substrates. Further same implantation process were performed under an externally applied magnetic field. The samples were subsequently annealing at temperature ranging from 200 – 600 °C. X-ray diffraction (XRD) analysis shows that even without annealing significant amount of ternary phase formation for ion implantation under external magnetic field. Further structural evolutions of ternary phases were observed with the annealing temperature. X-ray photoelectron spectra show core-level (Fe 2p_{3/2} & 3s) spectral asymmetry and splitting in these transition metal compounds. We believe this is the direct evidence of high Density of State (DOS) at valance band and a local moment in the ternary compounds.

AS-ThP9 Using ToF-SIMS to Characterize Surface Contamination in Sandia's Z Machine. *James Ohlhausen, B. Clark, R. Tang, D. Lamppa, D. Susan, R. Sorensen*, Sandia National Laboratories

The Z machine at Sandia National Laboratories is the world's most powerful and efficient laboratory X-ray radiation source. It generates 3-MV, 100-ns, 20-MA current pulses to compress target loads and produce high temperatures, high pressures, and 300-TW X-ray pulses for research in high energy density science. The Z machine target is fed by four parallel Magnetically-Insulated Transmission Lines (MITLs). The MITLs and target load hardware must be located in a high-vacuum chamber because of the exceptionally high electric- and magnetic-field stresses. The MITL electrode surfaces must be as clean as possible to maximize current delivery to the load. Residue from hardware handling, post-shot debris, and other environmental contaminants may generate electrode plasmas that contribute to current losses exceeding 6 MA for certain types of loads. Decreases in current delivery negatively affect all aspects of Z shot performance.

This analysis is part of a larger experiment to evaluate the efficacy of *in-situ* plasma cleaning within the Z machine's load region. Witness samples taken from different steps during hardware preparation and installation are used to characterize surface contaminants. ToF-SIMS is uniquely suited to perform analysis of these surfaces owing to its ability to image large areas while measuring elemental and chemical information. Both organic and inorganic species were detected in the form of particles and films. Contaminants found during the Z machine load hardware lifecycle were characterized before and after plasma cleaning to determine the effectiveness of plasma processing on the specific contaminants found. Methods of acquisition, analysis and quantification will be shown. Preliminary findings from the ToF-SIMS analysis will be presented.

**Sandia National Laboratories is a multi-program laboratory managed and operated by Sandia Corporation, a wholly owned subsidiary of Lockheed Martin Corporation, for the U.S. Department of Energy's National Nuclear Security Administration under contract DE-AC04-94AL85000.

AS-ThP10 Going Beyond Visualization: Exploiting Synergies Between Electron Microscopy and ToF-SIMS, Kathryn Lloyd, C.D. Chan, J.R. Marsh, D.J. Walls, S. Subramoney, DuPont Corporate Center for Analytical Sciences

As is most often the case with research and development characterization challenges, no one analytical technique is able to “tell the complete story”. The combination of inorganic and organic layers and components in today’s advanced materials and display systems requires new sample preparation and analytical strategies. Natural systems such as leaves and seeds, as well as hair and skin, require molecularly specificity. A common analytical need is to be able to distinguish phases or layers at sub-micron lateral resolution, based on molecular signatures.

Electron microscopy (SEM or TEM) is often the first step towards sub-micron visualization. ToF-SIMS (secondary ion mass spectrometry) provides mass spectral data, and thus molecular specificity, with typically 1 micron lateral resolution. Since the lateral resolution of EDS, often used in conjunction with SEM to provide elemental maps, is also around 1 micron, the two techniques can be combined with the secondary electron images to provide a more complete chemical picture. Organic contamination in metal powder synthesis and feed granule coatings provide two examples.

Cross-sectional sample preparation using Focused Ion Beam (FIB) technology has allowed SEM and TEM visualization of layers and defects that could not be achieved using more traditional sample preparation approaches. A companion analysis for these types of samples is top-down ToF-SIMS depth profiling, as the depth resolution in this type of experiment is typically tens of nanometers or less. Combining the information from these two approaches is challenging and not always straightforward. Examples from displays and other layered structures will be shown.

AS-ThP11 The Benefits of Using All of the Measured Mass Channels During MVSA of ToF-SIMS Data Sets, Vincent Smentkowski, General Electric Global Research Center, M.R. Keenan, Independent Scientist, H. Arlinghaus, ION-TOF GmbH

Time of flight secondary ion mass spectrometry (ToF-SIMS) data sets are very large and contain a wealth of information about the material being analyzed. A typical image data set can be comprised of 256 x 256 pixels with a 0 to 900 amu (or greater) mass spectrum collected at high ($M/\Delta M \sim 10,000$) mass resolution at every pixel. Data sets are often comprised of $>1 \times 10^{15}$ spectral channels. The challenge for a ToF-SIMS analyst is to scrutinize all of the measured information without bias in order to provide for the most robust understanding of the material being analyzed; this is especially important in an industrial setting where unknown samples are analyzed. Multivariate statistical analysis (MVSA) algorithms have assisted in ToF-SIMS data work up [1,2], however commercially available software is not able to handle data sets this large and the analysts often select mass intervals to utilize and/or degrades the mass resolution prior to MVSA analysis. In this poster, we will report first results obtained using MVSA software that is able to handle massive ToF-SIMS data sets. We demonstrate two important benefits of unbiased analysis of the massive ToF-SIMS data sets: (1) finding unexpected elements in real world samples (this is a reason why the authors never use peak lists for MVSA analysis) and (2) the ability to obtain high mass resolution results from data sets collected at nominal mass resolution (e.g., the beam alignment pulsing mode on ION-TOF instruments). The importance of these two benefits will be highlighted.

References: [1] Surface and Interface Analysis, Special issue on Multivariate Analysis. Volume 41, issue 2 Feb 2009

[2] Surface and Interface Analysis, Special issue on Multivariate Analysis II. Volume 41 issue 8, Aug 2009

AS-ThP12 Electron Gun Tilting and Shifting with O-Ring Stack System, In-Yong Park, B. Cho, KRIS, Korea, C. Han, KBSI, Korea, D. Lee, S.J. Ahn, KRIS, Korea

Most of the charged particle instruments (CPBIs) have the gun which generates a charge particle beam and column which controls a beam direction. In CPBIs, the precise alignment between gun and column is very important to get a best performance, such as high imaging resolution and patterning resolution. Generally, mechanical moving and electro-magnetic deflection are adopted to adjust beam path relatively in the each component. Most mechanical alignment operations use sliding single O-ring or thin metal bellows, which allow motion while preserving the internal vacuum. However, single O-ring allows the only small changes of shifting and tilting. For the double-deflector, an electronic part controlling the applied voltage or current is necessary, a fairly difficulty to assemble double-deflector part inside a vacuum chamber included. In this work, we center around on a simple and cheap electron gun alignment method in the laboratory experiment and early stages of CPBIs development.

To monitor the electron beam movement controlled by flange motion, we use a thermionic electron source and maintained a vacuum pressure of approximately 10^{-5} Pa with a combination of a rotary pump and a turbo-molecular pump which ran in tandem. In order to accelerate the generated electron beam, the electron gun system is floated at a negative 20 kV and the filament is heated by adjusting the current flow. Finally, the accelerated electrons hit the phosphor screen and make the visible light. We stacked ten O-rings and insert the metal center rings between O-rings to maintain the structure stably. We assembled four identical structures, all of which can shift the gun flange vertically and horizontally with clamping screws and separate it azimuthally with an equal space on the flange, which is under the O-rings. We monitored the beam position at the phosphor screen in real time shifting and tilting the flange on which electron gun is installed. Also, we get the nearly identical values comparing the experiment result and theoretical calculation result. This means that we can control the electron beam direction precisely with O-ring stack system maintaining the inside vacuum pressure steadily. We demonstrate a tilting angle of $\pm 2.55^\circ$ with shifts of ± 2 mm experimentally¹, values which are generally sufficient for application to CPBI gun alignment, as this adjustable range can cover the error range when the parts are made and assembled. It can also be applied when insulation is needed between the flanges while maintaining some degree of freedom.

[1] I.-Y. Park, B. Cho, C. Han, S. Shin, D. Lee and S. J. Ahn, Rev. Sci. Instrum. 86, 016110 (2015).

AS-ThP13 Covalent Surface Modification of Silicon Oxide Substrate using Aliphatic Alcohols and Microwave Radiation, Austin Lee, B.D. Gates, Simon Fraser University, Canada

Microwave radiation is used to react alcohols with silicon oxide surfaces to form self-assembled monolayers (SAMs). Advantages of using alcohols as building blocks for the formation of SAMs include their widespread availability, ease of handling, and stability against side reactions. Challenges to preparing monolayers of aliphatic alcohols on silicon oxide surfaces include the relatively high temperatures and slow reaction kinetics of the alcohol condensation reaction. Microwave radiation delivers sufficient thermal energy for the condensation reaction to occur in a fast, efficient manner. To demonstrate this capability, monolayers of 1-butanol, 1-octanol, and 1-octadecanol were successfully formed with the assistance of a microwave oven, and the monolayers were evaluated using Soxhlet extraction, WCA, AFM, and XPS. We optimized this reaction to render the silicon oxide surfaces hydrophobic, and successfully coated alcohols onto both the native oxide of silicon substrates and glass microscope slides.

AS-ThP16 XPS Analysis of Polycrystalline Samples $(\text{Bi}_3\text{M})(\text{Sb}_3\text{M})\text{O}_{14}$ type Pyrochlore with $\text{M} = \text{Cu, Co and Zn}$, Lazaro Huerta, R. Escamilla, M. Romero, Universidad Nacional Autonoma de Mexico, M. Flores, Universidad de Guadalajara, Mexico, A. Duran, Universidad Nacional Autonoma de Mexico

The general formula of the oxide pyrochlores can be written as $\text{A}_2\text{B}_2\text{O}_6\text{O}'$ with four crystallographically nonequivalent atom sites. These compounds have potential applications in a variety of applications as catalysis, magnetic and ionic conducting materials. A particular pyrochlore-type phase with $\text{Bi}_{1.5}\text{ZnSb}_{1.5}\text{O}_7$ stoichiometry is used in ZnO-based varistors, a polyphasic ceramic with property based on the grain boundary phenomenon. Here, we synthesized the polycrystalline samples of $(\text{Bi}_3\text{M})(\text{Sb}_3\text{M})\text{O}_{14}$ with $\text{M} = \text{Cu, Co and Zn}$ by solid state reaction. The samples were characterized by X-ray diffraction, Raman spectroscopy and X-ray photoelectron spectroscopy. X-ray diffraction studies revealed that the a lattice parameter increases with Cu, Co and Zn respectively. On the other hand, the Cu 2p, Co 2p, Zn 2p, Bi 4f and O1s core levels were analysed and the valence bands respective were studied.

AS-ThP17 XPS Analysis of CN_x Thin Films, Niklas Hellgren, Messiah College, R. Haasch, University of Illinois at Urbana-Champaign, S. Schmidt, L. Hultman, Linköping University, Sweden, I. Petrov, University of Illinois at Urbana-Champaign

X-ray photoelectron spectroscopy (XPS) has for decades been one of the most widely used techniques for analyzing the quantity and bonding states of nitrogen in carbon-nitride compounds, in particular hard carbon-nitride films in wear-protective applications, and more recently for analyzing nitrogen doping states in graphene used for electronic applications. Interpretation of the C1s and N1s spectra, however, can be very challenging due to the many possible bonding configurations of N and C, combined with the inevitable interaction with oxygen and hydrogen on the film surface. A corresponding debate over interpretation has accompanied the field.

In this study we report on XPS studies of magnetron sputtered CN_x thin films, with x ranging from ~ 0.1 to 0.6. Different growth conditions result in films of different structures, from amorphous to graphite-like and fullerene-

like. In order to address some of the above-mentioned difficulties, films were analyzed by angular-resolved XPS, first *in-situ* in the growth and analysis chamber, then after air exposure, and finally after Ar ion etching using ion energies ranging from 500 eV to 4 keV.

The as-deposited films typically exhibit two strong N1s peaks at ~398-398.5eV (usually assigned to pyridine-like nitrogen, C-N=C), and ~400-400.7eV (graphitic nitrogen, -N<), with some nitrile contribution (-C≡N) in between, at ~399eV. Interestingly, the in-situ spectra also show a shoulder in the 402-404 eV range, which is typically attributed to oxidized nitrogen (N-O). However, this peak does not increase upon air exposure, which shows that a different assignment is required for this peak. Instead, air exposure results in the gap between the two main peaks being filled, presumably due to an increase in pyrrole-like nitrogen (>N-H) and/or amino-like nitrogen (>NH₂). Meanwhile, the C1s peak broadens on the high-energy side which indicates that the 5-10 at.% oxygen uptake on the film surface is primarily in the form of C-O and possibly H₂O, but not N-O.

Argon ion etching readily removes surface oxygen, but also results in a strong preferential sputtering of nitrogen. The N/C ratios rapidly approach equilibria of 0.05-0.2, depending on the initial concentration and the Ar⁺ beam energy. Furthermore, changes in the N1s peak shape indicate that ion etching causes amorphization of the film surface. Both effects are more pronounced at higher ion energies, and the damage does not appear to be reversible with subsequent low-energy etching. The best methods for evaluating the as-deposited film structure and composition with *ex-situ* XPS will be discussed.

Friday Morning, October 23, 2015

Electronic Materials and Processing

Room: 211C - Session EM+AS+EN+NS-FrM

Nanoparticles for Electronics and Photonics

Moderator: Jessica Hilton, Mantis Deposition, Joseph G.

Tischler, U.S. Naval Research Laboratory

8:20am EM+AS+EN+NS-FrM1 Elimination of Bias-stress Effect in Ligand-free Quantum Dot Field-effect Transistors, *Matt Law*, UC Irvine **INVITED**

Colloidal quantum dot (QD) solids are the subject of active research with applications emerging in light-emitting diodes, field-effect transistors, and solar cells. In this talk, I describe the use of atomic layer deposition (ALD) infilling to engineer the surfaces and interfaces of PbSe QD films in order to produce high-performance QD field-effect transistors (FETs) that completely lack bias-stress effect (i.e., drain current transients caused by charge trapping near the dielectric/channel interface). This ALD “matrix engineering” approach includes steps designed to manage ligand concentrations, passivate surface states, and arrest ionic motion within the films, resulting in the first high-mobility ($\sim 14 \text{ cm}^2 \text{ V}^{-1} \text{ s}^{-1}$), environmentally stable, and transient-free PbX QD transistors. Two bias-stress mechanisms in QD FETs are identified and discussed. The implications of these mechanisms for the operation of QD solar cells is highlighted.

9:00am EM+AS+EN+NS-FrM3 Ultra High Sensitive CO Sensors with Less Overhead: Influence of Doping Methods and Dopants on the CO Sensitivity of Cu, Pt and Pd Doped SnO₂ Pellets, *Karthik Tangirala, M.A. Olvera*, CINVESTAV-IPN, Mexico

In this work, we report the synthesis, characterization and manufacturing of Cu, Pt and Pd doped SnO₂ pellets with ultra high sensitivities for CO atmospheres. To the best of our knowledge, we have accounted for the first time the ultra high CO sensitivities for Cu doped than Pt and Pd doped SnO₂ pellets. In order to obtain high sensitivities, we have employed novel methods, which are the mixture of chemical and physical synthesis methods. Non-spherical SnO₂ structures were prepared via two chemical synthesis routes using Urea (R1) and ammonia (R2) as precipitation agents. The resultant SnO₂ powders were doped with transition metal, Cu, and noble metals like Pt and Pd via two doping methods D1 and D2. In D1, the powders were bulk doped and then ball milled, whereas in D2, the powders were ball milled and then surface doped. All the powders obtained were later pressed using manual pressing machine to manufacture the SnO₂ pellets. The effect of synthesis routes, doping methods and dopants, on the structural, morphological and also on CO sensing were studied by different characterization techniques and reported with their detailed explanations. Interestingly, the Cu-SnO₂ pellets manufactured from the powders obtained by method D1R1, showed highest sensitivity around 1783 due to various reasons like uniform and small particle size, necks formation, inter-particle conductance and high oxygen adsorption due to stacking faults. All the reasons mentioned above were demonstrated by comparing the established sensor theory with our different experimental results obtained using XRD, Raman, SEM, HRTEM and sensitivity analysis.

9:20am EM+AS+EN+NS-FrM4 Selective Nucleation of Quantum Dots on Spontaneously Nanopatterned Surfaces, *Davide Del Gaudio, S. Huang, L. Aagesen, K. Thornton, R.S. Goldman*, University of Michigan, Ann Arbor

Controlled lateral ordering of self-assembled semiconductor quantum dots (QDs) is desirable for a wide range of solid-state applications, including solar cells, lasers, and telecom devices. To date, lateral alignment of QDs has been demonstrated for multilayers of QDs.^[1]

In these cases, the first layer of QDs is isotropically distributed; subsequently, during the growth of QD stacks, the accumulation of anisotropic strain often results in lateral QD alignment. However, a significant remaining question concerns the *direct* influence of spontaneous surface patterning on the selective nucleation of QDs.

In this work, we use a combined experimental-computational approach to directly examine correlations between buffer surface morphology and QD nucleation. For this purpose, we exploit a surface instability induced by the anisotropy of the surface diffusion constant of ad-atoms (the Ehrlich-Schwöbel effect^[2]) which leads to the formation of elongated ripples, often termed “mounds”. For epitaxial growth of InAs QDs on GaAs, Ye et al. reported a preference for in-plane QD alignment along the mound lengths^[1]. Here, our one-dimensional phase-field model reveals a preference for QD nucleation in regions of positive curvature,^[3] such as on the sides of the

mounds and/or in the “valleys” between the mounds. In our experiments, we explore the formation of InAs QDs on AlGaAs mounds using various substrate temperatures and indium exposure times.

We explore the use of fixed geometry indium evaporation as an approach to restrict QD nucleation to one side of the AlGaAs mounds, resulting in the formation of 1D QD chains.^[4] Specifically, for substrate temperature of 580°C, a high density of AlGaAs mounds is observed along [0-11]. For 3 monolayer (ML) of InAs deposition, we achieved selective positioning of QDs, with an average diameter of 16nm, on one side of the mounds.

We will discuss the influence of the As species (As₂ vs As₄) and growth interrupts on the size, density, and spatial arrangement of QDs. We will also present a detailed analysis of the surface instabilities that induce ripple formation, and the As adsorption kinetics, which lead to the anisotropic nucleation.

References

- [1] W. Ye, S. Hanson, M. Reason, X. Weng, and R. S. Goldman. (2005). *J. Vac. Sci. Technol. B* **23**, 1736-1740.
- [2] Schwöbel, R. L., & Shipsey, E. J. (1966). *J. App. Phys.*, **37**(10), 3682–3686.
- [3] Seol, D. J., Hu, S. Y., Liu, Z. K., Chen, L. Q., Kim, S. G., & Oh, K. H. (2005) *J. Appl. Phys.*, **98**(4), 044910.
- [4] Arciprete, F., Placidi, E., Magri, R., Del Gaudio, D., Patella, F. (2013) *J. Mat. Res.* **28**(23), 3201–3209

9:40am EM+AS+EN+NS-FrM5 Tailor-made Gas Phase based Nanoparticles with Functional Properties, *Gert ten Brink, B. Kooi, G. Palasantzas*, University of Groningen, The Netherlands **INVITED**

Using a home modified Mantis dedicated nanocluster[®] source we have the possibility to produce nanoparticles (NPs) of a great variety of materials with relatively small size dispersion and with properties that can be novel and different from their bulk counterpart. The system works on the principle of inert gas condensation and magnetron sputtering. We have produced a whole range of different NPs with size and motif control.

Covalent bonded NPs, in particular carbon;

Metallic NPs: Cu¹, Fe, Mg, Mo, Co, Al, Ag, Nb, Ti, Pd;

Semiconductor NPs, in particular Ge;

Bimetallic NPs: MgNi, MoCu, MgTi with several compositions;

Ternary alloy NPs, e.g. GeSbTe with several compositions and with amorphous and crystallinity control.

The particles can be deposited on most surfaces provided they have good vacuum compatibility.

The applications range from novel:

Wetting phenomena; Cu NPs covered surfaces giving rose petal effect²;

Bimetallic Mo-Cu NPs which are bulk immiscible but in NPs fully miscible³;

Bimetallic NPs for hydrogen storage⁴: MgNi, MgTi, MgCu;

Magnetic NPs: Fe-Fe₃O₄ core-shell particles for medical applications.

1. Brink, G. H. ten, Krishnan, G., Kooi, B. J. & Palasantzas, G. Copper nanoparticle formation in a reducing gas environment. *J. Appl. Phys.* **116**, 104302 (2014).

2. Ten Brink, G. H., Foley, N., Zwaan, D., Kooi, B. J. & Palasantzas, G. Roughness controlled superhydrophobicity on single nanometer length scale with metal nanoparticles. *RSC Adv.* **5**, 28696–28702 (2015).

3. G. Krishnan, M.A. Verheijen, G.H. ten Brink, G. Palasantzas, B.J. Kooi, Tuning structural motifs and alloying of bulk immiscible Mo-Cu bimetallic nanoparticles by gas-phase synthesis, *Nanoscale* **5**, 5375-5383 (2013).

4. Krishnan, G. *et al.* Synthesis and exceptional thermal stability of Mg-based bimetallic nanoparticles during hydrogenation. *Nanoscale* **6**, 11963-11970 (2014).

10:20am EM+AS+EN+NS-FrM7 A New Surfactant for Directed Deposition of Carbon Nanomaterials, *Hanna Nilsson*, University of Maryland, *L. de Knoop*, Chalmers University, *J. Tacey, B. Meany, Y. Wang*, University of Maryland, *E. Olsson*, Chalmers University, *J. Cumings*, University of Maryland

We show the results of using a new surfactant, ammonium laurate (AL), to suspend and deposit carbon nanostructures. In a recent publication¹, we show that multi-walled carbon nanotubes (MWCNTs) can be suspended in AL with much better shelf stability as compared with the common surfactant sodium dodecyl sulfate (SDS). AL differs from SDS only by the

choice of ionic species, but the deposition process with AL is more reliable and cleaner than with SDS. We use a process of producing a charged self-assembled monolayer on the substrate and then exposing the substrates to the aqueous surfactant solution of MWCNTs to achieve directed deposition of clean individual MWCNTs, which can then be used for fabrication of individual nanotube devices. In addition to these results, we show results for single-walled carbon nanotubes (SWCNTs) in AL, which show that nanotubes deposited from AL have lower electrical contact resistance as compared to those deposited from SDS. Photoluminescence results also show that SWCNTs with specific chirality are preferentially suspended in AL, which may present a separation and purification pathway. We will also present extensions of the work to single and few layer graphene sheets, where AL can be used to make clean depositions from aqueous solution onto sensitive substrates.

(1) Nilsson, H. M.; Meany, B.; Tacey, J.; Sun, C.-F.; Wang, Y.; Cumings, J. Ammonium Laurate Surfactant for Cleaner Deposition of Carbon Nanotubes. *Langmuir* **2015**, *31*, 6948-6955.

10:40am **EM+AS+EN+NS-FrM8 Compositional Control and Doping Uniformity in Spray Pyrolyzed CZTS Nanoparticles and Films**, *Stephen Exarhos, A. Alvarez, J. Hernandez, L. Mangolini*, University of California - Riverside

An innovative and scalable synthesis approach to the formation of stoichiometric $\text{Cu}_2\text{ZnSnS}_4$ (CZTS) nanocrystals has been developed using aerosol spray pyrolysis. This quaternary phase material is a potential replacement for currently commercialized semiconductors such as CdTe and CIGS that are used in photovoltaic devices. However, sustainability and environmental issues threaten long-term viability of these materials. Based upon earth abundant constituents and low chemical toxicity, CZTS, with a reported bandgap of ~ 1.5 eV^[1], appears to be a superior alternative to these other materials. Additional research and development is necessary to increase the efficiency of CZTS-based cells from the current record (12.6% by Wang *et al.*^[2]) to the >18% necessary to be considered commercially viable. Our work demonstrates the controllable, cost-effective, and reproducible synthesis of high-quality CZTS nanoparticles and films. A modified spray pyrolysis method involving decomposition of copper, zinc, and tin diethyldithiocarbamate precursors allows uniform incorporation of dopants (such as sodium) that are known to increase crystal grain growth during nanoparticle sintering^[3]. Once formed, the nanoparticles are deposited onto a substrate from a methanol dispersion using an "ink-spray" process with an argon-driven airbrush. To form an efficient absorber layer in a photovoltaic device, the coating is then annealed in a sulfur-vapor atmosphere resulting in a thin film with uniformly large crystal grain morphology throughout the film thickness (~ 1 -2 μm). The deposited films are characterized with respect to crystalline phase, stoichiometry, and overall film quality. Further preliminary results regarding the formation of $\text{Cu}_2\text{ZnSn}_{(1-x)}(\text{IV})_x\text{S}_4$ by means of this processing approach will be reported.

^[1] H. Wang. "Progress in Thin Film Solar Cells Based on $\text{Cu}_2\text{ZnSnS}_4$," International Journal of Photoenergy 2011 (2011).

^[2] Wang, Wei, Mark T. Winkler, *et al.* "Device Characteristics of CZTSSe Thin-Film Solar Cells with 12.6% Efficiency." *Advanced Energy Materials* **4**, no. 7 (2014).

^[3] Johnson, M., S. V. Baryshev, *et al.* "Alkali-Metal-Enhanced Grain Growth in $\text{Cu}_2\text{ZnSnS}_4$ Thin Films." *Energy & Environmental Science* **7**, no. 6 (2014): 1931-38.

Scanning Probe Microscopy Focus Topic

Room: 212A - Session SP+AS+MI+NS+SS-FrM

Probe-Sample Interactions

Moderator: Carl Ventrice, Jr., SUNY Polytechnic Institute

8:20am **SP+AS+MI+NS+SS-FrM1 Direct Visualization of Magnetoelectric Domains in Hexagonal Manganites**, *Weida Wu*, Rutgers University **INVITED**

Multiferroics are materials with coexisting magnetic and ferroelectric orders, where the cross-coupling between two ferroic orders can result in strong magnetoelectric effects [1-4]. Therefore, it is of both fundamental and technological interest to visualize cross-coupled magnetoelectric domains and domain walls in multiferroics. Recently, intriguing topological defects with six interlocked structural antiphase and ferroelectric domains merging into a vortex core were revealed in multiferroic hexagonal REMnO_3 (R =rare earths) [5, 6]. Many emergent phenomena, such as enhanced conduction and unusual piezoelectric response, were observed in charged ferroelectric domain walls protected by these topological defects [7-9]. More interestingly, alternating uncompensated magnetic moments were

discovered at coupled structural antiphase and ferroelectric domain walls in hexagonal manganites using cryogenic magnetic force microscopy (MFM) [10], which demonstrates the cross-coupling between ferroelectric and magnetic orders. Here we present the application of a magnetoelectric force microscopy (MeFM) technique that combines MFM with *in situ* modulating high electric fields. This new microscopy technique allows us to image the magnetoelectric response of the domain patterns in hexagonal manganites directly [11, 12]. We find that this response changes sign at each structural domain wall, a result that is corroborated by symmetry analysis and phenomenological modelling, and provides compelling evidence for a lattice-mediated magnetoelectric coupling. The direct visualization of magnetoelectric domains at mesoscopic scales opens up explorations of emergent phenomena in multifunctional materials with multiple coupled orders.

References

- [1] N. A. Spaldin, and M. Fiebig, *Science* **309**, 391 (2005).
- [2] W. Eerenstein, N. D. Mathur, and J. F. Scott, *Nature* **442**, 759 (2006).
- [3] S-W. Cheong, and M. Mostovoy, *Nat. Mater.* **6**, 13 (2007).
- [4] N. A. Spaldin, S-W. Cheong, and R. Ramesh, in *Physics Today*(2010), pp. 38.
- [5] T. Choi *et al.*, *Nature Materials* **9**, 253 (2010).
- [6] T. Jungk *et al.*, *Appl. Phys. Lett.* **97**, 012904 (2010).
- [7] E.B. Lochocki *et al.*, *Appl. Phys. Lett.* **99**, 232901 (2011).
- [8] D. Meier *et al.*, *Nat. Mater.* **11**, 284 (2012).
- [9] W. Wu *et al.*, *Phys. Rev. Lett.* **108**, 077203 (2012).
- [10] Y. Geng *et al.*, *Nano Letters* **12**, 6055-6059 (2012).
- [11] Y. Geng, and W. Wu, *Rev. Sci. Instrum.* **85**, 053901 (2014).
- [12] Y. Geng *et al.*, *Nat. Mater.* **13**, 163 (2014).

9:00am **SP+AS+MI+NS+SS-FrM3 Kelvin Probe Force Microscopy Studies of Magnetic Atoms on Ultrathin Insulating MgO Film**, *Taeyoung Choi, W. Paul, S. Baumann, C.P. Lutz, A. Heinrich*, IBM Almaden Research Center

The interplay of single atoms and their local environment on surfaces influences the atoms' spin excitations and dynamics, which can be utilized in progress toward atomic-scale memory and quantum information processing. We find that spin-excitation energy of Fe atoms on an insulating MgO film shifts depending on the tip-to-atom separation. This may be attributed to the electric field across the tunneling junction, as well as to local charge and structural changes around the atom. The Kelvin Probe Force Microscopy (KPFM) has been very useful tool to measure changes of local contact potential differences between a tip and a sample at the atomic level [1]. In this talk, we employ tuning fork KPFM/STM and show preliminary results on the charge character and spin excitations of Fe atoms.

This work is supported by grants from IBM.

[1] Leo Gross *et al.*, *Phys. Rev. B* **90**, 155455 (2014).

9:20am **SP+AS+MI+NS+SS-FrM4 Nanoscale Schottky Barrier Height Mapping Utilizing Ballistic Electron Emission Microscopy**, *C. Durcan, W. Nolting*, College of Nanoscale Science and Engineering, *Vincent LaBella*, SUNY Polytechnic Institute

The Schottky barrier is the electrostatic barrier between a metal and a semiconductor that results in rectification and is found in many types of devices such as source drain contacts to sub 20-nm-node transistors. Naturally, the Schottky barrier height can fluctuate across the interface due to variations in bonding, compositional fluctuations in the materials, and the presence of defects. However measuring and mapping these electrostatic fluctuations is impossible with bulk IV or CV techniques. This presentation will demonstrate how the Schottky barrier height can be mapped to nanoscale dimensions using an STM based technique called ballistic electron emission microscopy (BEEM). The STM tip is positioned on a regularly spaced grid and BEEM spectra are acquired from which the barrier height can be extracted. A map and histogram is then generated by measuring and fitting thousands of these spectra. These maps provide detailed insight into the electrostatic fluctuations occurring at the buried interface with nanoscale resolution that cannot be accomplished with other bulk measurements.

9:40am **SP+AS+MI+NS+SS-FrM5 Electron Transport Studies of Metal Films Utilizing Ballistic Electron Emission Microscopy**, *Christopher Durcan*, SUNY College of Nanoscale Science and Engineering, *V. LaBella*, SUNY Polytechnic Institute

Understanding scattering of electrons in nanometer thick metal films is of fundamental and technological importance. One method to study electron scattering is with ballistic electron emission microscopy (BEEM), which is

a three terminal STM based technique that measures both scattering through a metal film and the Schottky barrier height for metal-semiconductor junctions with both nanometer spatial resolution and meV energy resolution. This presentation will describe our work at understanding the relationship between the metal resistivity and the electron scattering lengths measured with BEEM by exploring metals with a range of resistivities from Ag (1.7 $\mu\Omega$ -cm) to Cr (12.6 $\mu\Omega$ -cm). In addition, nanoscale mapping of the Schottky barrier height of these metals to silicon will also be presented to understand the spatial uniformity of the transport.

10:00am **SP+AS+MI+NS+SS-FrM6 Utilizing Ballistic Electron Emission Microscopy to Study Sidewall Scattering of Electrons, Westly Nolting, C. Durcan, R. Balsano**, College of Nanoscale Science and Engineering, University of Albany, *V. LaBella*, College of Nanoscale Science and Engineering, SUNY Polytechnic Institute

Sidewall scattering of electrons within aggressively scaled metallic interconnects increases the resistance since the mean free path (~40 nm) is larger than the dimensions of the material. One method to study hot-electron scattering in nm-thick metallic films is Ballistic Electron Emission Microscopy (BEEM), which is an STM based technique. In this work, we perform BEEM scattering measurements on lithographically patterned fin structures with a Schottky diode interface to determine its ability to measure sidewall scattering. This is accomplished by acquiring BEEM spectra on a regularly spaced grid and fitting the results to determine both the Schottky barrier height and the slope of the spectra. The slope of the spectra is related to the scattering in the film and interface. The position of fin structures are then determined by mapping both the Schottky height and slope over a square micron to observe scattering at the interface caused by the patterned structures. The poster will discuss the fabrication of the patterned 50-nm-pitched sidewall structures that are used for mapping the sidewall scattering. In addition, it will present the preliminary BEEM measurements on these structures.

10:20am **SP+AS+MI+NS+SS-FrM7 Progress in Nanoscale Magnetic Resonance Imaging, Daniel Rugar**, IBM Research Division **INVITED**

Nuclear magnetic resonance (NMR) is the basis of powerful spectroscopic and imaging techniques, but extension to nanoscale samples has been a longstanding challenge due to the insensitivity of conventional detection methods. We are exploring the use of individual, near-surface nitrogen-vacancy (NV) centers in diamond as atomic-size magnetometers to detect proton NMR in organic material located external to the diamond. Using a combination of electron spin echoes and proton spin manipulation, the NV center senses the nanotesla field fluctuations from the protons, enabling both time-domain and spectroscopic NMR measurements on the nanometer scale. By scanning a small polymer test object past a near-surface NV center, we have recently demonstrated proton magnetic resonance imaging (MRI) with spatial resolution on the order of 10 nm.

One key issue in NV-NMR experiments is the loss of spin coherence when the NV center is located near the diamond surface. Although this loss of coherence is frequently attributed to the effect of magnetic noise emanating from unpaired spins on the diamond surface, we will show evidence that electric field noise from fluctuating surface charge may be the dominant factor.

Work performed in collaboration with M. Kim, H. J. Mamin, M. H. Sherwood, C. T. Rettner, K. Ohno, and D. D. Awschalom

11:00am **SP+AS+MI+NS+SS-FrM9 Reactive Intermediates Created and Analyzed by Scanning Probe Microscopy, Bruno Schuler**, IBM Research - Zurich, Switzerland, *N. Pavliček*, IBM Research - Zurich, *S. Collazos*, CIQUS, Universidade de Santiago de Compostela, *N. Moll*, *S. Fatayer*, IBM Research - Zurich, *D. Pérez*, *E. Guitán*, CIQUS, Universidade de Santiago de Compostela, *G. Meyer*, IBM Research - Zurich, *D. Peña*, CIQUS, Universidade de Santiago de Compostela, *L. Gross*, IBM Research - Zurich

Reactive intermediates are involved in most chemical transformations. However, their characterization is a great challenge because of their short lifetime and high reactivity.

Here we report on the creation of single radicals and diradicals on a thin insulating surface by means of atomic manipulation. Importantly, the thin insulating film facilitates the stabilization of these reactive intermediates at cryogenic temperatures. The molecules were characterized by atomic-resolution atomic force microscopy (AFM) imaging with a CO functionalized tip [1] and scanning tunneling microscopy (STM) orbital imaging [2]. We show that the molecules' reactivity is preserved even at low temperatures by performing different on-surface reactions by atomic manipulation. As an example, the generation of aryne is discussed, a very reactive intermediate caught for the first time [3].

References:

[1] L. Gross et al. *Science* **325**, 1110 (2009)

[2] J. Repp et al. *Phys. Rev. Lett.* **94**, 026803 (2005)

[3] N. Pavliček et al. On-surface generation and imaging of arynes by atomic force microscopy. (submitted)

11:20am **SP+AS+MI+NS+SS-FrM10 The Negative Stiffness and Positive Damping of Squeezed Air in Dynamic Atomic Force Microscopy, x. Yu, M. Tao, Nancy Burnham**, Worcester Polytechnic Institute

By oscillating a micro-sized cantilever beam at a certain frequency and observing its interaction with the sample surface, dynamic mode atomic force microscopy (AFM) has gained attention for characterizing mechanical properties of a variety of materials at the micro and nano scales. The thin air film, confined between the oscillating cantilever beam and the stationary sample surface, causes the so-called "squeeze-film effect" when the gap between the two boundaries is less than a hundred microns. Although studies have shown that the squeeze film can act as a spring and a damper in accelerometers and microelectromechanical systems [1], the influence of the squeeze-film effect on the dynamics of an AFM cantilever has not been previously explored, to the authors' knowledge. In this project, the stiffness and damping properties of the squeeze film between an oscillating AFM cantilever and a glass slide were calculated from the cantilevers' amplitude and phase responses as recorded by the AFM digital system. The smaller the cantilever-sample gap, the larger the absolute values of the stiffness and the damping of the squeeze film. Results from different cantilevers (consequently having different spring constants and resonant frequencies) indicated that the air film exhibited **negative stiffness and positive damping**, with normalized changes from free values of up to 40%. Theoretical analysis was conducted using an equivalent-circuit model [2] along with the phasor diagram, and the derived stiffness and damping values were in excellent agreement with the experimental ones. Interestingly, a rotation angle between 20° and 30° in the fit of the data to the model reveals a phase *lead* of the squeeze-film damping before the usual air damping when the cantilever is far from a surface: the maximum squeeze-film damping occurs before the maximum velocity of the cantilever because air becomes less dense as it rushes out of the tip-sample gap. The surprising sign of the stiffness is thus explained by the phase lead. Future work includes incorporating the squeeze-film effect into more accurate measurements of a material's stiffness and damping properties using dynamic AFM.

References:

1. Starr, James B. "Squeeze-film damping in solid-state accelerometers." *Solid-State Sensor and Actuator Workshop, 1990. 4th Technical Digest., IEEE. IEEE, 1990.*

2. Veijola, Timo. "Compact models for squeezed-film dampers with inertial and rarefied gas effects." *Journal of Micromechanics and Microengineering* 14.7 (2004): 1109.

Tribology Focus Topic

Room: 230B - Session TR+AS+BI+NS-FrM

Nanoscale Wear and Biotribology

Moderator: J. David Schall, Oakland University

8:20am **TR+AS+BI+NS-FrM1 2D or not 2D? The Impact of Nanoscale Roughness and Substrate Interactions on the Tribological Properties of Graphene, James Batteas**, Texas A&M University **INVITED**

Control of friction and wear is a ubiquitous challenge in numerous machined interfaced ranging from biomedical implants, to engines, to nano- and micro-scaled electromechanical systems (MEMS) devices. While lubricant additives are one approach to the development of surface coatings that can impede wear and reduce friction, in some cases, such approaches are simply not amenable and the development of ultrathin films are required. Recently, the robust mechanical properties of graphene has made it a material of interest as a means of modifying surface frictional properties. While graphene can readily adapt to surface structure on the atomic scale, when deposited on substrates with nanoscopic roughness (~10 – 20 nm rms as is common in many machined interfaces) a conformal coating cannot be fully formed due to competition between adhesion to substrate nanoscopic asperities and the bending strain of the graphene. This often leaves a mixture of supported and unsupported regions which respond differently to applied load and shear strain. Here we describe a combination of AFM nanomechanical and confocal Raman microspectroscopy studies of graphene on silica surfaces with controlled nanoscopic roughness to examine the how this impacts the frictional properties of graphene. Composite interfaces where graphene is supported on self-assembled

alkylsilane monolayers will also be described along with the synergistic influence of such mixed interfaces on the frictional properties of the surface.

9:00am **TR+AS+BI+NS-FrM3 Atomic-Scale Wear and Wear Reduction Mechanisms Elucidated by *In Situ* Approaches**, R.W. Carpick, University of Pennsylvania, **Tevis Jacobs**, University of Pittsburgh
INVITED

As technologies shrink to nanometer length scales, tribological interactions play an increasingly dominant role. A lack of fundamental insight into the origin of friction and wear at the nanoscale hinders the advancement of such technologies. Furthermore, macroscopic tribological applications often involve contact between nanostructured materials or at nanoscale asperities, due to surface roughness. Observing and understanding the nanoscale mechanisms at play is inhibited by the hidden nature of the buried interface and the challenge of performing observations at the nanometer scale. Recent advances in *in situ* methods are enabling tribological mechanisms at previously inaccessible interfaces to be studied with unprecedented resolution and sensitivity. We will discuss the application of two *in situ* experimental methods to develop new physical insights into tribological processes. The first approach addresses contact and wear phenomena at the atomic scale by *in situ* sliding in a transmission electron microscope [1], and the second addresses the generation of tribofilms from anti-wear additives using atomic force microscopy while immersed in additive-infused oil [2].

References:

[1] Jacobs, T.D.B. and Carpick, R.W. "Nanoscale Wear as a Stress-Assisted Chemical Reaction," *Nature Nanotech.*, 8, 2013, 108-112.

[2] Gosvami, N.N., Bares, J. A., Mangolini, F., Konicek, A.R., Yablon D.G., and R. W. Carpick. "Mechanisms of Antiwear Tribofilm Growth Revealed *In Situ* by Single Asperity Sliding Contacts," *Science*, 348, 2015, 102-106.

9:40am **TR+AS+BI+NS-FrM5 Influence of Polysaccharide Conformation on Friction and Adhesion**, **Rowena Crockett**, Empa, Switzerland
INVITED

The friction behavior of the polysaccharide dextran has been investigated on surfaces coated with PLL-dextran brushes as well as randomly orientated covalently attached chains in aqueous solution. It was found that while there was a strong dependence of friction on load for the dextran brushes, the randomly orientated chains showed a more constant friction coefficient. Polysaccharides play an important role in bioadhesion, but are also used in the mining industry to assist in the separation of minerals. Despite the high adhesion associated with polysaccharides, investigations showing that they can be used to achieve low friction have also been reported. It was proposed that this transition from low friction to high adhesion is achieved as a result of hydrogen bonding. That is, as the load increases, water is forced out of the contact and the number of hydrogen bonds between the polysaccharide and surface increase, inducing a transition to high adhesion.

10:20am **TR+AS+BI+NS-FrM7 Tribological Rehydration of Cartilage: A New Insight into an Old Problem**, **David Burris**, A.C. Moore, University of Delaware
INVITED

The bulk of cartilage lubricity is due to its multi-phasic structure and the pressurization of interstitial fluid during loading. Unfortunately, the same pressure gradients that support load and lubricate the contact also drive fluid from the tissue over time. This observation led McCutchen, the researcher responsible for the discovery of this unusual lubrication mechanism, to ponder how the joint prevented the loss of interstitial fluid over time. He proposed that articulation intermittently exposes the loaded zone to the bath, thus allowing the tissue to imbibe fluid. It wasn't until 2008 that Caligaris and Ateshian showed that interstitial pressure can be maintained if the contact migrates across cartilage more quickly than the diffusive speed of fluid in the tissue; because the joint involves a migrating contact, they proposed that this discovery resolved any uncertainty about how the joint maintains lubrication. However, joints spend only a fraction of the day articulating and the majority of the day exuding fluid in static compression. If the migrating contact simply prevents the loss of fluid by moving quicker than the fluid can respond, we contend that it cannot explain long-term maintenance of interstitial fluid in the joint; there must be an active uptake mechanism in which articulation drives fluid back into the cartilage surface at a rate that outpaces exudation. This paper explores the origins of this mechanism and in doing so uncovers several phenomena that cannot be explained by existing theory. Contrary to existing theory, we show that stationary contacts are able to sustain fluid pressures in a manner similar to the migrating contact. Furthermore, we demonstrate active recovery of interstitial fluid in a stationary contact without exposing the loaded zone to the bath. The results demonstrate that sliding alone, even at sub-physiological speeds, forces fluid back into the cartilage at rates that outpace exudation rates. The results suggest that interstitial or weeping

lubrication is the primary lubrication mechanism in the joint and that hydrodynamic effects prevent the loss of this mechanism in the long-term.

11:00am **TR+AS+BI+NS-FrM9 Biomimetic Aspects of Lubrication with Polymer Brushes and Gels**, **C. Mathis**, **L. Isa**, **Nicholas Spencer**, ETH Zürich, Switzerland

The role of the solvent is crucial in lubrication with polymer brushes and gels. Firstly it is important in maintaining the structure of the brush or gel layer in an unloaded state. Under loading, however, a new phenomenon becomes crucial, namely the Darcy flow of the solvent through the porous system. This aspect brings in a new set of properties to consider: the viscosity of the solvent determines the rate at which the solvent is forced through the porous network, and the sliding speed determines the extent to which the solvent is expelled from beneath the contact. The very act of expulsion of solvent is actually a process that bears a portion of the load. This phenomenon is well known in cartilage, and has been dubbed "fluid load support". This presentation will illustrate the ways in which this biomimetic approach can be utilized to protect polymer brushes and gels from wear, thus increasing their attractiveness as applicable lubricating systems, and will describe the approaches that can be used to quantify the process.

Authors Index

Bold page numbers indicate the presenter

— A —

Aagesen, L.: EM+AS+EN+NS-FrM4, 99
Abbas, A.: EN+AS+EM+NS+SE+SS+TF-MoM10, 8
Abdulgalil, A.G.M.: SS+AS-WeA2, 63
Abe, Y.: TF+AS+SS-MoM8, 15
Abel, A.J.: EN+AS+EM+SE+SS-TuM5, **31**
Abel, M.-L.: AS-MoA10, 19
Abelson, J.R.: SD+AS+EM-ThM2, 72
Abu-Husein, T.: TF+AS+SS-MoM1, 14
Abuzairi, T.: SM+AS+BI+PS-ThM5, 74
Adams, D.P.: TF+AS+EM+EN+MN-WeA3, 66; TF+AS+EM+EN+MN-WeA4, **66**
Addadi, L.: BI+AS-MoM5, 4
Afonso, C.R.M.: TF+AS+BI-WeA7, 65
Agarwal, A.: IS+AS+SA+SS-MoA10, 27
Ager, J.W.: EN+AS+EM+SE+SS-TuM10, **32**; SS+AS+EM+EN-ThA6, 89
Ahn, S.J.: AS-ThP12, 97
Akaishi, A.: TF+AS+SS-MoM9, 15
Akiba, C.: SS+AS+EN-TuM1, 35
Akselrud, L.: AC+AS+MI-WeM10, 43
Alam, T.: SS+AS+EN-MoM10, 14
Alarcon Llado, E.: EN+AS+EM+SE+SS-TuM2, 31; SS+AS+EM+EN-ThA6, 89
Alaydrus, M.: SS+AS+EN-MoM9, 14
Alayoglu, S.: IS+AS+SA+SS-WeM4, 46
Al-Azizi, A.: TR+AS+NS+SS-ThA9, 93
Alcantara Ortigoza, M.: SS+AS-WeA3, **63**
Alexander, M.R.: AS+BI-TuA3, 38
Alkemade, P.: HI+AS+SS+NS-ThM13, **72**
Allen, F.I.: HI+AS+NS-ThA10, **85**; HI+AS+NS-ThA8, 84
Alling, B.: TF+AS+NS+SA-ThA1, 90
Allred, D.D.: EL+AS+BI+EM-ThA11, **83**
Aloni, S.: NS+AS+SP-MoA8, 28
Altman, E.I.: SS+AS+EN-MoM5, 13
Altoe, M.V.P.: TR+AS+NS+SS-ThA1, 92
Alvarez, A.: EM+AS+EN+NS-FrM8, 100
Amati, M.: IS+AS+SA+SS-MoA7, 26
Amspacher, L.: AS-ThM2, 69
Amster, O.: SP+AS+NS+SS-WeM5, 48
Anand, B.X.: EN+AS+EM+NS+SE+SS+TF-MoA1, 24
Andersen, J.N.: IS+AS+SS-MoM11, 11
Anderson, T.J.: EM+AS+MS+SS-WeA12, 56; EM+AS+MS+SS-WeA7, 55
Anderson, V.: TF+AS+NS+SA-ThM13, **79**; TF+AS+NS+SA-ThM6, 78
Ankem, S.: AP+AS-MoA3, 17
Ansari, N.: TR+AS+NS+SS-ThA10, 93
Antunez, P.D.: EN+AS+EM+NS+SE+SS+TF-MoM2, 7
Apkarian, V.A.: IS+AS+SA+SS-WeM3, 46
Appy, D.: SS+AS+EN+NS-TuM6, 34
Arlinghaus, H.: AS-ThP11, 97
Arlinghaus, H.F.: AS+BI-TuA3, 38
Armocost, M.D.: IS+AS+SA+SS-MoA10, 27
Arnadottir, L.: SS+AS+EN-TuA10, **41**
Arndt, M.: SE+AS+NS+TR-MoM4, 12
Artyushkova, K.: AS+SS-ThA1, 81; AS-MoA5, **18**
Ashby, P.: NS+AS+SP-MoA8, 28
Ashurst, W.R.: TR+AS+NS+SS-ThA10, 93
Aspera, S.M.: SS+AS+EN-MoM9, **14**
Atanassov, P.: AS-MoA5, 18
Atiganyanun, S.: TF+AS+NS+SA-ThA9, **92**
Auerbach, D.J.: SS+AS-WeA7, **64**
Auzely-Velty, R.: BI+AS-MoA7, 21
Avila-Bront, L.G.: SS+AS+EM+EN-ThA8, 89
Aydil, E.S.: EN+AS+EM+NS+SE+SS+TF-MoA9, **25**
Aydogan, P.: EN+AS+EM+NS+SE+SS+TF-MoM9, 8

— B —

Ayers, J.E.: TF+AS+NS+SA-ThA6, 91
Babaeva, N.Yu.: SM+AS+BI+PS-ThA1, 87
Babar, S.: SD+AS+EM-ThM2, 72
Babinsky, K.: AP+AS-MoA5, 17
Baddorf, A.P.: SP+2D+AS+NS+SS-WeA7, 61; SP+AS+NS+SS-WeM6, 48; SS+AS+EN+NS-TuM10, 35
Badylak, S.F.: BI+AS-MoA3, 20
Baer, D.R.: AS-ThM5, **69**
Bagus, P.S.: AC+AS+MI-WeA10, **52**
Baker, B.: TF+AS+BI-WeA9, **65**
Balasubramanian, K.: SE+AS+NS+TR-MoM9, 12
Ballard, J.: SD+AS+EM+PS-ThA8, **86**
Balsano, R.: SP+AS+MI+NS+SS-FrM6, 101
Bañares, M.A.: IS+AS+SA+SS-WeM5, **47**
Banos, A.K.: AC+AS+MI-ThM10, **68**
Bao, W.: NS+AS+SP-MoA8, **28**
Bao, Z.: AC+AS+MI-WeM3, 43
Baratoff, A.: TR+AS+NS+SS-ThA7, 93
Barback, C.: BI+AS-MoA9, 21
Bar-David, Y.: AS+NS-TuM12, 30
Barlow, A.: AS+SS-ThA1, 81
Barlow, D.E.: BI+AS-MoA2, 20; BI+AS-MoM6, **4**
Barner-Kowolik, C.: AS-ThP6, 96
Barnes, T.M.: EN+AS+EM+NS+SE+SS+TF-MoM10, 8
Bartels, L.: SS+AS+NS-WeM1, 49
Bartynski, R.A.: SS+AS+EN-TuM10, 36
Baski, A.A.: SS+AS+EM+EN-ThM13, 77
Basov, D.N.: NS+AS+SP-MoA5, **28**
Batra, V.: TF+AS+NS+SA-ThA3, **91**
Batteas, J.D.: TR+AS+BI+NS-FrM1, **101**
Batzill, M.: SS+AS+EN-MoM3, **13**
Bauerdick, S.: HI+AS+SS+NS-ThM6, **71**
Baugh, D.: IS+AS+SA+SS-WeM2, **46**
Baumann, S.: SP+2D+AS+NS+SS-WeA9, 61; SP+AS+MI+NS+SS-FrM3, 100
Baxter, J.B.: EN+AS+EM+NS+SE+SS+TF-MoA5, **24**; EN+AS+EM+SE+SS-TuM5, 31
Beach, J.D.: EN+AS+EM+NS+SE+SS+TF-MoM10, 8
Bearden, B.E.: EN+AS+EM+NS+SE+SS+TF-MoA1, 24
Beasor, S.: TF+AS+NS+SA-ThM11, 79
Bedzyk, M.J.: AS+NS-TuM6, 30
Beeby, S.: EM+AS+SS-MoA1, 22
Belianinov, A.: IS+AS+SS-TuA11, 40
Belkadi, A.: EM+AS+SS-MoM1, 5
Belkin, M.A.: NS+AS+SP-MoA3, **27**
Bell, L.D.: AS+SS-WeA7, **53**
Belsey, N.A.: AS-WeM5, 45
Benck, J.D.: EN+AS+EM+SE+SS-TuM3, 31
Bencoe, D.: SS+AS+EN-MoM10, 14
Bendikov, T.: AS-ThP3, 95
Bent, S.F.: SD+AS+EM+PS-ThA10, 87; SD+AS+EM+PS-ThA6, 86; SS+AS+EM+EN-ThM1, 76; SS+AS+EM+EN-ThM5, **77**
Bergsman, D.S.: SD+AS+EM+PS-ThA6, 86
Beyer, A.: HI+AS+NS-ThA4, 84; SS+AS+EN+NS-TuM5, 34
Bhattacharjee, S.: SM+AS+BI+PS-ThM5, 74
Bhatti, A.S.: EL+AS+BI+EM-ThA9, **83**
Biffinger, J.C.: BI+AS-MoM6, 4
Biol, T.: EM+AS+SS-MoA5, 23
Blackman, G.S.: AS-ThM2, 69
Blair, S.: BI+AS-MoA9, 21
Blomfield, C.J.: AS+SS-WeA10, 54; AS-ThP3, 95; AS-WeM3, 45

Bluestein, B.M.: BI+AS-MoA5, **21**; BI+AS-MoM11, 5
Bluhm, H.: AS+SS-WeA9, 54; IS+AS+SS-MoM5, 10; SS+AS+EN-TuA3, 41
Bokor, J.: HI+AS+NS-ThA10, 85
Bolt, P.J.: EN+AS+EM+NS+SE+SS+TF-MoM8, 8
Bolvardi, H.: SE+AS+NS+TR-MoM2, 11
Bonifacio, C.S.: IS+AS+SS-TuA8, 40
Bonnell, D.: SP+AS+NS+SS-ThM6, 76
Bonnesen, P.: SS+AS+EN+NS-TuM10, 35
Booth, C.H.: AC+AS+MI-WeA9, 52
Booth, J.C.: EM+AS+SS-MoA5, 23
Borovsky, B.P.: TR+AS+NS+SS-ThA10, 93
Borowik, L.: SP+AS+NS+SS-WeM4, 48
Borros, S.: SM+AS+BI+PS-ThM10, **75**
Borys, N.: NS+AS+SP-MoA8, 28
Boswell, R.: HI+AS+SS+NS-ThM5, **71**
Bousquet, A.: TF+AS+NS+SA-ThM1, **78**
Boutaud, B.: PS+AS+SS-WeA11, 59
Bowen, K.: SS+AS+EN-TuA3, 41
Boxford, W.: AS-ThP3, 95
Boyer, N.: TF+AS+EM+EN+MN-WeA12, **67**
Brady, P.: EM+AS+SS-MoM1, 5; EM+AS+SS-MoM6, 6
Brazzini, T.: SS+AS+EM+EN-ThA6, **89**
Briley, C.: EL+AS+BI+EM-ThA4, **83**
Britto, R.: EN+AS+EM+SE+SS-TuM3, 31
Broderick, A.: IS+AS+SA+SS-TuM2, 33
Brongersma, H.: TF+AS+NS+SA-ThM10, 79
Bruchhaus, L.: HI+AS+SS+NS-ThM6, 71
Bruener, P.: AS-MoM3, 2; TF+AS+NS+SA-ThM10, 79
Brumbach, M.: SS+AS+EN-MoM10, **14**
Brumfeld, V.: BI+AS-MoM5, 4
Brundle, C.R.: AS+NS-TuM3, **30**
Brunns, M.: AS-ThP6, **96**
Bryan, S.R.: AS+SS-ThA8, **81**; AS-MoM8, 3
Burgener, N.J.: SS+AS+EM+EN-ThM10, 77
Burnham, N.A.: SP+AS+MI+NS+SS-FrM10, **101**
Burriss, D.: TR+AS+BI+NS-FrM7, **102**
Busby, Y.: AS+SS-WeA12, 54
Bushell, A.: AS-ThP4, **95**
Butt, H.J.: BI+AS-MoA4, 20
Buyanin, A.: NS+AS+SP-MoA8, 28

— C —

Cabrera, W.: SD+AS+EM-ThM10, 73
Cabrini, S.: NS+AS+SP-MoA8, 28
Caciuffo, R.: AC+AS+MI-WeM11, 44; AC+AS+MI-WeM3, 43
Cacovich, S.: AS+SS-WeA12, 54
Cai, W.: SS+AS+EN+NS-TuM11, 35
Cai, Z.B.: AS-ThP2, 95
Cairney, J.M.: AP+AS+MC+MI+NS-MoM6, 1; AP+AS-TuM3, 29
Cairns, E.: EN+AS+EM+SE+SS-TuM13, 32
Caldwell, R.: TF+AS+BI-WeA9, 65
Campbell, C.T.: SS+AS+EN-WeA7, **62**
Canal, C.: SM+AS+BI+PS-ThA3, **87**
Canepa, P.: IS+SS+NS+BI+VT+MN+AS-WeA9, 57
Cant, D.J.H.: AS-WeM5, **45**
Cantu, D.C.: SS+AS+EN-TuM11, 36
Cao, B.: IS+SS+NS+BI+VT+MN+AS-WeA4, 57
Carencio, S.C.: IS+AS+SS-TuA8, **40**
Carman, G.: TF+AS+NS+SA-ThA11, 92
Carreiro, K.: NS+AS+SP-MoA9, 28
Carpick, R.W.: AS-MoA9, 19; TR+AS+BI+NS-FrM3, 102; TR+AS+NS+SS-ThA4, 93
Carr, D.: AS+SS-WeA3, **53**

Carr, R.H.: AS-MoA10, 19
Casey, S.M.: SS+AS+EM+EN-ThM10, 77
Cassidy, A.: TF+AS+SS-MoM2, 14
Castle, J.E.: AS-MoA1, 18; AS-MoA10, 19
Castner, D.G.: AS-MoA7, 19; BI+AS-MoA1, 20; BI+AS-MoA3, 20; BI+AS-MoA4, 20; BI+AS-MoM3, 4; BI+AS-MoM8, 5
Ceccone, G.C.: BI+AS-MoM9, 5
Cellier, J.: TF+AS+NS+SA-ThM1, 78
Cha, J.: SS+AS+EN-MoM5, 13
Chabal, Y.J.: EN+AS+EM+NS+SE+SS+TF-MoA1, 24; IS+SS+NS+BI+VT+MN+AS-WeA10, 57; IS+SS+NS+BI+VT+MN+AS-WeA9, 57; SD+AS+EM+PS-ThA8, 86; SD+AS+EM-ThM10, 73; SS+AS+EM+EN-ThM2, 76; SS+AS+EM+EN-ThM4, 77
Chagarov, E.: EN+AS+EM+NS+SE+SS+TF-MoM1, 7
Chakhranont, P.: EN+AS+EM+SE+SS-TuM3, 31
Chalker, P.R.: EM+AS+SS-MoA1, 22
Chambers, S.A.: EM+AS+SS-MoM11, 7
Chan, C.D.: AS-ThP10, 97
Chang, J.P.: TF+AS+NS+SA-ThA11, 92
Chang, S.H.: SM+AS+BI+PS-ThM4, 74
Chaudhary, S.: IS+AS+SS-MoM11, 11
Chen, C.: SS+AS-WeA8, 64
Chen, D.A.: SS+AS+EN-WeA1, 62
Chen, J.: IS+SS+NS+BI+VT+MN+AS-WeA3, 57
Chen, J.-R.: SD+AS+EM-ThM1, 72
Chen, K.: AS-SS-ThA10, 82
Chen, L.: SS+AS+EN-WeA10, 63
Chen, M.J.: SM+AS+BI+PS-ThM4, 74
Chen, M.S.: SS+AS+EN-TuM13, 37
Chen, P.: IS+AS+SA+SS-TuM10, 33
Chen, R.: SS+AS+EN-TuA2, 41; SS+AS+EN-WeA4, 62
Chen, X.: IS+AS+SS-MoM3, 9
Chen, Z.Z.: SS+AS+EN-TuA2, 41; SS+AS+EN-WeA4, 62
Cheon, S.: SP+2D+AS+NS+SS-WeA4, 60
Chevalier, N.: SP+AS+NS+SS-WeM4, 48
Chiang, N.: NS+AS+SP-MoA7, 28
Chiang, S.: SS+AS+NS-WeM6, 60
Chin, M.: EM+AS+SS-MoM9, 6
Chintalapalle, R.V.: EN+AS+EM+NS+SE+SS+TF-MoA8, 25
Chirita, V.: SE+AS+NS+TR-MoM3, 11
Cho, B.: AS-ThP12, 97
Cho, K.J.: SS+AS+EM+EN-ThM2, 76; SS+AS+EM+EN-ThM4, 77; SS+AS+EN-WeA4, 62
Choi, B.D.: EN+AS+EM+NS+SE+SS+TF-MoM6, 8
Choi, B.J.: SD+AS+EM+PS-ThA9, 86
Choi, T.: SP+2D+AS+NS+SS-WeA9, 61; SP+AS+MI+NS+SS-FrM3, 100
Chopra, S.: SD+AS+EM-ThM11, 73
Chopra, T.P.: SS+AS+EM+EN-ThM2, 76
Chou, H.: SM+AS+BI+PS-ThM5, 74
Chu, J.P.: SM+AS+BI+PS-ThM4, 74
Chudzicki, M.: AS-MoM1, 2
Chulhai, D.: NS+AS+SP-MoA7, 28
Church, J.: AS-MoM10, 3
Chyntara, S.: SM+AS+BI+PS-ThM4, 74
Cieslar, M.: AC+AS+MI-WeM12, 44
Cieslinski, R.: AS+BI-TuA7, 38
Ciolan, M.A.: SM+AS+BI+PS-ThM5, 74
Clark, B.: AS-ThP9, 96
Clark, R.: SD+AS+EM+PS-ThA11, 87
Claus, T.: AS-ThP6, 96
Cleaves, H.J.: SS+AS+EN+NS-TuM10, 35
Closser, R.G.: SD+AS+EM+PS-ThA6, 86
Coad, B.R.: SM+AS+BI+PS-ThA6, 88
Cockrell, A.L.: BI+AS-MoM6, 4
Cohen, H.: AS+NS-TuM13, 30
Cohen, S.R.: BI+AS-MoM5, 4
Cola, B.A.: EM+AS+SS-MoA4, 23
Colinauro, E.: AC+AS+MI-WeM11, 44
Collazos, S.: SP+AS+MI+NS+SS-FrM9, 101
Collet, G.: SM+AS+BI+PS-ThM1, 74
Collings, M.P.: SS+AS-WeA2, 63
Collins, R.: SS+AS+EM+EN-ThA11, 90
Colpo, P.: TF+AS+BI-WeA1, 65
Conley, J.F.: TF+AS+NS+SA-ThA2, 91
Conley, Jr., J.F.: EM+AS+SS-MoM10, 7
Consiglio, S.: SD+AS+EM+PS-ThA11, 87
Cook, D.: BI+AS-MoM6, 4
Cornaby, S.: TF+AS+EM+EN+MN-WeA12, 67
Coultais, S.J.: AS+SS-WeA10, 54; AS-ThP3, 95; AS-WeM3, 45
Counsell, J.D.P.: AS+SS-WeA10, 54; AS-ThP3, 95; AS-WeM3, 45
Craver, B.: IS+AS+SA+SS-MoA10, 27
Creighton, R.: TF+AS+EM+EN+MN-WeA12, 67
Criscenti, L.: SS+AS+EN-MoM10, 14
Crockett, R.: TR+AS+BI+NS-FrM5, 102
Crommie, M.F.: HI+AS+NS-ThA10, 85
Crozier, P.A.: IS+AS+SS-TuA1, 39
Cruden, C.: TF+AS+SS-MoM5, 15
Crumlin, E.J.: IS+AS+SA+SS-TuM12, 33; IS+AS+SA+SS-TuM3, 33
Cui, J.: AP+AS-MoA7, 17
Culter, P.H.: EM+AS+SS-MoM5, 6
Cumings, J.: EM+AS+EN+NS-FrM7, 99
Cumpson, P.: AS+SS-ThA1, 81
Curk, T.: BI+AS-MoA7, 21
Cushman, C.V.: AS-MoM3, 2
Cybart, S.A.: HI+AS+NS-ThA6, 84

— D —

Da, B.: SS+AS+EN+NS-TuM13, 35
Dalmou-Mallorqui, A.: EN+AS+EM+SE+SS-TuM2, 31
Dameron, A.A.: AS-MoA8, 19
Daniel, C.: AP+AS-TuM11, 29
Danis, S.: AC+AS+MI-WeM3, 43
Darny, T.: SM+AS+BI+PS-ThM1, 74
D'Arrigo, C.: NS+AS+SP-MoA1, 27
Das, L.: AS+BI-TuA8, 38
Davis, R.: EM+AS+MS+SS-WeA3, 55
Davis, R.C.: TF+AS+BI-WeA11, 66; TF+AS+EM+EN+MN-WeA12, 67; TF+AS+EM+EN+MN-WeA9, 66
Davis, R.F.: EM+AS+MS+SS-WeA4, 55
de Knoop, L.: EM+AS+EN+NS-FrM7, 99
De Lucia, F.C.: IS+AS+SA+SS-MoA10, 27
Deeks, C.: AS+SS-ThA4, 81; AS-MoM9, 3; AS-ThP4, 95
Degeorge, V.: AP+AS-MoA7, 17
Deilmann, T.D.: SP+AS+NS+SS-WeM3, 48
Dekhter, R.: AS+NS-TuM13, 30
Del Gaudio, D.: EM+AS+EN+NS-FrM4, 99
Delaittre, G.: AS-ThP6, 96
Delgass, W.N.: IS+AS+SS-MoM8, 10
DeMasi, A.: TF+AS+NS+SA-ThM13, 79; TF+AS+NS+SA-ThM6, 78
Denecke, M.A.: AC+AS+MI-ThM1, 68
Deng, X.: SS+AS+NS-WeM11, 50; SS+AS+NS-WeM12, 51
Denys, R.V.: AC+AS+MI-WeM10, 43
Derouin, J.: SS+AS+EN-MoM1, 13; SS+AS+EN-MoM2, 13; SS+AS+NS-WeM13, 51
Deskins, N.A.: SP+AS+NS+SS-ThM4, 75
Desmet, C.: TF+AS+BI-WeA1, 65
Deutsch, T.: EN+AS+EM+SE+SS-TuM12, 32
Devaraj, A.: AP+AS+MC+MI+NS-MoM5, 1; AP+AS-MoA4, 17; AP+AS-MoA7, 17
Dhlamini, S.: AS-ThP7, 96
Dhoubhadel, M.: AS-ThP8, 96
di Carlo, A.: AS+SS-WeA12, 54
Dick, D.: SD+AS+EM+PS-ThA8, 86; SD+AS+EM-ThM10, 73
Dick, K.A.: SS+AS+EM+EN-ThA9, 90
Diebold, A.C.: EL+AS+BI+EM-ThA2, 82; EL+AS+BI+EM-ThA6, 83; TF+AS+NS+SA-ThM12, 79
Diercks, D.R.: EN+AS+EM+NS+SE+SS+TF-MoM10, 8
Diest, K.: EM+AS+SS-MoM9, 6
Dietler, G.: NS+AS+SP-MoA1, 27
Ding, Y.: IS+SS+NS+BI+VT+MN+AS-WeA4, 57
Ding, Z.J.: SS+AS+EN+NS-TuM13, 35
Diroll, B.T.: EN+AS+EM+NS+SE+SS+TF-MoA5, 24
Ditze, S.: SS+AS+NS-WeM2, 49
Divis, M.: AC+AS+MI-WeM12, 44
Divitini, G.: AS+SS-WeA12, 54
Dixit, D.: EL+AS+BI+EM-ThA6, 83
Diyatmika, W.: SM+AS+BI+PS-ThM4, 74
Dohnalek, Z.: SP+AS+NS+SS-ThM4, 75; SS+AS+EN-TuM2, 36; SS+AS+EN-TuM3, 36; SS+AS+EN-WeA10, 63
Dohnálek, Z.: SS+AS+EN-TuM11, 36; SS+AS+EN-TuM4, 36
Dombrowski, E.: SS+AS-WeA1, 63
Dong, X.: AS-ThM3, 69
Dong, Y.: SS+AS+EN-TuA9, 41
Donnelly, V.M.: PS+AS+SS-WeA3, 58
Doscher, H.: EN+AS+EM+SE+SS-TuM12, 32
Downey, B.: EM+AS+MS+SS-WeA9, 56; TF+AS+NS+SA-ThM6, 78
Dowsett, D.: HI+AS+SS+NS-ThM10, 71
Dozias, S.: SM+AS+BI+PS-ThM1, 74
Drozdhenko, D.: AC+AS+MI-WeM12, 44
Du, X.: BI+AS-MoA10, 22
Du, Y.: SP+AS+NS+SS-ThM4, 75
Dubacheva, G.V.: BI+AS-MoA7, 21
Ducati, C.: AS+SS-WeA12, 54
Duke, A.S.: SS+AS+EN-WeA1, 62
Dunn, R.F.: AS-ThM4, 69
Dupuis, V.: IS+AS+SS-MoM3, 9
Duran, A.: AS-ThP16, 97
Durand, C.: SP+2D+AS+NS+SS-WeA3, 60
Durcan, C.: SP+AS+MI+NS+SS-FrM4, 100; SP+AS+MI+NS+SS-FrM5, 100; SP+AS+MI+NS+SS-FrM6, 101
Dussart, R.: PS+AS+SS-WeA11, 59

— E —

Eaton, A.: AP+AS-MoA3, 17
Eddy, C.: TF+AS+NS+SA-ThM6, 78
Eddy, Jr., C.R.: TF+AS+NS+SA-ThM13, 79
Eddy, Jr., C.R.: EM+AS+MS+SS-WeA7, 55
Edel, R.: SS+AS+EM+EN-ThA8, 89
Eder, K.: AP+AS+MC+MI+NS-MoM6, 1
Edström, D.: SE+AS+NS+TR-MoM3, 11
Egger, D.A.: TF+AS+SS-MoM1, 14
Eichhorn, B.: AS-MoA4, 18; IS+AS+SS-MoM5, 10; SS+AS+EN-TuA3, 41
Einstein, T.L.: SS+AS+EM+EN-ThA4, 89
Ekerdt, J.: SD+AS+EM-ThM11, 73
El Hafni-Rabbi, B.: SM+AS+BI+PS-ThM1, 74
Ellinger, C.R.: EM+AS+SS-MoA9, 23
Ellsworth, A.A.: AS-MoM4, 2; SS+AS+EN+NS-TuM2, 34
Eloirdi, R.: AC+AS+MI-WeM11, 44
Emmrich, D.: HI+AS+NS-ThA4, 84
Encinas, N.: BI+AS-MoA4, 20
Engberg, D.L.J.: AP+AS-TuM10, 29
Engelhard, M.: AS-ThP1, 95
Engstrom, J.R.: SD+AS+EM-ThM1, 72
Eom, T.: SD+AS+EM+PS-ThA9, 86
Eren, B.: IS+AS+SA+SS-MoA5, 26
Eriguchi, K.: PS+AS+SS-WeA10, 59
Eriksson, F.: SE+AS+NS+TR-MoM8, 12
Escamilla, R.: AS-ThP16, 97

- Escorihuela, J.: AS+BI-TuA4, 38
 Evans, J.E.: AS+BI-TuA11, 39;
 IS+SS+NS+BI+VT+MN+AS-WeA1, 56
 Evans, J.W.: SS+AS+EN+NS-TuM6, 34
 Ewing, P.R.: IS+AS+SA+SS-MoA10, 27
 Ewsuk, K.: SS+AS+EN-MoM10, 14
 Exarhos, S.: EM+AS+EN+NS-FrM8, 100
- **F** —
 Facsko, S.: HI+AS+SS+NS-ThM12, 71
 Fadley, C.S.: AS+SS-WeA9, 54
 Fairley, N.: AS+SS-ThA3, 81
 Fallet, M.: TR+AS+NS+SS-ThA9, 93
 Fan, Q.T.: TF+AS+BI-WeA10, 66
 Fan, W.: NS+AS+SP-MoA8, 28
 Farber, R.G.: SS+AS+EN-MoM1, 13;
 SS+AS+EN-MoM2, 13; SS+AS+NS-
 WeM13, 51
 Farhaoui, A.: TF+AS+NS+SA-ThM1, 78
 Fartmann, M.: TF+AS+NS+SA-ThM10, 79
 Fattayer, S.: SP+AS+MI+NS+SS-FrM9, 101
 Faulk, D.M.: BI+AS-MoA3, 20
 Favaro, M.: IS+AS+SA+SS-TuM12, 33;
 IS+AS+SA+SS-TuM3, 33
 Fears, K.: BI+AS-MoM1, 4
 Feigelson, B.N.: EM+AS+MS+SS-WeA12,
 56
 Felfer, P.J.: AP+AS+MC+MI+NS-MoM6, 1
 Fennie, C.J.: EM+AS+SS-MoA5, 23
 Fenton, J.: AS+SS-ThA10, 82
 Fernandes, G.E.: EM+AS+SS-MoM9, 6
 Field, D.: TF+AS+SS-MoM2, 14
 Filippov, A.: TR+AS+NS+SS-ThA7, 93
 Fisher, E.R.: SM+AS+BI+PS-ThM13, 75;
 SS+AS+NS-WeM10, 50
 Fisher, G.L.: AS+SS-ThA8, 81; AS+SS-
 WeA3, 53
 Fitzell, K.: TF+AS+NS+SA-ThA11, 92
 Flater, E.: TR+AS+NS+SS-ThA10, 93
 Fletcher, J.S.: AS-WeM12, 46
 Flores, M.: AS-ThP16, 97
 Fonctuberta i Morral, A.:
 EN+AS+EM+SE+SS-TuM2, 31
 Fong, K.D.: EN+AS+EM+SE+SS-TuM3, 31
 Forbes, T.P.: AS+SS-ThA11, 82
 Fordham, J.L.:
 EN+AS+EM+NS+SE+SS+TF-MoA5, 24
 Foster, M.: IS+AS+SS-MoM6, 10
 Frau, E.: EN+AS+EM+SE+SS-TuM2, 31
 Frenkel, A.: IS+AS+SA+SS-MoA3, 26;
 IS+AS+SA+SS-MoA8, 27;
 IS+AS+SA+SS-WeM10, 47
 Frenkel, D.: BI+AS-MoA7, 21
 Frenken, J.W.M.: IS+AS+SS-MoM4, 10
 Freund, H.: SS+AS+EN-TuM5, 36
 Fridmann, J.: HI+AS+SS+NS-ThM6, 71
 Friedman, S.L.: SP+AS+NS+SS-WeM5, 48
 Frijters, C.: EN+AS+EM+NS+SE+SS+TF-
 MoM8, 8
 Fu, E.: BI+AS-MoA6, 21
 Fuentes-Cabrera, M.: SS+AS+EN+NS-
 TuM10, 35
 Fuentesf, E.: IS+SS+NS+BI+VT+MN+AS-
 WeA9, 57
 Fukasawa, M.: PS+AS+SS-WeA8, 59
 Fukutani, K.: SS+AS+EN-TuA1, 40;
 SS+AS-WeA10, 64
 Fulghum, J.: AS+SS-ThA1, 81
 Furuta, R.: SM+AS+BI+PS-ThA11, 88
- **G** —
 Gai, Z.: SP+AS+NS+SS-WeM6, 48
 Galante, D.: NS+AS+SP-MoA1, 27
 Galhenage, R.P.: SS+AS+EN-WeA1, 62
 Galindo, J.: EN+AS+EM+NS+SE+SS+TF-
 MoM5, 8
 Gall, D.: SE+AS+NS+TR-MoM9, 12;
 TF+AS+NS+SA-ThA4, 91
 Gamble, L.J.: BI+AS-MoA5, 21; BI+AS-
 MoM11, 5; BI+AS-MoM8, 5
 Gao, F.: SS+AS+EM+EN-ThM3, 76
 Gao, H.: TR+AS+NS+SS-ThA3, 93
 Gao, Y.: IS+SS+NS+BI+VT+MN+AS-
 WeA10, 57
 Garcia, J.C.: SP+AS+NS+SS-ThM4, 75
 Gash, A.E.: TF+AS+EM+EN+MN-WeA11,
 67
 Gates, B.D.: AS-ThP13, 97
 Gaulding, E.A.:
 EN+AS+EM+NS+SE+SS+TF-MoA5, 24
 Ge, Q.: SS+AS+EN-TuM4, 36
 Geller, A.: AS-MoA4, 18
 Gerstl, S.A.: AP+AS-TuM3, 29
 Ghaffar, F.: EM+AS+SS-MoA2, 22
 Ghosez, P.: EM+AS+SS-MoA5, 23
 Giardini, S.: EM+AS+SS-MoM9, 6
 Gillen, G.: AS+SS-ThA11, 82
 Gillette, E.: AS+SS-ThA9, 81
 Gilliland, D.: BI+AS-MoM9, 5
 Gilmore, I.S.: AS+BI-TuA12, 39; AS+BI-
 TuA9, 38
 Ginger, D.S.: EN+AS+EM+NS+SE+SS+TF-
 MoA7, 24
 Giovannini, M.: AC+AS+MI-WeM10, 43
 Giovannozzi, A.: AS+BI-TuA3, 38
 Girolami, G.S.: SD+AS+EM-ThM2, 72
 Givon, A.: AS+NS-TuM13, 30
 Glatzel, T.: TR+AS+NS+SS-ThA7, 93
 Glezakou, V.A.: SS+AS+EN-TuM11, 36
 Gnecco, E.: TR+AS+NS+SS-ThA7, 93
 Gofryk, K.: AC+AS+MI-WeM5, 43
 Goian, V.: EM+AS+SS-MoA5, 23
 Goldman, R.S.: EM+AS+EN+NS-FrM4, 99
 Gölzhäuser, A.: HI+AS+NS-ThA4, 84;
 SS+AS+EN+NS-TuM5, 34
 Gonzalez, D.: TF+AS+BI-WeA7, 65
 Goodson, W.J.: BI+AS-MoM6, 4
 Goorsky, M.: TF+AS+NS+SA-ThA10, 92
 Gopalan, V.: EM+AS+SS-MoA5, 23
 Gordon, J.M.: EM+AS+SS-MoM4, 6
 Gordon, L.: AP+AS-MoA4, 17
 Gordon, R.: SD+AS+EM-ThM3, 72
 Goto, K.: SM+AS+BI+PS-ThM12, 75
 Gottfried, J.M.: TF+AS+BI-WeA10, 66
 Gouder, T.: AC+AS+MI-WeM3, 43
 Gougousi, T.: SS+AS+EM+EN-ThM11, 77
 Gounder, R.: IS+AS+SS-MoM8, 10
 Graham, D.J.: BI+AS-MoA4, 20; BI+AS-
 MoM11, 5; BI+AS-MoM8, 5
 Grant, J.T.: AS-MoM5, 3; AS-ThM12, 70
 Greczynski, G.: SE+AS+NS+TR-MoM8, 12
 Greeley, J.: IS+AS+SS-MoM8, 10
 Green, A.: EL+AS+BI+EM-ThA8, 83;
 TF+AS+NS+SA-ThM12, 79
 Green, M.F.B.G.: SP+AS+NS+SS-WeM3,
 48
 Greene, J.E.: SE+AS+NS+TR-MoM3, 11;
 TF+AS+NS+SA-ThA1, 90
 Greenlee, J.D.: EM+AS+MS+SS-WeA12, 56
 Gregoratti, L.: IS+AS+SA+SS-MoA7, 26
 Grehl, T.: AS-MoM3, 2; TF+AS+NS+SA-
 ThM10, 79
 Grevin, B.: SP+AS+NS+SS-WeM4, 48
 Griesser, H.J.: SM+AS+BI+PS-ThA6, 88
 Griesser, S.S.: SM+AS+BI+PS-ThA6, 88
 Griffith, W.B.: AS-ThM1, 69
 Griveau, J.C.: AC+AS+MI-WeM11, 44
 Groot, I.M.N.: IS+AS+SS-MoM4, 10
 Gross, L.: SP+AS+MI+NS+SS-FrM9, 101
 Gstrein, F.: SD+AS+EM+PS-ThA3, 85
 Gu, G.: SP+2D+AS+NS+SS-WeA7, 61
 Guelcher, S.A.: AS-ThM4, 69
 Guerette, M.J.: SE+AS+NS+TR-MoM9, 12
 Guglietta, G.W.:
 EN+AS+EM+NS+SE+SS+TF-MoA5, 24
 Guitán, E.: SP+AS+MI+NS+SS-FrM9, 101
 Guo, D.: SS+AS+EN-TuM1, 35
 Guo, J.-H.: EN+AS+EM+SE+SS-TuM13,
 32; IS+AS+SA+SS-WeM1, 46
 Guo, Q.Y.: SE+AS+NS+TR-MoM10, 12
- **H** —
 Haasch, R.: AS-ThP17, 97
 Habelitz, S.: NS+AS+SP-MoA9, 28
 Hafeez, M.A.: EL+AS+BI+EM-ThA9, 83
 Hagenhoff, B.: AS+BI-TuA1, 38
 Hahn, C.J.: EN+AS+EM+SE+SS-TuM3, 31
 Hahn, R.: SE+AS+NS+TR-MoM11, 13
 Haight, R.A.: EN+AS+EM+NS+SE+SS+TF-
 MoM1, 7;
 EN+AS+EM+NS+SE+SS+TF-MoM2, 7
 Haislmaier, R.: EM+AS+SS-MoA5, 23
 Halberstadt, L.: SS+AS+EN-TuA10, 41
 Halevy, I.: AC+AS+MI-WeM10, 43;
 AC+AS+MI-WeM11, 44
 Hall, S.: EM+AS+SS-MoA1, 22
 Halls, M.D.: SD+AS+EM-ThM10, 73;
 SS+AS+EM+EN-ThM2, 76
 Hamaguchi, S.: PS+AS+SS-WeA8, 59;
 SM+AS+BI+PS-ThM12, 75
 Hammond, J.S.: AS+SS-ThA8, 81; AS-
 MoM8, 3
 Hamra, P.: AS+NS-TuM12, 30
 Han, C.: AS-ThP12, 97
 Han, S.E.: TF+AS+NS+SA-ThA9, 92
 Han, S.M.: TF+AS+NS+SA-ThA9, 92
 Han, Y.: SS+AS+EN+NS-TuM6, 34
 Harker, M.: TF+AS+EM+EN+MN-WeA12,
 67
 Harrison, E.: AS-MoA7, 19
 Harrison, J.A.: TR+AS+NS+SS-ThA11, 93;
 TR+AS+NS+SS-ThA9, 93
 Harshan, V.N.: TF+AS+NS+SA-ThA3, 91
 Hartl, M.: AS+SS-WeA9, 54; IS+AS+SS-
 MoM5, 10
 Hashemi, F.H.: SD+AS+EM+PS-ThA10, 87
 Hashizume, H.: SM+AS+BI+PS-ThA11, 88
 Haslberger, P.: AP+AS-MoA5, 17
 Hasz, K.: TR+AS+NS+SS-ThA4, 93
 Hatayama, T.: TF+AS+SS-MoM9, 15
 Hathaway, M.: TF+AS+NS+SA-ThM10, 79
 Haukka, S.: SD+AS+EM+PS-ThA1, 85
 Havela, L.: AC+AS+MI-WeM10, 43;
 AC+AS+MI-WeM12, 44; AC+AS+MI-
 WeM3, 43
 Havelund, R.: AS+BI-TuA12, 39
 Hawker, M.J.: SM+AS+BI+PS-ThM13, 75
 Head, A.R.: IS+AS+SS-MoM11, 11;
 IS+AS+SS-MoM5, 10; SS+AS+EN-
 TuA3, 41
 Healy, K.E.: SM+AS+BI+PS-ThA8, 88
 Hedström, P.: AP+AS-MoA1, 17
 Heeren, R.M.A.: AS+SS-ThA8, 81
 Hehn, L.: TF+AS+SS-MoM1, 14
 Heinrich, A.: SP+2D+AS+NS+SS-WeA9,
 61; SP+AS+MI+NS+SS-FrM3, 100
 Helal, Y.H.: IS+AS+SA+SS-MoA10, 27
 Heldebrant, D.: IS+AS+SA+SS-TuM13, 34
 Heller, R.: HI+AS+SS+NS-ThM12, 71
 Hellgren, N.: AS-ThP17, 97
 Hellman, O.: TF+AS+NS+SA-ThA1, 90
 Hellstern, T.R.: EN+AS+EM+SE+SS-TuM3,
 31
 Hemminger, J.C.: EN+AS+EM+SE+SS-
 TuM6, 32; IS+AS+SA+SS-TuM5, 33;
 SS+AS+EN-MoM8, 13
 Hen, A.: AC+AS+MI-WeM11, 44
 Henderson, M.A.: SP+AS+NS+SS-ThM4, 75
 Henegar, A.J.: SS+AS+EM+EN-ThM11, 77
 Heo, S.: EN+AS+EM+NS+SE+SS+TF-
 MoM6, 8
 Herman, G.: BI+AS-MoA10, 22
 Hernandez, J.: EM+AS+EN+NS-FrM8, 100
 Herrera-Gomez, A.: AS-MoM2, 2
 Hersam, M.C.: AS+NS-TuM6, 30;
 NS+AS+SP-MoA7, 28
 Hicks, Z.: SS+AS+EN-TuA3, 41
 High, E.: SS+AS-WeA1, 63
 Hilbert, J.: AS-MoA9, 19

- Hirayama, H.: SS+AS+NS-WeM5, **50**
Hite, J.K.: EM+AS+MS+SS-WeA7, 55;
TF+AS+NS+SA-ThM13, 79
Hjort, M.: SS+AS+EM+EN-ThA9, 90
Hlawacek, G.: HI+AS+SS+NS-ThM12, 71
Hobart, K.D.: EM+AS+MS+SS-WeA12, 56;
EM+AS+MS+SS-WeA7, 55
Hobbs, M.: TF+AS+EM+EN+MN-WeA4,
66
Hockenbery, D.: BI+AS-MoA5, 21
Hodges, D.R.:
EN+AS+EM+NS+SE+SS+TF-MoM5, **8**
Hofer, C.: AP+AS-MoA5, 17
Hofmann, T.: EL+AS+BI+EM-ThA3, 83;
EL+AS+BI+EM-ThA4, 83
Högborg, H.: SE+AS+NS+TR-MoM8, **12**
Holmlid, L.: EN+AS+EM+SE+SS-TuM1, 31
Hong, J.: HI+AS+NS-ThA10, 85
Hono, K.: AP+AS+MC+MI+NS-MoM1, 1
Hook, A.L.: AS+BI-TuA3, 38
Hori, M.: SM+AS+BI+PS-ThA11, 88
Hosemann, P.: HI+AS+NS-ThA10, 85;
HI+AS+NS-ThA8, 84
Hou, M.: EM+AS+MS+SS-WeA8, **55**
Hourani, R.: SD+AS+EM-ThM10, 73
Howansky, A.: SS+AS+EN-TuM10, 36
Hsieh, J.H.: SM+AS+BI+PS-ThM3, 74
Hsu, J.X.: SS+AS+EM+EN-ThM4, 77
Hu, J.: SS+AS+EN-TuM13, 37
Hu, X.: TR+AS+NS+SS-ThA1, 92
Hua, X.: AS+BI-TuA11, 39;
IS+SS+NS+BI+VT+MN+AS-WeA4, 57
Huang, J.J.: SS+AS+EN-TuM13, 37
Huang, L.: SE+AS+NS+TR-MoM9, 12
Huang, S.: EM+AS+EN+NS-FrM4, 99
Huang, W.C.: SM+AS+BI+PS-ThM4, 74
Huang, Y.: TF+AS+NS+SA-ThA2, 91
Hubbard, L.R.: EL+AS+BI+EM-ThA1, **82**
Huerta, L.: AS-ThP16, **97**
Huffman, E.S.: SS+AS+NS-WeM6, 50
Hultman, L.: AP+AS-TuM10, 29; AS-
ThP17, 97; SE+AS+NS+TR-MoM3, 11;
SE+AS+NS+TR-MoM8, 12;
TF+AS+NS+SA-ThA1, 90
Hus, S.: SP+2D+AS+NS+SS-WeA3, 60
Hussain, H.: EL+AS+BI+EM-ThA9, 83
Hussain, Z.: IS+AS+SA+SS-TuM12, 33;
IS+AS+SA+SS-TuM3, 33
Hutton, S.J.: AS+SS-WeA10, 54; AS-ThP3,
95
Hwang, C.S.: SD+AS+EM+PS-ThA9, 86
— **I** —
Iberi, V.: IS+AS+SS-TuA11, 40
Iddawela, G.: EL+AS+BI+EM-ThA6, 83
Iida, S.: AS+SS-WeA3, 53
Iijima, T.: HI+AS+NS-ThA3, 84
Iijima, T.: HI+AS+NS-ThA3, 84
Ikeda, Y.: SM+AS+BI+PS-ThA10, **88**
Illiberi, A.: EN+AS+EM+NS+SE+SS+TF-
MoM8, **8**
Interlandi, G.: AS-MoA7, 19
Isa, L.: TR+AS+BI+NS-FrM9, 102
Isheim, D.: AP+AS+MC+MI+NS-MoM3, **1**
Ishiguro, M.: PS+AS+SS-WeA12, **60**
Ishikawa, K.: SM+AS+BI+PS-ThA11, **88**
Isobe, M.: SM+AS+BI+PS-ThM12, 75
Ito, M.: SM+AS+BI+PS-ThA11, 88
Itsuki, D.: SM+AS+BI+PS-ThM12, 75
Iverson, B.D.: TF+AS+BI-WeA11, **66**;
TF+AS+EM+EN+MN-WeA12, 67
— **J** —
Jacobs, T.D.B.: TR+AS+BI+NS-FrM3, **102**
Jain, G.: AS+SS-ThA10, 82
Janakiraman, S.:
EN+AS+EM+NS+SE+SS+TF-MoA6, 24
Jang, J.E.: EM+AS+SS-MoA3, **22**
Janke, S.M.: SS+AS-WeA7, 64
Janoschek, M.J.: AC+AS+MI-WeM1, **43**
Jaramillo, T.F.: EN+AS+EM+SE+SS-TuM3,
31
Jasieniak, M.: SM+AS+BI+PS-ThA6, 88
Jede, R.: HI+AS+SS+NS-ThM6, 71
Jensen, B.D.: TF+AS+BI-WeA11, 66
Jensen, L.: NS+AS+SP-MoA7, 28
Jeon, B.: IS+AS+SA+SS-TuM3, 33
Jeong, B.: IS+AS+SA+SS-TuM12, **33**
Jiang, N.: NS+AS+SP-MoA7, 28
Jiang, X.: EM+AS+SS-MoA10, 23
Jin, M.: NS+AS+SP-MoA3, 27
Jinno, M.: SM+AS+BI+PS-ThA10, 88
Joghee, P.: EM+AS+SS-MoM9, 6
Johansson, N.: IS+AS+SA+SS-MoA4, 26;
IS+AS+SS-MoM11, **11**
Johansson-Jöesaar, M.P.: AP+AS-TuM10,
29
Johar, M.A.: EL+AS+BI+EM-ThA9, 83
Johnson, L.J.S.: AP+AS-TuM10, 29
Johnson, M.D.: AS-MoM4, 2
Johnson, N.: EN+AS+EM+NS+SE+SS+TF-
MoM9, **8**
Johnson, S.D.: TF+AS+NS+SA-ThM13, 79;
TF+AS+NS+SA-ThM6, 78
Jones, J.G.: AS-ThM12, 70
Joshi, S.: EM+AS+SS-MoM1, 5
Joy, D.C.: IS+AS+SS-TuA11, 40
Ju, H.X.: EN+AS+EM+NS+SE+SS+TF-
MoA7, **24**; EN+AS+EM+SE+SS-
TuM13, 32
Jung, H.: SD+AS+EM-ThM12, 73
Jung, M.: SP+2D+AS+NS+SS-WeA8, 61
Junk, C.P.: AS-ThM2, 69
Junquera, J.: EM+AS+SS-MoA5, 23
Juurlik, L.B.F.: SS+AS+NS-WeM13, 51
— **K** —
Kabir, S.: AS-MoA5, 18
Kakalios, J.: EN+AS+EM+NS+SE+SS+TF-
MoA9, 25
Kalan, M.: SS+AS+EN-MoM10, 14
Kalhor, N.: HI+AS+SS+NS-ThM13, 72
Kamba, S.: EM+AS+SS-MoA5, 23
Kamei, M.: PS+AS+SS-WeA10, 59
Kaminen, V.M.: EL+AS+BI+EM-ThA6, **83**
Kaminski, P.M.:
EN+AS+EM+NS+SE+SS+TF-MoM11,
9
Kandratsenka, A.: SS+AS-WeA7, 64
Kang, H.J.: EN+AS+EM+NS+SE+SS+TF-
MoM6, 8
Kang, M.: EM+AS+SS-MoM9, 6
Karahashi, K.: PS+AS+SS-WeA8, 59
Karslioglu, O.: AS+SS-WeA9, **54**;
IS+AS+SS-MoM5, 10
Kasai, H.: SS+AS+EN-MoM9, 14
Kaspar, T.C.: EM+AS+SS-MoM11, 7
Kasprzak, D.J.: AS-ThM2, 69
Kaub, T.: TF+AS+NS+SA-ThA8, 91
Kava, D.: EN+AS+EM+NS+SE+SS+TF-
MoM5, 8
Kawai, S.: TR+AS+NS+SS-ThA7, 93
Kawamura, M.: TF+AS+SS-MoM8, **15**
Kawase, A.: EN+AS+EM+SE+SS-TuM13,
32
Kay, B.D.: SS+AS+EN-WeA10, 63
Keagy, J.: SS+AS+EN+NS-TuM12, 35
Keely, D.: AS-ThM1, 69
Keenan, M.R.: AS-ThP11, 97
Keller, N.: EL+AS+BI+EM-ThA2, 82
Kelley, M.J.: AS+BI-TuA8, 38
Kemp, C.A.J.: AS-ThM3, 69
Kessels, W.M.M.: SS+AS+EN-TuM12, 37
Keszler, D.: TF+AS+NS+SA-ThA2, 91
Keylin, V.: AP+AS-MoA7, 17
Khadra, G.: IS+AS+SS-MoM3, 9
Khalifa, Y.: IS+AS+SA+SS-TuM2, 33
Khan, A.A.: EM+AS+SS-MoA2, 22
Kiba, T.: TF+AS+SS-MoM8, 15
Kibsgaard, J.: EN+AS+EM+SE+SS-TuM3,
31
Kieda, C.: SM+AS+BI+PS-ThM1, 74
Kieffer, B.: AS-MoA5, 18
Kikuchi, H.: IS+SS+NS+BI+VT+MN+AS-
WeA12, 58
Killelea, D.R.: SS+AS+EN-MoM1, **13**;
SS+AS+EN-MoM2, 13; SS+AS+NS-
WeM13, 51
Kim, H.: SD+AS+EM-ThM12, 73
Kim, H.-J.: SD+AS+EM-ThM12, 73
Kim, J.K.: AS-WeM11, 45
Kim, K.B.: EM+AS+SS-MoM9, 6
Kim, K.H.: TF+AS+SS-MoM8, 15
Kim, S.H.: TR+AS+NS+SS-ThA9, 93
Kim, T.H.: SP+2D+AS+NS+SS-WeA12, 61
Kim, T.-H.: SP+2D+AS+NS+SS-WeA4, **60**
Kimmel, G.A.: SP+AS+NS+SS-ThM4, 75;
SS+AS+EN-WeA9, 62
Kim-Ngan, N.-T.H.: AC+AS+MI-WeM12,
44
Kimura, K.: SP+AS+NS+SS-WeM12, **49**
Kind, M.: TF+AS+SS-MoM1, 14;
TF+AS+SS-MoM11, **16**
King, S.W.: EM+AS+MS+SS-WeA3, **55**
Kipreos, M.: IS+AS+SS-MoM6, **10**
Kjoller, K.: BI+AS-MoM6, 4
Klein, E.: BI+AS-MoM5, 4
Klingner, N.: HI+AS+SS+NS-ThM12, **71**
Knippenberg, T.: TR+AS+NS+SS-ThA9, 93
Knowles, T.P.J.: NS+AS+SP-MoA1, 27
Knudsen, J.: IS+AS+SS-MoM11, 11
Knutsson, J.: SS+AS+EM+EN-ThA9, 90
Ko, C.: NS+AS+SP-MoA8, 28
Kobayashi, H.: SS+AS-WeA10, 64
Kobayashi, K.: SP+AS+NS+SS-WeM12, 49
Koehler, A.D.: EM+AS+MS+SS-WeA7, 55
Koirala, P.: SS+AS+EM+EN-ThA11, 90
Koitaya, T.: IS+SS+NS+BI+VT+MN+AS-
WeA12, 58
Kokubo, I.: SS+AS+NS-WeM5, 50
Kolb, M.J.: SS+AS+NS-WeM13, 51
Koller, C.M.: SE+AS+NS+TR-MoM11, **13**
Kolli, R.: AP+AS-MoA3, 17
Kolmakov, A.: IS+AS+SA+SS-TuM4, **33**
Kolomiets, A.: AC+AS+MI-WeM10, 43
Koložsvári, S.: SE+AS+NS+TR-MoM11, 13
Komissar, A.: IS+AS+SA+SS-MoM12, 47
Kondo, H.: SM+AS+BI+PS-ThA11, 88
Kondo, T.: SS+AS+EN-TuM1, **35**; SS+AS-
WeA11, 64
Kooi, B.: EM+AS+EN+NS-FrM5, 99
Kooi, S.: EM+AS+SS-MoM9, 6
Koper, M.T.M.: SS+AS+NS-WeM13, 51
Koshiishi, A.: PS+AS+SS-WeA9, 59
Kotru, S.: TF+AS+NS+SA-ThA3, 91
Kotter, D.: EM+AS+SS-MoM1, 5
Kourkoutis, L.F.: EM+AS+SS-MoA5, 23
Kriegner, D.: AC+AS+MI-WeM12, 44
Krooswyk, J.D.: SS+AS+EN-WeA3, 62
Krueger, P.: SP+AS+NS+SS-WeM3, 48
Kruppe, C.M.: SS+AS+EN-WeA3, 62
Kub, F.J.: EM+AS+MS+SS-WeA12, 56
Kudo, C.: TF+AS+SS-MoM8, 15
Kujofsa, T.: TF+AS+NS+SA-ThA6, **91**
Kuk, Y.: SP+2D+AS+NS+SS-WeA1, **60**
Kulkarni, G.: AP+AS-MoA4, 17
Kumagai, T.: IS+AS+SA+SS-WeM2, 46
Kummel, A.C.: BI+AS-MoA9, 21;
EN+AS+EM+NS+SE+SS+TF-MoM1, 7;
EN+AS+EM+NS+SE+SS+TF-MoM2, 7
Kungas, R.: SP+AS+NS+SS-ThM6, 76
Kushner, M.J.: SM+AS+BI+PS-ThA1, **87**
Kuwauchi, Y.: IS+AS+SS-TuA3, 39
Kwolek, E.J.: SS+AS+EN+NS-TuM6, 34
Kwon, J.: EN+AS+EM+SE+SS-TuM6, **32**;
SS+AS+EN-MoM8, 13
Kyung Lee, W.: BI+AS-MoM6, 4

— L —

La Spina, R.: BI+AS-MoM9, 5
 LaBella, V.: SP+AS+MI+NS+SS-FrM4, **100**; SP+AS+MI+NS+SS-FrM5, 100; SP+AS+MI+NS+SS-FrM6, 101; TF+AS+NS+SA-ThM12, 79
 Labuda, A.: SP+AS+NS+SS-WeM13, **49**
 Lahav, M.: TF+AS+SS-MoM3, **15**
 Lai, J.: BI+AS-MoM8, 5
 Lai, K.: SP+AS+NS+SS-WeM10, **49**
 Lakshantha, W.: AS-ThP8, **96**
 Lamma, D.: AS-ThP9, 96
 Landa, A.: AC+AS+MI-ThM3, **68**
 Lane, B.: PS+AS+SS-WeA9, **59**
 Lang, D.: AP+AS-MoA5, 17
 Langford, J.M.: SS+AS+EN-MoM8, **13**
 Lanigan, D.: EN+AS+EM+NS+SE+SS+TF-MoA10, 25
 Lao, D.: AS+BI-TuA11, 39; IS+AS+SA+SS-TuM13, 34
 Lashuel, H.: NS+AS+SP-MoA1, 27
 Lasne, J.: TF+AS+SS-MoM2, 14
 Lau, K.K.S.: EN+AS+EM+NS+SE+SS+TF-MoA6, 24
 Laudrel, E.: PS+AS+SS-WeA11, **59**
 Lauritsen, J.V.: SS+AS+EN-TuA4, 41
 Law, M.: EM+AS+EN+NS-FrM1, **99**
 Leary, A.: AP+AS-MoA7, 17
 Lechner, B.A.J.: SS+AS+EN-TuA12, **42**
 Lee, A.: AS-ThP13, **97**
 Lee, C.H.: EM+AS+SS-MoA5, 23
 Lee, C.M.: SM+AS+BI+PS-ThM4, 74
 Lee, D.: AS-ThP12, 97
 Lee, D.H.: EN+AS+EM+NS+SE+SS+TF-MoM6, 8
 Lee, H.L.: EN+AS+EM+NS+SE+SS+TF-MoM6, 8
 Lee, J.: IS+AS+SA+SS-TuM12, 33; IS+AS+SA+SS-WeM3, **46**; SS+AS+NS-WeM11, 50; SS+AS+NS-WeM12, **51**
 Lee, J.-H.: AP+AS+MC+MI+NS-MoM8, 1
 Lee, K.: SP+2D+AS+NS+SS-WeA8, 61
 Lee, S.B.: AS+SS-ThA9, 81
 Lee, S.-H.: SP+2D+AS+NS+SS-WeA4, 60
 Lee, S.-Y.: EM+AS+SS-MoA7, **23**
 Lee, Y.-B.: SD+AS+EM-ThM12, 73
 Lee, Y.J.: SS+AS+EM+EN-ThM4, 77
 Lee, Y.T.: SM+AS+BI+PS-ThM3, **74**
 Lefauchaux, P.: PS+AS+SS-WeA11, 59
 Lehmann, S.: SS+AS+EM+EN-ThA9, 90
 Lei, H.: SS+AS+EN+NS-TuM6, 34
 Leighton, C.: EN+AS+EM+NS+SE+SS+TF-MoA9, 25
 Leijtens, T.: EN+AS+EM+NS+SE+SS+TF-MoA3, **24**
 Leinen, P.L.: SP+AS+NS+SS-WeM3, 48
 Lemay, J.C.: SS+AS+EN-TuA9, **41**
 Leone, S.R.: SS+AS+EM+EN-ThM12, 77
 Lepper, M.: SS+AS+NS-WeM2, 49
 Lerner, P.B.: EM+AS+SS-MoM5, **6**
 LeRoy, B.J.: SP+2D+AS+NS+SS-WeA10, **61**
 Lesser, J.: AS+SS-ThA10, 82
 Leusink, G.: SD+AS+EM+PS-ThA11, 87
 Levermann, M.: HI+AS+SS+NS-ThM2, 70
 Lewin, E.: SE+AS+NS+TR-MoM1, 11
 Lewis, A.: AS+NS-TuM12, 30; IS+AS+SA+SS-WeM12, **47**
 Lewis, D.: IS+AS+SA+SS-WeM12, 47
 Li, A.-P.: SP+2D+AS+NS+SS-WeA12, 61; SP+2D+AS+NS+SS-WeA3, 60; SP+2D+AS+NS+SS-WeA7, 61; SP+AS+NS+SS-WeM6, 48
 Li, C.: SM+AS+BI+PS-ThM3, 74; TF+AS+NS+SA-ThA10, **92**
 Li, E.: SS+AS+NS-WeM1, 49
 Li, H.: PS+AS+SS-WeA8, **59**
 Li, J.: EN+AS+EM+NS+SE+SS+TF-MoM10, **8**; IS+AS+SA+SS-MoA3, 26;

IS+SS+NS+BI+VT+MN+AS-WeA10, 57; IS+SS+NS+BI+VT+MN+AS-WeA9, 57
 Li, M.: EN+AS+EM+NS+SE+SS+TF-MoA9, 25; SS+AS+EM+EN-ThA10, **90**
 Li, S.: EN+AS+EM+NS+SE+SS+TF-MoA5, 24
 Li, Y.: BI+AS-MoA10, 22; SS+AS+EN+NS-TuM11, 35
 Liberman, A.: BI+AS-MoA9, 21
 Lietz, A.M.: SM+AS+BI+PS-ThA1, 87
 Lin, S.: EM+AS+SS-MoM10, **7**
 Lin, X.: SS+AS+EN-TuM11, 36
 Linden, A.: HI+AS+SS+NS-ThM2, **70**
 Lindhorst, K.: TF+AS+BI-WeA8, 65
 Linford, M.R.: AS-MoM3, 2
 Linh, N.H.: SS+AS+EN-MoM9, 14
 Linh, T.P.T.: SS+AS+EN-MoM9, 14
 Linic, S.: SS+AS+EN+NS-TuM3, **34**
 Liriano, M.L.: SS+AS+EN-WeA12, 63
 Liu, J.: AP+AS-MoA3, 17; AP+AS-MoA4, **17**; IS+AS+SA+SS-MoA8, 27
 Liu, L.: SP+2D+AS+NS+SS-WeA7, 61
 Liu, L.-H.: EN+AS+EM+NS+SE+SS+TF-MoA1, 24; SD+AS+EM-ThM10, 73; SS+AS+EM+EN-ThM4, 77
 Liu, Q.: IS+AS+SS-TuA1, 39
 Liu, S.: IS+AS+SA+SS-WeM2, 46
 Liu, X.: SS+AS+EN-TuA2, **41**; SS+AS+EN-WeA4, 62
 Liu, X.Z.: TR+AS+NS+SS-ThA4, 93
 Liu, Z.: IS+AS+SA+SS-TuM12, 33; IS+AS+SA+SS-TuM3, 33
 Lloyd, K.G.: AS-ThM2, 69; AS-ThP10, **97**
 Lo, M.: BI+AS-MoM6, 4
 Long, R.: EM+AS+MS+SS-WeA11, 56
 Longo, R.C.: SS+AS+EM+EN-ThM2, 76; SS+AS+EM+EN-ThM4, 77
 Lopez, T.: PS+AS+SS-WeA2, **58**
 Lovinger, D.: SS+AS+NS-WeM6, 50
 Lu, D.: EM+AS+SS-MoM6, 6
 Lu, F.: NS+AS+SP-MoA3, 27
 Lubinevsky, H.: BI+AS-MoM5, 4
 Lucci, F.R.: SS+AS+EN-WeA11, **63**; SS+AS+EN-WeA12, 63
 Ludwig, K.F.: TF+AS+NS+SA-ThM13, 79; TF+AS+NS+SA-ThM6, 78
 Lukes, J.R.: AS-MoA9, 19
 Lum, P.: HI+AS+NS-ThA10, 85
 Lund, J.M.: TF+AS+BI-WeA11, 66
 Luo, H.: AS-ThP2, 95
 Luo, Z.: EM+AS+SS-MoA1, 22
 Lutz, C.P.: SP+2D+AS+NS+SS-WeA9, 61; SP+AS+MI+NS+SS-FrM3, 100
 Lyubinetzky, I.: SP+AS+NS+SS-ThM4, **75**; SS+AS+EN-TuM11, 36; SS+AS+EN-TuM3, 36; SS+AS+EN-TuM4, 36

— M —

Ma, C.: AS-ThP2, 95; SP+2D+AS+NS+SS-WeA7, **61**
 Maas, D.: HI+AS+SS+NS-ThM13, 72
 Maayan, E.: IS+AS+SA+SS-WeM12, 47
 Mack, P.: AS+SS-ThA4, 81; AS-MoM9, 3; AS-ThM13, **70**
 Mackova, A.: AC+AS+MI-WeM3, 43
 Maes, J.W.: SD+AS+EM+PS-ThA1, 85
 Magnani, N.: AC+AS+MI-WeM11, 44
 Maier, S.: SS+AS+EN-TuA12, 42
 Maksymovych, P.: SS+AS+EN+NS-TuM10, 35
 Malko, A.V.: EN+AS+EM+NS+SE+SS+TF-MoA1, 24
 Mandal, H.: TF+AS+BI-WeA9, 65
 Mangolini, F.: AS-MoA9, **19**
 Mangolini, L.: EM+AS+EN+NS-FrM8, 100; PS+AS+SS-WeA2, 58
 Mann, J.E.: AS-MoM8, **3**
 Mann, W.F.: SS+AS+NS-WeM6, 50

Manno, M.: EN+AS+EM+NS+SE+SS+TF-MoA9, 25
 Manoharan, H.C.: SP+AS+NS+SS-WeM1, **47**
 Mansergh, R.H.: TF+AS+NS+SA-ThA2, 91
 Mao, S.F.: SS+AS+EN+NS-TuM13, 35
 Marbach, H.: SS+AS+NS-WeM2, 49
 Marchione, D.: SS+AS-WeA2, 63
 Marcinkowski, M.D.: SS+AS+EN-WeA12, **63**
 Marini, J.: SS+AS+EM+EN-ThM13, 77
 Mariolle, D.: SP+AS+NS+SS-WeM4, 48
 Markowski, L.: SS+AS-WeA9, **64**
 Marks, T.J.: AS+NS-TuM6, 30
 Marschewski, E.: HI+AS+NS-ThA4, 84
 Marsh, J.R.: AS-ThM2, 69; AS-ThP10, 97
 Marsh, R.: PS+AS+SS-WeA1, 58
 Martens, R.L.: SE+AS+NS+TR-MoM10, 12; TF+AS+NS+SA-ThA8, 91
 Martin, N.: HI+AS+SS+NS-ThM5, 71
 Martini, A.: TR+AS+NS+SS-ThA1, **92**; TR+AS+NS+SS-ThA3, 93; TR+AS+NS+SS-ThA4, 93
 Mashaal, H.: EM+AS+SS-MoM4, **6**
 Maskova, S.: AC+AS+MI-WeM10, **43**
 Matanovic, I.: AS-MoA5, 18
 Matej, Z.: AC+AS+MI-WeM12, 44
 Mathis, C.: TR+AS+BI+NS-FrM9, 102
 Matsukuma, M.: PS+AS+SS-WeA9, 59
 Matsumoto, M.: SS+AS-WeA10, 64
 Matteocci, F.: AS+SS-WeA12, 54
 Matthews, T.: AS+BI-TuA7, **38**
 Mattrey, R.: BI+AS-MoA9, 21
 Matyi, R.J.: TF+AS+NS+SA-ThM12, 79
 Maynicke, E.: HI+AS+SS+NS-ThM2, 70
 Mayrhofer, P.H.: SE+AS+NS+TR-MoM11, 13; SE+AS+NS+TR-MoM4, 12; SE+AS+NS+TR-MoM5, **12**
 Mazarov, P.: HI+AS+SS+NS-ThM6, 71
 Mazumber, B.: AP+AS-TuM11, **29**
 Mburu, S.: AP+AS-MoA3, 17
 McBreen, P.H.: SS+AS+EN-TuA9, 41
 McClimon, J.B.: AS-MoA9, 19; IS+AS+SA+SS-MoA4, 26
 McCoustra, M.R.S.: SS+AS-WeA2, **63**; TF+AS+SS-MoM2, 14
 McDaniel, F.: AS-ThP8, 96
 McGehee, M.D.: EN+AS+EM+NS+SE+SS+TF-MoA3, 24
 McGuire, M.: SP+2D+AS+NS+SS-WeA3, 60
 Mchenry, M.: AP+AS-MoA7, 17
 McIntyre, P.C.: EM+AS+MS+SS-WeA11, 56; SS+AS+EN+NS-TuM11, 35
 McNamara, J.D.: SS+AS+EM+EN-ThM13, **77**
 Meany, B.: EM+AS+EN+NS-FrM7, 99
 Mei, A.B.: TF+AS+NS+SA-ThA1, **90**
 Meier, T.: TR+AS+NS+SS-ThA7, 93
 Melaet, G.: IS+AS+SA+SS-WeM4, 46
 Meng, S.: AP+AS+MC+MI+NS-MoM5, 1
 Meyer III, H.: AS-ThP2, **95**
 Meyer, D.: TF+AS+NS+SA-ThM6, 78
 Meyer, E.: TR+AS+NS+SS-ThA7, 93
 Meyer, G.: SP+AS+MI+NS+SS-FrM9, 101
 Meysing, D.M.: EN+AS+EM+NS+SE+SS+TF-MoM10, 8
 Michael, T.: HI+AS+SS+NS-ThM2, 70
 Michalak, D.J.: SD+AS+EM-ThM10, 73; SS+AS+EM+EN-ThM4, 77
 Michl, T.D.: SM+AS+BI+PS-ThA6, 88
 Migliori, A.: AC+AS+MI-WeA7, **52**
 Mikkelsen, A.: SS+AS+EM+EN-ThA9, 90
 Miliyanchuk, K.: AC+AS+MI-WeM10, 43
 Miller, B.K.: IS+AS+SS-TuA1, 39
 Miller, C.J.: SS+AS+NS-WeM10, 50
 Miller, J.: IS+AS+SS-MoM8, 10
 Mills, A.: SS+AS-WeA8, 64

- Minaye Hashemi, F.H.: SD+AS+EM+PS-ThA6, 86
- Minelli, C.: AS-WeM5, 45
- Minor, A.M.: HI+AS+NS-ThA10, 85
- Mirabal, A.: SS+AS+EN-MoM10, 14
- Miskovsky, N.M.: EM+AS+SS-MoM5, 6
- Mitrovic, I.Z.: EM+AS+SS-MoA1, 22
- Mitzi, D.B.: EN+AS+EM+NS+SE+SS+TF-MoM1, 7
- Miyamoto, S.: SM+AS+BI+PS-ThM12, 75
- Miyayama, T.: AS+SS-WeA3, 53
- Mock, A.: EL+AS+BI+EM-ThA3, 83; EL+AS+BI+EM-ThA4, 83
- Moddel, G.: EM+AS+SS-MoM1, 5; EM+AS+SS-MoM3, 6
- Moffitt, C.: AS-WeM3, 45
- Mohanty, D.: AP+AS-TuM11, 29
- Mohimi, E.: SD+AS+EM-ThM2, 72
- Moll, N.: SP+AS+MI+NS+SS-FrM9, 101
- Mon, H.H.: SM+AS+BI+PS-ThA6, 88
- Monazami, E.: IS+AS+SA+SS-MoA4, 26
- Moore, D.W.: AS-WeM11, 45
- Mooney, P.: EM+AS+MS+SS-WeA1, 54
- Moore, A.C.: TR+AS+BI+NS-FrM7, 102
- Mora, J.R.: AS+SS-ThA3, 81
- Morales-Acosta, M.D.: SS+AS+EN-MoM5, 13
- Morales-Cifuentes, J.R.: SS+AS+EM+EN-ThA4, 89
- Mork, F.: EN+AS+EM+NS+SE+SS+TF-MoA9, 25
- Morrish, F.M.: BI+AS-MoA5, 21
- Motley, J.: BI+AS-MoA10, 22
- Moulder, J.F.: AS-MoM8, 3; AS-WeM1, 44
- Mousa, M.B.: SD+AS+EM+PS-ThA7, 86
- Mu, R.T.: SS+AS+EN-TuM11, 36; SS+AS+EN-TuM3, 36
- Mueller, T.: NS+AS+SP-MoA9, 28
- Mukai, K.: IS+SS+NS+BI+VT+MN+AS-WeA12, 58
- Mulckhuysen, W.: HI+AS+SS+NS-ThM13, 72
- Muller, D.A.: EM+AS+SS-MoA5, 23
- Muller, T.: NS+AS+SP-MoA1, 27
- Mullet, C.H.: SS+AS+NS-WeM6, 50
- Mulligan, C.P.: SE+AS+NS+TR-MoM9, 12
- Mun, B.S.: IS+AS+SA+SS-TuM12, 33
- Mundy, J.A.: EM+AS+SS-MoA5, 23
- Muramoto, S.: AS+SS-ThA11, 82
- Murari, N.: EM+AS+SS-MoM10, 7; TF+AS+NS+SA-ThA2, 91
- Murphy, C.J.: SS+AS+EN-WeA12, 63
- Murphy, N.R.: AS-ThM12, 70; EN+AS+EM+NS+SE+SS+TF-MoA8, 25
- Murphy, R.D.: TF+AS+EM+EN+MN-WeA3, 66
- Murray, C.B.: EN+AS+EM+NS+SE+SS+TF-MoA5, 24
- Muscat, A.J.: EL+AS+BI+EM-ThA1, 82
- Music, D.: SE+AS+NS+TR-MoM2, 11
- Myoui, A.: SM+AS+BI+PS-ThM12, 75
- N —
- Nadzeyka, A.: HI+AS+NS-ThA4, 84; HI+AS+SS+NS-ThM6, 71
- Nagahata, K.: PS+AS+SS-WeA8, 59
- Nagashima, K.: HI+AS+NS-ThA9, 85
- Nagatsu, M.: SM+AS+BI+PS-ThM5, 74
- Naitou, Y.: HI+AS+NS-ThA3, 84
- Nakakubo, Y.: PS+AS+SS-WeA10, 59
- Nakamura, J.: SS+AS+EN-TuM1, 35; SS+AS-WeA11, 64; TF+AS+SS-MoM9, 15
- Nakanishi, H.: SS+AS+EN-MoM9, 14
- Nakatsujii, K.: SS+AS+NS-WeM5, 50
- Nallan, H.: SD+AS+EM-ThM11, 73
- Nam, J.G.: EN+AS+EM+NS+SE+SS+TF-MoM6, 8
- Nandasiri, M.L.: AP+AS-MoA4, 17
- Narasimham, A.J.: TF+AS+NS+SA-ThM12, 79
- Narasimhan, M.: TF+AS+EM+EN+MN-WeA1, 66
- Nascente, P.A.P.: TF+AS+BI-WeA7, 65
- Neese, C.F.: IS+AS+SA+SS-MoA10, 27
- Negara, M.: EM+AS+MS+SS-WeA11, 56
- Nelin, C.J.: AC+AS+MI-WeA10, 52
- Nelson, A.J.: AC+AS+MI-ThM6, 68
- Nelson, S.F.: EM+AS+SS-MoA9, 23
- Nemanich, R.: EM+AS+MS+SS-WeA3, 55
- Nemsak, S.: AS+SS-WeA9, 54
- Nepal, N.: EM+AS+MS+SS-WeA7, 55; TF+AS+NS+SA-ThM13, 79; TF+AS+NS+SA-ThM6, 78
- Netzer, F.P.: SS+AS+EN-TuM2, 36
- Newberg, J.: IS+AS+SA+SS-TuM2, 33
- Ngo, T.: SD+AS+EM-ThM11, 73
- Nguyen, L.: IS+AS+SA+SS-MoA3, 26; IS+AS+SA+SS-MoA8, 27; IS+AS+SA+SS-WeM13, 47
- Nicotera, E.: SS+AS-WeA1, 63
- Nie, Y.: EM+AS+SS-MoA5, 23
- Niemeyer, T.C.: TF+AS+BI-WeA7, 65
- Nilsson, H.M.: EM+AS+EN+NS-FrM7, 99
- Nolting, W.: SP+AS+MI+NS+SS-FrM4, 100; SP+AS+MI+NS+SS-FrM6, 101
- Nomura, T.: SM+AS+BI+PS-ThA11, 88
- Nonnenmann, S.S.: SP+AS+NS+SS-ThM6, 76
- Norberg, S.A.: SM+AS+BI+PS-ThA1, 87
- Nordeen, P.: TF+AS+NS+SA-ThA11, 92
- Nouvellet, F.: HI+AS+NS-ThA4, 84
- Novotny, Z.: SS+AS+EN-TuM2, 36
- Ntwaeaborwa, O.M.: AS-ThP7, 96
- Nune, S.: IS+AS+SA+SS-TuM13, 34
- Nunney, T.S.: AS+SS-ThA4, 81; AS-MoM9, 3; AS-ThP4, 95; AS-ThP6, 96
- O —
- O'Mullane, S.: EL+AS+BI+EM-ThA6, 83
- O'Brien, L.: EN+AS+EM+NS+SE+SS+TF-MoA9, 25
- Ocola, L.E.: HI+AS+SS+NS-ThM1, 70
- Odén, M.: AP+AS-TuM10, 29
- Odqvist, J.: AP+AS-MoA1, 19
- Ogawa, S.: HI+AS+NS-ThA3, 84
- Ogawa, T.: SS+AS-WeA11, 64
- Ogletree, D.: NS+AS+SP-MoA8, 28
- Ogliore, R.C.: HI+AS+NS-ThA9, 85
- Ogura, S.: SS+AS-WeA10, 64
- Oh, I.K.: SD+AS+EM-ThM12, 73
- Oh, T.: SP+AS+NS+SS-ThM6, 76
- O'Hayre, R.: AS-MoA8, 19; EM+AS+SS-MoM9, 6
- Ohkubo, T.: AP+AS+MC+MI+NS-MoM1, 1
- Ohlhausen, J.A.: AS-ThP9, 96
- Ohno, S.: SS+AS+EN-TuA1, 40; SS+AS-WeA10, 64
- Ohta, T.: SM+AS+BI+PS-ThA11, 88
- Ojea, I.: BI+AS-MoM9, 5
- Okada, M.: SM+AS+BI+PS-ThM5, 74
- Okamoto, T.: SS+AS+EN+NS-TuM5, 34
- Olafsson, S.: EN+AS+EM+SE+SS-TuM1, 31
- Olsson, E.: EM+AS+EN+NS-FrM7, 99
- Olvera, M.A.: EM+AS+EN+NS-FrM3, 99
- O'Meara, D.: SD+AS+EM+PS-ThA11, 87
- Omote, H.: IS+AS+SS-TuA3, 39
- Omrani, A.A.: HI+AS+NS-ThA10, 85
- O'Mullane, S.: EL+AS+BI+EM-ThA2, 82
- Ono, K.: PS+AS+SS-WeA10, 59
- Opasanont, B.: EN+AS+EM+SE+SS-TuM5, 31
- Opila, R.L.: AS-MoM10, 3
- Orion, I.: AC+AS+MI-WeM11, 44
- Orloff, N.D.: EM+AS+SS-MoA5, 23
- Osgood, R.M.: EM+AS+SS-MoM9, 6
- Ouyang, W.: TR+AS+NS+SS-ThA7, 93
- Ovchinnikova, O.S.: AS+NS-TuM10, 30; IS+AS+SS-TuA11, 40
- Overzet, L.J.: PS+AS+SS-WeA7, 59
- Ozsdolay, B.D.: SE+AS+NS+TR-MoM9, 12
- P —
- Pacholski, M.L.: AS-ThM1, 69
- Page, S.C.: AS-ThP3, 95
- Pak, D.M.: SS+AS+EM+EN-ThM4, 77
- Palasantzas, G.: EM+AS+EN+NS-FrM5, 99
- Pan, M.: SS+AS+EN+NS-TuM10, 35
- Pang, Z.: SP+AS+NS+SS-ThM5, 76
- Parameswaran, L.: EM+AS+SS-MoM9, 6
- Paraskevoulakos, C.: AC+AS+MI-ThM5, 68
- Parikh, P.: AP+AS+MC+MI+NS-MoM5, 1
- Park, C.: SP+AS+NS+SS-WeM6, 48
- Park, C.-G.: AP+AS+MC+MI+NS-MoM8, 1
- Park, G.S.: EN+AS+EM+NS+SE+SS+TF-MoM6, 8
- Park, I.-Y.: AS-ThP12, 97
- Park, J.: SP+2D+AS+NS+SS-WeA7, 61; SP+2D+AS+NS+SS-WeA8, 61; SP+AS+NS+SS-WeM6, 48
- Park, J.B.: EN+AS+EM+NS+SE+SS+TF-MoM6, 8
- Park, J.H.: SS+AS+EM+EN-ThM4, 77
- Park, K.: SP+AS+NS+SS-ThM3, 75; SS+AS+EN-TuM4, 36
- Park, W.: EM+AS+SS-MoM6, 6
- Parsons, G.N.: SD+AS+EM+PS-ThA7, 86
- Partes, C.: TF+AS+SS-MoM11, 16
- Patel, A.M.: EN+AS+EM+SE+SS-TuM5, 31
- Patel, N.H.: HI+AS+NS-ThA10, 85
- Pateron, A.: PS+AS+SS-WeA1, 58
- Patil, S.K.: TF+AS+NS+SA-ThM11, 79
- Patscheider, J.: SE+AS+NS+TR-MoM1, 11
- Paukov, M.: AC+AS+MI-WeM12, 44
- Paul, M.: AS+BI-TuA7, 38
- Paul, W.: SP+2D+AS+NS+SS-WeA9, 61; SP+AS+MI+NS+SS-FrM3, 100
- Paven, M.: BI+AS-MoA4, 20
- Pavliček, N.: SP+AS+MI+NS+SS-FrM9, 101
- Pawlak, R.: TR+AS+NS+SS-ThA7, 93
- Pearse, A.J.: AS+SS-ThA9, 81
- Pegalajar-Jurado, A.: SM+AS+BI+PS-ThM13, 75
- Pehrsson, P.E.: BI+AS-MoM6, 4
- Pei, L.: TF+AS+EM+EN+MN-WeA12, 67
- Peixoto, T.: SD+AS+EM-ThM10, 73
- Pekin, T.C.: HI+AS+NS-ThA10, 85
- Pelster, A.: AS+BI-TuA3, 38
- Pelz, B.: EM+AS+SS-MoM1, 5; EM+AS+SS-MoM3, 6
- Peña, D.: SP+AS+MI+NS+SS-FrM9, 101
- Peng, W.N.: EN+AS+EM+NS+SE+SS+TF-MoA1, 24; SS+AS+EM+EN-ThM4, 77
- Perea, D.E.: AP+AS-MoA3, 17
- Perez, C.: SP+AS+NS+SS-ThM6, 76
- Pérez, D.: SP+AS+MI+NS+SS-FrM9, 101
- Periasamy, P.: EM+AS+SS-MoM9, 6
- Perkins, R.T.: EL+AS+BI+EM-ThA11, 83
- Persson, O.: SS+AS+EM+EN-ThA9, 90
- Peterson, E.: SS+AS-WeA1, 63
- Petrik, N.G.: SP+AS+NS+SS-ThM4, 75; SS+AS+EN-WeA9, 62
- Petrov, I.: AS-ThP17, 97; SE+AS+NS+TR-MoM3, 11; TF+AS+NS+SA-ThA1, 90
- Phillip, N.D.: IS+AS+SS-TuA11, 40
- Phumisithikul, K.L.: SS+AS+EM+EN-ThM13, 77
- Pimpinelli, A.: SS+AS+EM+EN-ThA4, 89
- Pireaux, J.-J.: AS+SS-WeA12, 54
- Poda, A.: TR+AS+NS+SS-ThA10, 93
- Poespawati, N.R.: SM+AS+BI+PS-ThM5, 74
- Pohlman, A.J.: SS+AS+EM+EN-ThM10, 77
- Polcik, P.: SE+AS+NS+TR-MoM4, 12
- Poodt, P.: EN+AS+EM+NS+SE+SS+TF-MoM8, 8

- Porter, L.M.: EM+AS+MS+SS-WeA4, **55**
Pouch, S.: SP+AS+NS+SS-WeM4, **48**
Pouvesle, J.-M.: SM+AS+BI+PS-ThM1, **74**
Powell, C.J.: AS-MoM1, **2**
Powell, T.: AS-ThM1, **69**
Pozzi, E.: NS+AS+SP-MoA7, **28**
Primig, S.: AP+AS-MoA5, **17**
Proksch, R.: SP+AS+NS+SS-WeM13, **49**
Pugmire, L.: AC+AS+MI-WeA9, **52**
Pujar, S.P.: SD+AS+EM-ThM10, **73**
Pujari, S.P.: TF+AS+SS-MoM10, **16**
Purnamaningsih, R.W.: SM+AS+BI+PS-ThM5, **74**
Pylypenko, S.: AS-MoA8, **19**
- **Q** —
Qi, J.: EM+AS+SS-MoA10, **23**
Qin, S.: SP+2D+AS+NS+SS-WeA12, **61**
Qiu, A.: TF+AS+NS+SA-ThM5, **78**
Qu, J.: AS-ThP2, **95**
Quan, J.: SS+AS-WeA11, **64**
Quick, A.S.: AS-ThP6, **96**
- **R** —
Race, J.: EL+AS+BI+EM-ThA2, **82**
Rai, R.: TF+AS+NS+SA-ThM11, **79**
Rakowska, P.D.: AS+BI-TuA12, **39**
Ralph, J.F.: EM+AS+SS-MoA1, **22**
Ralston, W.: IS+AS+SA+SS-WeM4, **46**
Ramana, C.V.: TF+AS+NS+SA-ThA3, **91**
Ramm, J.: SE+AS+NS+TR-MoM11, **13**
Randall, J.: SD+AS+EM+PS-ThA8, **86**
Rangan, S.: SS+AS+EN-TuM10, **36**
Rangel, E.: SS+AS+EN+NS-TuM10, **35**
Rastgar, N.: PS+AS+SS-WeA1, **58**
Ratner, B.D.: BI+AS-MoA3, **20**
Reese, M.O.: EN+AS+EM+NS+SE+SS+TF-MoM10, **8**
Reeves, R.V.: TF+AS+EM+EN+MN-WeA11, **67**; TF+AS+EM+EN+MN-WeA3, **66**; TF+AS+EM+EN+MN-WeA4, **66**
Rehman, S.: EL+AS+BI+EM-ThA9, **83**
Reifsnnyder Hickey, D.: AS+SS-ThA10, **82**
Reinke, P.: IS+AS+SA+SS-MoA4, **26**
Rementer, C.: TF+AS+NS+SA-ThA11, **92**
Reshchikov, M.A.: SS+AS+EM+EN-ThM13, **77**
Ribeiro, F.: IS+AS+SS-MoM8, **10**
Richter, R.P.: BI+AS-MoA7, **21**
Ridou, L.: SM+AS+BI+PS-ThM1, **74**
Rieth, L.W.: TF+AS+BI-WeA9, **65**
Rigutti, L.: AP+AS+MC+MI+NS-MoM10, **2**
Rios, L.: IS+AS+SA+SS-WeM3, **46**
Robert, E.: SM+AS+BI+PS-ThM1, **74**
Roberts, A.J.: AS+SS-ThA3, **81**; AS+SS-WeA10, **54**; AS-ThP3, **95**
Robinson, R.: BI+AS-MoA6, **21**
Rockett, A.: EN+AS+EM+NS+SE+SS+TF-MoM9, **8**; SS+AS+EM+EN-ThA11, **90**; TF+AS+NS+SA-ThA1, **90**
Rodriguez, M.: SS+AS+EN-MoM10, **14**
Rogalev, A.: AC+AS+MI-WeM11, **44**
Rogers, B.R.: AS-ThM4, **69**
Rohlfing, M.R.: SP+AS+NS+SS-WeM3, **48**
Rokholt, J.A.: EM+AS+MS+SS-WeA4, **55**
Romano, A.: TF+AS+NS+SA-ThM5, **78**
Romero, M.: AS-ThP16, **97**
Romming, N.: SP+2D+AS+NS+SS-WeA9, **61**
Romolino, K.L.: SS+AS+EM+EN-ThM10, **77**
Rondinone, A.J.: IS+AS+SS-TuA11, **40**
Rosner, F.: SS+AS+EN-MoM8, **13**
Ross, P.N.: IS+AS+SA+SS-TuM12, **33**; IS+AS+SA+SS-TuM3, **33**
Rossi, F.J.: BI+AS-MoM9, **5**; TF+AS+BI-WeA1, **65**
Rosu-Finsen, A.: TF+AS+SS-MoM2, **14**
Rothschild, M.: EM+AS+SS-MoM9, **6**
- Rousseau, R.: SP+AS+NS+SS-ThM4, **75**; SS+AS+EN-TuM11, **36**; SS+AS+EN-TuM3, **36**
Roussel, P.: AC+AS+MI-WeA11, **53**
Rout, B.: AS-ThP8, **96**
Rowley, J.T.: TF+AS+EM+EN+MN-WeA12, **67**
Roy, A.: AS+BI-TuA7, **38**
Rubloff, G.W.: AS+SS-ThA9, **81**
Rudzinski, A.: HI+AS+SS+NS-ThM2, **70**
Rue, C.: HI+AS+SS+NS-ThM3, **71**
Rugar, D.: SP+AS+MI+NS+SS-FrM7, **101**
Ruggeri, F.S.: NS+AS+SP-MoA1, **27**
Russell, Jr., J.N.: BI+AS-MoM6, **4**
Ryan, K.E.: TR+AS+NS+SS-ThA9, **93**
Ryu, S.: SS+AS+EN+NS-TuM11, **35**
- **S** —
Saidi, W.A.: SS+AS+EM+EN-ThA3, **89**
Saito, J.: SS+AS+EN+NS-TuM5, **34**
Saji, S.: SS+AS+EN-TuM1, **35**
Sakaue, M.: SS+AS+EN-MoM9, **14**
Sakudo, A.: SM+AS+BI+PS-ThM5, **74**
Salagaj, T.: EM+AS+MS+SS-WeA4, **55**
Saldin, L.T.: BI+AS-MoA3, **20**
Salmeron, M.B.: IS+AS+SA+SS-MoA5, **26**; IS+AS+SA+SS-WeM1, **46**; IS+AS+SS-TuA8, **40**; NS+AS+SP-MoA8, **28**; SS+AS+EN-TuA12, **42**
Salvo, C.R.: SS+AS+EN+NS-TuM12, **35**
Sampat, S.C.: EN+AS+EM+NS+SE+SS+TF-MoA1, **24**
Samuelsson, M.: SE+AS+NS+TR-MoM8, **12**
Sana, C.O.: EN+AS+EM+NS+SE+SS+TF-MoM5, **8**
Sanchez-Castillo, A.: SS+AS+EN+NS-TuM10, **35**
Sandoval, T.E.: SS+AS+EM+EN-ThM1, **76**
Sangiiovanni, D.G.: SE+AS+NS+TR-MoM3, **11**; TF+AS+NS+SA-ThA1, **90**
Sardashti, K.: EN+AS+EM+NS+SE+SS+TF-MoM1, **7**; EN+AS+EM+NS+SE+SS+TF-MoM2, **7**
Sasaki, T.: AP+AS+MC+MI+NS-MoM1, **1**; TF+AS+SS-MoM8, **15**
Sauter, A.J.: EN+AS+EM+NS+SE+SS+TF-MoA6, **24**
Saw, C.K.: AC+AS+MI-ThM6, **68**
Sbrockey, N.M.: EM+AS+MS+SS-WeA4, **55**
Schall, J.D.: TR+AS+NS+SS-ThA11, **93**
Schenter, G.A.: SS+AS+EN-TuM3, **36**
Scherrer, B.: AP+AS-TuM3, **29**
Schlepütz, C.M.: TF+AS+NS+SA-ThA1, **90**
Schlögl, R.: IS+AS+SA+SS-MoA1, **25**
Schlom, D.G.: EM+AS+SS-MoA5, **23**
Schmidt, D.: EL+AS+BI+EM-ThA4, **83**
Schmidt, S.: AS-ThP17, **97**
Schmüser, L.: BI+AS-MoA4, **20**
Schnadt, J.: IS+AS+SA+SS-MoA4, **26**; IS+AS+SS-MoM11, **11**
Schneider, J.M.: SE+AS+NS+TR-MoM2, **11**
Schneider, W.F.: IS+AS+SS-MoM8, **10**; SS+AS+EM+EN-ThA1, **88**
Schreiber, D.K.: AP+AS-TuM1, **29**; EM+AS+SS-MoM11, **7**
Schubert, E.: EL+AS+BI+EM-ThA3, **83**; EL+AS+BI+EM-ThA4, **83**
Schubert, M.: EL+AS+BI+EM-ThA3, **83**; EL+AS+BI+EM-ThA4, **83**
Schuck, P.: NS+AS+SP-MoA8, **28**
Schuler, B.: SP+AS+MI+NS+SS-FrM9, **101**
Schuster, S.: TF+AS+SS-MoM1, **14**; TF+AS+SS-MoM11, **16**
Schwarm, S.: AP+AS-MoA3, **17**
Seah, M.P.: AS+BI-TuA12, **39**
Sedghi, N.: EM+AS+SS-MoA1, **22**
Seebauer, E.: SS+AS+EM+EN-ThA10, **90**
Seideman, T.: NS+AS+SP-MoA7, **28**
Seidl, W.M.: SE+AS+NS+TR-MoM4, **12**
- Seifert, S.: IS+AS+SS-MoM3, **9**
Sekine, M.: SM+AS+BI+PS-ThA11, **88**
Sekora, D.: EL+AS+BI+EM-ThA3, **83**
Sen, R.: AS+BI-TuA4, **38**
Senesky, D.G.: EM+AS+MS+SS-WeA8, **55**
Seo, S.: SD+AS+EM-ThM12, **73**
Seol, J.-B.: AP+AS+MC+MI+NS-MoM8, **1**
Serov, A.: AS-MoA5, **18**
Sezen, H.: IS+AS+SA+SS-MoA7, **26**
Shahedipour-Sandvik, F.: SS+AS+EM+EN-ThM13, **77**
Shahriar, S.: EN+AS+EM+NS+SE+SS+TF-MoM5, **8**
Shamim, A.: EM+AS+SS-MoA2, **22**
Shan, B.: SS+AS+EN-TuA2, **41**; SS+AS+EN-WeA4, **62**
Shan, Z.W.: HI+AS+NS-ThA8, **84**
Shao, D.: SS+AS+EN+NS-TuM6, **34**
Shard, A.: AS-MoA3, **18**; AS-WeM5, **45**
Sharma, R.: TF+AS+BI-WeA9, **65**
Shavorskiy, A.: AS+SS-WeA9, **54**
Shayesteh, P.: IS+AS+SA+SS-MoA4, **26**
Shehzad, M.A.: EL+AS+BI+EM-ThA9, **83**
Shen, J.: SS+AS+EN-MoM5, **13**
Shen, K.M.: EM+AS+SS-MoA5, **23**
Shepelenko, M.: BI+AS-MoM5, **4**
Shi, G.H.: AS-ThM3, **69**
Shibuya, R.: SS+AS+EN-TuM1, **35**
Shick, A.B.: AC+AS+MI-WeM11, **44**
Shih, C.K.: SP+2D+AS+NS+SS-WeA12, **61**
Shin, H.-J.: SP+2D+AS+NS+SS-WeA8, **61**
Shishikura, K.: SS+AS+NS-WeM5, **50**
Shuh, D.K.: AC+AS+MI-WeA3, **52**
Shutthanandan, V.: AP+AS-MoA4, **17**; HI+AS+NS-ThA9, **85**
Sibener, S.J.: SS+AS+EM+EN-ThA8, **89**
Siekhaus, J.: AC+AS+MI-ThM6, **68**
Sijbrandij, S.: HI+AS+SS+NS-ThM10, **71**
Simpson, R.: AS-ThP4, **95**
Smallwood, C.: IS+SS+NS+BI+VT+MN+AS-WeA1, **56**
Smekal, W.: AS-MoM1, **2**
Smentkowski, V.: AS-ThP11, **97**
Smith, N.: HI+AS+SS+NS-ThM5, **71**
Smith, N.J.: AS-MoM3, **2**
Smith, R.S.: SS+AS+EN-WeA10, **63**
Smolin, Y.Y.: EN+AS+EM+NS+SE+SS+TF-MoA6, **24**
Smulders, M.M.J.: TF+AS+SS-MoM10, **16**
Snezhkova, O.: IS+AS+SS-MoM11, **11**
So, C.: BI+AS-MoA2, **20**
Soares, J.: SS+AS+EM+EN-ThA11, **90**
Sohn, S.-D.: SP+2D+AS+NS+SS-WeA8, **61**
Somorjai, G.A.: IS+AS+SA+SS-WeM4, **46**; IS+AS+SS-MoM1, **9**
Sorensen, R.: AS-ThP9, **96**
Sorensen, S.G.: SS+AS+EN-TuA4, **41**
Sorenson, S.: TR+AS+NS+SS-ThA10, **93**
Sorescu, D.: SS+AS+NS-WeM11, **50**; SS+AS+NS-WeM12, **51**
Sorouh, M.: EN+AS+EM+NS+SE+SS+TF-MoA6, **24**
Spampinato, V.: BI+AS-MoM9, **5**
Spencer, N.D.: TR+AS+BI+NS-FrM9, **102**
Spolenak, R.: AP+AS-TuM3, **29**
Spool, A.: AS+SS-WeA11, **54**
Springell, R.: AC+AS+MI-WeM3, **43**
Spurgeon, S.R.: EM+AS+SS-MoM11, **7**
Sriraman, S.: PS+AS+SS-WeA1, **58**
Stacchiola, D.J.: AS-ThM10, **69**
Stach, E.: IS+AS+SS-TuA8, **40**
Stark, M.: SS+AS+NS-WeM2, **49**
Stayton, P.S.: BI+AS-MoM8, **5**
Steinrück, H.-P.: SS+AS+NS-WeM2, **49**
Stenger, B.H.: SS+AS+NS-WeM6, **50**
Stephens, C.J.: AS-ThP4, **95**
Sterrer, M.: SS+AS+EN-TuA7, **41**
Stevens, E.: SD+AS+EM+PS-ThA7, **86**
Stevie, F.: AS+SS-WeA1, **53**

- Stickle, W.F.: AS-MoM4, 2
 Stine, R.: BI+AS-MoA2, 20
 Stout, P.J.: IS+AS+SA+SS-MoA10, 27
 Stuckert, E.P.: SS+AS+NS-WeM10, **50**
 Subramoney, S.: AS-ThP10, 97
 Sugimoto, S.: SM+AS+BI+PS-ThM12, 75
 Suh, J.: NS+AS+SP-MoA8, 28
 Sui, X.: IS+AS+SA+SS-TuM13, 34;
 IS+SS+NS+BI+VT+MN+AS-WeA3, **57**;
 IS+SS+NS+BI+VT+MN+AS-WeA4, 57
 Sullivan, K.T.: TF+AS+EM+EN+MN-
 WeA11, 67
 Sumiya, M.: PS+AS+SS-WeA12, 60
 Sumpter, B.: SS+AS+EN+NS-TuM10, 35
 Sun, L.: AS-ThM12, 70
 Surman, D.: AS-WeM3, 45
 Susan, D.: AS-ThP9, 96
 Suzer, S.: EN+AS+EM+NS+SE+SS+TF-
 MoM9, 8
 Suzuki, A.: PS+AS+SS-WeA9, 59
 Syed, A.: EM+AS+SS-MoA2, 22
 Sykes, E.C.H.: SS+AS+EN-WeA11, 63;
 SS+AS+EN-WeA12, 63
 Syme, D.B.: TF+AS+BI-WeA11, 66;
 TF+AS+EM+EN+MN-WeA12, 67
 Szakal, C.: AS-WeM10, **45**
- **T** —
 Tadjer, M.J.: EM+AS+MS+SS-WeA7, 55
 Taha, H.: AS+NS-TuM12, 30
 Tait, S.L.: SS+AS+NS-WeM3, **50**
 Takeda, K.: SM+AS+BI+PS-ThA11, 88
 Takeda, S.: IS+AS+SS-TuA3, **39**
 Takei, H.: SS+AS+EN+NS-TuM5, **34**
 Takeuchi, I.: EM+AS+SS-MoA5, 23
 Tallarida, N.: IS+AS+SA+SS-WeM3, 46
 Tan, K.: IS+SS+NS+BI+VT+MN+AS-
 WeA10, 57;
 IS+SS+NS+BI+VT+MN+AS-WeA9, **57**
 Tan, S.: HI+AS+NS-ThA1, **84**
 Tanatsugu, Y.: SM+AS+BI+PS-ThM4, 74
 Tang, M.: SS+AS+EN-TuM4, 36
 Tang, R.: AS-ThP9, 96
 Tang, X.: SS+AS+EN-TuA3, 41
 Tangirala, V.K.: EM+AS+EN+NS-FrM3, **99**
 Tao, C.: SS+AS-WeA8, **64**
 Tao, F.: IS+AS+SA+SS-MoA3, 26;
 IS+AS+SA+SS-MoA8, 27;
 IS+AS+SA+SS-WeM13, **47**
 Tao, M.: SP+AS+MI+NS+SS-FrM10, 101
 Tapily, K.: SD+AS+EM+PS-ThA11, **87**
 Tardio, S.: AS-MoA10, **19**
 Tathireddy, P.: TF+AS+BI-WeA9, 65
 Tatsumi, T.: PS+AS+SS-WeA8, 59
 Tautz, F.S.T.: SP+AS+NS+SS-WeM3, 48
 Taviot-Gueho, C.: TF+AS+NS+SA-ThM1,
 78
 Taylor, A.J.: BI+AS-MoA3, **20**
 Temirov, R.T.: SP+AS+NS+SS-WeM3, **48**
 ten Brink, G.H.: EM+AS+EN+NS-FrM5, **99**
 Tengdelius, L.: SE+AS+NS+TR-MoM8, 12
 Teplyakov, A.V.: SS+AS+EM+EN-ThM3,
 76
 Tereshina, E.: AC+AS+MI-WeM3, **43**
 Terfort, A.: TF+AS+BI-WeA8, **65**;
 TF+AS+SS-MoM1, 14; TF+AS+SS-
 MoM11, 16
 Terry, J.: TF+AS+NS+SA-ThM3, **78**
 Tesch, P.: HI+AS+SS+NS-ThM5, 71
 Thayer, R.: HI+AS+NS-ThA10, 85
 Thevuthasan, S.A.: AP+AS-MoA4, 17
 Thiel, P.A.: SS+AS+EN+NS-TuM6, **34**
 Thimsen, E.: EN+AS+EM+NS+SE+SS+TF-
 MoA10, **25**
 Thissen, A.: IS+AS+SA+SS-MoA9, **27**
 Thissen, P.: SS+AS+EM+EN-ThM2, 76
 Thompson, G.B.: SE+AS+NS+TR-MoM10,
 12; TF+AS+NS+SA-ThA8, 91
 Thonhauser, T.:
 IS+SS+NS+BI+VT+MN+AS-WeA10,
 57; IS+SS+NS+BI+VT+MN+AS-WeA9,
 57
 Thornton, K.: EM+AS+EN+NS-FrM4, 99
 Thorpe, R.: SS+AS+EN-TuM10, **36**
 Thron, A.: NS+AS+SP-MoA8, 28
 Thuvander, M.: AP+AS-MoA1, **17**; AP+AS-
 TuM10, 29
 Tian, W.: SM+AS+BI+PS-ThA1, 87
 Ticey, J.: EM+AS+EN+NS-FrM7, 99
 Tillocher, T.: PS+AS+SS-WeA11, 59
 Timm, R.: SS+AS+EM+EN-ThA9, **90**
 Tkach, I.: AC+AS+MI-WeM12, 44
 Tobin, J.G.: AC+AS+MI-ThM12, **68**
 Tokesi, K.: SS+AS+EN+NS-TuM13, 35
 Tomasella, E.: TF+AS+NS+SA-ThM1, 78
 Tompa, G.S.: EM+AS+MS+SS-WeA4, 55
 Tongay, S.: NS+AS+SP-MoA8, 28
 Torregrosa, I.G.: EN+AS+EM+SE+SS-
 TuM5, 31
 Toth, J.: SS+AS+EN+NS-TuM13, 35
 Treacy, J.P.W.: AS+SS-ThA4, **81**; AS-
 MoM9, 3; AS-ThP4, 95
 Trenary, M.: SS+AS+EN-WeA3, **62**
 Tringides, M.C.: SS+AS+EN+NS-TuM6, 34
 Trinh, B.: SD+AS+EM-ThM2, 72
 Trogler, W.: BI+AS-MoA9, 21
 Troian, A.: SS+AS+EM+EN-ThA9, 90
 Trotochaud, L.: IS+AS+SS-MoM5, **10**;
 SS+AS+EN-TuA3, 41
 Tshabalala, M.A.: AS-ThP7, 96
 Thuillon-Combes, J.: IS+AS+SS-MoM3, 9
 Turek, I.: AC+AS+MI-WeM12, 44
 Turk, C.: AP+AS-MoA5, 17
 Turley, R.S.: EL+AS+BI+EM-ThA11, 83
 Turner, J.: EN+AS+EM+SE+SS-TuM12, 32
 Turrissi, R.: AS+NS-TuM6, 30
 Tuteja, M.: SS+AS+EM+EN-ThA11, **90**
 Tutt, L.W.: EM+AS+SS-MoA9, 23
 Tyler, B.J.: AS+BI-TuA3, **38**
 Tyo, E.: IS+AS+SS-MoM3, 9
 Tysoe, W.T.: TR+AS+NS+SS-ThA3, 93
- **U** —
 Uecker, R.: EM+AS+SS-MoA5, 23
 Unocic, R.R.: IS+AS+SS-TuA11, 40
 Urbakh, M.: TR+AS+NS+SS-ThA7, 93
 Urpelainen, S.: IS+AS+SA+SS-MoA4, 26
 Urrabazo, D.: PS+AS+SS-WeA7, 59
 Utz, A.L.: SS+AS-WeA1, **63**
- **V** —
 Vaid, A.: EL+AS+BI+EM-ThA6, 83
 Vaida, M.E.: SS+AS+EM+EN-ThM12, **77**
 Vaish, A.: BI+AS-MoM10, 5
 Vajda, S.: IS+AS+SS-MoM3, 9
 Vallejo, E.: SS+AS+EN+NS-TuM10, 35
 Valsesia, A.: TF+AS+BI-WeA1, 65
 van Asten, A.C.: AS+SS-ThA11, 82
 Van Duyne, R.P.: NS+AS+SP-MoA7, 28
 van Spronsen, M.A.: IS+AS+SS-MoM4, **10**
 van Zijll, M.S.: SS+AS+NS-WeM6, 50
 Vandalon, V.: SS+AS+EN-TuM12, **37**
 Vanderah, D.: BI+AS-MoM10, 5
 Vanfleet, R.: TF+AS+BI-WeA11, 66;
 TF+AS+EM+EN+MN-WeA12, 67
 Varagas, M.: TF+AS+NS+SA-ThA3, 91
 Vargas, M.: EN+AS+EM+NS+SE+SS+TF-
 MoA8, **25**
 Venhaus, J.: AC+AS+MI-WeA9, 52
 Ventzek, P.: PS+AS+SS-WeA9, 59
 Veyan, J.-F.: SD+AS+EM-ThM10, 73
 Viani, M.: SP+AS+NS+SS-WeM13, 49
 Vieker, H.: SS+AS+EN+NS-TuM5, 34
 Viswan, A.: SM+AS+BI+PS-ThM5, 74
 Vitova, T.: AC+AS+MI-WeA1, **52**
 Vlassioui, I.: SP+2D+AS+NS+SS-WeA3,
 60
 Vohs, J.: SP+AS+NS+SS-ThM6, 76
 Vollmer, D.: BI+AS-MoA4, 20
 von Borany, J.: HI+AS+SS+NS-ThM12, 71
- Vukajlovic, J.: EN+AS+EM+SE+SS-TuM2,
 31
 Vummaneni, K.: TR+AS+NS+SS-ThA11, 93
- **W** —
 Wächter, T.: TF+AS+SS-MoM11, 16
 Wagner, C.W.: SP+AS+NS+SS-WeM3, 48
 Wagner, M.: NS+AS+SP-MoA9, **28**
 Wahl, K.: BI+AS-MoA2, 20
 Wajda, C.: SD+AS+EM+PS-ThA11, 87
 Walker, A.: AS+NS-TuM6, 30
 Walker, A.V.: AS-MoM4, **2**;
 SS+AS+EN+NS-TuM2, 34
 Walker, F.J.: SS+AS+EN-MoM5, 13
 Walker, M.: BI+AS-MoM10, **5**
 Wallingford, M.: SS+AS+EN+NS-TuM6, 34
 Walls, D.J.: AS-ThP10, 97
 Walls, J.M.: EN+AS+EM+NS+SE+SS+TF-
 MoM10, 8;
 EN+AS+EM+NS+SE+SS+TF-MoM11,
 9
 Walper, S.: BI+AS-MoA2, 20
 Walter, J.: EN+AS+EM+NS+SE+SS+TF-
 MoA9, 25
 Walters, D.: SP+AS+NS+SS-WeM13, 49
 Wan, L.: SE+AS+NS+TR-MoM10, 12
 Wang, C.-Z.: SS+AS+EN+NS-TuM6, 34
 Wang, G.: SS+AS-WeA11, 64
 Wang, H.: IS+SS+NS+BI+VT+MN+AS-
 WeA10, 57;
 IS+SS+NS+BI+VT+MN+AS-WeA9, 57
 Wang, J.: BI+AS-MoA9, **21**;
 SS+AS+EN+NS-TuM10, **35**
 Wang, Y.: EM+AS+EN+NS-FrM7, 99;
 SS+AS+EN+NS-TuM11, **35**;
 TF+AS+NS+SA-ThA11, 92
 Wang, Y.-G.: SS+AS+EN-TuM3, 36
 Wang, Y.C.: BI+AS-MoA1, **20**
 Wang, Z.: TF+AS+SS-MoM10, **16**
 Wang, Z.J.: HI+AS+NS-ThA10, 85;
 HI+AS+NS-ThA8, **84**
 Wang, Z.-T.: SP+AS+NS+SS-ThM4, 75;
 SS+AS+EN-TuM11, 36; SS+AS+EN-
 TuM3, 36; SS+AS+EN-TuM4, 36
 Wasio, N.A.: SS+AS+EN-WeA12, 63
 Watanabe, K.: SS+AS+EN+NS-TuM5, 34
 Watts, J.F.: AS-MoA10, 19
 Weatherup, R.S.: IS+AS+SS-MoM10, **10**
 Weber-Bargioni, A.: NS+AS+SP-MoA8, 28
 Weerakkody, A.D.: EM+AS+SS-MoA1, 22
 Wegener, M.: AS-ThP6, 96
 Weidner, T.: BI+AS-MoA4, 20
 Weiner, S.: BI+AS-MoM5, 4
 Weitering, H.H.: SP+2D+AS+NS+SS-
 WeA12, 61
 Welle, A.: AS-ThP6, 96
 Wen, Y.W.: SS+AS+EN-TuA2, 41
 Wepf, R.: AP+AS-TuM3, 29
 Werner, W.S.M.: AS-MoM1, 2
 Westerfield, G.: TF+AS+NS+SA-ThA2, 91
 White, L.J.: BI+AS-MoA3, 20
 White, R.G.: AS-ThP5, **95**
 Wiggins, B.: SS+AS+EM+EN-ThA8, **89**
 Wilde, M.: SS+AS+EN-TuA1, 40; SS+AS-
 WeA10, 64
 Wilhelm, F.: AC+AS+MI-WeM11, 44
 Willis, B.G.: EM+AS+SS-MoA10, 23
 Wilson, J.T.: BI+AS-MoM8, 5
 Windig, W.: AS+SS-ThA6, 81
 Winter, B.: IS+SS+NS+BI+VT+MN+AS-
 WeA7, **57**
 Winter, C.H.: SD+AS+EM-ThM5, **73**
 Wireklint, N.: TF+AS+NS+SA-ThA1, 90
 Wirtz, T.: HI+AS+SS+NS-ThM10, **71**
 Wise, B.: AS+SS-ThA6, **81**
 Wodtke, A.M.: SS+AS-WeA7, 64
 Wolden, C.A.:
 EN+AS+EM+NS+SE+SS+TF-MoM10,
 8
 Wolf, M.: IS+AS+SA+SS-WeM2, 46

- Womack, G.: EN+AS+EM+NS+SE+SS+TF-MoM11, 9
- Wood III, D.: AP+AS-TuM11, 29
- Wood, K.N.: AS-MoA8, 19
- Wrench, J.S.: EM+AS+SS-MoA1, 22
- Wu, C.H.: IS+AS+SA+SS-WeM1, 46
- Wu, J.: NS+AS+SP-MoA8, 28
- Wu, R.: SP+2D+AS+NS+SS-WeA12, 61
- Wu, W.: SP+AS+MI+NS+SS-FrM1, 100
- Wu, Z.: IS+AS+SS-TuA9, 40
- **X** —
- Xia, Y.: SP+AS+NS+SS-ThM3, 75; SS+AS+EN-TuM4, 36
- Xiao, Z.: AS-ThM3, 69
- Xie, K.: SS+AS+EN-WeA1, 62
- Xin, H.L.: IS+AS+SS-TuA8, 40
- Xu, H.: SS+AS+EN+NS-TuM13, 35
- Xu, J.: EM+AS+SS-MoM9, 6
- Xu, Q.: TF+AS+NS+SA-ThA11, 92
- **Y** —
- Yamada, H.: SP+AS+NS+SS-WeM12, 49
- Yamaguchi, K.: SS+AS+NS-WeM1, 49
- Yan, H.: SS+AS+EN-WeA1, 62
- Yang, B.: IS+AS+SS-MoM3, 9
- Yang, J.C.: IS+AS+SS-TuA8, 40; SS+AS+EM+EN-ThA3, 89
- Yang, K.: SP+2D+AS+NS+SS-WeA9, 61
- Yang, Y.: SP+AS+NS+SS-WeM5, 48
- Yano, J.: IS+AS+SA+SS-TuM3, 33
- Yao, A.: SP+AS+NS+SS-WeM12, 49
- Yao, J.: IS+AS+SA+SS-TuM13, 34
- Yao, Y.: EM+AS+MS+SS-WeA4, 55
- Yao, Z.: TF+AS+NS+SA-ThA11, 92
- Yarmoff, J.A.: SS+AS+EM+EN-ThA7, 89; SS+AS+EN+NS-TuM12, 35
- Yarrington, C.D.: TF+AS+EM+EN+MN-WeA3, 66
- Yartys, V.: AC+AS+MI-WeM10, 43
- Yates, P.: AS+NS-TuM5, 30
- Ye, Y.F.: EN+AS+EM+SE+SS-TuM13, 32
- Ye, Z.: TR+AS+NS+SS-ThA4, 93
- Yeom, H.W.: SP+2D+AS+NS+SS-WeA4, 60
- Yoo, C.: SD+AS+EM-ThM12, 73
- Yoon, J.: SD+AS+EM-ThM12, 73
- Yoon, M.: SP+AS+NS+SS-WeM6, 48
- Yoon, Y.: SP+AS+NS+SS-ThM4, 75; SS+AS+EN-TuM3, 36
- Yoshida, H.: IS+AS+SS-TuA3, 39
- Yoshiike, Y.: SS+AS+NS-WeM5, 50
- Yoshikwa, H.: SM+AS+BI+PS-ThM12, 75
- Yoshinobu, J.: IS+SS+NS+BI+VT+MN+AS-WeA12, 58
- Yoshiomoto, S.: IS+SS+NS+BI+VT+MN+AS-WeA12, 58
- Young, C.N.: AS-MoM4, 2
- Young, J.: EN+AS+EM+SE+SS-TuM12, 32
- Yu, C.: SM+AS+BI+PS-ThM4, 74
- Yu, J.: AS+BI-TuA11, 39; IS+SS+NS+BI+VT+MN+AS-WeA4, 57
- Yu, K.-H.: SD+AS+EM+PS-ThA11, 87
- Yu, x.: SP+AS+MI+NS+SS-FrM10, 101
- Yu, X.-Y.: AS+BI-TuA11, 39; AS-WeM4, 45; IS+AS+SA+SS-TuM13, 34; IS+SS+NS+BI+VT+MN+AS-WeA3, 57; IS+SS+NS+BI+VT+MN+AS-WeA4, 57
- Yu, Y.: IS+AS+SS-MoM5, 10; SS+AS+EN-TuA3, 41
- Yuan, S.: EM+AS+SS-MoM1, 5
- Yurek, P.: AS+SS-ThA10, 82
- **Z** —
- Zegkinoglou, I.: AS+SS-WeA9, 54
- Zeitler, T.: SS+AS+EN-MoM10, 14
- Zeng, L.: AS+NS-TuM6, 30
- Zhang, H.: SS+AS+EN-TuM13, 37
- Zhang, J.: IS+SS+NS+BI+VT+MN+AS-WeA4, 57; NS+AS+SP-MoA8, 28
- Zhang, L.: AS-ThM2, 69; IS+AS+SS-TuA1, 39; SS+AS+NS-WeM2, 49
- Zhang, S.: IS+AS+SA+SS-MoA8, 27
- Zhang, W.: SD+AS+EM-ThM1, 72
- Zhang, X.: EN+AS+EM+NS+SE+SS+TF-MoA9, 25; SP+2D+AS+NS+SS-WeA3, 60
- Zhang, Y.: NS+AS+SP-MoA8, 28; SP+2D+AS+NS+SS-WeA12, 61
- Zhang, Z.: SD+AS+EM-ThM11, 73; SP+AS+NS+SS-ThM3, 75; SS+AS+EN-TuM4, 36
- Zharnikov, M.: TF+AS+SS-MoM1, 14; TF+AS+SS-MoM11, 16; TF+AS+SS-MoM4, 15
- Zheng, H.: SS+AS-WeA8, 64
- Zheng, P.Y.: TF+AS+NS+SA-ThA4, 91
- Zhernokletov, D.: EM+AS+MS+SS-WeA11, 56
- Zhou, L.: TF+AS+NS+SA-ThM11, 79
- Zhou, M.: TF+AS+NS+SA-ThA9, 92
- Zhou, W.: SS+AS+EM+EN-ThA7, 89
- Zhou, X.: TF+AS+NS+SA-ThA8, 91
- Zhou, Y.: AS+BI-TuA11, 39; IS+AS+SA+SS-TuM13, 34; IS+SS+NS+BI+VT+MN+AS-WeA3, 57; IS+SS+NS+BI+VT+MN+AS-WeA4, 57
- Zhu, J.: SP+AS+NS+SS-ThM6, 76
- Zhu, J.F.: EN+AS+EM+NS+SE+SS+TF-MoA7, 24; EN+AS+EM+SE+SS-TuM13, 32; TF+AS+BI-ThA10, 66
- Zhu, K.: SP+AS+NS+SS-ThM3, 75; SS+AS+EN-TuM4, 36
- Zhu, Q.: SS+AS+EM+EN-ThA3, 89
- Zhu, X.: SS+AS+EN-MoM5, 13
- Zhu, Y.: EM+AS+SS-MoA5, 23
- Zhu, Z.: AS+BI-TuA11, 39; AS-WeM4, 45; IS+AS+SA+SS-TuM13, 34; IS+SS+NS+BI+VT+MN+AS-WeA3, 57; IS+SS+NS+BI+VT+MN+AS-WeA4, 57; SP+AS+NS+SS-ThM4, 75
- Zinoviev, O.: IS+AS+SA+SS-WeM12, 47
- Zojer, E.: TF+AS+SS-MoM1, 14
- Zoubian, F.: TF+AS+NS+SA-ThM1, 78
- Zuilhof, H.: AS+BI-TuA4, 38; SD+AS+EM-ThM10, 73; TF+AS+SS-MoM10, 16
- Zuluaga, S.: IS+SS+NS+BI+VT+MN+AS-WeA10, 57; IS+SS+NS+BI+VT+MN+AS-WeA9, 57